



SAPIENZA
UNIVERSITÀ DI ROMA

Multi-performance evaluation of traditional and low-damage non-structural components

**Sapienza University of Rome,
Department of Geotechnical and Structural Engineering**

A thesis submitted in partial fulfilment of the requirements for the Degree of Doctor of Philosophy by

Eng. Simona Bianchi

Supervisor
Prof. Eng. Stefano Pampanin

February 2020

Abstract

Non-structural components include all the building elements not part of the main load-bearing system of a structure or an industrial facility. These components are designed to provide specific performance, such as controlling the passage of heat or resisting to fire, while the seismic behaviour is typically neglected in the design process. Nevertheless, the response of these elements can significantly affect the building functionality after earthquakes, even for low-intensity events, and their poor performance can result in substantial economic losses and business interruption. Consequently, the non-structural damage has a severe impact on the post-earthquake building recovery in addition to the potential risk to life safety.

As either the earthquake engineering community or the public demand a higher level of earthquake protection, improving the seismic performance of structural systems is not enough and the expectation of advanced seismic behaviour for non-structural components is demanded. The need for reduction of non-structural seismic risk is thus being recognized fundamental in the decision-making process and in the performance-based seismic design the attention is nowadays focusing on both the harmonization of structural/non-structural performance and the development of damage-control or low-damage non-structural systems.

Considering the previous background, this Thesis mainly aims to: 1) provide evidence on the convenience of implementing innovative low-damage technologies for non-structural components, 2) highlight the importance of including the study of the seismic performance of new or retrofitted elements within an integrated multi-performance design approach.

The Thesis initially provides an overview of the damage states/mechanisms evolving during earthquake shakings in different typologies of non-structural elements, i.e. architectural

elements, building services and contents. Fragility curves developed from past experimental research are also collected; in fact, determining which parameters mainly influence the failure modes and when a damage condition is achieved can help in the proposal of new solutions.

Then, a literature review can be found on the innovative damage-mitigation technologies developed during the last decades for both structural and non-structural components. These solutions can be combined to define an integrated high-performance earthquake-proof building system. The Thesis also describes the experimental investigations (1D shake-table testing) carried out on a new earthquake-resistant solution proposed with the aim of reducing the seismic demand on non-structural systems anchored to concrete structures, i.e. supplemental damping is added to post-installed fasteners. The test results confirm the beneficial effects of this solution to seismically protect the non-structural elements for expansion or chemical fasteners in both un-cracked and cracked concrete.

The convenience of implementing low-damage systems is thus investigated through numerical and experimental studies. Cost/performance-based evaluations of multi-storey buildings comprising different traditional vs. low-damage structural systems (frames, walls) and non-structural elements (facades, partitions, ceilings) are performed to highlight that these solutions are able to withstand earthquake shakings with negligible damage, consequently reducing the expected losses in terms of repair costs and downtime. The high performance of such types of technologies, and particularly of the integrated system, is also proved through 3D shake-table tests of a 1:2 scale two storey-two bay building, consisting of a low-damage timber-concrete structural skeleton and high performance or damage-control non-structural components/envelopes. The experimental campaign is fully described from the design of the specimen and of its structural/non-structural detailing, to the construction and assembly phases, to the test setup. Preliminary experimental results are provided, focusing on the seismic demand/performance of all the tested non-structural components.

Finally, the importance of implementing a multi-performance design approach for non-structural components is presented in the last part of the Thesis. An integrated seismic & energy cost/performance investigation of traditional vs. low-energy and/or low-damage façade systems is initially carried out, to highlight that the dynamic behaviour of these systems must be studied to better design the non-structural detailing. Furthermore, a multi-criteria decision analysis, including all the non-structural performance (structural, architectural, long-term) and the initial cost as criteria/sub-criteria, is proposed and developed in order to drive decisions on non-structural systems, i.e. defining the best solution/detailing among alternatives.

Acknowledgements

These three years of Ph.D. have been an amazing and wonderful experience, and this would not be possible if I had not met again Professor Pampanin that fateful day. I had the opportunity to redirect myself towards a path that I already knew I wanted to take. I would like to thank Professor Pampanin for his technical guidance, for inspiring me in making this research and mainly for giving me the possibility to make a unique and unforgettable experience. I have grown professionally and personally with an indescribable gain for myself.

During this intense path, I have met so special friends and very nice persons. In Rome, thanks to all my old friends, my colleagues, my old and new flatmates for the time spent together having fun and leaving out problems related to work or study. I would also like to acknowledge all the staff from Sapienza University for their assistance in some situations. In Amsterdam, I would like to thank Michele Palmieri, for giving me the opportunity to spend 10 months in ARUP Nederland, that experience opened my mind inspiring me towards new research challenges. And, thanks to all the amazing friends and persons I met there, for all the laughter we had during our barbeques in the parks, you made unique that period. In Lisbon, thanks to the friends I also found there, for distracting me during hard periods of work, as well as to all the technicians and engineers of the LNEC who provided me support during the experimental campaign. I do not want to list all your names; however, I cannot help thanking Jonathan Ciurlanti. Really thanks to my special friend, you have accompanied me throughout all this path, working together on different topics. Thanks for your support during easy or hard periods, both in the work and life, and many thanks for making me have so much fun.

Finally, I would like to acknowledge the support of my family. Thanks for your understanding and encouragement during the periods abroad; this Thesis is dedicated to you.

Table of contents

1. Introduction

1.1	Background and research motivation.....	1.1
1.1.1	Post-earthquake non-structural damage.....	1.3
1.1.2	Improving the seismic performance of non-structural elements.....	1.4
1.1.3	Development of an integrated structural & non-structural high-performance system.....	1.5
1.2	Objectives and scopes of the research.....	1.6
1.3	Organisation of the Thesis.....	1.8
1.4	References.....	1.11

2. Overview of non-structural elements: typologies and overall performance

2.1	Introduction.....	2.1
2.2	Typologies of non-structural components.....	2.1
2.2.1	Exterior enclosures.....	2.2
2.2.1.1	Cladding systems.....	2.3
2.2.1.1.1	Curtain walls.....	2.4
2.2.1.1.2	Cladding walls.....	2.8
2.2.1.2	Infill walls.....	2.13
2.2.1.3	Mix systems.....	2.16
2.2.1.4	Summary: exterior enclosures.....	2.17
2.2.2	Partitions.....	2.18

2.2.3	Ceiling systems.....	2.25
2.2.4	Building services and contents.....	2.28
2.3	Performance of non-structural elements.....	2.29
2.3.1	Structural performance.....	2.29
2.3.1.1	Static.....	2.29
2.3.1.2	Dynamic.....	2.30
2.3.1.3	Fire.....	2.31
2.3.2	Architectural performance.....	2.32
2.3.2.1	Thermal.....	2.32
2.3.2.2	Acoustic.....	2.33
2.3.2.3	Weather tightness.....	2.34
2.3.3	Long-term performance.....	2.35
2.3.3.1	Durability.....	2.35
2.3.3.2	Sustainability.....	2.36
2.4	Summary: overall performance.....	2.37
2.5	Conclusions.....	2.39
2.6	References.....	2.41

3. Seismic performance of non-structural components

3.1	Introduction.....	3.1
3.2	Post-earthquake damage.....	3.2
3.2.1	Damage to exterior enclosures.....	3.3
3.2.1.1	Curtain walls.....	3.3
3.2.1.2	Cladding walls.....	3.4
3.2.1.3	Infill walls.....	3.5
3.2.2	Damage to partitions.....	3.6
3.2.3	Damage to ceiling systems.....	3.7
3.2.4	Damage to building services and contents.....	3.9
3.3	Investigations on seismic behaviour.....	3.12
3.3.1	Exterior enclosures.....	3.13
3.3.1.1	Curtain walls.....	3.13
3.3.1.2	Cladding walls.....	3.18
3.3.1.3	Infill walls.....	3.25
3.3.2	Partitions.....	3.29
3.3.3	Ceiling systems.....	3.34

3.3.4	Building services.....	3.37
3.3.5	Building contents.....	3.39
3.4	Conclusions.....	3.43
3.5	References.....	3.45

4. Development of innovative low-damage technologies

4.1	Introduction.....	4.1
4.2	Damage-Control design approach.....	4.1
4.3	Overview on damage-mitigation solutions.....	4.3
4.3.1	Low-damage structural elements.....	4.3
4.3.2	Low-damage non-structural elements.....	4.6
4.3.2.1	Exterior enclosures.....	4.7
4.3.2.1.1	Cladding systems.....	4.7
4.3.2.1.2	Infill walls.....	4.9
4.3.2.2	Partitions.....	4.11
4.3.2.3	Ceiling systems.....	4.12
4.3.2.4	Building services and contents.....	4.13
4.3.3	Integrated low-damage system.....	4.14
4.4	Experimental investigation on innovative earthquake-resistant fasteners....	4.15
4.4.1	Previous research.....	4.15
4.4.2	Development of the EQ-Rod concept.....	4.16
4.4.3	Experimental campaign on the EQ-Rod 2.0.....	4.18
4.4.3.1	General overview.....	4.18
4.4.3.2	Test setup.....	4.19
4.4.3.3	Monitoring system.....	4.21
4.4.3.4	Input motions and test matrix.....	4.22
4.4.3.5	Testing protocol.....	4.24
4.4.3.6	Test results.....	4.25
4.4.3.7	Conclusions from the experimental campaign.....	4.33
4.5	Conclusions.....	4.35
4.6	References.....	4.39

5. Convenience of implementing damage-resistant building systems

5.1	Introduction.....	5.1
5.2	Cost/performance evaluation of low-damage systems.....	5.2

5.2.1	Description of the case-study buildings.....	5.3
5.2.2	Design of the structural systems.....	5.5
5.2.3	Building performance points.....	5.7
5.2.4	Fragility specifications.....	5.11
5.2.4.1	Low-damage structural elements.....	5.12
5.2.4.2	Low-damage non-structural elements.....	5.12
5.2.5	Loss assessment analysis.....	5.15
5.2.5.1	Repair costs.....	5.16
5.2.5.2	Downtime.....	5.19
5.2.6	Further studies.....	5.21
5.2.7	Summary of the cost/performance analysis.....	5.29
5.3	Risk assessment analysis of precast concrete cladding systems: Traditional vs. Low-damage solution.....	5.31
5.3.1	Case-study building.....	5.31
5.3.2	Numerical investigation.....	5.32
5.3.2.1	Push-over analysis.....	5.32
5.3.2.2	Incremental dynamic analysis.....	5.34
5.3.2.3	Development of fragility curves.....	5.35
5.3.3	Summary of the risk assessment analysis.....	5.37
5.4	Conclusions.....	5.38
5.5	References.....	5.40

6. 3D shake-table tests on an integrated low-damage building system: Test Building design and construction

6.1	Introduction.....	6.1
6.2	Proposed EU-funded SERA project.....	6.1
6.3	Description of the experimental campaign.....	6.3
6.3.1	Test Building design.....	6.5
6.3.1.1	Connection design.....	6.9
6.3.1.2	Structural members.....	6.12
6.3.1.3	Non-structural detailing.....	6.14
6.3.2	Construction and assembly.....	6.21
6.3.2.1	Fabrication and transportation.....	6.21
6.3.2.2	Assembly of structural system.....	6.22
6.3.2.3	Assembly of non-structural components.....	6.27

6.4	Conclusions.....	6.38
6.5	References.....	6.40
7.	3D shake-table tests on an integrated low-damage building system: test setup and experimental results	
7.1	Introduction.....	7.1
7.2	Experimental set-up.....	7.1
7.2.1	Shaking table.....	7.2
7.2.2	Instrumentation plan.....	7.2
7.2.2.1	Phase 1: Skeleton Building.....	7.3
7.2.2.2	Phase 2: Skeleton Building with internal partitions.....	7.7
7.2.2.3	Phase 3: Integrated system.....	7.9
7.2.3	Ground motion selection.....	7.13
7.2.4	Test matrix.....	7.15
7.2.5	Signal processing and data acquisition.....	7.17
7.2.6	Timeline of the experimental tests.....	7.17
7.3	Shake table testing results.....	7.18
7.3.1	Phase 2 testing.....	7.18
7.3.1.1	Test results.....	7.19
7.3.1.2	Damage description.....	7.23
7.3.1.3	Dynamic identification.....	7.27
7.3.2	Phase 3 testing.....	7.29
7.3.2.1	Test results.....	7.30
7.3.2.2	Damage description.....	7.36
7.3.2.3	Dynamic identification.....	7.38
7.4	Conclusions.....	7.41
7.5	References.....	7.42
8.	Integrated seismic & energy cost/performance-based evaluation	
8.1	Introduction.....	8.1
8.2	Energy efficiency of buildings.....	8.1
8.2.1	Thermal performance.....	8.3
8.2.2	Energy efficiency evaluation.....	8.7
8.2.3	Innovative energy efficiency solutions.....	8.10
8.2.3.1	Energy-efficient solutions for buildings.....	8.10

8.2.3.2	Energy-efficient solutions for components.....	8.16
8.3	Integrated seismic & energy approach.....	8.20
8.3.1	Previous research.....	8.21
8.3.2	Application: seismic & energy cost/performance evaluation of building systems.....	8.22
8.3.2.1	Case-study building.....	8.24
8.3.2.2	Seismic performance.....	8.27
8.3.2.3	Energy performance.....	8.28
8.3.2.4	Integrated seismic & energy performance.....	8.36
8.4	Conclusions.....	8.43
8.5	References.....	8.44

9. Multi-criteria decision-analysis for non-structural components

9.1	Introduction.....	9.1
9.2	Overall non-structural performance.....	9.1
9.2.1	Static performance.....	9.2
9.2.2	Dynamic performance.....	9.3
9.2.3	Fire performance.....	9.4
9.2.4	Thermal performance.....	9.6
9.2.5	Acoustic performance.....	9.6
9.2.6	Weather tightness.....	9.9
9.2.7	Durability performance.....	9.11
9.2.8	Sustainability performance.....	9.13
9.3	Multi-criteria decision-making approach.....	9.15
9.3.1	General aspects of MCDM.....	9.15
9.3.2	MCDM for non-structural components.....	9.17
9.3.3	Application of the proposed MCDM.....	9.22
9.4	Conclusions.....	9.29
9.5	References.....	9.30

10. Conclusions and recommendations for future work

10.1	Introduction.....	10.1
10.2	Research conclusions.....	10.2
10.2.1	Study of the seismic behaviour of non-structural elements.....	10.2

10.2.2 Provide evidences on the benefits of innovative low-damage technologies.....	10.4
10.2.3 Definition of a multi-performance design approach for non-structural components.....	10.7
10.3 Future developments.....	10.9

Appendix A:

Shake-table tests on post-installed fasteners: Testing procedure and experimental results

A.1 Introduction.....	A.1
A.2 Testing procedure.....	A.1
A.3 Test results.....	A.7
A.4 References.....	A.21

Appendix B:

SLaMA-based analytical procedure for the cost/performance-based evaluation of buildings

B.1 Introduction.....	B.1
B.2 Evaluation of building response within the PBEE methodology.....	B.1
B.3 Validation of the SLaMA-based analytical procedure.....	B.4
B.3.1 Case-study buildings.....	B.5
B.3.2 Design of structural system.....	B.6
B.3.3 Building seismic response.....	B.7
B.3.4 Loss assessment analysis.....	B.9
B.4 Conclusions.....	B.13
B.5 References.....	B.14

Appendix C:

Shake-table tests on an integrated low-damage building system (SERA Project): Seismic design and structural verifications of the Test Building

C.1 Introduction.....	C.1
C.2 Test building design.....	C.1
C.2.1 Building data.....	C.1
C.2.2 Seismic demand.....	C.6
C.2.3 DDBD procedure.....	C.7

C.2.3.1	Frame system.....	C.9
C.2.3.2	Wall system.....	C.16
C.2.4	Initial numerical analysis.....	C.18
C.3	Test building detailing.....	C.19
C.4	References.....	C.25

Appendix D:

Shake-table tests on an integrated low-damage building system (SERA Project): Construction of the non-structural systems

D.1	Introduction.....	D.1
D.2	Fiber reinforced gypsum walls (Option 1).....	D.1
D.3	Glass fiber reinforced concrete facades (Option 2).....	D.5
D.4	Spider glazing facades (Option 2).....	D.7
D.5	Masonry infill partition (Option 2).....	D.9

Appendix E:

Thermal performance analysis of façade systems

E.1	Introduction.....	E.1
E.2	Thermal analysis.....	E.1

1. Introduction

1.1 Background and research motivation

Non-structural components comprise all the elements not part of the primary system of a building. These components are generally classified into three broad categories (Villaverde 2004), namely: 1) architectural elements, such as facades, partitions or ceilings (Figure 1.1 - left); 2) mechanical and electrical equipment, as piping systems, ducts or escalators; 3) building contents, including as example bookshelves or computers and desktop equipment. These systems are usually specified by architects, mechanical engineers and electrical engineers or may be installed directly by the building owners or tenants.

Non-structural components can be affected by numerous external actions during their life, due to environmental climatic factors (temperature, wind, rain, sun radiation) or other factors (fire, noise, earthquake). Therefore, as initially presented by Riccio (2010), these systems must be designed to provide satisfactory levels of performance to all these actions (thermal, acoustic, weather tightness, fire, static, dynamic) and a multi performance-based design approach should be adopted. E.g. for façade systems, the overall performance and the system detailing (e.g. panel thickness, sub-frame system, connection devices) must be designed taking into account the aesthetic image of the building, the capacity of controlling the passage of light and heat and avoiding thermal bridging, the property of preventing air leakage, the capability of controlling the passage of the sound, as well as other functions like the capacity of adjusting thermal expansions, resisting to movements due to wind, creep or earthquakes, resisting to fire and weather conditions (Baird et al. 2011a). Consequently, the

optimal design of a non-structural component should be carried out following a multi-criteria decision-making process, including also evaluations on the durability and sustainability properties of the element (Figure 1.1 - right).



Figure 1.1. Example of architectural components (left: Baird 2014, centre: www.appliedworkplace.co.uk) and overall non-structural performance (right).

Nevertheless, a complete multi-performance design approach is still missing in the common practice, and mainly the capacity of resisting against seismic actions is not yet taken into account or is certainly less investigated than the other performance measures. Nowadays, money is in fact invested to build a very high energy efficient façade, however, this may not represent the best choice if the component will be seriously damaged or destroyed after an earthquake. While, if during the design procedure is paid attention to the system connection details, simple measures could provide both energy and seismic efficient capabilities without increasing (significantly) the component investment cost. Non-structural components can, in fact, be subjected to large seismic forces during earthquakes and must withstand the accelerations and displacements arising from the structural response. Economic losses due to non-structural damage generally exceed the structural losses, even for low-seismic intensity motions, whilst damaged non-structural elements can severely limit the functionality of critical facilities. Therefore, it is fundamental to include the seismic study into the design process of non-structural systems.

1.1.1 Post-earthquake non-structural damage

Damage reports from past or more recent earthquakes (L'Aquila 2008, Darfield 2010, Christchurch 2011, Kaikoura 2016) have continuously highlighted that non-structural

components are very vulnerable to earthquake shakings (Figure 1.2 - left). Non-structural damage occurs at low-to-moderate seismic intensities and can be very high, leading to a substantial increase in the total building losses, as also presented in Bradley et al. (2009) (Figure 1.2 - right), in terms of both repair costs and business interruption. Furthermore, the failure of non-structural elements can become a potential risk to life-safety while their survival is essential to provide emergency services in the aftermath of a seismic event.

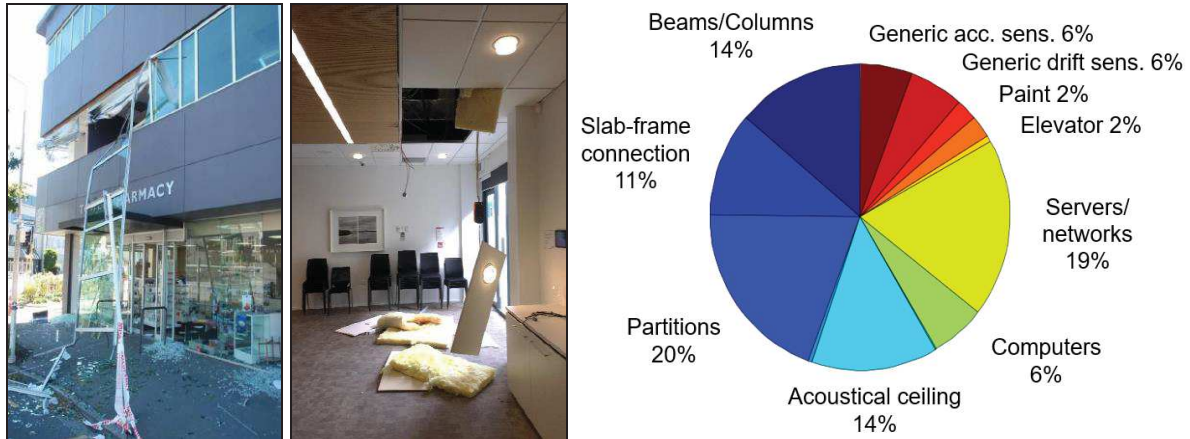


Figure 1.2. Examples of damage to non-structural elements: 1) disconnection of a light-medium weight cladding (left, Baird et al. 2011b), 2) fallen lightweight ceiling tiles (centre, Baird and Ferner 2017); example of percentage of non-structural contribution to the building seismic loss (right, Bradley et al. 2009).

In the past, earthquake engineers have mainly focused on improving the seismic performance of structural systems and more comprehensive standards developed as well as expectations of advanced seismic behaviour increased. Both the earthquake engineering community and the society demand a higher level of protection against earthquakes thus, it becomes fundamental to investigate the seismic behaviour of non-structural components. Therefore, a great research effort has been dedicated in the last decades to better understand the damage states of the non-structural systems taking into account post-earthquake damage reports, carrying out experimental tests or performing numerical investigations. The knowledge of these damage states can address the definition of technological solutions with higher performance.

As can be found in FEMA P-58 (2012) or as recently proposed by NIST within the ATC-120 Project (NIST GCR 17-917-44 2017), a collection of the key parameters describing the seismic behavior of non-structural components is needed. Moreover, in order to facilitate the proposal of practical and efficient damage-resistant technologies, the collection of information in terms of mechanisms and damage states is not enough, and the fragility

curves associated with the different damage conditions are required. In fact, notwithstanding fragility functions vary depending on the component details (i.e. for a glass façade they are a function of the framing detailing, glass-to-frame clearance, system type, glass type, panel dimensions, glass thickness) general considerations on the expected behavior of a system can be identified. Thus, new solutions can be proposed taking into account the fragility specifications and defining levels of inter-storey drift ratio or floor acceleration to be achieved during the design of the non-structural detailing.

1.1.2 Improving the seismic performance of non-structural elements

With the development of the performance-based earthquake engineering philosophy, it becomes important the harmonization of the performance levels between structural and non-structural components (Filiatrault and Sullivan 2014). If the structural system allows immediate occupancy after a seismic event, it must be avoided that the behaviour of non-structural components lowers the entire building performance. This aim can be reached by providing specific guidance to the design of non-structural components and adopting non-structural details that can guarantee the achievement of acceptable performance levels.

Regarding the seismic design, more investigations have been recently developed on the study of design provisions for non-structural systems, as the work carried out by NIST through the ATC-120 Project (NIST GCR 17-917-44 2017; NIST GCR 18-917-43 2018) whose intent is recommending improvements to these requirements that can have a large impact to public safety and economic welfare. New design philosophies are also developing, like the one conceived by the same ATC-120 (NIST GCR 18-917-43 2018) based on the concepts of capacity-based design or the methodology proposed by Filiatrault et al. (2018) i.e. the application of a direct displacement-based design procedure for non-structural elements.

Concerning the non-structural details, protective measures can be easily applied to reduce the seismic hazard to non-structural elements, e.g. in the FEMA E-74 (2011) different measures are indicated for improving the protection against earthquakes of different typologies of non-structural systems. Nevertheless, in the spirit of the performance-based earthquake engineering, protective solutions are efficient if they either improve the system performance or reduce the related socio-economic losses and business interruption. Consequently, innovative damage-mitigation techniques (damage-control or low-damage technologies) have been recently developed for non-structural elements to achieve this goal.

However, these systems need further investigations and standardized details should be defined to be applicable in the common construction practice.

1.1.3 Development of an integrated structural & non-structural high-performance system

The performance-based seismic design should move towards the development of an integrated approach controlling the performance of the whole building system (superstructure, non-structural components and soil/foundation system) from the design process to the construction phases. Due to the increased public consciousness of seismic risk, targeting life-safety is not enough for the design of new buildings and a paradigm shift towards damage-control design philosophy and technologies is needed (Pampanin 2012, 2015). Therefore, innovative cost-affordable low-damage technical solutions are developing to meet this higher public expectation and an integrated damage-resistant structural & non-structural system should be realized (Figure 1.3).

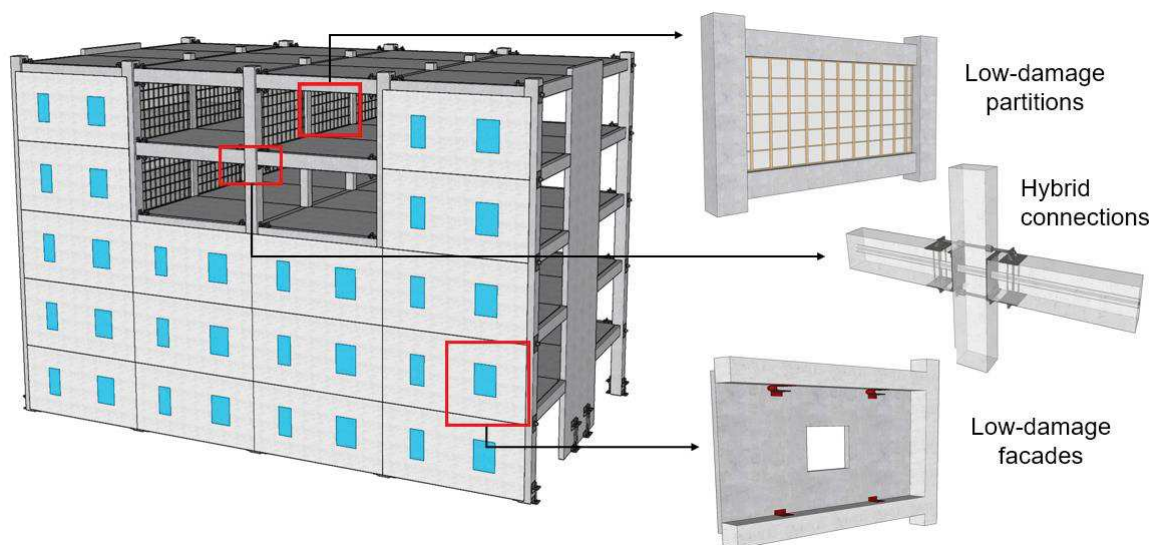


Figure 1.3. Integrated low-damage system (Bianchi et al. 2018).

The low-damage concept was initially conceived and developed for the structural skeleton (Stanton et al. 1997; Priestley et al. 1999), then, in order to target this integrated low-damage building system able to sustain earthquakes with negligible damage and limited socio-economic losses, i.e. the “ultimate earthquake-proof” building that the society expects (Pampanin 2015), innovative solutions have been recently proposed for architectural non-structural components (Baird et al. 2013; Tasligedik et al. 2014; Tasligedik and Pampanin

2016; Pourali et al. 2017). However, substantial evidence on the benefits of this integrated system, in terms of increasing the seismic performance and reducing the seismic socio-economic losses, is still missing. The convenience of implementing such a type of solution must instead be proved to either the society or the decision-makers.

1.2 Objectives and scopes of the research

Considering the background and motivations described in the previous section, the research aims to achieve different scopes and objectives, herein identified.

Scope S1. Study of the seismic behaviour of non-structural components.

A literary review is developed to investigate the seismic response of non-structural components, focusing on architectural systems (facades, partitions, ceilings). The objectives related to this scope are:

OB1.1 Study and collect the mechanisms and damage states developing in the components during earthquakes, gathering data from damage reports, laboratory testing, analytical/numerical investigations.

OB1.2 Collect the fragility specifications for different typologies of non-structural components. The fragility data can be used to implement loss assessment analyses or as a reference to propose new damage-mitigation solutions.

Scope S2. Provide evidence on the benefits of innovative low-damage technologies.

Further investigations are required to prove the efficiency of such systems in improving the seismic performance (mitigating the risk to damage) and consequently reducing the expected losses. The study is focused on either the non-structural elements or the entire integrated structural & non-structural system. The main objectives to be achieved for this scope are listed below.

OB2.1 Estimate and quantify the post-earthquake loss reductions (repair cost and downtime) due to the application of low-damage technologies.

OB2.2 Prove the high seismic performance of the integrated low-damage structural & non-structural system through experimental investigations.

Scope S3. Definition of a multi-performance design approach for non-structural components.

Non-structural components should be designed following a multi-criteria approach including the overall performance of the component (thermal, acoustical, weather tightness, seismic, fire, wind, durability, sustainability). This approach is not yet applied in the common practice, while it can allow the definition of the optimal component details depending on the priority given during the design (criteria weights assigned to each performance).

OB3.1 Study of the combined seismic&energy cost/performance to obtain the overall economic losses in the building life and to better design the non-structural details.

OB3.2 Proposal of a Multi-Criteria Decision Analysis (MCDA) for the design of non-structural components.

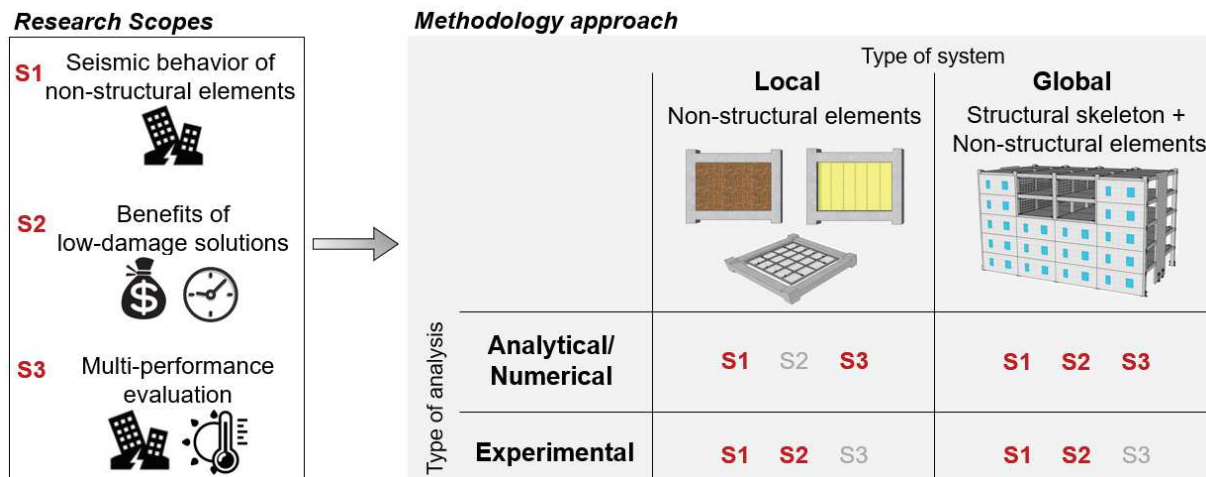


Figure 1.4. Research scopes and matrix of the methodology approach.

The research objectives are broad to be applied to all the currently available non-structural systems, therefore, focusing on architectural components and referring to new design, research boundaries have been established in order to provide manageable scopes. Among all the possible typologies, the research is limited to some non-structural elements (for facades: spider glazing systems, precast concrete cladding systems; unreinforced masonry infill walls; for partitions: masonry partitions and gypsum steel framed partitions; for ceilings: fully floating suspended ceilings; for contents: building elements fixed through post-installed fasteners). All the components taken into account are differently investigated depending on the objective to be achieved.

Other boundaries have been assigned concerning the performance to be investigated for these non-structural components. Although the initial idea was to study the influence of each performance into the common design (thermal, acoustical, weather tightness, seismic, fire, wind, durability, sustainability), due to the broad research fields involved, detailed investigations have been focused on the study of the seismic behaviour as well as of the combined seismic and thermal performance. In fact, the main aim of the research is to highlight the importance of including the seismic analysis into the design process of these building elements as well as of adopting a multi-performance design for the definition of non-structural details. An initial multi-criteria approach is thus defined and applied, mainly using analytical approaches, while more rigorous numerical investigations are carried out in order to study the seismic and the energy performance.

1.3 Organisation of the Thesis

The thesis is divided into ten chapters which are organized in four main parts, briefly described as follows:

- Highlight the importance of introducing the study of the seismic performance of non-structural systems into the common design process. An initial background explaining this consideration is provided, then a state-of-the-art overview of the different typologies of non-structural systems and of their expected seismic behaviour (mechanisms/damage states) is presented. (**Chapters 1, 2, 3**)
- Investigate the convenience of implementing damage-resistant (low-damage) technologies for non-structural components through experimental and numerical investigations (**Chapters 4, 5**).
- Experimentally investigate the performance of an integrated structural & non-structural building system (**Chapters 6, 7**).
- Define an approach for the multi-performance design of non-structural systems, focusing on the study of the combined seismic-energy performance, and provide the conclusion of the research (**Chapters 8, 9, 10**).

Examining each individual Chapter:

Chapter 1. An introduction to the research, its background and motivations as well as to the research scopes/objectives, can be found in this Chapter.

Chapter 2. It contains an overview of the typologies of non-structural components currently available for new design and in use in existing buildings, focusing the study on architectural elements (facades, partitions, ceilings). A description of all the performance measures affecting the non-structural behaviour is also provided.

Chapter 3. Referring to post-earthquake damage reports and to past numerical/experimental investigations, an overview of the non-structural damage states and mechanisms developing during seismic actions, as well as a collection of fragility curves for different typologies of systems, are reported within this Chapter.

Chapter 4. It contains an overview of the recently developed low-damage technologies for non-structural components. Experimental investigations (shake-table tests) on an earthquake-resistant solution for the anchorage system (post-installed anchors) of non-structural elements attached to reinforced concrete structures are also presented.

Chapter 5. Cost/performance-based analyses of multi-storey buildings consisting of different traditional vs. low-damage solutions (structural, non-structural, structural&non-structural) are carried out to highlight the seismic potentiality of low-damage technologies and quantify the great reduction of post-earthquake losses (repair cost, downtime) due to their application. The investigation is implemented considering case-study buildings located in both high and low seismicity zones. Further analyses are also performed for the specific case of precast concrete cladding systems to study a low-damage solution, based on the introduction of U-shape flexural plates, in terms of probability of damage not being exceeded.

Chapter 6. An experimental campaign (3D shake-table tests) of an integrated low-damage structural&non-structural system is herein described. The Chapter focuses on the description of the specimen design, its detailing, and the construction phases.

Chapter 7. The test set-up, as well as preliminary results from the experimental campaign (3D shake-table tests), are presented within this Chapter. The study focuses on the seismic behaviour of all the non-structural components included within the low-damage skeleton, i.e. fiber-reinforced gypsum partitions, masonry infill walls, glass fiber-reinforced concrete facades and glass (spider glazing) curtain walls.

Chapter 8. Numerical cost/performance-based investigations involving both the seismic and energy performance of different typologies of façade systems are carried out.

Chapter 9. A multi-criteria decision analysis for the design of new or retrofitted non-structural elements is proposed and developed for some example cases.

Chapter 10. This Chapter summarises the conclusions of the research and provides recommendations for future work.

1.4 References

- Baird A. (2014). Seismic Performance of Precast Concrete Cladding Systems, *Ph.D. Thesis*, University of Canterbury, Christchurch, New Zealand.
- Baird A., Palermo A., Pampanin S. and Riccio P. (2011a). Focusing on reducing the earthquake damage to Façade Systems, *Bulletin of New Zealand Society of Earthquake Engineering*, 44(2): 108-120.
- Baird A., Palermo A., Pampanin S. (2011b). Façade damage assessment of multi-storey buildings in the 2011 Christchurch earthquake, *Bulletin of New Zealand Society of Earthquake Engineering*, 44(4): 368-376.
- Baird A., Palermo A., Pampanin S. (2013). Controlling Seismic Response using Passive Energy Dissipating Cladding Connections, *Proceedings of 2013 NZSEE Conference*, Wellington, New Zealand.
- Baird A. and Ferner H. (2017). Damage to Non-structural elements in the 2016 Kaikoura earthquake, *Bulletin of the NZ Society for Earthquake Engineering*, 50(2): 187-193.
- Bianchi S., Ciurlanti J. and Pampanin S. (2018). A cost/performance-based evaluation of low-damage building system, *Proceedings of 16th European Conference on Earthquake Engineering*, Thessaloniki, Greece.
- Bradley B.A., Dhakal R.P., Cubrinovski M., MacRae G.A., and Lee D.S. (2009). Seismic loss estimation for efficient decision making, *Bulletin of the New Zealand Society for Earthquake Engineering*, 42(2): 96-110.
- Federal Emergency Management Agency (2011). *Reducing the Risks of Nonstructural Earthquake Damage – A Practical Guide, Fourth Edition*, prepared by the Applied Technology Council for the Federal Emergency Management Agency, FEMA E – 74, Washington, D.C., USA.
- Federal Emergency Management Agency (2012). *Seismic Performance Assessment of Buildings, Volume 1 - Methodology*, prepared by the Applied Technology Council for the Federal Emergency Management Agency, FEMA P-58-1, Washington, D.C., USA.
- Filiatrault A. and Sullivan T. (2014). Performance-based seismic design of nonstructural building components: The next frontier of earthquake engineering, *Earthquake Engineering and Engineering Vibration*, 13(1): 17-46.
- Filiatrault A., Perrone D., Merino R.J, Calvi G.M. (2018). Performance-Based Seismic Design of Nonstructural Building Elements, *Journal of Earthquake Engineering*, 13(1): 17-46.
- NIST GCR 17-917-44 (2017). *Seismic Analysis, Design, and Installation of Nonstructural Components and Systems – Background and Recommendations for Future Work*, National Institute of Standards and Technology, ATC 120, U.S. Department of Commerce.
- NIST GCR 18-917-43 (2018). *Recommendations for Improved Seismic Performance of Nonstructural Components*, National Institute of Standards and Technology, ATC 120, U.S. Department of Commerce.

- Pampanin S. (2012). Reality-check and renewed challenges in earthquake engineering: Implementing low-damage structural systems - from theory to practice, *Bulletin of New Zealand Society for Earthquake Engineering*, 45(4): 137-160.
- Pampanin S. (2015). Towards the “Ultimate Earthquake-Proof” Building: Development of an Integrated Low-Damage System, *Perspectives on European Earthquake Engineering and Seismology* (A. Ansal, ed.), Geotechnical, Geological and Earthquake Engineering 39, Springer Nature, Switzerland.
- Pourali A., Dhakal R.P., MacRae G.A. and Tasligedik A.S. (2017). Fully-floating suspended ceiling system: experimental evaluation of the effect of mass and elastic isolation, *Proceedings of 16th World Conference on Earthquake Engineering*, Santiago, Chile.
- Priestley M.J.N., Sritharan S., Conley J.R. and Pampanin S. (1999). Preliminary Results and Conclusions From the PRESSS Five-Story Precast Concrete Test Building, *PCI Journal*, 44(6): 42–67.
- Riccio, P. (2010). Multi performance-based design of facade systems in timber buildings, *Master Thesis*, Politecnico di Milano, Milan, Italy.
- Stanton J.F., Stone W.C., Cheok G.S. (1997). A hybrid reinforced precast frame for seismic regions, *PCI Journal*, 42(2): 20–32.
- Tasligedik A.S. and Pampanin S. (2016). Rocking Cantilever Clay Brick Infill Wall Panels: A Novel Low Damage Infill Wall System, *Journal of Earthquake Engineering*, 21(7): 1023-1049.
- Tasligedik A.S., Pampanin S. and Palermo A. (2014). Low damage seismic solutions for non-structural drywall partitions, *Bulletin of Earthquake Engineering*, 13(4): 1029–1050.
- Villaverde R. (2004). *Seismic Analysis and Design of Nonstructural Elements*, In *Earthquake Engineering: from Engineering Seismology to Performance Based Engineering*, Bozorgnia Y, Bertero V (editors), CRC Press LLC: Boca Raton, FL.

2. Overview of non-structural elements: typologies and overall performance

2.1 Introduction

This Chapter provides a description and classification of the typologies of non-structural components, which are in consensus currently. After this initial overview of the non-structural configurations, focusing on architectural systems (facades, partitions, ceilings), a background to the overall performance (structural, architectural, long-term) characterizing these building elements can be found.

The knowledge of the various typologies of non-structural systems and their specific detailing, e.g. panel modularity or connection to the primary structure, allow to better understand the seismic behaviour of traditional - construction practise - non-structural elements. This can facilitate the proposal of innovative technological solutions and strategies based on simple detailing modifications, as the techniques presented in Chapter 4, able to control the damage of non-structural components and consequently reducing the expected post-earthquake losses.

2.2 Typologies of non-structural components

As already stated, non-structural systems include all those building elements not part of the primary structure, namely: 1) architectural components, i.e. façades, partitions, ceilings; 2) building utility services, i.e. mechanical and electrical equipment; 3) building contents.

A description of the currently available technologies for both vertical and horizontal non-structural components is herein provided. Concerning vertical elements, the overview focuses on different types of exterior enclosures, from cladding systems to infill walls to mixed systems, and on various configurations of internal light and heavy partitions. While, for the case of horizontal elements, a classification of the ceiling systems typically applied in buildings is also introduced.

Building mechanical and electrical systems as well as contents highly contribute to the multi-performance evaluation of a structure, mainly for strategical buildings like hospitals, however they are not described in detail because outside the scope of this Thesis.

2.2.1 Exterior enclosures

The exterior enclosures can be grouped into three main categories: cladding systems, infill walls and a combination of both. The essential difference is related to the way of non-structural/structural connection, i.e. cladding enclosures are attached externally to the structural skeleton, while infill walls are built within the building frames.

As described by Riccio (2010) and summarized in Table 2.1, the primary aspects defining an exterior enclosure are:

- *Panel modularity.*

This property describes the degree to which a panel can be separated and recombined. Two different typologies of panel system are available: 1) mono-panel, where the degree of separation is equal to the infill dimension, and 2) multi-panel, i.e. the degree of separation is not equal to the infill dimension and both vertical panels, horizontal panels or a mix can be used.

- *Connection devices.*

The connection between non-structural component and primary structure can be implemented through alternative solutions: 1) bounding elements, such as mortar filling, into the corners of the building frame; 2) continuous elements; 3) metal punctual elements.

- *Connection modularity.*

This non-structural property describes the degree to which a connection can be separated and recombined. Two types of connection can be considered: 1)

continuous connection, where no interruption of the infill is introduced and the continuity can be in all parts or horizontally only; 2) discontinuous connection, where the connection to the primary structure is discrete.

Table 2.1. Summary of primary aspects for exterior enclosures.

Exterior Enclosures	
Panel modularity	<p>Monopanel Multipanel (vertical, horizontal or both)</p>
Connection devices	<p>Bounding Continuous Punctual</p>
Connection modularity	<p>Continuous Discrete</p>

2.2.1.1 Cladding systems

Cladding systems are non-load-bearing walls hanging from the face of the floor slabs. They are designed to withstand their own self weight and the forces due to wind or earthquake actions. Many configurations of cladding systems are available and the choice of the best typology for a specific building system depends on different variables (CMHC 2004): 1) cost/budget of the structure (design life, use, size, shape), 2) architectural design (aesthetics and fire safety) and 3) location (seismic, wind, weather/climate, acoustic).

The typologies of cladding systems are increasing over the years, in fact new configurations are always proposed from companies to fulfil advanced performance. The spectrum of available cladding solutions is boundless and various classifications can be defined depending on the field of interest. For example, as described in Das 1986, from the contractor's perspective, these components are categorized in function of their assembly and installation. Therefore, three groups are identified: 1) unit assemblies, fully prefabricated and

floor-to-floor installed; 2) grid assemblies, made of mullions and transoms built up on site; 3) built-up assemblies, for systems with brick or stone veneer.

From the engineer's perspective the cladding systems are differently categorised, and a state-of-the-art overview of the main configurations used around the world is herein presented.

2.2.1.1.1 Curtain walls

Curtain wall usually consists of a lightweight metal gridwork with some combination of transparent or opaque infill panels. The grid can be either assembled on site as individual pieces or pre-assembled in a factory and it is typically connected to the floor slabs at discrete points. In function of the erection system, glazing method and type of connection, curtain walls can be classified into four main categories:

- Stick curtain;
- Unitised curtain;
- Structural or semi-structural glazing;
- Spider glazing.

STICK CURTAIN

Stick curtain systems are formed by continuous vertical mullions and horizontal transoms, usually aluminium members, infilled with glass or opaque panels (Figure 2.1). These lightweight systems represent the most popular option adopted in multi-storey buildings.

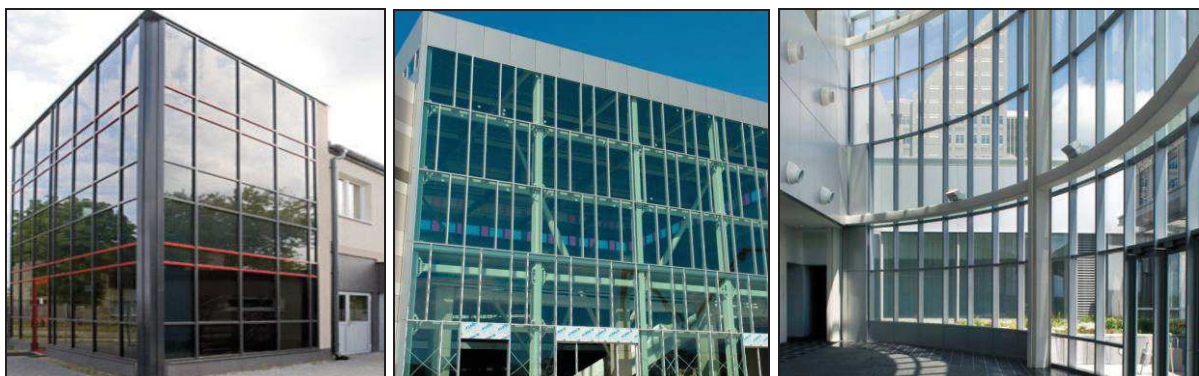


Figure 2.1. Examples of stick curtain systems (source: www.archiexpo.com, www.unicelarchitectural.com).

Each element of the stick system is produced in a factory, while the assembly and installation are realized directly on site. Skilled workers firstly connect the mullions to each floor using appropriate metal joints bolted to the primary structure, then the transoms between mullions are fixed using bolts and finally the infill units are fitted (Figure 2.2).



Figure 2.2. Stick curtain system: example of connection detail and installation of the façade (Eisenmann 2014).

The track between mullions and transoms is designed for static and energy issues. The system details also allow in-plane movements, thus the differential displacements between glass and frame can be accommodated. Silicone sealant helps guarantee this movement while keeping the water tightness.

UNITISED CURTAIN

This enclosure comprises prefabricated cells of glazing and opaque panels fixed into aluminium or steel frames and these units are fully assembled in factory and installed on site (Figure 2.3). Although there are great savings in terms of manpower costs and construction time, the unitised cladding systems can be more expensive than other typologies of façade and financial benefits should be obtained for only large projects.



Figure 2.3. Examples of unitised curtain systems (source: www.clearviewfacade.com, www.archiexpo.com).

The unitised systems are made of double skin panels of glazing or opaque material, which create an internal cavity and improve the building thermal performance. The system cells are attached to the building floor by bolted metal elements, properly detailed also to allow the differential dilatation between façade and floor (Figure 2.4).



Figure 2.4. Unitised curtain system: example of connection detail and installation of the façade (source: www.archiexpo.com).

STRUCTURAL OR SEMI-STRUCTURAL GLAZING

This cladding system is characterized by a metallic frame completely covered by glazing panels attached through structural adhesive (Figures 2.5 and 2.6). Two categories of structural glazing are available: 1) sided structural silicone, where two edges of the infill are adhered to the frame using structural silicone sealant while the other two are mechanically fixed with pressure plates; 2) 4-sided structural silicone, i.e. all the four edges of the infill are attached using structural silicone sealant. For quality control the 4-sided structural silicone is pre-installed before arriving on site.



Figure 2.5. Examples of structural glazing systems (source: www.argofacades.com).



Figure 2.6. Structural glazing system: example of connection detail and installation of the façade (source: www.gip-glazing.com).

Small horizontal ledges are usually introduced at the base of the glazing panels to help maintain the self-weight, while the sealant provides support against the stresses due to shear or developing in the pression and de-pression wind zones.

SPIDER GLAZING

Spider glazing curtain walls are suspended assemblies where a continuous glass surface is connected to the primary structure through discrete connections (Figure 2.7). These facades are typically used for tall building envelopes and installed on site by skilled worked.



Figure 2.7. Examples of spider glazing systems (source: www.glasxperts.com, www.neelkamalfacades.com).

Large glass panels are constrained by metal devices called “rotules” which transfer the loads to the secondary structure made of “spider connectors”, appropriately designed and bolted to structural components, as beams and columns or to an additional reticular structure comprising steel pipes or cables (Figure 2.8). The “rotules” have a spherical joint creating a hinge to avoid a rigid connection between glass and metal element. Tempered glass is

usually preferred for this type of connection because it offers great resistance to the local stresses forming around the holes of the glazing panel, i.e. where the bolts for the spider-glass connection are placed.

In the spider glazing curtain walls, the supporting system is completely separated from the glass façade. In fact, the glazing panels are located in a different in-plane position and this aspect guarantees an independent movement of the façade, which is also able to accommodate the relative movement between structural skeleton and non-structural system. While, silicone sealant between the glass panels helps limit the differential dilations between spider connector and glass.



Figure 2.8. Spider glazing system: example of connection to the primary building and installation of the façade (source: www.glassarchservicesng.com).

2.2.1.1.2 Cladding walls

Exterior enclosures are composed of cladding panels specifically designed to provide thermal insulation and weather resistance. E.g. rainscreen claddings, consisting of an outer weather-resistant skin fixed to an underlying structure by supporting grid, can be used to maintain a ventilated and drained cavity between cladding and structure.

A wide range of materials can be adopted for the panels and four categories of cladding walls can be identified:

- Lightweight cladding;
- Brick veneer;
- Precast concrete cladding;
- Monolithic cladding.

The cladding systems generally consist of a structural framing member, the attachment between structure and connection, the connector body and the attachment between connector body and cladding panel (Pinelli et al. 1993). The connector body represents the structural panel-building link and is realized using steel components and bolts. Different types of connector body are available (bearing, tie-back, slotted, fixed or dissipative, see Chapter 3) and this part of the cladding system is generally the weakest one. Therefore, it must be appropriately designed to accommodate in-plane movement and provide out-of-plane restraint.

LIGHTWEIGHT CLADDING

Lightweight panel cladding is one of the most popular and cost-effective solution for low-rise buildings and consists of frame, sub-frame and finishes (Figure 2.9).



Figure 2.9. Examples of lightweight cladding systems (source: www.ebmsupplies.com, www.hunker.com).

The panels are attached to the sub-frame by metal joints and insulation is placed between cladding and frame structure (Figure 2.10). Different materials can be used to build the cladding panels: 1) wood coverings, typically durable and with natural resistance to moisture; 2) metal claddings, formed by aluminium and zinc profiles which require low-maintenance; 3) fiber-cement panels, a composite material with more strength and durability; 4) brick slips or stone tiles; 5) PVC claddings, lighter than fiber-cement and with very high thermal resistance.

Lightweight sheet claddings tend to rely on the flexibility of the fixings to the frame to accommodate lateral distortions of the building, however expected cracking may still occur at sheet junctions when the lateral actions are strong.



Figure 2.10. Lightweight cladding system: example of connection detail and installation of the façade (source: www.ebmsupplies.com).

BRICK VENEER

Brick veneer walls are heavy claddings suitable for low-rise buildings and are composed of panels of clay or concrete bricks connected to a steel or timber frame (Figures 2.11 and 2.12). A single layer of masonry is separated from the main structure by an air cavity, which maintains the water tightness addressing the water penetrating the veneer to the bottom of the cavity where it is expelled by weep holes. The air cavity is also filled by an insulation increasing the thermal performance of the façade.



Figure 2.11. Examples of brick veneer cladding system (source: www.brickslips.co.uk).

The brick veneer cladding does not contribute to increase the building strength during wind or earthquake loads and needs horizontal ties to the structure to guarantee out-of-plane restraint against these actions.



Figure 2.12. Brick veneer cladding system: example of connection detail and installation of the façade (source: www.mattrisinger.com).

PRECAST CONCRETE CLADDING

Precast concrete panels are heavy cladding systems with height equal to the building inter-storey and width less or equal to the structural bay length (Figure 2.13).



Figure 2.13. Examples of precast concrete cladding systems (source: www.turnerconstruction.com, www.ciaprecast.com).

The panels are designed to resist against 1) the horizontal forces due to wind loads, 2) the seismic forces related to the system self-weight, 3) the vertical forces due to the self-weight. Reinforcement design is dominated by the control of cracking which can develop from the panel construction and erection or from thermal dilatations. Discrete connections are used to connect the panels to the primary structure. Cladding panels are usually attached by bearing connections, transferring the vertical load to the frame, and by tie-back or slotted connections, maintaining the panel in the vertical position and resisting to seismic and wind loads perpendicular to the panel (Figure 2.14).

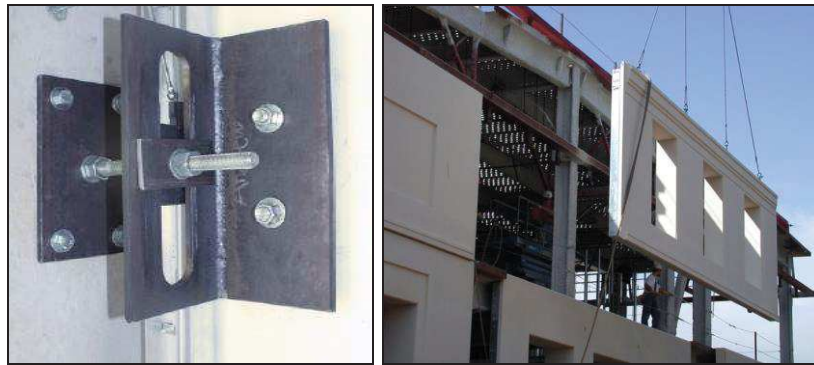


Figure 2.14. Precast concrete cladding system: example of connection detail and installation of the façade (source: www.designingbuildings.co.uk).

MONOLITHIC CLADDING

The oldest monolithic cladding system is stucco, that is a reinforced sand/cement mix applied on a thin fiber-cement or over building paper. Continuous concrete footings around the edge support the outside walls minimizing the movement. Modern monolithic systems include Exterior Insulated Finishing System (EIFS), made of polystyrene insulation and reinforced plaster, and fiber-cement sheets, where the edges are filled with a reinforced plaster mix to create a uniform finish. The finish coat can be either cement plaster or acrylic type texture and provides water tightness and a face seal impervious to moisture (Figures 2.15 and 2.16).



Figure 2.15. Examples of monolithic cladding system (source: www.constructionspecifier.com).

This cladding solution is very brittle and vulnerable to cracking. Each crack forming needs to be immediately repaired to ensure that the cladding system remains watertight.



Figure 2.16. Monolithic cladding system: particular of EIFS and construction of the monolithic stucco façade (source: www.consumer.org.nz).

2.2.1.2 Infill walls

Infill walls are exterior enclosures built between the structural members of a building. The structural skeleton supports the system, while the infill wall provides a separation between internal and external environment. Infill panels are not designed to be load-bearing systems, however they have to support their own weight and resist to the horizontal forces due to both wind and earthquake loads. Furthermore, infill walls provide weather resistance, fire resistance and thermal and sound insulation.

This typology of external wall is generally categorized in function of the material composing the system. Consequently, the following classification can be used:

- Masonry infill panel;
- Timber infill panel;
- Steel infill panel.

MASONRY INFILL PANEL

This type of heavy infill wall has been largely used in the past in reinforced concrete buildings and consists of clay brick or concrete blocks with solid or cavity shape bounded together and to the primary structure using mortar (Figure 2.17).

Masonry infill walls are built as multi-layer panels considering that thermal resistance must be ensured by external enclosures. As a matter of fact, the panels are isolated by different ways (externally, internally or in the cavity between two layers of the wall) and covered inside or outside the building by concrete plasterwork and paint.



Figure 2.17. Examples of masonry infill walls (source: www.structuremag.org).

Reinforced masonry walls are also available and can be adopted for increasing the structural performance of the infill panel. In fact, reinforcing bars can be distributed into the wall to provide better structural performance: 1) horizontal bars, lied on the mortar; 2) vertical bars, inserted before the wall construction and placed into the holes of the bricks.

TIMBER INFILL PANEL

Timber infill walls, usually indicated as “balloon frames”, are made of linear vertical timber members connected to horizontal timber guides, which in turn are attached to the building primary structure by nails. Insulation material is inserted between the vertical elements, while the external timber sheets are attached to the mullions by nails (Figure 2.18).

Timber infill walls are lightweight and rapidly-built structures reducing the installation time and cost, nevertheless they have less strength and are not suitable for the construction of tall sections or walls with large openings.



Figure 2.18. Examples of timber infill walls (source: www.canadawood.org).

An engineered wood product, as the plywood, can be also used to build infill walls. In fact, this economical material is obtained from sheets of wood glued together in alternating directions and it does not warp or crack due to changes in atmospheric moisture. Thermal insulation is often required to be attached to the plywood in order to provide good acoustic performance since the system is very light. The plywood panels are connected to each other and to the structural members by discrete metal elements.

STEEL INFILL PANEL

Lightweight steel infill wall panels are usually adopted for multi-storey framed constructions (Figure 2.19). This infill system is economic, easy and fast to install, capable of resisting to wind loads and supporting a range of cladding types (brickwork, insulated render, rain-screed). Large windows, parapets and other architectural features can be also incorporated within the steel infill walls.

The system is formed by vertical C-shaped studs spanning between the floors of the primary structure and attached by screws to horizontal U-shaped steel tracks connected to the building floors. Thermal insulation material is introduced between the mullions and an elastic element is included between the panels to provide better air tightness.

Among the different typologies of steel infill walls, the aqua-panel system proposed by Knauf USG is one of the most performing. In fact, the aqua-panel, made of Portland concrete and mineral aggregates on glass fiber concrete sheets, is a very sustainable panel with also good performance under rain and vapor exposure.



Figure 2.19. Examples of steel infill walls (source: www.designingbuildings.co.uk).

2.2.1.3 Mix systems

The infill and cladding wall configurations can be combined to create a mix façade system (Figure 2.20). It is highlighted that both the monolithic cladding and the brick veneer systems are grouped into the “cladding wall” category. Nevertheless, they are attached by ties or fasteners, respectively, to an internal steel or timber sub-frame inserted into the structural skeleton, thus, they can be also indicated as “mix systems”. However, “mix systems” are herein intended as a combination between masonry infill walls and exterior cladding enclosure. This combination creates the so-called ventilated façade system, i.e. an exterior enclosure with very high thermal performance and able to improve the internal comfort.



Figure 2.20. Examples of mix systems (source: www.sistemainvolucro.it).

The ventilated façade has an internal cavity between the infill wall and the cladding panel (Figure 2.21), where a natural circulation of the air is obtained through convective motions generating from the openings on the top and bottom parts of the exterior panel. The air circulation minimizes the heat dispersion during winter season while ejects the hot air for the chimney effect during summer season.

After the construction of the masonry infill wall, additional thermal insulation is attached on the bricks and specific devices are introduced for the connection to the external cladding. The connection devices are usually metal elements discretely inserted into the masonry wall while the type of device depends on the cladding enclosure (typically brick, ceramic, concrete or aluminum).



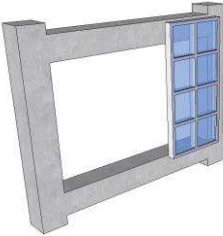

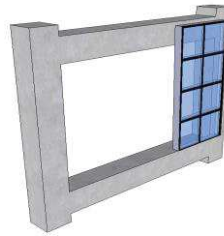
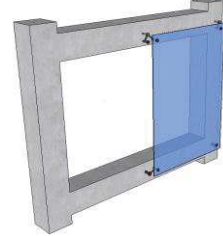
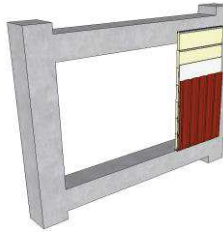
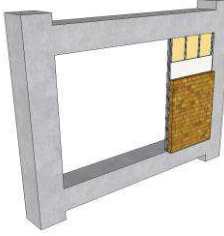
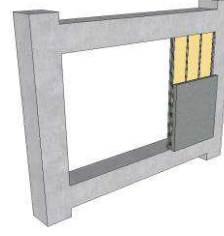

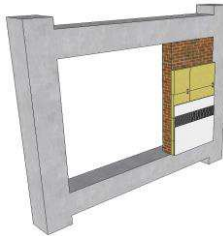
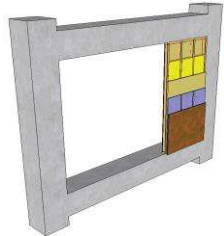

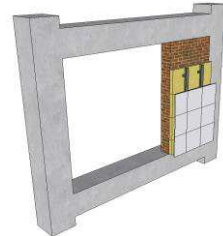
Figure 2.21. Ventilated façade: connection detail and assembly of the façade (source: www.walkingalmaty.com).

2.2.1.4 Summary: exterior enclosures

Table 2.2. Typologies and general aspects of the exterior enclosures.

Enclosure system	Typology of component	Panel modularity	Connection device	Connection modularity
Curtain wall	Stick curtain	Multi-panel	Punctual	Discrete
	Unitised curtain	Multi-panel	Punctual	Discrete
	Structural or semi-structural glazing	Multi-panel	Punctual	Discrete
	Spider glazing	Multi-panel	Punctual	Discrete
Cladding wall	Lightweight claddings	Multi-panel	Punctual	Discrete
	Brick veneers	Multi-panel	Punctual	Discrete
	Precast concrete claddings	Multi-panel	Punctual	Discrete
	Monolithic cladding	Mono-panel	Punctual	Discrete
Infill wall	Masonry infill	Mono-panel	Bounding	Continuous
	Timber infill	Multi-panel	Punctual	Continuous or Discrete
	Steel infill	Multi-panel	Punctual	Continuous
Mix system	Mix system	Mono-panel Multi-panel	Bounding Punctual	Continuous Discrete

Table 2.3. Exterior enclosures: summary of alternative configurations.

CURTAIN WALL			
<p><i>Stick curtain (SC)</i></p> 	<p><i>Unitised curtain (UC)</i></p> 	<p><i>Structural glazing (StrG)</i></p> 	<p><i>Spider glazing (SpG)</i></p> 
CLADDING WALL			
<p><i>Lightweight claddings (LC)</i></p> 	<p><i>Brick veneers (BV)</i></p> 	<p><i>Precast concrete claddings (PCC)</i></p> 	<p><i>Monolithic cladding (MC)</i></p> 
INFILL WALL			MIX SYSTEM
<p><i>Masonry infill (MI)</i></p> 	<p><i>Timber infill (TI)</i></p> 	<p><i>Steel infill (SI)</i></p> 	<p><i>Mix system (MS)</i></p> 

2.2.2 Partitions

Partition walls are vertical non-structural components with the function of internally separate a building into rooms or corridors. They are non-load bearing elements classified in terms of the material adopted for the wall panel. Light or more heavy solutions are available, and the choice of the best configuration is mainly related to the building function. For example, steel framed drywalls or glass partitions are typically adopted within commercial buildings, while timber framed drywalls in residential houses.

As described by Arora and Gupta (1988), a good partition must be thin in cross-section to maximize the floor area to be utilized, economical and simple in construction, built using durable and sound insulated materials, providing sufficient resistance to fire and being rigid enough to take the vibrations due to loads.

In this paragraph, the partitions are classified following the terminology and description proposed by Purnia et al. (2012), namely:

- Brick partition;
- Clay brick partition;
- Glass partition;
- Concrete partition;
- Metal partition;
- Plaster slab partition;
- Timber partition;
- Wood wool partition;
- Strawboard partition.

BRICK PARTITION WALL

Brick partitions can be built using plain bricks, reinforced bricks or brick noggin (Figure 2.22).



Figure 2.22. Examples of brick partition walls (source: www.pdgtugla.com, [mchrenewalproject](http://mchrenewalproject.com)).

In plain brick partitions, the bricks are bounded using cement mortar and plastered on both sides, and the wall is strong and resistant if properly realized. In reinforced brick partitions, hoop iron or wire mesh strips are placed at every third or fourth course; these walls are stronger than plain brick partitions and usually adopted when the wall must support

other super-imposed loads. Brick noggin partition wall consists of brickwork plastered on both sides built within a framework of wooden elements, which provide stability to the partition against lateral loads and vibrations.

CLAY BRICK PARTITION WALL

Clay brick partitions are made of clay or terracotta, solid or hollow blocks (Figure 2.23). Hollow brick partitions are typically used because they are economic, light in weight, strong and provide good sound insulation. The blocks are bounded together using mortar and grooves are provided at each edge of the block to improve the bond with the plaster.



Figure 2.23. Examples of clay brick partition walls (source: www.theconstructor.org).

GLASS PARTITION WALL

Glass partition walls consist of glass sheets or hollow glass blocks and are mainly used in offices (Figure 2.24). Glass walls are light-weight systems, easy to build, allow lighting and provide a good heat and sound insulation.



Figure 2.24. Examples of glass partition walls (source: www.architizer.com).

Glass sheet partition walls are formed by strong sheets of glass in a wooden framework dividing the area into a certain number of panels. While, hollow glass partitions consist of hollow glass blocks, light and manufactured with various sizes and thickness, with jointing edges painted internally and sanded externally to help the bond between mortar and glass blocks. For high glass blocks, metal strip reinforcement is also inserted between every third or fourth course.

CONCRETE PARTITION WALL

Concrete partition walls are formed by cast-in-situ or precast concrete slabs supported by vertical elements (Figure 2.25).



Figure 2.25. Examples of concrete partition walls (source: www.gharpedia.com).

Cast-in-situ concrete partitions walls have internal reinforcement in the middle of the section and more reinforcing is placed into the internal columns in which is divided. These non-economic walls are rigid and strong in both vertical and horizontal directions. Precast concrete partitions are made of precast concrete slabs secured by special precast posts and bounded using mortar.

METAL PARTITION WALL

Metal partition walls, mainly used for offices and industrial buildings, are lightweight, easy to build, strong and fire-resistant walls (Figure 2.26). The system is made of vertical elements (studs) attached to the horizontal channels which, in turn, are connected to the floor slabs. Insulated material is introduced between the studs and metal lathes are also inserted in front of the frame, appropriately supported and fixed by wires.



Figure 2.26. Examples of metal partition walls (source: www.diy-extra.co.uk).

PLASTER SLAB PARTITION WALL

Plaster slab walls are composed of burnt gypsum or plaster of paris mixed with sawdust or other material (Figure 2.27). 5-10 cm thick plaster boards are attached by nails or screws to timber or metal frames and they are also equipped with lateral grooves creating rigid joints into the wall system.



Figure 2.27. Examples of plaster partition walls (source: www.indiamart.com).

TIMBER PARTITION WALLS

This typology of partition consists of a timber frame with vertical studs and horizontal elements attached to the building floors and to the lateral walls (Figure 2.28). Both the sides of the timber frame are plastered or covered by boarding. These partitions are light in weight and easy to build whilst not sound- or fire-proof.



Figure 2.28. Examples of timber partition walls (source: www.indiamart.com).

WOOD WOOL PARTITION WALL

Wood wool partitions are prepared from a mixture of Portland cement and wood wool or wood shavings and sometimes a small quantity of gypsum is added (Figure 2.29). The slabs are joint by cement mortar and they have a rough surface painted or distempered. These partitions are lightweight, economical, durable, sustainable and provide a very good sound, fire and heat barrier.

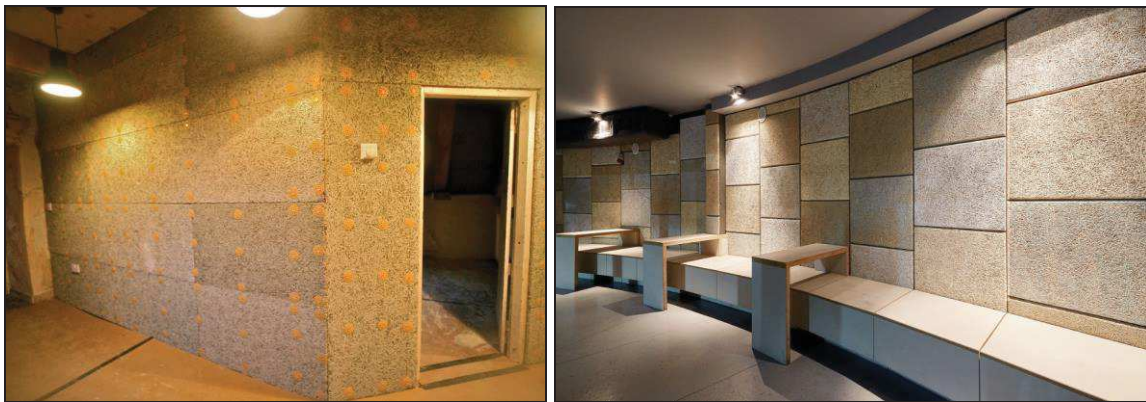


Figure 2.29. Examples of wood wool partition walls (source: www.theconstructor.org).

STARWBOARD PARTITION WALL

Strawboard partitions are easy-to-build system, mainly used when the removal of partitions is frequent. The walls are made of compressed straw covered by thick paper or hardboard. This type of partition is very sound and heat proof (Figure 2.30).



Figure 2.30. Examples of strawboard partition walls (source: www.ivotek.co.uk).

SUMMARY: PARTITION WALLS

Table 2.4. Partition walls: summary of alternative configurations.

PARTITION WALLS		
<p>Brick partition (BP)</p>	<p>Clay brick partition (CBP)</p>	<p>Glass partition (GP)</p>
<p>Concrete partition (CP)</p>	<p>Plaster slab partition (PSP)</p>	<p>Metal partition (MP)</p>
<p>Timber partition (TP)</p>	<p>Wood wool partition (WWP)</p>	<p>Strawboard partition (SP)</p>

2.2.3 Ceiling systems

The ceilings are horizontal architectural non-structural components creating an enclosure and separation between building internal spaces. These systems provide good aesthetics to the building interior and have different properties: provide a control of the light diffusion, reduce high inter-storey heights, improve the thermo-acoustical comfort and the fire performance of the building flooring systems, have resistant properties facilitating the insertion of building services which are hidden by the ceilings.

Many types of ceiling systems are available, and they can be classified in function of the connection typology (adherent, suspended or self-supporting) or of the type of substructure (on sight, hidden or semi-hidden/ closed or opened/ inspected or non-inspected). As described by the UNI EN 13964 (2007), the main components of a ceiling are: a supporting (bearing) structure, a superior fixing system, a suspended element, a supporting component, the panels and the perimeter frame (Figure 2.31).

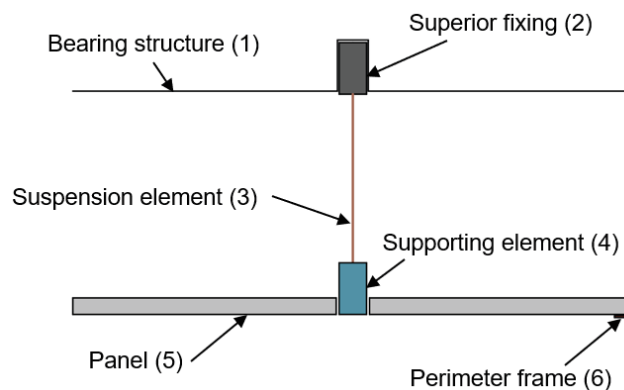





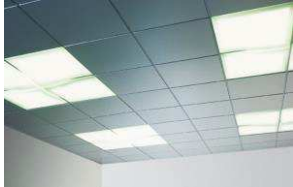




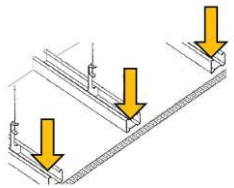
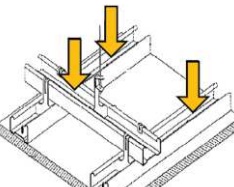
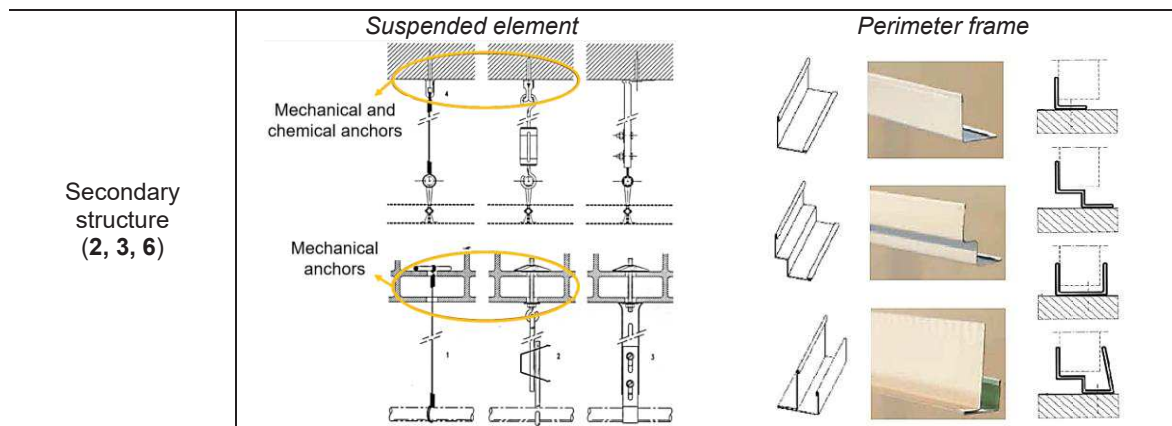


Figure 2.31. Ceiling system configuration.

The substructure of the ceiling system is formed by the primary structure, including the elements connecting panels and secondary structure to the building, and a secondary structure, which guarantees continuity to the panels and connects them to the primary structure. The horizontal panels can also be categorized in terms of configurations (panels, slats, grids, strips, coffered) or material (timber, metal, gypsum, fibre-reinforced gypsum, reinforced mineral fibre). A summary of all the typologies of ceiling components can be found in the following Table 2.5.

Table 2.5. Components composing a ceiling system and related classification (source: Gottfried 2002).

Component	Classification	
<p>Panels (5)</p>	<p style="text-align: center;"><i>Material</i></p> <ol style="list-style-type: none"> 1. Timber  2. Metal  3. Gypsum  4. Fibre reinforced gypsum  5. Reinforced mineral fibre  	<p style="text-align: center;"><i>Configuration</i></p> <ol style="list-style-type: none"> 1. Panel  2. Slats  3. Grids  4. Strips  5. Coffered 
	<p>Supporting element (4)</p>	<p style="text-align: center;"><i>Framework</i></p> <ol style="list-style-type: none"> 1. Simple  2. Double 



For the scope of this Thesis, the ceilings are classified considering the way they are connected to the primary structure. As previously anticipated and referring to the UNI EN 13964 (2007), three main typologies are identified: 1) adherent ceiling, where a metal grid is punctually fixed to the floor using specific hooks; 2) suspended ceiling, i.e. panels and secondary structure are supported by steel tie rods; 3) self-supporting ceiling, where the metal frame is not attached to the floor above but directly fixed to the lateral walls using perimeter guides. While, in function of the structure and load bearing system, the suspended ceilings can be also classified as: perimeter-fixed system, with one or more edges connected to the lateral walls or floating ceiling systems, attached using only braces to the floor above (Figure 2.32).

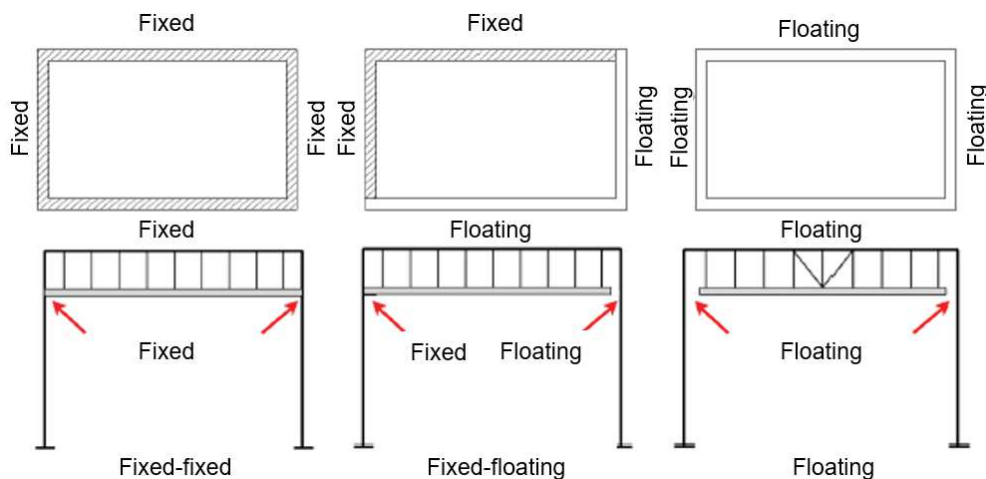
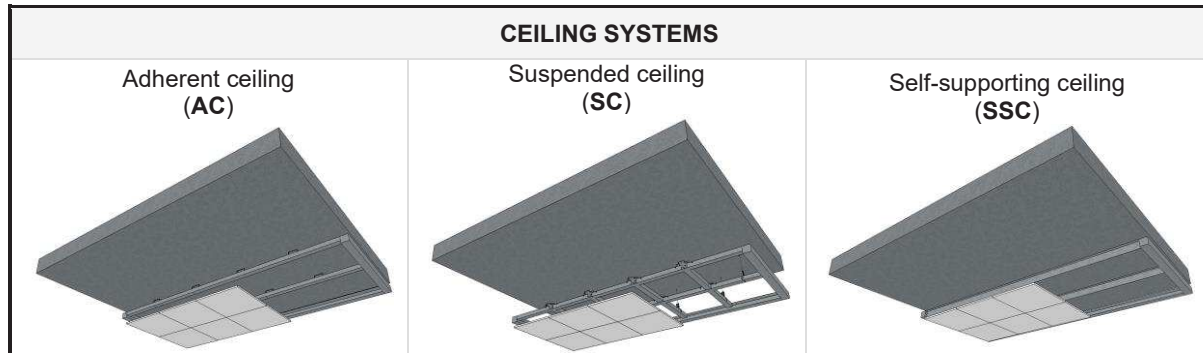


Figure 2.32. Schematic representation of different types of suspended ceiling (Dhakal et al. 2016).

SUMMARY: CEILING SYSTEMS

Table 2.6. Ceiling systems: summary of alternative configurations.



2.2.4 Building services and contents

Non-structural components also include all the mechanical and electrical equipment, the egress systems, and the contents placed on the building floors (Figure 2.33).



Figure 2.33. Examples of building services and contents (source: www.benincaprogetti.it).

As described by Taghavi and Miranda (2003), 1) the mechanical systems include piping, fire protection, heating and cooling systems and all the ducts in the building, 2) the electrical equipment includes lighting and power, power generator and wiring systems, 3) the egress systems indicate the elevators and stairs, while 4) the building contents mean furniture and accessories, like bookcases, modular office work stations or vertical cabinets. A broad category of alternative components is available for these elements, which are connected to the building structural skeleton through fasteners properly designed.

2.3 Performance of non-structural elements

Non-structural components should be designed following a multi-performance approach taking into account all the structural, architectural and long-term properties affecting the non-structural response. During their entire life, non-structural elements can be subjected to various external loads, therefore the design of these systems should be developed with the aim of achieving a specific target to each performance.

This paragraph provides an overview of all the performance describing the non-structural behaviour. Either the external actions (loads due to environment or casual factors) acting on the components and their effects or the parameters contributing to the component capacity are herein described.

2.3.1 Structural performance

Structural performance refers to the behaviour of non-structural components against loads like self-weight, wind and earthquake. These actions produce vertical, out-of-plane or in-plane movements creating deflections and differential inter-storey drift ratios. Another performance to be considered as structural is represented by the capacity to resist to fire.

2.3.1.1 Static

All the non-structural systems must support their own weight, while vertical floor-to-floor components must also accommodate the live load deflections of the floor slabs. Exterior enclosures are also subjected to wind and thermal loads, therefore out-of-plane supports are usually introduced and designed for the maximum deflection which can be achieved. As example, for the case of infill wall systems out-of-plane devices are introduced at the top and possibly along the sides of the panel, while in curtain wall systems splice joints are inserted to allow either the deflection or the thermal expansion.

In any case, the action of wind does not usually have a significant effect in heavy systems, whilst can change the performance of lightweight components, especially for tall buildings. Figure 2.34 presents some cases of damage due to an incorrect design for wind actions, i.e. dislodgment of some parts of the external building cladding.



Figure 2.34. Damage to non-structural components due to wind loads (source: www.weather.gov).

2.3.1.2 Dynamic

The dynamic behaviour of non-structural elements is related to earthquake actions, which generate inter-storey drift ratios and demand forces to the building frames and consequently displacements and accelerations to non-structural elements. Depending on the component configuration and connection devices, non-structural systems behave differently under seismic actions. Thus, understanding which parameter mostly influences the seismic performance of a component, an appropriate capacity design can be developed to define a non-structural solution with higher seismic performance.

Although non-structural elements are not typically designed to resist seismic actions, these systems are very vulnerable to earthquake shaking (Figure 2.35).



Figure 2.35. Damage to non-structural components due to earthquakes (De Sortis et al. 2009).

Considering that post-earthquake non-structural damage is generally greater than the damage due to structural members, innovative technological solutions have been proposed

and developed in the past decades to improve the seismic performance of these elements and reduce the subsequent repair cost and time after earthquakes (Chapter 4).

2.3.1.3 Fire

Fire has the potentiality to cause damage to non-structural components through burning, whilst generates a transition phase of the affected mass when the flame is hot enough (Figure 2.36). As described in the Italian Circolare CVVF 5043 (2013) and for the case of façade systems, the probability of fire and its propagation must be limited and during a fire the falling of façade parts must be avoided, to not compromise both the safety of the depopulation and the safety of the assistance measures.

The fire performance of a non-structural component is described by the fire resistance rating, representing the duration in time for which the system can withstand a fire resistance test. The fire resistance of any component is defined by the following properties: 1) stability, i.e. the capacity to maintain the mechanical resistance under fire action and is proper of those components representing primary elements within a fire cell, like the exterior walls; 2) integrity, provided by secondary elements like fire separations between internal walls, means the capacity to avoid the release or production of hot vapours or gas on the not-exposed side; 3) insulation, guaranteed by either the primary or the secondary elements and represents the capacity of reducing the time of heat propagation.



Figure 2.36. Damage to non-structural components due to fire load (source: www.wikiwand.com).

2.3.2 Architectural performance

Architectural performance refers to those properties of non-structural components generating indoor comfort to people. Consequently, good architectural performance means the capacity to reduce heat and sound transmission (thermal performance, acoustic performance) as well as the capacity to withstand the entrance of air, vapor and water inside the building (weather tightness).

As for the structural performance, the architectural one is herein briefly described in terms of both demand actions and related capacity of non-structural components.

2.3.2.1 Thermal

Thermal performance is mainly due to the difference between external and internal temperature in a building. External temperature depends on many factors, like the building site, and temperature variations are influenced by the specific season, month, day or hour. While, internal temperature is related to the temperature that people want inside a building and is again function of all the aspects previously indicated. External and internal temperatures influence the performance of an exterior enclosure, while the internal temperature also affects the performance of the internal partition walls.

The thermal capacity of a component is evaluated in terms of resistance or transmittance to the heat transfer. Thermal transmittance is generally used to describe the thermal performance of a building system, representing the rate of heat transfer through one square meter of a component divided by the difference of temperature across all the layers composing the element. A description of the methods to estimate the thermal performance of a system can be found in Chapter 8. Finally, an important aspect to consider for thermal evaluations is the presence of thermal bridges, forming when poor insulation materials come in contact allowing the heat to flow through the path created, i.e. as in the contact part between masonry infill walls and reinforced concrete columns. Thermal bridges must be avoided to prevent heat loss or gain, inserting insulating components and specific detailing measures.

As presented in Figure 2.37, the effects on the building due to temperature action can be: 1) the development of surface moisture due to condensation, 2) the growth of mould in humid environments and 3) the thermal expansion of the elements.



Figure 2.37. Damage to non-structural components due to temperature load (source: www.emmetisistemi.it).

2.3.2.2 Acoustics

Acoustic performance is an important aspect for the everyday welfare and represents one of the main parameters influencing the economic value of a building. The acoustic performance of a non-structural element is associated with the propagation of sound through the system. The sound propagation is altered by the presence of any kind of component, either extended surfaces or bodies with limited extension; in fact, sound can travel in solid structures as exterior walls or be transmitted through windows. Architectural elements limiting a room must avoid undesired sounds, the so-called noise, coming from outside spaces while must guarantee an appropriate sound inside the room. The acceptable level of sound inside a building depends on its use.

The propagation and perception of sound is related to mechanical vibrations. The sound waves, consisting of particles vibrating around their mean position not with the same phase, are customary described through the velocity of the particles and the sound pressure, which is the difference between the instantaneous and static pressure. Various equations govern the problem (conservation of momentum, conservation of mass) and define the wave equation, depending on the sound pressure, density and temperature variations. Nevertheless, the acoustic performance of a façade is practically defined using the so called “sound pressure level”, expressed in Decibel, and more specifically with the “sound insulation”, i.e. the difference between the external and the internal sound pressure levels.

2.3.2.3 Weather tightness

Weather tightness mainly characterizes the exterior enclosures indicating the resistance of a component against air, water and water vapor.

Tightness against air is determined experimentally and is useful to identify the air leakage sites on a component. The presence of pressure differences between the two sides of a façade has the effect of pushing the air to penetrate into the holes eventually located on the building enclosure, therefore knowing the air tightness of the system, the building pressures can be controlled. The limitation of the air leakage through the building envelope is very important for controlling moisture problems, energy efficiency, noise transfer, smoke propagation, indoor air quality and durability (Becker 2009).

Water tightness represents the attitude of the component to resist to the penetration of water. For example, a façade is subjected to the action of a precipitation and water could enter inside the building if the passage of water is not restricted, thus water can reach the inner face or other parts of the façade not designed to be wet. Water tightness is evaluated experimentally and defined in terms of the pressure corresponding to the infiltration of water inside the component. Infrared thermography is the best method to identify water losses or intrusions in a building, because infrared camera, measuring the thermal characteristics of wet materials and defining the moisture damage, can distinguish between wet and dry zones. Figure 2.38 presents some pictures where the effect of water infiltration is shown.



Figure 2.38. Damage to non-structural components due to weather tightness (source: www.vitorealizza.com).

The tightness against water vapor is the attitude of a component to let the passage of water vapor and is evaluated in terms of equivalent air thickness, calculated multiplying the

thickness and resistance of the component material to the vapor flux compared to the resistance of one meter of air. More a component is breathable, more it is durable because the probability that condensation and related problems develop on the surface of the component is very low and the integrity of the system is not compromised.

2.3.3 Long-term performance

Other performance measures characterizing non-structural elements are the durability and sustainability of a system. These aspects are related to long-term evaluations and have a great impact in the building financial assessment, building planning and cost/benefit analysis. The durability and sustainability of a component should be included in the common practice evaluations to address the decisional and operational processes during the design of a new system as well as for making decisions on retrofit interventions for existing components.

2.3.3.1 Durability

As described in the UNI 11156-2 (2006), the durability is the capacity of a component to perform the functions required during a specified time period, under the influence of the actions expected during the building operation. A maintenance plan consisting of inspections and maintenance operations is defined during the building design to guarantee that each component can maintain its geometry, material properties, thus its functionality, aesthetic aspect and resistance. An adequate durability is achieved taking into account the following correlated factors: the building use, the predictable environment conditions, the shape and details of the components, the quality of the execution, particular protective measures and the probable maintenance during the expected component life (NTC 2018). Effects of durability damage due to the obsolescence of the materials for the exposure to external environmental conditions are presented in Figure 2.39.

Each component has a natural drop in performance during the time and, reached a specific threshold value, the component has not any more the functions for which it has been designed, thus its life ends. Following the definitions provided in the UNI 11156-3 (2006), each element has a service life, that is the time period after the installation during which the component maintains performance levels greater or equal to acceptable limits, defined by customers and considering a minimum level of maintenance. The service life is divided into: 1) the assessment of the reference service life, expected in reference operational conditions

where the term “reference” indicates plausible boundary conditions assumed by the manufacturer certifying the durability of the product, and 2) the estimated service life, evaluated by the designer introducing coefficients which modify the reference conditions and consider the influence of material, design, environment, use and maintenance, according to the specific project context. The estimated service life is the parameter considered for the estimation of the durability of non-structural components.



Figure 2.39. Damage to non-structural components due to material obsolescence (source: www.infobuild.it).

2.3.3.2 Sustainability

During the last years the effect of building construction towards the environment, in terms of energy, materials, natural resources and costs, is gaining more attention in the construction sector. The construction of buildings represents a relevant part of the economy of a nation using a lot of resources and producing very high economic, social and environment impacts. The sustainability level of a building can be evaluated through green evaluation systems, i.e. methodologies determining the environmental sustainability through an analysis of the energy consumptions, the site properties, the internal comfort and the effects on human health. Evaluation systems on a voluntary based have been developed in national and international level, such as the ITACA protocol in Italy, the LEED protocol in the United States and the BREEAM system in United Kingdom.

The sustainability of a component is determined through the Life-Cycle Assessment (LCA), defining the environmental implications of a product during all its life cycle moving from the extraction and processing of raw materials, to the fabrication phase, transportation and distribution, to the use and eventually re-use of the product, finally to the storage, recovery and final waste disposal (Figure 2.40). The main advantage of an LCA is that it

makes possible the quantification of the impacts on the environment not limited to energy or CO₂ emissions, moreover including the use of other renewable and non-renewable resources, covering the emission of many organic and non-organic compounds into the air, water, and soil, as well as ionizing radiation (Caruso et al. 2017).

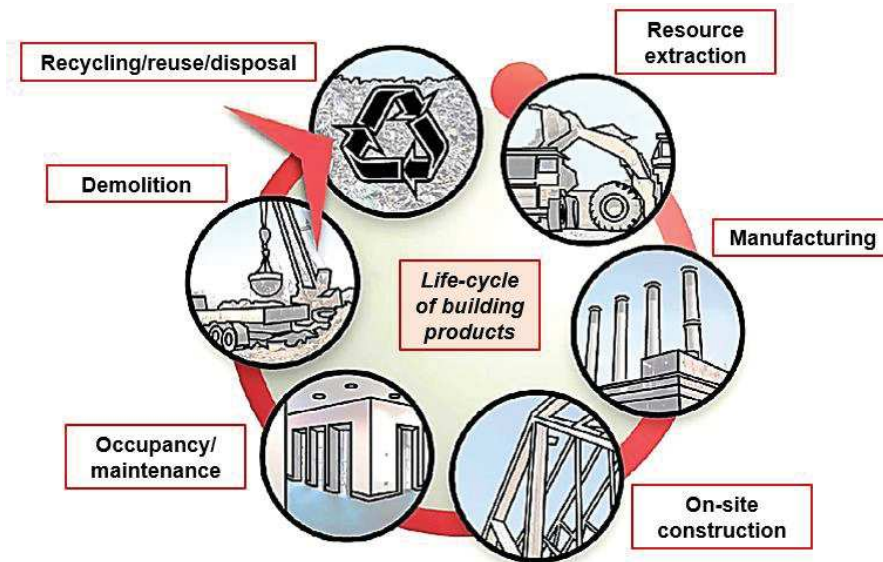










Figure 2.40. Schematic representation of the Life-Cycle of a building product (source: www.greenbuildings.com).

2.3.4 Summary: overall performance

Table 2.7 summarizes the overall performance (structural, architectural and long-term) of non-structural components and, particularly, the demand and capacity to be considered for each performance into the design process of a component/system can be found. Referring to the Italian and European context, the codes/guidelines to be taken into account for the determination of these demands and capacities are also indicated.

Table 2.7. Summary of the overall performance: Demand vs. Capacity.

Performance	Demand	Capacity
<p>Wind</p> 	<p>Definition of the wind pressure load acting on external and internal surfaces, function of basic velocity pressure and exposition coefficients</p> <p>Reference codes: NTC (2018), UNI EN 1991-1-4 (2005)</p>	<p>Analytical or numerical determination of the deflection (v)</p> <p>Reference codes: UNI EN 13116 (2005)</p>
<p>Seismic</p> 	<p>Definition of the design spectra and of the horizontal force applied to the non structural component</p> <p>Reference codes: NTC (2018), UNI EN 1998-1 (2005)</p>	<p>Analytical, numerical or experimental determination of the inter-storey drift (θ) or floor acceleration (a)</p> <p>Reference codes: NTC (2018), UNI EN 1998-1 (2005)</p>
<p>Fire</p> 	<p>Definition of the design fire load and density of fire load</p> <p>Reference codes: NTC (2018), UNI EN 1991-1-2 (2004)</p>	<p>Tabulated values or experimental determination of the fire resistance (REI)</p> <p>Reference codes: CVVF 5043 (2013), DM 16/02/2007 (2007), UNI EN 1991-1-2 (2004)</p>
<p>Thermal</p> 	<p>Determination of the external and internal air temperature and its distribution into the components</p> <p>Reference codes: NTC (2018), UNI EN 1991-1-5 (2004)</p>	<p>Analytical or numerical determination of the transmittance (U)</p> <p>Reference codes: UNI EN 13947 (2007)</p>
<p>Acoustic</p> 	<p>Determination of the sound pressure levels and the reverberation time</p> <p>Reference codes: D.P.C.M. 05/12/1997 (1997)</p>	<p>Analytical or experimental determination of the sound insulation (D)</p> <p>Reference codes: ISO 3382 (1975), UNI EN ISO 140-5 (2000), D.P.C.M. 05/12/1997 (1997)</p>
<p>Weather tightness</p> 	<p>-</p>	<p>Experimental evaluation of the air and water tightness and analytical determination of the vapor tightness in terms of equivalent air thickness (S_D)</p> <p>Reference codes: UNI EN 12152 (2003), UNI EN 12208 (2000), UNI EN ISO 13788 (2013)</p>

Performance	Demand	Capacity
Durability 	-	Durability criteria and analytical determination of the estimated service life (ESL) Reference codes: UNI EN 11156-3 (2006), NTC (2018)
Sustainability 	-	Life-Cycle Assessment for the evaluation of the sustainability level Reference codes: ISO 14040 (2006)

2.4 Conclusions

This Chapter has provided a background to all the existing typologies of non-structural components. The classification of each element is required to better understand how each system works, which components govern the behaviour of the system and how non-structural elements are connected to the primary building (structural skeleton).

After the description of alternative typologies, focusing on architectural elements, a brief overview is provided on the structural, architectural and long-term performance quantities characterizing the non-structural elements' behaviour. Understanding the targets to be achieved for each performance is fundamental to better design a specific component. In fact, as presented in Chapter 9 of the Thesis, a multi-criteria decision analysis including rating systems for each of this non-structural performance should be adopted for addressing the design of non-structural components. E.g. a wall system should resist to many different forces during its own life, consequently it represents a suitable separation of indoor and outdoor environments if the system: has structural strength and stiffness, withstands wind deflections, resists the spread of fire, controls heat flow, air flow and water vapor flow, controls sound and vibration, controls the exterior precipitation and sun radiation, is durable.

Following the above description, Table 2.8 summarizes the performance measures and related loads affecting the non-structural behaviour.

Table 2.8. Non-structural performance and external loads.

Performance		Load	Non-structural elements			
			Exterior enclosures	Partitions	Ceiling systems	Services, contents
Structural	Static	Gravity	✓	✓	✓	✓
		Wind	✓			
		Temperature	✓	✓	✓	✓
	Dynamic	Earthquake	✓	✓	✓	✓
	Fire	Fire	✓	✓	✓	✓
Architectural	Thermal	Temperature	✓	✓	✓	✓
	Acoustic	Noise	✓	✓	✓	✓
	Weather tightness	Wind	✓			
		Rain	✓			
		Vapor	✓	✓		
Long-term	Durability	Temperature	✓	✓	✓	✓
		Wind	✓			
		Rain	✓			
		Vapor	✓	✓		
	Sustainability	-	✓	✓	✓	✓

2.5 References

- Arora N.L., Gupta B.R. (1988). *Building construction*, Eds. Satya Prakashan, New Delhi, India.
- Becker R. (2009). Air Leakage of Curtain Walls – Diagnostics and Remediation, *Journal of Building Physics*, 34(1).
- Caruso M.C., Menna C., Asprone D., Prota A., Manfredi G. (2017). Methodology for Life-Cycle Sustainability Assessment of Building Structures, *ACI Structural Journal*, 114(2).
- CVVF 5043 (2013). *Requisiti di sicurezza antincendio delle facciate negli edifici civili – Aggiornamento*, Lettera circolare, Dipartimento dei Vigili del Fuoco, del Soccorso Pubblico e della Difesa Civile, Rome, Italy.
- CMHC (2004). *Glass and metal curtain walls. Best practise guide, building technology*, Canada Mortgage and Housing Corporation, Canada, USA.
- Das S. K. (1986). A Study of Exterior Facades – Problems and Solutions. *Paper presented at the Application and Performance of Structural Materials and Exterior Facades*, Boston, USA.
- De Sortis A., Di Pasquale G., Dolce M., Gregolo S., Papa S., Rettore G.F. (2009). *Linee guida per la riduzione della vulnerabilità di elementi non strutturali arredi e impianti*, Presidenza del Consiglio dei Ministri, Dipartimento della Protezione Civile, Rome, Italy.
- Dhakal R.P., MacRae G.A., Pourali A. and Paganotti G. (2016). Seismic fragility of suspended ceiling systems used in NZ based on component tests, *Bulletin of the New Zealand Society for Earthquake Engineering*, 49(1).
- DM 16/02/2007 (2007). *Classificazione di resistenza al fuoco di prodotti ed elementi costruttivi di opere da costruzione*, Suppl. Ord. G.U. n. 74 29/03/2007, Rome, Italy.
- DPCM 05/12/1997 (1997). *Determinazione dei requisiti acustici passivi degli edifici*, Italian standards, Italy.
- Eisenmann R. (2014). *Glass Curtain Wall Installation*.
- Gottfried A. (2002). *Quaderni del manuale di progettazione edilizia. I rivestimenti*. Editor: Hoepli.
- ISO 3382 (1975). *Acoustics - Measurement of reverberation time in auditoria*, International Organization for Standardization, Ginevra, Switzerland.
- ISO 14040 (2006). *Environmental Management - Life Cycle Assessment - Principles and Framework*, International Standards Organization, Geneva, Switzerland.
- NTC (2018). *Aggiornamento delle Norme Tecniche per le Costruzioni*, Suppl. Ord. G.U. n 42 20/02/2018, serie generale, Rome, Italy.
- Pinelli J.P., Craig J.I., Goodno B. J., Hsu C.C. (1993). Passive control of building response using energy dissipating cladding connections, *Earthquake Spectra*, 9(3): 529-546.
- Pumnia B.C., Ashok J., Arun J. (2012). *Building construction*, Eds: Laxmi Publications (P) Ltd., New Delhi, India.

- Riccio P. (2010). Multi-performance based design of facade systems in timber buildings, *Master Thesis*, Politecnico di Milano, Milan, Italy.
- Taghavi S. and Miranda E. (2003). *Response assessment of nonstructural building elements*, Pacific Earthquake Engineering Research Center, Berkley, California.
- UNI 11156-2 (2006). *Valutazione della durabilità dei componenti edilizi - Parte 2: Metodo per la valutazione della propensione all'affidabilità*, Italian standards, Milan, Italy.
- UNI 11156-3 (2006). *Valutazione della durabilità dei componenti edilizi - Parte 3: Metodo per la valutazione della durata (vita utile)*, Italian standards, Milan, Italy.
- UNI EN 12152 (2003). *Facciate continue - Permeabilità all'aria - Requisiti prestazionali e classificazione*, Italian standards, Milan, Italy.
- UNI EN 12208 (2000). *Finestre e porte - Tenuta all'acqua - Classificazione*, Italian standards, Milan, Italy.
- UNI EN 13116 (2005). *Facciate continue - Resistenza al carico del vento - Requisiti prestazionali*, Italian standards, Milan, Italy.
- UNI EN 13947 (2007). *Prestazione termica delle facciate continue - Calcolo della trasmittanza termica.*, Italian standards, Milan, Italy.
- UNI EN 13964 (2007). *Controsoffitti - Requisiti e metodi di prova*, Italian standards, Milan, Italy.
- UNI EN 1991-1-2 (2004). *Eurocodice 1 - Azioni sulle strutture - Parte 1-2: Azioni in generale - Azioni sulle strutture esposte al fuoco*, Italian standards, Milan, Italy.
- UNI EN 1991-1-4 (2005). *Eurocodice 1 - Azioni sulle strutture - Parte 1-4: Azioni in generale - Azioni del vento*, Italian standards, Milan, Italy.
- UNI EN 1991-1-5 (2004). *Eurocodice 1 - Azioni sulle strutture - Parte 1-5: Azioni in generale - Azioni termiche*, Italian standards, Milan, Italy.
- UNI EN 1998-1 (2005). *Eurocodice 1 - Progettazione delle strutture per la resistenza sismica - Parte 1: Regole generali, azioni sismiche e regole per gli edifici*, Italian standards, Milan, Italy.
- UNI EN ISO 13788 (2013). *Prestazione igrotermica dei componenti e degli elementi per edilizia - Temperatura superficiale interna per evitare l'umidità superficiale critica e la condensazione interstiziale - Metodi di calcolo*, Italian standards, Milan, Italy.
- UNI EN ISO 140-5 (2000). *Acustica - Misurazione dell'isolamento acustico in edifici e di elementi di edificio - Misurazioni in opera dell'isolamento acustico per via aerea degli elementi di facciata e delle facciate*, Italian standards, Milan, Italy.

3. Seismic performance of non-structural components

3.1 Introduction

This Chapter focuses on the study of the seismic performance of non-structural components. Gathering data from post-earthquake reconnaissance and damage reports and/or past research studies (analytical/numerical/experimental), the expected seismic behaviour and damage mechanisms of different typologies of non-structural elements can be collected. Therefore, a paragraph on the seismic damage observed after earthquakes for the non-structural components classified in the previous Chapter is firstly reported. Then, the Chapter presents a literature review on the investigations, mainly experimental testing, developed in the past or recently to study the seismic response of these building elements.

Due to the high contribution of non-structural damage to increasing the socio-economic losses after earthquakes, research in the Seismic Engineering field has recently aimed to better investigate the dynamic behaviour of these elements and fragility curves, describing the achievement of specific damage states, have been developed to describe their seismic vulnerability. A state-of-the-art overview of research works dealing with the development of fragility functions is thus presented, being the component seismic vulnerability fundamental to define at which seismic demand level damage states are expected within a component. The knowledge of fragility functions is crucial to understand the expected behaviour of a system under seismic shakings as well as can help in the proposal of new solutions/strategies to improve this behaviour, i.e. moving the achievement of damage states towards higher demand values (inter-storey drift ratios and/or floor accelerations).

3.2 Post-earthquake damage

As described in the FEMA E-74 (2011), seismic actions can cause damage to non-structural elements in four different ways:

- *Inertial effects producing sliding, rocking or overturning.*

Inertia forces produced during an earthquake shaking push the non-structural elements back and forth in a direction opposite to the ground shaking direction and if a system is unrestrained or marginally restrained, effects on the components can be sliding, rocking, striking other objects or overturning.

- *Building deformation.*

During earthquakes structural elements deform and any non-structural component rigidly attached to them deforms or displaces the same amount. Components made of brittle materials, like glass or masonry infill, cannot tolerate significant deformations and when the crack develops, the inertia forces in the out-of-plane direction can cause problems related to dislodgements and falling of element parts. The structural/non-structural interaction must be appropriately studied because stiff non-structural components can be the cause of structural damage or collapse, as shown in Magenes and Pampanin (2004) for heavy infill walls.

- *Separation or pounding between structures.*

Non-structural damage can also be produced by pounding or movement across separations between adjacent structures or building portions, where often architectural finishes terminate. Non-structural elements must be designed to accommodate the seismic movement developing at these locations and resist to the related pounding effects when the gap size is not enough.

- *Interaction with other systems.*

Many non-structural systems are not isolated components into a building while share the same place with other elements. Therefore, the interaction between these elements during earthquake motions can be the cause of damage, such as the impact of mechanical equipment against a partition.

Many factors affect the seismic performance and the damage extension of these building elements, such as the location into the building, the type of ground motion, the connection devices

used, and this session provides a description of the typical damage that can be expected after earthquakes to all the typologies of non-structural systems previously described.

The non-structural damage states herein presented refer to reports from L'Aquila 2008, Darfield 2010, Christchurch 2011, Kaikoura 2016 earthquakes, respectively found in De Sortis et al. (2009), Dhakal (2010), Dhakal et al. (2011), Baird et al. (2011a, 2011b), Baird and Ferner (2017) and from the damage description by the FEMA E-74 (2011) and Filiatrault and Sullivan (2014).

3.2.1 Damage to exterior enclosures

Exterior enclosures can be classified as heavy or light components depending on the impact associated to their failure: heavy façades, for which the failure will likely threaten the people life safety, such as masonry infill walls or precast concrete claddings; light facades, for which the failure may not cause danger to life-safety but economic losses in terms of repair and replacement could be very high. Glazing systems are commonly considered lightweight claddings, although the risk to life safety could be high for pedestrians.

Exterior enclosures (facades) are systems attached or built between building floors, therefore, displacement incompatibilities can be produced by the inter-storey drift ratios during earthquakes. These incompatibilities can be initially taken by gaps, elastic or inelastic deformations or moving elements, then local stresses concentrate in some parts of the component and damage develops. The weakest part of the system determines the seismic behaviour, for example in precast concrete claddings the connections govern the seismic response instead of the panels.

Damage data from past earthquake reports highlight how the current façade design, usually not including the exterior enclosures in the seismic design process, as well as the common construction practice are insufficient to guarantee reduced direct and indirect seismic losses.

3.2.1.1 Curtain walls

Concerning curtain walls, typical damage consists of falling glass breaking for the presence of an insufficient allowable movement of the panels (Figure 3.1). The risk of falling glass represents a very high hazard to people outside the buildings and can be reduced by the application of laminated or tempered glass. Laminated glass prevents the glass to break and fall in a lot of pieces, however during earthquakes the entire panel could fall representing a significant hazard to pedestrians. Tempered glass breaks into thousands of small glass fragments and the related hazard to human life is very low, but it must be accepted that the glass is going to break and fall under seismic actions.



Figure 3.1. Damage to curtain walls related to broken glass (left and centre: Baird et al. 2011b; right: FEMA E-74 2011).

Another observed damage to curtain wall systems is represented by the warping of the steel or aluminium frame and its total or partial disconnection from the structural system. This damage is correlated to the presence of metal connections not appropriately designed to sustain the displacement incompatibilities between cladding and sub-frame.

Notwithstanding the spider glazing system represents a curtain wall with good seismic behaviour, because it moves independently from the structural skeleton, concentration of stresses into local zones can produce the local breaking of glass during earthquakes.

3.2.1.2 Cladding walls

Referring to post-earthquake reconnaissance, various damage mechanisms can be identified based on the cladding configuration. Lightweight panels usually damage for the absence of allowance to the relative movement between structural system and component; the damage consists of cracking, tearing or disconnection of the panel and typically occurs at the interface between panels. In brick veneer cladding systems, if there is an insufficient lateral restraint made of a limited number of ties, the out-of-plane failure of panels can be observed and connections with not sufficient flexibility to accommodate seismic movements may distort while veneer units may crack, spall, or dislodge and fall. Observed damage to monolithic cladding systems consists of cracking to the monolithic finish, mainly located around window corners.

Finally, concerning the heavy precast concrete claddings (Figure 3.2), main damage states can be identified: cracking of the panels; corner crushing mainly due to pounding between panels; if the bolts suffer the distortions due to inter-storey deformations and are not able to slide, bolts can fail and panel disconnection can happen; ejection or rupture of sealing joints. Connections and panels can also damage due to beam elongation effects.



Figure 3.2. Damage to heavy precast concrete walls (left and centre: FEMA E-74 2011; right: Baird et al. 2011b).

3.2.1.3 Infill walls

Infill walls highlighted a very poor seismic performance during past or more recent earthquakes compared to other typologies of façade systems. Concerning lightweight infill walls, i.e. timber or steel infill walls, these systems were usually damaged due to the absence of in-plane movement allowance. While, in case of masonry infill walls, the high post-earthquake damage associated with this type of façade (Figure 3.3) was mainly attributed to the structural/non-structural interaction developing under seismic shakings.



Figure 3.3. Damage to masonry infill walls (left: Baird et al. 2011b; centre: Tasligedik et al. 2011; right, Tasligedik 2014).

Masonry infill walls are very stiff and strong systems, consequently, they interact with the structural skeleton affecting the building response during earthquakes. The interaction with the primary structure can lead to unexpected effects both at local level, such as failure in columns or damage of joint regions, and at global level, like the formation of soft storey mechanisms. Therefore, the damage of these components can limit severely the building functionality increasing the risk to life safety.

3.2.2 Damage to partitions

During past earthquakes many buildings suffered moderate-to-extensive damage to partitions (Figure 3.4). High economic losses were related to these non-structural elements because they needed extensive repairs or complete replacement and the failure of these components also blocked corridors and endangered occupants trying to exit from a damaged building.

Lightweight partitions may be damaged as a result of in-plane or out-of-plane effects if not properly detailed. As observed from past earthquake reports, the most current damages to lightweight partitions are: fastener damage at top and bottom connections, dislodgments of studs, linings cracked or detached from the framing, failure of anchorage between partition frame and structural members. Diagonal and vertical cracking can occur at the upper corners of doors and window openings as well as at the intersections of beams and walls.



Figure 3.4. Damage to lightweight partitions (left: FEMA E-74 2011; centre and right: Tasligedik 2014)

Heavy partitions like masonry walls may affect and change the overall response of the building to earthquakes and are both acceleration and displacement sensitive, falling for either in-plane or out-of-plane movements if not properly detailed (Figure 3.5). Masonry walls may crack and spall, creating debris which is particularly hazardous in stairwells and elevator shafts.

Glazing systems may be very vulnerable to seismic actions if they do not have lateral support and if they are not isolated from the movement of the primary structure. Typical damage includes broken glass, damage to the mullions, gaskets or setting block, cracking and spalling of finishes, deformation of partition frame and failure of connections. Glazed partitions may also be damaged by the impact of not properly anchored furniture or contents or suspended systems. Considering the case of glass block panel assemblies, when rigid mortar is used along all the four sides of the block

and in the mortar joints, the damage of these rigid elements may result in breakage of glass blocks, falling of block units or failure of the panel (Figure 3.6).



Figure 3.5. Damage to heavy partitions (left: FEMA E-74 2011; right: De Sortis et al. 2009).

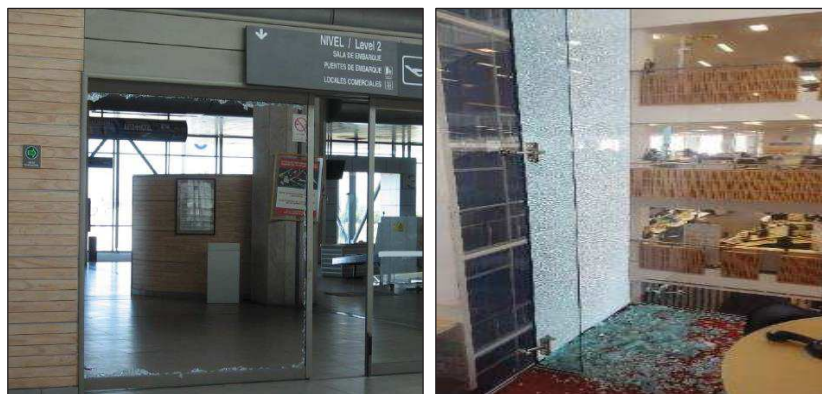


Figure 3.6. Damage to glazing partitions (left: FEMA E-74 2011; right: Baird and Ferner 2017).

3.2.3 Damage to ceiling systems

Damage to ceiling systems represents one of the widespread consequences after earthquakes, as reported in different data collections (Figure 3.7).

Referring to suspended ceiling systems, typical damage includes dislodging and breaking of tiles, failure of grid members, connections and perimeter angles, displacement incompatibilities, interaction with the structure or other systems. Many t-rails were observed to fail mainly for large ceiling areas due to inertia forces on the component greater than the system capacity; this fact was related to the presence of perimeter fixing of the grid to the structure and ceiling rails inadequate for the area they had to provide restraint to. While, the interaction between the suspended ceiling and other components, such as services, partitions and primary structure, produced damage to ceiling

tiles and grid. This indicated the not adequate system design, not considering the relative movements between these adjacent components, or the not proper design of the other systems relying on the suspended ceilings. Light and heavy tiles were observed to fall, and especially the failure of heavy components represented a risk to the life safety of building occupants.



Figure 3.7. Damage to suspended ceilings (FEMA E-74 2011).

Extended damage to suspended ceilings was also observed where various services were attached to the ceiling system. This damage was related to the absence of a grid system not strong enough to support these additional elements. Many damage cases also referred to ceilings and services not well designed or not correctly installed. This is a significant issue to be solved through investigation and enforcement of consistent methods and installation of ceilings (Dhakal et al. 2016).

Concerning ceiling systems directly applied to structural elements, if the finish material is not well anchored to the structure, this may pose a falling hazard (Figure 3.8). Typical damage for this ceiling solution is related to panel cracking or cracking located around the edges between ceiling and walls or the seismic joints.



Figure 3.8. Damage to ceilings adherent to the building floors (FEMA E-74 2011).

Heavy suspended ceilings represent a high risk to the life safety of occupants if the systems break and both the finish material and the furring grid fall (Figure 3.9). Both accelerations and deformations may cause damage to these components, in fact accelerations may produce lost or deformation of the connectors, while differential movements between the system and primary structure or other non-structural elements may also damage the ceilings.



Figure 3.9. Damage to heavy ceilings (FEMA E-74 2011).

3.2.4 Damage to building services and contents

Widespread post-earthquake damage was also observed in the past to services and contents in multiple buildings. Suspended services, such as HVAC or electrical, almost caused damage to suspended ceilings, since they were not braced, and the ceilings were not strong enough to sustain the service falling from above. The relative displacement between services and ceilings determined the falling of the ceiling systems.

Taghavi and Miranda (2004) describe the following main damage conditions to some mechanical and electrical services due to earthquakes (Figure 3.10):

- *Cooling systems*: unanchored systems may move and fall. Usually, air conditioning systems require minor repair, pipes often break or shift, equipment pads usually crack.
- *Ducts*: they often shift or fall during earthquakes. They can rotate during the shaking action and the joints between ducting fail. Other damage is related to other equipment that shift or fall onto the ducting.
- *Fire protection*: damaged piping usually characterizes sprinkler systems. Piping fails due to the impact of other elements and pipe hangers fail for other components falling into

them or for shearing of fasteners. The movement of the ceilings during seismic motions also stresses and damages the sprinkler.

- *Tanks*: anchorages suffer damage and bolts may shear, and in the worst-case tanks may move off supports and topple over, also causing damage to other components connected to them. Tank falling may cause flooding, especially when it is located on the roof of the building.
- *Plumbing*: connections and pipes usually break, due to their own movement or to the hitting of other elements, and plumbing damage results in water damage to other systems.
- *Heating system*: damage can involve ductwork and plumbing; thus, the system loses its functions. Boiler foundations may be damaged and boiler can shift, causing damage to other components nearby.
- *HVAC*: equipment can break, shift and fall, also causing damage to equipment connected to it or to components below. System damage includes falling ducts and diffusers, separation of system components, damage to pump fittings.
- *Communication services*: after earthquakes communication equipment doesn't work, due to power failures or damage to system components, like antenna or cables. Transmission equipment may shift and fall inside a building, telecommunication lines often damaged.
- *Generators and transformers*: when the power is out, generators are needed after earthquakes. These components may not work without being damaged because of the damage of other component from which they depend on, as example if the generator needs cooling water to operate whilst the water tanks are damaged. Common damage includes their shifting, which can damage anchorages and other elements.



Figure 3.10. Damage to building services (left: Baird and Ferner 2017; centre and right: FEMA E-74 2011).

Regarding the egress systems (Figure 3.11), as described by the same authors (Taghavi and Miranda 2004) the most common damage associated with stairs is to the walls in the stairwell, initiating with the cracking of the plaster that may become severe and crack the wallboard or infill when the ground motions intensify. While, elevators are often temporarily inoperable after earthquakes due to mechanical failure or a loss of power. Therefore, they may be out of commission despite having no damage and the damage usually is attributed to components involved into the mechanical process, such as controllers, motor generators, governor anchors, stabilizers, machines as well as their specific supports and anchorages.



Figure 3.11. Damage to egress systems (left: Taghavi and Miranda 2004; centre and right: FEMA E-74 2011).

Concerning building contents, the extent of the related damage (Figure 3.12) depends on the use and location into the building. For example, in residential houses damaged contents may be objects such as racks, fragile items, television sets, in offices the equipment can include printers, monitors, modular office desks, bookcases. Notwithstanding these items are easily substituted and cleaned up after earthquakes, the extent of furniture represents economic losses and a potential for people injury within the building, therefore also these elements must be appropriately restrained.



Figure 3.12. Damage to building contents (left: Dhakal 2010; right: Baird and Ferner 2017).

3.3 Investigations on seismic behaviour

The evaluation of damage to architectural non-structural components, building services and contents is an essential part of the performance and loss assessment of a structure. Damage data can be collected from post-earthquake reports, laboratory experiments or numerical analyses of the components. The identification of the damage states from these sources allows the definition of the fragility curves, representing the probability that a specific component response to various seismic excitations exceeds performance limit states.

Non-structural elements can be sensitive to acceleration, inter-storey drift ratio or both, e.g. ducts, boilers or tanks are acceleration-sensitive components, partitions or masonry walls are drift-sensitive components, while precast elements or fire sprinklers are sensitive to both (Taghavi and Miranda 2004). The damage states characterizing a component can be associated with these response parameters and converted into fragility curves. A non-structural system consists of many individual elements linked together, thus the system fragility depends on the fragility of each component as well as on their connection.

Fragility curves are described by a relation between the Engineering Demand Parameter (EDP) and the probability of exceeding a specific damage state. Different fragility curves can be defined for each component depending on the modes of failure of the system. Fragility functions take the form of lognormal cumulative distribution functions and are mathematically described as:

$$F_i(D) = \Phi \left(\frac{\ln(D/\theta_i)}{\beta_i} \right)$$

Where: $F_i(D)$ is the conditional probability that the component will be damaged to damage state “i” as a function of a demand parameter (D), Φ indicates the standard normal (Gaussian) cumulative distribution function, θ_i denotes the median value of the probability distribution, and β_i denotes the logarithmic standard deviation. The dispersion represents the uncertainty in the value of demand at which a damage state is likely to initiate and when fragilities are determined from a limited set of test data it can be computed as:

$$\beta = \sqrt{\beta_r^2 + \beta_u^2}$$

Where: β_r is the random variability observed in the test data, β_u is a measure of the uncertainties associated with the actual physical construction details and loading conditions on the building as compared to the component testing conditions in the laboratory.

Depending on the available data, different methods exist to determine the fragility parameters, i.e. the actual demand data, the bounding demand data, the capable demand data, the derivation, expert opinion, as also described in the FEMA P-58 (2012). Concerning non-structural damage from post-earthquake surveys, data collections are available to support the development of the fragility functions, such as the MCEER database containing data from the Alaska earthquake of 1964 (Song and Vender 1999). However, experimental testing is one of the most reliable sources of data to evaluate the damage progress of a component subjected to defined loads. In fact, everything is monitored during an experiment and reports on the mode of failure of the non-structural components as well as the corresponding level of loading or deformation can be generally found.

Obviously, fragility curves vary in function of the system details, i.e. for a glass façade these functions depend on the framing detailing, glass-to-frame clearance, system type, glass type, panel dimensions, glass thickness, however general considerations on the expected behaviour of a system can be identified. Furthermore, the knowledge of fragility functions can help in the proposal of new solutions/strategies to improve this behaviour.

3.3.1 Exterior enclosures

A documentation on the main findings from past experimental investigations, carried out to study the seismic behaviour of façade systems and determine fragility functions, is herein provided.

3.3.1.1 Curtain walls

a) Experimental studies

Initial investigations on the in-plane movement of glass panels were proposed by Bouwkamp, that in 1960 conducted in plane-loading tests on 39 glass window panels (Bouwkamp 1961). He found that the glass panels move in two different phases: 1) the supporting frame deflects, and the internal glass panel within the frame translates until the opposite corners of the glass and the frame come into contact (rigid body slip); 2) then the glass panel rotates in the enclosing frame until it is seated in the two diagonal opposite corners (Bouwkamp and Meehan 1960). An analytical formulation was later proposed by Sucuoglu and Vallabhan (1997) to determine the total lateral

deformation of the window panel due to rigid body motion, in terms of geometrical properties of the panel.

Lim and King (1991), Thurston and King (1992) performed a three-year research program from the Building Research Association of New Zealand (BRANZ) to study the behaviour of curtain wall glazing systems subjected to inter-storey drift ratios which can be expected during earthquakes. Four types of facades (neoprene gasket dry-glazed system, unitized 4-sided structural silicone glazed system, two-sided silicone glazed system, mechanically fixed patch plate systems with toughened glass) in five different configurations (single storey specimen with zero adjacent inter-storey drift, single storey specimen with full adjacent inter-storey drift, double storey specimen with zero adjacent inter-storey drift, double storey specimen with full adjacent inter-storey drift, corner specimen with zero adjacent inter-storey drift) were tested. These static tests proved the development of the two mechanisms previously described. The research also concluded that it is possible to accurately determine the racking capacities of full-scale curtain walls through controlled in-plane displacement loading in the laboratory.

Behr et al. (1995 a, 1995b), Behr and Belarbi (1996) performed experimental serviceability tests, ultimate tests and dynamic-crescendo tests to investigate the behaviour of various types of architectural glass and related glazing systems commonly used in mid-rise buildings under simulated earthquake conditions. The laboratory tests were developed from 1996 at the Building Envelope Research Laboratory at the University of Missouri-Rolla. The results determined the effects of glass surface prestress, lamination, wall system type, and dry versus structural silicone glazing, and the dynamic drift limits for glass cracking and fallout in the tested configurations (Behr 1998).

In 2004 Memari et al. carried out research on mid-rise curtain wall systems by dynamically racking different asymmetric insulating glass units, concluding that the polyvinyl butyral (PVB) interlayer thickness, glass thickness, and glass type variables do not have significant effects on the cracking or fallout of the annealed inner glass panes, the serviceability of the outer annealed laminated panes or the entire unit fallout limit state. Another research work was developed by Memari et al. (2006), who performed full-scale dynamic racking tests of glass panel curtain walls. The authors also proposed a vulnerability mitigation measure consisting of modification of corner geometry and edge finishing (rounding the glass corners), considering that glass edges and corner finishing mainly influence the glass cracking and the system fallout.

Weggel et al. (2007) experimentally studied a conventional mullion system with laminated glass panels subjected to static and transient dynamic service loads. The same authors also developed a finite element model taking into account the obtained experimental results.

Real scale in-plane racking laboratory tests on typical point fixed glass façade systems were conducted by Sivanerupan et al (2010, 2014), as shown in Figure 3.13, left. These experimental tests allowed to study the seismic behaviour of such type of glazing facade. Detailed finite element models were also proposed and analysed to evaluate the drift contributions of each racking mechanism, such as rigid body translation of the glass panels at the oversize holes due to construction tolerance, spider arm rotation and spider arm deformation. Most of the drift capacity was found to be attributed to the first of these mechanisms.



Figure 3.13. Left: experimental tests on spider glazing configurations (Sivanerupan et al. 2010); Right: Test setup of a full-scale stick curtain wall and lateral load application by a hydraulic jack (Caterino et al. 2017).

The seismic behaviour of full-scale stick curtain walls was studied by Caterino et al. (2017) through full-size in-plane experimental tests (Figure 3.13, right) at the laboratory of the Construction Technologies Institute (ITC) of the Italian National Research Council (CNR). A finite element modelling was also proposed to properly describe the effect of aluminium frame and transom-to-mullion connection stiffness, the clearance between glass panels and frame, the local stiffness in the glass-to-frame interaction and the gasket-to-glass friction.

b) Fragility curves

The typical load-drift relationship from experimental static tests of a curtain wall system has the shape presented in Figure 3.14, and a very similar behaviour can be found from static and dynamic cyclic racking tests. Different damage states can be identified along the curve and consequently

related fragility functions. Typical damage states for glazing facades include: 1) gasket degradation, 2) initial glass cracking and crushing, and 3) glass fallout.

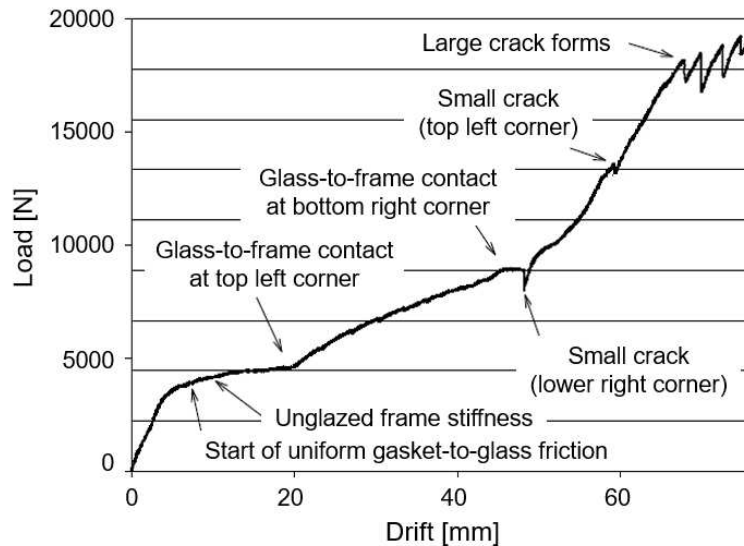


Figure 3.14. Example of load-displacement diagram from experimental static tests (Memari et al. 2014).

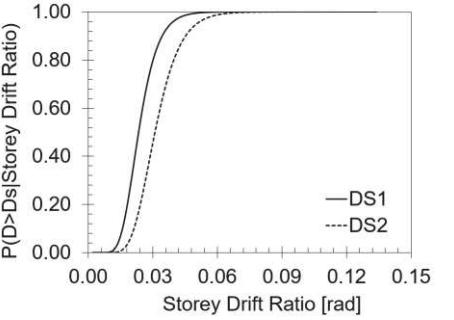
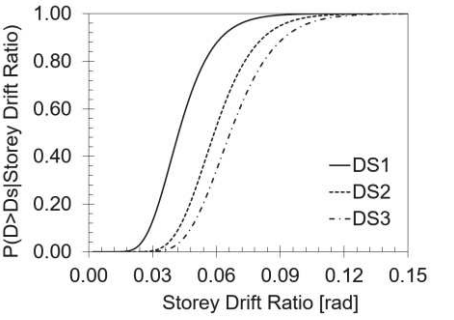
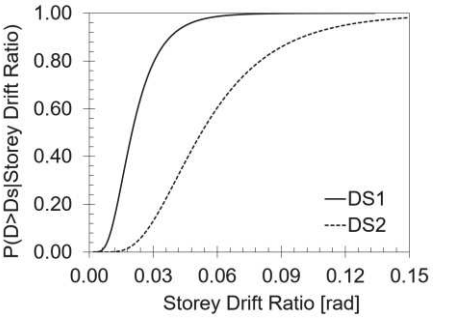
The degradation of the perimeter gasket seal can be due to various conditions (distortion, pull-out, push-in and shifting), as described by Behr et al. (1995a), and is considered a serviceability damage state not posing risk to life safety whilst allowing air and water infiltrations. Initial glass cracking and crushing is also considered as a serviceability failure not compromising life safety, however it can allow air leakage, water infiltration, and other indirect damages which can increase the cost to building owners and occupants. Finally, glass fallout is an ultimate damage state posing potential life safety hazard, thus causing many indirect economic consequences.

Fragility functions can be used to describe the behaviour of a component if the glass system under consideration has the same detailing of the element for which the fragility curves have been developed, i.e. framing detailing, glass-to-frame clearance, system type, glass type, panel dimensions, glass thickness. Otherwise, modifications of the fragilities must be introduced, as described in O'Brien (2009), providing fragility modification methods for glass configurations varying in framing, glass-to-frame clearance and aspect ratio.

Fragility curves for glazing systems in terms of damage probability as a function of the drift were developed by O'Brien et al. (2012) referring to experimental in-plane racking tests available from literature. Particularly, 24 selected types of curtain walls experimentally studied at the Pennsylvania State University and University of Missouri were considered for the development of these fragility

functions. Referring to the study by O'Brien et al. (2012), to the fragility database of FEMA P-58 2012 or considering damage states from other experimental tests (e.g. Sivanerupan 2014), all the available fragility curves can be collected. Some examples of fragility specifications for different typologies of glazing systems can be found in Table 3.1.

Table 3.1. Examples of fragility curves for curtain wall systems (source: O'Brien et al. 2012, FEMA P-58 2012).

Component type	Description	Fragility curves
Stick curtain	Insulated glass unit, 6 mm inner/outer annealed glass, aluminium frame 11 mm glass-to-frame clearance, square corners, cut corner and edge finish, 6:5 aspect ratio	 <p>DS1: Glass cracking DS2: Glass fallout</p>
Storefront	Insulated glass unit, 6 mm inner/outer annealed glass, aluminium frame 15 mm glass-to-frame clearance, square corners, cut corner and edge finish, 6:5 aspect ratio	 <p>DS1: Gasket degradation DS2: Glass cracking DS3: Glass fallout</p>
Spider glazing	12 mm toughened glass, 8 mm silicon weather sealant, fixed K-type spider arm, 7 mm horizontal and 17.5 mm vertical gaps for M10 bolted connections	 <p>DS1: Gasket degradation DS2: Glass fallout</p>

3.3.1.2 Cladding walls

Among the cladding systems presented in the previous Chapter, most of the research focused on the study of the seismic behaviour of heavy precast concrete cladding facades. Therefore, a literature review on the main experimental works on these non-structural components is herein presented, focusing on the study of both connection and system level (cladding panel connected to a structural system).

a) *Experimental studies*

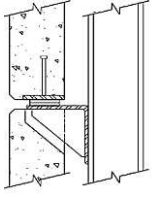
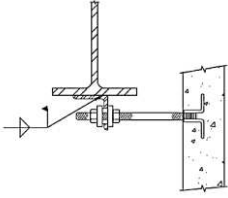
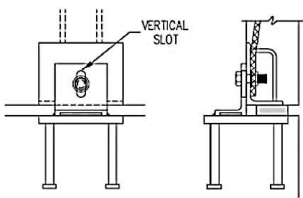
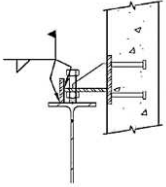
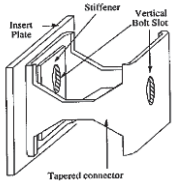
The influence of cladding systems in the structural strength and stiffness of multi-storey buildings has been highly investigated during the last years. These architectural systems are connected to structural members and designed assuming negligible interaction with the primary structure, however this interaction may be beneficial or detrimental to the seismic performance of the building (Goodno 1983). The interaction between structural system and cladding panels is related upon the design and detailing of panels and connection devices. For example, when the connections are not well designed, such as overstrained connections, gaps too small, slotted holes too short, cladding panels may damage and fail, or structural damage may result (Pinelli et al. 1995).

Experimental investigation on these architectural components can involve testing on either the single components (cladding panel or connection devices) or the overall cladding-structure system. Tests on cladding panels are usually performed in order to evaluate the architectural properties, i.e. weather tightness or thermal rating, while, many past experimental investigations have been carried out to study the seismic behaviour of different types of connection devices as well as to the study the structural/non-structural interaction through large scale testing.

- Connection-level investigations

As presented by Pinelli et al. (1993), cladding systems are composed of five main elements: the structural framing member, the attachment between structure and connection, the connector body, the attachment between connector body and the cladding panel. The weakest link in a cladding system is generally represented by the connector body. Various typologies of connector devices, as summarized in Table 3.2 and described in PCI (2007), are available and must be designed to accommodate the lateral displacement as well as to provide out of plane restraint.

Table 3.2. Summary of connection systems as described in PCI (2007).

Bearing connection (PCI 2007)	Tie-back connection (PCI 2007)	Slotted connection (PCI 2007)
		
Fixed connection (PCI 2007)	Dissipative connection (Pinelli et al. 1995)	
		

- **Bearing connections.** Usually bolted steel angles, they are intended to transfer the vertical loads to the supporting structure. These connections are typically inserted at no more than two points per panel to avoid the development of an indeterminate force distribution of the gravity loads and can be inserted in the plane of the panel on the bottom edge or eccentric, using continuous or localized reinforced concrete corbels or haunches, cast-in steel shapes, or attached panel brackets.
- **Tie-back connections:** These devices are made of threaded rods bolted or welded to angle or tube steel sections attached to the structural members. Their primary function is keeping the panel into the vertical position and resisting against horizontal forces perpendicular to the panel. They can be also designed against in-plane horizontal forces and often used to isolate the panel allowing independent distortions and not participation in the building lateral response.
- **Slotted connections.** They have an oversized hole or slot which guarantees the sliding of the bolt and the accommodation of the drift level. They keep the panel in the vertical position, also providing both in-plane and out-of-plane movements and isolating the panel from the entire building response.
- **Fixed connections.** Similar to bearing connections whilst designed to carry the panel self-weight as well as to resist loads imposed from each direction. They have a stiff and strong body, hence, the panel itself can accommodate the horizontal movements.

- *Dissipative connections.* Dissipative connections take advantage of the structural/non-structural interaction to dissipate energy, thereby reducing the response of the main structure. These connections also limit the forces transmitted into the panel, consequently reducing the expected damage.

Several experimental investigations focusing on the study of the connection behaviour can be found in literature and some of them are herein described.

Rihal (1988) studied the behaviour of precast claddings and connection devices in medium-rise steel-framed buildings, performing cyclic tests on a cladding panel with bearing connections at the bottom and threaded rod push-pull connections at the top. The threaded-rod connections provided evidence of strain-hardening, showing the susceptibility of these devices to low-cycle fatigue.

In-plane dynamic loading tests of connection elements were performed by Sack et al. (1989). The connection tests included rod components connected through steel angles to the structure and threaded inserts in the concrete. The connections showed an elastic perfectly plastic behaviour and the dissipation property was due to the combination of inter-storey drift and plastic load limits.

The lateral stiffness, energy dissipation and ductility of steel inserts in cladding panels was investigated by Craig et al. (1986) and Pinelli and Craig (1989). The initial tests in 1986 found a failure related to the concrete fracture which suggested to improve the component design integrating the insert with the panel reinforcing steel. In the latest tests of 1989, cyclic loads revealed pinching in the hysteretic loops, explained by the interaction between the steel insert and the surrounding concrete, while the brittle failure of concrete was found in many cases, mainly due to lack of confinement. This last aspect led to initiation of great displacements for the connections and to failure of the weld between steel plate and reinforcement.

Full-scale threaded rod tie-back and welded plate cladding connections were tested by McMullin et al. (2004a) to determine their force-deformation behaviour. A ductile behaviour was observed for the connections, achieving deformations of 150 mm without loss of strength, however this ductility was overestimated due to the application of only monotonic loading not able to capture the cyclic actions as well as the strength and stiffness degradation.

Finally, it is cited the work by Okazaki et al. (2007), who investigated the behaviour of flexible or sliding connections attached to autoclaved lightweight aerated concrete (ALC) panels. These connections successfully isolated the panels from the structure, even under a large inter-storey drift of 4%.

Several studies were also proposed to investigate the behaviour of advanced connections using the interaction between panels and building structure to dissipate energy. These devices can reduce the deformations of the main structure and prevent the damage to both structural and non-structural elements. Among these studies, it is acknowledged the research on elastomeric connections by Kemeny and Lorant (1989), on the friction-damped connection by Pall (1989), on the advanced tapered connection by Craig et al. (2000), Goodno et al. (1998), Pinelli et al. (1995).

- System-level investigations

Craig et al. (1989) carried out initial experimental tests on a precast cladding subsystem made of cladding panels with bolt-insert and ductile rod push-pull connections to confirm the analytical models proposed for this type of connection. Then, in 1989 Goodno and Craig performed experimental tests to validate numerical investigations where cladding systems affected the building lateral stiffness. Particularly, ambient vibration measurements and force vibration testing were applied to high-rise buildings in order to determine the building natural frequencies, modal shapes and damping, highlighting how the global behaviour was mainly influenced by the connections instead of the panels.

In-plane dynamic tests of a large precast concrete panel connected to a steel frame structure were carried out by Rihal (1989). The author studied the system displacements and vibration modes, showing that the great mass of the tested 115 mm thick cladding overcame the additional stiffness offered to the structure and reduced the system periods of vibration.

A full-scale six-storey two-bays steel structure was studied during a US-Japan program started in 1979 (Wang 1986, 1987; Wang and Bassler 1992) to analyse the seismic performance of non-structural elements, e.g. exterior claddings, and their interaction with the primary structure. The non-structural elements reduced the building natural period by 30%, but it was observed that after 8 cycles of testing at a storey drift of 0.3% most of this additional stiffness was lost due to the damage of non-structural elements. Different cladding connections were tested (angle bearing connections and long-rod lateral connections; tube bearing connections and slotted lateral connections) and the results showed that the sliding connections were the first to deteriorate and the slot was inadequate to accommodate the drift, the long-rod connections performed well and had significant ductility. Finally, some cracking of the panels was also observed.

In 2011 a full-scale five-storey steel frame building with full-scale precast concrete cladding panels with slotted connections (NEES/Tips Project) was tested on the E-Defence shake table facility in Japan (Soroushian et al. 2012; McMullin et al. 2012). The façades were designed considering

vertical slots in the connections to allow rocking actions developing during horizontal actions. The research focused on the evaluation of inter-storey drifts and accelerations on the cladding systems. The experimental results found that claddings behaved accordingly to the design with no damage observed in the panels.

At the University of California (San Diego) in 2012 the Building Non-structural Components and Systems (BNCS) Project involved the seismic testing of a five-story building completely furnished with non-structural elements, including a functioning passenger elevator, partition walls, cladding and glazing systems, piping, HVAC, ceiling, sprinklers, building contents, as well as passive and active fire systems (Chen et al. 2012; Hutchinson et al. 2015; Pantoli et al. 2013, 2016). The building was composed of two different facades: 1) lightweight metal stud system overlaid with stucco (bottom half of building) and a precast concrete cladding system (top half of building) with different typologies of connection (sliding, flexing and a new yielding connection) (Figure 3.15).



Figure 3.15. Five-storey Test Building (left) and cladding system details (Pantoli et al. 2013).

Flexing and sliding tieback connections with three different lengths were tested and flexing connections generally showed better performance than sliding connections. In fact, plastic deformation was caused by the bending of the rod and sliding of the rod inside the oversized installation hole, which minimized permanent displacement from developing in the panels. These observations led to the conclusion that for both types of connections the actual working mechanism involved both sliding and bending. The sliding connections, made of a rod and an oversized hole in the support clip angle, were affected by good performance especially with the adoption of short and medium-length rods. During these tests a new corner connection for the precast panels with a ductile fuse mechanism was also proposed and tested.

Experimental tests on a full scale, single-bay, single-storey frame subassembly with bearing and different tie-back connections were carried out by Baird et al. (2012), Baird (2014) (Figure 3.16). Long threaded rod connections, slotted connections and short threaded rod connections were tested to investigate the hysteresis behaviour of such type of devices and to determine the cladding damage limit states. Concerning the experimental results, the long-threaded rods were found to fail during the 1.5-2.0% inter-storey drift cycles, while no connection failure was observed in the slotted connections. Nevertheless, when the slot length was exceeded cracking started developing in the panel and the short-threaded connections were found to repeatedly fail during the 1.5% drift cycle.

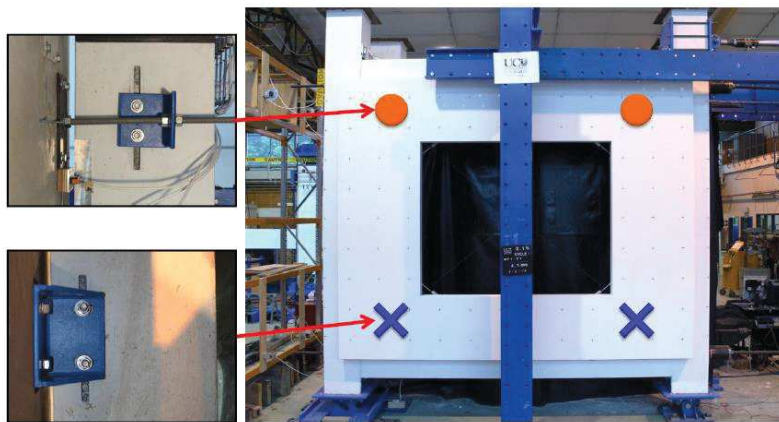


Figure 3.16. Experimental test frame and connection assemblies (Baird et al. 2012).

During the SAFECCLADDING Project, developed with the aim of improving the connection system between cladding panels and precast reinforced concrete buildings in seismic-prone areas, static and pseudo-dynamic tests at both serviceability and ultimate limit states were performed on a two-bays one-storey building with cladding systems, considering different types of connection between panels and frame as described in Negro et al. (2017). The experimental results highlight that: 1) considering panels as simple masses without stiffness is far from the real system behaviour, even using devices to uncouple panels and frame displacements; 2) bearing high loads transferred by the frame through connections lead to create weak points into the system; 3) the dissipative solution provides the best results, combining lower relative displacements with limited loads within the connections, avoiding both the compatibility problems and excessive forces.

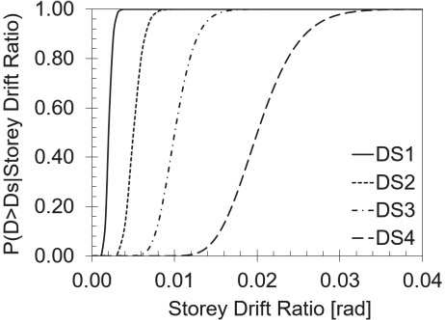
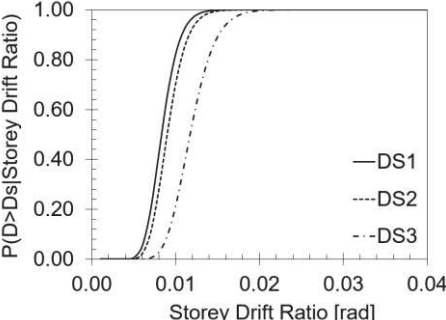
Belleri et al. (2016) investigated the in-plane performance of horizontal precast reinforced concrete cladding panels through quasi-static cyclic loading. An experimental campaign was conducted on four full scale cladding panel to column subassemblies with typical connections used in the Italian territory. Different types of connection were tested: 1) two bottom bearing connections,

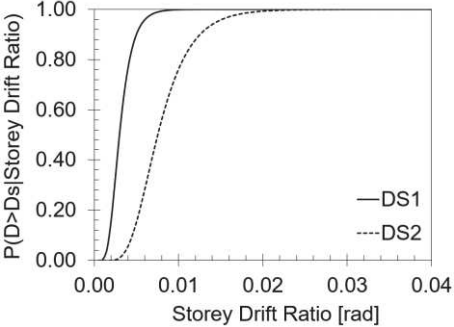
i.e. a stocky steel element partially inserted into a steel pocket inside the column and a rotating steel plate; 2) top retaining connections, characterized by a vertical anchor channel embedded in the column allowing for vertical tolerances, a slotted steel profile anchored into the panel for horizontal tolerances and a connecting flat head bolt with washers and nuts. The experimental results highlighted failure mechanisms associated with the top connections.

b) Fragility curves

Different damage states can be identified depending on the system configuration, panel properties, type of connection and its design. However, for the cladding panels the following damage conditions can be generally identified: 1) first visible cracking of the panel; 2) minor cracking, less than 0.3mm for Serviceability Limit State; 3) major cracking, crushing at connections; 4) disconnection of the panel. While for connections the damage states typically include: 1) undamaged condition, pre-yielding or within the slot capacity; 2) visible damage, post-yielding or exceedance of slot capacity; 3) severe damage to connections; 4) rupture of the rod (Table 3.3).

Table 3.3. Example of fragility curves for precast concrete panel systems (source: Baird 2014).

Component type	Description	Fragility curve
Threaded connection	Rod diameter of 20 mm, Rod length of 250 mm, Interstorey height of 3000 mm	 <p>DS1: Pre-yielding DS2: Post-yielding DS3: Severe damage to connections DS4: Rupture of rod</p>
Slotted connection	Bolt diameter of 20 mm, Slot length of 70 mm, Interstorey height of 3000 mm	 <p>DS1: Within the slot capacity DS2: Exceedance of slot capacity DS3: Severe damage to connections</p>

Component type	Description	Fragility curve
Panel	Dual panel configuration, Short threaded rod connections, Interstorey height of 3000 mm, 3775 x 2975 mm panel dimension, 12 mm panel thickness	 <p data-bbox="901 660 1356 750"> DS1: First visible cracking of the panel DS2: Minor cracking, less than 0.3mm for Serviceability Limit State </p>

3.3.1.3 Infill walls

Concerning infill walls and focusing on heavy systems, some of the main experimental results found in literature are herein reported.

a) *Experimental studies*

At the University of L'Aquila, Colangelo (1999, 2003) carried out in-plane pseudo-dynamic tests on infilled one-storey 1:2 scaled frames (Figure 3.17, left), either designed for gravity only, thus typical of the Italian construction practice before the introduction of modern seismic design provisions, or designed accordingly to the Eurocode 8 (1998). Several types of infill were tested (either vertically or horizontally hollowed bricks, arranged in a single or double panel) and results confirmed the increase of the initial stiffness and strength, respectively one order and two orders more when compared to the bare frame system.

Pseudo-dynamic tests on a full scale four-storey 3D infilled frame were performed at the European Laboratory for Structural Assessment (ELSA) of the Joint Research Centre in Ispra (Figure 3.17, right) by Negro (1995). Three different solutions were tested (bare frame, uniformly infilled frame and partially infilled frame) to study the influence of the infill walls on the global building dynamic behaviour. The pseudo-dynamic tests were complemented by shaking table tests at the University of Bristol to investigate the importance of the out-of-plane forces (Negro and Taylor 1996) and the results suggested that the out-of-plane collapse of infill walls can be controlled by good detailing.

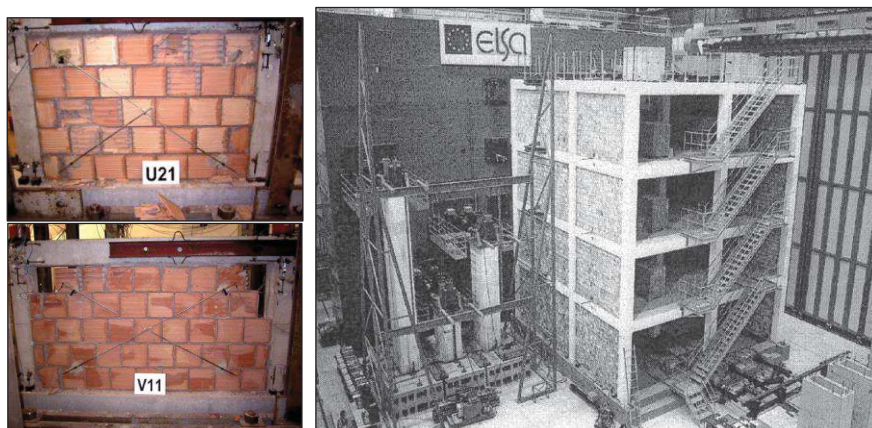


Figure 3.17. Pseudo dynamic tests on one-storey 1:2 scaled frames (left) by Colangelo (1999) and on a full scaled RC frame with uniform infill distribution (right) by Negro (1995).

Mosalam et al. (1997) carried out quasi-static testing of single-storey, one and two-bay steel frames, infilled with unreinforced masonry walls with and without openings. The results showed that the presence of openings led to a more ductile behavior and larger post-cracking force ratio compared to infill panels without openings.

In 2001, Calvi and Bolognini investigated through quasi-static testing the behaviour of four different reinforced concrete frame configurations (bare frame, infilled frame with unreinforced clay bricks, infilled frame with clay bricks with horizontal reinforcement in mortar layers, infilled frame with clay bricks with reinforcing mesh on the surface), showing how the reinforcing mesh on the surface can improve either the in-plane or the out-of-plane response. The brittle failure of the infill material was prevented, and a ductile post-peak response was achieved.

The effect of masonry infills on the structural response was also studied by Pujol and Fick (2010). The authors carried out reverse-cyclic quasi-static testing on a full-scale three-storey reinforced concrete flat slab building with unreinforced masonry brick infill walls. The damage states associated with the infill walls during the tests were also investigated.

Other experimental tests were performed by Tasnimi and Mohebkah (2011). The authors tested six full-scale, single-storey, single-bay steel frame specimens with and without infill walls. Different orientations of the openings in the panels were analyzed, showing that the ductility of infill walls with openings is not always higher than the ones without openings.

Finally, it is acknowledged the work by Tasligedik and Pampanin (2016), that performed 2D quasi static testing on a as-built unreinforced clay brick infill wall within a reinforced concrete one-storey one-bay frame. The progress of damage in the infill panel was studied and the research

highlighted the contribution of the non-structural component to the beam elongation occurring in the structural frame.

b) Fragility curves

Several studies focused on the development of fragility curves for masonry infill walls as a function of the inter-storey drift ratio for the in-plane seismic behaviour and of the peak floor acceleration for the out-of-plane response. Some of these research works are herein cited.

Cardone and Perrone (2015) determined fragility curves from 55 experimental tests of laboratory specimens comprising reinforced-concrete/steel frames with masonry infills realized with hollow clay bricks and pine-wood sub-frames with ordinary plan dimensions. Fragility curves were identified for exterior masonry infill walls without openings, exterior masonry infill walls with openings and exterior masonry infill walls with French windows, considering four different damage states (light cracking, extensive cracking, corner crushing, collapse; Figure 3.18). The authors used the inter-storey drift ratios directly obtained from the experimental results for developing the fragility specifications, neglecting the differences between the test specimens in terms of aspect ratio and typology of masonry. Some of the fragility functions proposed by the authors for the in-plane condition are presented in Table 3.4.

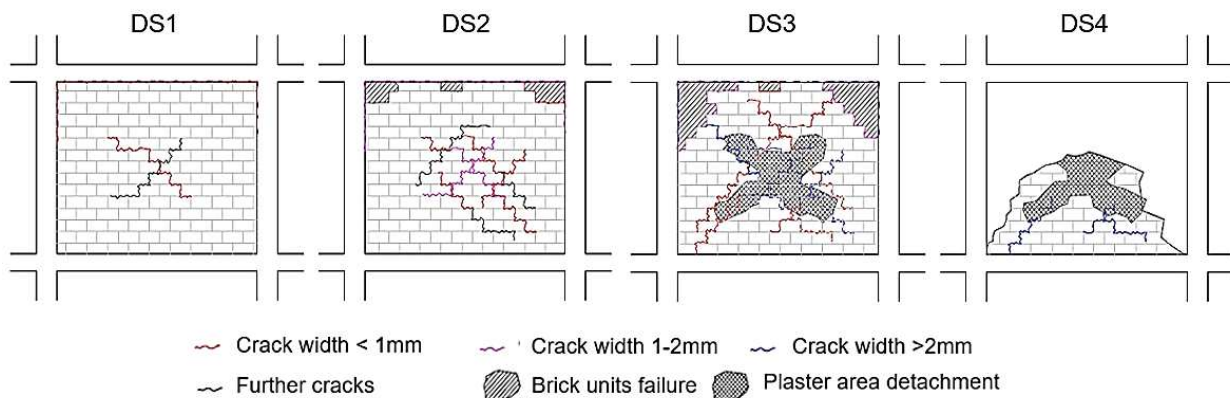


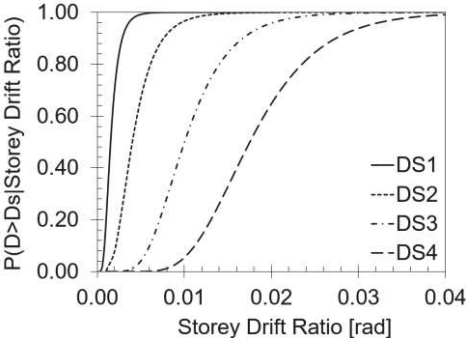
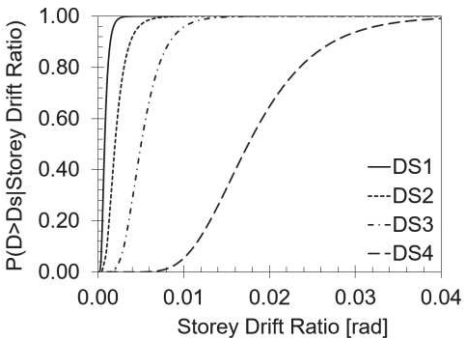
Figure 3.18. Damage states of masonry infill walls without opening (Cardone and Perrone 2015).

Sassun et al. (2015) collected data from an extensive set of experimental tests (conducted in Europe, the Middle East and the United States and including solid and hollow clay brick or concrete block infills, constructed within either reinforced concrete or steel framing) and determined fragility functions for the in-plane performance of masonry infills. The results showed that masonry infills can exhibit first signs of damage at drifts as low as 0.2% but may not suffer complete failure until drifts

as high as 2.0%. Authors also highlight that masonry fragility changes significantly according to the type of infill masonry.

Chiozzi and Miranda (2017) developed drift-based fragility functions for in-plane loaded masonry infills. The fragility input data were derived from a comprehensive experimental dataset gathered from current literature, comprising 152 specimens of infilled RC or steel frames tested under lateral cyclic loading, with different types of masonry blocks (solid clay bricks, hollow clay bricks and concrete masonry units). Fragility curves were defined referring to three different damage states (light cracking, moderate cracking and heavy cracking) and four sources of uncertainty were investigated into the fragility results (specimen-to-specimen, finite-sample, measured mortar compression strength and prism compression strength, presence of openings).

Table 3.4. Fragility function parameters of masonry infills (source: Cardone and Perrone 2015).

Component type	Description	Fragility curve
Exterior walls without openings	Masonry infills with French window	 <p>DS1: Detachment of infill, Light diagonal cracking DS2: Extensive diagonal cracking DS3: Corner crushing and sliding of mortar joints DS4: Global collapse in-plane</p>
Exterior walls with openings	Masonry infills with French window	 <p>DS1: Detachment of infill, Light diagonal cracking DS2: Extensive diagonal cracking DS3: Corner crushing and sliding of mortar joints DS4: Global collapse in-plane</p>

3.3.2 Partitions

Focusing on drywall partitions, widely adopted around the world, an overview of the main experimental studies found from a literature review is presented below.

a) Experimental studies

First experimental tests on seventeen drywalls made of different materials and different connection types (stud to track connection by friction or pop-rivets) were performed by Freeman in 1971. Using a transportable racking test setup, he studied the cyclic behaviour and the energy absorption properties of drywalls. In 1980, Rihal performed quasi-static loading protocol tests on similar drywall configurations confirming the results obtained by Freeman. Then, quasi-static testing on partitions inserted within a full scale six storey steel structure was carried out by Wang in 1987 during a joint project between US and Japan. In this research, US practice and Japan practice were compared.

McMullin and Merrick (2001) performed a set of seventeen experimental tests for determining the cost-damage relationship of residential gypsum wallboard partition walls. Different variables were considered during the experiments (fastener types and spacing, loading protocol, boundary conditions, opening and fenestration features, repairing methods) and it was observed that the maximum loads were sustained at 1 to 1.5% drift. Two dominant failure modes were noticed: 1) the loosening of wallboard from the framing systems due to the pulling of fasteners; 2) the racking movement of the individual panels.

Lee et al. (2006) tested 4 full-scale light gauge steel framed drywall partitions following Japan's practice within a modified racking test setup. The tests studied the effect of a door or an intersecting wall, showing how the damage typically concentrated to perimeter regions in contact with ceiling, floor or columns. The research work concluded that repair costs after 2.0% inter-storey drift reached almost the initial cost of construction for a new drywall infill.

In 2007 McMullin and Merrick conducted 11 tests using full scale timber framed drywalls with diagonal straps as bracing elements, reporting two different failure modes, i.e. joint failure with the individual gypsum linings racking and pier rotation where all the gypsum linings in a pier rotated as a unit. It was also observed a maximum load occurring at drift levels between 0.68% and 1.87% while the initial cracking at 0.25%.

Filiatrault et al. (2010) tested 36 steel studded gypsum drywall partitions using a typical racking setup (Figure 3.18, left). The experimental results showed that the application of slip tracks and gaps at the top end of the drywalls reduced the seismic damage of the drywall panels attached in the vertical direction, however the damage concentrated within the vertical joints between drywalls in the orthogonal direction.

Shaking table tests were performed by Magliulo et al. (2014) in order to investigate the seismic response of plasterboard partitions. The tests were carried out considering simultaneous shaking into the two horizontal directions and referring to a wide range of interstorey drift demand and seismic damage. The tested plasterboard partitions exhibited a good seismic behaviour, both in their own plane and out of plane, showing limited damage up to 1.1% inter-storey drift ratio (Figure 3.19, right).

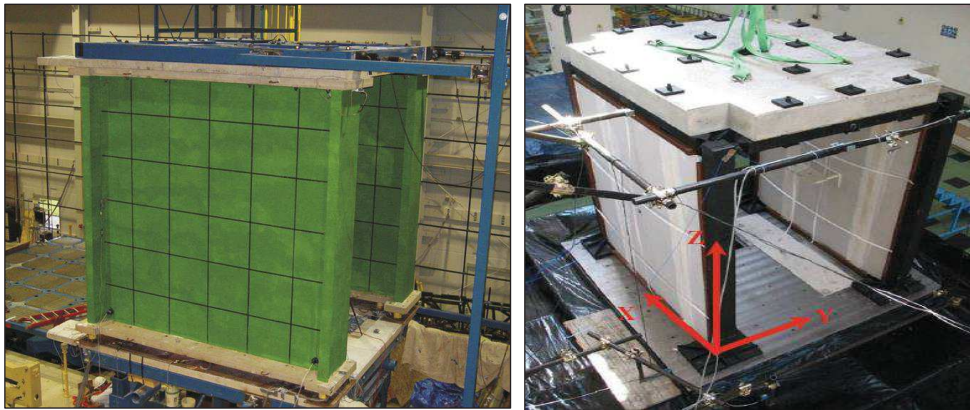


Figure 3.19. Left: racking setup for tests on drywall partitions by Filiatrault et al. (2010). Right: shaking table test setup on plasterboard partitions carried out by Magliulo et al. (2014).

Reverse cyclic quasi-static loading tests on steel or wood framed drywall partitions with typical construction practise details were performed by Tasligedik et al. (2014). Test results showed that the steel framed drywall specimen tended to behave in a ductile manner, while the timber framed drywall specimen tended to behave in a brittle manner. After 1.5% drift, both drywall types were characterized by the same cyclic behaviour and residual strength (approximately 40kN). The importance of considering the effect of interaction between the structural system and the non-structural walls, even when considering light steel or timber framed drywalls, was also highlighted.

Petrone et al. (2016) performed quasi-static tests to evaluate the out-of-plane seismic performance of plasterboard internal partitions with steel studs. Following the FEMA 461 testing protocol, four tall specimens (i.e. 5 m high) were tested. Results showed a significant nonlinear pinched behaviour of the specimens, caused by the damage in the screwed connections, and the board typology and amount of screwed connections influenced the system stiffness and strength.

b) Fragility curves

Several studies focused on the development of fragility curves for drywall partitions.

Bersofsky (2004) investigated the fragility functions of tall light-gauge metal-studded gypsum partition walls through in-plane shear testing of sixteen specimens. The following damage states were identified to develop fragility curves: 1) minor damage, to be repaired using just tape, mud and paint (drift ratios in the range 0.05-0.5%); 2) a second damage state which requires sections of gypsum to be cut out and replaced (not observed in all the tests performed); 3) a third damage level corresponding to walls damaged beyond repair (drift ratios in the range 1.5-3%).

McMullin et al. (2004b) developed fragility curves of wood frame walls using different testing protocol for the experiments (displacement-controlled monotonic, static cyclic, and dynamic cyclic). Nineteen interior partition walls were tested and built from double-sided 12 mm gypsum wallboard. The partition damage thresholds were related to the drift applied to the wall and they included damage at fastener heads, cracking at wall openings, crushing and/or cracking at perimeter walls, cracking of the panel joints, local buckling of sheathing, and global buckling of sheathing.

Lang and Restrepo (2005) determined the fragility curves of gypsum metal stud partitions through experimental testing of two full scale specimens. The research objectives were the assessment of the influence of wall configurations and boundary conditions in the seismic performance as well as the determination of a parametric fragility model relating the inter-storey drift to the decision-making intensity measures (repair costs or downtime).

Petrone et al. (2015) developed fragility curves for plasterboard internal partitions, representing typical partitions in industrial and commercial buildings in the European area. Quasi-static tests were performed on six 5-m-high internal partitions and experimental results showed that the typical failure mode of the specimens was the buckling of a steel stud. Damage states of the partition walls were studied, and fragility functions developed in terms of inter-storey drift ratios (median values of 0.28%, 0.81%, and 2.05% for DS1, DS2, and DS3 respectively).

Petrone et al. (2017) defined fragility functions of four different partition typologies (a classic partition, composed of 18-mm-thick wooden panel; a steel partition, consisting of an 18-mm-thick plasterboard panel, encased in 1-mm-thick steel panel with the edges suitably shaped to allow the connection to the vertical studs; a P85 partition, similar to steel partition, except the internal steel structure; a glass partition, composed of laminated glass panels, included within steel or aluminium frames that are shaped to allow the connection to vertical studs). Shaking table tests were performed

and for standard specimens it was observed minor damage for drift in the range of 0.41–0.65%, moderate and major damage states in the range 0.51–0.95% (Figure 3.20).

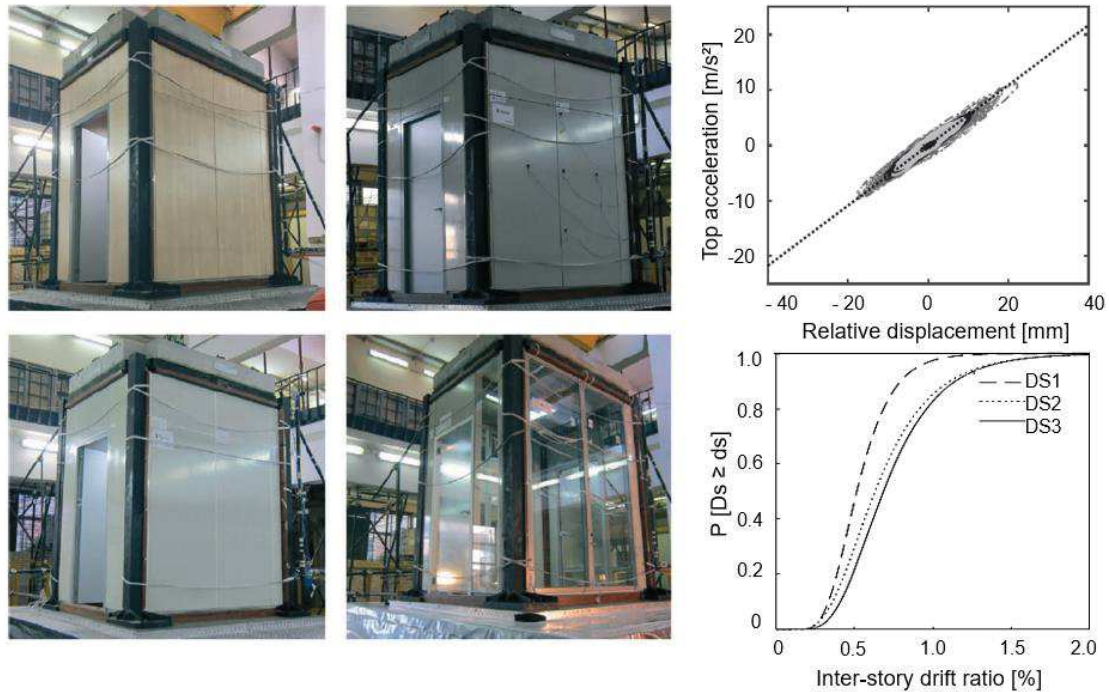
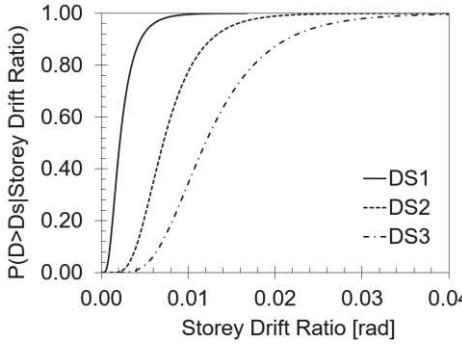
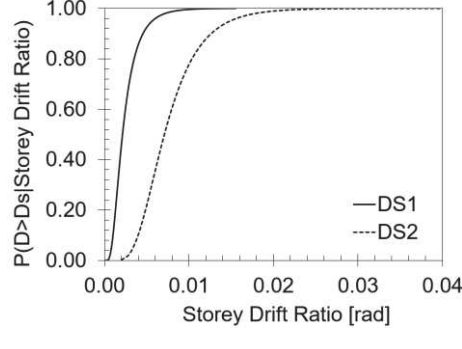


Figure 3.20. Specimen configurations and experimental results (acceleration versus relative displacement of the classic partition; fragility curves of the standard partition walls) by Petrone et al. (2017).

Rahmanishamsi et al. (2016) performed component level testing to characterize the out-of-plane response and damage mechanisms of stud-to-track connections in non-structural steel-framed partition walls. The authors studied the performance of connections with various stud-to-track gap dimensions, stud and track thicknesses, and screw-attachment configurations. The experimental data were used to generate capacity fragility curves in terms of displacement and force and nonlinear numerical hinge models were developed and calibrated to represent the out-of-plane hysteresis behaviour of stud-to-track connections.

Example of fragility functions for drywall partitions extrapolated from the FEMA P-58 (2012) database can be found in Table 3.5.

Table 3.5. Fragility curves of drywall partitions (source: FEMA P-58 2012).

Component type	Description	Fragility curve
Metal framed wall partition	Gypsum with metal studs, Full height, Fixed below and above	 <p>DS1: Screws pop-out, minor cracking of wall board, warping or cracking of tape DS2: Moderate cracking or crushing of gypsum wall boards (typically in corners and in corners of openings) DS3: Significant cracking and/or crushing of gypsum wall boards- buckling of studs and tearing of tracks</p>
Wood framed wall partition	Gypsum with wood studs, Full height, Fixed below and above	 <p>DS1: Cracking of paint over fasteners or joints DS2: Local and global buckling out-of-plane and crushing of gypsum wallboards. Studs are typically not damaged by failure of the gypsum wallboard</p>

3.3.3 Ceiling systems

This paragraph provides a description of the main experimental studies carried out on suspended ceilings. During past earthquakes suspended ceilings have generally sustained major damage, therefore the literature review focuses on this typology of ceiling solution.

a) Experimental studies

First experimental studies on ceilings were performed by ANCO Engineers Inc. in 1983, that conducted tests on a 3.6 x 8.5 m suspended ceiling system with intermediate-duty runners and lay-in tiles. The non-structural component was subjected to the 1953 Taft earthquake ground motion and the experimental results showed that the most common locations for damage of these components was around the perimeter of a room at the wall/ceiling intersection. Vertical struts were found to be ineffective and pop rivets were discovered to be more effective than sway wires in reducing the post-earthquake damage.

Rihal and Granneman (1984) investigated the effectiveness of current building code provisions and installation practices for braced and unbraced suspended ceilings with and without partitions in a series of dynamic tests. The results showed that the addition of vertical struts reduced the vertical displacement response, preventing the tiles from crashing down but damage was caused by pounding of cross tees to perimeter angles.

In 1993, ANCO Engineers Inc. performed new earthquake tests for Armstrong World Industries Inc. on a 7.31 x 4.26 m ceiling system using ground motions representative of specific American seismic zones and earthquake histories developed to represent the expected motions of the third and sixth floors of a six-storey moment-resisting steel frame structure located on a soft soil site.

Yao (2000) investigated the vibration characteristics and seismic capacity of a 1.2 x 4.0 m suspended ceiling using experimental and analytical methods. The study revealed how the introduction of 45° sway wires in each direction do not produce an increase of the system seismic capacity, while the seismic behaviour could be improved adding edge hanger wires.

Armstrong World Industries Inc. undertook an extensive series of earthquake tests on suspended ceiling systems in the years 2001-2005 at the Structural Engineering and Earthquake Simulation Laboratory (SEESL) of the State University 10 of New York at Buffalo (Badillo et al. 2002; Kusumastuti et al. 2002; Badillo et al. 2003a, 2003b). Different types of ceiling systems were tested using a set of combined horizontal and vertical earthquake excitations for qualification purposes (Figure 3.21). During these tests two damage limit states were identified for the seismic qualification of ceilings (loss of tiles and failure of suspension system) and experimental results showed that more failures occurred for the first type of damage. An important conclusion of the experiments was that the addition of retention clips represented a cost-effective strategy to improve the performance of ceiling systems, even under very strong earthquake shaking.



Figure 3.21. Test frame (left) and system detailing (right) (Badillo et al. 2006).

Gilani et al. (2008) performed seismic qualification and fragility tests to characterize the seismic performance of manufacturer engineering components intended for use at the perimeter of the ceiling system, with the aim of defining susceptible components, modes of failure, and performance levels. Shaking table tests were performed at the University at Buffalo's Structural Engineering and Earthquake Simulation Laboratory and main conclusions from the experiments were that ceilings using alternate installation components performed as well or better than the code installations.

b) Fragility studies

Many experimental tests have been performed in order to determine the fragility curves of either single components or entire ceiling systems (e.g. in Table 3.6) and some of them are herein presented.

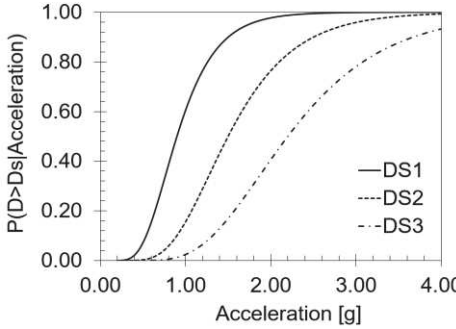
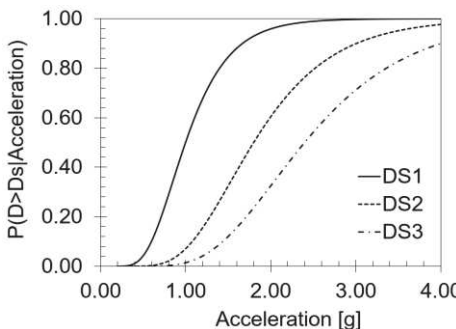
Badillo et al. (2007) conducted full-scale dynamic testing of suspended ceiling systems to obtain fragility data suitable for performance-based assessment and design. Authors evaluated the effect of size and weight of tiles, use of retainer clips, the installation of compression posts, and physical condition of grid components on the ceiling performance. Four limit states were proposed to identify the damage observed in the systems and the threshold peak floor accelerations associated with each limit state were found.

Echevarria et al. (2012) developed fragility curves through numerical modelling. The authors proposed a finite element model to study the behaviour of suspended ceiling systems with acoustic tiles, considering smaller and larger area ceiling systems in braced and unbraced conditions. Fragility curves were based on unseating of the grid and dislodgment of ceiling tiles and results showed how

the probability of damage in unbraced system was very high due to the unseating of the tee beam grid at the ceiling perimeter.

Dhakal et al. (2016) derived component failure fragility curves on typical New Zealand suspended ceilings, considering loading in tension, compression and shear. The experiments focused on grid members -main tees and cross tees- as well as connections including cross tee connections, main tee splices and end fixing rivets. They also presented a simple method to analyse perimeter-fixed ceilings using peak floor acceleration, allowing the definition of the ceiling system fragility from component fragilities.

Table 3.6. Fragility curves of suspended ceilings (source: FEMA P-58 2012).

Component type	Description	Fragility curve
Suspended lay-in acoustic tile ceiling	Area < 250 sf, Vertical hanging wires only	 <p>DS1: 5 % of tiles dislodge and fall DS2: 30% of tiles dislodge and fall, t-bar grid damaged DS3: Total ceiling collapse</p>
	Area < 250 sf, Vertical hanging wire, diagonal wires, and compression posts, 2-inch-wide ledger support angles at wall and oversize holes around tile openings	 <p>DS1: 5 % of tiles dislodge and fall DS2: 30% of tiles dislodge and fall, t-bar grid damaged DS3: Total ceiling collapse</p>

3.3.4 Building services

a) *Experimental studies*

As reported in Filiatrault et al. (2001), several studies have been performed in the past on building services, such as elevator systems (e.g. Yang et al. 1983; Suarez and Singh 1996, 1998; Kelly and Tsai 1985), mechanical, electrical and appliance equipment (e.g. Ohtani et al. 1992; Mroz and Soong 1997), piping systems (e.g. Nims and Kelly 1990; Tsuruta and Kojima 1988) and computer equipment (e.g. Meyer et al. 1998; Jin and Astaneh-Asl 1998). While, some of the investigations developed in recent years are described below.

Goodwin et al. (2004) investigated the seismic behaviour of piping systems typically used in hospital facilities to determine the capacity, weak points and failure modes of such type of component. Shaking table tests were performed considering the AC156 testing protocol and cable-braced and unbraced systems were tested. The main finding of the research was that bracing systems limit the displacement demands, while the acceleration amplifications were similar to those of the unbraced systems.

Fathali and Filiatrault (2008) carried out investigations to study the seismic performance of Isolation/Restrain (I/R) systems for light mechanical equipment through shaking table tests. After the campaign it was observed that: reducing the displacements of the equipment through the I/R system amplifies the peak equipment accelerations; reducing the gap size, the seismic performance of the I/R system improves; increasing the thickness of the rubber snubbers the seismic performance of the I/R system increases, but both accelerations and displacements in the equipment can increase.

Filiatrault et al. (2010) carried out experimental tests for developing seismic fragility curves for first leakage of sprinkler piping systems (Figure 3.22). Cyclic testing on different T sprinkler piping joints were initially proposed with the aim of developing fragility curves and defining an appropriate numerical model in order to describe the hysteretic behaviour. Shaking table tests of the sprinkler piping sub-system were also performed with the same objectives.

Wang et al. (2017) investigated the seismic performance of a functional traction elevator as part of a full-scale five-storey building shake table test program. A suite of earthquake input motions of increasing intensity was applied to study the behaviour of an elevator system placed in three different configurations by varying the vertical location of its cabin and counterweight. During the test a complete report of the component damage and operability was defined, and results proved how the application of well-restrained guide shoes prevents the cabin and counterweight from derailment

during high-intensity shakings. In any case, differential displacements induced by the building imposed undesirable distortion of the elevator components and their surrounding support structure, which caused damage and inoperability of the elevator doors.

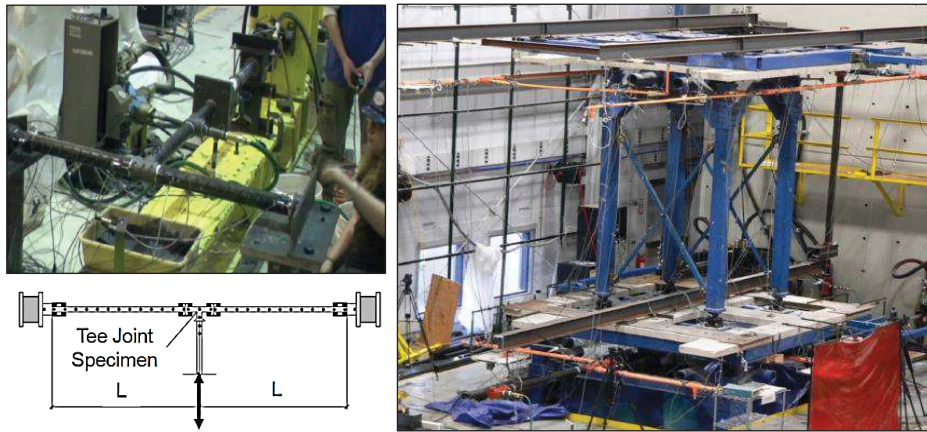


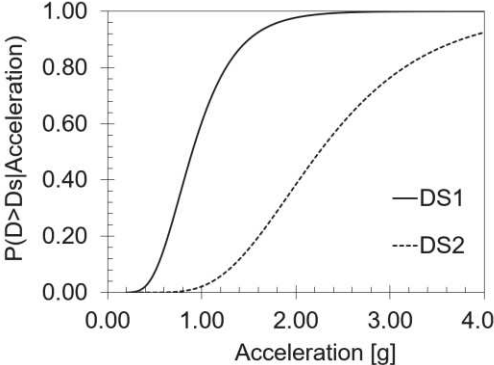
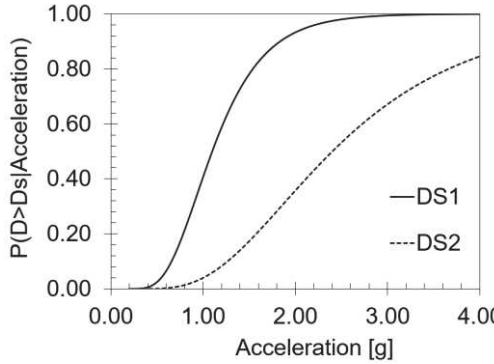
Figure 3.22. Cyclic testing of sprinkler piping joints (left) and seismic testing of sprinkler piping subsystems (right) by Filiatrault et al. (2010).

b) Fragility curves

A large database of fragility curves describing the seismic vulnerability of building services can be found in the FEMA P-58 (2012) and some examples are shown in Table 3.7.

Table 3.7. Fragility curves of building services (source: FEMA P-58 2012).

Component type	Description	Fragility curve
Cold water piping	Diameter > 2.5 inches, SDC A or B	<p>DS1: Minor leakage at flange connections 1 leak per 1000 feet of pipe DS2: Pipe Break 1 break per 1000 feet of pipe</p>

Component type	Description	Fragility curve
HVAC ducting	Galvanized sheet metal ducting less than 6 sq. ft in cross sectional area, SDC A or B	 <p>DS1: Individual supports fail and duct sags – 1 failed support per 1000 feet of ducting DS2: Several adjacent supports fail and sections of ducting fall - 60 feet of ducting fail and fall per 1000 foot of ducting</p>
Fire sprinkler water piping	Horizontal mains and branches, thin wall steel, no bracing, SDC A or B	 <p>DS1: Spraying & Dripping Leakage at joints - 0.02 leaks per 20 ft section of pipe DS2: Joints Break - Major Leakage - 0.02 breaks per 20 ft section of pipe</p>

3.3.5 Building contents

a) Experimental studies

When looking at the experimental research works developed in the past on building contents, one of the first studies was implemented by Rihal (1994). The author determined a test method for the investigation of the in-plane and out-of-plane seismic behaviour of cantilever library shelving. Then, in 1991 Filiatrault carried out experimental evaluations on the seismic performance of modular office furniture systems. Shaking table tests were performed and test results showed that the structural integrity of the system was not compromised during any of the earthquake ground motions

considered, although a larger torsional response was observed when the furniture was oriented parallel to the ground shaking. Books located on the shelves of the unit toppled and could have caused injuries to occupants.

White (1999) performed 49 shake table tests on building contents, during a program related to the assessment of the seismic vulnerability of non-structural components. Horizontal and vertical input motions were considered, and results highlighted that equipment restrained with properly design methods performed very well, while unrestrained equipment suffered extensive damage.

Konstantinidis and Makris (2005) conducted experimental studies to evaluate the seismic response of freestanding and restrained laboratory equipment. One incubator and two refrigerators were tested considering freestanding and chained configurations for uni-directional shaking table tests. During the tests it was observed that the peak equipment accelerations of the restrained equipment were significantly larger than those observed in the freestanding ones, therefore the risk of damage may increase for restraining acceleration sensitive laboratory equipment.

Hutchinson and Chaudhuri (2006a) conducted earthquake testing to study the seismic response of bench and shelf-mounted equipment and contents. Different integral bench-shelf configurations were assembled with details representative of typical biological and chemical laboratories in science buildings. Transverse and longitudinal bench configurations, using both single and double benches were constructed, and uni-strut support members were used to connect the bench-shelving system to each other and to a concrete floor and timber ceiling system. Test results indicated that the supporting bench (or shelf) dynamic characteristics play an important role in the overall response of the small rigid equipment and it was observed how this equipment are generally sliding-dominated.

Finally, it is acknowledged the work developed in recent years by Di Sarno et al. (2014). The authors carried out shaking table tests to study the seismic demand, capacity and properties of hospital contents (Figure 3.23). The limit states of a typical health care room were determined through experiments on a full-scale three-dimensional model of an ambulatory room composed of different building contents (1-window and 2-windows cabinets, a desktop computer, a desk, different glass contents included in the cabinets). Test results allowed the definition of proper fragility functions for these elements. For example, it was observed that the peak shake table acceleration that caused the rocking mechanism initiation and the overturning in both the cabinets ranges between 0.37 g and 0.61 g for the first type of mechanism or is larger than 1.00 g for the second type of mechanism.

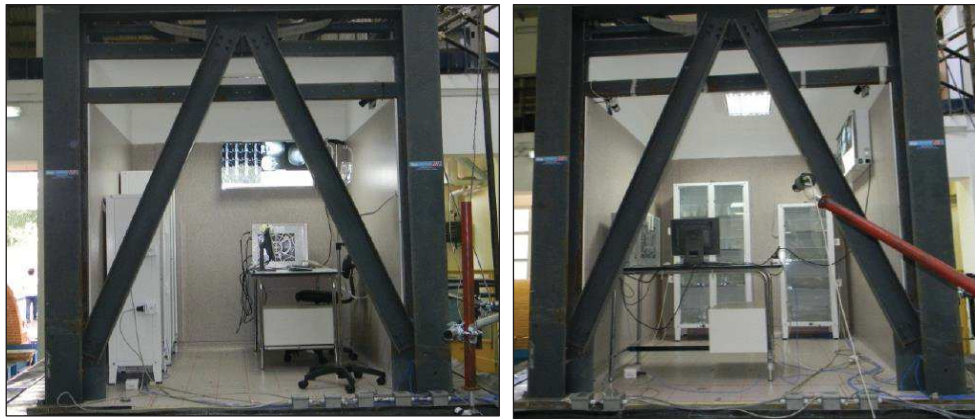


Figure 3.23. Photos of the two different configurations tested during the experimental campaign (Di Sarno et al. 2014).

b) Fragility curves

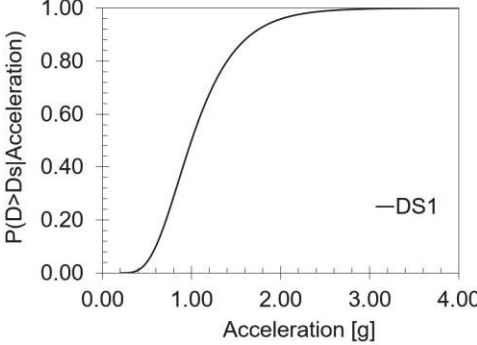
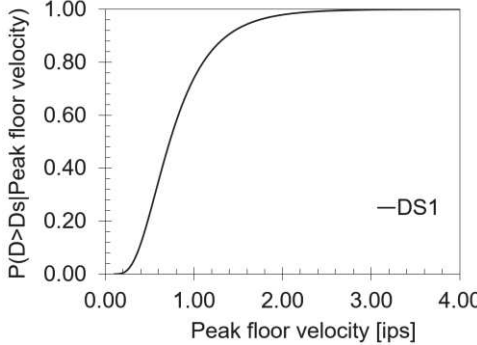
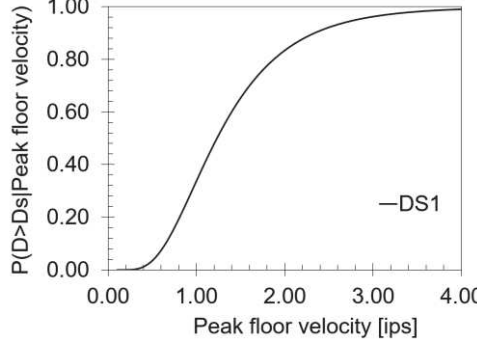
Different studies have been developed with the aim of deriving fragility curves for building contents. Some of these research works are reported below.

Hutchinson and Chaudhuri (2006b) performed analytical studies to find approximate fragility curves for different unattached equipment and building contents, focusing the study on rigid scientific equipment placed on top of ceramic laboratory benches. Authors proposed approximate equations to estimate fragility curves parameters for bench-mounted sliding-dominated components within multi-storey reinforced concrete or steel structures, also considering a range of surface's frictional coefficients. The same authors also studied experimentally and analytically the seismic fragility of storage glassware that can typically be found in hospitals and laboratories. During the tests it was finally investigated the effect of both amount and density of the liquid contained in the glassware. The experiments demonstrated that the seismic response of glassware was mainly dominated by sliding and the seismic fragility by the building flexibility properties.

Haider et al. (2006) presented the fragility curves of building contents in terms of probability of overturning. They analysed objects for a given object dimensions, dynamic characteristics of the building and location of the object within the building. While, Jaimes et al. (2012) presented a methodology to assess the seismic vulnerability of inventories of contents to multiple failure modes using an ordering method to find out the probabilities of failure of a conditional mode upon the survival of other modes. The procedure considers the statistical correlation of failure modes due to contents dynamic response (sliding and overturning), and failure modes due to non-structural components.

Examples of fragility curves for different building contents are presented in Table 3.8.

Table 3.8. Fragility curves of building contents (source: FEMA P-58 2012).









Component type	Description	Fragility curve
Modular office work-stations	Diameter > 2.5 inches, SDC A or B	 <p>DS1: Wall units need to be adjusted and straightened. Some elements are bent / damaged and need to be replaced</p>
Bookcase	2 shelves, 12-5/8" deep x 29" tall, unanchored laterally	 <p>DS1: Bookcase falls over and contents are scattered. Likely damage to bookcase</p>
Vertical filing cabinet	2 drawer, unanchored laterally, 15" deep x 24" tall	 <p>DS1: Filing cabinet falls over and contents are scattered. Likely damage to file cabinet</p>

3.4 Conclusions

This Chapter has provided a description of the seismic behaviour of different typologies of non-structural components. The typical post-earthquake damage states affecting each system are initially presented and for the case of architectural components, primary investigated within this Thesis, a summary of these damage conditions can be found in Table 3.9.

Table 3.9. Typical seismic damage to architectural non-structural elements (source: Baird et al. 2011b; FEMA E-74 2011, Tasligedik 2014; Baird and Ferner 2017)

Non-structural component	Typical damage
Curtain walls	<div style="display: flex; justify-content: space-around;"> <div style="text-align: center;">  <p><i>Broken glass</i></p> </div> <div style="text-align: center;">  <p><i>Frame dislocation</i></p> </div> </div>
Cladding walls	<div style="display: flex; flex-direction: column; align-items: center;"> <div style="display: flex; justify-content: space-around; width: 100%;"> <div style="text-align: center;">  <p><i>Cracking</i></p> </div> <div style="text-align: center;">  <p><i>Corner crushing</i></p> </div> </div> <div style="display: flex; justify-content: space-around; width: 100%; margin-top: 10px;"> <div style="text-align: center;">  <p><i>Connection failure</i></p> </div> <div style="text-align: center;">  <p><i>Panel disconnection</i></p> </div> </div> </div>
Infill walls	<div style="display: flex; flex-direction: column; align-items: center;"> <div style="display: flex; justify-content: space-around; width: 100%;"> <div style="text-align: center;">  <p><i>Cracking</i></p> </div> <div style="text-align: center;">  <p><i>Corner crushing</i></p> </div> <div style="text-align: center;">  <p><i>Interface separation</i></p> </div> </div> <div style="display: flex; justify-content: space-around; width: 100%; margin-top: 10px;"> <div style="text-align: center;">  <p><i>Out-of-plane</i></p> </div> <div style="text-align: center;">  <p><i>Damage to structure</i></p> </div> </div> </div>

Non-structural component	Typical damage		
Partitions	 <p data-bbox="647 521 743 551"><i>Cracking</i></p>	 <p data-bbox="863 521 1072 551"><i>Panel dislodgement</i></p>	 <p data-bbox="1121 521 1342 551"><i>Damage to structure</i></p>
Ceiling systems	 <p data-bbox="655 797 743 826"><i>Cracking</i></p>	 <p data-bbox="847 797 1088 826"><i>Failure of components</i></p>	 <p data-bbox="1126 797 1326 826"><i>Connection failure</i></p>
	 <p data-bbox="719 1037 911 1066"><i>Panel dislocation</i></p>	 <p data-bbox="935 1037 1262 1066"><i>Interaction with other elements</i></p>	

Then, an overview of past experimental investigations carried out on alternative components to study their seismic behaviour and determine fragility functions is reported. In fact, in the definition of non-structural damage-mitigation solutions, the knowledge of the single-component/global-system vulnerability is fundamental to determine which parameters mainly influence the failure modes and at which demand level a damage state is expected to be achieved. The seismic performance of non-structural components can influence the behaviour of the main structure (skeleton system) in many cases and, as observed from past earthquake experiences, non-structural damage substantially increases the expected losses in terms of both repair costs and business interruption, even for low-intensity ground motions. For this reason, many tools have been recently developed to take into account the contribution of non-structural elements in the loss estimation (e.g. PACT of FEMA P-58 2012) as well as innovative damage mitigation solutions have been proposed and studied.

3.5 References

- ANCO Engineers Inc. (1983). *Seismic Hazard Assessment of Non-Structural Ceiling Components: Phase I*. Report No. 1249.12, Grant 8114155, National Science Foundation, Culver City, California, USA.
- ANCO Engineers Inc. (1993). *Earthquake testing of a suspended ceiling system*, Culver City, CA, USA.
- Badillo-Almaraz H., Kusumastuti D., Reinhorn A.M., Whittaker A.S. (2002). *Testing for Seismic Qualification of Suspended Ceiling Systems, Part I, Report No. UB CSEE/SEESL-2002-01*, State University of New York at Buffalo, Buffalo, New York, USA.
- Badillo-Almaraz H., Whittaker A. S., Reinhorn A. M. (2003a). *Testing for Seismic Qualification of Suspended Ceiling Systems, Part III, Report No. UB CSEE/SEESL-2003-02*, State University of New York at Buffalo, Buffalo, New York, USA.
- Badillo-Almaraz H., Whittaker A.S., Reinhorn A.M. (2003b). *Testing for Seismic Qualification of Suspended Ceiling Systems, Part IV, Report No. UB CSEE/SEESL-2003-01*, State University of New York at Buffalo, Buffalo, New York, USA.
- Badillo-Almaraz H., Whittaker A.S., Reinhorn A.M., Cimellaro G.P. (2006). *Seismic Fragility of Suspended Ceiling Systems, Report MCEER-06-0001*, MCEER/SUNY/Buffalo.
- Badillo-Almaraz H., Whittaker A.S., Reinhorn A.M. (2007). Seismic fragility of suspended ceiling systems, *Earthquake Spectra*, 23(1) :21–40.
- Baird A. (2014). Seismic Performance of Precast Concrete Cladding Systems, *Ph.D. Thesis*, University of Canterbury, Christchurch, New Zealand.
- Baird A., Palermo A., Pampanin S. and Riccio P. (2011a). Focusing on reducing the earthquake damage to Façade Systems, *Bulletin of New Zealand Society of Earthquake Engineering*, 44(2): 108-120.
- Baird A., Palermo A. and Pampanin S. (2011b). Façade damage assessment of multi-storey buildings in the 2011 Christchurch earthquake, *Bulletin of New Zealand Society of Earthquake Engineering*, 44(4): 368-376.
- Baird A., Palermo A., Pampanin S. (2012). Experimental and numerical validation of seismic interaction between cladding systems and moment resisting frames, *Proceedings of 15th World Conference on Earthquake Engineering*, Lisbon, Portugal.
- Baird A and Ferner H (2017). Damage to Non-structural elements in the 2016 Kaikoura earthquake, *Bulletin of the NZ Society for Earthquake Engineering*, 50(2): 187-193.
- Behr R.A., Belarbi A., Brown A.T. (1995a), Seismic performance of architectural glass in a storefront wall system, *Earthquake Spectra*, 11(3): 367-391.
- Behr R.A., Belarbi A., Culp J.H. (1995b), Dynamic racking tests of curtain wall glass elements with in-plane and out-of-plane motions, *Earthquake Engineering Structural Dynamics*, 24(1): 1-14.
- Behr R.A. and Belarbi A (1996), Seismic test methods for architectural glazing systems, *Earthquake Spectra*., 12(1): 129-143.

- Behr R.A. (1998), Seismic performance of architectural glass in mid-rise curtain wall, *Journal of Arch. Eng.*, 4(3): 94-98.
- Belleri A., Torquati M., Marini A., Riva P. (2016). Horizontal cladding panels: in-plane seismic performance in precast concrete building, *Bulletin of Earthquake Engineering*, 14 (4): 1103-1129.
- Bersofsky A.M. (2004). A Seismic Performance Evaluation of Gypsum Wallboard Partitions. *M.S. Thesis*, University of California, San Diego, USA.
- Bouwkamp J. G. (1961). Behavior of Window Panel Under In-Plane Forces, *Bulletin of the Seismological Society of America*, 51(1): 85-109.
- Bouwkamp J. G. and Meehan J. F. (1960), Drift limitations imposed by glass, *Proceedings of the 2nd World Conference on Earthquake Engineering*, Tokyo, Japan.
- Calvi G.M. and Bolognini D. (2001). Seismic Response of Reinforced Concrete Frames Infilled with Weakly Reinforced Masonry Panels, *Journal of Earthquake Engineering*, 5: 153-185.
- Cardone D. and Perrone G. (2015). Developing fragility curves and loss functions for masonry infill walls, *Earthquakes and Structures*, 9(1): 257-279.
- Caterino N., Del Zoppo M., Maddaloni G., Bonati A., Cavanna G., Occhiuzzi A. (2017). Seismic assessment and finite element modelling of glazed curtain walls, *Structural Engineering and Mechanics*, Vol.61(1): 77-90.
- Chen M., Pantoli E., Wang X., Espino E., Mintz S., Conte J., Hutchinson T., Marin C., Meacham B., Restrepo J., Walsh K., Englekirk R., Faghihi M., Hoehler M. (2012). Design and Construction of a Full-Scale 5-Story Base Isolated Building Outfitted with Nonstructural Components for Earthquake Testing at the UCSD-NEES Facility, *Structure Congress 2012*: ASCE.
- Chiozzi A., Miranda E. (2017). Fragility functions for masonry infill walls with in-plane loading, *Earthquake Engineering Structural Dynamics*, 46(15): 2831-2850.
- Colangelo F. (1999). Qualificazione, risposta sismica pseudodinamica e modelli fenomenologici di portali di c.a. tamponati con laterizio, DISAT.
- Colangelo F. (2003). Experimental Evaluation of Member-by-Member Models and Damage Indices for Infilled Frames, *Journal of Earthquake Engineering*, 7 (1): 25-50.
- Craig J.I., Goodno B.J., Keister M.J., Fennel C.J. (1986). Hysteretic behaviour of precast cladding connections, *Proceedings of 3rd ASCE Engineering Mechanics Specialty Conference on Dynamic Response of structures*, UCLA, CA, USA.
- Craig J. I., Leistikow R., Fennell C. J. (1989). Experimental studies of the performance of precast cladding connections, *Proceedings of Ninth World Conference on Earthquake Engineering*, Tokyo, Japan.
- Craig J. I., Goodno B., Towashiraporn P., & Dogan, T. (2000). Ductile Cladding Systems for Seismic Design, *Proceedings of 12th World Conference on Earthquake Engineering*, Auckland, New Zealand.

- De Sortis A., Di Pasquale G., Dolce M., Gregolo S., Papa S., Rettore G.F. (2009). *Linee guida per la riduzione della vulnerabilità di elementi non strutturali arredi e impianti*, Presidenza del Consiglio dei Ministri, Dipartimento della Protezione Civile, Rome, Italy.
- Dhakal R.P. (2010). Damage to Non-Structural Components and Contents in 2010 Darfield Earthquake, *Bulletin of the NZ Society for Earthquake Engineering*, 43(4): 404-411.
- Dhakal R.P., MacRae G.A., Hogg K. (2011). Performance of ceilings in the February 2011 Christchurch earthquake, *Bulletin of the New Zealand Society for Earthquake Eng.*, 44(4): 379-389.
- Dhakal R.P., MacRae G.A., Pourali A., Paganotti G. (2016). Seismic fragility of suspended ceiling systems used in NZ based on component tests, *Bulletin of the New Zealand Society for Earthquake Eng.*, 49(1).
- Di Sarno L., Petrone C., Magliulo G., Maddaloni G., Protà A. (2014). Shake table tests to evaluate the seismic demand, capacity and dynamic properties of hospital contents, Proceedings of the 2nd European Conference on Earthquake Engineering and Seismology, Istanbul, Turkey.
- Echevarria A., Zaghi A. E., Soroushian S., Maragakis M. (2012). Seismic Fragility of Suspended Ceiling Systems, *Proceedings of 15th World Conference on Earthquake Engineering*, Lisbon, Portugal.
- Fathali S., Filiatrault A. (2008). Effect of Elastomeric Snubber Properties on Seismic Response of Vibration-Isolated Mechanical Equipment: An Experimental Study. *Earthquake Spectra*, 24(2): 387-403.
- Federal Emergency Management Agency (2007). *Interim Testing Protocols for Determining the Seismic Performance Characteristics of Structural and Nonstructural Components*. FEMA 461, Washington, USA.
- Federal Emergency Management Agency (2011). *Reducing the risks of non-structural earthquake damage – a practical guide*. FEMA E-74, Washington, USA.
- Federal Emergency Management Agency (2012). *Seismic Performance Assessment of Buildings, Volume 1 - Methodology*, prepared by the Applied Technology Council for the Federal Emergency Management Agency, FEMA P-58-1, Washington, D.C., USA.
- Filiatrault A. (1991). Seismic Evaluation of Modular Office Furniture System, *Earthquake Spectra*, 7(4): 529-541.
- Filiatrault A., Christopoulos C., Stearns C. (2001). Guidelines, Specifications, and Seismic Performance Characterization of Nonstructural Building Components and Equipment, PEER Report 2002/05, College of Engineering, University of California, Berkeley, USA.
- Filiatrault A., Mosqueda G., Retamales R., Davies R., Tian Y., Fuchs J. (2010). Experimental Seismic Fragility of Steel Studded Gypsum Partition Walls and Fire Sprinkler Piping Subsystems, presented at the *ASCE Structures Congress*, Orlando, Florida, USA.
- Filiatrault A. and Sullivan T. (2014). Performance-based seismic design of nonstructural building components: The next frontier of earthquake engineering, *Earthquake Eng. & Eng. Vibration*, 13: 17-46.
- Freeman S.A. (1971). *Third Progress Report on Racking Tests of Wall Panels*, University of California, Berkeley, USA.

- Gilani A.S.J., Reihorn A., Ingratta T., Glasgow B. (2008). Earthquake Simulator Testing and Evaluation of Suspended Ceilings: Standard and Alternate Perimeter Installations, *Proceedings of American Society of Civil Engineers (ASCE) structural congress*, Vancouver, USA.
- Goodno B. J. (1983). *Cladding-structure interaction in highrise buildings: Schools of Civil and Aerospace Engineering*, Georgia Inst. of Technology, Atlanta, USA.
- Goodno B. J., Craig J. I. (1989). Historical Overview of Studies on the Contribution of Cladding to Lateral Resistance of Buildings, *Paper presented at the Architectural Precast Concrete Cladding - Its Contribution to Lateral Resistance of Buildings*, Chicago, IL., USA.
- Goodno B.J., Craig J.I., Dogan T., Towashiraporn P. (1998). *Ductile Cladding Connection Systems for Seismic Design*, Building and Fire Research Laboratory, NIST, Gaithersberg, MD.
- Goodwin E., Maragakis E., Itani A. (2004). Seismic Evaluation of Hospital Piping Systems, *Proceedings of 13th World Conference on Earthquake Engineering*, Vancouver, B.C., Canada, USA.
- Haider A.A., Nelson T.K.L., Emad F.G. (2006). Seismic fragility curves for damage to building contents, *Earthquake Engineering in Australia*, Canberra, Australia.
- Hutchinson T. C. and Chaudhuri S. R. (2006a). Bench–shelf system dynamic characteristics and their effects on equipment and contents, *Earthquake Engineering Structural Dynamics*, 35(13): 1631 – 1651.
- Hutchinson T. C. and Chaudhuri S. R. (2006b). Simplified Expression for Seismic Fragility Estimation of Sliding-Dominated Equipment and Contents, *Earthquake Spectra*, 22(3): 709-732.
- Hutchinson T., Pantoli E., McMullin K., Hildebrand M., Underwood G. (2015). *Seismic Drift Compatibility of Architectural Precast Concrete Panels and Connections: A Design Guide for Engineers*, Department of Structural Engineering, University of California, San Diego, California, USA.
- ICC (2010). *Acceptance Criteria for Seismic Qualification by Shake-Table Testing of Nonstructural Components*, Report AC156, ICC Evaluation Service Inc.
- Jaimes M.A., Reinoso E., Esteva L. (2012). Seismic vulnerability of building contents for a given occupancy due to multiple failure modes, *Proceedings of the 15th World Conference on Earthquake Engineering*, Lisbon, Portugal.
- Jin M., Astaneh-Asl A. (1998). Study of Seismic Resistance of Desktop Computers, *Proceedings of the ATC-29 Seminar and Workshop on Seismic Design and Performance of Equipment and Nonstructural Components in Buildings and Industrial Structures*, Applied Technology Council, Redwood City, CA, USA.
- Kelly J.M., Tsai H.C. (1985). Seismic Response of Light Internal Equipment in Base-Isolated Structures, *Earthquake Engineering and Structural Dynamics*, 13(6): 711-732.
- Kemeny Z. A., Lorant J. (1989). Energy Dissipating Elastomeric Connections, *Paper presented at the Architectural Precast Concrete Cladding - Its Contribution to Lateral Resistance of Buildings*, Chicago, IL., USA.
- Konstantinidis D., Makris N. (2009). Seismic response analysis of multidrum classical columns, *Earthquake Engineering and Structural Dynamics*, 34(10): 1243–1270.

- Kusumastuti D., Badillo H., Reinhorn A.M., Whittaker A.S. (2002). *Testing for Seismic Qualification of Suspended Ceiling Systems, Part II, Report No. UB CSEE/SEESL-2002-02*, State University of New York at Buffalo, Buffalo, New York, USA.
- Lang A. F., Restrepo J. I. (2005). *Performance Evaluation of Gypsum Wallboard Partitions*. Berkeley, Pacific Earthquake Engineering Research Center (PEER).
- Lee T.H., Kato M., Matsumiya T., Suita K., Nakashima M. (2006). Seismic Performance Evaluation of Non-Structural Components: Drywall Partitions, *Earthquake Engineering and Structural Dynamics*, 36(3).
- Lim K.Y.S. and King A.B. (1991), The behavior of external glazing systems under seismic in-plane racking, *Building Research Association of New Zealand*, BRANZ.
- Magenes G., and Pampanin S. (2004). Seismic response of gravity-load design frames with masonry infills, *Proceedings of 13th World Conference on Earthquake Engineering*, Vancouver, B.C., Canada.
- Magliulo G., Petrone C., Capozzi V., Maddaloni G., Lopez P., Manfredi G. (2014). Seismic performance evaluation of plasterboard partitions via shake table tests, *Bulletin of Earthquake Engineering*, 12(4): 1657-1677.
- McMullin K.M. and Merrick D.S. (2001). *Seismic Performance of Gypsum Walls-Experimental Test Program*, Woodframe Research at San Jose State University.
- McMullin K., Wong Y., Choi C., Chan K. (2004a). *Seismic Performance States of Precast Concrete Cladding Connections*, Proceedings of 13th World Conference on Earthquake Engineering Conference, Vancouver, B.C., Canada, USA.
- McMullin K., Merrick D., Karim S., Davis R. (2004b). Fragility curves of woodframe walls for residential construction, *Proceedings of 13th World Conference on Earthquake Engineering Conference*, Vancouver, B.C., Canada, USA.
- McMullin K.M. and Merrick D.S. (2007). Seismic Damage Thresholds for Gypsum Wallboard Partition Walls, *Journal of Architectural Engineering*, 13: 22-29.
- McMullin K.M., Ortiz M., Patel L., Yarra S., Kishimoto T., Stewart C., Steed B. (2012). Response of Exterior Precast Concrete Cladding Panels in NEESTIPS/NEES-GC/E-Defense Tests on a Full Scale 5-story Building, *Proceedings of the ASCE Structures Congress*, ASCE, Pennsylvania, United States.
- Memari A.M., Behr R.A., Kremer P.A. (2004), Dynamic racking crescendo tests on architectural glass fitted with anchored pet film, *Journal Arch. Eng.*, 10(1), 5-14.
- Memari A.M., Kremer P.A., Behr R.A. (2006), Architectural glass panels with rounded corners to mitigate earthquake damage, *Earthquake spectra*, 22(1), 129-150.
- Memari A.M., Shirazi A., Kremer P.A., Behr R.A. (2014). Seismic Vulnerability Evaluation of Architectural Glass in Curtain Walls, *J. Civil Eng. Architect. Res.*, 1(2): 110-128.
- Meyer J.D, Soong T.T., Hill R.H. (1998). Retrofit Seismic Mitigation of Mainframe Computers and Associated Equipment: A Case Study, *Proceedings of the Seminar on 93 Seismic Design, Retrofit, and Performance of Non-Structural Components*, ATC-29-1, San Francisco, CA, USA.

- Mosalam K.M., White R.N., Gergely P. (1997). Static Response of Infilled Frames Using Quasi-Static Experimentation, *Journal of Structural Engineering*, 123: 1462-1469.
- Mroz M.P. and Soong T.T. (1997). Fire Hazards and Mitigation Measures Associated with Seismic Damage of Water Heaters. *Proceedings of the NEHRP Conference and Workshop on Research on the Northridge, California Earthquake of January 17, 1994*, 805-812.
- Negro P., Anthoine A., Combescure D., Magonette G., Molina J., Pegon P., Verzeletti G. (1995). *Tests on Four-Storey Full-Scale Reinforced Concrete Frame with Masonry Infills: Preliminary Report*, Special publication No. I.95.54, European Commission, Joint Research Centre, Ispra, Italy.
- Negro P., Taylor C.A. (1996). Effect of infills on the global seismic behaviour of RC frames: results of pseudo-dynamic and shaking table tests, *Proceedings of 11th World Conference on Earthquake Engineering*, Acapulco, Mexico.
- Negro P., Tornaghi M.L. (2017). Seismic response of precast structures with vertical cladding panels: The SAFECLADDING experimental campaign, *Engineering Structures*, 132: 205–228.
- Nims D.K., Kelly J.M. (1990). Experimental Study of Alternative Support Systems for the Seismic Restraint of Piping, *Proceedings of the ATC-29 Seminar and Workshop on Seismic Design and Performance of Equipment and Nonstructural Components in 94 Buildings and Industrial Structures*, Applied Technology Council, Redwood City, CA, USA.
- O'Brien W.C. (2009). Development of a closed-form equation and fragility curves for performance-based seismic design of glass curtain wall and storefront systems, *Master Thesis*, The Pennsylvania State University, USA.
- O'Brien W.C., Memari A.M., Kremer P.A. and Behr R.A. (2012). Fragility Curves for Architectural Glass in Stick-Built Glazing Systems, *Earthquake Spectra*, 28(2), 639-665.
- Okazaki T., Nakashima M., Suita K., Matusmiya T. (2007). Interaction between cladding and structural frame observed in a full-scale steel building test, *Earthquake Engineering & Structural Dynamics*, 36(1): 35-53.
- Ohtan, K., Shibata H., Watabe M., Kawakami M.S., Ohno T. (1992). Seismic Proving Tests for Nuclear Power Plant No. 1, *Proceedings of the 10th World Conference on Earthquake Engineering*, Rotterdam, The Netherlands.
- Pall A. S. (1989). Friction Damped Connections for Precast Concrete Cladding. *Paper presented at the Architectural Precast Concrete Cladding - Its Contribution to Lateral Resistance of Buildings*, Chicago, IL., USA.
- Pantoli E., Wang X., Chen M., Hutchinson T., Meacham B., Park H. (2013). Shake Table Testing of a Full-Scale Five-Story Building: Performance of the Major Nonstructural Components - Egress and Facades, *Structures Congress 2013*: ASCE.
- Pantoli E., Hutchinson T.C., McMullin K.M., Underwood G.A., Hildebrand M.J., PCI (2007). *Architectural Precast Concrete*, Chicago, IL., USA: PCI Architectural Precast Concrete Manual Committee.
- Pantoli E., Chen M.C., Wang X., Astroza R., Ebrahimian H., Hutchinson T.C., Conte J.P., Restrepo J.I., Marin C., Walsh K.D., Bachman R.E., Hoehler M.S., Englekirk R., Faghihi M. (2016). Full-scale structural and

non-structural building system performance during earthquakes: Part II-NSC damage states, *Earthquake Spectra*, 32(2): 771-794.

PCI (2007). *Architectural precast concrete*, Chicago, IL., USA: PCI Architectural Precast Concrete Manual Committee.

Petrone C., Magliulo G., Lopez P., Manfredi G. (2015). Seismic fragility of plasterboard partitions via in-plane quasi-static tests, *Earthquake Engineering Structural Dynamics*, 44(14): 2589:2606.

Petrone C., Magliulo G., Lopez P., Manfredi G. (2016). Out-of-Plane Seismic Performance of Plasterboard Partition Walls via Quasi-Static Tests, *Bulletin of the New Zealand Society for Earthquake Engineering*, 49(1): 125-137.

Petrone C., Magliulo G., Manfredi G. (2017). Shake table tests on standard and innovative temporary partition walls, *Earthquake Engineering and Structural Dynamics*, 46(10): 1599-1674.

Pinelli J. P., Craig J. I., Goodno B. J., Hsu C. C. (1993). Passive control of building response using energy dissipating cladding connections, *Earthquake Spectra*, 9(3), 529-546.

Pinelli J. P., Craig J. I., Goodno B. J. (1995). Energy-Based Seismic Design of Ductile Cladding Systems, *Journal of Structural Engineering*, 121(3): 567-578.

Pinelli J.P. and Craig J.I.(1989). *Experimental Studies on the Performance of Mexican Pre-cast Cladding Connections*, *Proc. Architectural Precast Concrete Cladding – Its Contribution to Lateral Resistance of Buildings*, PCI, Chicago, Illinois, USA.

Pujol S., Fick D. (2010). The Test of a Full-Scale Three-Story RC Structure with Masonry Infill Walls, *Engineering Structures*, 32: 3112-3121.

Rahmanishamsi E., Soroushian S., Maragakis E.M. (2016). Evaluation of the out-of-plane behavior of stud-to-track connections in nonstructural partition walls, *Thin-Walled Structures*, 103: 211–224.

Rihal S.S. (1980). *Racking Tests of Non-Structural Building Partitions*, California Polytechnic State University, USA.

Rihal S.S. and Granneman G. (1984). *Experimental Investigation of the Dynamic Behavior of Building Partitions and Suspended Ceilings during Earthquakes*. Report No. ARCE R-84-1, California Polytechnic State University, San Luis Obispo, California, USA.

Rihal S. S. (1988). Earthquake resistance and behavior of architectural precast cladding and connections, *Paper presented at the Symposium on Architectural Precast Concrete Cladding*, Chicago, IL., USA.

Rihal S. S. (1989). Earthquake Resistance and Behavior of APCC and Connections, *Paper presented at the Architectural Precast Concrete Cladding - Its Contribution to Lateral Resistance of Buildings*, Chicago, IL., USA.

Rihal, S. (1994). Assessment of Seismic Safety Standards for Library Shelving, *Proceedings of the 5th US National Conference on Earthquake Engineering*, Chicago, USA.

- Sack, R. L., Beers, R. J., & Thomas, D. L. (1989). Seismic Behavior of Architectural Precast Concrete Cladding, *Paper presented at the Architectural Precast Concrete Cladding - Its Contribution to Lateral Resistance of Buildings*, Chicago, IL., USA.
- Sassun K., Sullivan T.J., Morandi P., Cardone D. (2015). Characterising the in-plane seismic performance of infill masonry, *Bulletin of the New Zealand Society for Earthquake Engineering*, 49(1).
- Sivanerupan S., Wilson J.L., Gad E.F. and Lam N.T.K. (2010). In-plane drift capacity of point fixed glass façade systems, *Proceedings of Australian Earthquake Engineering Society 2010 Conference*, Perth, Western Australia.
- Sivanerupan S., Wilson J.L., Gad E.F. and Lam N.T.K. (2014). Drift Performance of Point Fixed Glass Façade Systems, *Advances in Structural Engineering*, 17(10): 1481-1495.
- Song A.K. and Vender A. (1999). *Nonstructural Damage Database, Technical Report MCEER-99-0014*, University at Buffalo, State University of New York, Buffalo, USA.
- Soroushian S., Ryan K.L, Maragakis M., Wieser J., Sasaki T., Sato E., Okazaki T., Tedesco L., Zaghi A.E., Mosqueda G., Alarez D. (2012). NEES/E-Defense Tests: Seismic Performance of Ceiling/Sprinkler Piping Nonstructural Systems in Base Isolated and Fixed Base Building, *Proceedings of the 15th World Conference on Earthquake Engineering*, Lisbon, Portugal.
- Suarez L.E., Singh P. (1996). Seismic Response of Rail-Counterweight Systems of Elevators, *Proceedings of the 11th World Conference on Earthquake Engineering*, Acapulco, Mexico.
- Suarez L.E., and Singh P. (1998). Dynamics and Response of Rail-Counterweight Systems Under Strong Seismic Motions, *Proceedings of the 6th U.S. National Conference on Earthquake Engineering*, Seattle, USA.
- Sucuoğlu H. and Vallabhan C.G. (1997), Behaviour of window glass panels during earthquakes, *Eng. Struct.*, 19(8): 685-694.
- Taghavi S. and Miranda E. (2003). *Response assessment of nonstructural building elements*. Pacific Earthquake Engineering Research Center, Berkley, California, USA.
- Tasligedik A.S. (2014). Damage mitigation strategies for non-structural infill walls. *PhD Thesis*, University of Canterbury, Christchurch, New Zealand.
- Tasligedik A.S., Pampanin S. and Palermo A. (2011). Damage Mitigation Strategies of 'Non-Structural' Infill Walls: Concept and Numerical-Experimental Validation Program, *Proceedings of the 9th Pacific Conference on Earthquake Engineering Building an Earthquake-Resilient Society*, Auckland, New Zealand.
- Tasligedik A.S., Pampanin S. and Palermo A. (2014). Low damage seismic solutions for non-structural drywall partitions, *Bulletin of Earthquake Engineering*, 13(4): 1029–1050.
- Tasligedik A.S. and Pampanin S. (2016). Rocking Cantilever Clay Brick Infill Wall Panels: A Novel Low Damage Infill Wall System, *Journal of Earthquake Engineering*, 21(7): 1023-1049.
- Tasnimi A.A. and Modebkhah A. (2011). Investigation on the Behavior of Brick-Infilled Steel Frames with Openings, Experimental and Analytical Approaches, *Engineering Structures*, 33: 968-980.

- Thurston S.J. and King A.B. (1992), *Two-directional cyclic racking of corner curtain wall glazing*, Building Research Association of New Zealand, BRANZ.
- Tsuruta K., and Kojima K. (1988). Dynamic Design Procedure for HVAC Ducts, *Journal of Pressure Vessel Technology*, 110: 413-421.
- Yang T.Y., Kullegowda H., Kapania R.K., Schiff A.J. (1983). Dynamic Response Analysis of Elevator Model, *Journal of Structural Engineering*, ASCE, 109(5): 1194-1210.
- Yao G.C. (2000). Seismic Performance of Direct Hung Suspended Ceiling Systems, *Journal of Architectural Engineering*, 6(1): 6-11.
- Wang M. L. (1986). *Nonstructural element test phase: U.S.-Japan Cooperative Research Project on a Full Scale Steel Test Frame*, Center for Environmental Design Research, Univ. of California, Berkeley.
- Wang M. L. (1987). Cladding performance on a full-scale test frame, *Earthquake Spectra*, 3(1), 119-173.
- Wang M. L., Bassler B. L. (1992). *Cladding / Council on Tall Buildings and Urban Habitat*, New York, NY., USA: McGraw-Hill.
- Wang X., Hutchinson T.C., Astroza R., Conte J.P., Restrepo J.I., Hoehler M.S., Ribeiro W. (2017). Shake Table Testing of an Elevator System in a Full-Scale Five-Story Building, *Earthquake Engineering Structural Dynamics*, 46(3): 391–407.
- Weggel D.C., Zapata B.J., Kiefer M.J. (2007). Properties and Dynamic Behavior of Glass Curtain Walls with Split Screw Spline Mullions, *Journal of Structural Engineering*, 133(10).
- White W. (1999). Reducing the Risk from Nonstructural Building Components in Earthquakes, *Proceedings of the 8th Canadian Conference on Earthquake Engineering*, Vancouver, Canada, USA.

4. Development of innovative low-damage technologies

4.1 Introduction

An overview of the low-damage technological solutions developed during the last decades for both structural and non-structural components is provided within this Chapter. After a brief and initial paragraph on the concept of damage-control approach, where it is highlighted the importance of moving towards this design level for meeting the modern society expectation, innovative damage-resistant technologies proposed and studied in past research works for either structural or non-structural elements are presented. Combining these low-damage solutions for skeleton, building envelope and fit-outs, an integrated low-damage building system can be defined, and this should represent the next generation of “earthquake-proof” resilient buildings.

Finally, experimental investigations on a new earthquake-resistant solution for expansion and chemical fasteners are described in the final section of this Chapter and in **Appendix A** of this Thesis. The proposed fastener solution represents a low-damage technique for non-structural elements attached to concrete structures through post-installed anchors.

4.2 Damage-Control design approach

Following a performance-based design framework, modern buildings are designed targeting Life-Safety criteria. Structures are conceived as ductile systems where inelasticity is concentrated within discrete plastic hinge regions (e.g. beam-to-column interface, column-to-

foundation and wall-to foundation connections) as per capacity-design principles and this structural system is designed for allowing buildings to sway and stand and people to evacuate. Notwithstanding these buildings performed as expected after earthquakes depending on the shaking intensity they were subjected to, the Life-safety design philosophy inherently accepts significant damage to both structural elements, such as beam hinging (Figure 4.1, left) or cracking in floor, and non-structural systems, as the damage described in the previous Chapter. Therefore, reparation of these structures may be uneconomical when compared to the cost of demolition and re-construction of the entire building system, both in terms of money and time, as also observed after the 22 February 2011 earthquake in Christchurch, New Zealand, where many buildings were demolished instead of being repaired (Kam et al. 2011).

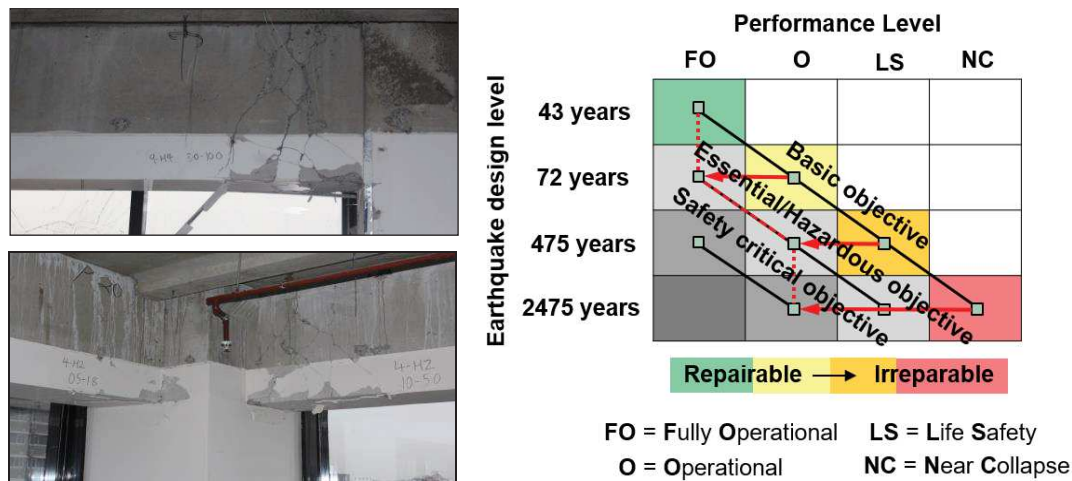


Figure 4.1. Left: Beam end hinging in a modern reinforced concrete building after the 22 February 2011 Christchurch earthquake (Kam et al. 2011); Right: Proposed modification of the Basic objective curve of the seismic performance design objective Matrix defined by SEAC Vision 2000 towards a damage-control approach (Pampanin 2012).

Targeting Life-Safety criteria for the design of new buildings is not enough for the current society and a shift towards damage-control design approaches and technologies is urgently required (Pampanin 2015). The expected or desired objective levels within the performance-based design framework need to be modified and the objectives and design methodologies of the new damage-control systems to be determined (Figure 4.1, right).

Due to the high socio-economic impact of moderate-to-strong earthquakes in terms of damage, dollars and downtime and the increased public awareness of seismic risk, the development and implementation of damage-control technologies, capable of sustaining low-level of damage and limited economic losses (repair cost and business interruption) after a

design level earthquake, is demanded. Moreover, the focus of the next generation of performance-based design framework should be directed towards the development of design tools and technical solutions for engineers and stakeholders to control the performance/damage of the entire building system, thus including superstructure, foundation systems and non-structural elements (Pampanin 2012).

4.3 Overview of damage-mitigation solutions

A brief overview of the innovative technologies developed within this damage-mitigation philosophy as well as of the high performance of these solutions compared to traditional systems is herein provided. These innovative elements do not increase significantly the building construction cost associated to the material only part, whilst reduce substantially the construction/erection time (and thus the other components of construction costs associated to time and financing), especially when considering the structural parts.

4.3.1 Low-damage structural elements

Apart from well-known damage-control technologies such as base isolation and supplemental dissipative braces, particular interest is being received by alternative and more recently developed “low-damage” systems. In this “low-damage” structural systems, the plastic hinge required by a traditional ductile design is substituted by a controlled rocking mechanism at the interface of the structural elements, i.e. beam-to-column, column-to-foundation or wall-to-foundation connections. The initial concept of this technology was developed by Stanton et al. (1997) and Priestley et al. (1991, 1999) and during the US PRESSS (PREcast Seismic Structural System) program at the University of San Diego in the 1990s (Figure 4.2, left). Jointed ductile connections were proposed, where precast components were jointed through unbonded post-tensioning tendons/bars creating a moment-resisting system.

Energy dissipation was then added to the system for ensuring the correct amount of ductility (Figure 4.2, right) by internally located mild steel bars - as per the *first-generation* technology -, or, more recently, using externally replaceable “Plug&Play” dissipators (Pampanin 2005; Marriott et al. 2008, 2009; Sarti et al. 2016), as presented on the left of Figure 4.3. The result is a hybrid connection made of both self-centering and energy dissipation capabilities whose behavior is described by the so-called “Flag Shape” hysteresis

rule (Figure 4.3, right). The properties of the system can be modified by designers by varying the ratio between the re-centering and dissipative (moment) contributions, provided by the post-tensioned tendons/bars (and/or axial load) and dissipaters respectively.



Figure 4.2. Left and centre: Five-Storey PRESSS Building tested at University of California, San Diego (Priestley et al. 1999); Right: concept of low-damage system (fib 2003).

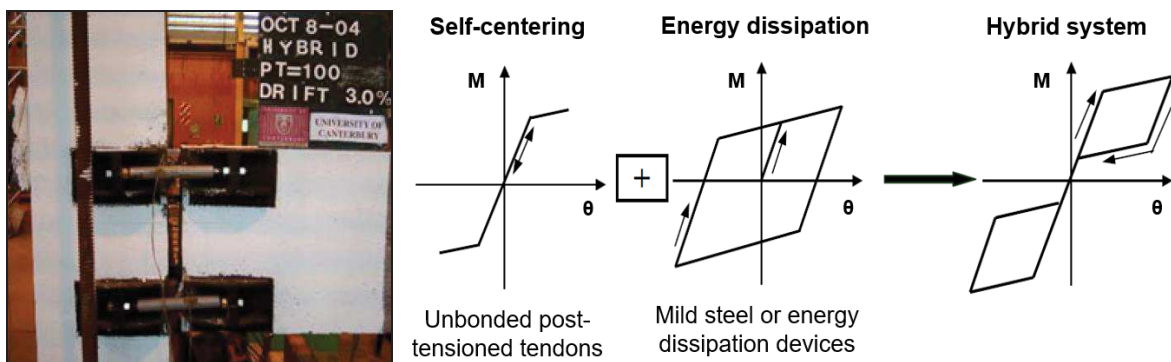


Figure 4.3. Left: Experimental tests on PRESSS concrete beam-column joints: configuration for Plug&Play dissipaters for beam-column joints (Marriott et al. 2008, 2009); Flag-shape hysteresis loop for a hybrid system (fib 2003).

During the earthquake shaking, the connections allow rocking motions by the opening and closing of the existing gaps, the dissipater devices ensure the correct system ductility, and the residual or permanent deformations are reduced. The structural skeleton of the building would thus remain undamaged after a major design level earthquake without any need for repairing actions.

Due to the self-centering capabilities of rocking systems, jointed ductile connections would suffer a constant and predictable beam elongation, also if lower than the equivalent cast-in-situ elongation. Therefore, for mitigating this problem and minimizing the damage to

floor systems guaranteeing a reliable diaphragm action, innovative solutions have been proposed, namely:

1. *Articulated floor solution.* A first application of this system was proposed by Priestley et al. (1999) that implemented discrete metallic connectors to concentrate the shear transfer mechanism between the diaphragms and the lateral resisting system of the Five-storey PRESSS Building tested in San Diego. Then, an articulated “jointed” floor system was developed by Amaris et al. (2007) (Figure 4.4) conceived as a double hinge mechanism at the beam-column interface, representing a shear key transfer mechanism, and sliding shear keys in the horizontal plane, used as connectors between the frame and floor systems.
2. *Non-Tearing floor solution.* In this system, beams and columns are separated by small gaps, which are partially grouted at the bottom to avoid geometrical beam elongation effects. This system would not prevent the tearing action in the floor due to gap opening at the top of the beam (Amaris et al. 2008) and no re-centring capabilities were provided due to the location and profile of the tendon. Therefore, improved concepts of the solution involve the combination of an inverted gap to prevent tearing in the floor and an antisymmetric tendon profile to solve the re-centring problem.

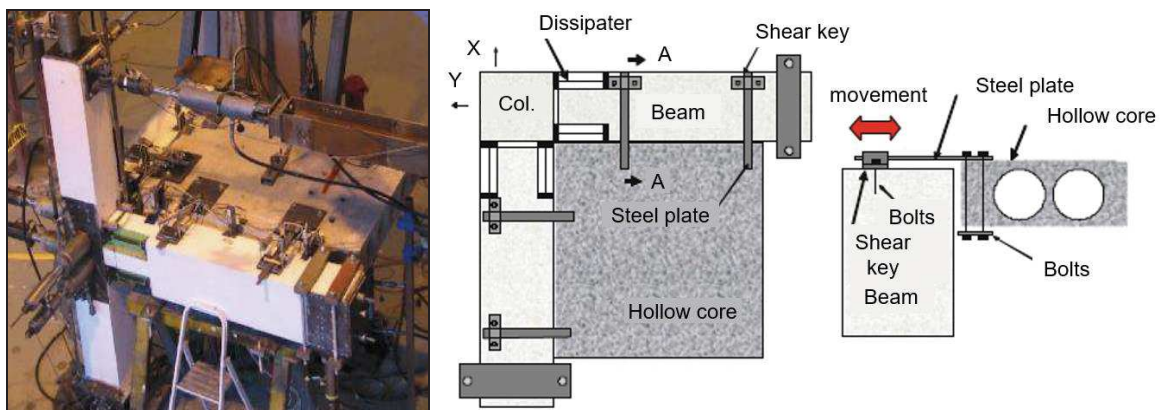


Figure 4.4. “Articulated floor” system by Amaris et al. (2007): response under uni-directional and bi-directional cyclic tests (left) and concept and connection details (right).

The high seismic performance of the jointed ductile connections, with negligible or no post-earthquake damage into the structural elements, led to the extension of the concept to different connection types (column-to-foundation or wall-to-foundation) and material (steel, timber or a combination of material, i.e. concrete-timber, steel-timber).

Referring to wood solutions, this system can be easily extended to engineered timber frame and wall multi-storey buildings (Palermo et al. 2005, 2006; Pampanin et al. 2006) leading to the Pres-Lam (Prestressed Laminated timber) technology. In fact, since 2004 extensive numerical investigations and experimental tests have been carried out on several subassemblies or large-scale systems at the University of Canterbury to apply this low-damage solution to timber structures. This experimental testing provided very good results and confirmed the high potentiality of this low-damage technology for timber constructions, creating high quality buildings with large open spaces, excellent living and working environments, and resistance to hazards such as earthquakes, fires and extreme weather events (Buchanan et al. 2011).

The rapid development of low-damage connections resulted in the implementation of a wide range of alternative arrangements available to designers and contractors for practical applications and different on-site implementations of this technology have started to be implemented in various seismic-prone countries around the world, e.g. U.S., Central and South America, Europe and New Zealand (Figure 4.5).



Figure 4.5. Left: Alan MacDiarmid Building at Victoria University of Wellington (New Zealand), first multi-storey PRESS building in New Zealand (Structural Engineers: Dunning Thornton Consultants; Cattanach and Pampanin 2008); Right: Nelson Marlborough Institute of Technology (New Zealand), world first Pres-Lam building (Structural Engineers: Aurecon, Devereux et al. 2011, Architects: Irving-Smith-Jack).

4.3.2 Low-damage non-structural elements

As a further step towards the development of a resilient integrated low-damage building system, not only the skeleton but also the non-structural elements should follow a similar approach. For this reason, in the last decade innovative damage-mitigation technologies have been proposed and developed to control and reduce the post-earthquake damage to

either vertical (facades, partitions) or horizontal (ceilings) non-structural elements. Various damage-resistant solutions found in literature are herein presented for different typologies of architectural systems.

4.3.2.1 Exterior enclosures

The connection of an exterior enclosure (façade system) to the primary structure is the critical aspect affecting the structural/non-structural interaction. Structural systems are typically designed neglecting non-structural elements thus the current approach is connecting the façade such that the interaction with the structural system is minimized. This means that the exterior envelope is considered as a simple dead weight and other systems are introduced to incorporate the stiffening and damping properties of the non-structural element with the structure.

Different strategies can be adopted for reducing the damage to façade systems (Baird et al. 2011), namely:

- disconnection from the primary structure, using seismic gaps or using connections allowing lateral movement;
- partial disconnection from the primary structure using dissipation devices designed to yield before the facade starts damaging;
- complete integration of the façade with the primary structure using strengthening, mainly adopted for masonry infill wall enclosures.

Taking into account the possible strategies for reducing the damage to these components and finding economical solutions easily applicable in the common practice, low-damage technologies have been proposed and initially investigated through numerical and experimental studies.

4.3.2.1.1 Cladding systems

As described in Chapter 2, cladding systems can be made of different materials and typologies (curtain walls, stick systems, double skin facades, spider glazing, monolithic claddings, lightweight or heavy cladding panels) and their seismic performance can be improved by designing appropriate gaps and connections to the structural frame. Concerning precast concrete cladding systems, the minimization of the cladding/skeleton interaction can

be guaranteed by the combination of bearing connections on the bottom of the panels, able to only transfer the vertical loads, and tieback or slotted connections on the upper part, which allow the lateral movement and are detailed with specific ductility and capacity to prevent failure (FEMA E-74: 2011; Baird et al. 2011).

Slotted or flexible tie-back connections are recommended by PCI (2007) to allow the in-plane movement of the panel. However, although designed according to the state-of-the-art design practice, these connections can increase the lateral stiffness of the building. Consequently, another solution for precast concrete cladding systems is taking advantage of this interaction to dissipate energy. Designed with proper ductility and damping properties, dissipative connections can provide significant benefits compared to more traditional systems (Goodno 1998; Pinelli et al. 1995). These connections should be able to dissipate the energy without failure during strong earthquakes limiting the demand forces transmitted to the panel.

Following this goal, Baird et al. (2013) developed and studied a low-damage solution for precast concrete cladding panels using U-shaped Flexural Plates (UFP) connections. These devices, initially proposed by Kelly et al. (1972) as a means of providing energy dissipation between structural walls, were introduced to dissipate the seismic energy and withstand the relative structure/panel displacement (Baird et al. 2014). The test results showed how the UFP connections have great potentiality as passive energy dissipation devices, representing a low-damage solution for such type of non-structural components. These connections are also able to limit the maximum displacements in a structure, reducing potential damage to other non-structural components.

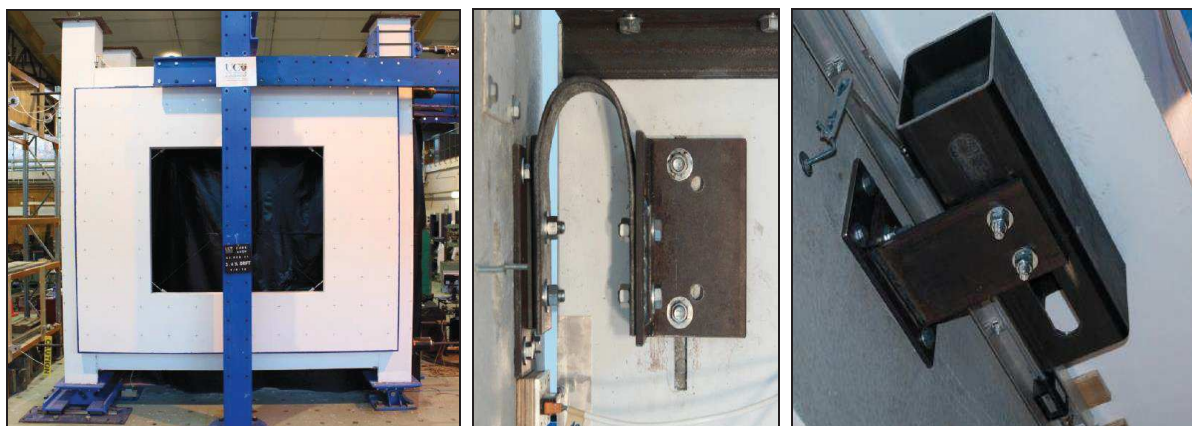


Figure 4.6. Left: experimental test on the low-damage precast concrete cladding system; Right: different configurations (unhoused or housed) of the UFP connections (Baird 2014).

As regards the curtain walls, a higher seismic performance can be obtained adopting advanced façade connections. These devices can provide a better uniformly distributed energy dissipation over the building height and are able to protect the façade limiting the force transmitted to the panels, as the friction damping connector proposed by Grigorian et al. (1993) or the visco-elastic dampers from Chang et al. (1998). However, as presented by Sivanerupan et al. (2014) for spider glazing systems, simple modifications of the non-structural detailing, as the adoption of K-type spider connectors with internal horizontal and vertical gaps in the steel plate assembly connected to the primary structure, can improve the seismic performance of these components.

4.3.2.1.2 Infill walls

Referring to exterior masonry infill walls, in consideration of the low deformation capacity causing brittle mechanisms, different solutions have been investigated.

An isolation system for masonry infill walls was analytically investigated by Aliaari and Memari in 2007. This solution, called Seismic Infill Wall Isolator Sub-frame (SIWIS), consisted of two vertical and one horizontal light-gauge steel studs connected to a surrounding frame and an isolator placed between the masonry infill and sub-framing. The isolator was designed to fail at the load after which the behaviour turned suddenly into bare frame behaviour. However, when this system was tested, it added a very brittle nature to the global behaviour, that may be considered to be an undesirable effect for such type of modifications.

Mohammadi and Mahalleh (2011) developed a new sliding system with low-to-moderate deformation capacity, made of horizontal panels connected by a frictional sliding fuse (FSF) avoiding undesirable failure mechanisms and addressing the damage to a ductile failure mode. The fuse acts before infill corner crushing and controls the infill so that it is not overloaded and, as a result, deformation capacity increases while strength deterioration decreases. In any case, friction slider adjustment should be properly designed otherwise crushing at the lower boundary of the wall can occur.

Following the same concept of dividing the masonry wall into horizontal panels, Preti et al. (2014) proposed a design solution with horizontal sliding joints, creating planes of weakness in the infill texture where the deformation concentrates. The infill-frame interaction is thus reduced, and the out-of-plane stability is ensured through a specific contact connection at the column-infill interface. The sliding joints provide a mechanism in the infill

wall governed by the hierarchy of strengths and capable of ensuring ductility and energy dissipation. Test results proved that this solution allowed to achieve 2.5% in-plane drift under quasi-static cyclic loading with negligible damage (Figure 4.7), stable hysteretic response and no strength degradation. Nevertheless, the interaction with a real reinforced concrete frame, the different size and shape of the openings, the layout of the sliding joints should be investigated before applying the technique in the design practice.

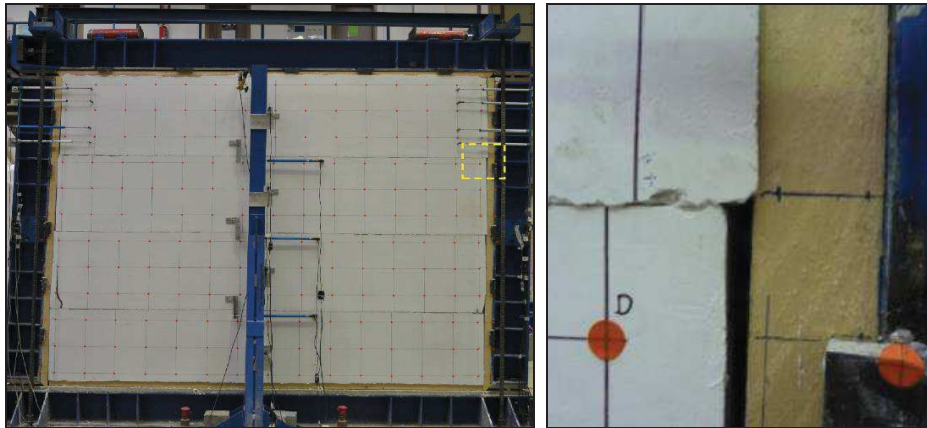


Figure 4.7. Left: Wall specimen at 2.5% drift; Right: detail of the compressive strain in the contact area between masonry and plank at a sub-portion corner (Preti et al. 2014).

Within the European FP7 Project “INSYSME”, Morandi et al. (2018) used the same concept of dividing the masonry infill wall into horizontal panels as seismic-resistant solution. The system was conceived considering a combined use of sliding joints inserted in the masonry and deformable joints at the wall-frame interface. Specific construction detailing was proposed and tested through in-plane cyclic tests on one-storey one-bay reinforced concrete frames with two different infill configurations (a solid wall and a wall with a central opening).

The previous systems based on the division of the panel into horizontal parts may have out-of-plane issues, not easily to be addressed in practical applications, and at high inter-storey drift levels, the system may induce shear failure at reinforced concrete columns. This represents the most relevant problem related to such type of solutions.

Another low-damage system was recently proposed by Tasligedik and Pampanin (2016). The infill wall was divided into vertical panels and moderate-to-high deformation capacity was achieved. The concept was based on the formation of a jointed system accommodating the inter-storey drift demands through a rocking mechanism between adjacent panels. The

solution investigated was able to sustain 2–2.5 % inter-storey drift, under quasi-static cyclic loading, corresponding to the maximum code allowed demand under a design level earthquake, without evident cracking/damage. The rocking infill wall consisted of internal gaps which minimized the structural/non-structural interaction until the achievement of a design drift level and the gaps were fully closed (Figure 4.8). It is highlighted that the advantage of this solution is the capability of an engineer to control the drift level after which the infill wall damage can be allowed.



Figure 4.8. Left: Low-damage rocking infill wall (Taslignedik 2014); Right: construction details (top-left: sub-frame system; bottom left: clay bricks infilled within the sub-frame; top-right: polyurethane foam in the lateral gaps; bottom-right: polyurethane structural joint sealant into the lateral gaps) as described in Taslignedik (2014).

4.3.2.2 Partitions

During the last years, several studies have aimed to define strategies able to reduce the damage to these non-structural components. Some of these investigations are herein described for the case of drywall gypsum partition walls.

After experimental testing on 36 steel studded gypsum drywall partitions, Filiatrault et al. (2010) concluded that slip tracks and gaps at top end of the panels lead to minor damage of drywalls attached between two floors. However, during the tests damage was concentrated into the vertical joints between panel and orthogonal direction.

Araya-Letelier et al. (2019) developed a sliding frictional connection to improve the seismic performance and mitigate the damage to these vertical elements. While a conventional drywall specimen suffered damage around 0.1%, with this sliding frictional connection type, the specimen stayed damage-free until 1.52% drift.

Petrone et al. (2017) developed and studied the influence of an innovative device on the seismic performance of drywall partitions. This innovative device avoids the unhooking of the panels from the supporting studs and is a locking system composed of a steel plate with two lateral flaps and a bolt. The locking device is placed into the stud and activated through the tightening of the bolt; once the bolt is tightened, lateral flaps adhere to the stud, reducing the width of the slots, which house panel hooks, and preventing the overturning of the panels, if they are subjected to both uplift and out-of-plane forces. Test results showed that the introduction of this device significantly increased the level of collapse (up to 1.45% drift).

Adopting the same concept previously described for infill wall facades, Tasligedik et al. (2014) investigated a low-damage drywall solution. Internal gaps and details modifications, not adding material and labour cost, were introduced into the system configuration to obtain a component able to achieve high drift levels before initial cracking and consequent loss of serviceability (Figure 4.9). In fact, the experimental tests carried out by Tasligedik et al. (2014) showed how the gap closed at around 1.5% drift level as per design, no damage was observed until 2.0% drift level and the drywall remained serviceable even at 2.5% drift level.



Figure 4.9. Left: experimental test on the low-damage drywall system (Tasligedik et al. 2014); Right: details of the wall construction (top-left: sub-frame system; bottom left: friction fitted interior fire-rated stud; top-right: installation of the gypsum lining to the steel studs; bottom-right: finished drywall partition) as described in Tasligedik (2014).

4.3.2.3 Ceiling systems

FEMA E-74 (2011) provides different mitigation strategies to reduce the damage to suspended ceiling systems, providing an unrestrained ceiling able to accommodate the movements using appropriate grid connectors, hangers, perimeter closure angles and edge clearance or providing a restrained ceiling with rigid or non-rigid bracing assemblies.

Referring to fully-floating systems, a high seismic performance solution was proposed by Pourali et al. (2017). The authors carried out experimental tests on a fully-floating ceiling with elastic acoustic isolation foam into the lateral gaps (Figure 4.10). Experimental results showed that the perimeter filling reduced the pounding impacts due to the horizontal displacements exceeding the gaps when the earthquake frequencies were close to the ceiling resonant frequency. The accelerations and displacements on the ceiling system were thus reduced and this effect led to mitigate the component damage.



Figure 4.10. Test specimen (left) and detail of isolation foam placed in the lateral gap (right) (Pourali et al. 2017).

4.3.2.4 Building services and contents

Considering all the possible damage states observed from past earthquake events, different techniques can be proposed to improve the restraint systems of such type of non-structural elements, e.g. the solutions defined in FEMA E-74 (2011).

However, focusing the attention on the fixings, commonly the weakest link in the restraint system, and following the goal of defining an integrated low-damage building including damage-mitigation details for services and contents, fasteners should be properly designed in order to reduce the demand (force and acceleration) on the connected non-structural element. Therefore, a new low-damage solution, initially proposed by Quintana-Gallo et al. (2018), has been further studied within this Thesis through experimental testing (shake table). Results from this investigation are presented in the next paragraph of this Chapter and further described in **Appendix A**.

4.3.3 Integrated low-damage system

In the previous section, a literature review of the low-damage solutions recently developed for both structural and non-structural elements, capable to withstand high levels of drift with negligible damage, can be found. All these systems have been refined and investigated independently and mostly under quasi-static testing.

The next generation of buildings should include all these solutions forming an integrated damage-resistant building system. However, more research studies are needed to investigate the seismic performance and feasibility of the integrated system as a whole, that is, including all the aforementioned technologies. With this scope, Johnston et al. (2014) carried out uni-axial shaking table tests on a half scaled two-storeys concrete frame building consisting of a post-tensioned rocking hybrid frame, incorporating an articulated floor (with U-shaped Flexural Plates), low-damage drywall infill and facades (Figure 4.11). Tested under different configurations and subjected to over 400 earthquakes of different intensity levels, no evident level of structural and non-structural damage was observed.

Nevertheless, comprehensive investigations should be carried out to prove the high seismic potentiality of the integrated low-damage structural/non-structural system as well as to refine both connections and construction details. Research is moving towards this direction, as lately presented by Pampanin et al. (2019) and Dhakal et al. (2019).

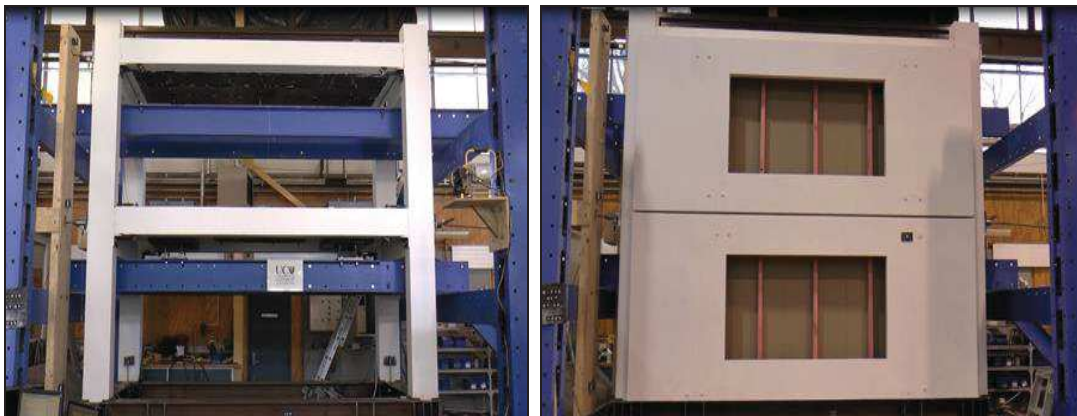


Figure 4.11. Test Building by Johnston et al. (2014): PRESSS Bare Frame (left) and complete structural & non-structural system with low-damage partitions and facades (right).

In particular, within an EU-funded SERA project (Pampanin et al. 2019), 3D large-scale shake-table tests (under 3 degrees of freedom input motions, two horizontal and one vertical components) of an integrated damage-resistant system have been carried out. As part of the

research of this Thesis, the EU-funded experimental campaign is described in Chapters 6 and 7 focusing on the design procedure of the specimen, its construction detailing and manufacturing, the experimental set-up as well as providing preliminary results.

4.4 Experimental investigation on innovative earthquake-resistant fasteners

Non-structural components, such as suspended ceilings, pipelines or mechanical equipment, are typically connected to reinforced concrete buildings using post-installed fasteners, usually preferred by designers for their flexibility and large field of possible applications compared to cast-in-place anchors. The study of the seismic behavior of this connection system is spreading, and research aims to better understand the seismic performance of the fasteners as well as its effect on the non-structural elements, through both experimental and numerical investigations. As highlighted several times, due to the increasing community expectations towards the reduction of post-earthquake non-structural damage, the study and improvement of the seismic behavior of post-installed fasteners is becoming fundamental.

4.4.1 Previous research

Over the past few decades, large amount of work has been done to study the behavior of different types of individual or groups of post-installed anchors subjected to quasi-static and dynamic force or displacement-controlled loading protocols in uncracked or cracked concrete (Eligehausen 1991, Eligehausen and Balogh 1995; Mahrenholtz and Eligehausen 2010; Hoehler et al. 2011; Vintzéléou and Eligehausen 2012; Mahrenholtz et al. 2016). In past years the dynamic behavior of post-installed fasteners has been also investigated through uniaxial or triaxial shake table excitations, like the tests performed by Rieder (2009), Mahrenholtz et al. (2014) and Abate (2015).

In the actual context of performance-based seismic design and with the aim of improving fastening techniques, a comprehensive experimental and numerical campaign has been carried out at the University of Canterbury to develop a new generation of post-installed fasteners able to resist to severe seismic events, referred to as EQ-Rod (Earthquake Resistant fastener), thus capable of reducing the damage to the non-structural component (Quintana-Gallo et al. 2018). This type of fastener relies upon the use of supplemental

damping, either viscous and/or hysteretic, added in series or in parallel to a traditional fastener to reduce the acceleration demand and consequently the force applied to the non-structural component and represents a first generation of low-damage system for this type of component (Figure 4.12).

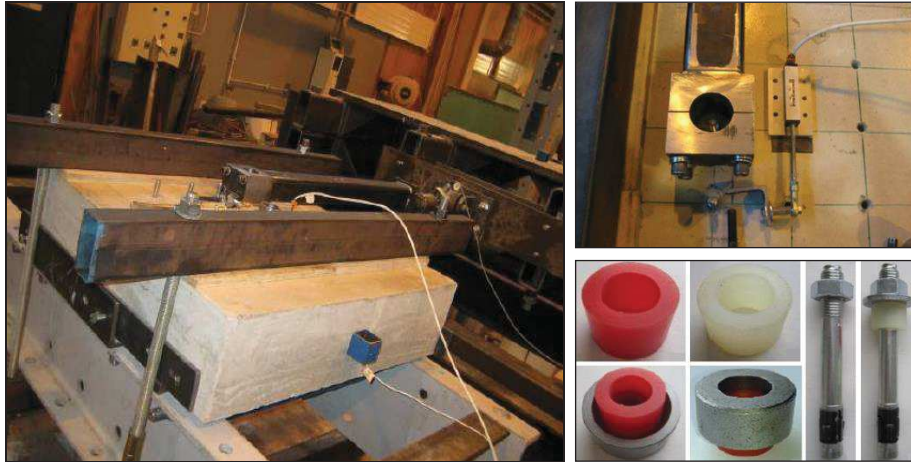


Figure 4.12. Details of the experimental campaign on traditional and EQ-Rod fasteners (left and top-right) and configurations adopted for the supplemental damping devices (bottom-right) (Quintana-Gallo et al. 2018; Pampanin et al. 2008).

Building on this original research, a second experimental campaign has been carried out at the Structural Laboratory of the University of Rome “La Sapienza” in 2017 with the aim of extending the previous investigation and propose solutions to a larger variety of fastening systems (traditional and low-damage expansion and chemical anchors), focusing on the behavior in both un-cracked and cracked concrete (Pampanin et al. 2017; Ciurlanti et al. 2019).

4.4.2 Development of the EQ-Rod concept

Fasteners can be grouped in function of the way they transfer tension loads to the anchorage material. Load-transfer mechanisms are typically identified as: 1) mechanical interlock, where the load is transferred by bearing the fastener onto the anchorage material; 2) friction, due to fasteners that have a geometry generating an expansion force, which in turn produces a friction force between the anchor and the sides of the drilled hole; 3) bond, where the tension load is transferred to the anchorage material by a chemical interlock (Eligehausen et al. 2006).

During an earthquake, a fastener may be subjected to tension, shear, combined tension-shear, and combined shear and bending cycling loading. Referring to a non-structural component anchored to a reinforced concrete structure using a fastener, during the seismic motion the anchor loads develop due to the inertial response of the non-structural element to the acceleration of the building floor to which is attached.

The seismic behaviour of acceleration-sensitive non-structural components is typically described by floor acceleration response spectra, which provide the maximum associated acceleration in function of the fundamental period of vibration of the element. The response spectra depend on the system viscous damping (non-structural component + connections), therefore increasing the value of the damping, the demands on the non-structural component can be reduced. Taking into account this concept and in order to achieve the seismic demand reduction, the idea of adding supplemental damping to the fasteners started to develop and a first innovative damage-resistant fastener was proposed and studied (Quintana-Gallo et al. 2018; Pampanin et al. 2008), the so-called EQ-Rod fastener. An external supplemental damper is added to a traditional anchor, increasing the system damping, and this results in reducing the amplitude of the spectral response and the acceleration on the non-structural element under a given ground motion (Figure 4.13).

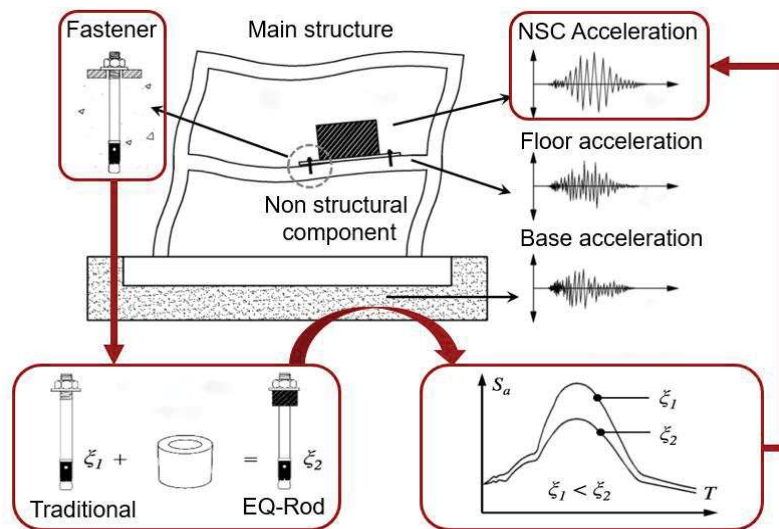


Figure 4.13. Effect of supplemental damping on fasteners in reducing the seismic demands of the attached non-structural component (Ciurlanti et al. 2019).

4.4.3 Experimental campaign on the EQ-Rod 2.0

Notwithstanding the first initial whilst comprehensive experimental campaign on the EQ-Rod solution for post-installed fasteners, further investigations are needed to confirm the beneficial effects of the concept of dissipative anchor rod to seismically protect the non-structural components for a greater variety of fastening systems (expansion and chemical anchors) in both un-cracked and cracked concrete.

The shaking table tests made in 2008 at the University of Canterbury focused the attention on just expansion fasteners in uncracked concrete, while it is important to extend the application of the low-damage solution to other typologies of fastener (expansion and chemical) and system conditions (uncracked and cracked concrete). In fact, fasteners can be located in a crack which either forms during an earthquake or has formed at some prior time and the crack width can typically change over the duration of an earthquake, therefore investigations are also needed to apply the low-damage strategy in cracked concrete.

In such a context, a new low-damage prototype (EQ-Rod 2.0) has been proposed by the industry supplier and in order to study the seismic performance of this solution a new research project has been developed between the University of Rome “La Sapienza”, the University of Natural Resources and Life Sciences (Vienna, Austria), and Fischer (Fischerwerke Artur Fischer GmbH & Co. KG). The testing setup, instrumentation, protocol and main outcomes of this experimental campaign are presented in this part of the Thesis and in **Appendix A**. However, more detailed information can be found in the report prepared by Pampanin S., Bianchi S. and Ciurlanti J. (2017).

4.4.3.1 General overview

Uni-axial shake table tests have been carried out to study the seismic behaviour of the proposed EQ-Rod 2.0 prototype, with the primary scope of investigating the potentiality and the efficiency of this solution when compared to a traditional fastener. Thus, a specific testing protocol capable of simulating, through shake table testing, the dynamic response of fasteners under seismic actions has been prepared at the Structural Engineering Laboratory of the University of Rome “La Sapienza”.

The experimental campaign has involved different phases:

- preparation of the ad-hoc test setup and monitoring system;

- preliminary tests on different types of anchors to confirm the correct functioning of the whole testing apparatus, including fastener installation, loading protocol, control and acquisition system, post-processing of the results;
- finally, further and comprehensive experimental tests have been performed according to a detailed test matrix on cracked and uncracked blocks.

Six different types of M12 anchors - i.e. two categories, expansion (FAZ II) and chemical (Superbond) anchors, in three configurations, i.e. traditional, EQ-Rod 2.0 and traditional with mortar filling - have been tested under real recorded earthquake ground motions, through shear loads to the anchors, to investigate the anchor behavior as well as the accelerations and displacements transferred to the attached non-structural component.

4.4.3.2 Test setup

The experimental Single-Degree of Freedom (SDOF) test setup comprised three parts: 1) a concrete block representing the floor slab; 2) a driving mass representing the attached non-structural element; 3) the anchorage system. The shake table reproduced the selected input motions, transmitted to the floor concrete block where the anchor rod was installed and connected through a lever arm to the driving mass, which was in turn excited. Details of the experimental test setup are shown in the following Figure 4.14.

The shake-table at the University of Rome “La Sapienza” is a uni-axial earthquake ground motion simulator (MOOG n. L081-324-011) consisting of a steel base plate (4250x1500 mm), an aluminum shaker table (1500x1500 mm), and a steel welded reaction bracket to take the hydraulic actuator. Furthermore, the test rig includes two guiding rails (RUE35) which are protected by stiff steel covers and movable protection covers and are designed for a travel of ± 200 mm (total stroke of 400 mm). MOOG servo-valves control the hydraulic actuator, and their capacity limits the velocity of the table in function of the frequency (the maximum value of the velocity is 200 cm/s and it can be reached only in the range 1.8-2 Hz).

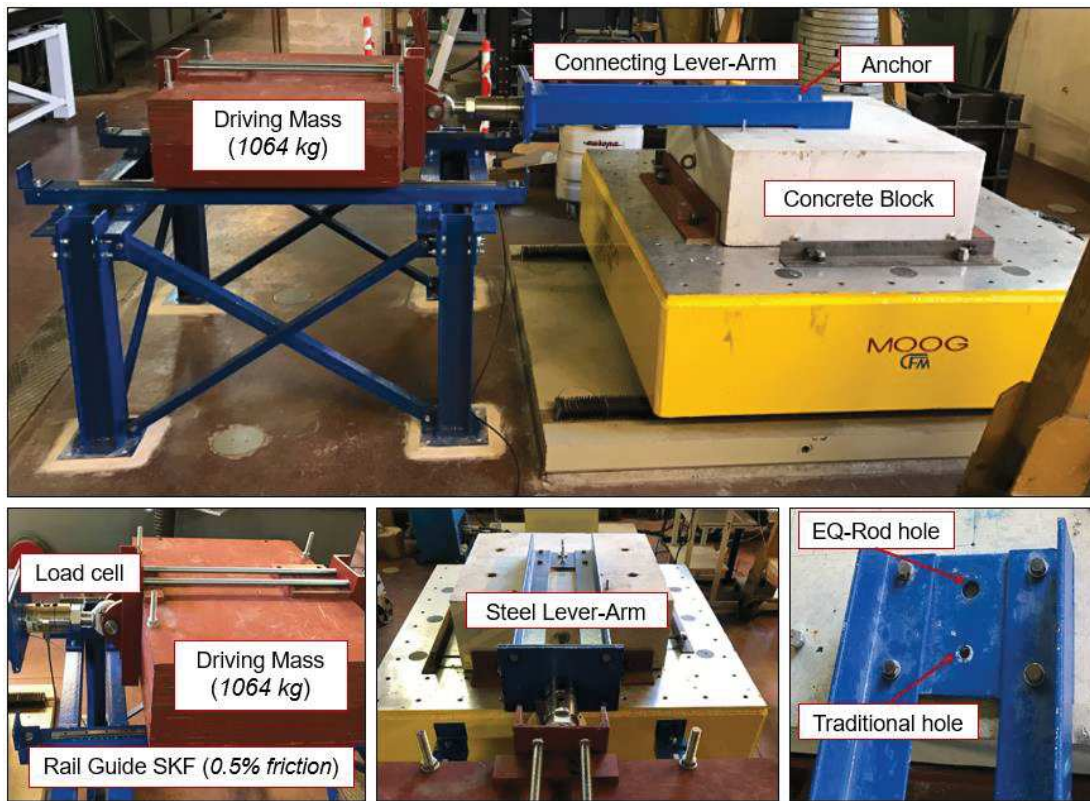


Figure 4.14. Details of the experimental test setup.

The concrete floor slab on which the anchor was installed was represented by a cracked or uncracked concrete block (80 x 80 x 30 cm) with characteristic compression strength, f_{ck} , of 20 MPa. The block was rigidly attached to the shake table as shown in the left of Figure 4.15. Lateral sliding was prevented by steel angles fixed on the shake table in both longitudinal and transverse directions. As part of this research investigation, cracked concrete blocks were intended to simulate the presence of a crack parallel to the shaking direction and on which the anchor was installed to be tested.

A driving mass of 1046 kg, made by assembling steel plates, represented the non-structural mass attached to the anchor rod and was located on two low-friction linear rail guides (LLT of SKF group), fixed on an exterior steel frame, to allow the movement along the shaking direction (Figure 4.15, right). These guides had precision-ground raceways and a carriage with four rows of balls in an X-arrangement, the dynamic coefficient of friction of the whole system was approximately $\mu_d=0.5\%$ while the maximum acceleration guaranteed was 75 m/s^2 .

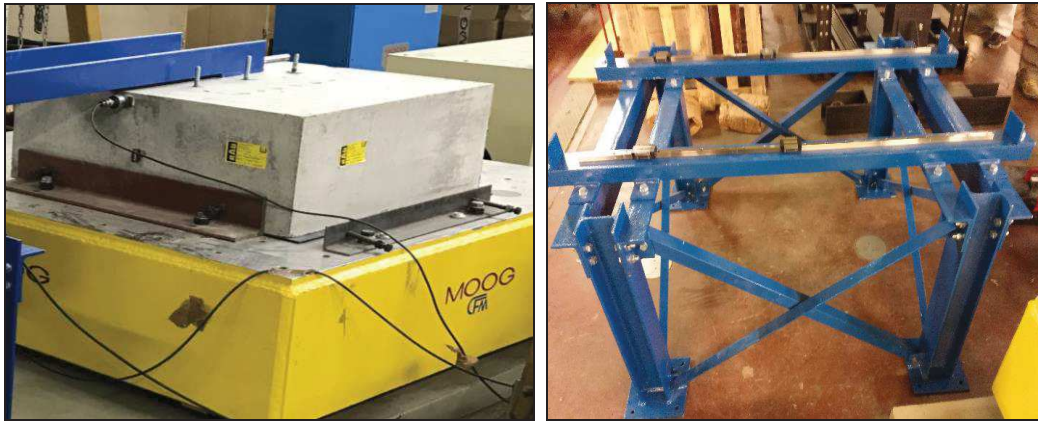


Figure 4.15. Left: Floor level concrete block; Right: Exterior steel frame with SKF Profile LLT Rail Guide.

A steel lever-arm connected the external driving mass to the anchor and consisted of L profiles of S355 steel settled to a steel plate where the load cell ended. The rigid lever arm spread the inertia force from the driving mass to the fastener allowing the inertia force to act in the centre of the non-structural element. Consequently, the vertical displacement of the anchor was not influenced by additional push and pull forces.

Finally, a steel plate comprising two different holes was located on the concrete block to install the fasteners. The greater hole was for the EQ-Rods and had a diameter of 24 mm, while the smaller one was for the traditional anchors and had a diameter of 14 mm.

4.4.3.3 Monitoring system

The monitoring system designed for the 1D shaking table tests is shown in Figure 4.16.

A load cell with maximum capacity of 200kN (tension and compression) was installed between the driving mass and the steel lever-arm for measuring the load transferred to the anchorage system. Three accelerometers were attached to the system in the shaking direction, i.e. on the driving mass, on the concrete block and on the shake table, for monitoring the accelerations of the system. The acceleration of the shake table was measured to compare the input record and the output signal of the table. The accelerations of the concrete block were collected to check the rigidity of the concrete/table connection. While, the accelerometer on the driving mass allowed the evaluation of the contribution of the fastener to the load transferring to the non-structural element.

Finally, three LVDT transducers were installed for controlling the relative displacements between the driving mass and the concrete block. In particular, the vertical displacement of

the anchor rod was monitored as well as the horizontal displacements of both the fastener and the steel plate. The difference between these horizontal displacements provided a measure of the internal gap between the two components.

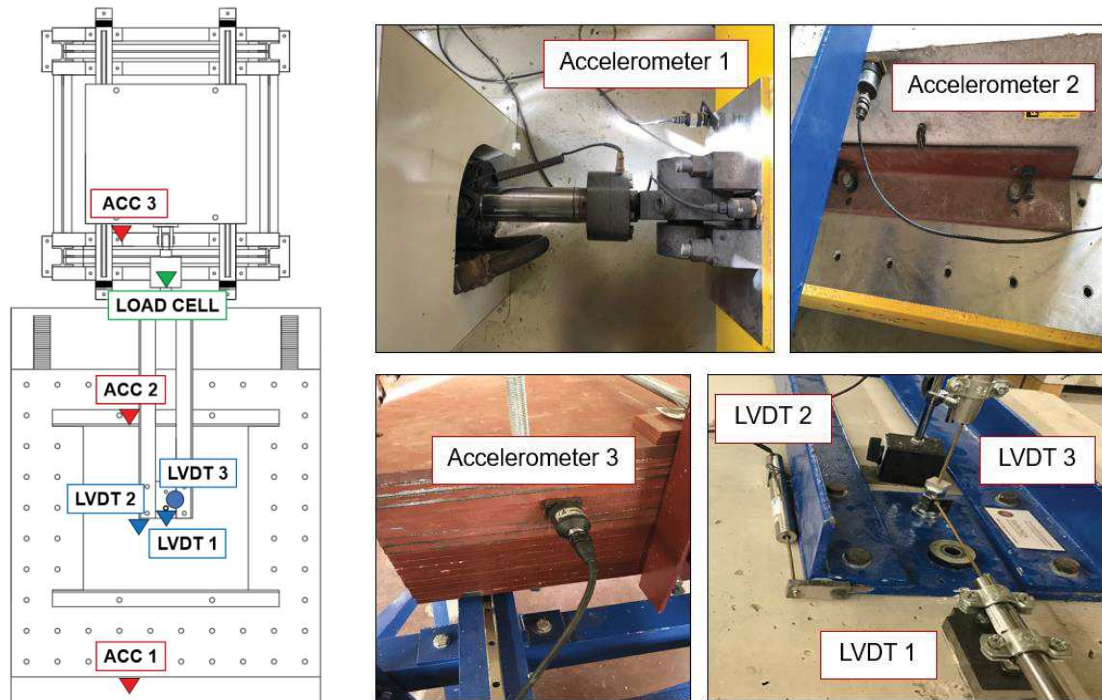


Figure 4.16. Instrumentation plan.

4.4.3.4 Input motions and test matrix

Different types of input signals were considered for the experimental campaign. Initially, sinusoidal inputs, either acceleration history with constant frequency and varying the amplitude (from 0.05 g to 0.5 g) or sweep signals with amplitude of 0.15g and 0.3g, a frequency range of 1-5 Hz and a time-period of 10s, were implemented to study the dynamic behaviour of the fasteners. Finally, the experimental tests were carried out using time-history earthquake inputs, selecting three Far Field and two Near Fault ground motions properly scaled. In fact, the records were scaled to satisfy the spectro-compatibility condition between the average spectrum and the target design spectrum, developed referring to Eurocode 8 and considering a high-seismicity zone in Italy (0.35g of PGA, Soil B).

The scaled acceleration spectra of the selected earthquake records are shown in Figure 4.17, while the main characteristics of the input motions can be found in Table 4.1.

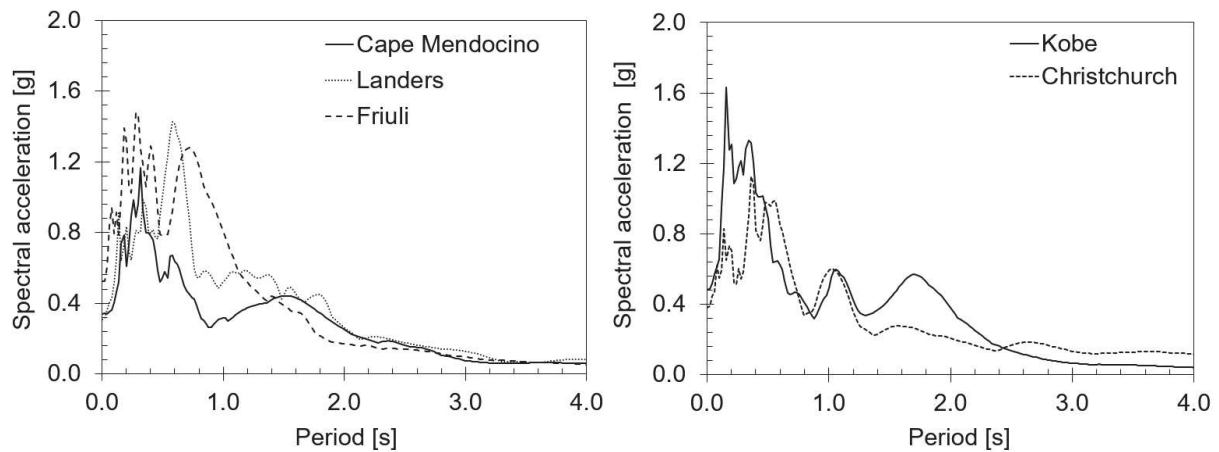


Figure 4.17. Acceleration response spectra for the Far Field (left) and Near Fault (right) input motions.

Table 4.1. Earthquake records selected for the shake-table tests.

Input name	Year	Station	M _w	Record ID
Cape Mendocino	1992	Eureka – Myrtle & West	7.0	EQ ₁
Landers	1992	Morongo Valley	7.3	EQ ₂
Friuli	1976	ST33	6.0	EQ ₃
Kobe	1995	CUE	6.8	EQ ₄
Christchurch	2011	CCCC	6.3	EQ ₅

The shaking table tests were performed following a specific test matrix including three different configurations of M12 expansion (*FAZ II*) and chemical (*Superbond*) post-installed fasteners anchored in uncracked and cracked concrete blocks: traditional anchor, traditional anchor with EQ-Rod and traditional anchor with mortar filling into the gap between the steel plate and the rod due to construction tolerances (Figure 4.18).

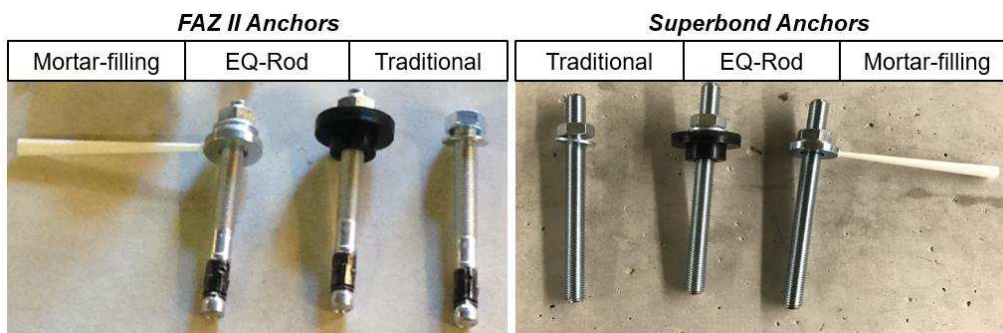


Figure 4.18. Different typologies (expansion – *FAZ II* - and chemical - *Superbond* -) and configurations (Traditional, with EQ-Rod and with mortar filling) of anchors.

Referring to the five input motions previously described (EQ_i) and to their simulated aftershocks (EQ_i-50), assumed as 50% of the input motion (amplitude-only reduction, same duration), for each expansion and chemical fastener the experimental test matrix in Table 4.2 was followed. For each typology of anchor and for each input motion (e.g. Traditional, $EQ_1 + EQ_1-50$), three fasteners were tested to have more reliable results (i.e. 15 tests x 3 times), therefore, in total, the test matrix of the experimental campaign consisted of 360 shake table tests (input + aftershocks), 180 for uncracked concrete and 180 for cracked concrete (see **Appendix A** for the complete Test Matrix).

Table 4.2. Test matrix considered for both FAZ II and Superbond fasteners in both un-cracked and cracked concrete.

Test ID	Input motion	Type of fastener
1	$EQ_1 + EQ_1-50$	Traditional
2	$EQ_1 + EQ_1-50$	Traditional with Mortar Filling
3	$EQ_1 + EQ_1-50$	EQ-Rod
4	$EQ_2 + EQ_2-50$	Traditional
5	$EQ_2 + EQ_2-50$	Traditional with Mortar Filling
6	$EQ_2 + EQ_2-50$	EQ-Rod
7	$EQ_3 + EQ_3-50$	Traditional
8	$EQ_3 + EQ_3-50$	Traditional with Mortar Filling
9	$EQ_3 + EQ_3-50$	EQ-Rod
10	$EQ_4 + EQ_4-50$	Traditional
11	$EQ_4 + EQ_4-50$	Traditional with Mortar Filling
12	$EQ_4 + EQ_4-50$	EQ-Rod
13	$EQ_5 + EQ_5-50$	Traditional
14	$EQ_5 + EQ_5-50$	Traditional with Mortar Filling
15	$EQ_5 + EQ_5-50$	EQ-Rod

4.4.3.5 Testing protocol

The installation of anchors was a crucial phase for the experimental testing. In fact, test results are directly affected by the installation operation of the fasteners, therefore for each type of anchors the installation procedure was applied in a rigorous manner before performing the shaking table tests.

Each M12 fastener was installed into the concrete following the procedure specified by the manufacturer. Regarding the concrete blocks, to study the seismic performance of anchor rods located along cracks parallel to the shaking direction, an appropriate apparatus was created to generate these cracks (Figure 4.19): a bar with a sharp edge was positioned and forced by an oil jack exactly between two cotters inserted in the concrete block and the crack was opened by blowing onto both cotters on the left and on the right of the bar until it reached 0.5 mm width.

More information about the testing protocol to be followed for each typology of anchor and for both un-cracked and cracked concrete can be found in **Appendix A**.

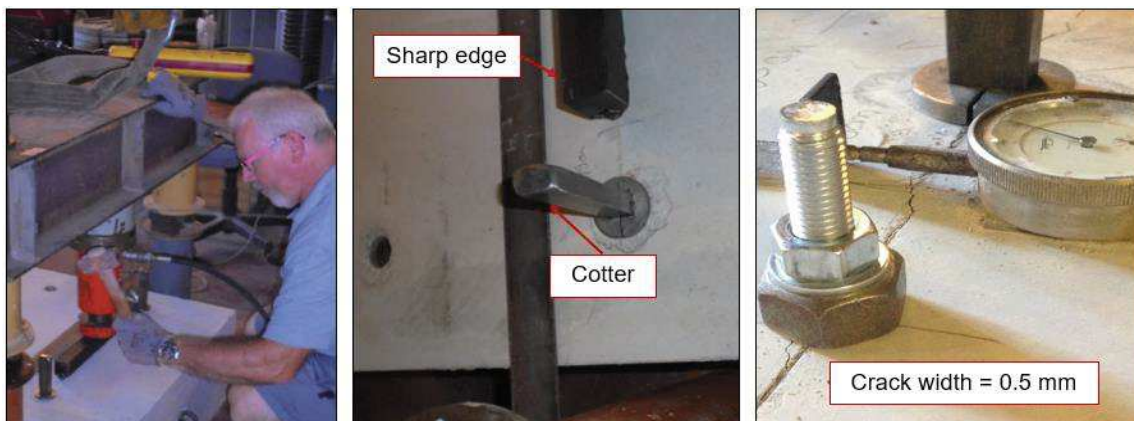


Figure 4.19. Testing protocol for opening the cracks in the concrete blocks.

4.4.3.6 Test results

Both the acceleration of the driving mass, representing the non-structural system, and the hysteretic behavior (force-displacement relationship) of the fastener anchored to the concrete block were determined as output from the experimental testing. The efficacy of the EQ-Rod prototypes in improving the seismic response of the system was thus determined as the capacity of reducing the acceleration demand on the connected non-structural component (driving mass) when compared to the same demand related to the application of traditional (expansion or chemical) fasteners.

The main findings from the experimental campaign are presented in this paragraph, however, a more complete report of all the obtained results can be found in Pampanin et al. (2017).

Concerning the data processing, it is observed that the data obtained from the high-speed logger connected to the shake table were filtered using a low pass (6th order Butterworth filter) with a cut off frequency of 20Hz to reduce external noise.

- **Sinusoidal input tests, FAZ II and Superbond anchors**
(PHASE 0 – October 2016/January 2017)

The preliminary experimental results from the sinusoidal input tests on uncracked concrete blocks are initially presented in terms of hysteretic loops for both Traditional anchor and EQ-Rod 2.0 considering either FAZ II or Superbond configurations (Figure 4.20).

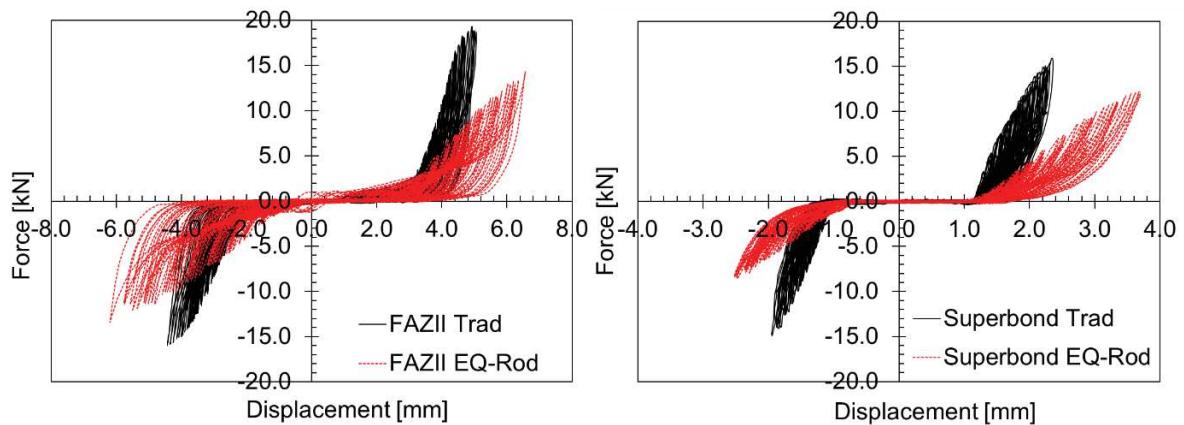


Figure 4.20. Comparison between FAZ II Traditional and FAZ II EQ-Rod (left) and Superbond Traditional and Superbond EQ-Rod (right) in terms of Hysteretic Loop for uncracked concrete.

The installation of each anchor followed the testing protocol, with the only difference that the application of the torque was reduced to 0 Nm - instead of 30Nm or 20 Nm - in order to simulate the complete loss of tightening torque due to long periods.

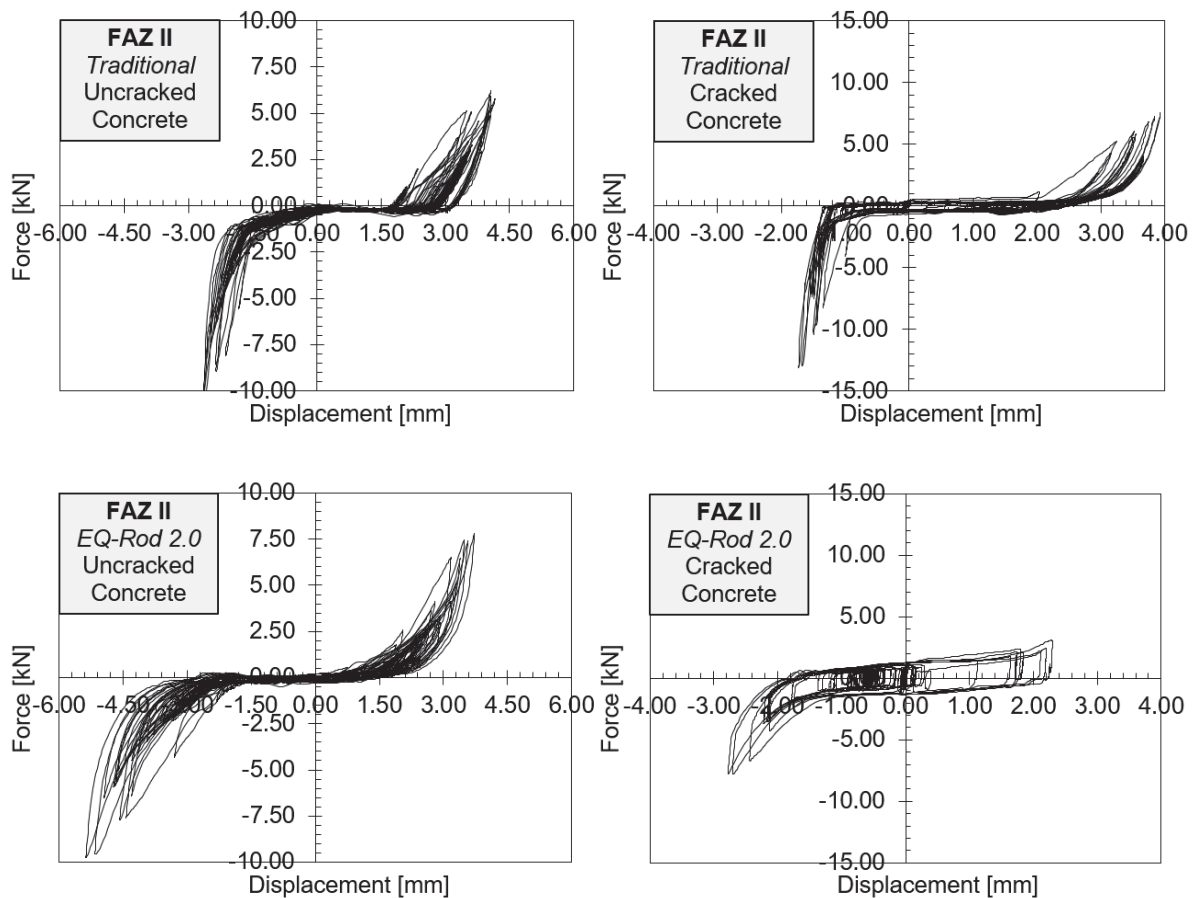
Analyzing the maximum force values determined on the non-structural system, the results showed a reduction in the range of 15-25% of the EQ-Rod solution compared to the FAZ II traditional one, while 20-35% of the EQ-Rod solution compared to the Superbond traditional system. These results are justified considering the large hysteretic energy of the EQ-Rod system, thus the greater displacement that this configuration reached during most of the cycles.

- **Ground motion input tests, FAZ II anchors**
(PHASE 1 – March 2017/May 2017)

Following the test matrix, the shake table tests were initially carried out for all the proposed configurations of expansion anchors in uncracked and cracked concrete.

In order to have more reliability on the results and make statistics on them (average, standard deviation) for each type of anchor (Traditional, EQ-Rod 2.0 and Mortar Filling) and earthquake motion (EQ_i and aftershock EQ_{i-50} for i=1,...,5) three different tests were performed, e.g. testing 3 Traditional anchors post-installed in different positions in the concrete block for just EQ₁ (see Test Matrix in **Appendix A** for more details).

Results in terms of force/displacement curves of the driving mass are shown in Figure 4.21 for just one test of an input record (EQ₁) for all the three types of anchors (FAZ II Traditional, FAZ II EQ-Rod, FAZ II with Mortar Filling), while in Figure 4.22 a comparison is made in terms of peak driving mass acceleration, where “positive” and “negative” refer to the directions of loading/motions.



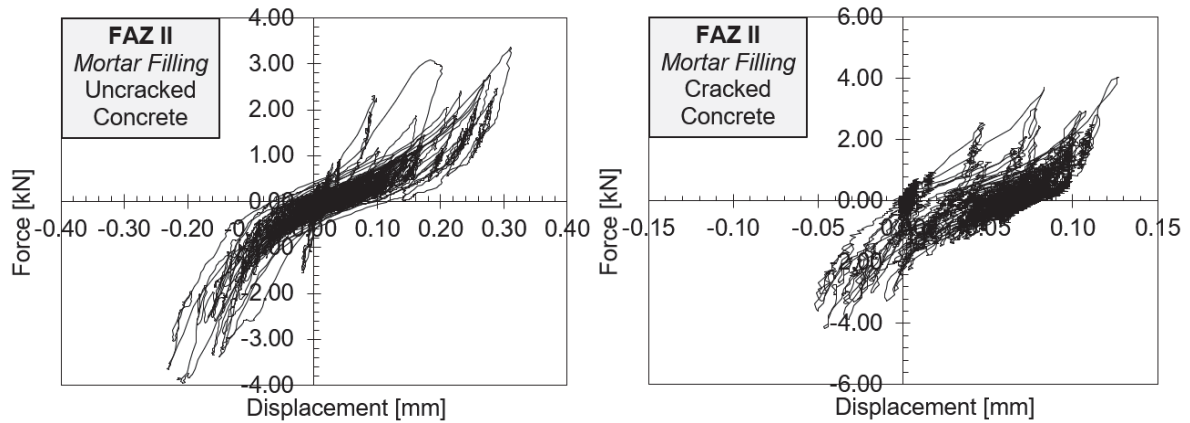


Figure 4.21. Force-displacement relationships for the FAZ II Traditional, FAZ II EQ-Rod, FAZ II Traditional with Mortar Filling in uncracked and cracked concrete (from one of the three tests with 100% EQ₁).

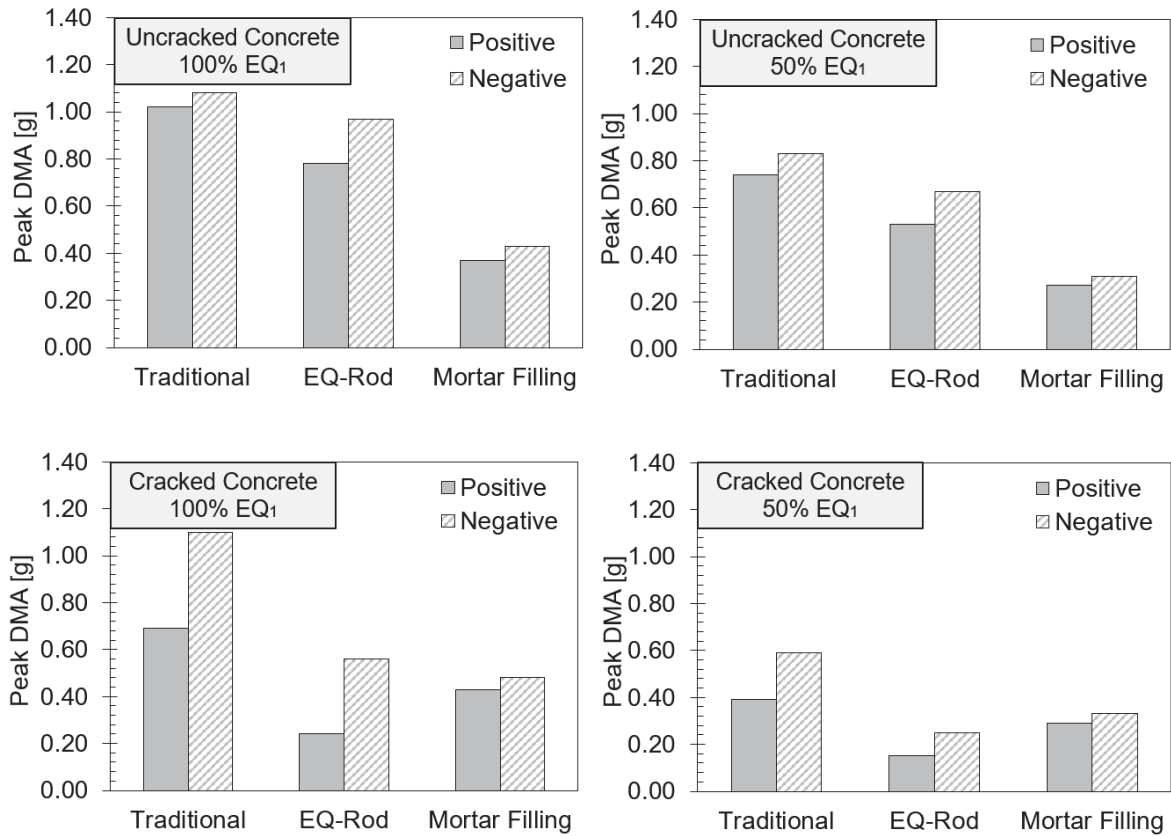


Figure 4.22. Peak Driving Mass Acceleration (DMA) for the FAZ II Traditional, FAZ II EQ-Rod, FAZ II Traditional with Mortar Filling in uncracked and cracked concrete (results from one test with 100% EQ₁ and its aftershock EQ₁-50).

The complete table with the results from all the earthquake motions in terms of peak driving mass accelerations, forces and displacements can be found in **Appendix A** as well as in the final research report (Pampanin et al. 2017). Elaborating the output data, i.e.

estimating the mean values, the main findings from Phase 1 of the experimental campaign are summarized.

✓ **Uncracked concrete blocks**

- *FAZ II Traditional anchor vs. FAZ II EQ-Rod*: reduction in terms of driving mass forces and accelerations in the range of 10-15% for the input signals and of 15-30% for the aftershocks;
- *FAZ II Traditional anchor vs. FAZII Traditional anchor with mortar filling*: reduction in terms of driving mass forces and accelerations in the range of 40-50% for the input signals and of 50-60% for the aftershocks.

The higher reduction related to the solution with mortar filling is mainly due to the lack of dynamic impact (pounding) for the presence of gaps between steel plate/anchor and concrete/anchor of the EQ Rod 2.0 prototype. The anchor with mortar filling thus acts as a more rigid element, while EQ-Rod allows for isolation and dissipation. It appears that a combination of the two concepts (filling the gap and adding a tight-fit EQ-Rod dissipative system) would be able to provide the best and most reliable benefits.

While, the appreciable increase in reduction of forces between Traditional anchor and EQ-Rod 2.0 solution for the aftershocks inputs when compared to the main shock is mostly due to the degradation of the EQ-Rod lowering and to the concrete crushing on contact. Even if apparently leading to a better performance of the non-structural system and protection of the anchor, this phenomenon is once again related to the dynamic impact due to the presence of gaps.

✓ **Cracked concrete blocks**

- *FAZ II Traditional anchor vs. FAZ II EQ-Rod*: reduction in terms of driving mass forces in the range of 20-30% and in terms of driving mass accelerations in the range of 25-40% for the input signals. The reduction is equal to 30-40% for both accelerations and forces considering the aftershocks;
- *FAZ II Traditional anchor vs. FAZII Traditional anchor with mortar filling*: reduction of driving mass forces and accelerations in the range of 50-60% for either the input signals or the aftershocks.

Overall, the performance and benefits of EQ-Rod 2.0 in cracked concrete appears superior to that in uncracked concrete. It should be noted that, in addition to the inherent

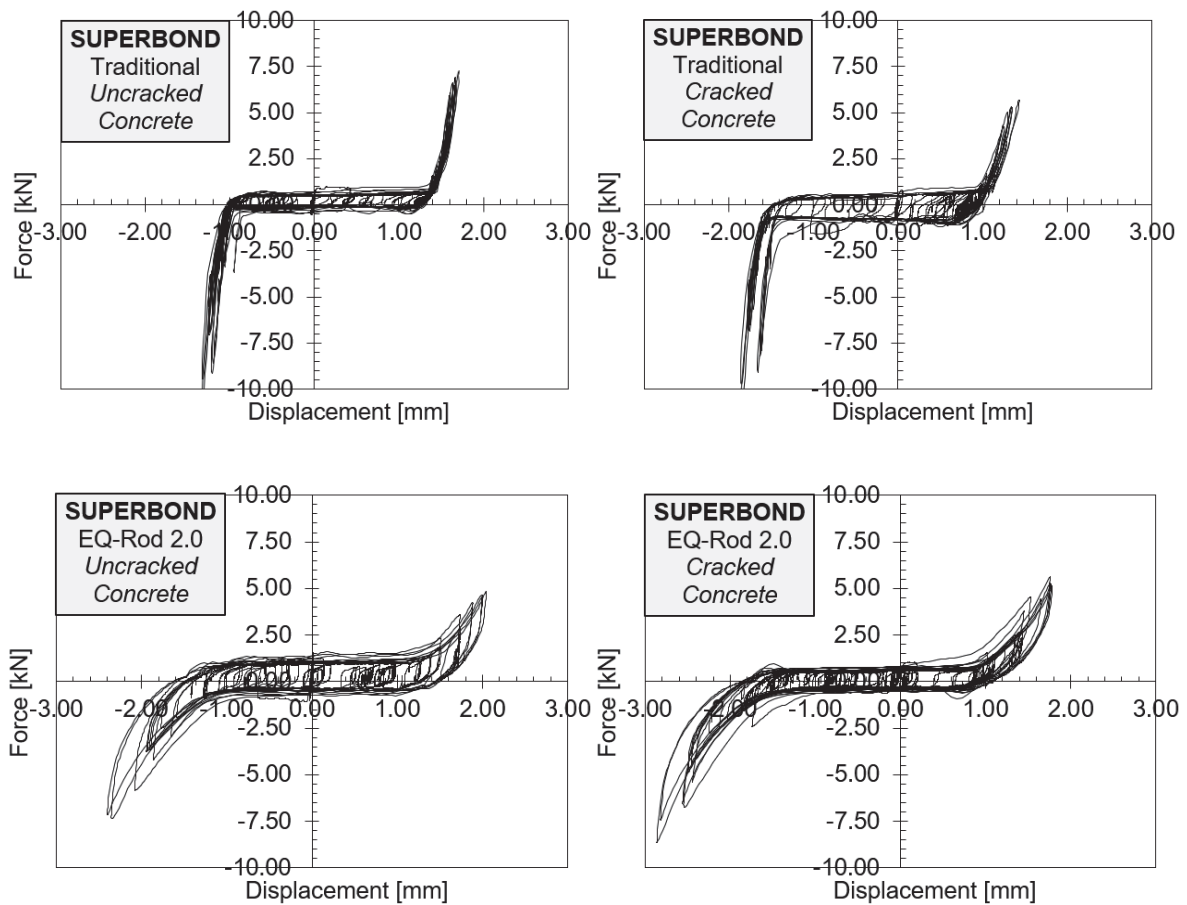
isolation-dissipation mechanism, EQ-Rod 2.0 anchor has greater displacements in cracked concrete. The system has thus lower frequencies (higher period) and attracts less forces moving towards the de-amplification part of the spectra.

- **Ground motion input tests, Superbond anchors**

(PHASE 2 – July 2017/September 2017)

In the second phase of the experimental campaign, shaking table tests were performed for all the proposed configurations of chemical anchors (Traditional, EQ-Rod 2.0 and Mortar Filling) in uncracked and cracked concrete.

As for the expansion anchors, also in this case more reliable results were provided performing for each input motion tests on three different fasteners of the same typology. Test results in terms of force/displacement curves of the driving mass are shown in Figure 4.23 for just one test of an input record (EQ₁) for all the three types of anchors. While, in Figure 4.24 a comparison is made in terms of peak driving mass acceleration, where “positive” and “negative” refer to the directions of loading/motions.



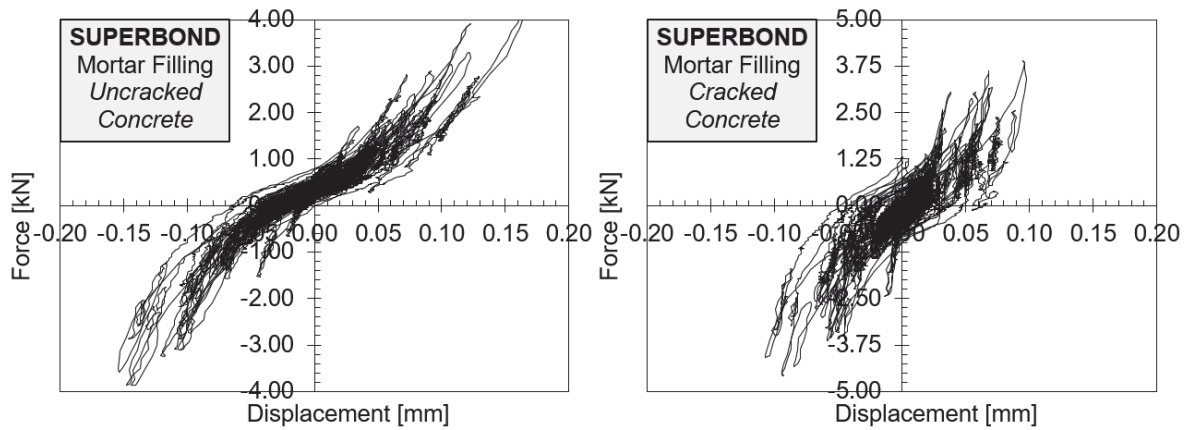


Figure 4.23. Force-displacement relationships for the Superbond Traditional, Superbond EQ-Rod, Superbond Traditional with Mortar Filling in uncracked and cracked concrete (from one test with 100% EQ1).

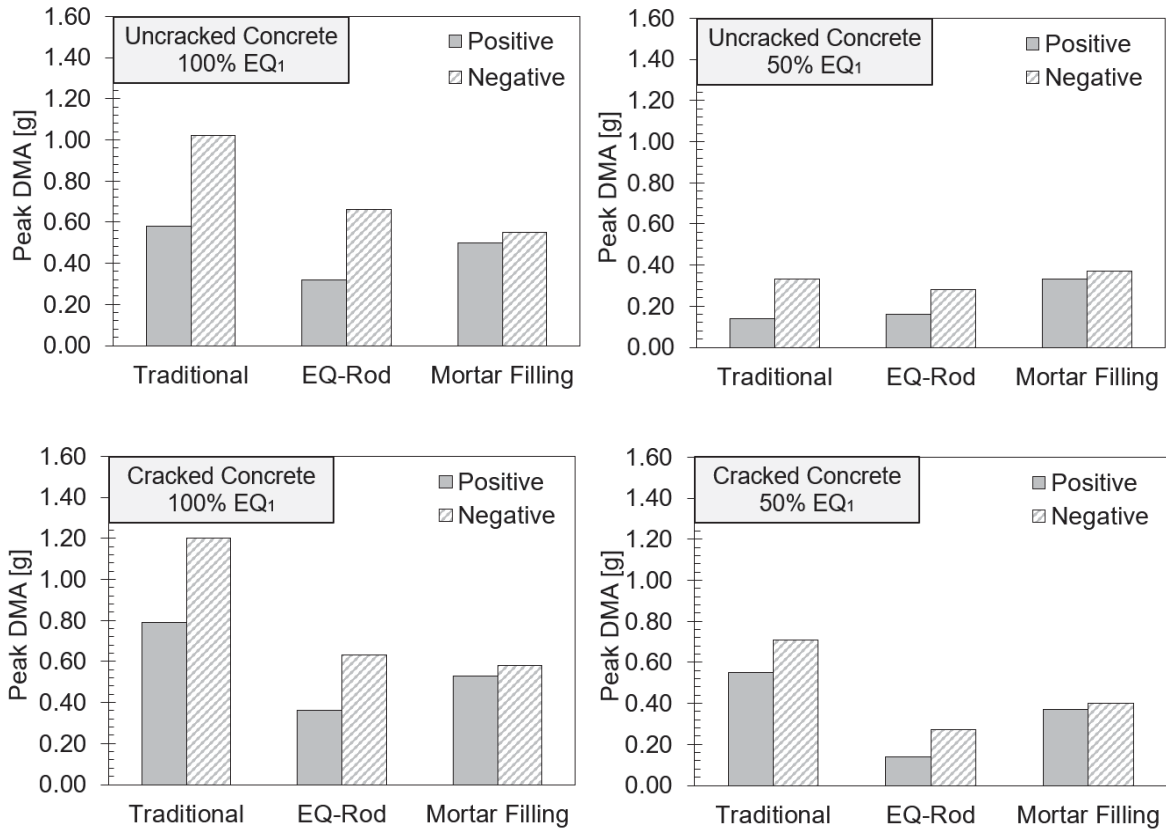


Figure 4.24. Peak Driving Mass Acceleration (DMA) for the Superbond Traditional, Superbond EQ-Rod, Superbond Traditional with Mortar Filling in uncracked and cracked concrete (from one tests with 100% EQ1 and its aftershock EQ1-50).

The complete table with the results from all the earthquake motions in terms of peak driving mass accelerations, forces and displacements can be found in **Appendix A** or in the final research report (Pampanin et al. 2017). Elaborating the output data, i.e. estimating the mean values, the main outcomes from Phase 2 of the experimental campaign are listed below.

✓ **Uncracked concrete blocks**

- *Superbond Traditional anchor vs. Superbond EQ-Rod*: the EQ-Rod solution provides a reduction in terms of driving mass forces in the range of 10-25% and in terms of driving mass accelerations in the range of 20-30% considering the input signals. The reduction is equal to 30-40% for accelerations and forces for the aftershocks;
- *Superbond Traditional anchor vs. Superbond Traditional anchor with mortar filling*: the mortar filling solution provides a reduction in terms of driving mass forces and accelerations in the range of 40-50% for both the input signals and the aftershocks.

These results can be justified taking into account the same considerations previously described for Phase 1 of testing.

✓ **Cracked concrete blocks**

- *Superbond Traditional anchor vs. Superbond EQ-Rod*: the EQ-Rod solution provides a reduction in terms of driving mass forces and accelerations in the range of 20-30% for the input signals and of 30-40% for the aftershocks;
- *Superbond Traditional anchor vs. Superbond Traditional anchor with mortar filling*: the mortar filling Solution provides a reduction in terms of driving mass forces and accelerations in the range of 40-50% for the input signals and the aftershocks.

Considering that the test setup was developed for shear-only tests and not for tension (extraction) tests, the shear behaviour of the system was not expected to be influenced by the cracking of the concrete block. No significant differences between cracked and uncracked blocks were noted.

4.4.3.7 Conclusions from the experimental campaign

The experimental test results confirmed how the concept of adding damping to a fastener can be adopted for improving the seismic performance of the system, because it is able to reduce the accelerations and forces on the connected non-structural component, thus it can be considered a damage-control solution for such a type of application.

Making a comparison between the two different research, made in New Zealand in 2008 and in Italy in 2017, the following considerations from the test results can be highlighted.

✓ *Difference between the tested FAZ II anchors*

The features of the FAZ II (M12) anchors used for the experimental campaign at the University of Canterbury in New Zealand (reported in Pampanin et al. 2008) were different from the FAZ II (M12) anchors used for the tests at Sapienza University of Rome. In fact, NZ FAZ II (M12) had an unthreaded part longer than the threaded part while the new FAZ II M12 has the threaded part as long as the fastener total length. Due to this change, the tolerance/gap between the fastener and the concrete is not present anymore so there is only a gap between the steel plate and the anchor. Furthermore, the gap/tolerance of 2mm is now reduced to 1mm (Figure 4.25, left).

✓ *Difference between the EQ-Rod prototypes*

Concerning the configuration with the EQ-Rod, the first generation of this solution was composed of a damper adherent to the rod, i.e. there was no gap between the anchor rod and the inner rubber EQ-Rod damper, while the new EQ-Rod 2.0 provided by Fischer incorporates a gap between the anchor rod and the inner diameter of the EQ-Rod (Figure 4.25, right) to facilitate its application in the common practice mainly for existing systems. However, as observed by different tests, this gap introduced significant dynamic effects which can impair the performance of the EQ-Rod mechanism (isolation and dissipation), leading in some cases to detrimental rather than beneficial effects. Overall, the dissipation mechanism of the system is reduced by this different mechanism. For this reason, an improvement of the system is recommended and suggested to fully exploit the novelty of the dissipative/isolation mechanism of the EQ-Rod solution and obtain a greater and robust reduction of the driving mass accelerations when compared to the traditional anchor (with or without mortar filling).

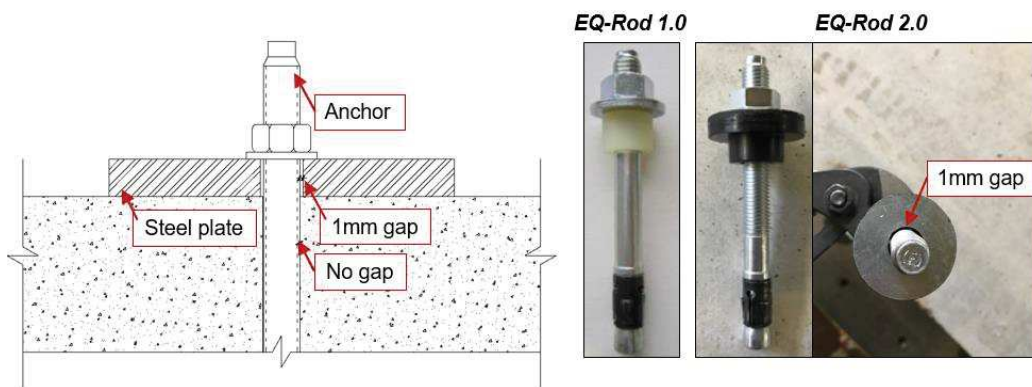


Figure 4.25. Left: Configuration with 1mm gap for the M12 FAZII anchors tested in Rome. Right: Difference between EQ-Rod 1.0 (no gap between dissipater and rod) and the EQ-Rod 2.0 (1mm gap between dissipater and rod).

✓ Bearing actions and permanent deformation of the damper

Due to the larger geometric tolerances between the EQ-rod and the fastener rod (inner tolerance/gap) as well as probably due to the different material of the new EQ-Rod when compared to the initial prototype, during the described tests the bearing stresses on the rubber material led sometimes to the yielding of the rubber damper with permanent deformations and amplifications of the dynamic effects (Figure 4.26).

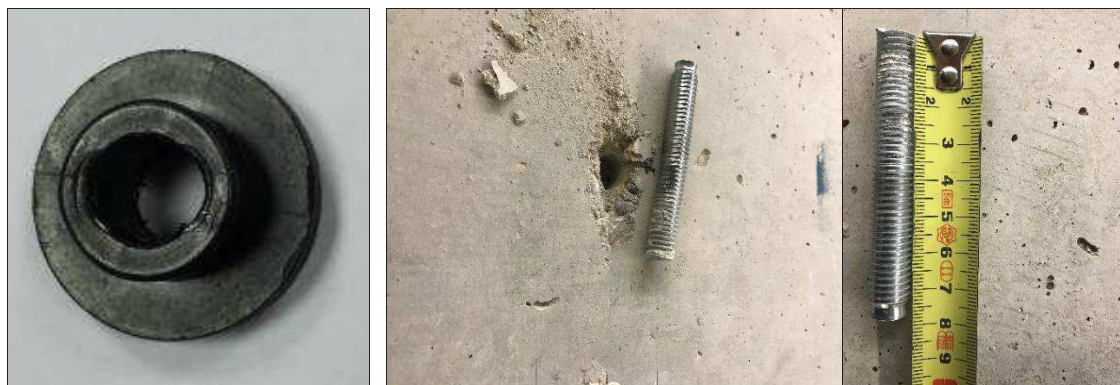


Figure 4.26. Left: Permanent deformation and enlargement of the inner diameter of the EQ-Rod. Right: Failure of the anchor rod after sinusoidal tests.

This in turns reduced the efficiency of the EQ-Rod system as a damping element but also compromised its fatigue (long-term) life. In fact, this behaviour produced a larger dynamic impact mechanism whereby the fastener surrounded by EQ-Rod could fracture at earlier stages (when compared to the traditional rod not equipped with EQ-Rod), as observed

during some sinusoidal tests. The lack of gap between steel rod and concrete might also played some role in increasing the impact shear forces on the steel section.

However, different solutions can be suggested (see Pampanin et al. 2017) for improving the behaviour of the EQ-Rod solution and mitigating all the problems previously highlighted.

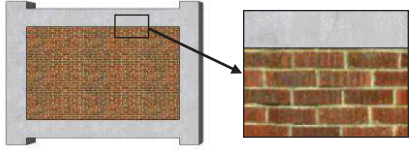
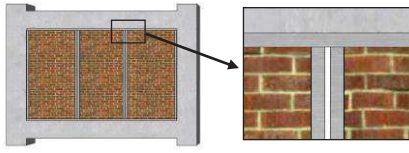
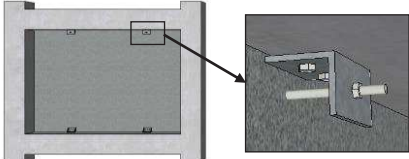
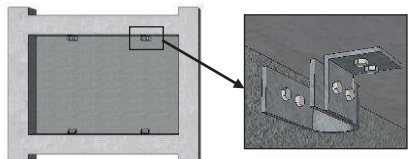
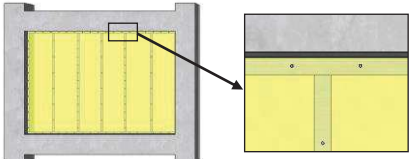
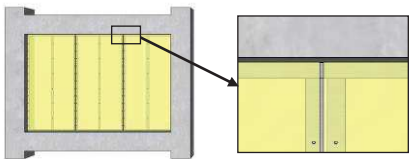

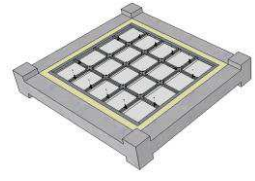
4.5 Conclusions

This Chapter has provided an overview of the innovative low-damage technologies developed in the last decades, and improved/refined or developed in more recent years, for both structural and non-structural components. These cost-affordable solutions can be properly designed to withstand higher level of inter-storey drift ratios, thus are capable of limiting the damage of these building elements after earthquakes, consequently reducing the expected losses in terms of either repair costs or downtime.

Low-damage systems based on post-tensioned rocking dissipative connections have been initially proposed for the structural skeleton. Despite these damage-resistant structural connections have been deeply studied in terms of seismic performance through both experimental and numerical investigations, refinements of this technology are still developing, as the application of the hybrid system to mixed material (e.g. timber-concrete connections). Furthermore, in recent years, building on the same damage-control concept and in order to target an integrated low-damage building system, innovative solutions have been proposed and initially studied for both vertical, e.g. infill walls, cladding systems, drywall partitions, and horizontal, e.g. ceilings, non-structural elements. These solutions rely upon connections detailed with relative movement between components and/or supplemental dissipation devices. Table 4.3 summarizes some of the low-damage solutions proposed for all these non-structural components.

Combining these damage-mitigation technologies (dry jointed ductile connections for frames and walls, articulated solutions for flooring systems, low damage infilled walls/facade/cladding connections and fit-outs), an integrated “earthquake proof” system can be identified. This system represents the next generation of buildings that our modern society is expecting. Although initial investigations on this low-damage structural/non-structural solution have been carried out, more research studies are needed to prove the higher seismic performance of the overall system when compared to a “traditional” building as well as to provide evidence on its benefits in terms of reducing the expected post-earthquake losses.

Table 4.3. Summary of available low-damage solutions for non-structural systems.

Component	Traditional system	Low-damage system
<p>Infill wall</p> <p>Monolithic masonry wall (bricks bounded by mortar)</p>	 <p>Masonry panels built into horizontal and vertical steel profiles with internal gaps (between panels, with the surrounding frame)</p>	 <p>Masonry panels built into horizontal and vertical steel profiles with internal gaps (between panels, with the surrounding frame)</p>
<p>Precast cladding</p> <p>Cladding panels connected using bearing connections (bottom) and tie-back or slotted connections (top)</p>	 <p>Cladding panels connected using bearing connections (bottom) and U-Shaped Flexural plates (top)</p>	 <p>Cladding panels connected using bearing connections (bottom) and U-Shaped Flexural plates (top)</p>
<p>Drywall partition</p> <p>Gypsum panel attached to both the horizontal tracks and vertical studs of the steel frame using screws</p>	 <p>Vertical gypsum panels separated by internal and lateral gaps and only attached to the vertical studs using screws</p>	 <p>Vertical gypsum panels separated by internal and lateral gaps and only attached to the vertical studs using screws</p>
<p>Suspended ceiling</p> <p>Fully floating system attached to the main structure through the suspended elements</p>	 <p>Fully floating suspended ceiling with an elastic isolation foam into the lateral gaps</p>	

Finally, in the last section of this Chapter, experimental tests (1D shake-table) on an innovative post-installed earthquake-resistant fastener are described. An anchor with a supplemental damping is proposed and studied with the aim of improving the seismic response of non-structural systems anchored to concrete structures. The first prototype of this solution was developed in 2008, while a new system (EQ-Rod 2.0) is now considered, conceived as an easily applicable solution for either expansion or chemical fasteners. The seismic performance of this system has been deeply studied through shake table tests using specific testing protocols for both uncracked and cracked concrete.

The efficiency of the EQ-Rod solution are evaluated in terms of driving mass (i.e. non-structural element) acceleration or force reduction when compared to the application of traditional (expansion - FAZ II - and chemical - Superbond -) fasteners. The experimental test results confirmed how the concept of adding damping to a fastener can be adopted to improve the seismic performance of the system. In fact, making elaborations of the experimental data, thus estimating mean values from all the results, the main outcomes are herein summarized:

- for the M12 **FAZ II anchors**, the EQ-Rod solution is able to reduce the acceleration and forces on the attached non-structural system in the range of **10-30%** for uncracked concrete and **20-40%** for the cracked concrete considering both input motions and aftershocks.
- for the M12 **Superbond anchors**, the EQ-Rod solution is able to reduce the acceleration and forces on the attached non-structural system in the range of **10-40%** for uncracked concrete and **20-40%** for the cracked concrete considering both input motions and aftershocks.

Nevertheless, when considering the results obtained when the traditional system is filled using mortar to close the existing gap between steel plate and anchor due to construction tolerances, the reductions are found to be in the range of 50-60%. This higher reduction, due to the lack of dynamic impact (pounding) for the presence of gaps between steel plate/anchor and concrete/anchor of the EQ Rod 2.0 prototype, suggests that a combination of the two concepts, i.e. filling the gap with mortar and adding a tight-fit EQ-Rod dissipative system, would be able to provide the best and most reliable benefits.

Finally, it is concluded that, notwithstanding greater advantages could be obtained improving the proposed EQ-Rod prototype, the concept of adding supplemental damping can

be considered as a damage-control solution for such type of applications. After earthquakes the damage to the connected non-structural element can be prevented and consequently the repair action of the system may consist only in the eventual substitution of the external dissipative device.

4.6 References

- Abate M. (2015). Seismic Behaviour of Post-Installed Anchors: Non-Structural Components and Art Objects Fastening, *PhD Thesis*, University of Padova, Padova, Italy.
- Aliaari M. and Memari A.M. (2007). Experimental Evaluation of a Sacrificial Seismic Fuse Device for Masonry Infill Walls, *Journal of Architectural Engineering*, 13: 111-125.
- Amaris A.D., Pampanin S., Bull D.K., Carr A.J. (2007). Development of a non-tearing floor solution for jointed precast frame systems, *Proceedings of 2007 NZSEE conference*, Palmerston North, New Zealand.
- Amaris A.D., Pampanin S., Bull D.K., Carr A.J. (2008) Solutions to control and minimize floor damage in precast concrete buildings under severe earthquake loading, *NZ Concrete Industry Conference*, Rotorua, New Zealand.
- Araya-Letelier G., Miranda E., Deierlein G. (2019). Development and Testing of a Friction/Sliding Connection to Improve the Seismic Performance of Gypsum Partition Walls, *Earthquake Spectra* 35(2): 653-677.
- Baird A., Palermo A., Pampanin S. and Riccio P. (2011). Focusing on reducing the earthquake damage to Façade Systems, *Bulletin of New Zealand Society of Earthquake Engineering*, 44(2): 108-120.
- Baird A., Palermo A., and Pampanin S. (2013). Controlling Seismic Response using Passive Energy Dissipating Cladding Connections, *Proceedings of 2013 NZSEE Conference*, Wellington, New Zealand.
- Baird A., Smith T., Palermo A., Pampanin S. (2014). Experimental and numerical Study of U-shape Flexural Plate (UFP) dissipators, *Proceedings of 2014 NZSEE Conference*, Auckland, New Zealand.
- Buchanan A.H., Palermo A., Carradine D.M. and Pampanin S. (2011). Post-Tensioned Timber Frame Buildings, *The Structural Engineer*, 89(17): 24-30.
- Cattanach A., Pampanin S. (2008). 21st century precast: the detailing and manufacture of NZ's first multi-storey PRESSS-building, *NZ Concrete Industry conference*, Rotorua, New Zealand.
- Chang K. C., Lin Y.Y., Lai M.L. (1998). Seismic analysis and design of structures with viscoelastic dampers, *Journal of Earthquake Technology*, 35(4): 180.
- Ciurlanti J., Bianchi S., Pampanin S. (2019). Shaking table tests on post-installed traditional and dissipative fasteners in uncracked and cracked concrete, *Proceedings of the 7th ECCOMAS Thematic Conference on Computational Methods in Structural Dynamics and Earthquake Engineering (COMPdyn)*, Crete, Greece.
- Devereux C.P., Holden T.J., Buchanan A.H., Pampanin S. (2011). NMIT arts & media building – damage mitigation using post-tensioned timber walls. Proceedings of the ninth Pacific conference on earthquake engineering, *Building an Earthquake-Resilient Society*, Auckland, New Zealand.

- Dhakal R.P., Muhammad R., Bhatta J., Sullivan T.J., MacRae G.A., Clifton G.C., Jia L.J. and Xiang P. (2019). Shake Table Tests of Multiple Non-Structural Elements in a Low – Damage Structural Steel Building, *4th International Workshop on the Seismic Performance of Non-Structural Elements (SPONSE)*, Pavia, Italy.
- Eligehausen R. (1991). Behavior, design and testing of anchors in cracked concrete, *ACI Structural Journal*, 130: 123-175.
- Eligehausen R. and Balogh T. (1995). Behavior of fasteners loaded in tension in cracked reinforced concrete, *ACI Structural Journal*, 92(35).
- Eligehausen R., Mallée R., Silva J.F. (2006). *Anchorage in Concrete Construction*, 1st Edition, Ernest and Sohn Publisher, Berlin, Germany.
- Federal Emergency Management Agency (2011). *Reducing the risks of non-structural earthquake damage – a practical guide, FEMA E-74*, Washington, DC
- fib (2003). *International Federation for Structural Concrete*, Bulletin No. 27, Lausanne, Switzerland.
- Filiatrault A., Mosqueda G., Retamales R., Davies R., Tian Y., and Fuchs J. (2010). Experimental Seismic Fragility of Steel Studded Gypsum Partition Walls and Fire Sprinkler Piping Subsystems, *presented at the ASCE Structures Congress*, Orlando, Florida.
- Goodno, B.J. (1998). *Ductile cladding connection systems for seismic design: National Institute of Standards and Technology*, Building and Fire Research Laboratory, Gaithersburg, MD.
- Grigorian C.E., Yang T.S., Popov E. (1993). Slotted Bolted Connection Energy Dissipators, *Earthquake Spectra*, 9(3): 491-504.
- Hoehler M. S., Mahrenholtz P., Eligehausen R. (2011). Behavior of Anchors in Concrete at Seismic-Relevant Loading Rates, *ACI Structural Journal*, 108(2): 238-247.
- Johnston H.C., Watson C.P., Pampanin S., Palermo A. (2014). Shake table testing of an integrated low-damage frame building, *Proceedings of 2014 NZSEE Conference*, Auckland, New Zealand.
- Kam W.Y., Pampanin S., Elwood K. (2011). Seismic performance of reinforced concrete buildings in the 22 February Christchurch (Lyttleton) earthquake, *Bulletin New Zealand Society of Earthquake Engineering*, 44(4): 239–279.
- Kelly, J.M., Skinner, R.I., Heine, A.J. (1972). Mechanisms of Energy Absorption in Special Devices for use in Earthquake Resistant Structures, *Bulletin of the New Zealand Society for Earthquake Engineering*, 5(3).
- Mahrenholtz P. and Eligehausen R. (2010). *Behavior of anchor groups installed in cracked concrete under simulated seismic actions. Fracture Mechanics of Concrete and Concrete Structures - Assessment, Durability, Monitoring and Retrofitting of Concrete Structures*, B. H. Oh, et al. (eds), Korea Concrete Institute, Seoul.
- Mahrenholtz P., Hutchinson T.C., and Eligehausen R. (2014). Shake Table Tests on Suspended Nonstructural Components in Cyclically Cracked Concrete, *Journal of Structural Engineering*, 140(11).

- Mahrenholtz P., Elgehausen R., Hutchinson T.C., Hoehler M.S. (2016). Behavior of post-installed anchors tested by stepwise increasing cyclic load protocols, *ACI Structural Journal*, 113: 997-1008.
- Marriott D., Pampanin S., Bull D., Palermo A. (2008). Dynamic testing of precast, post-tensioned rocking wall systems with alternative dissipating solutions, *Bulletin of New Zealand Society Earthquake Engineering*, 41(2): 90–103.
- Marriott D., Pampanin S., Palermo A. (2009). Quasi-static and pseudo-dynamic testing of unbonded post-tensioned rocking bridge piers with external replaceable dissipaters, *Earthquake Engineering Structural Dynamics*, 38(3): 331–354.
- Mohammadi M. and Mahalleh R.M.G. (2011). A new infilled steel frame with engineering properties, *Proceedings of the Institution of Civil Engineers*, London, England.
- Morandi P., Milanese R.R., Magenes G. (2018). Innovative solution for seismic-resistant masonry infills with sliding joints: in-plane experimental performance, *Engineering Structures*, 176: 719-733.
- Palermo A., Pampanin S., Buchanan A.H., Newcombe M.P. (2005). Seismic design of multi-storey buildings using Laminated Veneer Lumber (LVL), *Proceedings of NZ Society for Earthquake Engineering conference*, Wairakei, New Zealand.
- Palermo A., Pampanin S., Buchanan A. (2006). Experimental investigations on LVL seismic resistant wall and frame subassemblies, *1st ECEES*, Geneva, Italy.
- Pampanin S. (2005). Emerging solutions for high seismic performance of precast -prestressed concrete buildings, *Journal of Advanced Concrete Technologies*, 3(2): 202–222.
- Pampanin S. (2012). Reality-check and renewed challenges in earthquake engineering: implementing low-damage structural systems – from theory to practice, *Bulletin of New Zealand Society and Earthquake Engineering*, 45(4): 137–160.
- Pampanin S. (2015). *Towards the “Ultimate Earthquake-Proof” Building: Development of an Integrated Low-Damage System*, Perspectives on European Earthquake Engineering and Seismology (A. Ansal, ed.), Geotechnical, Geological and Earthquake Engineering 39, Springer Nature, Switzerland.
- Pampanin S., Palermo A., Buchanan A., Fragiacomio M., Deam B (2006). Code provisions for seismic design of multi-storey post-tensioned timber buildings, *CIB Workshop*, Florence, Italy.
- Pampanin S., Moghaddasi M., Quintana-Gallo P., Rieder A. (2008). *EQ-Rod a New Generation of Earthquake-Resistant Fasteners. Report prepared for Fischerwerke Artur Fischer GmbH & Co. KG*, University of Canterbury, Christchurch, New Zealand.
- Pampanin S., Bianchi S., Ciurlanti J. (2017). *Shake table tests of post-installed anchors with supplemental damping (EQ-Rod 2.0)*, Report prepared for Fischerwerke Artur Fischer GmbH & Co. KG, Sapienza University of Rome, Rome, Italy.
- Pampanin S., Ciurlanti J., Bianchi S., Palmieri M., Grant D., Granello G., Palermo A., Correia A. (2019). Overview of SERA Project: 3D shaking table tests on an integrated low-damage building

- system, *Proceedings of 4th International Workshop on the Seismic Performance of Non-Structural Elements (SPONSE)*, Pavia, Italy.
- PCI (2007). *Architectural Precast Concrete*, Chicago, IL., USA: PCI Architectural Precast Concrete Manual Committee.
- Petrone C., Magliulo G., Manfredi G. (2017). Shake table tests on standard and innovative temporary partition walls, *Earthquake Engineering and Structural Dynamics*, 46(10).
- Pinelli, J.P., Craig, J.I., & Goodno, B.J. (1995). Energy-Based Seismic Design of Ductile Cladding Systems, *Journal of Structural Engineering*, 121(3): 567-578.
- Pourali A., Dhakal R.P., MacRae G.A., and Tasligedik A.S. (2017). Fully-floating suspended ceiling system: experimental evaluation of the effect of mass and elastic isolation, *Proceedings of 16th World Conference on Earthquake Engineering*, Santiago, Chile.
- Preti M., Migliorati L., Giuriani E. (2014) Experimental testing of engineered masonry infill walls for post-earthquake structural damage control, *Bulletin of Earthquake Engineering*, 13: 2029–2049.
- Priestley M.J.N. (1991). Overview of PRESSS Research Program, *PCI Journal*, 36(4): 50–57.
- Priestley M.J.N., Sritharan S., Conley J.R., and Pampanin S. (1999). Preliminary Results and Conclusions From the PRESSS Five-Story Precast Concrete Test Building, *PCI J.*, 44(6): 42–67.
- Quintana-Gallo P., Moghaddasi M., Pampanin S. and Bergmeister K. (2018). Shake table tests of post-installed fasteners in concrete with supplemental damping, *ACI Structural Journal*, 115(3): 595-606.
- Rieder (2009). Seismic Response of Post-Installed Anchors in Concrete. *PhD Dissertation*, University of Natural Resources and Life Sciences, Vienna, Austria.
- Sarti F., Palermo A. and Pampanin S. (2016). Fuse-Type External Replaceable Dissipaters: Experimental Program and Numerical Modeling, *Journal of Structural Engineering*, 142(12).
- Sivanerupam S., Wilson J.L., Gad E.F., and Lam N.T.K. (2014). Drift Performance of Point Fixed Glass Façade Systems, *Advances in Structural Engineering*, 17(10): 1481-1495.
- Stanton J.F., Stone W.C., Cheok G.S. (1997). A hybrid reinforced precast frame for seismic regions, *PCI Journal*, 42(2): 20–32.
- Structural Engineers Associate of California (1995). *Performance-based seismic engineering*, SEAOC Vision 2000, Sacramento, California, USA.
- Tasligedik A.S. (2014). Damage-Mitigation Strategies for Non-structural Infill Walls, *PhD Thesis*, University of Canterbury, Christchurch, New Zealand.
- Tasligedik A.S., Pampanin S. and Palermo A. (2014). Low damage seismic solutions for non-structural drywall partitions, *Bulletin of Earthquake Engineering*, 13(4): 1029–1050.
- Tasligedik A.S. and Pampanin S. (2016). Rocking Cantilever Clay Brick Infill Wall Panels: A Novel Low Damage Infill Wall System, *Journal of Earthquake Engineering*, 21(7): 1023-1049.

Vintzéleou E. and Eligehausen R. (2012). Behaviour of Fasteners under Monotonic or Cyclic Shear Displacements, Anchors in Concrete – Design and Behavior, *ACI Special Publication*, 130(7): 181-204.

5. Convenience of implementing damage-resistant building systems

5.1 Introduction

This Chapter investigates the cost/performance benefits due to the application of innovative low-damage technologies for both structural and non-structural systems. Although these solutions have been proposed in order to reduce the post-earthquake damage, thus different numerical and experimental studies on their seismic performance are available in literature, investigations are needed to quantify how much they can reduce the seismic losses (in terms of repair cost, downtime).

Therefore, cost/performance-based evaluations of reinforced concrete multi-storey buildings (3, 5, 7 storeys) comprising alternative damage-resistant solutions (low-damage structural; low-damage non-structural; integrated low-damage structural/non-structural system) and different structural configurations (frames, walls) and non-structural components (heavy or light facades, heavy or light partitions, ceilings) are performed. The results in terms of seismic performance and post-earthquake losses are provided and discussed. Moreover, further studies are carried out to highlight the benefits of applying low-damage technologies for buildings located in either low or high seismicity zones. Finally, more investigations on the seismic performance are carried out for the case of precast concrete claddings with the aim of implementing risk assessment analysis, thereby proving the convenience of low-damage systems also in terms of probability of not being damaged compared to more traditional solutions.

5.2 Cost/performance evaluation of low-damage systems

The current seismic assessment and design of buildings follow the performance-based earthquake engineering philosophy (Cornell et al. 2002; Krawinler et al. 2004), whose rigorous and probabilistic approach is summarized in Figure 5.1.

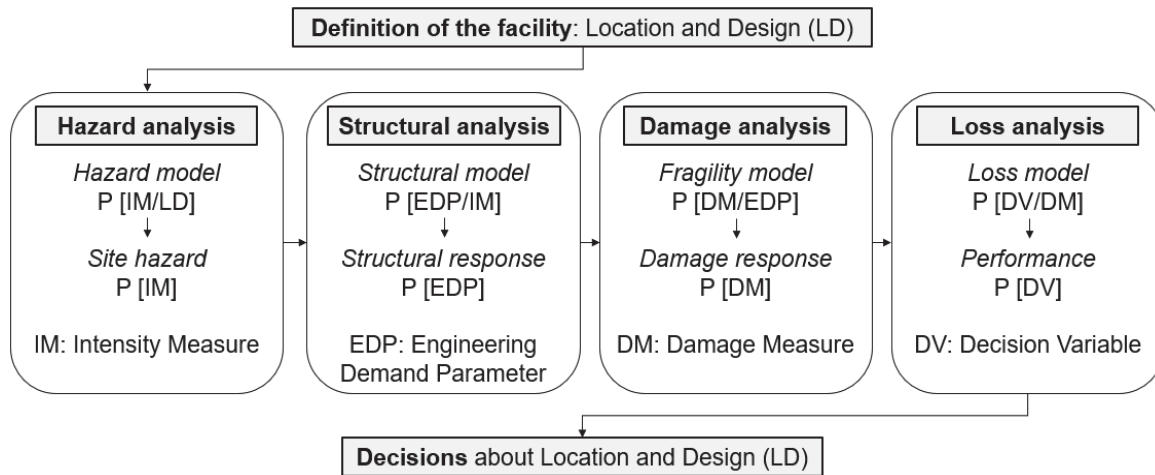


Figure 5.1. Framework of the Performance-Based Earthquake Engineering (PBEE) methodology (modified after Porter 2003).

The decision-making process of seismic risk has been improved through the application of validated procedures that aim to define performance metrics which are relevant to stakeholders to make informed decisions (Moehle and Deierlein 2003). In fact, performance measures significant for decision makers are repair costs, downtime and casualties, not only the building seismic response in terms of typical engineering parameters such as inter-storey drift ratios or floor accelerations. The performance-based earthquake engineering was initially expressed in form of design seismic intensity levels for either structural or non-structural components, as presented in SEAOC Vision 2000 in 1995. Then, more refined procedures were implemented to probabilistically determine the building seismic damage and related socio-economic losses and practical tools were developed to apply the methodology (e.g. Performance Assessment Calculation Tool of FEMA P-58 2012).

The low-damage technologies proposed for both structural and non-structural elements are able to mitigate the post-earthquake damage, consequently reduced direct and indirect losses are expected. The low-damage structural solutions have been extensively studied in terms of seismic performance through experimental tests and numerical investigations, and recent research has moved towards cost/benefit evaluations of the structural system (Garro 2017; Bianchi et al. 2018; Nuzzo et al. 2018). Nevertheless, cost/performance evaluations are needed to better investigate the

benefits related to the application of low-damage non-structural solutions and, specifically, to the implementation of integrated damage-resistant structural/non-structural systems.

With this aim, cost/performance-based investigations of multi-storey reinforced concrete buildings consisting of alternative low-damage building configurations are carried out and the results of these analyses (seismic performance, post-earthquake losses) are herein reported. In order to study the influence of the seismic hazard in the definition of the optimal low-damage configuration, the same cost/performance-based investigation is proposed for a building designed with reference to two different seismic zones (low and high seismicity).

Moreover, it is observed that the cost/performance-based evaluations are implemented adopting a Capacity Spectrum Method and non-linear static analysis. This pushover-based approach is a practical method accepted within the FEMA P-58 (2012) methodology, as an alternative to the application of simplified linear static analyses or more sophisticated non-linear time-history analyses. Considering that non-linear static analyses are arguably the best compromise between accuracy and simplicity and that several analyses are involved in the implemented study, the estimation of storey drift ratios and floor accelerations is carried out through this approach. Another non-linear static procedure that may be adopted for the cost/performance-based evaluations of multiple buildings is the Simplified Lateral Mechanism Analysis (SLaMA) - based approach. Although outside the scopes of the Thesis, this methodology is proposed and investigated in **Appendix B** as a promising tool for a daily use of practicing engineers for a rapid evaluation of economic losses for both the seismic assessment of existing buildings and the initial feasibility studies of new structures.

5.2.1 Description of the case-study buildings

Cost/performance-based evaluations are implemented for three reinforced concrete structures respectively of 3, 5 and 7 storeys. Considering the reference 5-storey building with global dimensions and plan geometry presented in Figure 5.2, the other two multi-storey structures are obtained parametrizing the number of storeys. The building use is commercial with a roof on the top floor and the structural system is composed of two seismic resistant four-bay frames in the longitudinal direction and two shear walls in the opposite direction. For implementing the proposed study, each building is combined with various non-structural components: three different exterior enclosures (cladding systems, infill walls, spider glazing); three cases of internal partitions (all light - gypsum - or heavy – masonry - partitions, mixed heavy/light partitions); suspended ceilings; building services and contents (Figure 5.3).

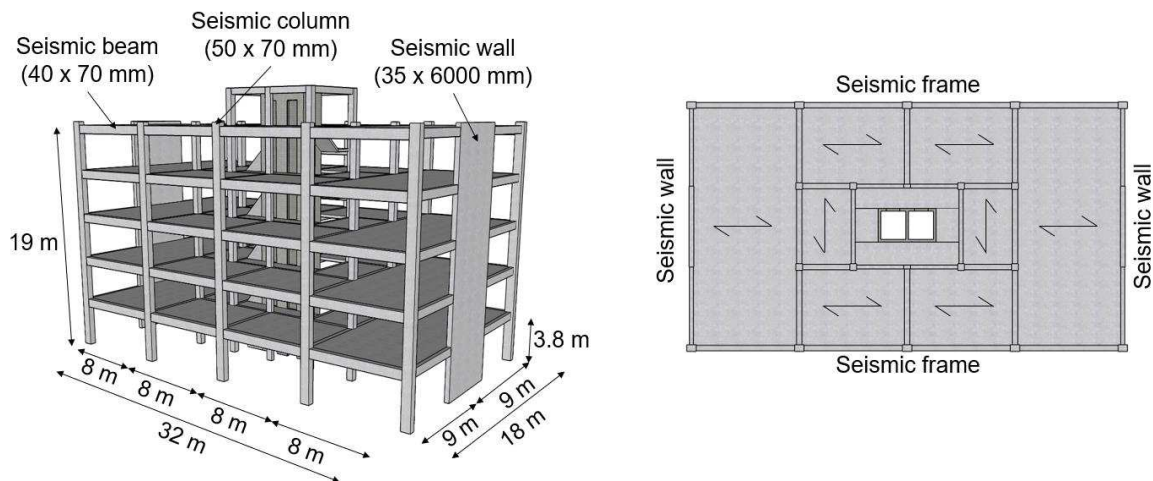


Figure 5.2. Dimensions and plan view of the structural system (Bianchi et al. 2018).

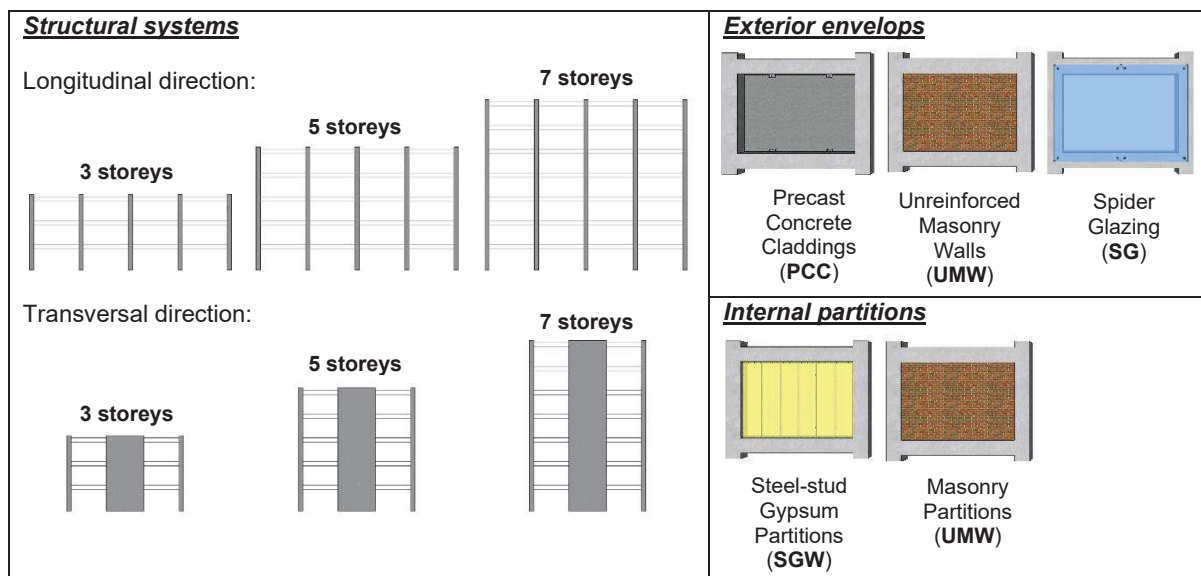


Figure 5.3. Structural systems (longitudinal views) and non-structural configurations (exterior enclosures, partitions) of the case-study buildings.

The buildings are designed referring to this structural scheme and related gravity loads (self-weight and live loads), moreover considering the seismicity from a high seismic area in Italy (Reggio Calabria). For each building (3, 5 and 7 storeys), both a monolithic structural skeleton and a low damage rocking dissipative (PRESSS) structure are designed, i.e. a total number of 6 different structural skeletons are obtained. All these structures are combined with traditional or low-damage non-structural systems, referring to the damage-resistant technologies for facades, partitions and ceilings previously presented and summarized in Table 4.3. As far as spider glazing curtain walls are also concerned, the application of K-type spider connectors with internal gaps proposed by Sivanerupan et al. (2014) is considered as low-damage solution for this building envelope, because

the façade has very high seismic performance compared to the use of more traditional X-type spider connectors. Consequently, four building configurations are identified for each case (3, 5 and 7 storeys):

- the monolithic cast-in-situ structure with traditional non-structural elements (benchmark structures);
- the low-damage structural skeleton with traditional non-structural elements;
- the monolithic building with low-damage non-structural components;
- the integrated structural/non-structural low-damage system.

All these cases (4 building systems) as well as the alternative configurations of exterior enclosures and partitions (3 monolithic or low-damage types of facades, 3 monolithic or low-damage partition wall configurations), define a total number of 108 cases (permutations) to be analysed for all the case-study structures (3, 5, 7 storeys).

5.2.2 Design of the structural systems

The design of both the monolithic and PRESSS structural skeletons is carried out at the Ultimate Limit State (ULS) level (475 years return period earthquake for an Importance Class 2) following the Direct Displacement-Based Design (DDBD) procedure developed by Priestley et al. (2007) and Pampanin et al. (2010). Referring to appropriate inter-story drift limits suggested by the design code (NTC 2018), good practice and/or material strain limits, the DDBD procedure consists of determining of the equivalent building Single Degree of Freedom (SDOF) system, with effective elastic stiffness (K_e), effective mass (m_e), effective height (H_e) and equivalent viscous damping (ξ_e) related to the target displacement (Δ_d). Reducing the 5% damped design spectrum (Figure 5.4, left) to account for the ductility/damping of the system, from the target displacement the effective period can be defined (T_e), as shown on the right of Figure 5.4, thus evaluating the SDOF effective stiffness (K_e) the building base shear can be calculated (V_b). Table 5.1 lists the parameters obtain by DDBD procedure for all the case-study structures.

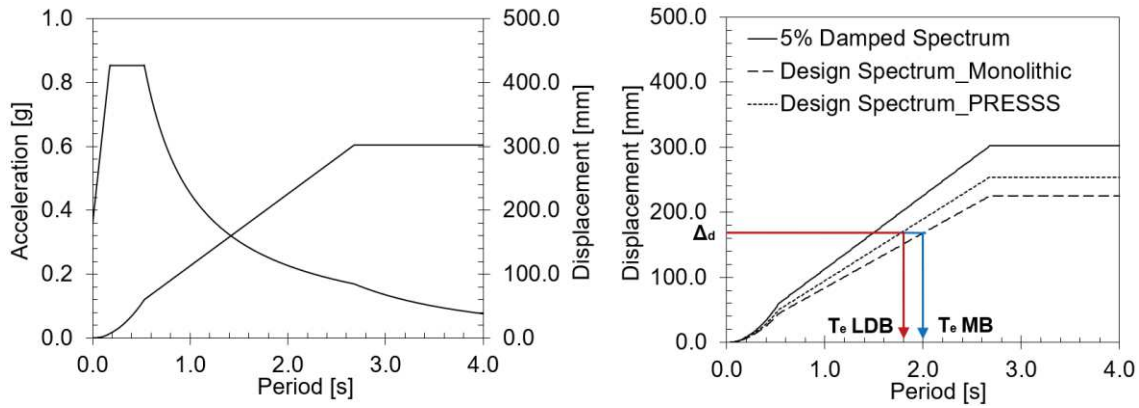


Figure 5.4. Left: 5% elastic spectrum at ULS (PGA of 0.27g, C soil type); Right: Design spectra for e.g. the frame systems of both monolithic and low-damage skeleton for the 5-storey case-study building and estimation of the effective periods from the design displacement.

Table 5.1. Parameters from DDBD procedure for all the case-study buildings (3, 5, 7 Storeys).

	Parameter	Monolithic Building (MB)		Low-damage Building (LDB)	
		Frame direction	Wall direction	Frame direction	Wall direction
3-Storey Building	θ_{design} [%]	2.0	1.0	2.0	1.0
	$\Delta_{yielding}$ [mm]	39.1	19.6	39.1	19.6
	Δ_{design} [mm]	170.9	85.4	170.9	85.4
	$m_{effective}$ [t]	1725.9	1725.9	1725.9	1725.9
	$H_{effective}$ [m]	8542.9	8542.9	8542.9	8542.9
	$\xi_{equivalent}$ [%]	20.7	20.6	12.0	12.0
	$T_{effective}$ [s]	2.0	1.0	1.8	0.9
	$K_{effective}$ [kN/m]	16472.1	65903.0	20986.0	83957.3
	V_{base} [kN]	2814.4	5630.0	3585.6	7172.4
5-Storey Building	θ_{design} [%]	2.0	1.2	2.0	1.2
	$\Delta_{yielding}$ [mm]	51.0	49.8	51.0	49.8
	Δ_{design} [mm]	222.97	162.3	222.97	162.3
	$m_{effective}$ [t]	2972.5	2831.4	2972.5	2831.4
	$H_{effective}$ [m]	13173.8	13526.5	13173.8	13526.5
	$\xi_{equivalent}$ [%]	20.7	18.4	12.0	10.4
	$T_{effective}$ [s]	2.7	1.9	2.4	1.7
	$K_{effective}$ [kN/m]	16658.3	31572.1	21223.3	40553.2
	V_{base} [kN]	3714.3	5124.7	4732.2	6582.5
7-Storey Building	θ_{design} [%]	1.5	1.3	1.5	1.3
	$\Delta_{yielding}$ [mm]	69.1	94.3	69.1	94.3
	Δ_{design} [mm]	230.6	238.1	230.6	238.1
	$m_{effective}$ [t]	4144.0	3947.6	4144.0	3947.6
	$H_{effective}$ [m]	18062.7	18543.5	18062.7	18543.5
	$\xi_{equivalent}$ [%]	18.6	16.1	11.0	9.4
	$T_{effective}$ [s]	2.7	2.7	2.4	2.4
	$K_{effective}$ [kN/m]	22777.5	21698.1	28618.2	27299.0
	V_{base} [kN]	5253.4	5165.7	6600.5	6499.1

Distributing the base shear throughout the structures, the internal actions to be used for the design of structural members can be determined, therefore, either the steel reinforcement of the monolithic connections or the dissipaters (internal fuse) and post-tensioned cables/tendons (initial force) of the PRESSSS connections can be designed. Low-damage elements are designed using a re-centering ratio λ equal to 1.25 (56% contribution from the unbonded post-tensioned tendons, 44% contribution from the dissipative devices).

It is finally highlighted that the structural design is implemented considering a C50/60 concrete, B 450C mild steel for both the internal reinforcement and the external dissipaters, and different types of cables/tendons for hybrid walls and beams depending on the dimensions available from commercial catalogues.

5.2.3 Building performance points

Numerical non-linear static (push-over and push-pull) analyses for all the case-study buildings (3, 5 and 7 storeys with both monolithic and PRESSSS structural skeleton) are carried out using Ruaumoko 2D software (Carr 2003) adopting a lumped plasticity approach. The monolithic structures are modelled by mono-dimensional elastic elements with plastic hinges at the end sections (Giberson elements), where the inelasticity is represented by appropriate moment-curvature relationships and stiffness-degrading hysteresis rules (i.e. Takeda). While, the PRESSSS structures are modelled through elastic members with two rotational springs working in parallel at the connection interfaces, one simulating the re-centering action of the post-tensioning cables/tendons (non-linear elastic), the other one representing the energy dissipation from the external mild steel dissipaters (elasto-plastic).

In addition to the bare frame models, for the building configurations with traditional external masonry walls, a second numerical model is implemented to take into account the contribution of these non-structural elements into the building response (the contribution to the global response of the other non-structural systems is not modelled). Consequently, infill walls are modelled through diagonal strut axial springs calibrated on the formulas proposed by Bertoldi et al. (1993) and using the Crisafulli (1997) hysteresis rule.

Push-over curves are obtained from non-linear static analyses and converted into acceleration-displacement curves in the Acceleration Displacement Response Spectra (ADRS) domain. Referring to the NTC 2018 code, four seismic intensity levels are considered (namely SLO, SLD, SLV, SLC, or, respectively Immediate Operational, Damage Control, Life Safety and Collapse Prevention) and

the related demand spectra were introduced into the same ADRS graph. The demand spectra are obtained from the elastic spectra using the η reduction factor supported by Priestley et al. (2007), in turn defined by the equivalent viscous damping from the building push-pull analyses.

Applying the Capacity Spectrum Method (ATC 40 1996), with the building equivalent viscous damping being derived from push-pull analyses, the maximum expected seismic displacements and accelerations (performance) of all the case-study buildings at each seismic intensity level can be identified (e.g. in Figure 5.5 for the 5-storey building in the ADRS domain, while in Tables 5.2 and 5.3 for the acceleration/displacement values of the Performance Points of all the case-study structures at SLV seismic intensity considering both the bare frame and infilled frame numerical modelling).

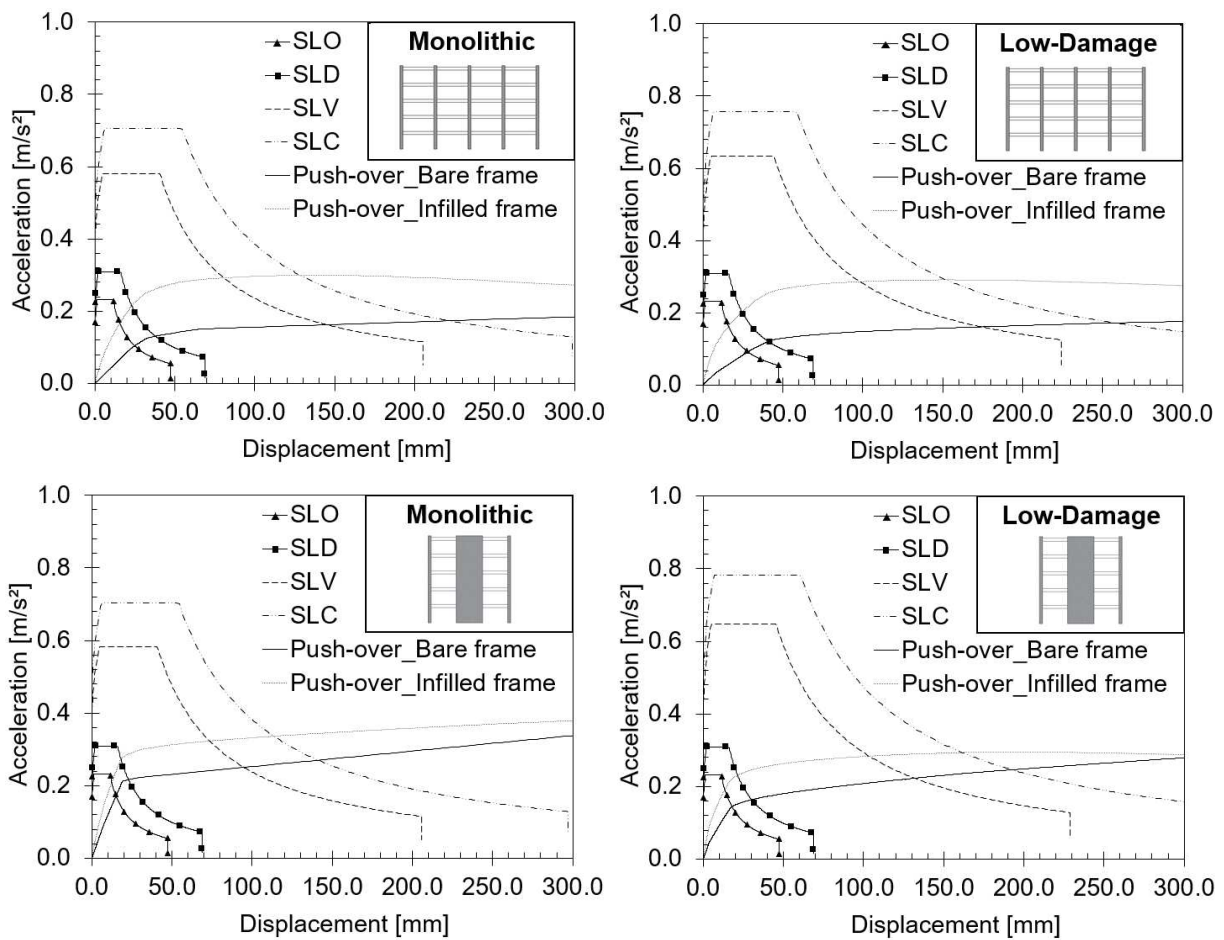


Figure 5.5. Building response of the 5-storey case-study buildings in the ADRS domain.

Table 5.2. Performance Points of all the case-study buildings at SLV limit state (Bare frame modelling).

N° storeys	Performance Point parameter	Monolithic Building (MB)		Low-damage Building (LDB)	
		Frame direction	Wall direction	Frame direction	Wall direction
3	Acceleration [g]	0.22	0.44	0.21	0.40
	Displacement [mm]	104.80	55.29	130.00	70.00
5	Acceleration [g]	0.16	0.25	0.16	0.23
	Displacement [mm]	145.40	95.58	179.50	135.00
7	Acceleration [g]	0.14	0.17	0.16	0.16
	Displacement [mm]	174.60	158.70	199.00	195.00

Table 5.3. Performance Points of all the case-study buildings at SLV limit state (Infilled frame modelling).

N° storeys	Performance Point parameter	Monolithic Building (MB)		Low-damage Building (LDB)	
		Frame direction	Wall direction	Frame direction	Wall direction
3	Acceleration [g]	0.40	0.49	0.34	0.48
	Displacement [mm]	56.91	52.20	75.06	57.15
5	Acceleration [g]	0.29	0.32	0.29	0.28
	Displacement [mm]	80.75	74.68	97.82	103.59
7	Acceleration [g]	0.24	0.23	0.26	0.21
	Displacement [mm]	102.70	119.50	117.15	146.12

Considering the drift performance point as Engineering Demand Parameter (EDP), Table 5.4 summarizes the results obtained for all the multi-story case-study buildings (3, 5, 7 stories) at the different intensity seismic levels (SLO, SLD, SLV, SLC, as per the Italian Code NTC 2018). These results are derived from the numerical investigations carried out using the bare-frame (monolithic or low-damage) models as well as considering the numerical analyses including the infill wall modelling. All these graphs and tables show how the hybrid connections can move the performance points of the monolithic connections towards higher displacements, especially at the ultimate limit states (ULS). It can be also noticed the effect of infill wall modelling, namely an increase of acceleration whilst a reduction of displacement for the performance points compared to the ones from the bare frame numerical results.

Table 5.4. Drift performance point of all the case-study buildings at the different seismic intensity levels.

Building	Intensity level	Monolithic Building (MB)		Low-damage Building (LDB)	
		Frame direction	Wall direction	Frame direction	Wall direction
<i>Bare-Frame modelling</i>					
3-storey building	SLO	0.22%	0.05%	0.22%	0.09%
	SLD	0.36%	0.07%	0.35%	0.21%
	SLV	1.38%	0.73%	1.52%	0.82%
	SLC	2.10%	1.15%	2.28%	1.22%
5-storey building	SLO	0.20%	0.12%	0.21%	0.13%
	SLD	0.30%	0.18%	0.30%	0.22%
	SLV	1.15%	0.75%	1.33%	1.00%
	SLC	1.79%	1.13%	2.00%	1.47%
7-storey building	SLO	0.17%	0.16%	0.21%	0.16%
	SLD	0.24%	0.23%	0.29%	0.24%
	SLV	0.98%	0.89%	1.10%	1.08%
	SLC	1.48%	1.34%	1.59%	1.58%
<i>Infilled-Frame modelling</i>					
3-storey building	SLO	0.12%	0.05%	0.14%	0.05%
	SLD	0.19%	0.07%	0.21%	0.08%
	SLV	0.75%	0.69%	0.88%	0.67%
	SLC	1.16%	1.03%	1.43%	1.01%
5-storey building	SLO	0.12%	0.10%	0.12%	0.10%
	SLD	0.18%	0.14%	0.18%	0.16%
	SLV	0.64%	0.59%	0.72%	0.77%
	SLC	0.99%	0.91%	1.11%	1.19%
7-storey building	SLO	0.11%	0.13%	0.11%	0.11%
	SLD	0.16%	0.19%	0.17%	0.17%
	SLV	0.58%	0.67%	0.65%	0.81%
	SLC	0.92%	1.03%	0.97%	1.28%

The performance points enable the definition of the floor accelerations and storey drift ratios which are input data for the subsequent loss estimation analyses. E.g. Figure 5.6 shows the storey drift ratios along the building height for the two structural systems (monolithic and PRESSS) considering the case of 5-storey building and the bare frame numerical modelling.

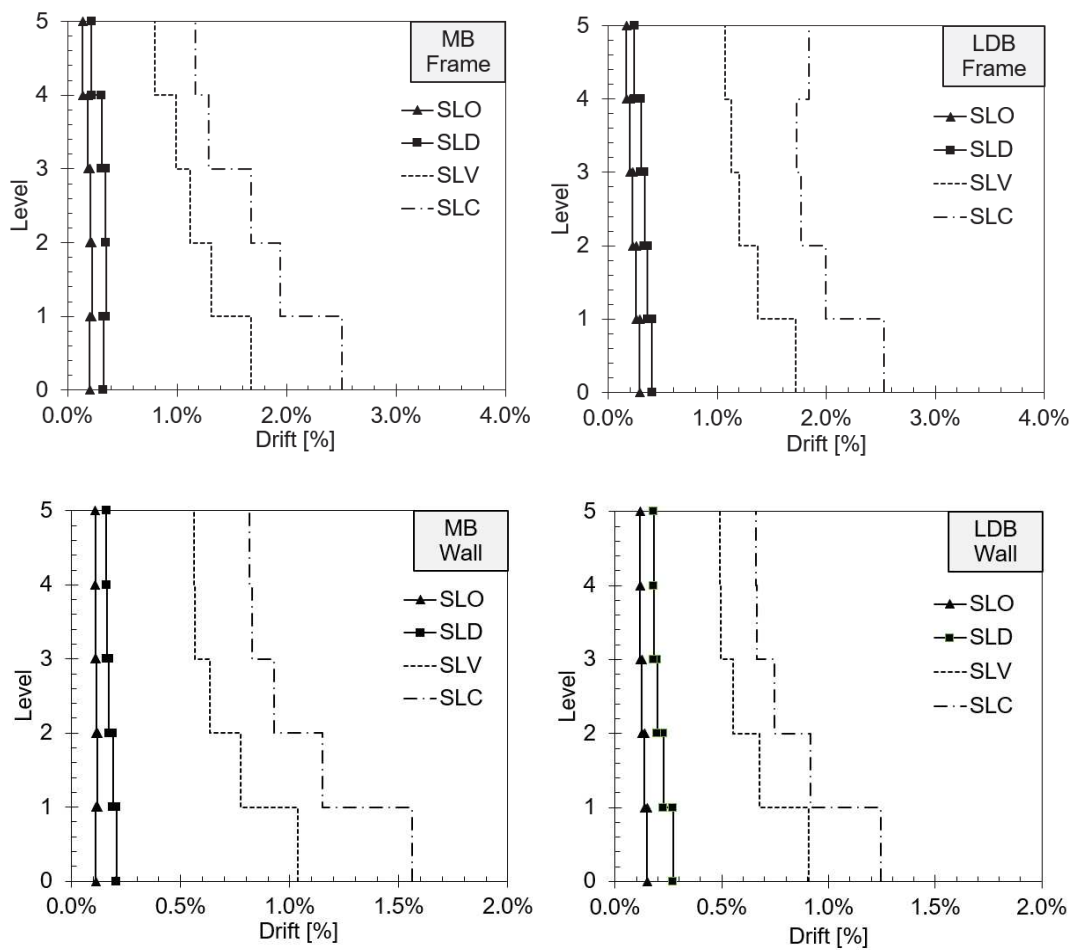


Figure 5.6. Storey drift ratios of the 5-storey reinforced concrete building for both the structural skeletons (Monolithic Building - MB - and Low-Damage Building - LDB -) and for the case of Bare Frame modelling.

5.2.4 Fragility specifications

The implementation of loss assessment analyses through the probabilistic methodology (PBEE) requires the identification of the potential damage states (fragility curves) and consequence functions (repair cost and time) for all the structural and non-structural elements. The fragility specifications of the monolithic building components can be found in the database provided by FEMA P-58 (2012). Just for the traditional infill walls the damage states/fragility curves were assumed as described by Cardone and Perrone (2015), also providing data for the consequence functions. While, equivalent curves (fragility and consequence) need to be defined for the low-damage components, i.e. for the hybrid connections (beam-column joints, wall-base, column-base) and for all the low-damage non-structural systems taken into account.

5.2.4.1 Low-damage structural elements

Due to the potentiality of the implemented numerical model in capturing the building behavior, the fragility curves of the hybrid connections are determined from the section analysis (moment-rotation curves) assuming the collapse of the external dissipaters as first damage state (DS1) and the yielding of the post-tensioned tendons as second damage state (DS2). The dispersion of these curves is assumed equal to 0.5 because the fragilities are not directly obtained from experimental data (although the numerical models considered for the hybrid connections have been extensively validated through experimental tests, e.g. Priestley et al. 1999). Figure 5.7 presents for the case of 5-storey building these functions compared to the fragility curves of monolithic connections (residual crack widths > 0.06 inches for DS1, initial spalling of cover concrete for DS2, possibility of having core concrete crushing, fracture or buckling of reinforcement for DS3), found in the FEMA P-58 (2012) database for similar element geometry.

Concerning the consequence functions, referring to the data available in the FEMA database, the DS2 of the hybrid connections is assumed equal to the DS3 of monolithic connections. Nevertheless, this assumption is conservative because the repair costs and time associated with low-damage connections, i.e. the simple substitution of the external damaged easy-replaceable dissipaters, can be less when compared to a monolithic connection.

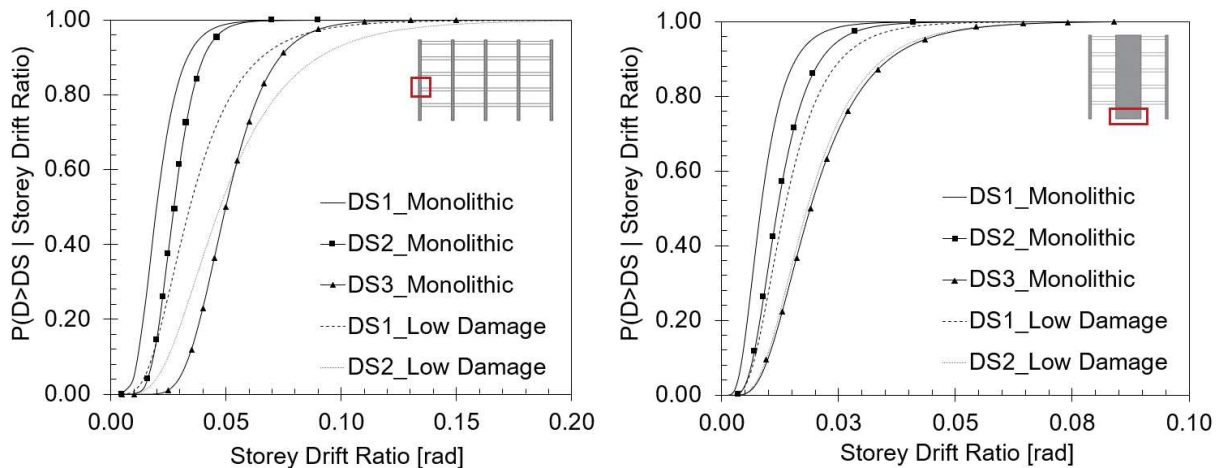


Figure 5.7. Comparison of fragility curves for monolithic and hybrid connections - 5 Storey building - for both beam-column joint connection (left) and wall-base connection (right).

5.2.4.2 Low-damage non-structural elements

Experimental tests are available to identify the damage states of the innovative non-structural solutions, i.e. the median values of drift ratio or acceleration to build the fragility curves, while the

dispersions of the damage levels can be assumed by judgement. A summary of the main outcomes from the experimental tests to which refer for identifying the damage states of the different low-damage non-structural systems is herein provided and the mean values/dispersions used for deriving the fragility functions are presented in the following Table 5.5.

For the case of low-damage infill walls, from the experimental tests carried out by Tasligedik and Pampanin (2016) on unreinforced clay brick walls (vertical rocking panels built inside a steel sub-frame) it can be observed how the structural/non-structural interaction is limited until 1.5% drift level, and the system remains serviceable even at 2.0-2.5% drift. For steel framed drywall partitions, Tasligedik et al. (2014) found as damage states 1) minor cracking occurring at 1.0% drift and 2) the anchor pull-out of the external steel studs at 2.0% drift.

The damage states for the low-damage precast concrete claddings with dissipative connections are provided by Baird et al. (2013). The full-scale test results demonstrated the effectiveness of U-shaped Flexural Plates (UFP) connections, when compared to more traditional tieback or slotted connections, proving during the experimental campaign that these systems remain undamaged and the transition to the Life Safety performance level is more related to the exceedance of the slot allowance of the connection, depending on the connection design, than to the risk of the system failure. The same authors also provide data on the repair costs and time associated with both the traditional and the innovative cladding configurations.

Sivanerupan et al. (2014) provide drift limits for spider glazing systems. For the classical glass façade with pinned X-type spider arms, the glass panel failure is reached at 2.1% drift, while for the solution with fixed K-type spider arms and internal vertical and horizontal gaps, referred in this research as low-damage system for such type of exterior enclosure, the same damage state is achieved at 5.25% drift.

Finally, concerning the suspended ceiling systems, shaking table test results from Pourali et al. (2017) were taken into account to develop tentative fragility curves. The tested fully-floating suspended ceiling with elastic perimeter isolation material showed a panel dislodgement, due to pounding effect against perimeter beams, for very high vertical accelerations (greater than 1g).

Table 5.5. Damage states of both traditional and low-damage non-structural elements implemented in the loss assessment investigations of all the case-study buildings (3, 5, 7 storeys).

Non-structural element	Type of system	Description of the system	Data for fragility curves
<i>Glazing façade:</i> Spider glazing	Traditional (Sivanerupan et al. 2014)	12 mm toughened glass, 8 mm silicon sealant, Pinned X-type spider arms	DS1. Glass fallout ($\theta = 2.1\%$, $\sigma = 0.5$)
	Low damage (Sivanerupan et al. 2014)	12 mm toughened glass, 8 mm silicon sealant, Fixed K-type spider arms with 7 mm horizontal and 17.5 mm vertical gaps	DS1. Gasket degradation ($\theta = 2.0\%$, $\sigma = 0.5$) DS2. Glass fallout ($\theta = 5.25\%$, $\sigma = 0.5$)
<i>Cladding façade:</i> Connection system for precast concrete panels	Traditional (Baird et al. 2014)	Threaded connection, Rod diameter 20 mm, Rod length 250 mm	DS1. Pre-yielding ($\theta = 0.2\%$, $\sigma = 0.2$) DS2. Post-yielding; visible cracking ($\theta = 0.5\%$, $\sigma = 0.2$) DS3. Severe cracking ($\theta = 1.0\%$, $\sigma = 0.2$) DS4. Rupture of rod ($\theta = 2.0\%$, $\sigma = 0.2$)
	Low damage (Baird et al. 2013)	UFP connection, 120 x 8 mm steel plate	DS1. Pre-yielding ($\theta = 0.18\%$, $\sigma = 0.2$) DS2. Post-yielding; visible cracking ($\theta = 2.7\%$, $\sigma = 0.2$)
<i>Infilled façade:</i> Masonry infill walls	Traditional (Cardone and Perrone 2015)	Masonry infills with French window and partitions with door	DS1. Detachment of infill, Light diagonal cracking ($\theta = 0.15\%$, $\sigma = 0.5$) DS2. Extensive diagonal cracking ($\theta = 0.4\%$, $\sigma = 0.5$) DS3. Corner crushing and sliding of mortar joints ($\theta = 1.0\%$, $\sigma = 0.4$) DS4 Global in-plane collapse ($\theta = 1.75\%$, $\sigma = 0.35$)
		Masonry infills with French window and partitions with door	
	Low damage (Tasligedik and Pampanin 2016)	Rocking walls with lateral gaps of 10 mm, 1.5 - 2 aspect ratio	DS1. Minor horizontal mortar cracking ($\theta = 1.5\%$, $\sigma = 0.5$) DS2. Light mortar cracking, minor toe-crushing ($\theta = 2.5\%$, $\sigma = 0.5$)
<i>Drywall partition:</i> Steel stud gypsum wall	Traditional (FEMA P-58 2012)	Gypsum with metal studs, Full height, Fixed below and above	DS1. Screws pop-out, minor cracking of wall board, warping or cracking of tape ($\theta = 0.21\%$, $\sigma = 0.6$) DS2. Moderate cracking or crushing of gypsum ($\theta = 0.71\%$, $\sigma = 0.45$) DS3. Significant cracking and/or crushing of gypsum, buckling of studs, tearing of tracks ($\theta = 1.2\%$, $\sigma = 0.45$)

Non-structural element	Type of system	Description of the system	Data for fragility curves
<i>Drywall partition:</i> Steel stud gypsum wall	Low damage (Tasligedik et al. 2014)	Gypsum with metal studs, 15 and 5 mm external and internal gaps, Gypsum boards attached only to the vertical studs	DS1. Minor plaster cracking ($\theta = 1.0\%$, $\sigma = 0.4$) DS2. Anchor pull out of the external studs ($\theta = 2.0\%$, $\sigma = 0.4$)
<i>Suspended ceiling</i> Suspended lay-in acoustic tile ceiling	Traditional (FEMA P-58 2012)	Area < 250 sf, Vertical hanging wires only	DS1. 5 % of tiles dislodge and fall ($a = 0.9g$, $\sigma = 0.4$) DS2. 30% of tiles dislodge and fall and t-bar grid damaged ($a = 1.5g$, $\sigma = 0.4$) DS3. Total collapse ($a = 2.2g$, $\sigma = 0.4$)
	Low damage (Pourali et al. 2017)	Elastic acoustic isolation material into the lateral gap	DS1. 5 % of tiles dislodge and fall ($a = 1.22g$, $\sigma = 0.4$)

As regards the consequence functions, these curves can be derived from the ones available in FEMA P-58 (2012) database for the corresponding traditional non-structural systems, apart from the precast concrete claddings comprising UFP connections for which consequence data can be found in Baird (2014).

5.2.5 Loss assessment analysis

The post-earthquake losses are estimated using the Performance Assessment Calculation Tool (PACT) of FEMA P-58 (2012). All the building structural/non-structural configurations are then compared in terms of repair costs and downtime, which are parameters useful to decision makers because linked to the building insurance premium estimation. The PACT directly provides both the repair cost as and the repair time, while the downtime can be estimated adding to these repair time the so-called “impeding factors” and utility disruption, determined according to the procedure proposed by Almufti and Willford (2013).

Taking into account previous works and data from on-site applications (e.g. Smith et al. 2009; Cattanaach and Pampanin 2008) loss analyses are implemented making the following assumptions for the replacement cost and time of the PRESSS structure: 1) the total replacement cost of a low-damage technology is considered 10% higher than the benchmark cost of a monolithic (cast-in-situ) building (assumed as about 1100 euro/m²); 2) the replacement time of a low-damage technology is assumed a 25% lower than the monolithic structure (790 days).

5.2.5.1 Repair costs

Considering time-based assessment analysis, the results in terms of Expected Annual Losses (EAL) are herein provided. As example, Figure 5.8 shows the loss estimation results obtained for the 5-storey building and alternative non-structural configurations.

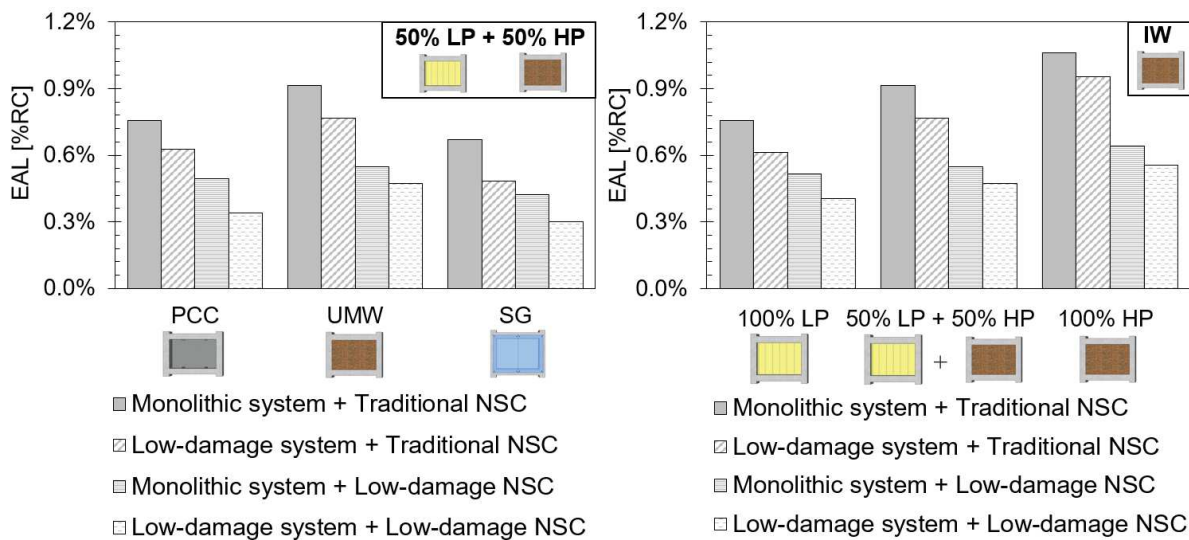


Figure 5.8. Considering the 5-storey case-study building: 1) EAL results (left) for 50% Light Partitions (LP) and 50% Heavy Partitions (HP) and all the exterior enclosure configurations (Precast Concrete Claddings – PCC; Unreinforced Masonry Infill Walls – UMIW; Spider Glazing – SG); EAL results (right) for external Infill Walls (IW) and different cases of internal partitions (all light or heavy or both).

From the previous graphs, it can be observed how the integrated low-damage building system, with all damage-resistant components (structural connections, exterior enclosures, partitions and ceilings, apart from building services and contents assumed to be the same traditional components for each building system), provides a great reduction of EAL compared to the benchmark building with all traditional elements (in the range of 48-55% for all the three types of façade) and the spider glazing curtain walls define the best cost-affordable integrated system (0.3% of EAL). Even the sole introduction of low-damage structural or non-structural systems determine high reductions (for this case of mixed light and heavy internal partitions, the reduction due to just low-damage structural members is between 17 and 28%, while the reduction due to damage-resistant non-structural elements is in the range 35-40% and a substantial contribution is given by low-damage masonry infill walls). It can be also observed how increasing the percentage of heavy partitions (50%, 100%) the EAL values of the monolithic traditional building increment. However, these EALs can be significantly reduced by the application of damage-mitigation infill walls.

Considering the EAL results from all the 108 cases, the savings in 50 years building-life due to the application of the alternative low-damage strategies (only low-damage structural components, only low-damage non-structural elements and integrated low-damage system) can be estimated, as presented in Figure 5.9 - left - for the 5-storey building.

When considering the maximum and minimum values of EAL for each building typology, from the benchmark (cast-in-situ) structure and the integrated system respectively, the maximum savings can be identified (Figure 5.9 – right – and Table 5.6). It can be observed that significant savings are obtained mainly for the building cases with external infill walls (mean value of around 200 €/m²).

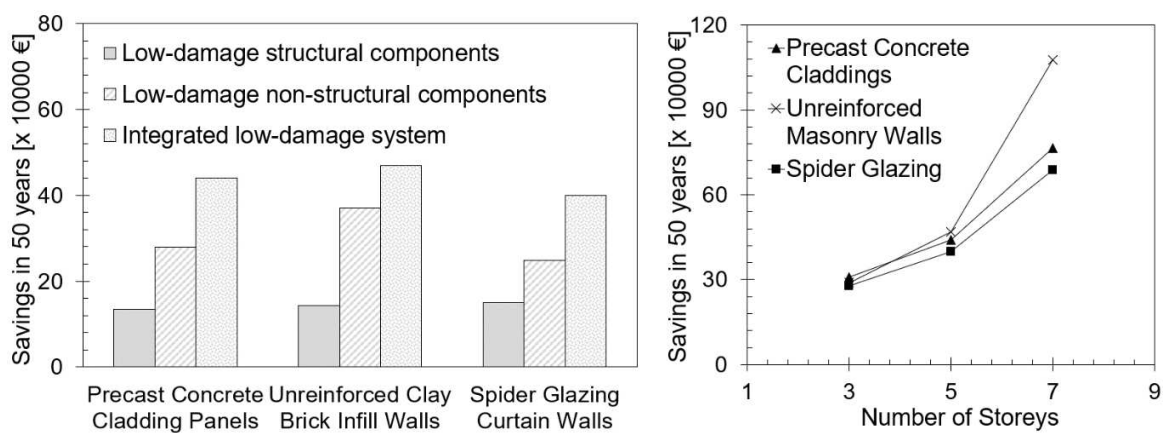


Figure 5.9. Savings in 50 years building-life: Left, considering the alternative low-damage systems (only low-damage structural components, only low-damage non-structural elements and integrated low-damage system) for the 5-storey reinforced concrete structure and all the exterior envelope configurations; Right, for all the case-study structures (3, 5, 7 storeys), all the envelope systems comparing the case of integrated system with the benchmark structures.

In order to highlight the convenience of implementing low-damage technologies at different seismic intensity levels and define the major contributions to losses, results from intensity-based assessment are also investigated. As example, for one of the 5-storey building configuration with precast concrete claddings and gypsum partitions Figure 5.10 shows the percentage contributions to the EAL values of the repair costs at the different intensity levels. It can be observed from this graph how the application of low-damage systems leads to very high benefits (greater than 60%) for the low-seismic intensity levels (SLO and SLD, respectively Immediate Operational and Damage Control), mainly due to damage-resistant non-structural components.

Table 5.6. Minimum (integrated low-damage system) and maximum (benchmark building) EAL values for all the case-study structures and total savings in 50 years of building life.

Parameter	Cladding panels			Infill walls			Spider glazing		
	100% L	50% L+H	100% H	100% L	50% L+H	100% H	100% L	50% L+H	100% H
3 Storey Case- Study Building									
EAL _{max} [%]	0.19	0.23	0.25	0.25	0.27	0.33	0.16	0.17	0.24
EAL _{min} [%]	0.44	0.50	0.58	0.46	0.55	0.64	0.35	0.45	0.53
Savings in 50 years [\$ /m ²]	184.6	203.6	242.0	155.3	206.5	228.2	141.9	207.8	215.7
5 Storey Case- Study Building									
EAL _{max} [%]	0.28	0.34	0.42	0.40	0.47	0.56	0.24	0.30	0.36
EAL _{min} [%]	0.56	0.76	0.94	0.76	0.91	1.06	0.47	0.67	0.87
Savings in 50 years [\$ /m ²]	124.3	185.1	230.3	155.4	195.5	224.4	99.28	163.2	227.4
7 Storey Case- Study Building									
EAL _{max} [%]	0.21	0.31	0.40	0.37	0.46	0.54	0.13	0.20	0.33
EAL _{min} [%]	0.51	0.78	1.15	0.91	1.14	1.45	0.39	0.61	1.01
Savings in 50 years [\$ /m ²]	131.9	208.5	329.6	239.7	299.3	404.0	115.6	184.8	301.4

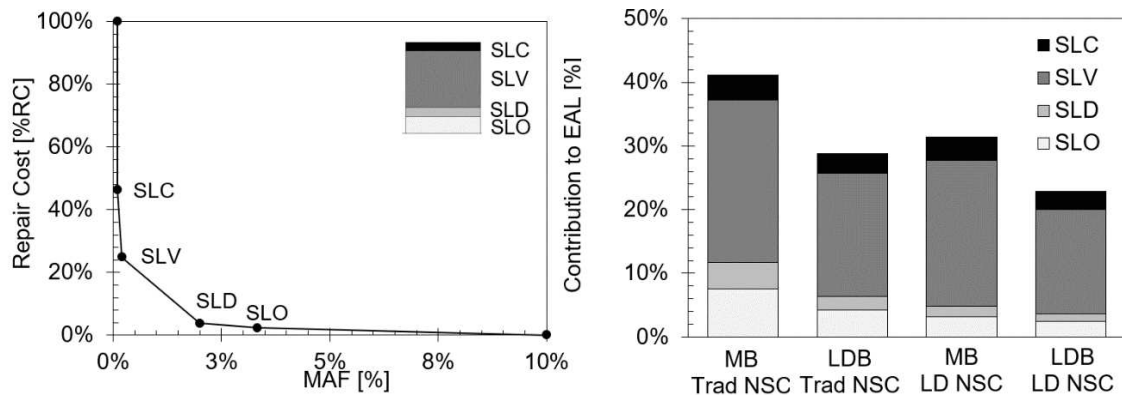


Figure 5.10. For the 5-storey reinforced concrete building with Precast Concrete Claddings (PCC) and Steel Gypsum partition Walls (SGW): Left, Repair cost (as percentage of the Replacement Cost) - Median Annual Frequency (MAF) curve of the benchmark building; Right, Contributions to the EAL values of all the intensity levels and for all the low-damage building configurations (Monolithic or Low-Damage Building, MB or LDB; Traditional or Low-Damage Non-Structural Components, Trad or LD NSC).

Grouping the different building components (structural elements, non-structural systems and building contents), their contribution to the seismic losses at each intensity level can be defined. Results highlight again the substantial reduction of repair costs due to the implementation of low-damage infill walls, as shown from Figure 5.11 for the 5-storey structure.

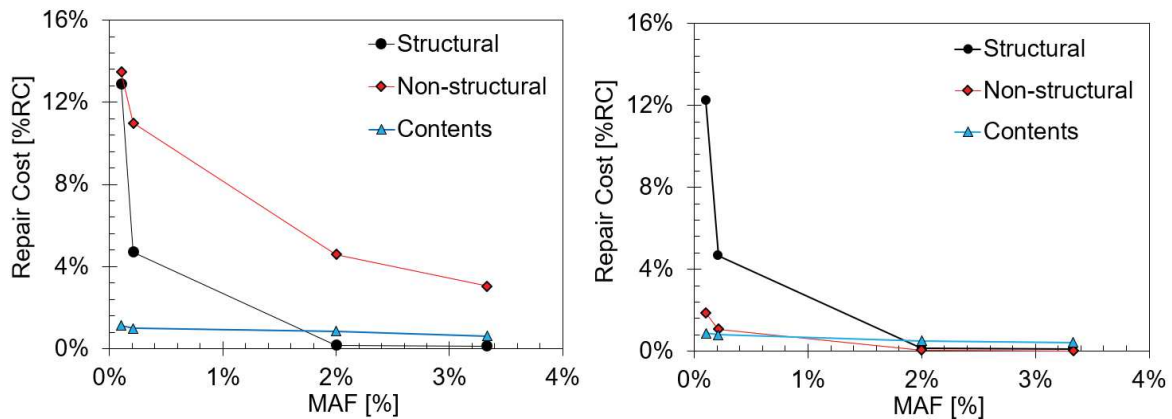


Figure 5.11. Contribution to losses of the building elements at each seismic intensity level (Repair costs/Median Annual Frequency curves) for the case of 5-Storey structure with Unreinforced Masonry Infill Walls (UMIW) and Steel Gypsum partition Walls (SGW) for the benchmark system (left) and the integrated structure (right).

5.2.5.2 Downtime

Besides the repair costs, the building configurations can be compared in terms of downtime, representing an important performance measure to be estimated mainly for buildings whose serviceability after earthquakes is fundamental, such as hospitals. Downtime can be calculated from the repair time of the PACT intensity-based results, properly modified in functions of the maximum number of workers that can be present in the working area simultaneously, adding 166 days of delay due to impeding factors (Almufti et al. 2013).

Figure 5.12 – left – shows the results in terms of business interruption for the case of 5-storey building (all exterior enclosures and gypsum partitions). While, Figure 5.12 – right – summarizes the average values of the downtime reductions at ULS seismic intensity (SLV) obtained for all the case-study buildings (3, 5 and 7 storeys) when the benchmark structures are compared to the integrated systems. The downtime estimations for all the analysed building systems are summarized in Table 5.7. It can be noticed that the downtime reduction is in the range of around 2 to 7 months. The results confirm the benefits of the design strategy of implementing low-damage solutions in reducing also the business interruption, especially for the configurations comprising infill wall enclosures and masonry wall partitions.

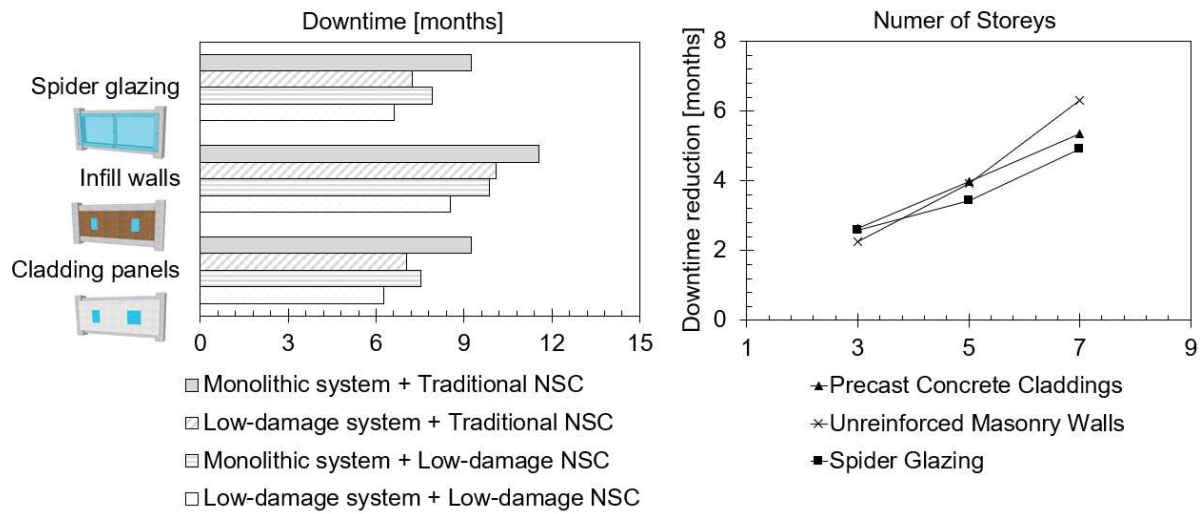


Figure 5.12. Left: Comparison of downtime values for all the building configurations considered for the 5-storey building and referring to the case of 100% gypsum partitions; Right: Downtime reductions of the integrated low-damage buildings when compared to the traditional structural/non-structural systems.

Table 5.7. Minimum (integrated low-damage system) and maximum (benchmark building) Downtime values for all the case-study structures and associated time savings.

Parameter	Cladding panels			Infill walls			Spider glazing		
	100% L	50% L+H	100% H	100% L	50% L+H	100% H	100% L	50% L+H	100% H
3 Storey Case- Study Building									
Downtime min [months]	5.5	6.1	6.6	6.6	7.4	7.9	5.8	6.4	6.8
Downtime max [months]	7.8	8.6	9.7	8.7	9.5	10.4	7.8	9.0	10.0
Savings [months]	2.2	2.5	3.1	2.1	2.1	2.6	2.0	2.6	3.2
5 Storey Case- Study Building									
Downtime min [months]	6.3	6.8	7.9	8.5	9.2	10.4	6.6	7.3	8.5
Downtime max [months]	9.3	10.6	13.1	11.6	13.2	15.0	9.2	10.5	12.9
Savings [months]	3.0	3.7	5.2	3.0	4.0	4.6	2.6	3.2	4.4
7 Storey Case- Study Building									
Downtime min [months]	6.3	7.5	9.0	9.7	10.9	12.5	6.6	7.8	9.4
Downtime max [months]	10.1	12.5	16.2	14.8	17.1	20.2	10.0	12.4	16.1
Savings [months]	3.8	5.1	7.2	5.1	6.2	7.7	3.4	4.6	6.7

5.2.6 Further studies

The benefits of low-damage building systems in increasing the seismic performance, limiting the post-earthquake damage and consequently reducing the expected economic losses, are herein investigated considering the influence of the seismic hazard. Referring to the same global dimensions and plan geometry of the 5-storey building previously studied, both the monolithic and PRESSS structural skeletons are now designed for two different seismic zones (low and high seismicity). With reference to the Ultimate Limit State (ULS) level (475 years return period earthquake for an Importance Class 2) the seismic demand associated with a low and a high seismic zone in Italy is taken into account for implementing the building design. The demand parameters of these zones are obtained as median values from five different locations in Italy for both low seismicity - i.e. Rufina (FI), Mirabello (FE), Troia (FG), Pennadomo (CH), Bronte (CT) - and high seismicity - i.e. Ferla (SI), Pedace (CO), Isernia, L'Aquila, Gemona (UD) - with PGAs of 0.224 g and 0.353 g respectively. The elastic design acceleration and displacement spectra (5% damped and Soil type C) at ULS of both seismic conditions are presented in Figure 5.13.

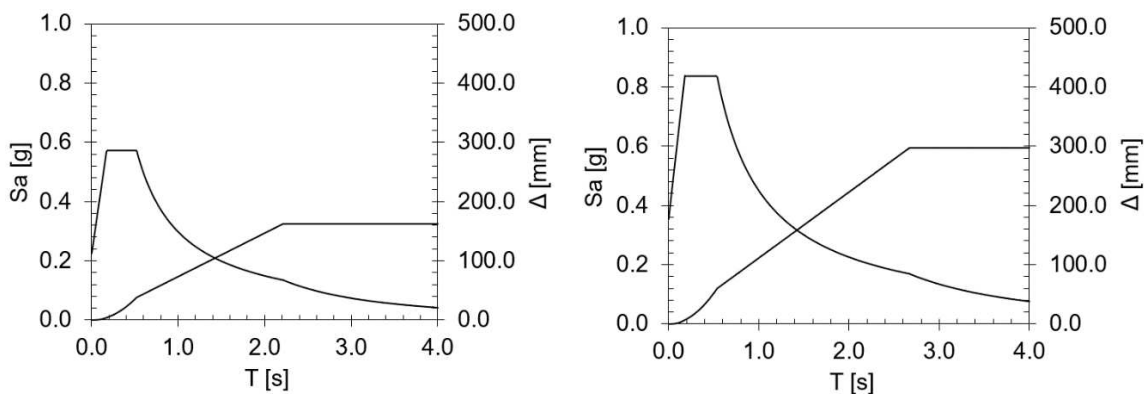


Figure 5.13. Elastic response spectra at ULS for the low (left) and high (right) seismic zones (Bianchi et al. 2019a).

The building use is now assumed as commercial for the first two floors and residential for the other two levels, while on the top floor there is a roof. Then, as developed for the previous study, both the monolithic and PRESSS structures in low and high seismicity are designed following the Direct Displacement Based Design (DDBD) procedure considering appropriate inter-story drift limits. The DDBD provides the internal actions on the structural members to consider for the design of the structural members. As in the previous work, the low-damage elements are designed using a re-centring ratio λ equal to 1.25 (56% contribution from the unbonded post-tensioned tendons, 44% contribution from the dissipative devices).

Table 5.8 lists the parameters obtained from the DDBD procedure for both structural systems. As can be noticed from the table, different design drift ratios are taken into account for developing the DDBD procedure of the buildings in the two seismic zones, however, these imposed drift values are maintained equal for the different structural systems (monolithic/low damage).

Table 5.8. Design parameters from DDBD procedure for monolithic and low-damage structural skeletons in low and high seismic zones (F_{LS} = Frame direction, Low Seismicity; F_{HS} = Frame direction, High Seismicity; W_{LS} = Wall direction, Low Seismicity; W_{HS} = Wall direction, High Seismicity).

Parameter	Monolithic structure				Low-damage structure			
	F_LS	F_HS	W_LS	W_HS	F_LS	F_HS	W_LS	W_HS
θ_{design} [%]	1.3	2.0	0.90	1.20	1.30	2.0	0.90	1.20
$\Delta_{yielding}$ [mm]	61.9	61.92	49.95	49.95	61.92	61.92	49.95	49.95
Δ_{demand} [mm]	143.56	223.10	121.90	162.53	143.56	223.10	121.90	162.53
$m_{effective}$ [t]	3028.54	3028.54	2883.36	2883.36	3028.54	3028.54	2883.36	2883.36
$H_{effective}$ [m]	13.19	13.19	13.54	13.54	13.19	13.19	13.54	13.54
$\mu_{Displacement}$	2.32	3.60	2.44	3.25	2.32	3.60	2.44	3.25
$\xi_{equivalent}$ [%]	15.30	19.19	15.80	18.37	9.58	11.31	9.80	10.94
$T_{effective}$ [s]	2.44	2.64	2.09	1.90	2.21	2.35	1.89	1.70
$K_{effective}$ [kN/m]	20004.99	17149.02	26044.60	31378.88	24453.50	21641.45	31986.84	39366.37
V_{base} [kN]	2871.99	3825.88	3174.85	5100.14	3510.63	4828.13	3899.21	6398.38

Cost/performance-based investigations are then implemented for all the building low-damage solutions (low-damage structural skeleton with traditional non-structural elements; monolithic building with low-damage non-structural components; integrated structural/non-structural low-damage system) and non-structural systems (for traditional or low-damage systems: precast concrete claddings or masonry infill walls or spider glazing systems as exterior enclosures, only gypsum steel studded walls as interior partitions and suspended ceilings as ceiling system; only traditional systems for building services and contents) considered in the preceding work. A total number of 24 cases, including the benchmark structure, is defined to be analysed.

Numerical results (Ruauumoko 2D) for the two buildings and both the bare frame and infilled frame modelling configurations are presented in Figures 5.14 and 5.15 in terms of push-over curves

in the ADRS domain. The maximum expected seismic displacements and accelerations (performance) at each intensity level (SLO, SLD, SLV, SLC) can be thus identified and the storey drift ratios and floor accelerations determined.

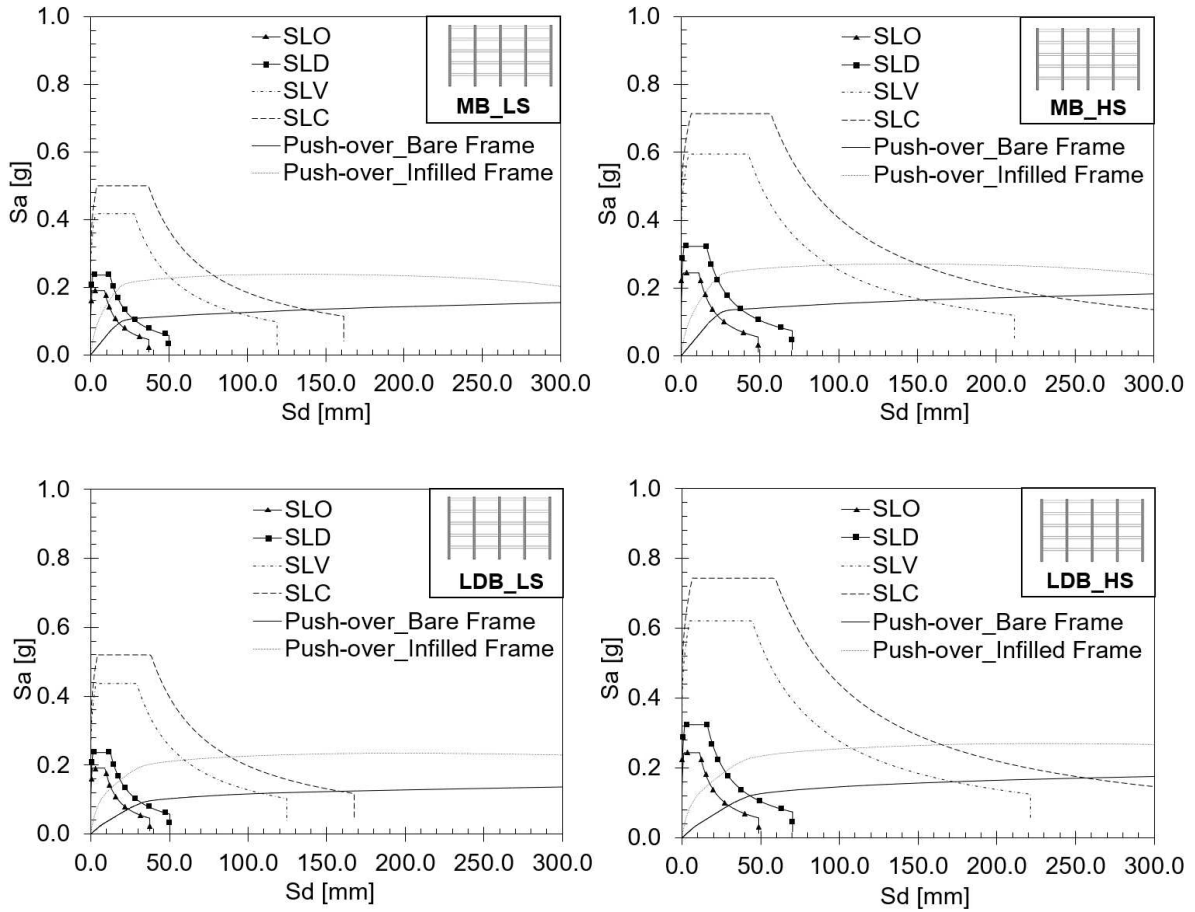
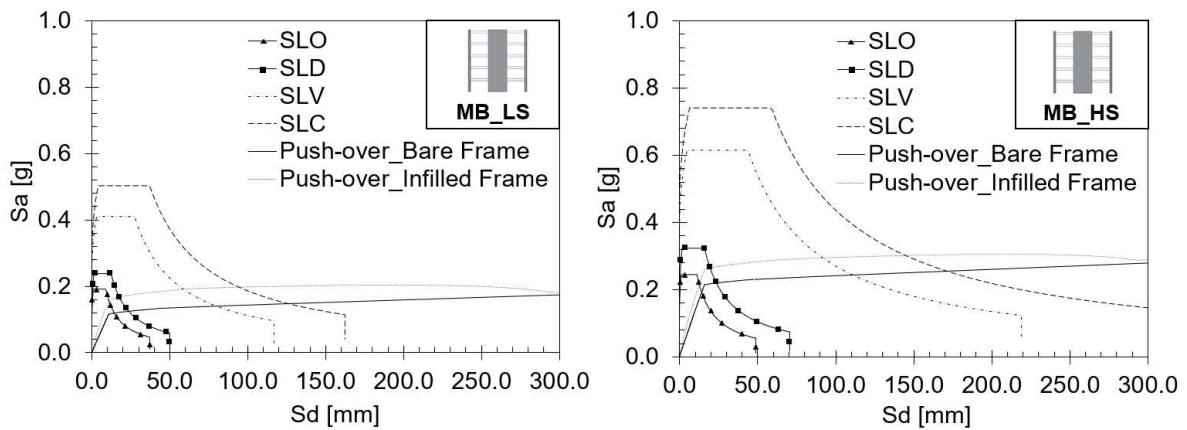


Figure 5.14. Building response in the ADRS domain for the frame direction of the 5-storey building in both low and high seismic zones (MB = Monolithic Building; LDB = Low Damage Building; LS = Low Seismicity; HS = High Seismicity).



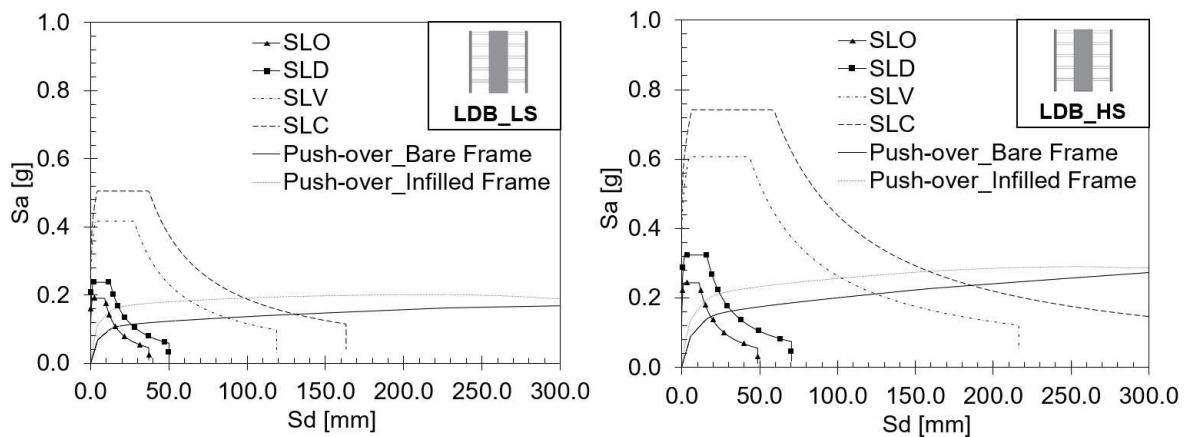


Figure 5.15. Building response in the ADRS domain for the wall direction of the 5-storey building in both low and high seismic zones (MB = Monolithic Building; LDB = Low Damage Building; LS = Low Seismicity; HS = High Seismicity).

Finally, loss assessment investigations are performed considering the same assumptions on the damage states and consequence functions as well as on the construction cost and time made in the previous study. The results obtained in terms of EAL are summarized in Figure 5.16 for all the case-study configurations. For both buildings in different seismicity conditions, great reduction of EAL due to the application of damage-resistant technologies are found: 1) the integrated low-damage solution, with all damage-resistant components (structural members, facades, partitions, ceilings), provides a great reduction of EAL when compared to the benchmark building with all traditional systems (reduction of around 50% for the precast concrete claddings and spider glazing configurations for both seismicity, and up to 70% and 85% for the infill wall configurations respectively for the high and low seismicity cases); 2) even the sole introduction of low-damage structural members or non-structural systems provide high reductions, especially when low-damage rocking infill walls are introduced (reduction of 60% and 70% respectively for the high and low seismicity cases).

Figure 5.16 also highlights that the presence of infill walls has a substantial influence on the seismic response of the 5-storey building located in the low seismic zone, i.e. the EALs associated to this condition are very high compared to the other façade systems. The same consideration is not valid for the high seismicity cases. Moreover, considering the maximum and minimum values of EAL, respectively from the benchmark structure and the integrated system, for each building typology the savings in 50 years building-life can be determined, as summarized in Figure 5.17 (left). Very significant savings can be obtained for the buildings with unreinforced masonry infill walls as exterior enclosures, that is around 220 euro per square meter for both low and high seismic zones.

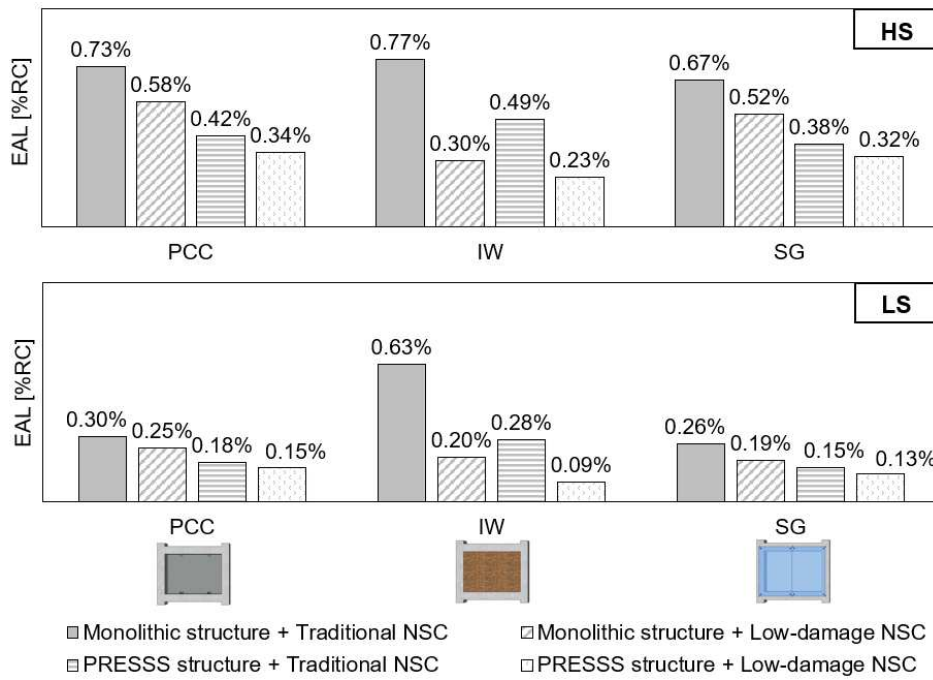


Figure 5.16. EAL values for all the building configurations (Monolithic or Low-damage (PRESSS) structure/Traditional or Low-damage Non Structural Components), all the exterior enclosures (Precast Concrete Claddings, Infill Walls, Spider Glazing systems) and seismicity conditions (Low Seismicity LS, High Seismicity HS).

Referring to the PACT intensity-based results, the downtime can be estimated adding 166 days of delay (impeding factors) to the repair time. Figure 5.17 (right) shows the reduction of downtime due to the integrated low-damage system compared to the traditional benchmark building for the case of ULS seismic intensity. The results confirm the benefits of this design strategy in reducing the business interruption, mainly for the configuration with infill wall exterior enclosures (around 8 months). When investigating the other seismic intensities, great reductions can be also noticed.

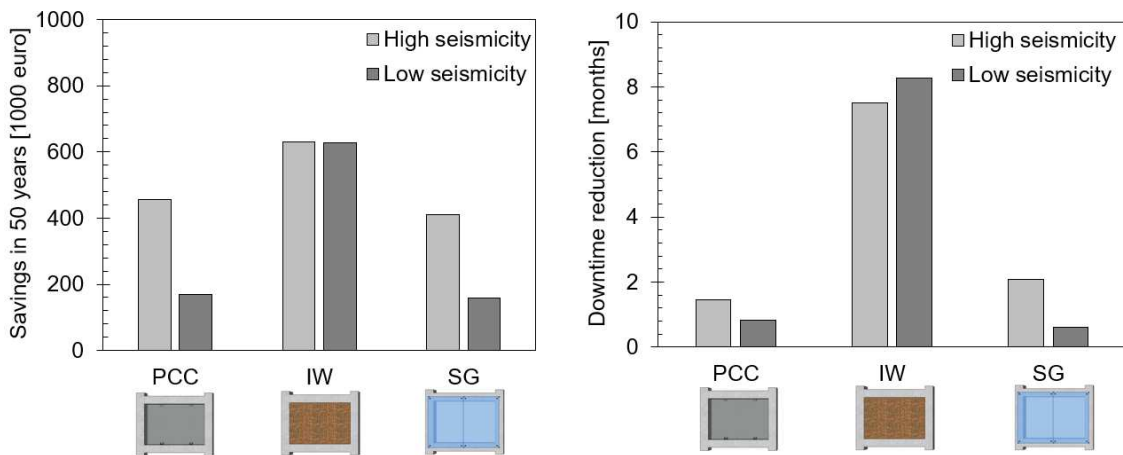


Figure 5.17. Savings in 50 years building-life (left) and downtime reductions (right) for the ULS seismic intensity comparing the solution of monolithic building made of all traditional non-structural systems with the integrated low-damage solution (Bianchi et al. 2019a).

Nevertheless, in this investigation the repair time is not simply calculated taking into account the maximum number of workers available in the building area, whilst business interruption is properly elaborated as proposed by the methodology found in REDi™ Rating system (Almufti et al. 2013).

In order to define a construction schedule and create a realistic repair sequence to achieve a specific recovery state (functional recovery), the various repairs occurring at each building floor as a function of time can be determined, as presented in Figure 5.18 for two different analysed configurations of the 5-storey building with external masonry walls (benchmark structure and integrated low-damage system). These Gantt charts are obtained taking into account the sequence of repairs (non-structural repair starts after the structural system has been repaired), the number of workers that are available to work on the same component type on each floor and simultaneously across multiple floors and the total number of workers which are able to work on-site simultaneously.

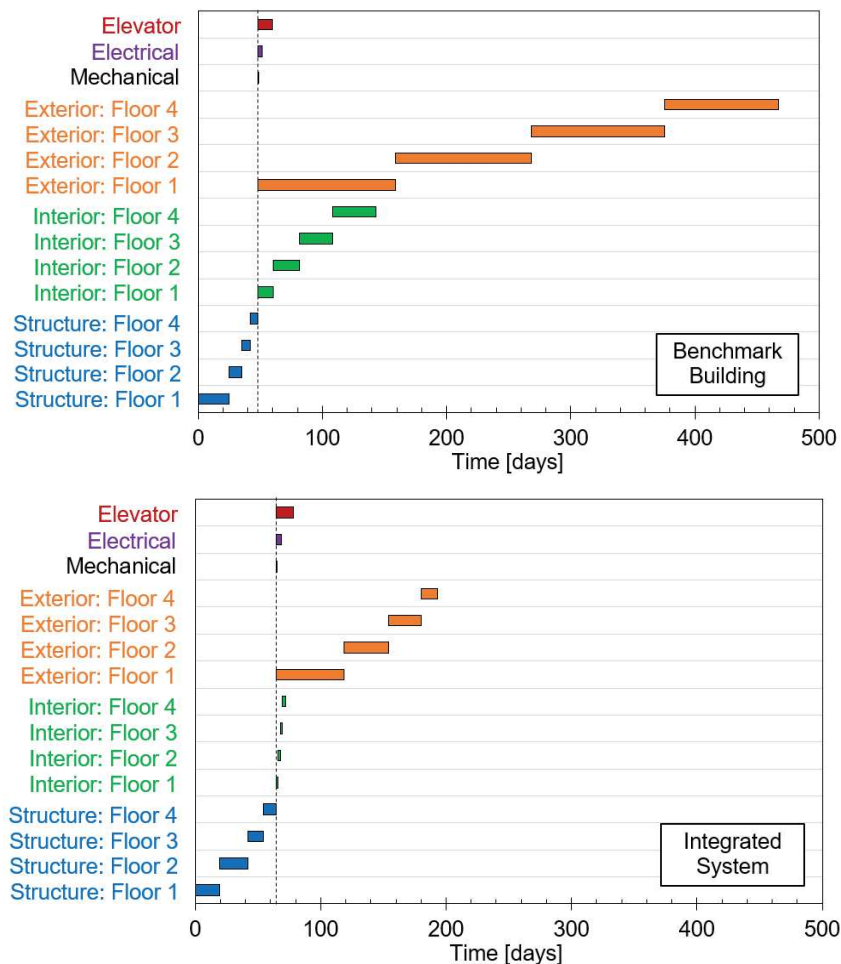


Figure 5.18. Repair schedule for two different building configurations of the infilled 5-storey structure located in high seismic zone (Benchmark Building - top - and Integrated Low-damage Building - bottom -) considering the methodology proposed by Almufti et al. (2013), where the repairs are divided in function of the building floor and component typology (Structure: structural connections; Interior: Piping, HVAC distribution, Partitions, Ceilings; Exterior: Enclosures; Mechanical equipment; Electrical equipment; Elevators).

Comparing the two previous charts, the benefits of low-damage non-structural technologies in reducing the repair time associated with exterior and interior non-structural components (i.e. exterior infill walls, gypsum partitions, ceilings) are confirmed again.

Finally, it is observed that the results could be presented in terms of resilience curves, where the building performance can be expressed in function of the recovery time. Resilience curves are often used to illustrate the resilient behaviour of an engineered system undergoing a disruptive event, such as an earthquake, defining the impacted area representing the performance loss after this event (i.e. the grey area in Figure 5.19).

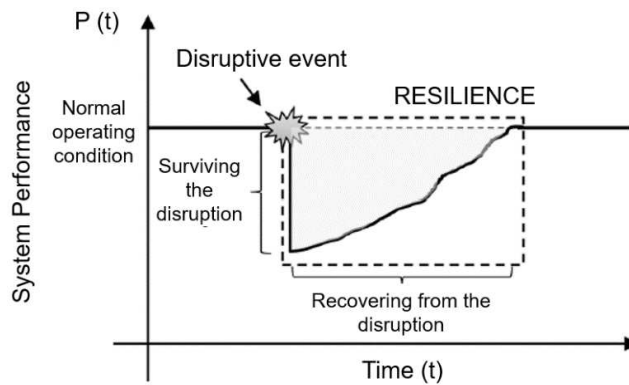


Figure 5.19. Engineering resilience behaviour following a disruptive event (Uday et al. 2015).

Using an equivalent approach, resilience-based curves can be calculated considering the downtime as the time needed for reaching a specific building functionality condition and the advantages of applying low-damage solutions can be read in the reduction of the impacted area forming. E.g. this approach is presented in Figure 5.20 through a simplified procedure for the 5-storey structure comparing the benchmark building to the integrated low-damage solution and considering as disruptive condition an event with 975 years return period (collapse seismic intensity, SLC). Considering the total recovery state (100% performance) as final objective, the curves are derived assuming the estimation of the Performance percentage P as follows:

$$P = 1 - \frac{R}{RC} [\%]$$

Where R is the building Repair cost and RC is the Replacement Cost (if the building is fully damaged, P is equal to 0%). While for the time values, after a constant trend due to the impeding factors, the line related to the building repair actions initiates, herein simply assumed with a stable linear profile.

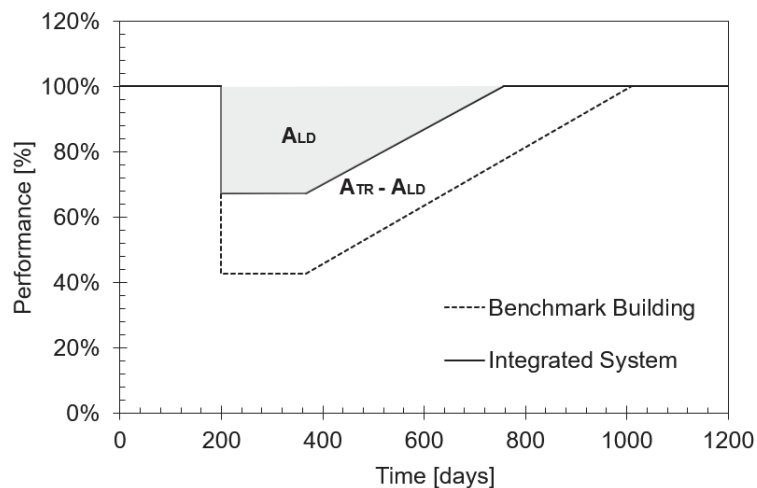


Figure 5.20. Simplified resilience curves for the 5 storey building (Benchmark structure vs. Integrated system) with exterior infill walls and interior gypsum partitions referring to the occurring of a 975 years return period event. In the graph the impacted area associated to the low-damage system (A_{LD}) as well as the reduction of the area of the traditional structure ($A_{TR} - A_{LD}$) are indicated.

Applying the proposed simplified approach, it can be observed a reduction of the impacted area due to the application of the integrated system equal to around 45% for this specific case-study.

5.2.7 Summary of the cost/performance analysis

The numerical study has investigated the impact of different traditional/low-damage structural/non-structural building systems through the application of cost/performance-based evaluations of multi-storey reinforced concrete buildings. The research has aimed to provide evidence on the socio-economic benefits related to the implementation of these innovative technologies, quantifying the expected losses in terms of both repair cost and downtime.

Considering the seismic performance, notwithstanding all the monolithic and PRESSS case-study buildings have been designed according to the DDBD which guarantees a more similar control in terms of expected inter-storey drift levels, the benefits in the use of hybrid connections are evident. In fact, at the same drift level the damage of low-damage members is lower than the one of monolithic elements, therefore the repair costs and time are reduced and linked to the simple substitution of the damaged and easily replaceable external dissipaters. Another benefit due to low-damage connections is the reduction of the residual inter-storey drift associated to the re-centring effect of the post-tensioned tendons. The convenience of applying low-damage non-structural systems is instead highlighted from the comparison in terms of damage states; similar damage states are

achieved for higher drift or acceleration values, depending on the sensitivity of the component, for the damage-resistant solutions when compared to more traditional systems.

Concerning the results in terms of economic losses, great beneficial effects (reduction of both EAL and downtime) are found for the integrated low-damage structural&non-structural building system. Taking into account the great percentage of economic losses related to non-structural damage, results highlight how the sole application of damage-mitigation non-structural solutions produce very high savings, especially for heavy infill walls. Although more case-study structures need to be investigated for making statistics on the results, an initial statistical study can be proposed considering the obtained savings in 50-years building life as well as the downtime reductions and including all the reinforced case-study buildings (3, 5, 7 storeys) in the category of mid-rise structures. The results of this investigation are shown in Figure 5.21.

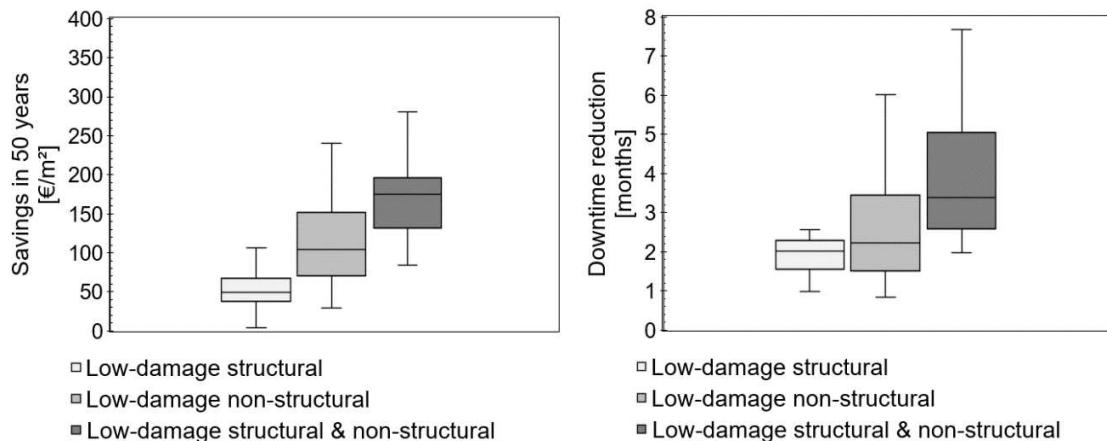


Figure 5.21. Statistical representation of the money savings (left) and downtime reductions (right) at ULS for all the low-damage building solutions (only low-damage structural skeleton, only damage-resistant non-structural elements, integrated system) when compared to the monolithic traditional structure.

From the previous tentative statistics, median values for both the money savings and downtime reduction can be calculated for the considered low-damage systems. Greater dispersions in the results are found to be related to the application of low-damage non-structural systems, due to the different alternative configurations adopted and herein simply grouped without distinctions. Finally, it is noticed that higher values of downtime reductions can be found if for all the case-study structures the complete methodology proposed in Almufti et al. (2013) for the estimation of the complete repair sequence, as presented in Figure 5.18 for the 5-storey structure in high seismicity zone, is applied.

The research has also studied the influence of the design in a low or high seismic zone on the loss assessment estimations. The benefits of low-damage solutions are evident for both seismicity

cases, yet, when considering low-seismicity condition, more substantial reductions of economic losses are obtained for the infill wall configurations.

5.3 Risk assessment analysis of precast concrete cladding systems: Traditional vs. Low-damage solution

With the aim of proving the high seismic capabilities of damage-resistant systems also in terms of probability of not being damaged when compared to more traditional systems, a risk assessment analysis is developed and herein presented. The study is implemented for the case of precast concrete cladding systems comprising different types of connections in order to define and compare the related fragility functions. Referring to an initial work proposed by Diafeira et al. (2011) and performing Incremental Dynamic Analyses, the damage probability of cladding systems with traditional tie-back (or slotted) connections after earthquakes of different intensities is determined. Then, the same investigation is developed introducing innovative connections (U-Shape Flexural plates, Baird et al. 2013) to highlight the benefits of adopting damage-resistant technologies for these non-structural systems.

5.3.1 Case-study building

The 5-storey reinforced concrete structure previously investigated is again taken into account. Nevertheless, the investigation focuses on the monolithic structural skeleton covered by precast concrete claddings. The building, designed at the Ultimate Limit State (ULS) level following the DDBD procedure, is now located in Norcia, Italy (PGAs of 0.341 g, Soil type C).

The precast concrete panels are 100 mm thick and include a central opening. The claddings are composed of dual-panel systems of 8 m total length in the frame direction (Figure 5.22) while mono-panel systems of 6 m in the wall direction. These panels are connected to the structural skeleton using two bearing (fixed) connections at the bottom of the panel while different types of connections are considered at the top (Figure 5.22- right): two traditional tie-back and/or slotted connections, designed considering a suggested drift of 0.2% (Baird et al. 2011), or dissipative U-Shaped Flexural Plate (UFP) connections (Baird et al. 2013), designed to yield at the same drift level of the other connection devices.

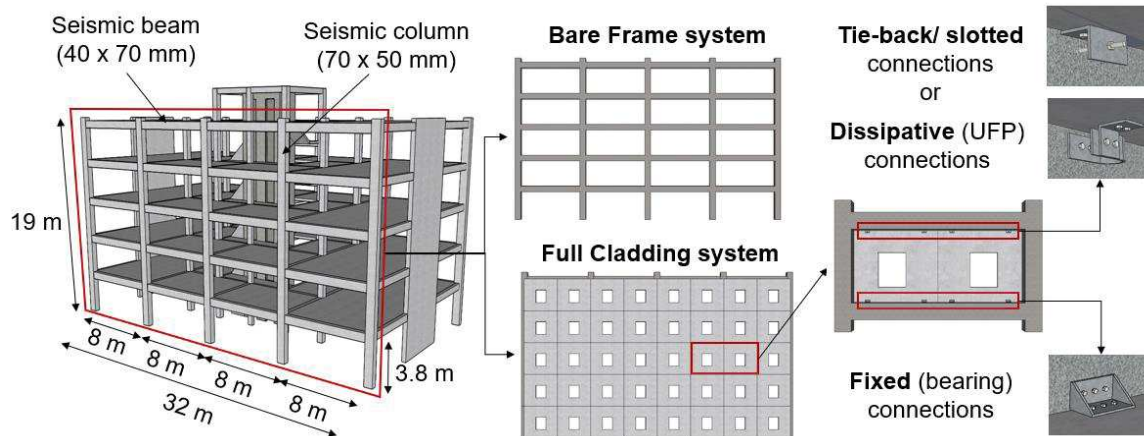


Figure 5.22. Case-study Building: global view and frame dimension (left); implemented numerical models (centre); configurations assumed for the cladding connections (right) (Bianchi et al. 2019b).

5.3.2 Numerical investigation

The longitudinal seismic frame of the structure, with first mode period of 0.86 s, is considered for implementing the proposed study.

5.3.2.1 Push-over analysis

Initial numerical non-linear static analyses are carried out using Ruaumoko 2D software (Carr 2003) and a lumped-plasticity approach with the aim of validating the system modelling, also highlighting the influence of non-structural systems in the global structural behaviour.

As described before, the structural skeleton is modelled by mono-dimensional elastic elements with plastic hinge regions at the end sections (Giberson elements). While, the precast concrete panels are modelled through an equivalent spring model consisting of a single linear spring representing the cladding panel and top and bottom connections described respectively by horizontal springs (tie-back or UFP - Bounded Ramberg Osgood - Figure 5.23, right) or dash-pots (slotted - Coulomb Dash-pot) and rigid links (bearing). The in-plane stiffness of the panel with a central opening as well as the properties of the connection elements are calibrated using the formulas proposed by Baird (2014). The rotations and axial displacements of these elements are restrained so that they can only deform horizontally.

Non-linear static pushover and push-pull analyses are initially performed, considering different connections at the top of the cladding panel: 1) tie-back connections made of long (250 mm) or short (50 mm) threader rods of 20 mm diameter; 2) slotted connections with 150 mm slot length; 3) UFP

connections composed of a 140 x 10 mm steel plate. The obtained push-over curves are presented in Figure 5.23 (left) and compared to the capacity curve of the bare frame system. This figure shows that the influence of such connection systems in the global response is limited. In fact, it can be observed how the stiffness and strength of the structure increase by a value of 3% for both the tie-back connections with long rods and slotted connections, 16% for the tie-back connections with short rods and 12% for the UFP connections.

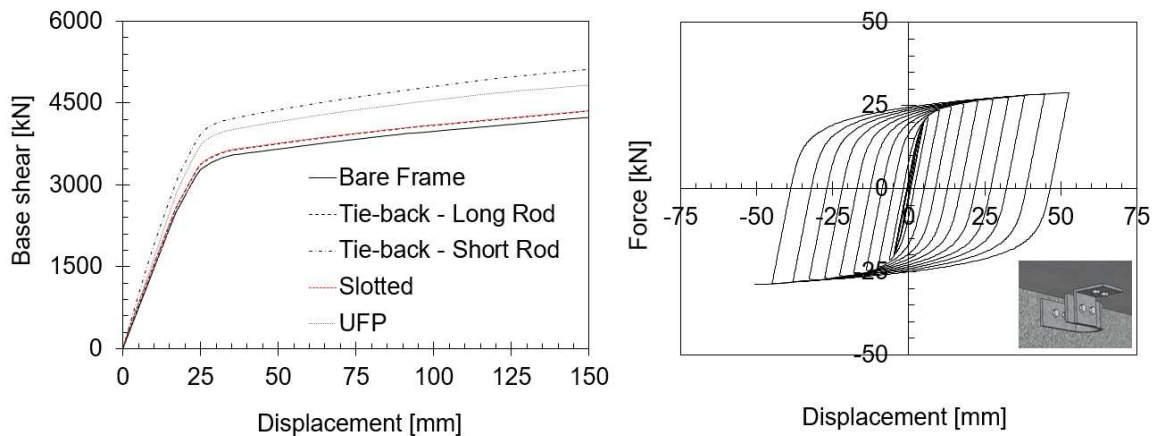


Figure 5.23. Numerical push-over curves (left) and hysteresis behaviour of UFP connection (right) (Bianchi et al. 2019b).

Notwithstanding the interaction with the structural system is very reduced, tie-back connections are expected to fail when a drift of 1.5-2% is reached. For slotted connections, if the displacement demand exceeds the slot capacity, the force transferred to the cladding system is much greater than the friction force alone and the connection becomes a fixed end threaded rod connection expected to fail at a certain point. When these connections fail, the heavy precast concrete panels may detach, and this damage condition may cause risk of hazard to human life. Consequently, substantial economic losses may develop.

Regarding the UFP connections, these dissipative systems take advantage of the interaction with the structural system to dissipate energy. Therefore, these connections reduce the demand on the panels and the consequent damage, moreover they are not expected to fail due to the achievement of a maximum displacement whilst for fatigue criteria (Kelly et al. 1972), that is in this case a minimum of 150 cycles (at the maximum stroke).

5.3.2.2 Incremental dynamic analysis

The probability of the connection damage can be calculated through seismic risk analyses. The reaching/overcoming of damage state conditions as well as the related fragility functions can be obtained through the implementation of the Incremental Dynamic Analysis (IDA) procedure proposed by Vamvatsikos and Cornell (2002). The connection behaviour can be identified from available experimental tests and expressed in terms of “connection drift”, representing the relative displacement of the connection divided by the inter-storey height. Therefore, the probability of reaching this Engineering Demand Parameter (EDP) as a function of an appropriate Intensity Measure (IM) can be found. The IDA investigation has been implemented considering a suite of 15 ground motion records representative of events likely to cause from moderate to severe shaking motions (up to 5.4 Moment Magnitude) in the Norcia area (Table 5.9).

Table 5.9. Suite of ground motion records used for the Incremental Dynamic Analysis.

N°	Event	Station	Mw	Soil	PGA [m/s ²]
1	Gubbio, 1984	CTC	5.6	B	0.489
2	Lazio Abruzzo, 1984	ST145	5.9	C	0.121
3	Lazio Abruzzo, 1984	ST1034	5.5	C	0.392
4	Umbria-Marche, 1997	AQK	5.7	B	0.043
5	Umbria-Marche, 1997	AQG	6.0	B	0.054
6	Umbria-Marche, 1997	ANNI	5.6	C	0.542
7	Umbria-Marche, 1997	ST229	5.5	D	0.134
8	Umbria-Marche, 1998	ST3177	5.4	B	0.299
9	L'Aquila, 2009	AQA	6.3	B	4.339
10	L'Aquila, 2009	AQF	5.6	B	0.772
11	Gran Sasso, 2009	AQA	5.4	B	0.568
12	Center Italy, 2016	NOR	6.5	C	3.574
13	Center Italy, 2016	NOR	6.5	B	5.216
14	Center Italy, 2016	AMT	6.0	B	8.508
15	Center Italy, 2016	NRC	6.0	B	3.668

The number of events selected are enough to provide sufficient accuracy in the estimation of seismic demands for mid-rise buildings, assuming an efficient IM, like the spectral acceleration

$Sa(T_1,5\%)$ (Shome and Cornell 1999). In fact, the IDA curves are obtained scaling the 15 accelerograms from 0.2g to 2g with a step of 0.2g in relation to their spectral acceleration $Sa(T_1,5\%)$ and a total of 150 analyses have been performed for every connection analysed.

5.3.2.3 Development of fragility curves

The fragility study is carried out referring to the case of long threaded rod tie-back connections. In fact, these systems have a better behaviour when compared to the short rod solution, as previously highlighted from the push-over curves. Moreover, these systems are more effectively described in the model than slotted connections, whose dash-pot components need to be adjusted to take into account the stiffness increase due to the achievement of the total slot length.

Taking into account that the performance of non-structural elements also depends on the response of the primary structure, the fragility curves have been prescribed to consider the occurrence building global collapse. Therefore, referring to the “total probability” (Jalayer 2003) both the conditions of building collapse, assumed as the achievement of 4% drift ratio as for the FEMA 356 (2000) recommendations, and no-collapse are considered. The functions describing the probability of occurrence building collapse/irreparability can be thus defined through a log-normal distribution (Figure 5.24 - left).

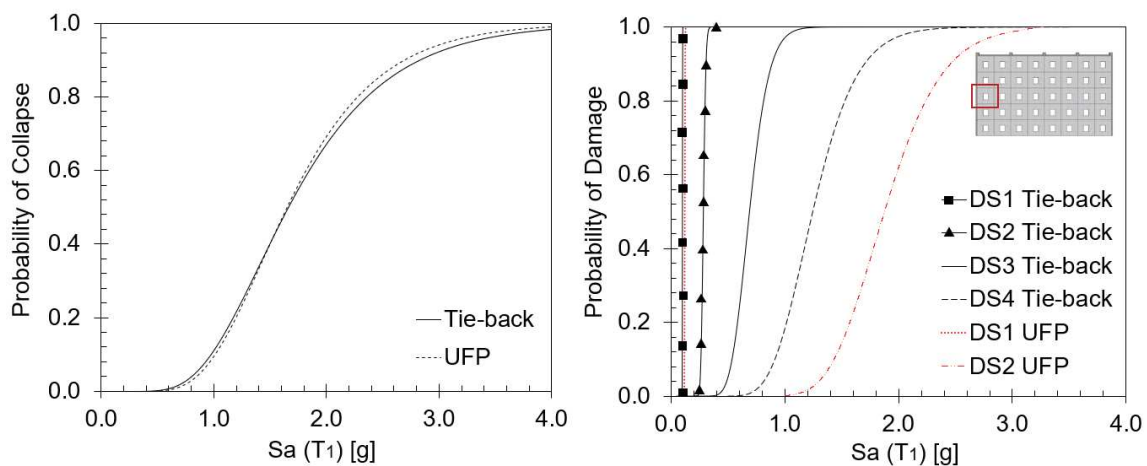


Figure 5.24. Left: Probability of occurrence collapse/irreparability of the Full Cladding system with tie-back or UFP connections; Right: Fragility curves of the traditional and low-damage connection of the lateral cladding on the third building floor (first connection which yields).

Based on this result, the fragility curves of the tie-back connections can be built taking into account the damage states presented in the previous Table 5.5 (DS1, pre-yielding; DS2, post-yielding and visible cracking; DS3, severe cracking; DS4, rupture of rod). These fragility functions

can be compared to the fragility curves estimated for the UFP connections adopted as an alternative solution, e.g. as shown in Figure 5.24 - right.

The previous graphs show that, notwithstanding the probability of collapse/irreparability of the building is very similar introducing tie-back or UFP connections at the top of cladding panels, the beneficial effects of the low-damage system in the fragility curves are evident. As previously described, the UFP connections fail for fatigue criteria however a damage state (DS2) due to the exceedance of the designed slot allowance of the connection can be assumed. Although both types of connections are designed to yield at 0.2% drift, it can be noticed that for example at 1.5g of S_a (T_1) the probability of being in DS4 for the tie-back connection is around 80% while for the UFP connection the probability of being in DS2 is around 10%.

Furthermore, the damage probabilities from the previous graph can be expressed in function of the annual frequency or return period of the earthquakes using the formula proposed by Maniyar et al. (2009). In this way, the probability of defined damage conditions not being exceeded for seismic demand of various annual probabilities can be determined (Figure 5.25).

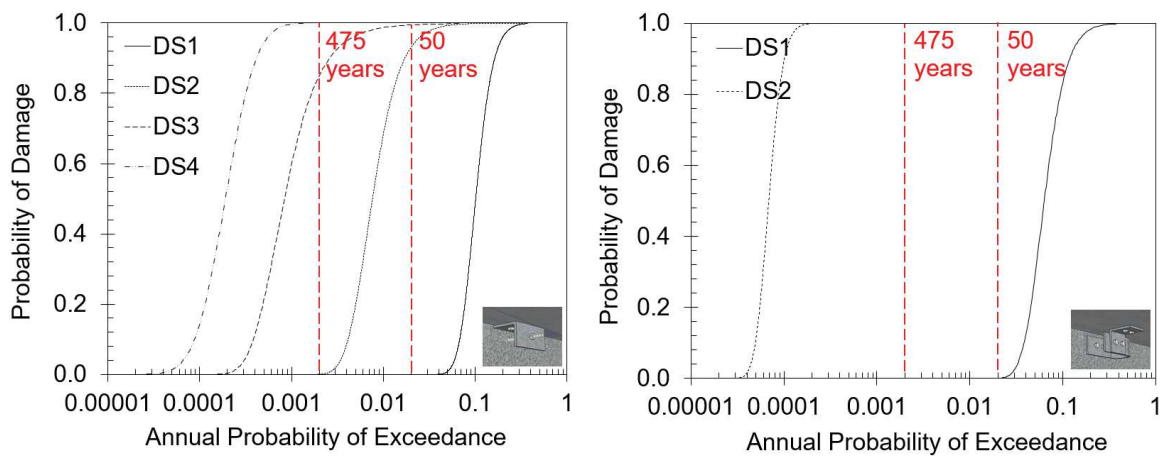


Figure 5.25. Probability of damage in relation of the annual probability of exceedance for both the tie-back connection (left) and UFP connection (right).

Referring to the seismic intensity levels of Damage Control (SLD, $T_R = 50$ years), it can be noticed that for the tie-back connection the probability of the damage states not being exceeded is around 90% for DS2 and almost 100% for DS3, while for the UFP connections the probability of not being exceeded is 100% for DS2. In the case of Life-Safety condition (SLV, $T_R = 475$ years) for the UFP connections the probability remains 100% whilst for the tie-back connections the probability for DS3 of not being exceeded becomes more than 80%. This highlights how the low-damage connections have a very high probability of not being damaged compared to the traditional system,

in addition to the fact that these solutions lead to very reduced post-earthquake non-structural damage, thus limited associated losses, because of their capability of dissipating the seismic energy.

5.3.3 Summary of the risk assessment analysis

The seismic performance of traditional (construction practice) non-structural systems can be improved introducing innovative low-damage solutions. These damage-mitigation solutions allow a reduction of the expected seismic losses due to the achievement of the corresponding damage states for very high displacements or accelerations, depending on the system sensitivity, when compared to more traditional systems. Therefore, with the aim of proving this concept, a qualitative risk assessment investigation is performed to show the convenience of implementing this new technology for the case, as example in the study, of heavy precast concrete cladding panels.

The results of the implemented investigation highlight that, although both the traditional and innovative connections are designed to yield at the same drift level, the collapse of the traditional system is achieved for very lower seismic intensities. While, the probability of damage conditions not being exceeded is very high for the low-damage solution when compared to the traditional system at different seismic demand levels.

5.4 Conclusions

This Chapter has provided evidence on the benefits of implementing structural and/or non-structural damage-mitigation solutions. In order to prove that these technologies are able to limit the post-earthquake damage withstanding higher seismic demand parameters (storey drift ratios or floor accelerations), thus reducing the expected socio-economic losses, cost/performance-based evaluations of different multi-storey reinforced concrete structures (3, 5, 7 storeys) are carried out. Considering alternative low-damage building systems (a low-damage structural skeleton with traditional non-structural elements; a monolithic cast-in-situ building with low-damage non-structural components; an integrated structural/non-structural low-damage system) and different typologies of non-structural components (precast concrete claddings or masonry infill walls or spider glazing curtain walls as exterior enclosures; gypsum or masonry walls as internal partitions; suspended ceilings; building services and contents) numerical investigations are implemented and numerical results are discussed in terms of either seismic performance (building performance points, fragility curves) or losses (repair costs and downtime). Further investigations are carried out considering the effect of the seismic hazard (building design in both low and high seismic areas) in the results.

The loss assessment results prove the benefits of the low-damage solutions in reducing the expected economic losses for both high and low seismicity zones, and this result is highlighted either from time-based results in terms of Expected Annual Losses or from intensity-based results, that is Downtime at ULS and repair costs, repair time and resilience curves at different intensity levels. Great reductions of the seismic losses are obtained for the integrated low-damage systems, i.e. savings of approximately 150-300 €/m² in 50 years building-life and downtime reduction at ULS of around 2-7 months when compared to the monolithic traditional solution. However, notwithstanding the benefits in the use of the sole damage-resistant structural members are evident, i.e. no residual deformations or structural repair simply related to the substitution of the easily replaceable external dissipaters, low-damage non-structural elements produce a considerable reduction of repair costs and downtime, especially for heavy infill walls for the condition of low-seismicity design (i.e. direct savings of about 220 €/m² in a 50-years building life, in addition to a downtime reduction of about 8 months under the design level earthquake - ULS seismic intensity).

Finally, the Chapter concludes with a final session on a qualitative risk assessment analysis of precast concrete cladding systems. Incremental Dynamic Analyses are performed to develop the fragility curves of cladding systems composed of traditional, i.e. tie-back, vs. low-damage, i.e. U-Shaped Flexural Plate, connections. The convenience of implementing the damage-resistant solution is shown in terms of both seismic performance and probability of damage levels not being exceeded at various intensity levels.

5.5 References

- Almufti I. and Willford M. (2013). *Resilience-based Earthquake Design Initiative for the Next Generation of Buildings*, (REDi™) Rating System, London, England.
- Applied Technology Council (1996). *Seismic evaluation and retrofit of concrete buildings, Volume 1, Technical Report ATC 40*, Redwood City, California, USA.
- Baird A., Palermo A., Pampanin S. and Riccio P. (2011). Focusing on reducing the earthquake damage to Façade Systems, *Bulletin of New Zealand Society of Earthquake Engineering*, 44(2): 108-120.
- Baird A., Palermo A., and Pampanin S. (2013). Controlling Seismic Response using Passive Energy Dissipating Cladding Connections, *Proceedings of 2013 NZSEE Conference*, Wellington, New Zealand.
- Baird A. (2014), Seismic Performance of Precast Concrete Cladding Systems, *Ph.D. Thesis*, University of Canterbury, Christchurch, New Zealand.
- Baird A., Smith T., Palermo A., Pampanin S. (2014). Experimental and numerical Study of U-shape Flexural Plate (UFP) dissipators, *Proceedings of 2014 NZSEE Conference*, Auckland, New Zealand.
- Bertoldi S. H., Decanini L. D. and Gavarini C. (1993). Telai tamponati soggetti ad azione sismica, un modello semplificato: confronto sperimentale e numerico, *Proceedings of 6th Convegno Nazionale ANIDIS*, Perugia, Italy.
- Bianchi S., Ciurlanti J., and Pampanin S. (2018). A cost/performance-based evaluation of low-damage building systems, *Proceedings of 16th European Conference on Earthquake Engineering*, Thessaloniki, Greece.
- Bianchi S., Ciurlanti J., and Pampanin S. (2019a). Cost/performance evaluation of traditional and low-damage structural & non-structural building configurations, *Proceedings of 4th International Workshop on the Seismic Performance of Non-Structural Elements (SPONSE)*, Pavia, Italy.
- Bianchi S., Ciurlanti J., and Pampanin S. (2019b). Seismic vulnerability of non-structural components: from traditional solutions to innovative low-damage systems, *Proceedings of Conference on Earthquake risk and engineering towards a resilient world*, SECED, London, England.
- Cardone D. and Perrone G. (2015). Developing fragility curves and loss functions for masonry infill walls, *Earthquakes and Structures*, 9(1): 257-279.
- Carr A.J. (2003). *Ruaumoko Program for Inelastic Dynamic Analysis - User Manual*, University of Canterbury, Christchurch, New Zealand.
- Cattanach A. and Pampanin S. (2008). 21st Century Precast: the Detailing and Manufacture of NZ's First Multi-Storey PRESSS-Building. *Proceedings of 2008 NZ Concrete Industry Conference*, Rotorua, New Zealand.
- Cornell C. A., Jalayer F., Hamburger R.O., Foutch D.A. (2002). Probabilistic basis for 2000 SAC Federal Emergency Management Agency steel moment frame guidelines, *ASCE Journal of Structural Engineering*, 128 (4): 526-533.
- Crisafulli F.J. (1997). Seismic behaviour of reinforced concrete structures with masonry infills, *Ph.D. Thesis*, University of Canterbury, Christchurch, New Zealand.

- Diaferia R., Baird A., Palermo A. and Pampanin S. (2011). Numerical Study on the Seismic Interaction Between 2D Seismic Resisting Frames and Claddings, University of Canterbury, New Zealand
- Federal Emergency Management Agency (2000). *Prestandard and Commentary for the seismic rehabilitation of buildings, Technical Report FEMA 356*, Washington, USA.
- Federal Emergency Management Agency (2012). *Seismic Performance Assessment of Buildings, Volume 1 – Methodology, Technical Report FEMA-P-58-1*, Washington, D.C., USA.
- Garro, A.E. (2017). Cost-Benefit Evaluation of Post-Tensioned Rocking-Dissipative Concrete Buildings, *Master Thesis*, Istituto Universitario di Studi Superiori, Pavia, Italy.
- Jalayer F. (2003). Direct Probabilistic Seismic Analysis: Implementing Non-Linear Dynamic Assessments, *Ph.D. Thesis*, Stanford University, United States.
- Kelly J.M., Skinner R.I. and Heine A.J. (1972). Mechanisms of energy absorption in special devices for use in earthquake resistant structures, *Bulletin of New Zealand Society for Earthquake Engineering*, 5(3): 63–88.
- Krawinkler H., Miranda E. (2004). *Performance-based earthquake engineering. Earthquake Engineering: from engineering seismology to performance-based engineering*, Bertero VV (eds), CRC Press: Boca Raton.
- Maniyar M., Khare R.K. and Dhakal R.P. (2009). Probabilistic Seismic Performance Evaluation of Non Seismic RC Frame buildings, *Structural Engineering and Mechanics*, 33(6).
- Moehle J. and Deierlein G. (2003). A framework methodology for performance-based earthquake engineering, *13th World Conference on Earthquake Engineering*, Vancouver, B.C., Canada.
- NTC (2018). *Aggiornamento delle Norme Tecniche per le Costruzioni*, Supplemento ordinario n°8 alle G.U. n° 42 del 20/02/2018, serie generale, Rome, Italy.
- Nuzzo I., Pampanin S., Caterino N. (2018). Proposal of a New Loss Ratio Performance Matrix in Seismic Design Framework, *16th European Conference of Earthquake Engineering*, Thessaloniki, Greece.
- Pampanin S., Marriott D., Palermo A. and New Zealand Concrete Society (2010). *PRESSS Design Handbook*, Auckland, New Zealand.
- Porter K.A. (2003). An Overview of PEER's Performance-Based Earthquake Engineering Methodology. *9th International Conference on Applications of Statistics and Probability in Civil Engineering*, San Francisco, California, USA.
- Pourali A., Dhakal R.P., MacRae G.A., and Tasligedik A.S. (2017). Fully-floating suspended ceiling system: experimental evaluation of the effect of mass and elastic isolation, *Proceedings of 16th World Conference on Earthquake Engineering*, Santiago, Chile.
- Priestley M.J.N., Sritharan S., Conley J.R., Pampanin S. (1999). Preliminary Results and Conclusions from the PRESSS Five-Story Precast Concrete Test Building. *PCI Journal*, 44(6): 42–67.
- Priestley M.J.N., Calvi G.M., Kowalsky M.J. (2007). *Direct Displacement-Based Seismic Design of Structures*, 1st edition, IUSS Press, Pavia, Italy.

- Shome N. and Cornell C.A. (1999). *Probabilistic seismic demand analysis of nonlinear structures*, Report No. RMS-35, RMS Program, Stanford University, Stanford, USA.
- Smith T., Fragiaco M., Pampanin S., Buchanan A.H. (2009). Construction Time and Cost for Post-tensioned Timber Buildings. *Construction Materials*, 162(4): 141-149.
- Sivanerupan S., Wilson J.L., Gad E.F. and Lam N.T.K. (2014). Drift Performance of Point Fixed Glass Façade Systems, *Advances in Structural Engineering*, 17(10): 1481-1495.
- Structural Engineers Associate of California (1995). Performance-based seismic engineering, SEAOC Vision 2000, Sacramento, California, USA.
- Tasligedik A.S. and Pampanin S. (2016). Rocking Cantilever Clay Brick Infill Wall Panels: A Novel Low Damage Infill Wall System, *Journal of Earthquake Engineering*, 21(7): 1023-1049
- Tasligedik A.S., Pampanin S. and Palermo A. (2014). Low damage seismic solutions for non-structural drywall partitions, *Bulletin of Earthquake Engineering*, 13(4): 1029–1050.
- Uday P. and Marais K. (2015). Designing Resilient Systems-of-Systems: A Survey of Metrics, Methods, and Challenges, *Systems Engineering*, 18(5): 491–510.
- Vamvatsikos D. and Cornell C.A. (2002). Incremental dynamic analysis, *Earthquake Engineering Structural Dynamics*, 31(3): 491-514.

6. 3D shake-table tests on an integrated low-damage building system: Test Building design and construction

6.1 Introduction

This Chapter describes the experimental campaign, fully funded within a European SERA project, carried out on an integrated structural/non-structural low-damage building system. A two-storey 1:2 scale fully prefabricated and dry-assembled timber-concrete low-damage structure comprising different non-structural systems (concrete and glass facades; gypsum and masonry partitions) has been designed to be tested on a 3D shaking table.

The specimen design, the structural and non-structural detailing as well as the manufacturing and assembly/construction of the Test Building is herein fully described. More detailed information on the design procedure, structural verifications and construction phases can be found in **Appendices C** and **D**. The description of the experimental campaign (test setup, monitoring system and preliminary results) will be completed in Chapter 7 of this Thesis.


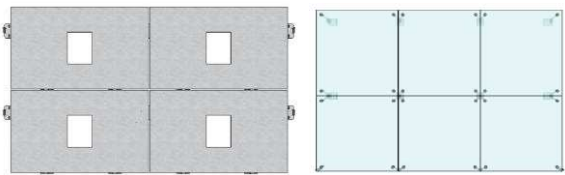

6.2 Proposed EU-funded SERA project

As largely explained in Chapter 4, targeting life-safety is arguably not enough for our modern society and communities. The performance-based design objectives need a paradigm shift towards a low-damage design philosophy with the final goal of developing a cost-affordable high-performance building system, including structural and non-structural elements, services and soil foundation systems. The integrated building system is therefore capable of sustaining a design level earthquake

with limited damage, controllable socio-economic losses and minimum disruption of business. This integrated structural/non-structural low-damage building system is rapidly moving towards the “ultimate earthquake proof” building that our society is expecting. Experimental shake-table tests on such an integrated system have been firstly carried out on a shake-table of a two-storey concrete frame structure under unidirectional 2D loading (Johnston et al. 2014). However, more comprehensive investigations are needed to demonstrate the high seismic performance of this type of buildings and refine connection and construction details. For this reason, as part of an EU-funded SERA project, 3D large-scale shake-table tests (under 3 degrees of freedom input motions, two horizontal and one vertical components) of a complete low-damage system have been carried out at the Laboratório Nacional de Engenharia Civil (LNEC) in Lisbon.

The SERA research project, titled “(Towards the) Ultimate Earthquake Proof Building System: development and testing of integrated low-damage technologies for structural and non-structural elements”, intended to promote a research effort within the European environment for the wider industry/community uptake of an integrated low-damage building system, including skeleton and non-structural components for the next generation of buildings. Particularly, a low-damage structural system combined with high performance or low-damage non-structural elements, as summarized in Table 6.1, was built to be tested experimentally.

Table 6.1. Structural and non-structural systems characterizing the Test Building.

Structural system	Non-structural system
<p data-bbox="204 1294 710 1328">Low-damage: PRESSS, PresLam technologies</p> 	<p data-bbox="762 1294 1417 1357">High seismic performance facade systems: Glass Fiber Reinforced Concrete claddings, Spider Glazing systems</p>  <p data-bbox="762 1585 1417 1648">High seismic performance and low-damage partition walls: Fiber Reinforced Gypsum walls, Unreinforced Masonry walls</p> 

Design methodologies and technical solutions for both the structural skeleton and the non-structural components were considered to define the Test Building. Employing modular demountable, replaceable and relocatable components facilitate the re-arrangement of internal

spaces, layout and exterior envelope of this typology of building systems. This in turn would allow in real constructions for potentially several changes of use during its lifetime with also potential re-usability and recyclability of obsolete or not anymore fit-for-purposes components.

The overall research project comprised analytical/numerical and experimental investigations focusing around the shake table tests of a 1:2 scale two storey-two bay low-damage building system, consisting of structural skeleton (frames in one direction and walls in the other) and non-structural components/envelope. Some of the research project phases, i.e. the design of the specimen and its detailing (structural/non-structural) as well as the manufacturing and construction processes are described within this Chapter.

6.3 Description of the experimental campaign

The experimental research focused on non-destructive shaking table tests (1D, 2D and 3D) of a timber-concrete low-damage building system, comprising self-centring and dissipative structural systems, combined with high-performance or low-damage non-structural technologies. The campaign involved three testing Phases, each of them characterized by a different system configuration as shown in Figure 6.1.



Figure 6.1. Test Building configurations: Skeleton Building (left), Option1 (centre), Option2 (right).

The three Test Building solutions are:

- Skeleton Building (SB)

The low-damage structural skeleton system was initially tested. The specimen consisted of post-tensioned timber beams, precast concrete columns and hybrid post-tensioned rocking-dissipative connections in one direction and post-tensioned rocking-dissipative low-damage timber walls in the orthogonal direction. External replaceable *Plug&Play* dissipaters were implemented in both frame and wall systems. Regarding the flooring systems, two different

typologies of timber-concrete slab were introduced, namely a Timber-Concrete Composite (TCC) flooring system on the first level and a Pre-stressed Timber-Concrete flooring system (3PT) on the second level of the Test Building.

- Option 1 (O1)

Fibre-reinforced gypsum partition walls with low-damage detailing were built on the first floor of the specimen. Therefore, the Skeleton Building with internal partition walls represented the second system to be tested.

- Option 2 (O2)

Finally, an integrated structural/non-structural solution was tested. The Skeleton Building was “dressed” using Glass Fiber Reinforced Concrete (GFRC) cladding systems in the frame direction and spider glazing curtain walls in the other direction, while the internal gypsum wall was substituted by an unreinforced masonry partition comprising low-damage detailing.

The SERA project was proposed trying to achieve three main objectives:

1. Development, refinement and validation of the seismic response of 3D innovative low-damage structural systems based on post-tensioned rocking dissipative solutions for multi-storey and open-space post-tensioned buildings with hybrid (concrete-timber) materials and structural systems (frames and walls).
2. Investigation on the seismic performance of different typologies of non-structural elements, including façade systems and partition walls made of high seismic performance or low-damage detailing.
3. Investigation of the full interaction between structural and non-structural components during simulated real-time seismic response under three directions. Particularly focusing on: displacement-incompatibility issues between frames, walls, floor systems and non-structural components; floor spectra and acceleration-displacement demand to non-structural components; validation and refinement of currently used non-linear macro-models; calibration of interface/local behaviour by using FEM micromodels; calibration of ‘elastic’ damping and hysteretic models for design purposes; performance assessment of various components vs. predictions (limit states, fragility curves, structural and economical/losses).

The experimental tests were carried out at the Laboratório Nacional de Engenharia Civil (LNEC) in Lisbon where a 5.60 x 6.20 m shaking table is available. The Test Building was subjected to earthquake motions of increasing level of intensity, considering alternatively input motions in the orthogonal directions, simultaneously in both directions as well as adding vertical shaking. The

selected input ground motions were representative of spectral-compatible earthquakes at various level of code-based limit states up to Collapse Prevention, as described in Chapter 7 of the Thesis.

6.2.1 Test Building design

The Test Building was designed considering a hypothetical full-scale Prototype Building (Figure 6.2) with typical structural dimensions of an inner core of multi-storey commercial buildings while ensuring the specimen could fit within the size and weight limitations of the shake table. Moreover, the Test Building had to be compatible to the size of the steel foundation already available in the laboratory LNEC of Lisbon.

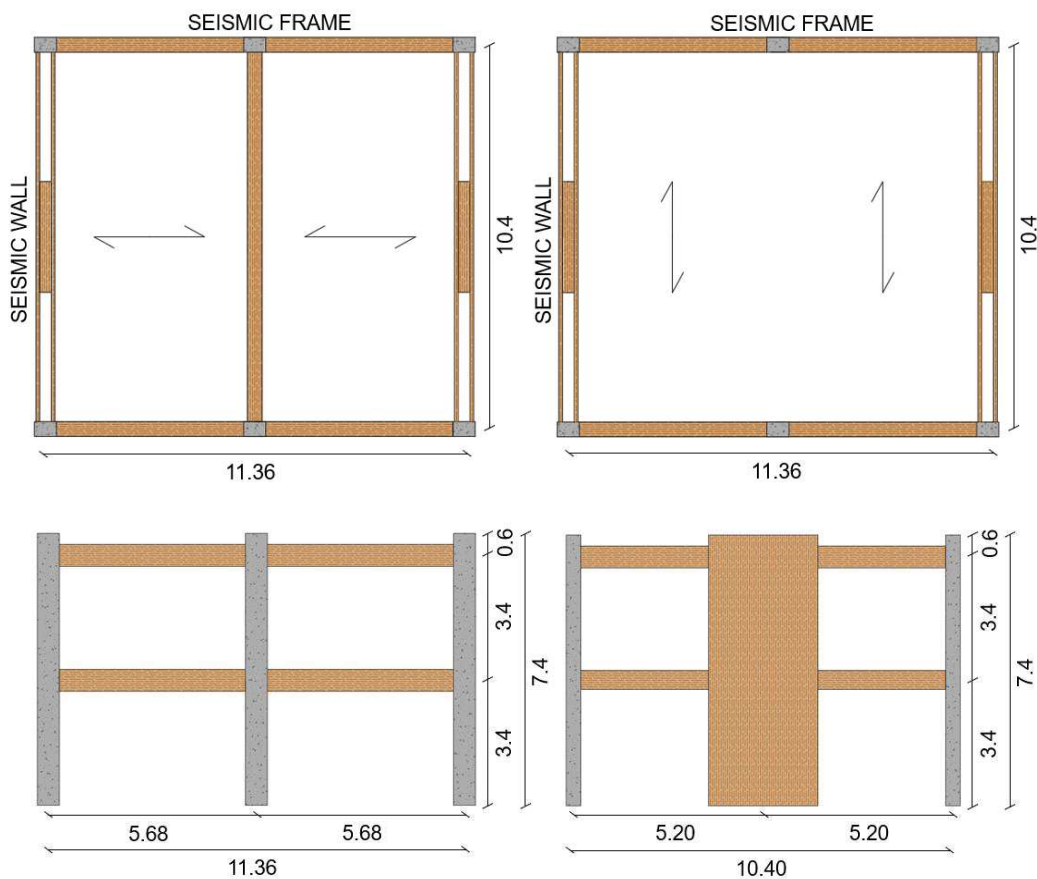


Figure 6.2. Plan and elevation views - Prototype Building.

The Prototype Building was a two-storey structure with two seismic resistant post-tensioned frames in the longitudinal direction (timber beams and concrete columns) and two post-tensioned timber walls in the transverse direction. It had a footprint (centre-to-centre) of 11.36 m x 10.4 m with 5.68 meters bay length in the frame direction, 10.4 meters bay length in the wall direction, and the total footprint was 11.96 m x 10.8 m. The inter-storey height was 3.4 m, while the total building height

was 7.4 m. The structural frames consisted of timber seismic beams with horizontal post-tensioned wire strands and mild steel external dissipaters (Steel S 355) and concrete columns with B 450C reinforcement bars and mild steel external dissipaters (Steel S 355). While, the re-centring timber walls in the transverse direction comprised a post-tensioned bar and mild steel external dissipaters (Steel S 355). Non-seismic timber beams were introduced in the wall direction: 1) edge or sandwich beams connected to the walls through a pinned connection; 2) a central gravity beam supporting the flooring system on the first level. A summary of the section geometry and type of material proper to each component is reported in Table 6.2.

Table 6.2. Section geometry and material of the structural components - Prototype Building.

Component	Section geometry	Material
Seismic beam	400 x 600 mm	Timber, GLULAM 32h
Seismic column	400 x 600 mm	Concrete, C 35/45
Seismic wall	316 x 3000 mm	Timber, XLam C24
Edge beams (sandwich beams)	100 x 520 (first level) or 600 mm (second level)	Timber, GLULAM 32h
Central beam (gravity beam)	400 x 600 mm	Timber, GLULAM 32h

Apart from the self-weight of the structural skeleton, the seismic design of the Prototype Building was implemented including the weight (G_1 and G_2) and live load (Q) of the flooring system on the two building levels, i.e. 1) a Timber-Concrete Composite floor with 120x440 mm timber joists 2000 mm-spaced, 25 mm plywood and 60 mm reinforced concrete slab and 2) a 3PT pre-stressed flooring system composed of 5 timber-concrete beams of 2152x240 mm (details of both flooring typologies can be found in the description of the specimen). The weight of the non-structural components, referring to the exterior enclosures and internal partitions to be subsequently included into the specimen, was finally added to refine the total mass value.

The seismic design at the Ultimate Limit States (475 years return period earthquake for an Importance Class 2) was carried out following the Direct-Displacement Based Design (DDBD) procedure by Priestley et al. (2007) and Pampanin et al. (2010) and considering the seismic demand associated with a seismicity representative of a high seismic zone in Italy. In fact, the demand parameters of the zone were obtained as mean values from 5 locations in Italy PGA of 0.353 g and the related elastic design acceleration and displacement spectra (5% damped and Soil type C) at ULS are presented in Figure 6.3.

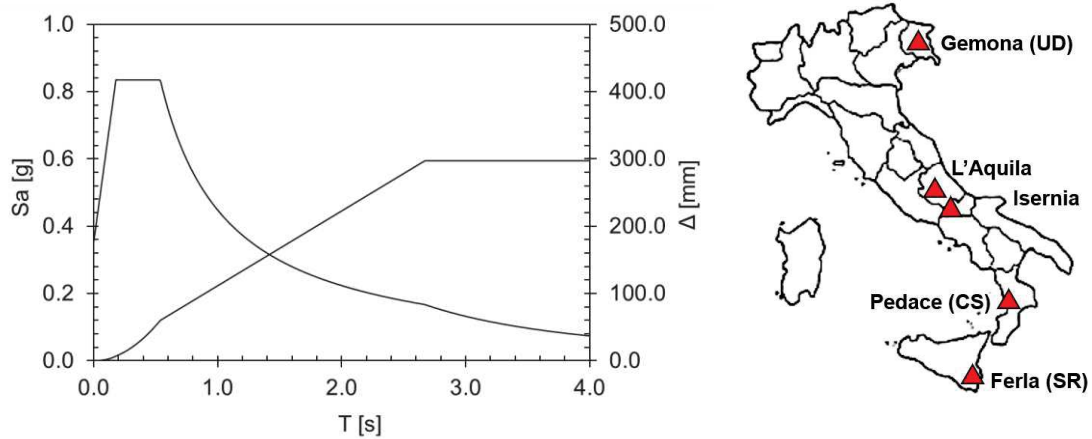


Figure 6.3. Left: Elastic acceleration and displacement spectra at ULS. Right: 5 locations contributing in the definition of the seismic demand parameters.

The DDBD procedure was implemented with reference to an inter-storey target drift of 1.5% and 1.0%, in the frame and wall direction, respectively, and the design parameters obtained for both building directions are listed in Table 6.3. Distributing the base shear throughout the structural system, the hybrid connections were designed considering a re-centering ratio λ equal to 1.25 (56% contribution from the unbonded post-tensioned tendons and 44% contribution from the dissipative external devices).

Table 6.3. Design parameters - Prototype Building.

Parameter	Frame Direction	Wall Direction
Design inter-storey drift θ_d [%]	1.5	1.0
Design displacement Δ_d [mm]	82.9	55.1
Effective mass m_e [t]	93.5	93.5
Effective height H_e [m]	5524.1	5524.1
Equivalent viscous damping ξ_{eq} [%]	13.4	14.7
Effective period T_e [s]	0.90	0.61
Effective stiffness K_e [kN/m]	4504.6	9761.7
Base shear V_b [kN]	373.3	538.3

Then, the Cauchy-Froude similitude of constant stress and constant acceleration was applied to determine the geometrical configuration of the 1:2 ($\lambda=0.5$) scale Test Specimen configuration. Therefore, the Test Building components were designed considering the scaled forces from the Prototype Building as well as applying the same DDBD procedure, as further verification. Additional masses (driving masses) were required to be added to the Test Specimen when compared to the

Prototype Building, representing the increased density due to scaling (8.6 tons for the first level, 7.2 tons for the second level). The global geometry of the Test Building can be found in Figure 6.4, while Table 6.4 presents the scaled dimensions and the material of each building component.

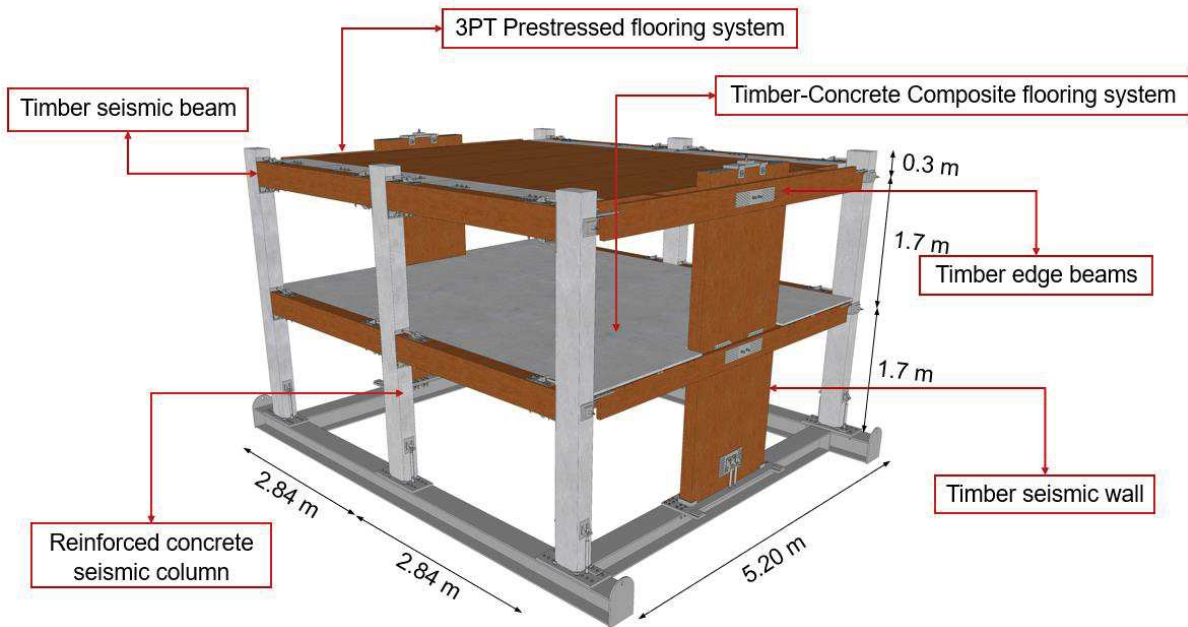


Figure 6.4. Global dimensions of the Test Building.

Table 6.4. Section geometry and material of the structural members - Test Building.

Component	Section geometry	Material
Seismic beam	200 x 300 mm	Timber, GLULAM 32h
Seismic column	200 x 300 mm	Concrete, C 35/45
Seismic wall	158 x 1500 mm	Timber, XLam C24
Edge beams (sandwich beams)	50 x 260 (first level) or 300 mm (second level)	Timber, GLULAM 32h
Central beam (gravity beam)	200 x 300 mm	Timber, GLULAM 32h

The design parameters for the specimen, obtained from the Cauchy-Froude similitude or from the implementation of the DDBD procedure, are summarized in Table 6.5. It is observed that the design inter-storey drift ratios may be higher for this typology of structures. However, in this specific case the design drifts were assumed taking into account material limitations for the wall direction due to the cracking limit of the XLam C24 timber. In general, the limited mass allowable for the specimen on the shake-table (31 tons, i.e. 40 tons minus the 9 tons of the existing heavy steel foundation) as well as the high number of components resisting to the seismic actions did not let to

move the design towards higher drift values. In fact, higher drift values would require dissipater sections so reduced to be unfeasible to build.

Table 6.5. Design parameters - Test Building.

Parameter	Frame Direction	Wall Direction
Design inter-storey drift θ_d [%]	1.50%	1.00%
Design displacement Δ_d [mm]	41.43	27.6
Effective mass m_e [t]	23.4	23.4
Effective height H_e [m]	2762.1	2762.1
Equivalent viscous damping ξ_{eq} [%]	13.4	14.69
Effective period T_e [s]	0.64	0.43
Effective stiffness K_e [kN/m]	2252.3	4880.9
Base shear V_b [kN]	93.3	134.6

6.2.1.1 Connection design

Considering the base shear from the DDBD procedure, the forces acting on each structural component were identified, thus the hybrid connections (beam-column joint, column-base and wall-base) could be designed. The connection design was developed following the procedure described in the NZCS PRESS Design Handbook (Pampanin et al. 2010) for the concrete elements and in the STIC Design Guidelines (Pampanin et al. 2013) for the timber components.

Table 6.6 provides the properties of the post-tensioned wire strands of the seismic beams and of the threaded bar inside the seismic walls. While, the external dissipaters of the structural elements were obtained from necking-down 16mm or 20mm mild steel bars (from 16 mm to 6.8/8.8 mm for the beam dissipaters, from 20 mm to 14/15.6 mm for the column dissipaters, from 16 mm to 11 mm for the wall dissipaters).

Table 6.6. Post-tensioned wire strands and threaded bars.

Structural member	Type of component	Diameter [mm]	Force [kN]
Beam - 1°floor	1/2" wire strands	12.5	~ 70
Beam - 2°floor	3/8" wire strands	9.3	~ 50
Wall	18WR threaded bar	17.5	~ 50

A complete description of the connection design is presented in **Appendix C**, however the Moment-Rotation curves obtained combining both the dissipation capability of the external

dissipators and the re-centring capability of the post-tensioned wire strands/bars (or only the contribution of axial load for the concrete columns) are shown in Figure 6.5.

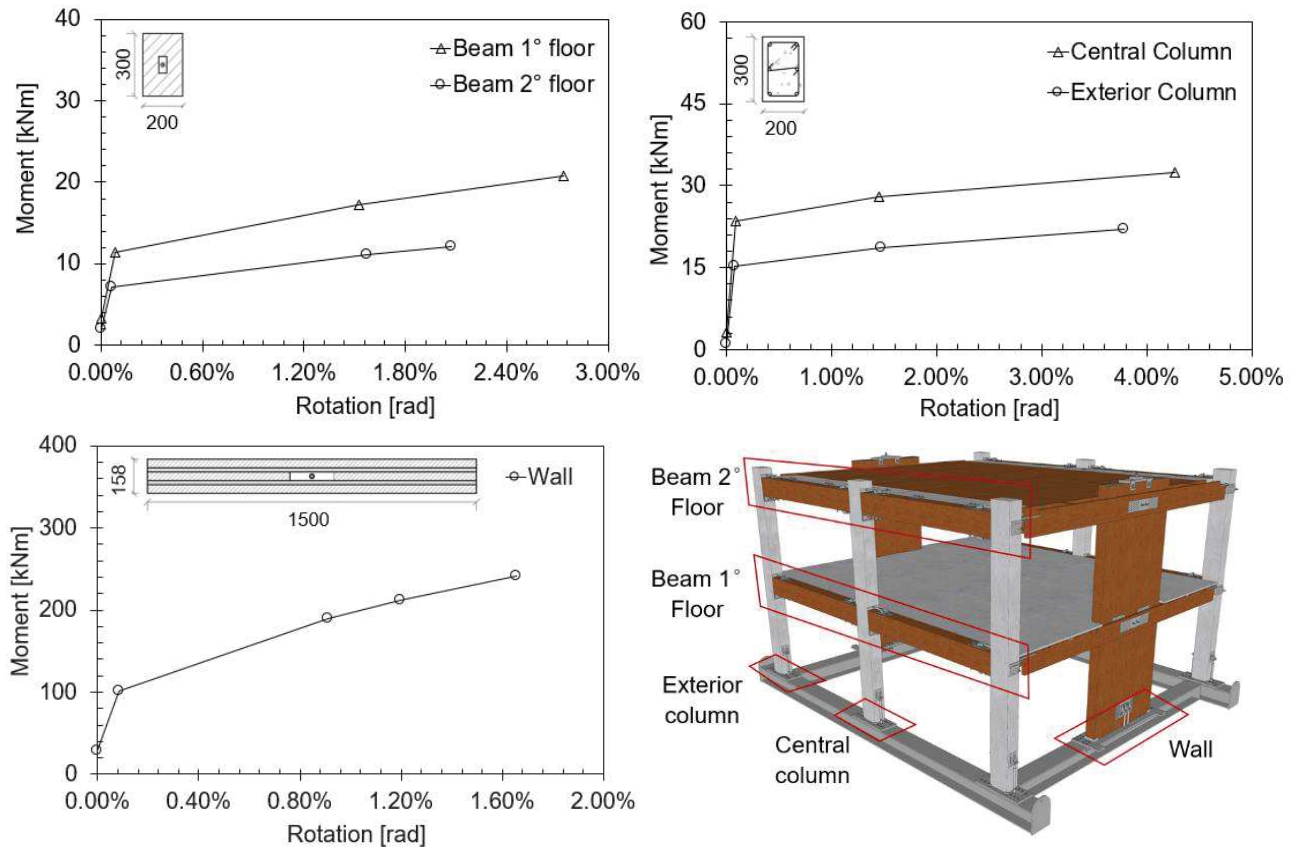


Figure 6.5. Moment-Rotation relationships for the beam-column (top-left), column-foundation (top-right) and wall-foundation connections (bottom-left), as indicated in the bottom-right picture.

In addition to the design of the post-tensioned tendons/cables, i.e. type and initial force, and the design of the external dissipaters, i.e. determination of diameter and internal fuse dimensions of the steel bar, it was very important to design the structural detailing, including all the steel assemblies (steel plates, bolts, screws, nails, welding) introduced for correctly realizing the hybrid connections. A summary of all the structural verifications implemented for the different components and details are reported in **Appendix C**, while in Figure 6.6 the hybrid connections are shown through renders.

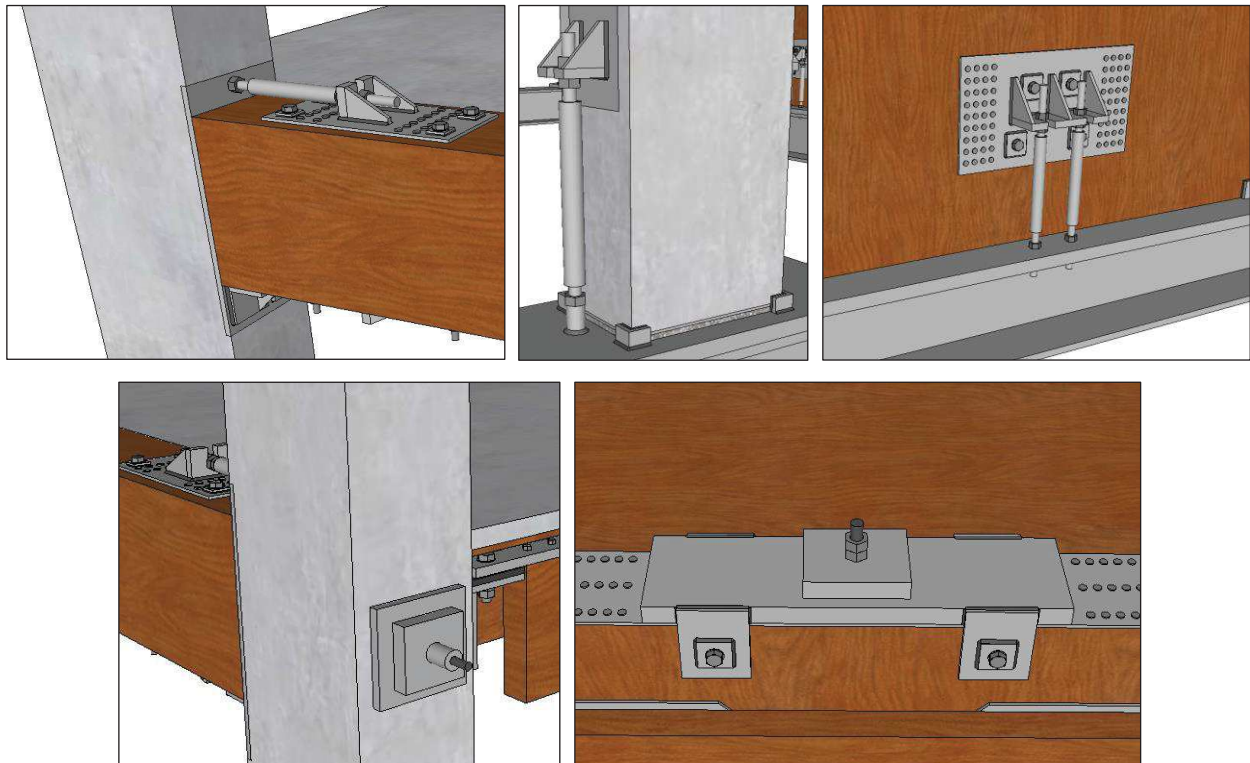


Figure 6.6. Detailing of the hybrid connections: connection of dissipaters to the beam and column in an external joint (top - left), connection of external dissipaters to the column/wall and to the steel foundation (top - centre and right), anchorage for the wire strands of the timber beams (bottom - left), upper anchorage of the post-tensioned bar of the wall (bottom - right).

Concerning the beam-column connection, the dissipator anchorage in the column was a coupling nut, which allowed the dissipater to be screwed into a reinforcing anchor bar. For the anchorage in the beam, a steel assembly was properly realized to bolt the dissipator. The anchorages were designed to locate the dissipaters away from the column face allowing them to be replaced easily, also ensuring no undesired interaction with the rocking beams. For the case of column/wall-foundation connection, the external dissipaters were screwed into welded couplers or directly bolted on the steel foundation plate, and a proper steel assembly was created to connect the dissipaters to the concrete column or to the timber wall. Finally, regarding the post-tensioned wire strands and the post-tensioned threaded bar, a specific anchorage system (assembly of steel plates) was realized on the external sides of the lateral columns and on the top/bottom of the timber wall/steel foundation respectively (Figure 6.6, bottom - left and right).

6.2.1.2 Structural members

Apart from the hybrid connections, many structural details were introduced: 1) to properly connect the steel foundation plates of columns and walls to the steel foundation available in the laboratory, 2) for positioning the seismic, edge and central beams, 3) to properly connect the edge (sandwich) beams to the wall (pinned connection) and to the lateral concrete columns, 4) for positioning the two flooring systems, 5) for connecting the floors to the lateral seismic resistant systems, thus allowing an appropriate transfer of forces to the structure. All these details are not herein presented (refer to the technical report of the project for more details), since the Thesis focuses on non-structural systems, however, they were fundamental for providing the correct functionality to the overall system. These structural detailing, including all the steel plates, shear keys, pins, bolts, screws, nails, welding, were verified referring to methodologies and formulas indicated in international codes (EN 1995-1-1 2004; EN 1993-1-8 2005; EN 1993-1-1 2005; NTC 2018; NZS 3404-1,2 1997; NZS 3404-1 2009; NZS 3101-1,2 2006; NZS 3603 1993; STIC 2012; STIC 2013; AS/NZS1170 2002), as also indicated in **Appendix C** of the Thesis.

The two lateral views of the Skeleton Building are shown in the following Figure 6.7 through rendering.

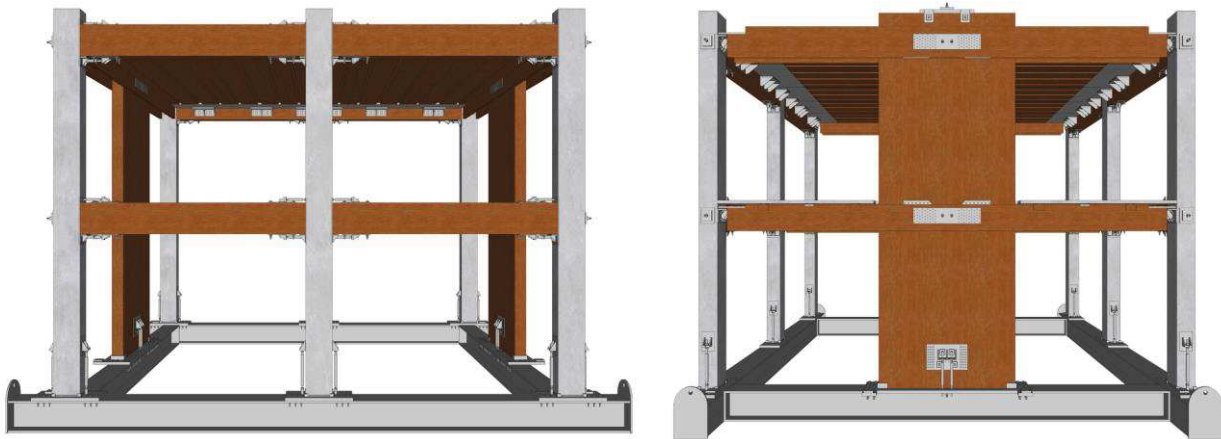


Figure 6.7. Elevation views of both the frame (left) and wall (right) directions of the Skeleton Building.

Concerning the flooring systems, the first floor of the specimen was a Timber-Concrete Composite (TCC) floor designed following the STIC (2012) and AS/NZS (2002) 1170 series, using a deflection control value of $L/\Delta > 300$, and consisting of 60 x 220 mm timber joists, 12.5 mm plywood and 30 mm concrete slab on the top (Figure 6.8). Reinforcing bars were designed to be introduced in the concrete slab for guaranteeing a correct diaphragm action to the floor itself. While, the second

floor was a 3PT prestressed timber-concrete floor (Palermo and Pampanin 2017) composed of 1076 x 120 mm timber-concrete beams with 3 wire-strands of 6.4 mm diameters (Figure 6.9). The wire-strands were located in a central hole at the bottom part of the timber or inside a steel tube casted into the concrete part. Detailing of the two flooring systems are not reported in this Thesis, however more information can be found in the structural report and drawings of the research project.

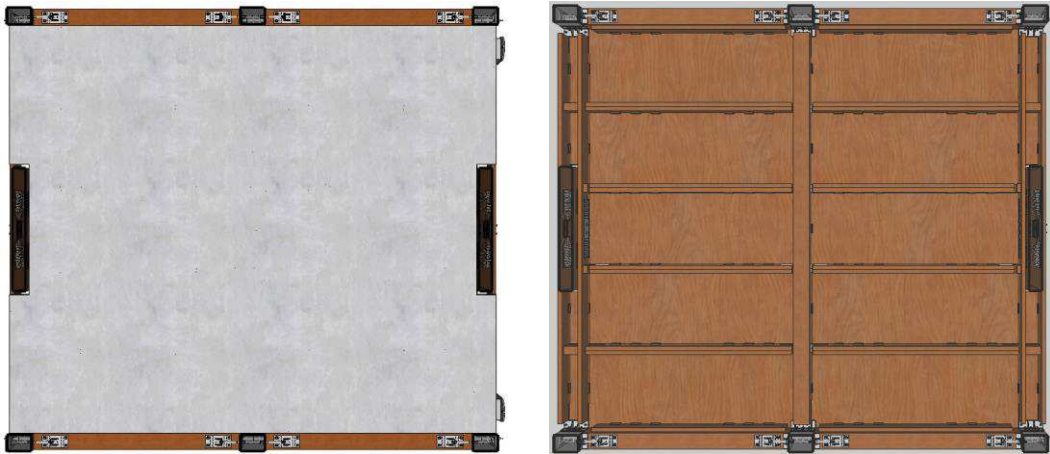


Figure 6.8. Timber-Concrete Composite floor on the first level of the Skeleton Building: view from the top (left) and view from the bottom (right).

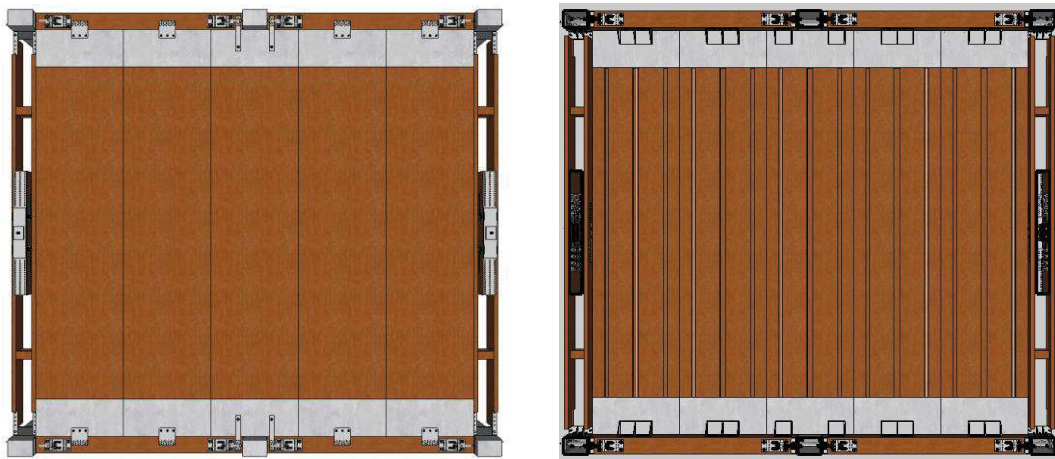


Figure 6.9. 3PT pre-stressing floor on the second level of the Skeleton Building: view from the top (left) and view from the bottom (right).

6.2.1.3 Non-structural detailing

This paragraph presents the details of the non-structural elements and their connection to the structural system. Apart from the masonry partition wall, fully designed following the low-damage concept thus applying the suggestions provided by Tasligedik and Pampanin (2016), the other non-structural systems were proposed by the related industry suppliers and their details were discussed to be adapted to the existing structural skeleton. In fact, the objective was to define an integrated structural/non-structural system to be applicable in the construction practice.

- **Fibre-reinforced gypsum partitions**

Concerning the fibre-reinforced gypsum wall partitions studied during the second testing phase (*Option 1*) and focusing on the partition system built in the wall direction, the system consisted of (Figures 6.10, 6.11):

- a steel sub-frame made of 40x75 mm horizontal channels and 49x74 mm vertical studs. The horizontal profiles were connected to the top floor using screws and to the bottom floor using post-installed anchors. The vertical profiles were not screwed to the horizontal channels whilst positioned with 600mm spacing being free to move inside the horizontal profiles, apart from the two vertical studs surrounding the door openings (400x800 mm) properly fixed to the top channel. Specific measurements were introduced during the construction of the partition, as shown later when describing the construction and assembly of the system. E.g. the non-structural detailing included: 1) 10/15 mm gaps, between the vertical studs and the horizontal profile on the top as well as between the horizontal channels and the lateral concrete columns; 2) timber frames creating the opening of the doors, properly connected to lateral steel studs which, in turn, were screwed to the bottom horizontal track while attached to the upper horizontal channel using a telescopic joint;
- 25 mm-thick fiber reinforced ceramic gypsum panels were finally inserted and connected between themselves using their male-female joints and adhesive glue, while the connection to the sub-frame system was realized screwing the panels to the vertical studs only.

As described in the next section, additional construction details were introduced in the system in order to define an earthquake-resistant solution. The same non-structural detailing was applied to the monolithic partition wall in the frame direction.

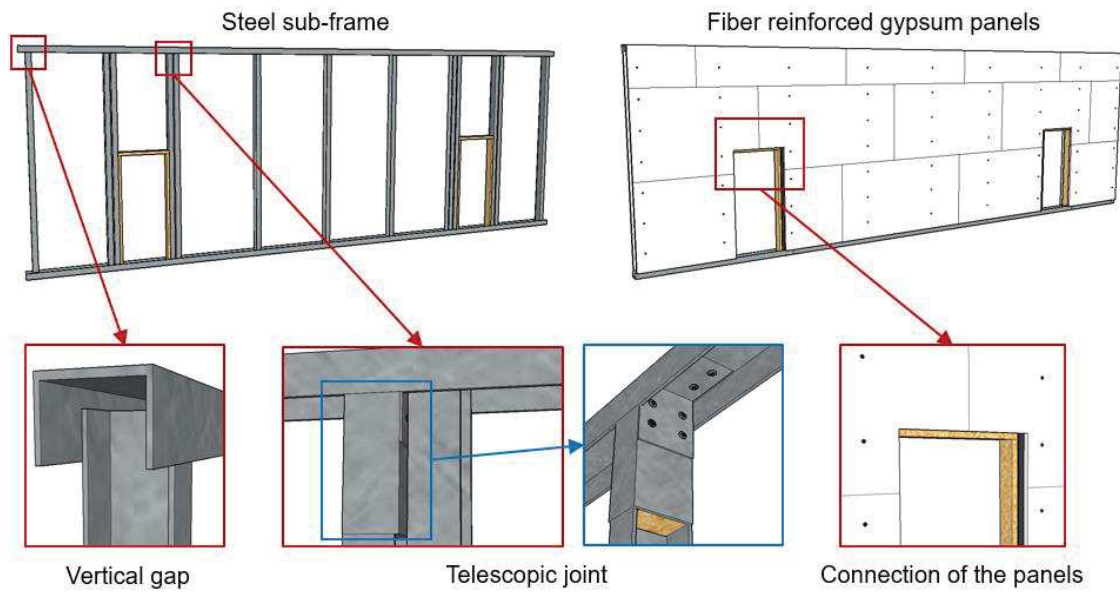


Figure 6.10. Detailing of the fiber-reinforced ceramic gypsum partition walls.



Figure 6.11. Renders of Option 1 configuration: global view (top - left), distribution in plan of the partitions (top - right), view of the wall with openings (bottom - left), view of the wall without openings (bottom - right).

- **Glass Fiber Reinforced Concrete (GFRC) facades**

GFRC cladding systems covered the structural skeleton in the frame direction during the third testing phase (*Option 2*). The 15 mm-thick GFRC panels with a central 500x650 mm opening defined a lightweight façade, connected through stirrups to a steel frame properly designed which, in turn, was attached to the structural members using restraint (bottom) and sliding (top) connections (Figure 6.12). The bottom connections had a restraint function only, i.e. the steel frame was inserted until half-length of the circular tube welded inside the bottom anchorage thus these connections maintained the façade in the correct position only (more detailing in the next section). These anchorages were welded and bolted on the steel foundation or screwed laterally to the timber beams of the first floor. The weight of the façade was fully transmitted to the concrete columns through the upper sliding connections, where the steel frame supporting the concrete claddings was located (Figure 6.13).

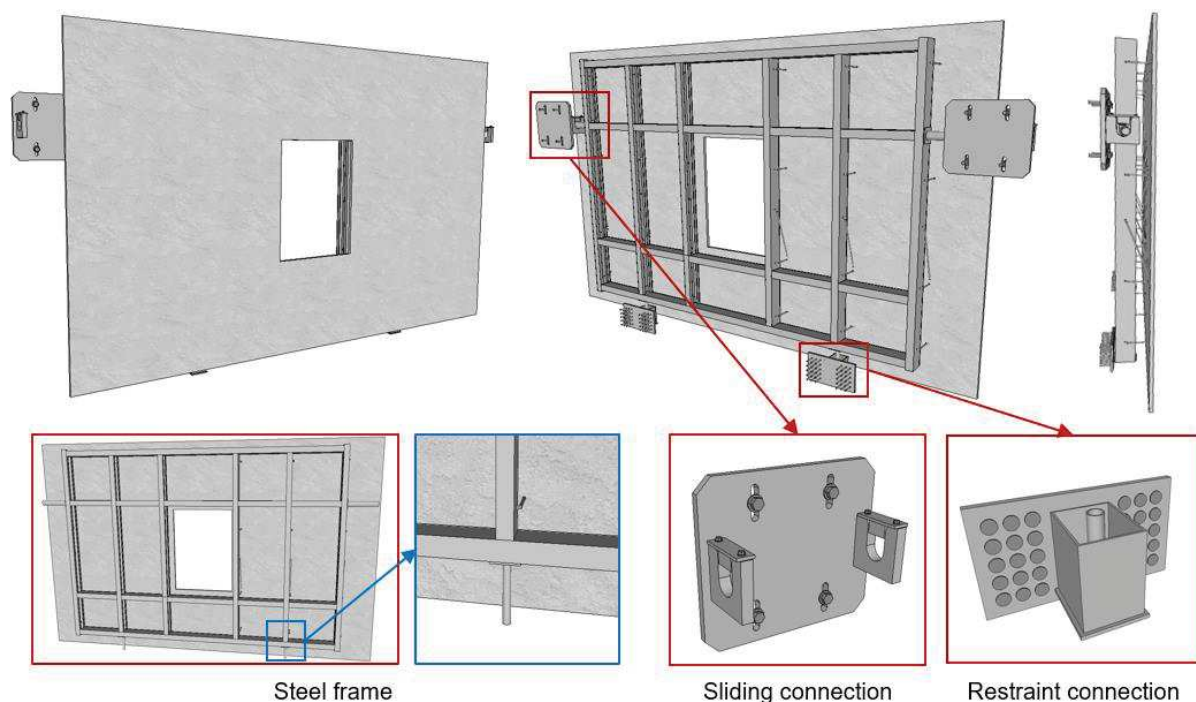


Figure 6.12. Detailing of a GFRC cladding system to be located within level 1 and 2 of Skeleton Building.

As indicated by the industry supplier, this façade system is generally designed to resist wind actions while no verification is implemented for seismic actions. Nevertheless, due to the introduced detailing a high seismic performance system is expected. In fact, the presence of GFRC panels with very reduced thickness whilst high compressive, flexural and tensile strength provides capacity to resist cracking. Furthermore, even if the sliding connections at the top of the panel are not dissipative

connections, these systems can provide good seismic performance during earthquake shakings if properly designed.

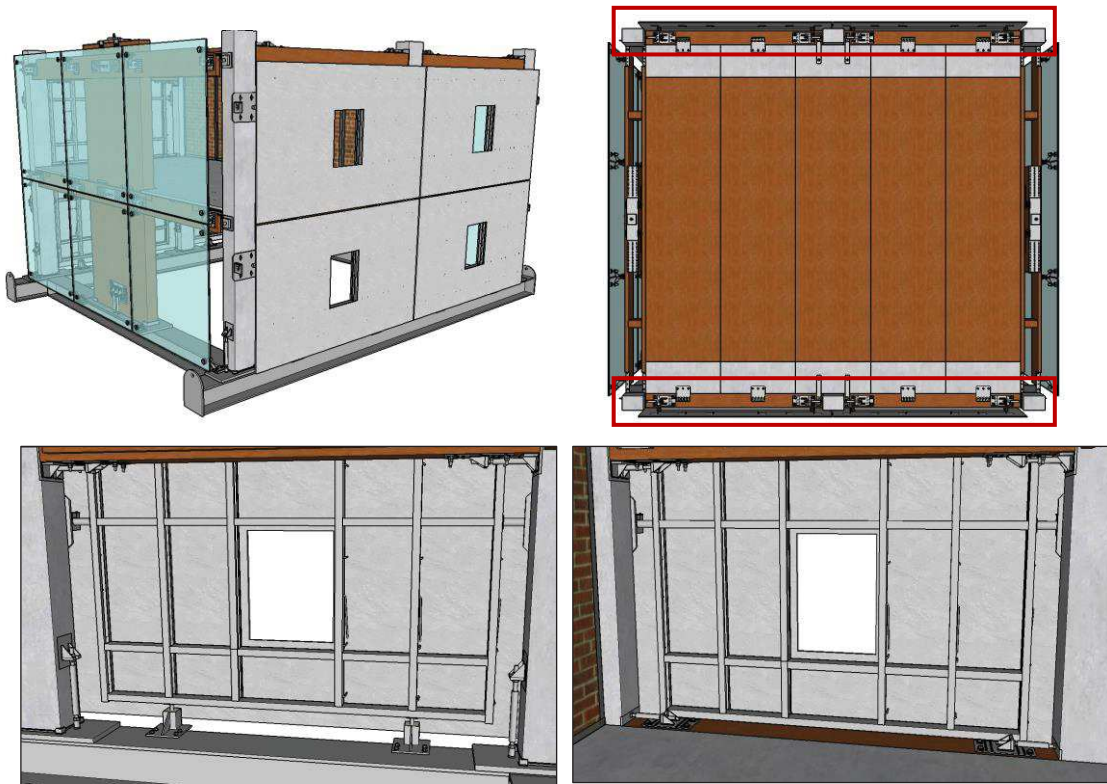


Figure 6.13. Renders of *Option 2* configuration: global view (top - left), distribution in plan of the GFRC facades (top - right), internal view of a precast panel between level 0 and 1 (bottom - left), internal view of a precast panel between level 1 and 2 (bottom - right).

- **Spider Glazing façades**

Spider glazing curtain walls covered the structural skeleton in the wall direction in the *Option 2* system configuration. The façades were composed of 10+1.52Pvb+10 mm glass with 13 mm gap between adjacent panels and were fixed to the edge beams and steel foundation using steel plates specifically realized. As shown in Figure 6.14, the façade system was made of articulated screws (rotules) consisting of spherical joints inserted within holes in the glass panels. These joints were bolted to spider connectors properly designed which, in turn, were connected to steel plates screwed to the structural system.

The glass façade was designed referring to the usual construction practice, the only difference was the connection to the structural skeleton. In fact, this typology of façade is generally used for multi-storey structures and additional structures/elements are introduced for supporting the weight of the glass panels (steel or concrete columns, additional glass profiles, use of cables). While, for fitting

the façade to the Test Building specific steel plates were designed to be connected to the lateral beams and to the steel foundation (Figure 6.15).

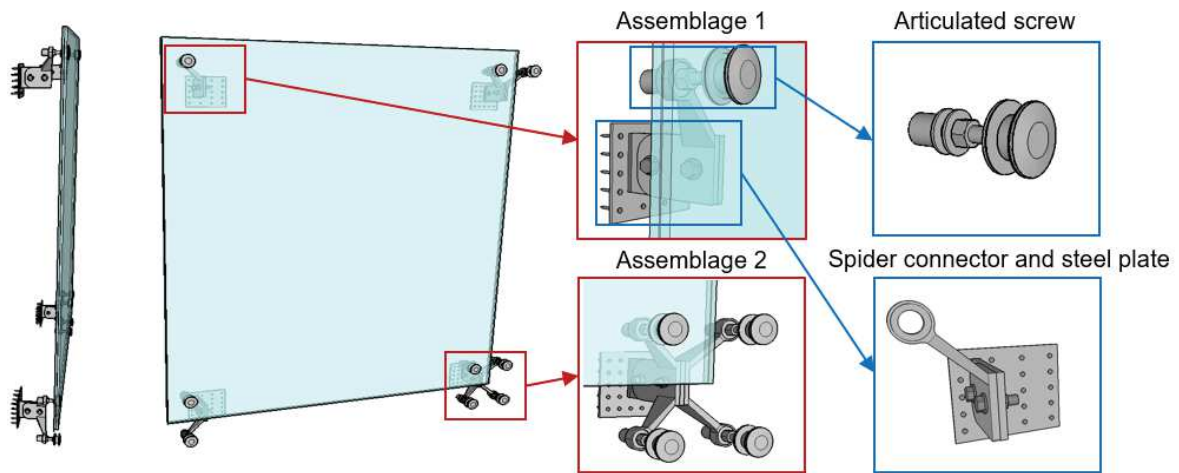


Figure 6.14. Detailing of a glass panel to be located within level 1 and 2 (upper left corner) of the Skeleton Building.

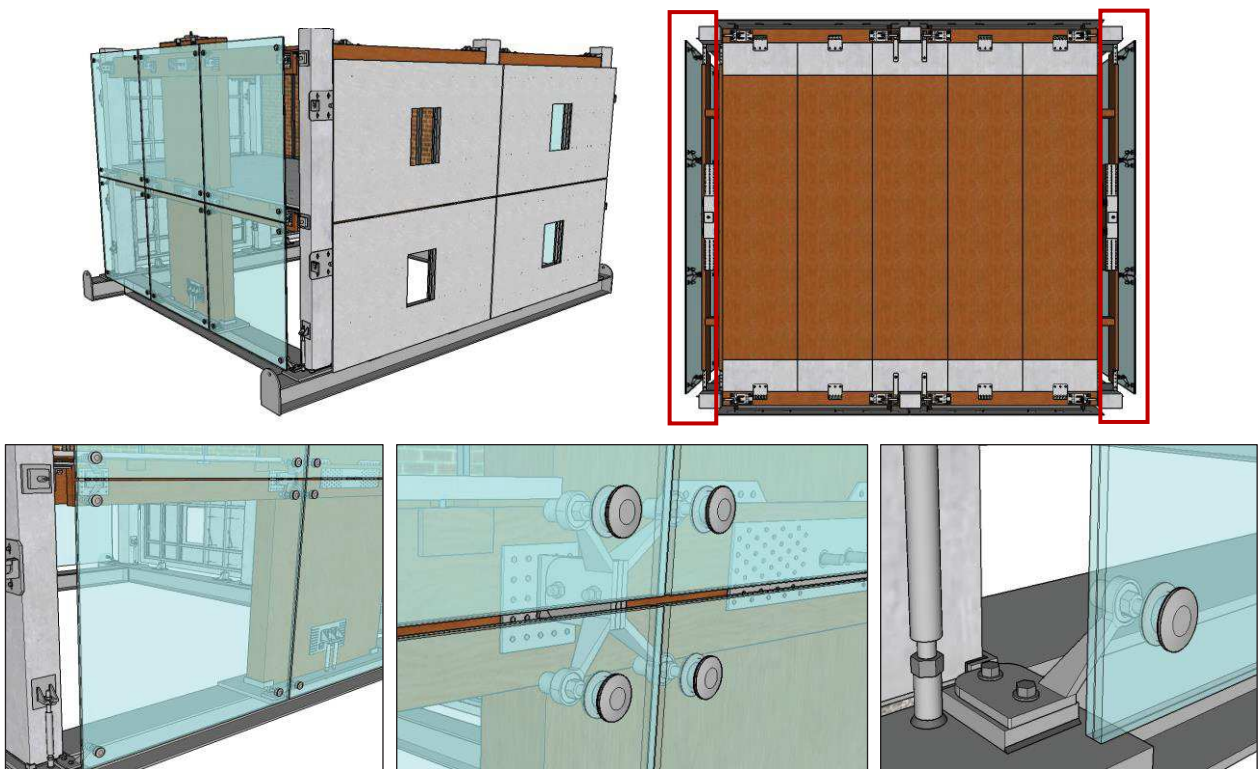


Figure 6.15. Renders of *Option 2* configuration: global view (top - left), distribution in plan of the glass facades (top - right), view of a glass panel between level 0 and 1 (bottom - left), detail of a connection to the timber beam (bottom - centre), detail of a connection to the foundation (bottom - right).

It is observed that this façade solution is typically designed to resist out-of-plane wind load, thus verifications on the maximum bending stress at the centre and edges of the panel are implemented, and to accommodate the in-plane building movement due to wind, thermal and earthquake loads, thus larger diameter holes to allow both relative vertical and horizontal movements are introduced. Although no method is available to façade engineers to calculate the in-plane drift capacity of the point fixed glass façades and to define the demand level to which the component resists, due to the system articulation allowing glass/connector movements and rotations of the panels, this typology of façade can be classified as a solution with high seismic performance. Moreover this consideration can be confirmed taking into account past damage reports or numerical/ experimental investigations on such type of systems.

- **Masonry partition walls**

The masonry partition was designed following the suggestions provided by Tasligedik and Pampanin (2016). A low-damage partition was defined, i.e. a system made of rocking vertical panels separated by horizontal gaps. In fact, the partition wall consisted of (Figure 6.16):

- a steel sub-frame system, composed of horizontal steel tracks bolted and screwed to the concrete slab and timber floor respectively, vertical steel studs with 994 mm spacing inserted inside the horizontal channels without connection, i.e. they were free to move inside the upper and lower steel profiles. Specific detailing was introduced in the low-damage solution: 5 mm of horizontal gap between the lateral vertical studs and the horizontal channels, 15 mm of vertical gap between all the steel studs and the horizontal channel connected to the second floor, 5 mm of horizontal gap between all the internal vertical studs.
- the masonry panels, made of 90 mm bricks bounded by mortar, were built inside the steel sub-frame without the introduction of mortar on the bottom and top of the panel infill zone as well as laterally to the steel sub-frame for providing an additional sliding effect. For completing the wall, the lateral gaps between the steel studs and with the lateral columns were finally filled using polyurethane joint foam.

The low-damage masonry wall was built on the first building floor to be tested during the third phase - *Option 2* - (Figure 6.17), therefore it substituted the previous fiber-reinforced gypsum partition demolished after the experimental tests on the *Option 1* configuration.

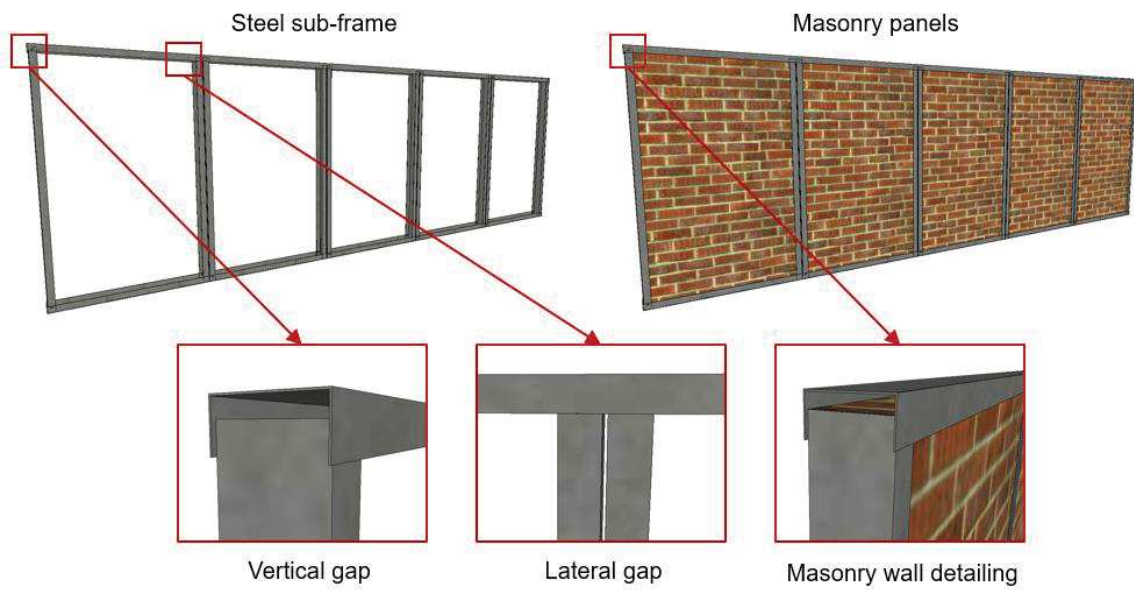


Figure 6.16. Detailing of the low-damage masonry infill wall.

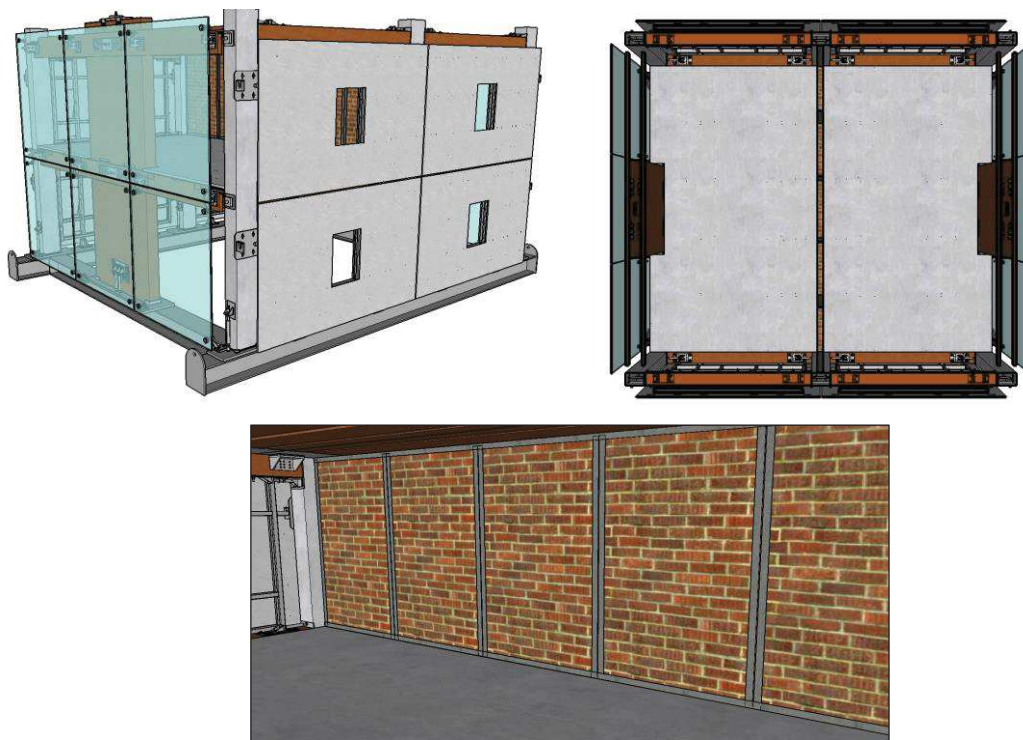


Figure 6.17. Renders of Option 2 configuration: global view (top - left), distribution in plan of the masonry partition wall (top - right), internal view of the partition (bottom).

6.2.2 Construction and assembly

This paragraph provides a description of the construction/assembly of the Test Building. The construction phases of the Skeleton Building are initially presented in general terms, then the description focuses on the assembly of the non-structural systems.

6.2.2.1 Fabrication and transportation

As part of the research project a consortium of Italian contractors and suppliers was organized for contributing to the supply of the structural elements (L.A. Cost Srl for the timber and steel components, Generale Prefabbricati Spa for the concrete columns) and of the non-structural components (Gessi Roccastrada Srl for the fiber reinforced gypsum, Generale Prefabbricati Spa for the GFRC panels, Glass Point Studio Srls and Cristal Vetri Srl for the glazing facade). All the components composing the specimen were fully fabricated in the related factories in Italy, thus they were shipped to Lisbon by road transport (Figures 6.18, 6.19).

The only components fully fabricated in Lisbon were the concrete slab of the TCC floor, the concrete blocks of the 3PT floor and the low-damage masonry infill wall. These parts of the specimen were directly built in the laboratory thanks to a Portuguese company (Jamosil Lda) providing both material and manpower. The same company was also involved in the assembly of the specimen in all the three testing phases.



Figure 6.18. Storage of material in the L.A. Cost factory before the transportation to Lisbon.



Figure 6.19. Transportation of the structural and non-structural components to the Laboratório Nacional de Engenharia Civil (LNEC) in Lisbon.

6.2.2.2 Assembly of structural system

The advantage of applying low-damage structures is also evident in the construction phases. Due to fact that this typology of buildings is conceived as a sort of “Lego” system, they are easy to be assembled and the construction/erection of the system is very rapid, consequently the time of construction is very reduced when compared to traditional monolithic structures. Different phases involved the construction of the Test Building, as summarized in Figure 6.20 and described as follows.

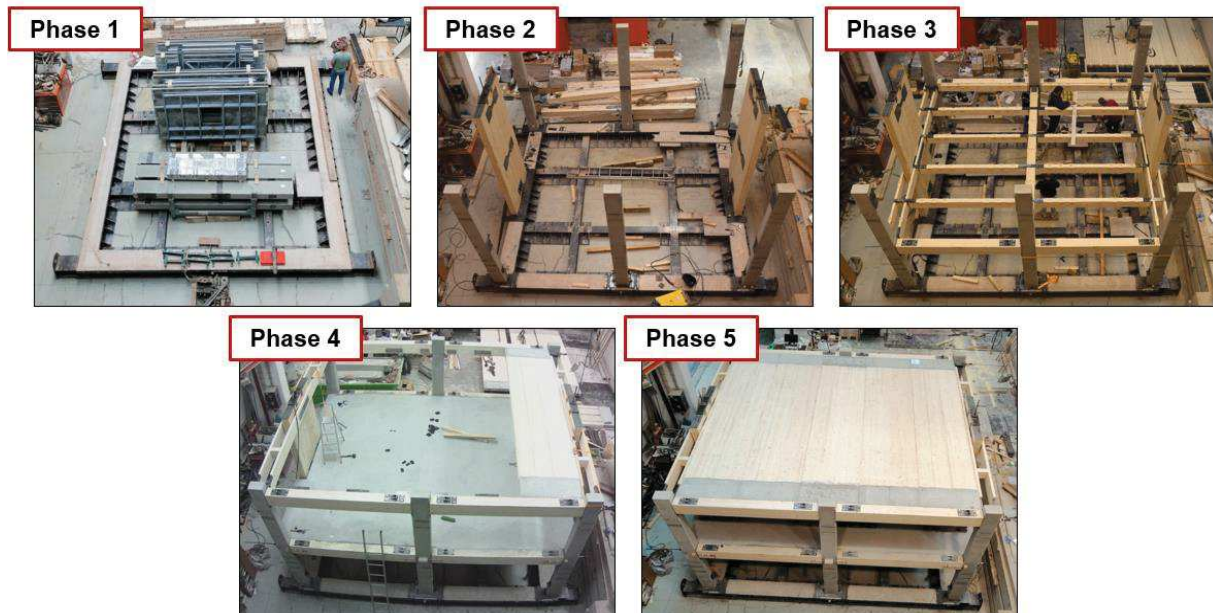


Figure 6.20. Construction phases of the Bare Frame system.

Phase 1: *Preparation of the steel foundation.*

The Skeleton Building was entirely built outside the shaking table on a steel foundation already available in the laboratory. The steel foundation consisted of HEB 300 profiles to be properly bolted on the shaking table creating a rigid connection, thus avoiding possible movements. Due to the presence of a UPN 400 profile welded on the perimetral steel profiles and filled with concrete on the top, specific measurements were taken to fix the steel foundation plates of the columns and walls to the existing foundation (Figure 6.21). Therefore, a solid connection was created to avoid possible movements between plates and foundation.



Figure 6.21. *Phase 1:* positioning of the steel foundation plates (left); welding of pieces of steel to fix the foundation plates to the UPN profile (centre); example (foundation plate of internal columns) of connection to the UPN profile (right).

Phase 2: *Erection of the vertical structural elements.*

The second phase involved the lifting and positioning of the columns and walls on the steel foundation (Figure 6.22). The vertical elements were craned in place and the distance between components was checked and eventually adjusted to be compliant to the structural drawings.

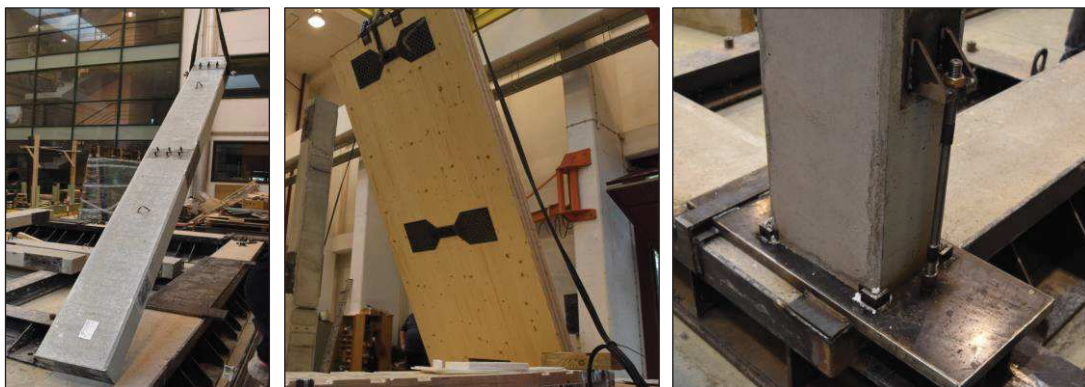


Figure 6.22. *Phase 2:* Lifting of concrete columns (left) and walls (centre); detailing of the column base connection (right).

Phase 3: *Positioning of the horizontal elements.*

The edge (sandwich) beams were craned in place and bolted through M14 anchors on steel plates attached to the concrete columns. It is observed that checking the position of these beams was fundamental for properly realizing the pinned connection, i.e. the pins had to be easily inserted into the provided holes (external edge beam/wall/internal edge beam).

Then, the central gravity beam in the wall direction was positioned and bolted on its sitting plates. Finally, the seismic beams were craned to be located on their steel corbels welded to the lateral plate casted into the concrete columns (Figure 6.23).

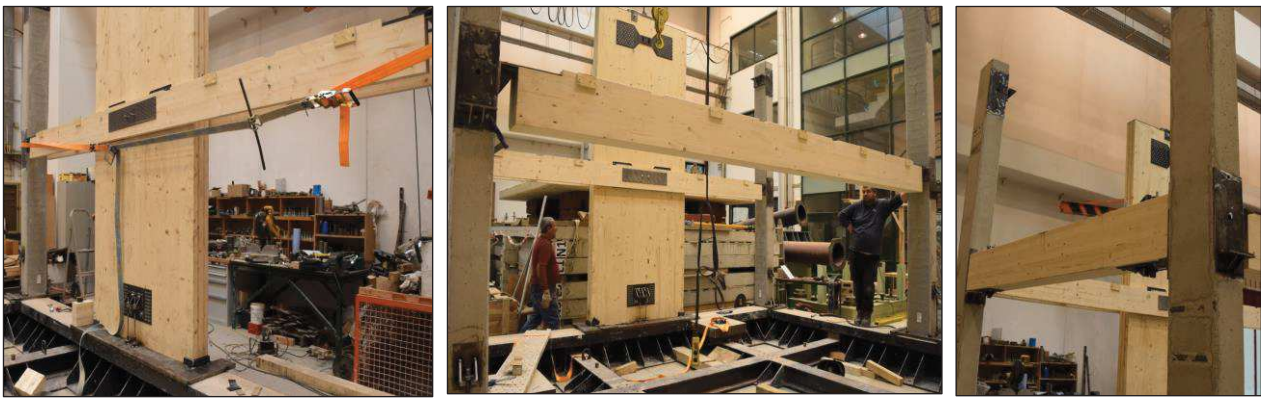


Figure 6.23. Phase 3: Edge beams (left), central beam (centre) and seismic beams (right) lifted into place.

Phase 4: *Construction of the Timber Concrete Composite (TCC) floor.*

The construction of the TCC floor on the first building level started with the positioning and connection of the timber joists. Then, 12.5 mm of plywood floor units were introduced on the top of the timber joists to create the base for the floor concrete slab (Figure 6.24).



Figure 6.24. Phase 4a: Positioning of timber joists (left) and introduction of the plywood floor units (right).

After realizing a timber formwork and correctly inserting the steel reinforcement, the 30 mm of concrete slab was casted in the laboratory (Figure 6.25). When the concrete was sufficiently dry, steel masses (4 masses of 1.2 tons and 6 masses of 0.6 tons) were bolted onto the concrete slab for simulating the additional mass (driving mass) required by scaling.



Figure 6.25. *Phase 4b: Casting of the concrete slab.*

Phase 5: Assembly of the 3PT timber concrete floor.

The final stage consisted in the assembly of the upper flooring system. The timber-concrete beams were craned to be located on their supporting plates attached laterally to the seismic beams. Then, the five beams of the floor were connected to the edge beams and each other using screws (Figure 6.26). Additional plates were introduced in the frame building direction for providing a better distribution of shear to the lateral-resistant system. The Skeleton Building was then ready to be lifted and placed on the shake-table (Figure 6.27). The additional (driving) mass of the second floor was introduced in this final configuration (6 masses of 1.2 tons).



Figure 6.26. *Phase 5: Lifting in place of the timber-concrete beams of the second floor (left) and final configuration of the second floor.*



Figure 6.27. Lifting of the Test Building (left) and positioning on the shaking table (right).

It is highlighted that the post-tensioning of the wire strands of both the seismic beams and the timber-concrete beams forming the 3PT floor as well as the post-tensioning of the threaded bar of the timber walls (Figure 6.28) were realized between phase 4 and 5 of the specimen construction, few days after the concrete casting of the first floor. Although it was planned to be made before the casting of the concrete, due to a time schedule to be strictly respected and for delays of the external company furnishing the jack, the post-tensioning was carried out within those days. However, to reduce the transmission of forces to the concrete slab, allowing the closing of the gaps at the rocking interfaces, the seismic beams were fully disconnected from the lateral joists of the TCC floor. Nevertheless, part of the post-tensioning force was transmitted to the slab, i.e. through the concrete columns, thus this must be taken into account when post-processing the experimental results and comparing them to the initial numerical studies.



Figure 6.28. Detail of the wire-strands and anchorage system of the beams of the 3PT floor (left) and of the first-floor seismic beams (right).

6.2.2.3 Assembly of non-structural components

The construction or assembly of each non-structural system was directly carried out with the specimen on the shaking table. Therefore, after the first testing phase (*Skeleton Building*) the internal fiber-reinforced gypsum partitions were built and the second testing phase was performed. Then, the internal partitions were demolished, the exterior enclosures attached and finally the internal masonry partition built, thus the last phase of the experimental tests was carried out.

The construction phases of each non-structural system are presented below, however the different construction sequences as well as more photos describing the assembly of these systems can be found in *Appendix D*.

- **Fiber-reinforced gypsum partitions**

The 5 m-long partition in the wall direction was firstly built. The construction started with the assembly of the steel sub-frame made of 40x75 mm horizontal channels connected to the building floors (through Akifix 3.5x45 mm black phosphated self-tapping screws to the timber slab while using Akifix 6x40 mm post-installed anchors to the concrete slab) and 49x74 mm vertical studs (Figure 6.29). The vertical profiles composing the frame were free to move inside the horizontal guides (only the vertical guides forming the opening of the doors were attached to the upper horizontal profile). The space between the vertical profiles was 650 mm, apart from the vertical studs near the columns and the 400x800 mm doors located 100 and 50 mm far from them respectively.



Figure 6.29. Construction of the steel sub-frame.

The following additional details were introduced during the construction of the steel frame (Figure 6.30 and Figure 6.31).

- Adhesive acoustic single- or double-sided tape was attached to both sides of the vertical studs and to the bottom part of the U-shape horizontal channels. Although this material has the function of improving the acoustic performance to the system, it was applied due to the influence it may have during seismic motions. In fact, the adhesive is typically only attached to the horizontal tracks, while the constructors of this partition also use it for the vertical profiles where the fibre-reinforced ceramic gypsum panels are screwed.
- As observed in the previous section, the lateral steel profiles of the openings had in the upper part an additional telescopic joint (slip joint) which was screwed to the top guide, while in the bottom part they were connected to the vertical extension of the horizontal guide properly realized for the base of the doors. A timber frame was also inserted to form the openings and this frame was connected to the lateral steel studs. For completing the frame of the doors, an additional assembly of steel profiles was introduced 15 mm from the top of the timber frame and properly connected to the lateral studs.
- 10/15 mm of lateral gaps were introduced within the system: 1) between the horizontal tracks and the concrete columns, 2) between the vertical studs and the upper horizontal channel.

After the assembly of the steel sub-frame, the 25 mm fibre-reinforced ceramic gypsum panels were introduced (Figure 6.32, left) and attached to both sides of the frame system. The 600x1200 mm panels (around 16 kg each) were properly cut to be fitted to the available space following a specific assemblage scheme and the panels were connected together through their male-female joints and additional adhesive glue (Figure 6.32, centre and right).



Figure 6.30. Steel frame construction: application of the adhesive (left); telescopic (slip) joint (centre); horizontal guides with the vertical extension forming base of the door frame (right).



Figure 6.31. Steel frame construction: timber frame of the door opening with the upper steel assembly (left); lateral gap between the horizontal guide and the concrete column (centre); gaps on the top between horizontal guide and column as well as between vertical guide and horizontal profile (right).



Figure 6.32. Detail of the fiber-reinforced gypsum panel (left) and assemblage of the panels through male-female joints (centre) and additional glue (right).

As shown in Figure 6.33, the gypsum boards were connected to the steel studs using Akifix 3.5x45 mm black phosphate self-tapping screws. However, the panels were not screwed to the vertical studs connected to the concrete columns and 10 mm of gap was left at each corner of the gypsum wall (i.e. panel-opening, panel-column, panel-top floor).

After the assemblage of the wall, the adhesive glue was applied to the overall surface and particularly to the corners of the gypsum panels creating a homogeneous and smooth wall. Then, silicone foam was inserted in the lateral gaps of the wall (i.e. panels-openings, panels-columns, panels-top floor) and, after the removal of the additional dried foam, joint cover tape was introduced in each corner of the wall and properly attached using adhesive glue. These lateral parts were finally covered by silicone sealant (Figure 6.34).



Figure 6.33. Insertion of the fiber-reinforced gypsum boards: final wall (left), first line of screws from the corners (centre) and lateral gap between wall and column (right).



Figure 6.34. Completion of the wall: insertion of adhesive glue on the entire wall surface (left); application of silicone foam (centre); introduction of additional joint cover tape in the corners (top - right); application of silicone sealant (bottom - right).

Regarding the 2.5m-long partition wall in the frame direction, the construction followed the same phases previously described. The only difference was related to the introduction of L-shape steel profiles connected using Teks screws to both sides of the bottom horizontal guide. These steel components are usually applied in the construction practice of this typology of system for allowing the passage of facilities under the wall, however it was not possible to introduce them in the longer wall due to the presence of the driving masses. It is finally observed that specific detailing (cut of profiles) was required for the connection of the vertical lateral stud to the timber wall, due to the presence of the internal edge beam (Figure 6.35, centre).



Figure 6.35. Construction of the partition wall in the frame direction: additional L-shape steel profiles (left), connection of the lateral vertical stud to the timber wall (centre), complete assembly of the panels (right).

- **Glass Fiber Reinforced Concrete (GFRC) facades**

Concerning the GFRC facades, the assembly operations were very easy to be carried out, and the construction started with the connection of the 15x300 x350 mm steel assemblies to the concrete columns (Figure 6.36, top - left). Cast-in channels located 455 mm from the centre of the beam-column joints allowed this connection through Halfen HS 40/22 M16x60, 4.6 hammer head bolts. These steel assemblies included U-shape plates forming the upper sliding anchorage of the precast cladding systems.

Then, the precast concrete panels were lifted and placed on these anchorages through the circular steel tubes leaking from the internal steel frame of the cladding systems (Figure 6.36, bottom - left). When making this operation, the correct position for the anchorages on the bottom of the panels was also checked, so that the steel frames could correctly be inserted into the circular tubes welded inside these bottom anchorages. Consequently, when found the correct position, these anchorages were appropriately fixed to the structural system (foundation, seismic beams). For the connection to the steel foundation, the steel plates were welded and bolted to the concrete filling on the top of the UPN profile using Hilti M12 expansion anchors, and fast-setting mortar was finally introduced in the rectangular steel tube ($>120 \text{ kg/cm}^2$ after 24 hours). While, for the connection to the timber beams, the steel plates were fixed using 6x80 mm screws, then the rectangular tubes were filled using fast-setting mortar (Figure 6.37).



Figure 6.36. Assembly of the precast concrete claddings: connection of the upper anchorage to the concrete columns (top - left), lifting of the panels (top - right), particular of the sliding anchorage (bottom - left), positioning of the last panel forming the façade (bottom - right).



Figure 6.37. Connection of the bottom anchorages to the structural system: connection to the steel foundation (left), connection to the timber beams (centre) and internal view of a bottom panel (right).

Finally, for completing the exterior enclosure small plates on the top of the U-shape plates were introduced and bolted to the steel profile for confining the anchorage system also in the vertical

direction (Figure 6.38). It is highlighted that the precast panels had 20 mm of gap between themselves in both the vertical and horizontal directions, as per design drawings.



Figure 6.38. Final configuration of the GFRC façade (left) and of the upper sliding anchorage (right).

- **Spider glazing façades**

The construction of the glazing facades involved few construction phases, however, accuracy and precision were required for the assembly of the system. The first construction operation consisted in the connection of the steel anchorages to the structural system. Assemblies comprising spider connectors already connected through M10 bolts to steel plates were properly positioned and fixed to the Bare Frame using 4.5x50 mm screws for the connection to the external timber beams or welding for the connection to the specimen foundation (Figure 6.39).

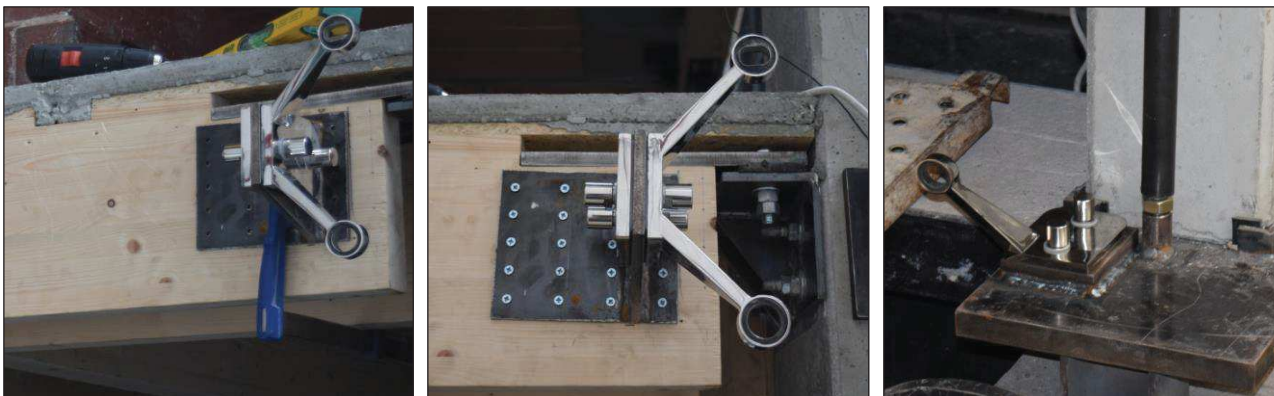


Figure 6.39. Construction of the glass wall: positioning of the steel plate/spider connector assembly (left); fixing of the steel assembly using screws (centre); welding of the base plate to the foundation (right).

For avoiding direct contact between glass and steel, an adhesive tape of 2 mm was attached on pieces of circular aluminium profiles covering the internal part of the ball joint (Figure 6.40, left). The ball joints (rotules) were thus introduced into the holes of each glass panel with 2-3 mm of internal

glass/steel tolerance (Figure 6.40, centre). Then, the panels were lifted and properly connected to the spider/plate system using their 24 mm diameter nuts (Figure 6.40, right).



Figure 6.40. Connection of the rotules to the glass panels: particular of the rotule covered by adhesive tape (left), insertion of the rotule into the hole of the glass panel (centre), rotule/spider/plate connection (right).

For realizing the overall façade, the glass panels of the bottom level were initially assembled starting from the central part, then the panels of the upper level were lifted in place and connected to the anchorage systems (Figure 6.41, left and centre). Internal gaps of around 13 mm were left between the glass panels in both the vertical and horizontal directions (Figure 6.41, right).

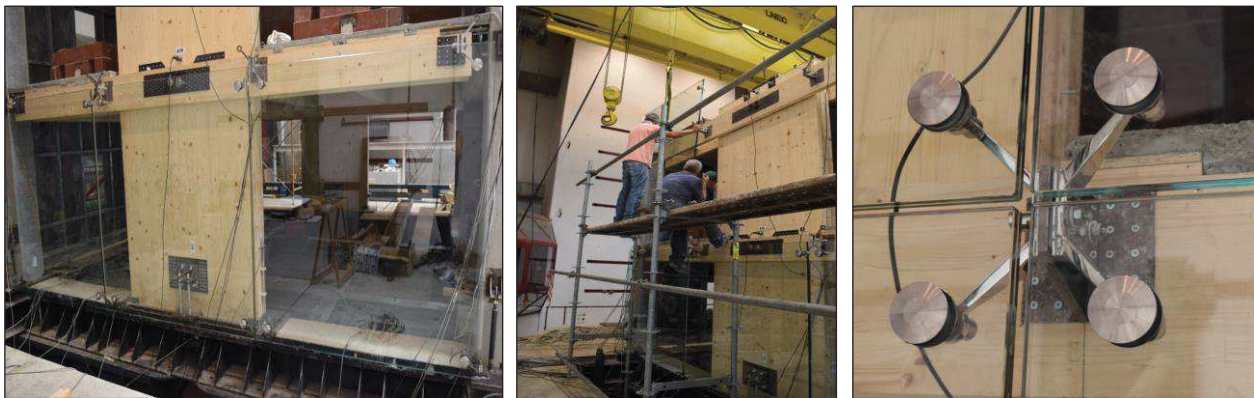


Figure 6.41. Assembly of the overall façade: lifting in place of the bottom panels (left), lifting in place of the upper panels (centre), particular of an internal connection (right).

For completing the wall, Wurth sealing tape VKP Plus was added in the lateral gaps surrounding the glass panels. Generally, this type of filling is made using silicone gaskets covered by silicone sealant, however this material was not furnished by the supplier. Considering that the function of the silicone gasket/sealant is to provide weather tightness and insulation properties to the façade system, it was however decided to fill the gaps using sealant tape, which is another solution used in the common practice for achieving this aim in different applications. The application of the sealing

tape mainly allowed to simulate the presence of an internal material avoiding potential contact between the glass panels during the earthquake motion (Figure 6.42).

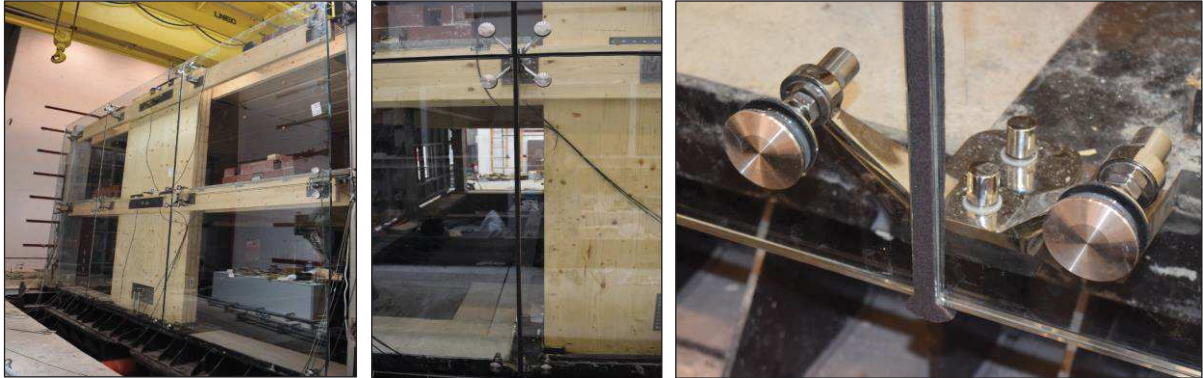


Figure 6.42. View of the entire glass façade (left) and application of the sealant tape inside the gaps (centre and right).

- **Masonry partition walls**

The construction of the 5 m low-damage masonry wall initiated with the assembly of the steel sub-frame made of 1.5x50x90 mm horizontal and vertical channels (Figure 6.43, left).



Figure 6.43. Assembly of the steel sub-frame of the masonry partition: global view (left) and detailing of the lateral (centre) and internal (right) gaps.

The horizontal tracks were connected to the structural system through Akifix 3.5x45 mm black phosphated self-tapping screws at the top while using Akifix 6x40 mm post-installed anchors at the bottom. As described in the previous section, horizontal and vertical gaps (Figure 6.43, centre and right) were introduced within the system to allow the proper movement of the rocking panels (5 mm gap between the horizontal channels and the concrete columns; 5 mm gap between the vertical studs forming the different masonry panels; 5 mm gap between the first steel studs and the horizontal channels; 15 mm vertical gap between the steel tracks and the upper horizontal channel).

It is observed that an angle of 45° was created at the base of each vertical stud in order to provide more freedom to the development of the rocking motion of the different masonry panels. The vertical steel profiles were also horizontally cut at the base to allow the insertion of the studs inside the horizontal channel (the problem was the same dimension of the horizontal and vertical profiles, not available of different sizes from the supplier company), as shown in Figure 6.44, right.



Figure 6.44. Detail of the base of the vertical steel profiles.

Finally, the unreinforced masonry partitions were built inside the steel frame using 90x190x300 mm bricks and 10 mm of mortar for both horizontal and vertical directions (5 masonry walls with 994 mm of width, 1560 mm of height and 90 mm of thickness). For building the masonry walls, no mortar was introduced between bricks and steel profiles for providing an additional sliding behaviour to the masonry rocking walls. It is also noticed that due to the presence of the 15 mm upper gap between masonry walls and horizontal steel channel, the last line of bricks was formed considering half of the brick section and adjusting the level of mortar below the last layer. In fact, for simplifying the realization of the wall, the sequence of construction on the top of the panels was suggested as: 1) insertion of the half-size bricks of the last line, 2) insertion of the bricks of the level below and 3) introduction of additional mortar between the two lines if required.

The wall was thus completed filling the horizontal gaps with polyurethane foam, i.e. between the vertical studs and between the studs and the concrete columns. While, a light white painting was applied to one of the two sides of the wall to help in checking the possible formation of the cracks on the masonry wall during the shaking tests.

Figure 6.45 shows some photos summarizing what is previously explained.



Figure 6.45. Construction of the masonry infill wall (top - left, centre) and final configuration of a panel (top - right); completion of the wall introducing polyurethane foam (bottom - left) and paint on one side (bottom - right).

6.4 Conclusions

This Chapter has provided a description of the first stages of the experimental campaign carried out at the Laboratório Nacional de Engenharia Civil (LNEC) in Lisbon, where the seismic performance of an integrated structural/non-structural building system has been investigated through shake-table testing. As part of an EU-funded SERA project, the research has intended to promote an effort within the European environment for the development of a low-damage building system, including skeleton and non-structural components, for the next generation of buildings.

The Chapter has initially presented the research objectives as well as the different testing phases, i.e. experimental studies on the *Skeleton Building* solution (**Phase 1**), then on *Option 1* configuration comprising internal fibre-reinforced gypsum partitions on the first building floor (**Phase 2**), finally on *Option 2* configuration representing a fully integrated structural/non-structural system where exterior enclosures (GFRC facades and spider glazing curtain walls) and masonry partitions are introduced (**Phase 3**). Then, the design of the 1:2 scale low-damage structural skeleton from the Prototype Building, i.e. a two-storey fully prefabricated and dry-assembled building with two bay timber-concrete low-damage seismic frames and post-tensioned rocking dissipative timber seismic

walls, can be found. All the detailing and measurements introduced in the Test Building, mainly focusing on the non-structural systems, are also provided.

Finally, in the last part of this Chapter the construction and assembly of the different specimen configurations are described, also including photos of the construction phases to provide more understanding of the specimen detailing. Due to the objectives of this Thesis, detailed information are provided for the non-structural systems tested during Phase 2 and Phase 3 of the experimental campaign (Figure 6.46).



Figure 6.46. Phase 2 (left) and Phase 3 (right) of the experimental campaign.

The dynamic shake table tests provided valuable information and confirmation on the seismic performance of the low-damage systems. The experimental campaign also allowed to investigate a) the 3D dynamic behaviour of an innovative composite-hybrid material solutions for post-tensioned rocking dissipative systems (timber-concrete), b) the performance of some of the latest developments in terms of low-damage floor-diaphragm system, c) the interaction between various combination of structural and non-structural element system, d) the design and construction feasibility as well as the actual (simulated) seismic behaviour of an integrated high performance low-damage building system.

The other stages of the experimental campaign, i.e. the testing setup (test matrix, monitoring system) and preliminary results on the seismic performance, focusing on the response of all the non-structural components, are described in the next Chapter.

6.5 References

- AS/NZS 1170 (2002). *Australian/New Zealand Standard 1170*, Standards Australia/Standards New Zealand.
- EN 1995-1-1 (2004). *Eurocode 5: Design of timber structures - Part 1-1: General - Common rules and rules for buildings*, The European Union Per Regulation 305/2011, Directive 98/34/EC, Directive 2004/18/EC.
- EN 1993-1-1 (2005). *Eurocode 3: Design of steel structures - Part 1-8: Design of joints*, The European Union Per Regulation 305/2011, Directive 98/34/EC, Directive 2004/18/EC.
- EN 1993-1-8 (2005). *Eurocode 3: Design of steel structures - Part 1-1: General rules and rules for buildings*, The European Union Per Regulation 305/2011, Directive 98/34/EC, Directive 2004/18/EC.
- Johnston H.C., Watson C.P., Pampanin S., Palermo A. (2014). Shake table testing of an integrated low-damage frame building, *Proceedings of 2014 NZSEE Conference*, Auckland, New Zealand.
- NTC (2008). *Norme Tecniche per le Costruzioni*, Supplemento ordinario n°30 alle G.U. n° 29 del 14/01/2008, serie generale, Rome, Italy.
- NZS 3101-1 (2006). *Concrete structures standard - The design of concrete structures*, Development Sponsored by the Earthquake Commission (EQC) and Department of Building and Housing (DBH), Standards New Zealand.
- NZS 3101-2 (2006). *Concrete structures standard – Commentary*, Development Sponsored by the Earthquake Commission (EQC) and Department of Building and Housing (DBH), Standards New Zealand.
- NZS 3404-1,2 (1997). *Steel structures Standard*, P 3404 Committee for the Standards Council established under the Standards Act 1988, Standards New Zealand.
- NZS 3404-1 (2009). *Steel structures Standard Part 1: Materials, fabrication, and construction*, Supersedes in part NZS 3404 Parts 1 and 2:1997, P 3404 Committee for the Standards Council established under the Standards Act 1988, Standards New Zealand.
- NZS 3603 (1993). *Timber Structures Standard*, Standards New Zealand.
- Palermo A., Pampanin S. (2017). Pre-stressed beams or panels (3PT), *United States Patent n. US9809979B2* (filed in 2014), *Japan Patent n. JP6373975B2* (filed in 2014), *Canada Patent n. CA2909402C*.
- Pampanin S., Marriott D., Palermo A. and New Zealand Concrete Society (2010). *PRESSS Design Handbook*, Auckland, New Zealand.
- Pampanin S., Palermo A. and Buchanan A. (2013). *Structural Timber Innovation Company Inc. (2013)*, Post-Tensioned Timber Buildings - Design Guide, Christchurch: Structural Timber Innovation Company.
- Priestley M.J.N., Calvi G.M., Kowalsky M.J. (2007). *Direct Displacement-Based Seismic Design of Structures*. 1st edition, IUSS Press, Pavia, Italy.
- Structural Timber Innovation Company (2012). *Design Guide Australia and New Zealand – Timber Concrete Composite Floor Systems*, STIC, New Zealand.

Structural Timber Innovation Company (2013). *Design Guide Australia and New Zealand – Timber Rivet Connections Design Guide*, STIC, New Zealand.

Tasligedik A.S. and Pampanin S. (2016). Rocking Cantilever Clay Brick Infill Wall Panels: A Novel Low Damage Infill Wall System, *Journal of Earthquake Engineering*, 21(7): 1023-1049.

7. 3D shake-table tests on an integrated low-damage building system: test setup and experimental results

7.1 Introduction

This Chapter further describes the experimental campaign (3D shake-table tests) on the half-scaled integrated low-damage structural/non-structural building, carried out at the Laboratório Nacional de Engenharia Civil (LNEC) in Lisbon, PT. After an overview of the experimental set-up, i.e. monitoring system (instrumentation layout) and test matrix (selection of input motions, sequence of testing), preliminary experimental results are provided in terms of floor accelerations and inter-storey drift ratios. Moreover, the description focuses on the seismic performance of the non-structural components - facades and partitions - in terms of dynamic behaviour and observed damage.

It is observed that, due to the timeline of experimental testing, only preliminary results from the data post-processing have been obtained to be included within this Thesis. However, more results/outcomes from the shake-table campaign can be found in the publications that will follow.

7.2 Experimental set-up

The Test Building was subjected to ground motion records from the shaking table. These earthquake records were properly scaled to account for both the spectrum-compatibility condition and the Cauchy-Froude similitude, as shown later. The seismic response of the specimen, i.e. either the global response or the local connection behaviour, was recorded using the sensors available in the laboratory and different instrumentation plans were designed for each testing phase.

7.2.1 Shaking table

The Laboratório Nacional de Engenharia Civil (LNEC) in Lisbon has a tri-axial shaking table (Figure 7.1) with an area of 5.60 m x 4.60 m extensible to 5.60 x 6.20 m, a table mass of about 40 t, a maximum allowable specimen weight of about 400 kN, a frequency range from 0 to 15 Hz, maximum accelerations of 1.1, 0.5 and 1.8 g for the transverse, vertical and longitudinal axis respectively, and maximum displacements of ± 175 mm for all the three axes. The three longitudinal, transverse and vertical actuators have respectively total force of 1250 kN, 750 kN and 375 kN. Moreover, detailed information on the characteristics of the shaking table can be found in Emilio et al. (1989).



Figure 7.1. Shake-table of the Laboratório Nacional de Engenharia Civil (LNEC): top view (left) and vertical hydraulic actuators (right).

7.2.2 Instrumentation plan

The instrumentation of the Test Building consisted of a combination of sensors: accelerometers, LVDT transducers, potentiometers, load cells, optical devices, strain gauges. The instrumentation was used to directly analyse the global behaviour of the building and to determine the local behaviour of the structural connections as well as of the non-structural elements, based on a combination of data and material behaviour assumptions. In fact, due to the specimen dimensions and to the high number of components involved during the experimental testing, a large number of sensors should be used for properly monitoring the seismic behaviour of the Test Building and its components. Nevertheless, considering the instrumentation available at the LNEC Earthquake Engineering and Structural Dynamics Division and mainly the available channels for the data acquisition, the monitoring system was designed trying to find the best solution during each testing phase.

7.2.2.1 Phase 1: Skeleton Building

Firstly, all the sensors were installed for monitoring the seismic response of the structural skeleton and its hybrid connections (beam-column, wall-base, column-base). Therefore, the instrumentation plan was defined as briefly described below.

- FOUNDATION LEVEL

3 accelerometers were used to collect the horizontal (**A3**: longitudinal, frame direction; **A2**: transverse, wall direction) and vertical (**A1**) accelerations of the steel foundation (Figure 7.2, centre). An additional accelerometer (**A4**) was attached nearby the base of a concrete column to study the impact effect developing during the rocking motion (Figure 7.2, right).

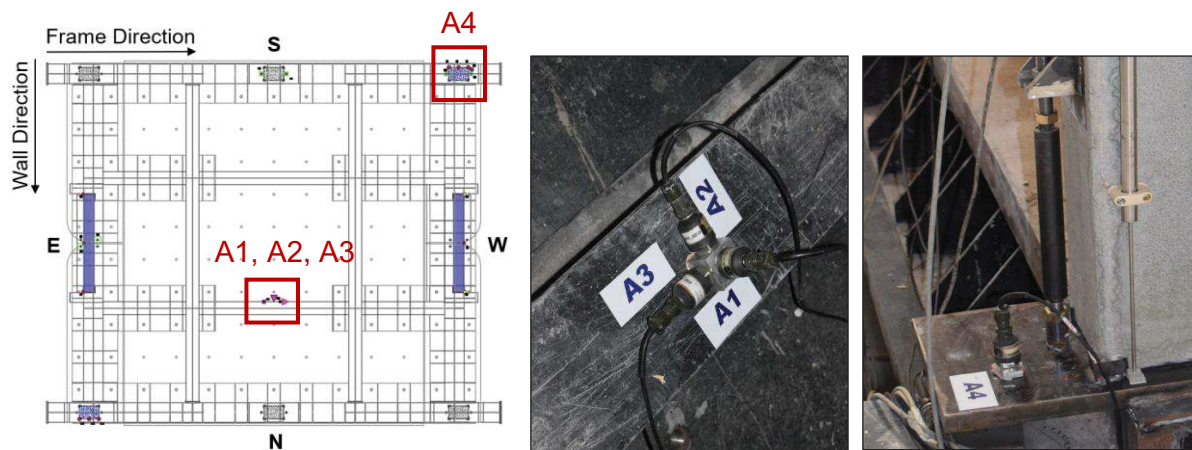


Figure 7.2. Accelerometers on the foundation level: accelerometers on the steel foundation (centre) and accelerometer on the column foundation plate (right).

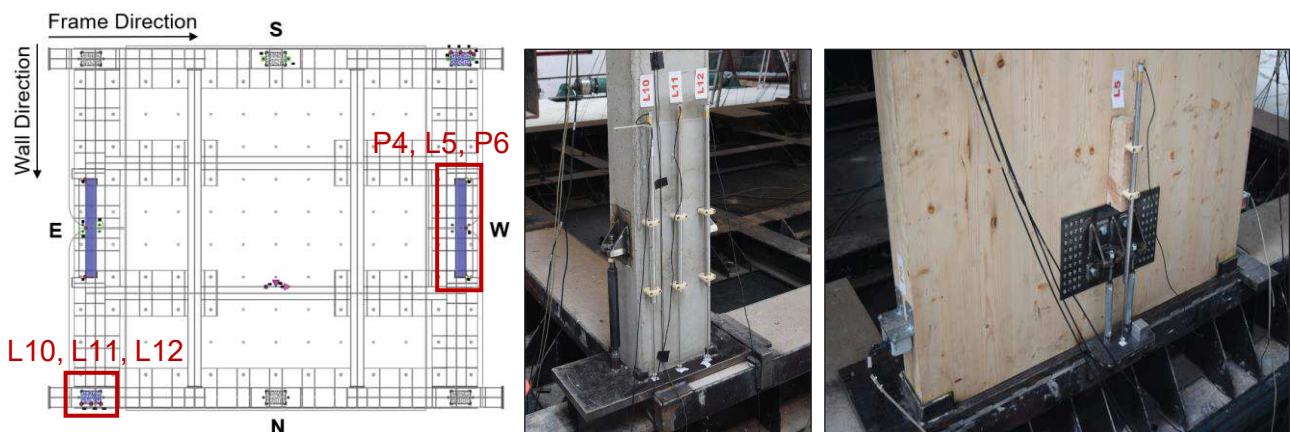


Figure 7.3. LVDTs and potentiometers on the foundation level: LVDTs of the column in the North-East corner (centre) and LVDT/potentiometers monitoring the West wall.

The rocking motion of the timber walls and of two opposite concrete columns was fully monitored using three LVDT transducers at each component base (**L1**, **L2** and **L3** for the East wall, **L7**, **L8**, **L9** for the column in the South-West corner, **L10**, **L11**, **L12** for the column in the North-East corner), apart from the wall in the West side for which the opening of the gap was recorded using two potentiometers and one LVDT (**P4**, **L5**, **P6**). Some of these sensors are shown in the previous Figure 7.3.

It is finally observed that strain gauges were attached to some of the external dissipaters for recording the force developing in their internal fuse during the earthquake simulations. The strain gauges were fixed to the internal fuse of the “*Plug & Play*” dissipaters using proper glue, thus the steel tube covering the internal fuse was inserted and filled using epoxy for anti-buckling and finally, before bolting these steel elements into their anchorages, the monitored dissipaters were subjected to tension testing with the aim of calibrating the strain gauges (Figure 7.4, left and centre). Figure 7.4 - right - presents in the plan view the monitored dissipaters at the base of the vertical elements, i.e. the two dissipaters of the external (**S5**, **S6**) and internal (**S3**, **S4**) columns in the South side and two opposite (external side/internal side) dissipaters of the East wall (**S1**, **S2**).

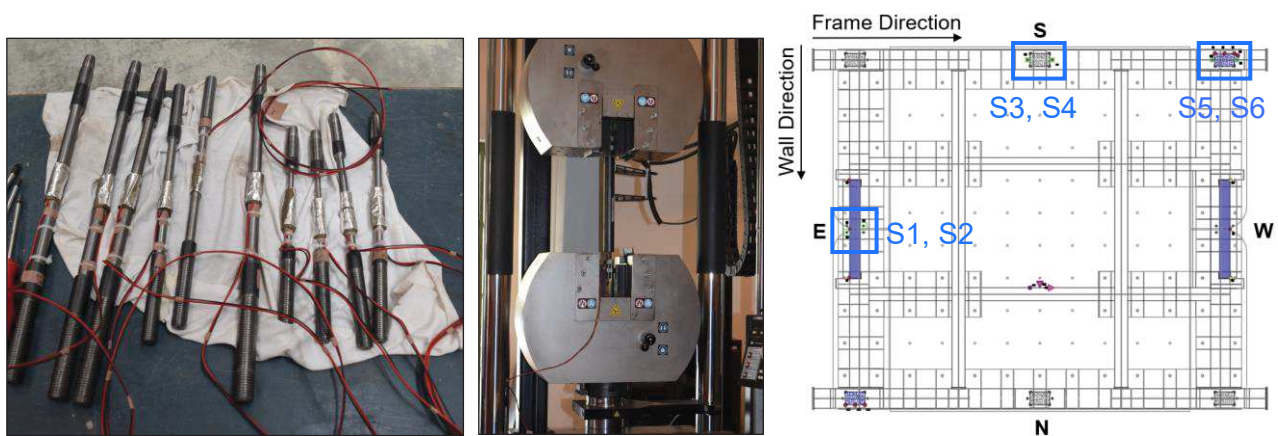


Figure 7.4. Monitored dissipaters: insertion of the strain gauges (left), tension test for calibrating the strain gauges (centre) and plan view of the monitored dissipaters in the foundation level (right).

- FIRST LEVEL

14 accelerometers were introduced for monitoring: the four lateral columns in both longitudinal and transverse directions (column in the South-East corner: **A5**, **A6**; column in the South-West corner: **A7**, **A8**; column in the North-West corner: **A11**, **A12**; column in the North-East corner: **A13**, **A14**); the two timber walls in both the in-plane and out-of-plane directions (West wall: **A9**, **A10**; East

wall: **A15**, **A16**); the vertical accelerations on the floor, positioning two accelerometers on two opposite points of the concrete slab (**A17** and **A18**).

6 LVDT transducers were used for recording the opening and closing of the horizontal gaps at the beam-column interface for two opposite corners (joint in the South-West corner: **L13**, **L14**, **L15**; joint in the North-East corner: **L16**, **L17**, **L18**). While, the force acting on the external dissipation devices located in the South-West corner was fully monitored using strain gauges (**S7**, **S8**), properly calibrated before the start of the experimental tests through tension testing of the “Plug & Play” dissipaters.

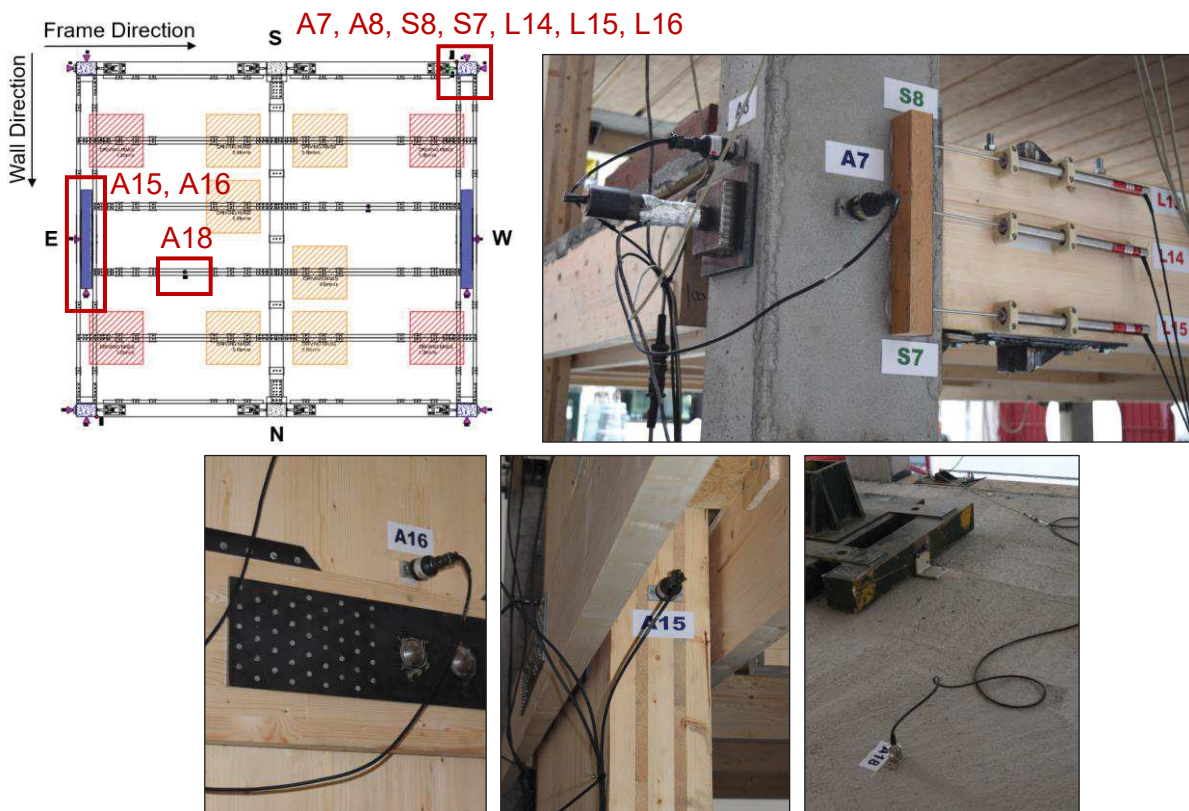


Figure 7.5. Monitoring system of the first level: external joint in the South-West corner (top - left), accelerometers on the East wall (bottom - left and centre), accelerometer on the concrete slab (bottom - right).

Two optical devices (**O1**, **O2**) were also used for controlling the vertical and horizontal displacements of the centre of the two beam-column joints in the North-East and North-West corners, thus for monitoring the movement of the frame system in the North side (Figure 7.6).

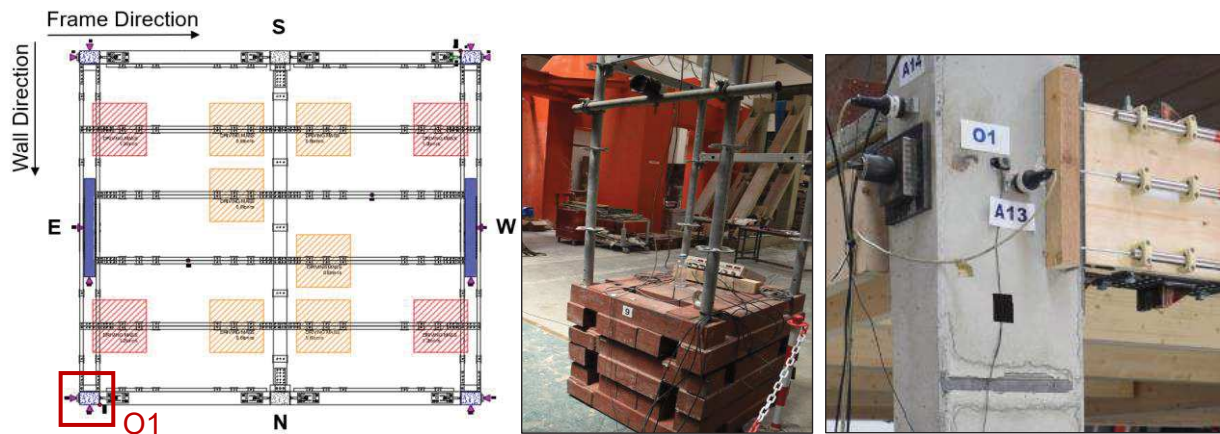


Figure 7.6. Optical devices in the North frame: external frame supporting the optical transducer (centre) and positioning of the controlled point in the beam-column joint of the North-East corner (right).

Finally, it is observed that load cells were introduced in the South-West and North-West corners for recording the force of the post-tensioned wire-strands of the timber beams. These load cells were connected to the tendons during the construction phases, that is before the initial post-tensioning.

- SECOND LEVEL

The instrumentation plan of the second level was designed to be similar to the one of the first level, as described below.

14 accelerometers were introduced for monitoring: the four lateral columns in both longitudinal and transverse directions (column in the South-East corner: **A19**, **A20**; column in the South-West corner: **A21**, **A22**; column in the North-West corner: **A25**, **A26**; column in the North-East corner: **A27**, **A28**); the two timber walls in both the in-plane and out-of-plane directions (West wall: **A23**, **A24**; East wall: **A29**, **A30**); the vertical accelerations on the floor, positioning two accelerometers on two opposite points of the slab (**A31** and **A32**). 6 LVDT transducers were used for recording the opening and closing of the horizontal gaps at the beam-column interface for two opposite corners (joint in the South-West corner: **L19**, **L20**, **L21**; joint in the North-East corner: **L22**, **L23**, **L24**). While, the force acting on the external dissipaters located in the South-West corner was monitored through strain gauges (**S9**, **S10**), properly calibrated through tension testing of the steel bars.

Load cells were introduced in the South-West and North-West corners for collecting the force of the post-tensioned wire-strands of the timber beams. These load cells were connected to the tendons during the construction phases and before the initial post-tensioning. Finally, other two available optical devices (**O3**, **O4**) were used for controlling the vertical and horizontal displacements

of the centre of the two beam-column joints in the North-East and North-West corners, thus for monitoring the second level of the frame system in the North side.

Some sensors of the second floor are shown in the following Figure 7.7.

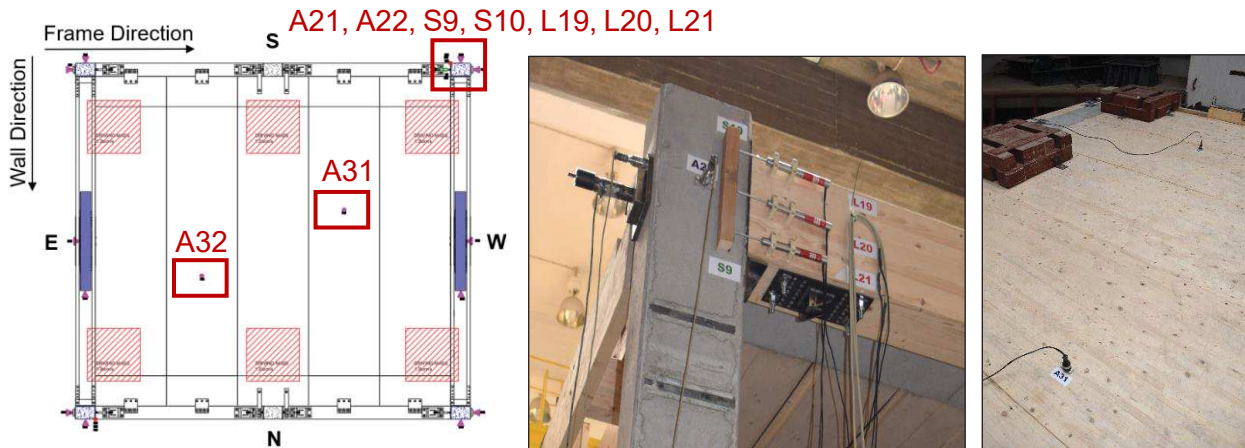


Figure 7.7. Monitoring system of the second level: external joint in the South-West corner (centre) and accelerometers on the flooring system (right).

7.2.2.2 Phase 2: Skeleton Building with internal partitions

Considering the limited number of sensors and due to the need for monitoring both the structural system and the internal partitions during the second testing phase, after the experimental tests on the Skeleton Building configuration 6 accelerograms and 8 LVDT transducers were removed from the structural system, i.e. the accelerometers **A4**, **A1**, **A17**, **A18**, **A31**, **A32** collecting the vertical accelerations and the LVDT in the centre of each column/wall/beam section (**L2**, **L5**, **L8**, **L11**, **L14**, **L17**, **L20**, **L23**), to be positioned on the non-structural components. Choosing to better control the behaviour of the partition wall built in the frame direction, the sensors were distributed as follows.

- 5 accelerometers were placed as presented in Figure 7.8 for recording the out-of-plane behaviour of the panel. One accelerometer was positioned at the centre of the wall (**A31**), while the others were installed along the vertical (**A17** and **A18**, around 200 mm from the building floors) and the horizontal (**A4** and **A1**, at respectively 1/4 and 3/4 of the partition length) directions in order to evaluate the acceleration distribution of the partition in the two orthogonal directions.
- 4 LVDT transducers were installed on the wall for monitoring the in-plane movement, i.e. two LVDTs in the vertical direction (**L17**, **L23**) and two LVDTs in the horizontal direction (**L2**, **L11**) in the opposite corners. These devices were used for evaluating the relative

displacements between the partition and the structural system (wall, floors) while **L11** monitored the relative displacement between the two orthogonal partitions.

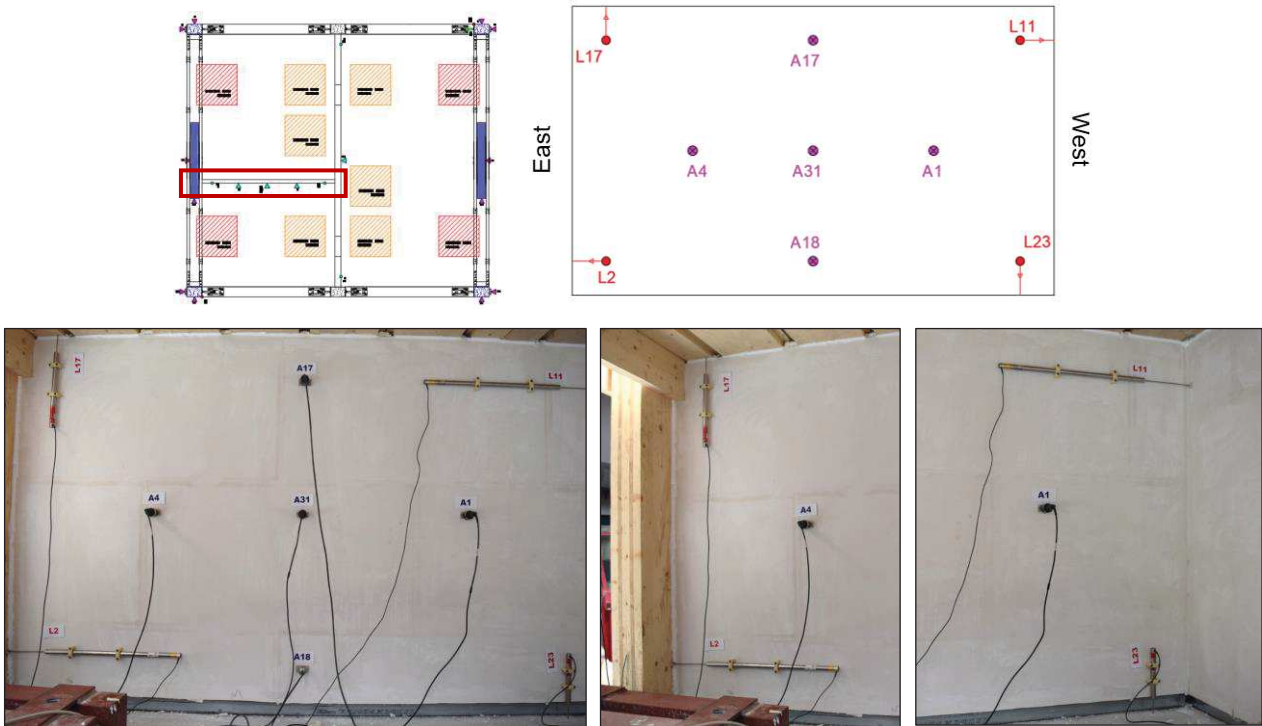


Figure 7.8. Instrumentation plan for the partition in the frame direction: schematic drawing (top) and photos (bottom).

While, for the longer partition wall in the opposite direction, the monitoring system was:

- 1 accelerometer (**A32**) located at the middle height of the panel where the two orthogonal walls intersected.
- 4 LVDT transducers, two in the vertical direction (**L5**, **L8**) and two in the horizontal direction (**L14**, **L20**). These devices were used for evaluating the displacements relative to the structural system (column, slab), therefore for determining the in-plane movement of the wall.

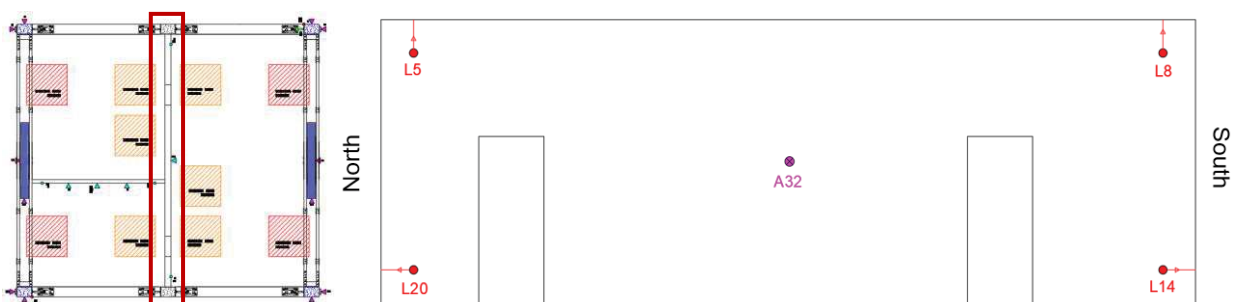




Figure 7.9. Instrumentation plan for the partition in the wall direction: schematic drawing (top) and photos (bottom).

7.2.2.3 Phase 3: Integrated system

Concerning the instrumentation plan designed for the last specimen configuration, due to the high number of components to be monitored, all the 22 LVDT transducers were removed from the structural system to be installed on the non-structural components, while additional accelerometers (from **A33** to **A40**) were introduced. Due to the increment of quantities to be recorded, the number of channels for the strain gauges was reduced and an additional extra board was installed in the data acquisition control unit.

Regarding the GFRC facades, the instrumentation was installed as follows (see also Figures 7.10 and 7.11):

- For the façade in the North side: 4 accelerometers were attached for monitoring the in plane accelerations of the first and second level (**A39**, **A40**) while the out-of-plane accelerations of an upper panel were also recorded (**A37**, **A38**); 4 LVDT transducers were installed for controlling the horizontal displacement of the upper and bottom panel (**L21**, **L22**) as well as the relative horizontal displacement (**L23**, **L24**) between the two levels of cladding.
- For the façade in the South side: just two LVDT transducers (**L11**, **L12**) were introduced to record the horizontal displacements of the upper and lower panels.

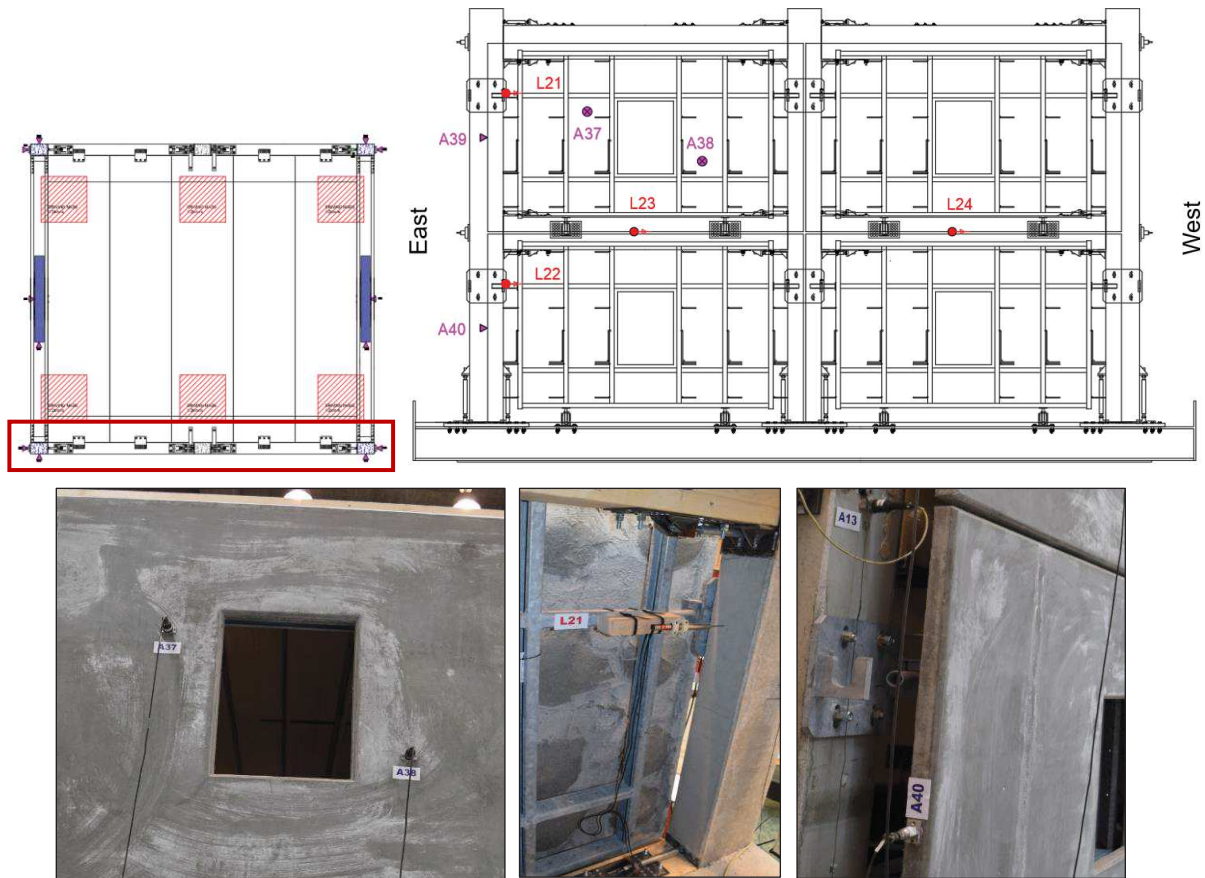


Figure 7.10. Instrumentation plan for the GFRG façade in the North side: schematic drawing (top) and photos (bottom).

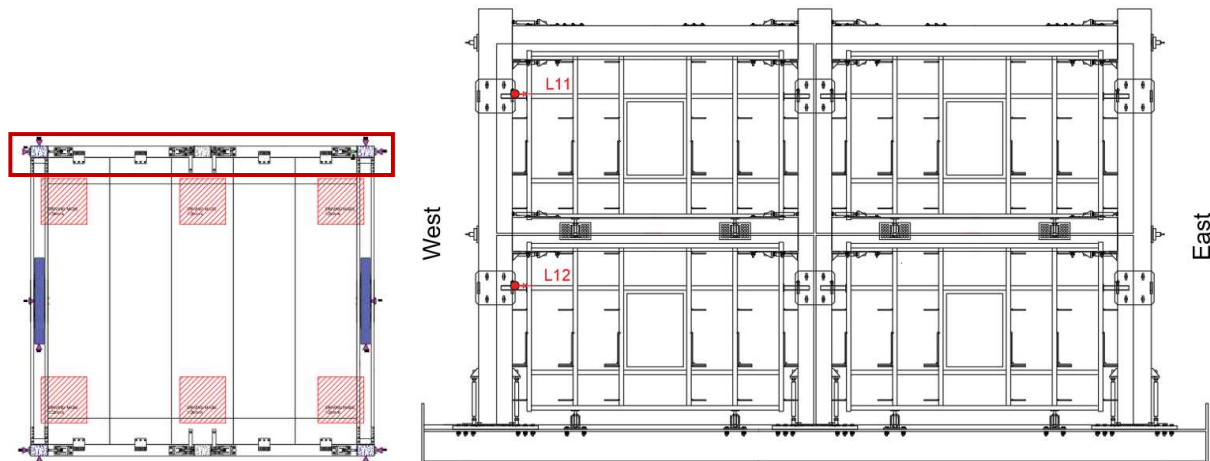


Figure 7.11. Instrumentation plan for the GFRG façade in the South side: schematic drawing.

Regarding the spider glazing facades, for the glass façade in the East direction the planned instrumentation is shown in Figure 7.12.

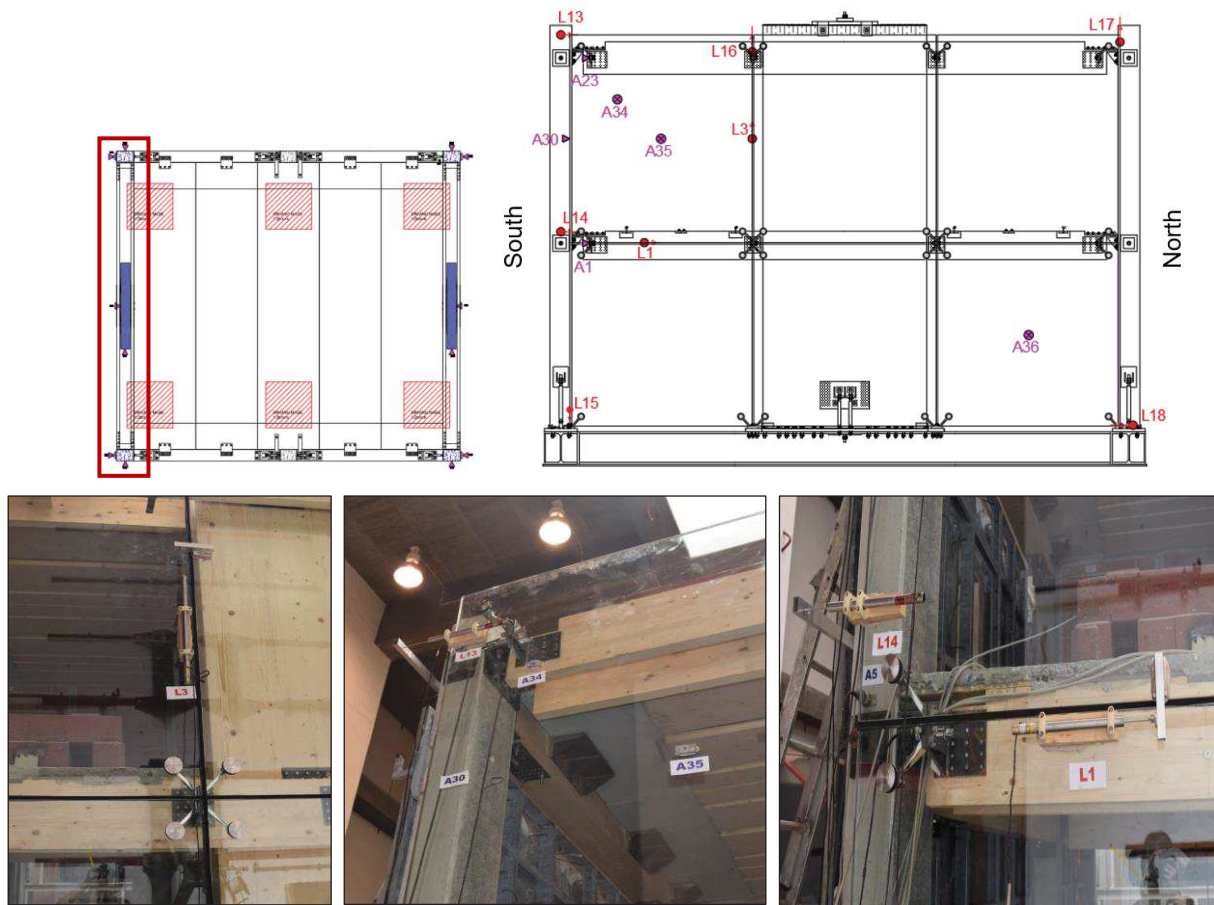


Figure 7.12. Instrumentation plan for the glass façade in the East side: schematic drawing (top) and photos (bottom).

The instrumentation of this glass façade comprised:

- 8 LVDTs for monitoring the horizontal and vertical movements of the façade: **L13** and **L14** monitored the relative horizontal displacement between the panel in the upper-left part and the concrete column; **L16** controlled the relative vertical displacement between the same panel and the timber beam of the second floor; **L1** and **L3** monitored the relative horizontal and vertical displacements of this panel compared to the two adjacent panels; **L15** and **L17** were used for recording the vertical displacement between the steel foundation and the panel in the bottom-left corner and between the column and the panel in the upper-right corner respectively; finally, **L18** measured the relative horizontal displacement between the panel in the bottom-right corner and the steel foundation.
- For the panel in the upper-left part of the façade, 5 accelerometers were installed: **A35** and **A34** for measuring the out-of-plane accelerations in the centre of the panel and along the diagonal direction respectively; **A30** for collecting the in-plane horizontal acceleration

in the middle of the panel; **A23** and **A1** for recording the accelerations on the upper and lower spider connector.

While, for the glass façade in the West direction only 2 LVDT transducers (**L19**, **L20**) were introduced for measuring the horizontal displacements of the glass panel in the upper-left part relative to the displacements of the concrete column (Figure 7.13).

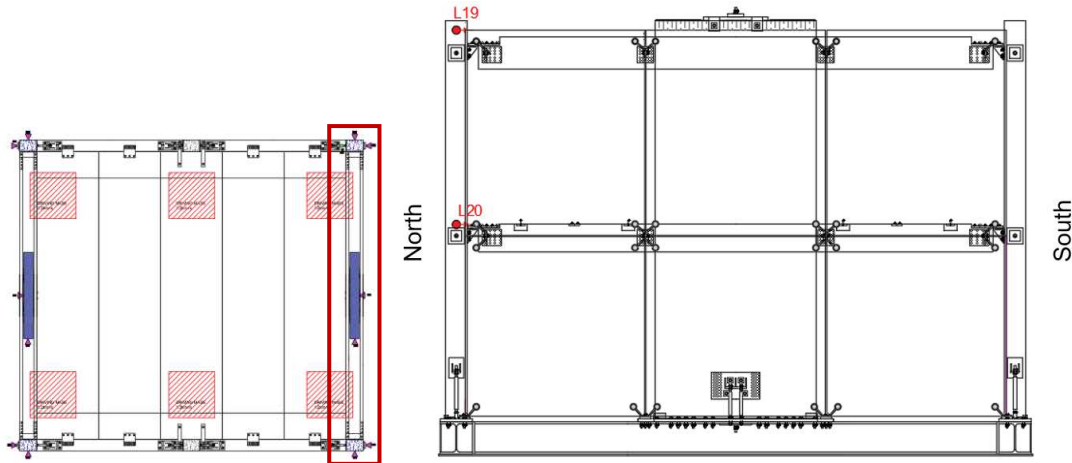


Figure 7.13. Instrumentation plan for the glass façade in the West side: schematic drawing.

Finally, the internal masonry partition wall was monitored (Figure 7.14) using the following devices:

- 6 LVDTs positioned in the East side of the wall: **L5** for measuring the vertical displacement in the North corner of the rocking wall relative to the second floor system; **L8** for monitoring the horizontal displacement of the same wall compared to the column; **L10** recorded the relative horizontal displacement between the two adjacent walls; **L2** for measuring the vertical displacement in the South corner of the rocking wall relative to the first floor system; **L7** collected the horizontal displacement of the same wall compared to the concrete column; **L9** monitored the relative horizontal displacement between the two adjacent walls.
- 2 accelerometers positioned in the West side of the wall (**A33** in the middle of the rocking wall in the North corner and **A4** in the middle of the rocking wall in the South corner).

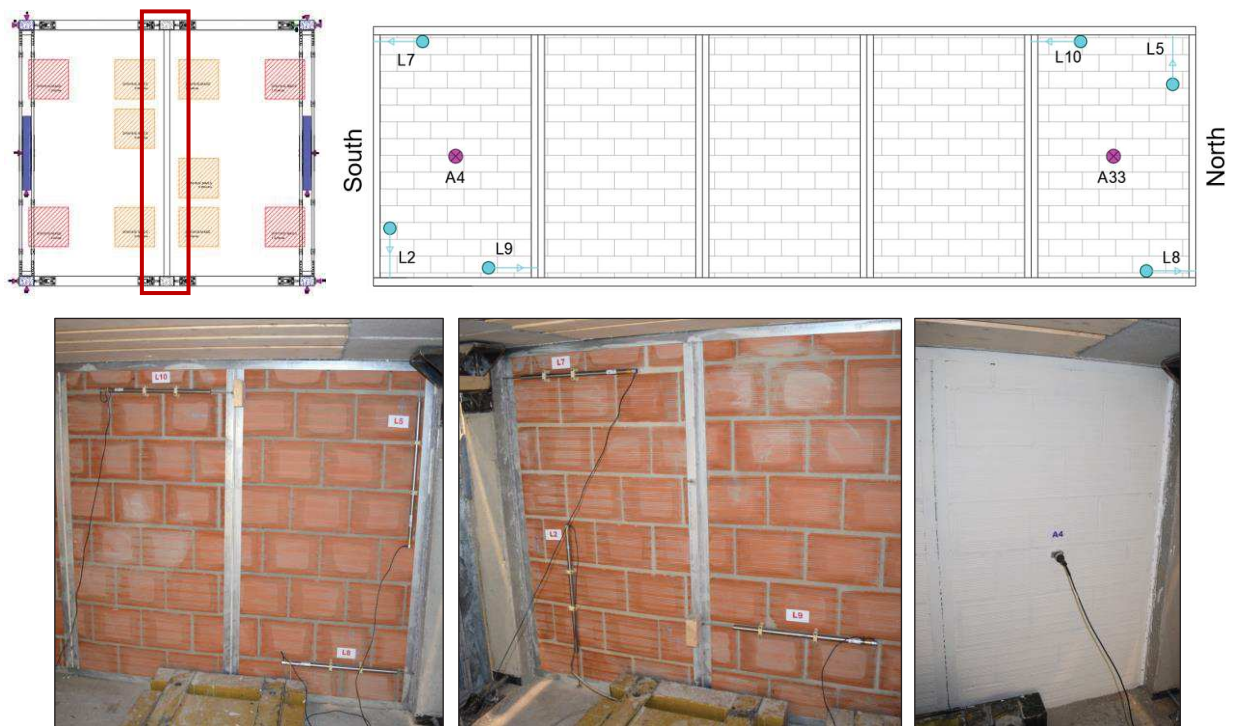


Figure 7.14. Instrumentation plan for the masonry infill wall: schematic drawing (top) and photos (bottom).

7.2.3 Ground motion selection

Four levels of earthquake intensity, corresponding to four values of probability of exceedance, were tested on the shaking table, namely: Limit State 1 (**LS1**), representing the Damage Control limit state of the Italian seismic code (NTC 2018) ($T_R = 50$ years); Limit State 2 (**LS2**), representing more than a Serviceability limit state ($T_R = 101$ years); Limit State 3 (**LS3**), corresponding to the Life Safety limit state ($T_R = 475$ years) of the Italian seismic code (NTC 2018); a last Limit State (**LS4**) representing the condition of $T_R = 1500$ years which is more than the Collapse Prevention limit state of the Italian code.

5 different ground motions were selected to be scaled at each of this seismic intensity level: 3 Far Field earthquakes (EQ_1, EQ_2, EQ_3) and 2 Near Fault records (EQ_4, EQ_5). An additional earthquake was introduced to represent an input motion with high vertical acceleration (EQ_6). All the cited earthquakes are summarized in the next Table 7.1.

Table 7.1. Selected earthquake motions.

ID	Event	Station	Record ID	Year	Mw
EQ ₁	Cape Mendocino	Eureka – Myrtle & West	FF02	1992	7.0
EQ ₂	Landers	Morongo Valley	FF03	1992	7.3
EQ ₃	Darfield	REHS	FF15	2010	7.1
EQ ₄	Imperial Valley-06	El Centro Array #4	NF01	1979	6.5
EQ ₅	Christchurch	CCCC	NF13	2011	6.3
EQ ₆	L'Aquila	AQV	AQ	2009	6.3

The ground motions were scaled using the scaling procedure included within the NZS 1170.5 (2004). The procedure consists in satisfying the following condition for the scale factor k_1 :

$$D_1 = \sqrt{\frac{1}{(1.3 - 0.4)T_1} \int_{0.4T_1}^{1.3T_1} \left[\log \frac{k_1 SA_{component}}{SA_{target}} \right]^2 dT} \leq \log(1.5)$$

That is, k_1 is the scale factor which minimizes in at least mean square sense the difference, D_1 , between the ground motion spectra ($SA_{component}$) and design spectra (SA_{target}) over the period range of interest. The period range of interest was determined from the building fundamental period T_1 , as $0.4 T_1 - 1.3 T_1$. The scale factors were limited to the range of 0.33 - 3.0 and the first period, T_1 , of 0.4s for the full-scale Prototype Building was used for implementing the procedure. Finally, the obtained records were further scaled in time for respecting similitude requirements, thus the time component of each motion was reduced by a factor of $\sqrt{0.5}$.

The scaling factors k_1 of the 5 records (3 Far Field and 2 Near Fault) were determined implementing this approach at the Life-Safety limit state, considering the design spectrum shown in the previous Figure 6.3. Then, the scaling (Table 7.2) of the different intensity levels was defined assuming the average spectrum from the earthquakes at the LS3 as the reference condition with scaling factor equal to 1.0. The scaling factors in Table 7.2 were used for all the three testing phases, i.e. no modification was introduced to these values to account for the effect of the building properties during *Option 1* e *Option 2* testing.

Table 7.2. Scaling factors for the different intensity levels.

Intensity name	Scaling factor
Limit State 1 - LS1	0.38
Limit State 2 - LS2	0.54
Limit State 3 - LS3	1.00
Limit State 4 - LS4	1.30

While for EQ_6 signal, different scaling factors were identified considering a spectrum-compatibility to the vertical design spectrum, defined according to the NTC 2018 code (0.15 for LS1; 0.23 for LS2; 0.60 for LS3; 1.06 for LS4). However, these scaling factors were so defined for the experimental tests on the Skeleton Building configuration, while they were assumed to be equal to the ones determined for the horizontal shakings when performing the other testing phases. As highlighted later, notwithstanding this signal (EQ_6) is representative of a different seismic shaking, it was combined with the other horizontal input motions with the aim of subjecting the specimen to a very high 3D earthquake excitation.

The average spectra of the 5 horizontal motions compared to the design spectrum of the various limit state conditions are shown in Figure 7.15 - left, while the acceleration spectrum of the EQ_6 input is presented in Figure 7.15 - right.

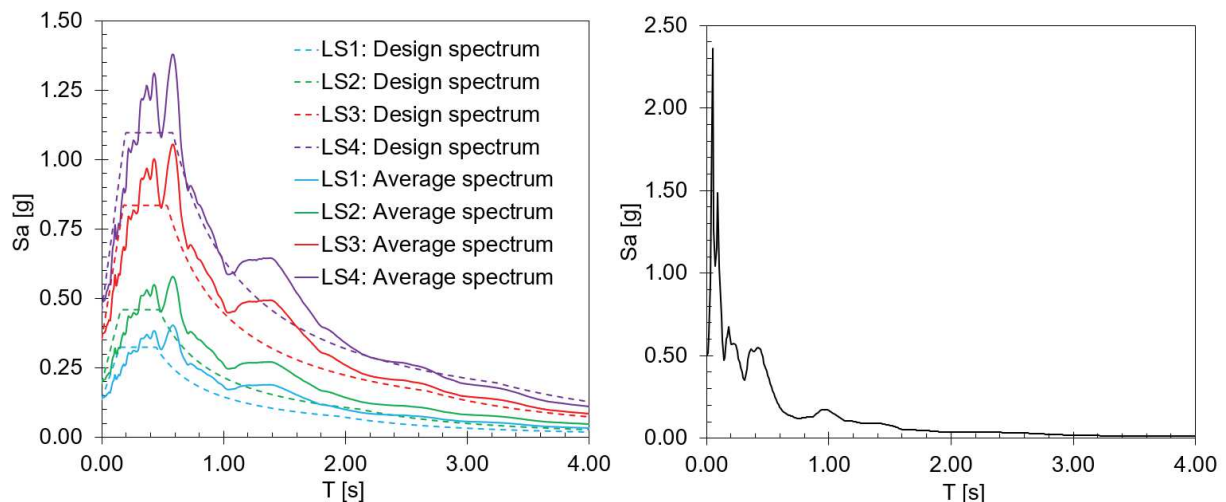


Figure 7.15. Left: design and average spectra of the 5 horizontal records at the different seismic intensities; Right: non-scaled vertical spectrum of EQ_6 .

7.2.4 Test matrix

The experimental campaign was carried out by incrementally increasing the seismic intensity in different directions, namely: the longitudinal (X) or frame direction, the transverse (Y) or wall direction, a direction corresponding to a 45° of inclination in the horizontal plane (XY), the vertical direction (Z). The test sequence was thus conceived as follow: 1) the building was initially subjected to 1D input motions in both the longitudinal and vertical directions; 2) then 2D input motions in the horizontal direction (XY) were performed, 3) finally 3D input motions were carried out considering the combination of the XY input with the vertical excitation (XY+Z). In addition to the ground motion

sequence, a white noise motion was run before and after each intensity level. Consequently, the test matrix was defined basing on these considerations.

Table 7.3 shows part of the Test Matrix and particularly provides the sequence adopted for each intensity seismic level. Each of the earthquake record presented in this table was properly scaled in function of the shaking level.

Table 7.3. Test sequence adopted for each seismic intensity level (i.e. for LS1, LS2, LS3 and LS4).

Record ID	Input motion description
H_EQ1_X	EQ1, X Direction
H_EQ1_Y	EQ1, Y Direction
H_EQ1_XY (45°)	EQ1, XY (45°) Direction
H_EQ2_X	EQ2, X Direction
H_EQ2_Y	EQ2, Y Direction
H_EQ2_XY (45°)	EQ2, XY (45°) Direction
H_EQ3_X	EQ3, X Direction
H_EQ3_Y	EQ3, Y Direction
H_EQ3_XY (45°)	EQ3, XY (45°) Direction
H_EQ4_X	EQ4, X Direction
H_EQ4_Y	EQ4, Y Direction
H_EQ4_XY (45°)	EQ4, XY (45°) Direction
H_EQ5_X	EQ5, X Direction
H_EQ5_Y	EQ5, Y Direction
H_EQ5_XY (45°)	EQ5, XY (45°) Direction
V_EQ6_Z	EQ6, Z Direction
H+V_EQ1_XY (45°) + EQ6_Z	EQ1, XY (45°) Direction + EQ6, Z Direction
H+V_EQ2_XY (45°) + EQ6_Z	EQ2, XY (45°) Direction + EQ6, Z Direction
H+V_EQ3_XY (45°) + EQ6_Z	EQ3, XY (45°) Direction + EQ6, Z Direction
H+V_EQ4_XY (45°) + EQ6_Z	EQ4, XY (45°) Direction + EQ6, Z Direction
H+V_EQ5_XY (45°) + EQ6_Z	EQ5, XY (45°) Direction + EQ6, Z Direction

The test sequence previously described was fully respected during the first phase of experimental tests on the *Skeleton Building* solution, while for studying the configurations with non-structural components (*Option 1* and *Option 2*) and mainly for time issues, the test matrix was reduced to three or two earthquakes for the horizontal shakings (2 or 1 Far Field and 1 Near Fault).

7.2.5 Signal processing and data acquisition

For the control of the LNEC 3D shake table, compatible displacement and acceleration time series are required, both sampled at 200Hz. Fourier filters, both low and high pass, integration,

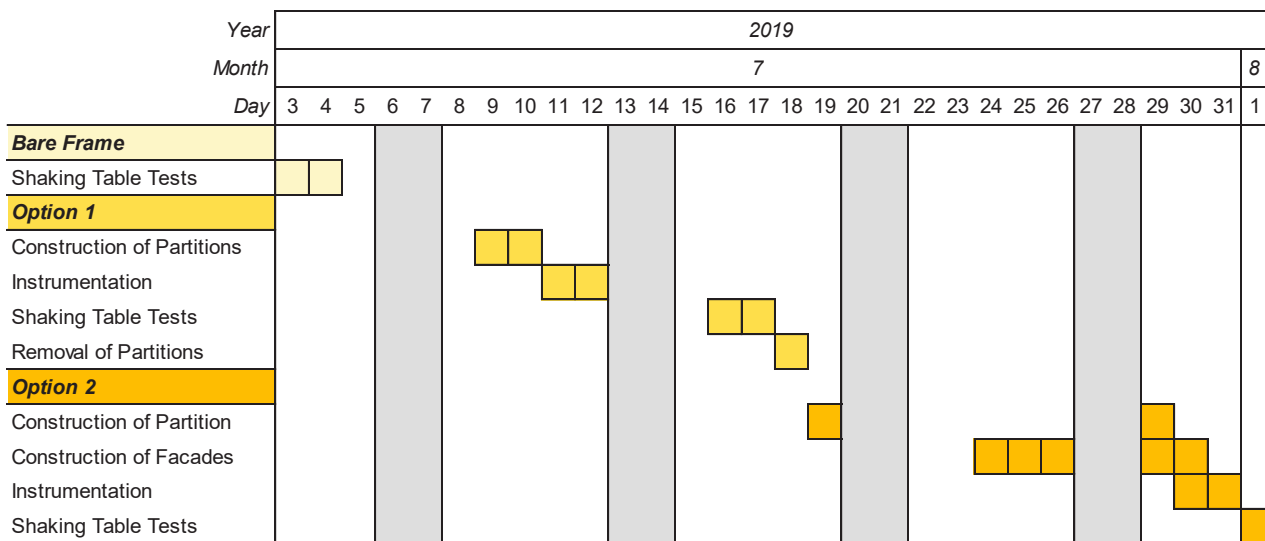
differentiation and detrending were used to achieve this. This digital signal processing, in both time and frequency domains, was carried out using the LNEC-SPA software developed at LNEC.

Shaking table data acquisition was collected via a high-speed logger and computer arrangement. All data was collected at a sample frequency of 200Hz to ensure a sufficient sample size for filter options during postprocessing and a Butterworth bandpass filter was applied to all recorded acceleration data across the frequencies of 0.1-20 Hz to eliminate noise outside of the range of building excitation.

7.2.6 Timeline of the experimental tests

The experimental tests were carried out in July 2019/beginning of August 2019, as presented in Table 7.4 where a Gantt diagram of the time period between the first tests on the *Skeleton Building* solution and the final tests on the Integrated system is presented.

Table 7.4. Timeline of the testing phases.



Due to the construction of an infill wall with low damage detailing to be tested in the third experimental phase, 20 days (or more) were not needed for the curing of the masonry, as typically expected for a traditional wall, while a period of 10 days was assumed. It is also highlighted that the construction of the masonry partition was split into two phases, i.e. 1) the first phase corresponding to the construction of the rocking walls inside the steel sub-frame and 2) the second phase representing the introduction of the polyurethane foam into the lateral gaps and the application of the light white painting on one side of the wall.

7.3 Shake-table testing results

This paragraph presents the results obtained from the experimental campaign of the half scaled structural/non-structural building system. Particularly, for the scope of this Thesis the description focuses on the study of the seismic performance of the non-structural components in the low-damage timber-concrete structural system, therefore on the second and third testing phases. Considering the two horizontal directions of the Test Building, results are provided in terms of peak floor accelerations and maximum inter-storey drift ratios for the global system, in terms of dynamic amplifications, relative displacements and damage description for the non-structural components. Elaborating the data from the white noise signals and the impact hammer testing, the natural periods of both the Test Building and the different non-structural components are also computed.

All the results reported within this section are only preliminary elaborations from an initial post-processing of the experimental data. However, more refined results will be developed and shown in future conference/journal papers.

7.3.1 Phase 2 testing

The second testing phase involved shaking table tests on the low-damage structural skeleton comprising the internal fibre-reinforced ceramic gypsum partitions. As previously stated, the Test Matrix was reduced when testing the configurations with non-structural components. Specifically, the sequence of testing included three different earthquakes (2 Far Field and 1 Near Fault, i.e. EQ₂, EQ₃ and EQ₅) for each intensity level. The Test Matrix was modified as:

- For **LS1** (Damage Control level of the NTC 2018, $T_R = 50$ years), the three earthquakes were simulated by the shaking table in both the structural directions (X and Y) as well as in the inclined 45° direction (XY);
- As for the previous limit state, for **LS2** (more than Serviceability limit state, $T_R = 101$ years), the three earthquakes were simulated in both the structural directions (X and Y) and in the inclined 45° direction (XY);
- For the **LS3** (Life Safety of the NTC 2018, $T_R = 475$ years), just EQ₂ was fully simulated in the X, Y and XY (45°) directions, while the other two records were directly considered in the combined XY + Z configuration, that is the application of the earthquake in the XY (45°) direction combined with the vertical input EQ₆;

- For the **LS4** (more than Near Collapse of the NTC 2018, $T_R = 1500$ years), just EQ₅ was applied in the XY + Z combined simulation, i.e. XY (45°) of EQ₅ combined with EQ₆ in the vertical direction.

7.3.1.1 Test results

First of all, results are presented in terms of seismic response of the overall low-damage structural skeleton including the fibre-reinforced gypsum partitions on the first floor. The inter-storey drift ratios and the floor accelerations are thus determined for each earthquake motion and intensity level and the maximum values of these demand parameters are summarized in Figures 7.16 and 7.17 for either the frame or the wall directions. Considering a specific simulated earthquake, for each structural direction and building level, average values of the inter-storey drift/acceleration are obtained taking into account all the sensors monitoring that direction/level. Then, considering all the earthquake sequence of a specific intensity level (LS_{*i*}, *i*=1,2,3,4) the maximum values of the demand parameters are calculated and used for building the following graphs. The demand parameters (accelerations, drift ratio) in these graphs are correlated to the spectral accelerations at the first natural periods (T_{1x} , T_{1y}) determined from dynamic identification studies (see 7.3.1.3 paragraph) and estimated considering the response spectra properly evaluated from the base accelerations.

Figures 7.16 and 7.17 highlight that the drift/acceleration values do not substantially increase when moving from LS2 to the higher intensity levels. In fact, due to the Test Matrix followed during this testing phase, combined XY + Z input motions are mainly simulated for LS3 and specifically for LS4 intensity level, therefore the combined action led to reduced drift/acceleration when compared to the mono-directional motion applied to X or Y, as for the LS1 and LS2 conditions.

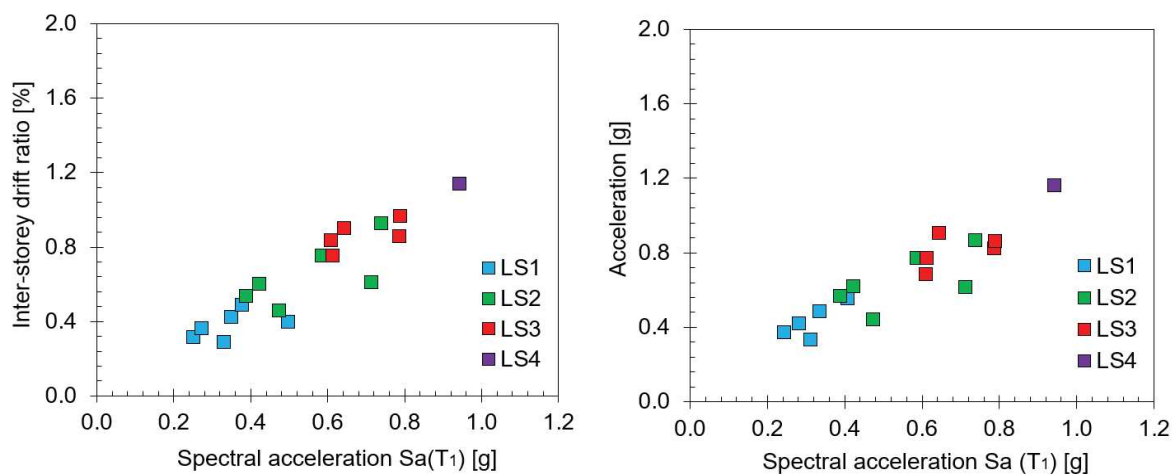


Figure 7.16. Frame direction: maximum inter-storey drift ratios (left) and peak floor accelerations (right).

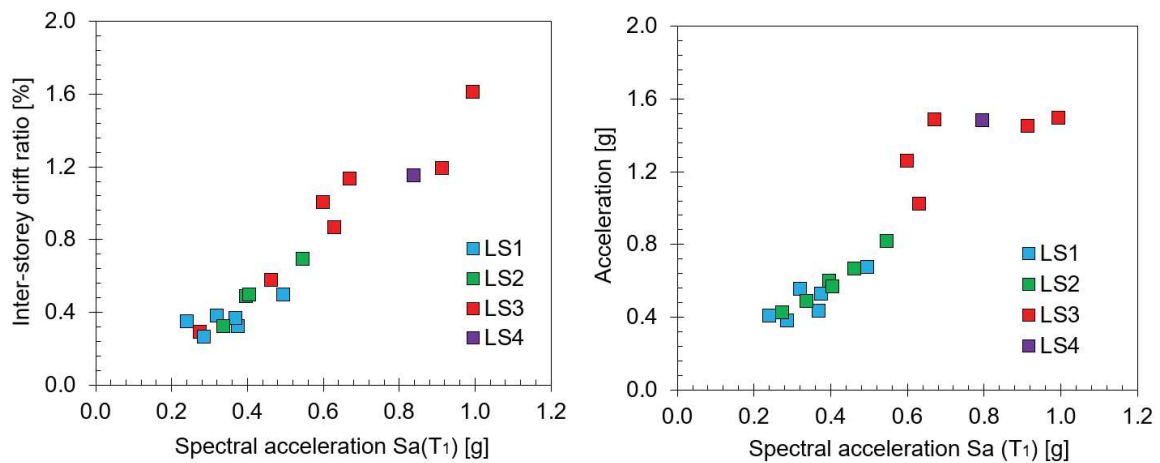


Figure 7.17. Wall direction: maximum inter-storey drift ratios (left) and peak floor accelerations (right).

It is observed that the results summarized in the previous figures are coherent with what defined during the design process of the Test Building.

Considering EQ_5 as input motion, representing the only record achieving the fourth limit state - LS4 - during this test phase, and referring to the output data from the devices monitoring the column in the North-West corner, as example Figures from 7.18 to 7.20 provide the results obtained for both building directions in terms of: 1) shaking table acceleration, 2) first floor acceleration, 3) drift ratio between level 1 and level 2.

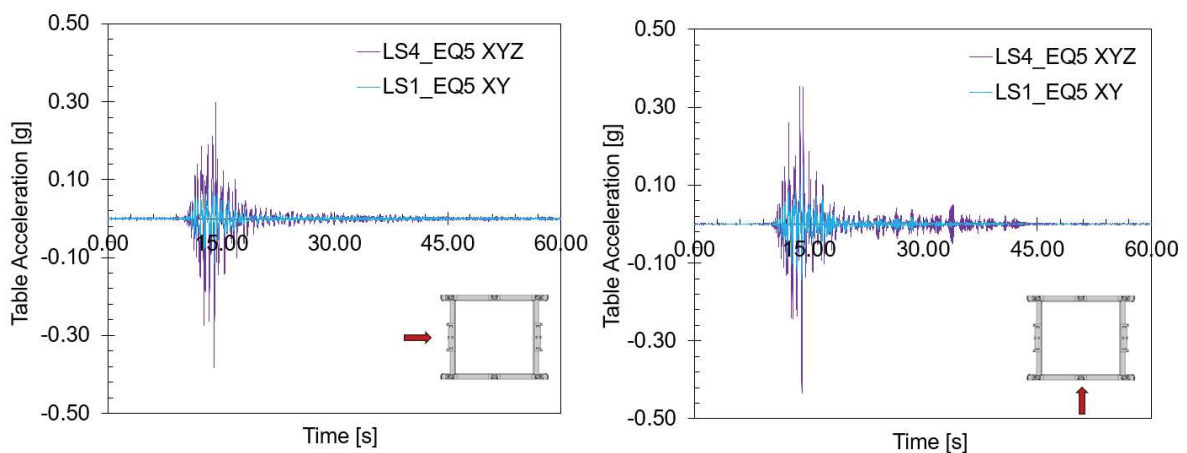


Figure 7.18. Considering EQ_5 earthquake and both the LS1 and LS4 intensity levels: table acceleration in the frame direction (left) and in the wall direction (right).

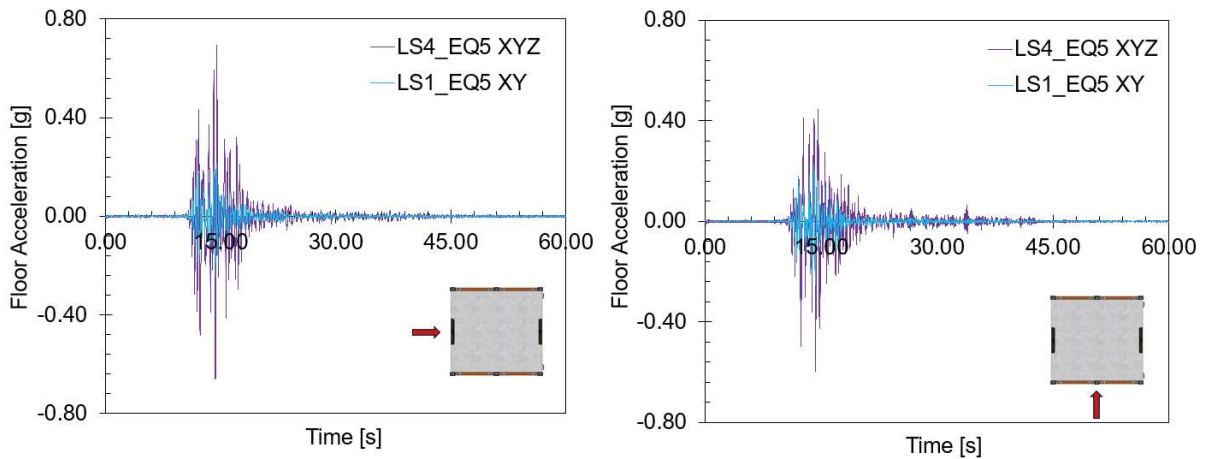


Figure 7.19. Considering EQ_5 earthquake, both the LS1 and LS4 intensity levels and referring to the column in the North-West corner: 1st floor acceleration in the frame direction (left) and in the wall direction (right).

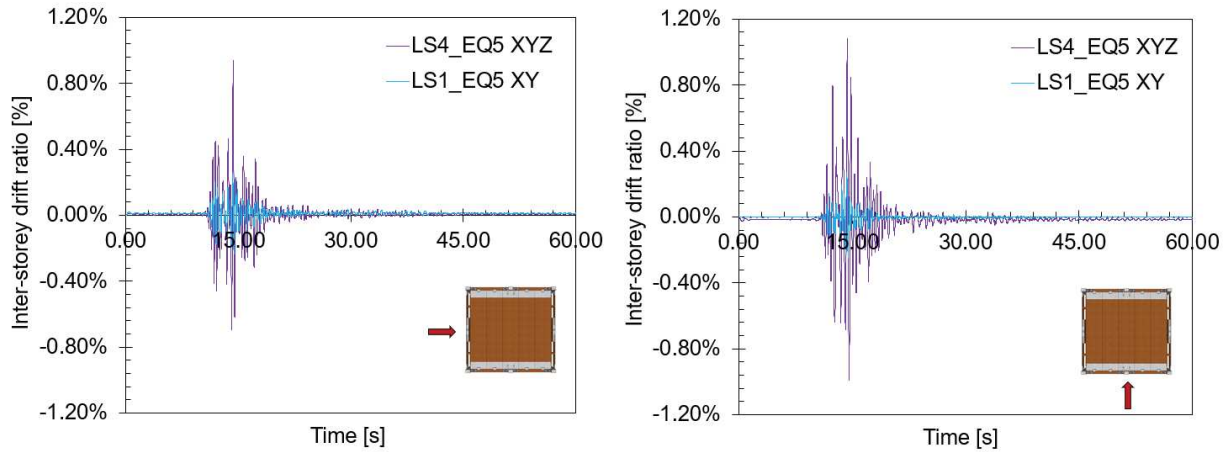


Figure 7.20. Considering EQ_5 earthquake, both the LS1 and LS4 intensity levels as well as referring to the column in the North-West corner: inter-storey drift ratio between level 1 and level 2 in the frame direction (left) and in the wall direction (right).

The results of the second test campaign are summarized in Table 7.5. For each intensity level and for both building directions, the table includes: 1) the peak accelerations of the table; 2) the peak accelerations at the first floor and second floor levels; 3) the maximum accelerations recorded on the partition wall; 4) the inter-storey drift ratios between the foundation level and the first floor as well between the two building levels; 5) the maximum relative displacements between the partition wall and the structural skeleton, i.e. partition/wall in the frame direction and partition/column in the wall direction.

Table 7.5. Maximum values of the recorded quantities for each limit state and building direction.

Intensity level	Direction	Acceleration [g]				Inter-storey drift ratios [%]		Relative displacement [mm]
		Table	Floor 1	Floor 2	Partition	Level 0/1	Level 1/2	Partition
LS1	Frame	0.17	0.35	0.55	0.53	0.46	0.40	5.49
	Wall	0.20	0.36	0.67	1.20	0.49	0.39	1.23
LS2	Frame	0.29	0.56	0.86	0.86	0.92	0.79	12.82
	Wall	0.25	0.42	0.82	1.27	0.69	0.56	1.67
LS3	Frame	0.35	0.63	0.90	0.99	0.96	0.86	14.01
	Wall	0.38	0.68	1.49	1.64	1.54	1.61	9.72
LS4	Frame	0.35	0.67	1.16	1.12	1.14	0.95	12.75
	Wall	0.43	0.65	1.48	1.68	1.11	1.07	6.48

Considering the partition in the frame direction, that is the 2.5 m long partition monitored using 5 accelerometers and 4 LVTD transducers (see previous Figure 7.8), if the amplification factor for the out-of-plane acceleration is evaluated, this is typically included between 2 and 3. Studying for the same partition the out-of-plane acceleration distribution, it is observed that the acceleration on the panel is almost the same at different locations characterized by the same height (i.e. A4, A31, A1) and maximum values are recorder for the accelerometer (A1) closer to the intersection zone with the orthogonal partition wall. Therefore, the partition deformed in the out-of-plane mainly along the vertical plane, whereas reduced deformations were recorded in the horizontal plane.

When taking into account the study of the LVDT responses for this partition wall, results highlight that the vertical displacements, recorded by L11 and L17, achieved a maximum recorded value of 3 mm and the displacement between the two orthogonal panels in the horizontal direction was negligible. While, the wall/partition relative displacement, recorded by L2, achieved values between 10 mm and 14 mm when performing the higher earthquake levels (LS3, LS4), meaning for the introduced non-structural detailing (lateral gap of 10-15 mm) an interaction with the structural system. Referring to a specific earthquake motion, an example of displacement recorded by the L2 transducer is shown in Figure 7.21.

Similar considerations on the dynamic amplification as well as on the vertical displacements are valid for the other partition wall built in the wall direction (5 m long partition). However, lower relative displacements were recorded between the partition and the seismic columns (less than 10 mm).

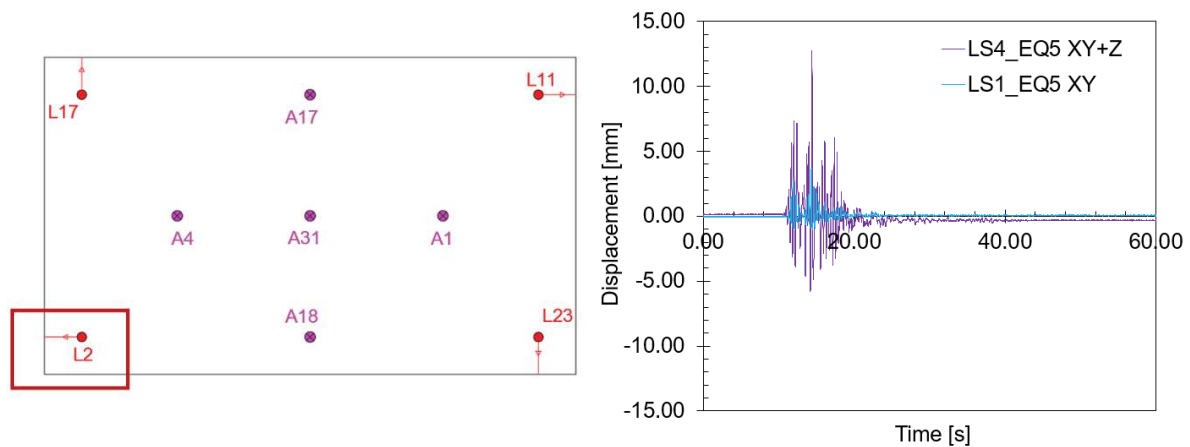


Figure 7.21. Considering EQ₅ earthquake, both the LS1 and LS4 intensity levels: displacement recorded by the L2 transducer on the partition wall in the frame direction.

7.3.1.2 Damage description

The fiber-reinforced gypsum partitions behaved very well during the experimental testing. Damage state conditions were achieved for higher demand parameters when compared to more traditional solutions and no detachment of the panels was observed after the full test sequence. However, during the shaking table tests the following damage levels were observed:

- After the **LS1 earthquakes** (inter-storey drift of around 0.4%).

Formation of cracks along the diagonals of the openings was observed for the partition wall in the South-North direction. The cracks were less than 0.04 mm and located on both sides of the openings (Figure 7.22, left).



Figure 7.22. Diagonal cracks in the East side (left) and vertical crack in the West side (right) of the North opening of the South-North wall.

Apart from these diagonal cracks, a vertical crack from the 3PT floor was observed in the West side of this wall (Figure 7.22, right). This crack formed in that position due to the influence of a crack already developed in the gypsum panel during the construction. In fact, the gypsum panel was repaired in this zone using additional joint tape attached to the wall using glue, therefore the crack seemed to be the continuation of the one already developed when the partition was built.

After the first stage of the shaking table tests, other damage was related to the initial detachment of the silicone-based sealant and adhesive (Figure 7.23) in the bottom corners of the partition.



Figure 7.23. Initial detachment of the silicone sealant and adhesive.

- After the **LS2 earthquakes** (inter-storey drift in the range of 0.5 - 0.8%).

The previous cracks continued to open reaching width values in the range of 0.10-0.30 mm (Figure 7.24). It was also observed additional detachment of the silicone sealant and loss of adhesive in the lateral parts of the corners connected to the columns and to the wall (Figure 7.25).



Figure 7.24. Diagonal cracks in the West side, North opening (left) and South opening (right) of the South-North wall.



Figure 7.25. Detachment of the silicone sealant and adhesive.

- After the **LS3 earthquakes** (inter-storey drift in the range of 0.8 - 1.6%).

The previous cracks extended reaching width values in the range of 0.15-0.65 mm and new cracks formed along both diagonal and horizontal directions of the longer partition wall. The silicone sealant and adhesive continued to detach at the bottom edges of the partitions in the connection part to the seismic columns and to the timber wall. These damage states are shown in the next figures (from Figure 7.26 to Figure 7.28).



Figure 7.26. Cracking of the South-North wall in the West side, North opening.



Figure 7.27. Cracking of the South-North wall in the East side, South opening.



Figure 7.28. Detachment of the silicone sealant and adhesive.

- After the **LS4 earthquakes** (inter-storey drift in the range of 0.9 - 1.1%).

The previous cracks reached width values greater than 2 mm. Crushing of the panels was observed in the bottom corners of the partition walls (connection to columns and wall as well as between the two orthogonal partitions), as also shown in Figure 7.29.



Figure 7.29. Cracking of the South-North wall in the East side, North opening (first photo) and crushing in the lateral corners of both wall partitions (other photos).

No additional damage, i.e. the buckling of the steel studs, was observed when the system was dismounted. The solution had a good seismic behaviour. No cracking was observed in the panels of the smaller partition in the frame building direction, apart from initial detachment of silicone or initial crushing in the wall/partition corner after LS3 events. While, for the longer partition in the wall building direction very limited cracking was observed along the diagonals of the openings until LS2.

7.3.1.3 Dynamic identification

Dynamic identifications of the specimen and of the non-structural element were planned after each intensity level sequence, performing low-intensity white noise signals (maximum amplitudes from 1.5 to 3 mm, duration of 165s) for all building directions and by impact hammer on the 2 m-long partition (maximum amplitudes of around 1g, duration more than 50s). Elaborating the acceleration data through the transfer function method, the natural frequencies of both the structure in the two building directions and of the partition wall can be identified. Table 7.6 lists the frequencies and periods of the first mode of vibration for either the building or the non-structural element obtained during the test campaign.

Table 7.6. Frequencies and periods of the first mode of vibration of the Test Building and of the partition.

	Frame direction		Wall direction		Partition	
	f1 [Hz]	T [s]	f1 [Hz]	T [s]	f1 [Hz]	T [s]
Initial	3.50	0.29	3.71	0.27	21.00	0.048
After LS1	3.37	0.30	3.12	0.32	20.00	0.050
After LS2	3.08	0.32	3.12	0.32	19.71	0.051
After LS3	3.03	0.33	2.59	0.39	19.06	0.052
After LS4	2.88	0.35	2.54	0.39	18.70	0.053

Due to a change of post-tensioned force in the wall between Phase 1 (*Bare Frame*) and Phase 2 (*Option 1*) of the experimental campaign, a direct comparison between the period of the structure with or without partitions cannot be made. However, due to the reduced additional mass of the partition when compared to the mass of the structure as well as for the introduced non-structural detailing, it can be assumed that the partitions had negligible impact on the stiffness of the building to lead to period modifications of the Bare Frame system.

The decreasing value of frequency highlights the evolving of damage in either the structure or the partition system. Particularly, the “damage” of the Test Building was due to the yielding and consequent permanent deformations of the external dissipaters, especially the ones at the base of the timber walls. Such typology of structures is designed for concentrating the damage into the dissipation devices, i.e. the only repair action after earthquakes is related to the substitution of the external dissipaters, estimated to be a cost of around 30-40 euros per dissipater. However, it is observed that the dissipaters started to loss capacity due to the high number of shakings to which they were subjected to (input motions + related iterations). Notwithstanding no collapse of the dissipaters was observed, they were completely substituted after the second testing phase of the experimental campaign to have a new structure to be tested during the last stage of the project (shaking table tests on the integrated structural/non-structural system, i.e. *Option 2*).

While, the evolving of frequency values in the non-structural system was due to the component damage previously described. Referring to the work of DiPasquale E. and Cakmak A.S. (1988), damage indices can be computed for the partition wall relating the period of the un-damaged component to the one of the damaged system (Figure 7.30, right).

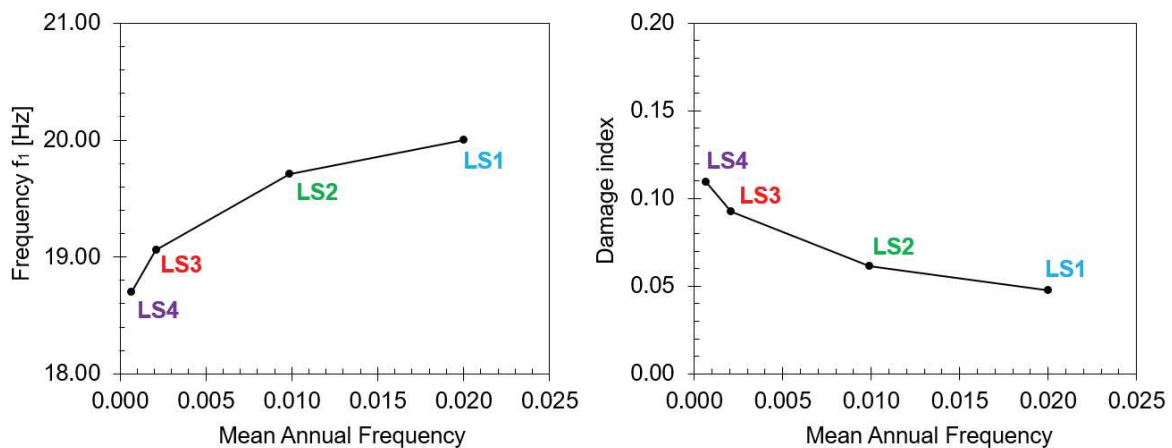


Figure 7.30. For the 2 m long partition wall: Frequency/MAF (left) and Damage index/MAF (right) relations.

The obtained damage indices confirm the good seismic behaviour of the non-structural element. In fact, the values are less than 0.1 until the LS3 intensity level, meaning an intact system, while the index becomes more than 0.1 (maximum value of 0.11) indicating a minor damage condition.

7.3.2 Phase 3 testing

The third testing phase involved shaking table tests on the integrated structural/non-structural building configuration comprising GFRC and glazing facades and an internal masonry partition.

As previously anticipated, the Test Matrix was reduced for testing the configurations with non-structural components. Particularly, the third testing phase included two different earthquakes (1 Far Field and 1 Near Fault, i.e. EQ₂ and EQ₅) considered at each intensity level as follows:

- For **LS1** (Damage Control level of the NTC 2018, $T_R = 50$ years), EQ₂ earthquake was simulated by the shaking table in both the structural directions (X and Y), in the inclined 45° direction (XY) and in the combined XY + Z configuration with EQ₆;
- For **LS2** (more than Serviceability limit state, $T_R = 101$ years), the two earthquakes were directly simulated in the combined XY + Z configuration;
- As for the previous level, for the **LS3** (Life Safety of the NTC 2018, $T_R = 475$ years), the two earthquakes were directly simulated in the combined XY + Z configuration;
- As for the previous level, for the **LS4** (more than Near Collapse of the NTC 2018, $T_R = 1500$ years), the two earthquakes were directly simulated in the combined XY + Z configuration.

7.3.2.1 Test results

The results are initially provided in terms of seismic response of the integrated low-damage structural skeleton comprising of envelopes and internal partition. The inter-storey drift ratios and the floor accelerations are determined for each earthquake motion and intensity level and the maximum values of these demand parameters are summarized in Figures 7.31 and 7.32 for either the frame or the wall building directions.

Considering a specific simulated earthquake, for each structural direction and building level, average values of the inter-storey drift/acceleration are obtained taking into account all the sensors monitoring that direction/level. Then, considering all the earthquake sequence of a determined intensity level (LS_{*i*}, *i*=1,2,3,4) the maximum values of the demand parameters are calculated and

used for building the following graphs. The graphs are built in terms of spectral accelerations (S_a) at the first natural periods (T_{1x}, T_{1y}), determined from dynamic identification studies. The $S_a(T_1)$ values are estimated from the response spectra properly evaluated for the base accelerations.

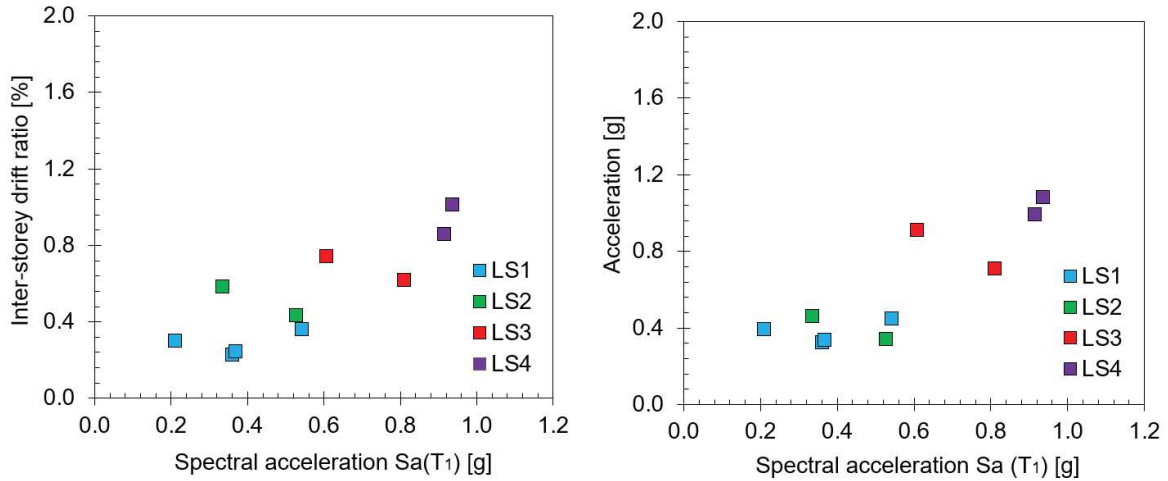


Figure 7.31. Frame direction: maximum inter-storey drift ratios (left) and peak floor accelerations (right).

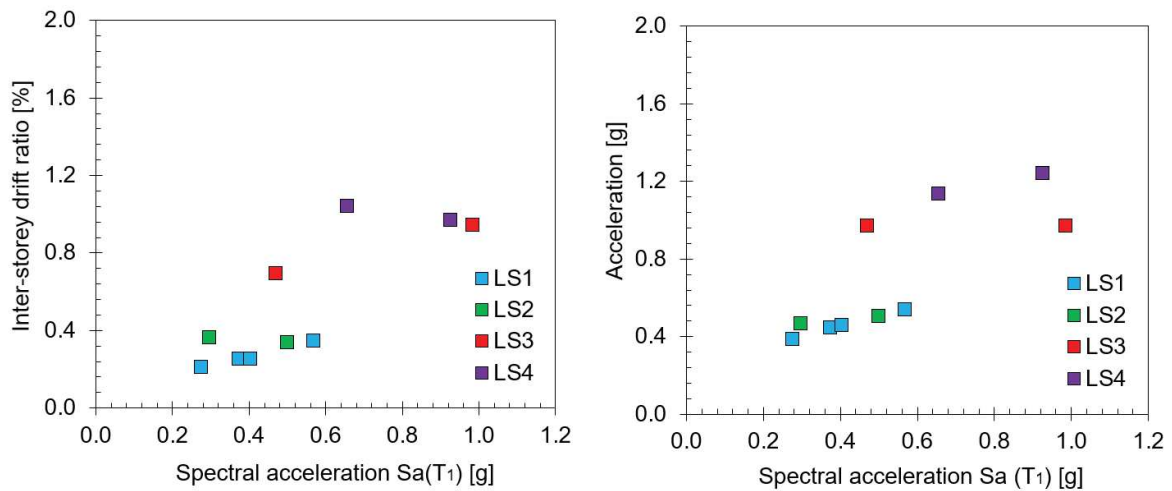


Figure 7.32. Wall direction: maximum inter-storey drift ratios (left) and peak floor accelerations (right).

Comparing the previous figures with the same graphs obtained for *Option 1*, it can be seen that the recorded inter-storey drift ratios and floor acceleration are now reduced for the wall direction, due to the influence of the non-structural systems. Considering EQ_5 as input motion and referring to the output data from the devices monitoring the North-West column, Figures from 7.33 to 7.35 present the results for both building directions in terms of shaking table and first floor acceleration, drift ratio between level 1 and level 2.

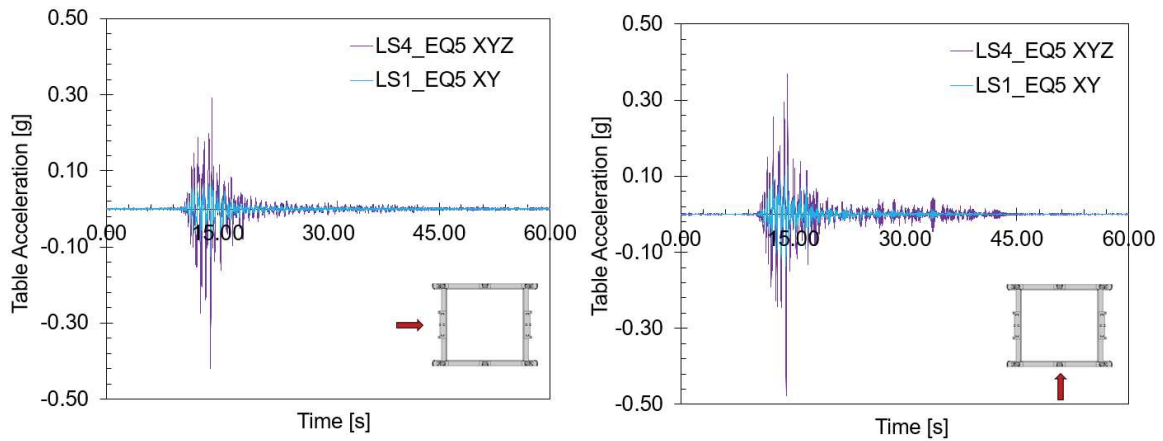


Figure 7.33. Considering EQ₅ earthquake and both the LS1 and LS4 intensity levels: table acceleration in the frame direction (left) and in the wall direction (right).

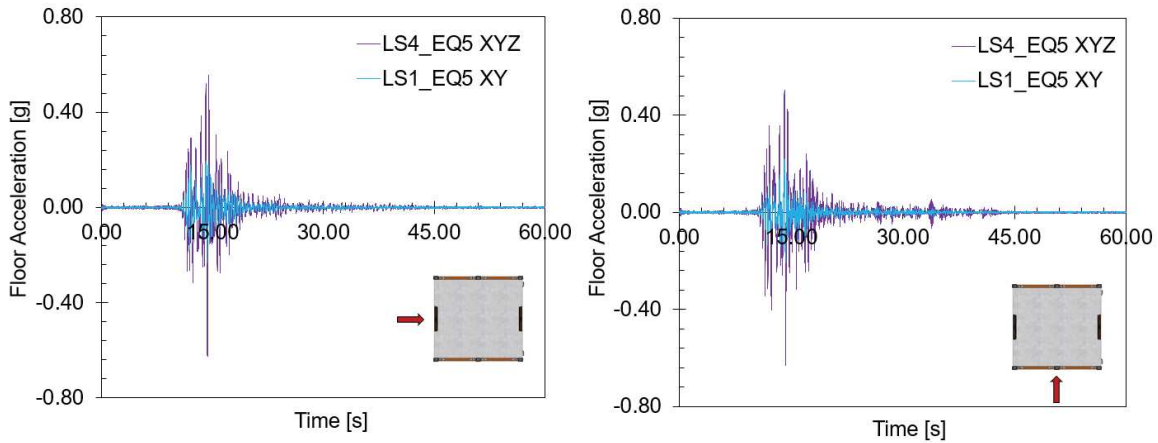


Figure 7.34. Considering EQ₅ earthquake, both the LS1 and LS4 intensity levels as well as referring to the column in the North-West corner: 1st floor acceleration in the frame direction (left) and in the wall direction (right).

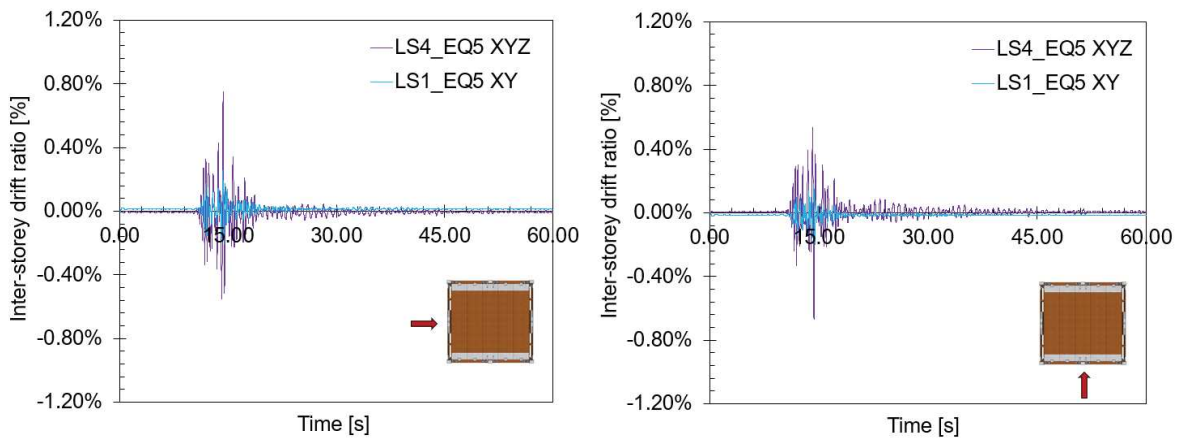


Figure 7.35. Considering EQ₅ earthquake, both the LS1 and LS4 intensity levels as well as referring to the column in the North-West corner: inter-storey drift ratio between level 1 and level 2 in the frame direction (left) and in the wall direction (right).

The results of the third test campaign are summarized in Tables 7.7 and 7.8. For each intensity level and for both building horizontal directions, the table includes: 1) the peak accelerations of the table; 2) the peak accelerations at the first floor and second floor levels; 3) the maximum accelerations recorded on each non-structural element; 4) the inter-storey drift ratios between the foundation level and the first floor as well as between the two building levels; 5) the maximum relative displacements between the non-structural systems and the structural skeleton, i.e. cladding/column, glass panel/column and partition/column.

Table 7.7. Maximum accelerations recorded for each limit state and building direction.

Intensity level	Direction	Acceleration [g]					
		Table	Floor 1	Floor 2	GFRC facade	Glass facade	Infill wall
LS1	Frame	0.14	0.26	0.44	-	0.59	0.40
	Wall	0.17	0.31	0.54	0.79	0.39	-
LS2	Frame	0.22	0.38	0.46	-	0.97	0.55
	Wall	0.17	0.28	0.50	0.79	0.35	-
LS3	Frame	0.34	0.53	0.91	-	1.09	0.82
	Wall	0.32	0.48	0.97	1.12	0.69	-
LS4	Frame	0.41	0.60	1.08	-	1.47	0.96
	Wall	0.47	0.59	1.24	1.52	0.99	-

Table 7.8. Maximum inter-storey drifts and relative displacements recorded for each limit state and building direction.

Intensity level	Direction	Inter-storey drift ratio [%]		Relative displacement [mm]		
		Table-Floor 1	Floor 1-Floor 2	GFRC facade	Glass facade	Infill wall
LS1	Frame	0.36	0.29	3.97	-	-
	Wall	0.57	0.32	-	2.76	3.02
LS2	Frame	0.55	0.58	5.52	-	-
	Wall	0.36	0.33	-	2.38	1.93
LS3	Frame	0.74	0.58	9.21	-	-
	Wall	0.94	0.69	-	4.55	6.53
LS4	Frame	1.01	0.76	12.15	-	-
	Wall	0.94	1.04	-	5.32	9.91

From the previous tables it can be noticed that the demand parameters are higher in some cases for LS1 when compared to LS2. This is related to the type of action simulated for that limit state, i.e. not only the combined XY + Z configuration while also the mono-directional earthquakes in both X and Y directions.

Elaborating the results and determining the amplification factor for the out-of-plane accelerations of all the non-structural systems, this is included between 2 and 3 for the exterior envelopes while is around 2 for the internal partition.

Analysing the seismic behaviour of each single non-structural system, particularly considering the in-plane movements of the non-structural systems during the seismic shakings, the following considerations can be made:

1. GFRC facades

Referring to the registrations obtained for the façade in the North side, more monitored than the other façade, the relative displacements between the top and bottom panels, measured by the L23 and L24 transducers (see previous Figure 7.10), are found to be less than 16 mm. A similar behaviour can be noticed when comparing the registrations of the LVDTs positioned in the two different spans of the frame system.

Regarding the measure of the displacement of the top (sliding) anchorage system related to the concrete column, the maximum recorded value is 12 mm. This displacement can be converted into “connection drift” value, as presented in the following Figure 7.36 for the EQ₂ input motion at LS4.

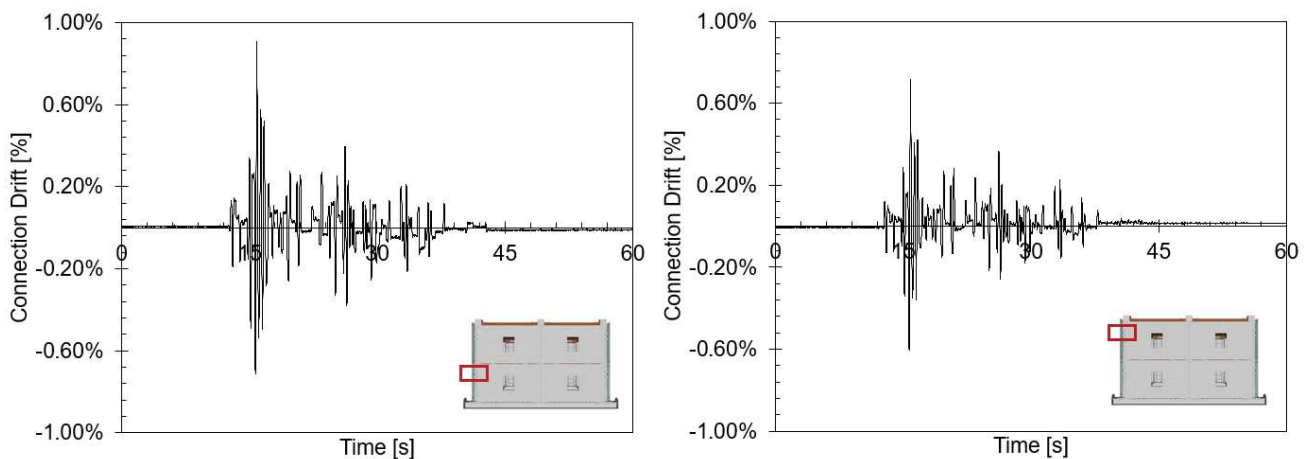


Figure 7.36. Considering as example EQ₂ at LS4 limit state: connection drifts for the precast concrete system in the North-East side for the first (left) or the second (right) cladding levels.

The maximum recorded connection drift was around 0.95% and no damage was observed until this value for the concrete panels.

As observed in the conclusions of the work, further studies are planned, particularly for determining the frictional effect of these sliding connections, thus calibrating proper numerical

models to study the influence of this non-structural component in the global building response.

2. *Glass facades*

Considering the output data of the East side façade, more monitored when compared to the other West glass wall, it can be noticed that the movement of the glass relative to the structural system, i.e. referring to the registrations of all the transducers monitoring the vertical and horizontal displacements of the glass panels relative to the columns, to the steel foundation or to the top floor (see previous Figure 7.12), is very reduced, achieving maximum values of around 6 mm. During the seismic actions the seismic forces were in fact primarily taken by the spider arms, thus the glass panels and the spider arms all rotated as rigid bodies while rotation did not occur because the frictional moment capacity of the spider arms was not exceeded.

As observed in the next section, the system performed very well in the in-plane direction, while in the out-of-plane movement, differential displacements leading to possible damage conditions were found to be.

3. *Infill wall partition*

Regarding the movement of the infill wall system, due to the available instrumentation of the laboratory registrations were collected for the two lateral infill panels only (see previous Figure 7.14). The movement of these two vertical panels was found to be quite similar with displacements between the wall and the column less than 10 mm, while reduced vertical displacements between the wall and the top slab as well as limited relative displacements between adjacent panels (lateral panel/internal one) were recorded (less than 4 mm).

Taking into account a specific earthquake input, the behaviour of the panel in the South corner is shown in the next Figure 7.37. Results highlight a cumulative residual horizontal displacement mainly due to the sliding of the panel inside the steel frame during the seismic motions, as also observed in the subsequent damage description.

For all the non-structural solutions tested during Phase 3, further studies are planned for better understanding the in-plane or out-of-plane movements of these components under seismic events, for calibrating specific numerical modelling to describe their seismic behaviour as well as for suggesting improvements to the non-structural detailing.

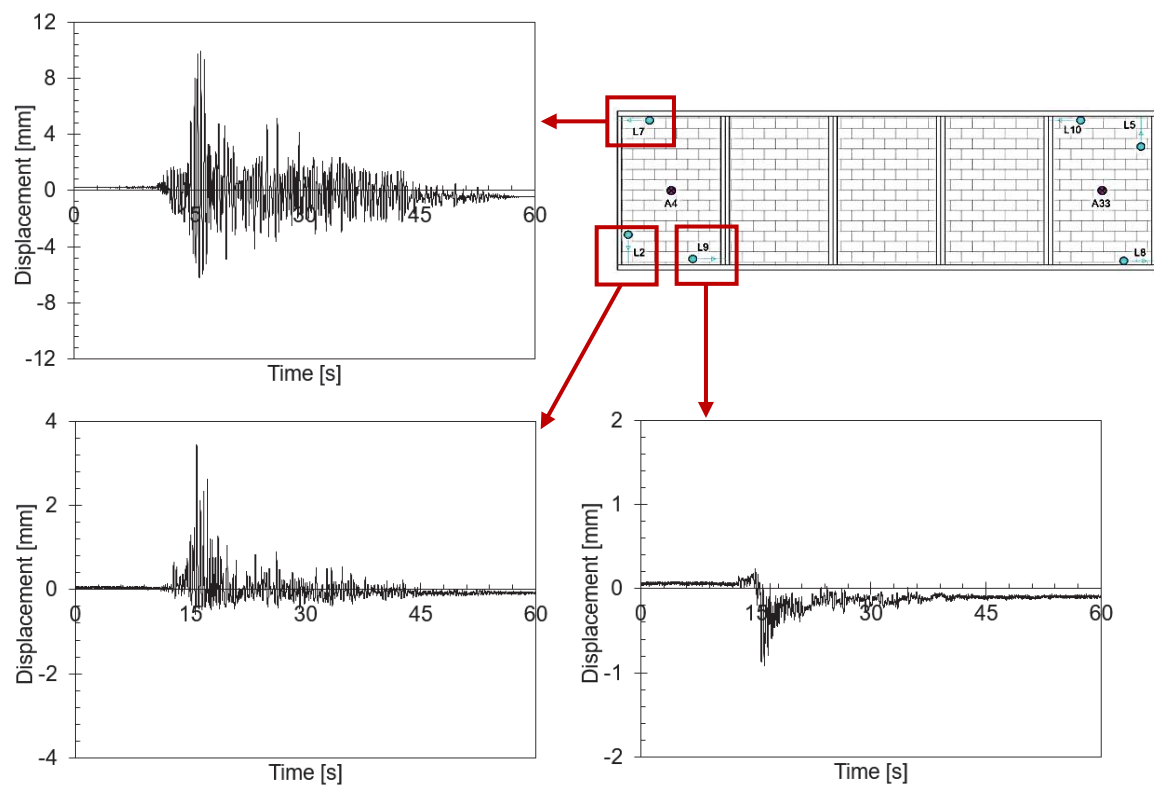


Figure 7.37. Considering EQ5 earthquake and LS4 limit state: movement of the infill panel in the South corner recorded by the different LVDT transducers.

7.3.2.2 Damage description

Concerning the GFRC facades covering the structural skeleton in the frame direction, these components had good seismic performance during the earthquake shakings at increasing intensities. No cracking was observed in the cladding panels after all the testing sequence, thus until the tested 1% of inter-storey drift level. No other damage condition was found to be associated with this typology of façade, apart from little misalignments of the panels in the out-of-plane direction, already observed during the construction of the façade. These misalignments were emphasized during the tests due to the movement of the low-damage structure, specifically due to the torsional response of the timber seismic beams.

Regarding the spider glazing systems in the wall direction, they behaved very well during the earthquake shakings. No failure of the glass panels was observed after all the testing sequence, as expected according to previous testing of this typology of facade. However, different aspects were highlighted analyzing the behaviour of these non-structural components.

- Great displacements in the out-of-plane direction of the glass panels relative to each other (maximum of around 14 mm) were found after the experimental campaign. These displacements were related to the yielding and elongation of the rotule bolt fittings (around 5 mm), subjected to high seismic forces in this direction due to the inertia of the glass wall (Figure 7.38, 7.39, 7.40). The out-of-plane displacement of the glass panels relative to each other induced a combined local bending and tensile stresses particularly around the bolt to glass panel which could result to initiation of cracking and consequent failure of the glass panel for higher intensity levels.



Figure 7.38. Out-of-plane movement of the panels.



Figure 7.39. Measurements of the out-of-plane movement of the panels after all the testing sequence.



Figure 7.40. Misalignment of the spider connector (left) and one of the rotules elongated during the tests (right).

- Compression of the PVC internal layer was observed in some holes of the glass panels. This damage condition was caused by the impacts of the rotule to the glass panel during the major earthquake motions.

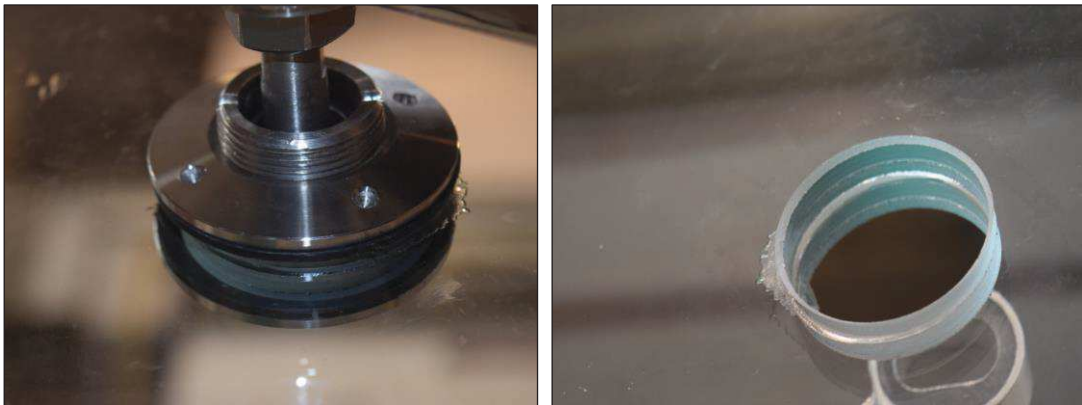


Figure 7.41. Damage to the PVC internal layer.

Finally, concerning the low-damage infill wall, the seismic behaviour of this solution confirmed the high potentiality of applying low-damage detailing to such type of partition wall. Overall, the infill wall did not suffer any serious in-plane damage and did not lose its out-of-plane capacity, which was due to the in-plane integrity of the clay brick infill wall and the integrity of the sub-frame system. In fact, no damage was observed after the first three levels of seismic intensity, while after the last seismic intensity sequence the following damages were found to be (Figure 7.42):

- initial detachment of the lateral silicone-sealant in the corner of the wall;

- sliding of the masonry wall inside the steel frame, observed thanks to the light white painting applied on one side of the masonry wall. This condition was already noticed after LS3 earthquake sequence;
- cracking of the mortar surrounding one brick located in the upper-left corner of the second rocking wall from the North direction.



Figure 7.42. Observed damage to the low-damage masonry wall.

7.3.2.3 Dynamic identification

Dynamic identifications of the entire specimen and of all the non-structural elements were planned after each intensity level sequence, performing low-intensity white noise signals (maximum amplitudes from 1.5 to 3 mm, duration of 165s) for all the building directions and by impact hammer on the GFRC panel in the upper-left part of the North façade, on the glass panel in the upper-left of the East façade and on the lateral infill wall in the North side (maximum amplitudes of around 1g, duration more than 50s). Elaborating the acceleration data through the transfer function method, the natural frequencies of both the structure in the two building directions and of the non-structural elements can be identified. Tables 7.9 and 7.10 list the frequencies and periods of the first mode of vibration for either the building or the non-structural components obtained during the test campaign.

Table 7.9. Frequencies and periods of the first mode of vibration of the Test Building.

	Frame direction		Wall direction	
	f1 [Hz]	T [s]	f1 [Hz]	T [s]
Initial	3.66	0.27	3.90	0.26
After LS1	3.53	0.28	3.87	0.26
After LS2	3.47	0.29	3.71	0.27
After LS3	3.35	0.30	3.32	0.30
After LS4	3.08	0.32	2.98	0.34

Table 7.10. Frequencies and periods of the first mode of vibration of all the non-structural elements.

	GFRC facade		Glass facade		Infill wall	
	f1 [Hz]	T [s]	f1 [Hz]	T [s]	f1 [Hz]	T [s]
Initial	16.27	0.061	69.00	0.014	37.35	0.027
After LS1	16.02	0.062	69.00	0.014	37.05	0.027
After LS2	-	-	-	-	32.44	0.031
After LS3	15.43	0.065	68.75	0.015	26.17	0.038
After LS4	15.27	0.065	68.59	0.015	15.02	0.067

Regarding the global system behaviour, it is observed a decrease of the natural period for both building directions when the initial *Option 2* configuration is compared with the initial *Option 1* system (frame direction: from 0.286s to 0.273s; for wall direction: from 0.270s to 0.256s), in fact the building had higher mass, however, the stiffness provided by the non-structural components reduced the period. While, the decreasing value of frequency for the entire system was mainly due to the yielding and consequent permanent deformations of the external dissipaters, especially the ones at the base of the timber walls, as already observed for Phase 2 testing.

The evolving of frequency values in the non-structural systems during the testing sequence was due to damage of the panels, also if not directly observed as for the infill wall system. Referring to the work of DiPasquale E. and Cakmak A.S. (1988), damage indices can be computed for each system, as shown in Figure 7.43, right.

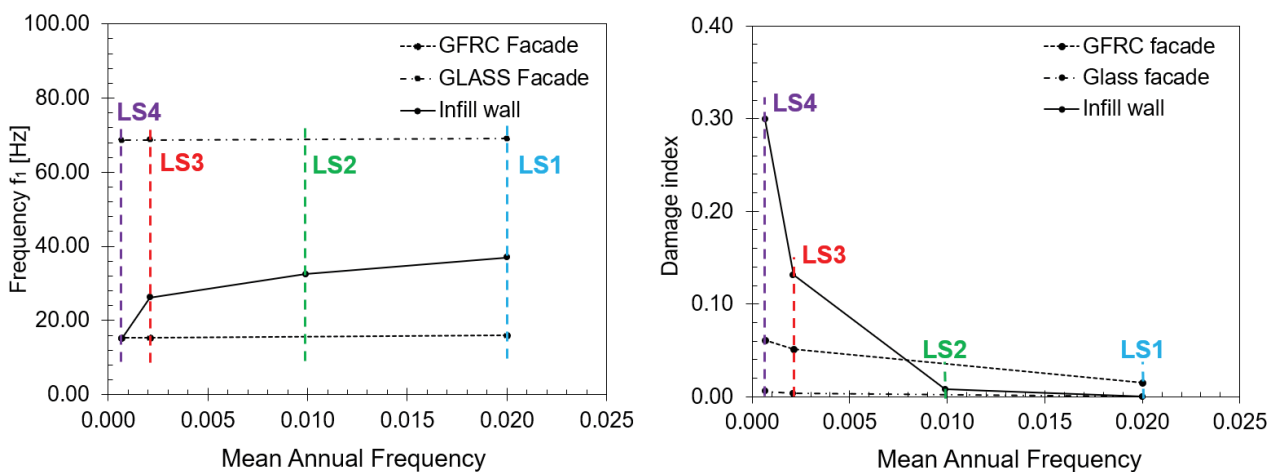


Figure 7.43. For all the non-structural elements: Frequency/MAF (left) and Damage index/MAF (right) relations.

It is observed that for either the GFRC system or the glass panel, no dynamic identification was carried out by impact hammer after the second limit state sequence, for this reason no value can be found in the Table 10 or Figure 7.43 at this intensity level.

The computed damage indices highlight as follows:

- For the GFRC panel, the damage index achieves values less than 0.10 indicating an intact (undamaged) component;
- For the Glass façade, the damage index assumes negligible value, in fact no modification in the frequency response was observed through the dynamic identification, i.e. the panel was completely intact after all the tests;
- For the infill wall partition, until the LS2 (more than Serviceability limit state) the damage index is almost zero, indicating the absence of damage, while from LS3 to LS4 minor damage (Damage Index less than 0.3) is found to be in the component.

7.4 Conclusions

This Chapter has finalized the description of the experimental campaign started in Chapter 6. Particularly, the setup of the shaking table tests (test matrix and monitoring system) as well as preliminary results, focusing on the study of the seismic demand and behaviour of all the tested non-structural systems, are provided.

The shaking table tests were carried out at the Laboratório Nacional de Engenharia Civil (LNEC) in Lisbon. The instrumentation plan was defined taking into account all the devices (accelerometers, LVDT transducers, strain gauges, load cells, optical devices) and channels available for monitoring the building response during the experimental tests. While, regarding the testing sequence, different input motions from Far Field and Near Fault registrations were chosen to be simulated, considering for them scaling factors defined in function of the limit state level to be achieved (spectrum-compatibility) and of the similitude to the Prototype structure (Cauchy-Froude). A specific test matrix was established, however it was fully followed for the *Skeleton Building* system only, to properly calibrate the behaviour of the primary structure, while for testing *Option 1* and *Option 2*, including non-structural components, the test matrix was reduced as indicated in this Chapter.

Preliminary results in terms of maximum inter-storey drift ratios and floor accelerations for the global system and in terms of maximum accelerations and relative displacements, damage

description and dynamic identification for the non-structural systems can be found for both Phase 2 and Phase 3 of the experimental campaign.

Further studies on the seismic performance of these non-structural components and on their interaction with the structural skeleton are needed and already planned. However, these preliminary results confirm the good seismic performance of such typology of envelopes and partition systems, even if some detailing should be improved. The experimental results mainly demonstrate the possibility of including these solutions in a low-damage building system to define a high performance integrated structural/non-structural system for the next generation of building solutions.

7.5 References

- DiPasquale E., Cakmak A.S. (1988). *Identification of the serviceability limit state and detection of seismic structural damage, Report NCEER-88-0022*, National Center for Earthquake Engineering Research, State University of New York at Buffalo, USA.
- Emílio F. T., Duarte R.T., Carvalhal, F. J., Costa C.O., Vaz C. T., Corrêa M.R. (1989). *The New LNEC Shaking Table for Earthquake Resistance Testing*, Memoire LNEC 757.
- NTC (2018). *Aggiornamento delle Norme Tecniche per le Costruzioni*, Supplemento ordinario n°8 alle G.U. n° 42 del 20/02/2018, serie generale, Rome, Italy.
- NZS 1170.5 (2004). *Structural design actions - Part 5: Earthquake actions*, Standards New Zealand.

8. Integrated seismic & energy cost/performance-based evaluation

8.1 Introduction

This Chapter describes the results obtained when an integrated seismic and energy cost/performance-based analysis is implemented. This combined approach can be very useful to identify the best alternative of non-structural component to be introduced in a building system.

A literature review on the methods generally adopted to study of the thermal performance of a building, thus, to determine either the energy efficiency of the overall building or the thermal properties of a single component, can be found in the initial part of this Chapter. Then, a state-of-the-art overview is provided on the energy-efficient solutions available at global (building) and local (envelope) level in order to limit the energy consumptions.

Ultimately, numerical investigations are carried out to study the energy performance of a case-study structure comprising alternative configurations of façade systems. This energy study is combined with the seismic investigation presented in the previous Chapter 5 and an integrated seismic & energy approach is developed with the aim of addressing the design of the non-structural detailing. Further results on the implemented study can be found in **Appendix E**.

8.2 Energy efficiency of buildings

Over the past twenty years, interest in reducing the energy demand of buildings is increasing.

As highlighted from a statistical analysis made within the United Nations Environmental Programme (2009), buildings nowadays generate approximately 40% of the world’s carbon emissions (22% for residential consumptions and 18% for commercial consumptions), as can be noticed from Figure 8.1. Therefore, different codes developed with the aim of raising the bar on the energy performance criteria for building envelopes and systems (e.g. ASHRAE Standard 90.1).

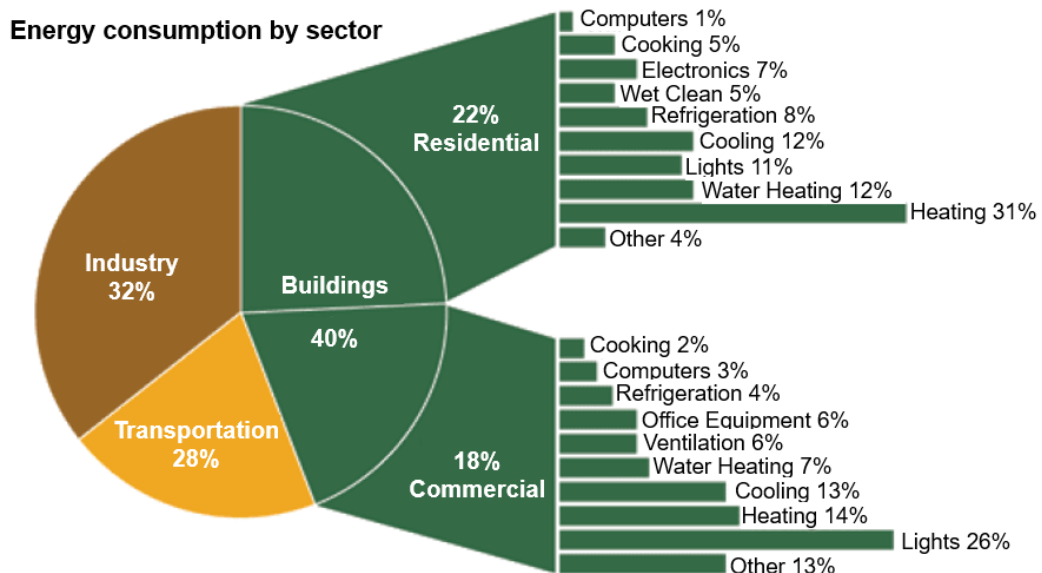


Figure 8.1. Percentage of energy consumptions by sectors (estrapolated from the report of the United Nations Environmental Programme 2009).

A sustainable policy in the construction field is required and energy efficiency is the final goal to be achieved. Consequently, in recent years the demand for “green” services is continuing to rise and designers are moving towards the finding and implementation of energy-efficient technologies and solutions. Buildings constructed in a sustainable manner are commonly perceived to incur higher cost than conventional buildings. However, for building owners investing money on energy efficiency solutions is a convenient choice if the related expected benefits are taken into account, i.e. including saving water and energy, reducing waste generation, improving indoor environmental quality and occupants’ comfort/productivity, reducing occupants’ medical cost, lowering building operation and maintenance cost, enhancing building quality, increasing financial returns (Kats 2003; Zhang et al. 2011).

Reducing energy consumptions is one of the main objectives for the actual building design and retrofiting phases. Energy consumptions are due to different sources in a building (i.e. facades, windows, roof, flooring systems, heating/cooling systems) and infrared thermography is generally adopted to identify where the maximum energy losses, mainly related to the presence of thermal

bridging, are located in the buildings. Energy estimations can be performed through different approaches (stationary, quasi-stationary and dynamic analyses) leading to the calculation of the energy consumptions. Based on these results, both the optimal strategy for improving the energy performance of existing structures and the best energy efficiency configuration for new buildings can be identified.

In order to provide more information on the issue of energy efficiency, a general description 1) of the factors affecting the estimation of the thermal performance of a system, 2) of the methodologies adopted for the evaluation of the building/components energy performance as well as an overview 3) of (some of) the innovative energy-efficiency solutions/technologies available for both the entire building system and the single components (e.g. facades) are herein reported.

8.2.1 Thermal performance

The building thermal performance refers to the process of modelling the energy transfer between the structure and the external environment. The knowledge of the different heat exchange processes developing in a building is required to determine the thermal performance. Heat flows by conduction through various building elements such as walls, roof, door, windows, etc. and the transferring of heat takes also place from different surfaces by convection and radiation (Figure 8.2).

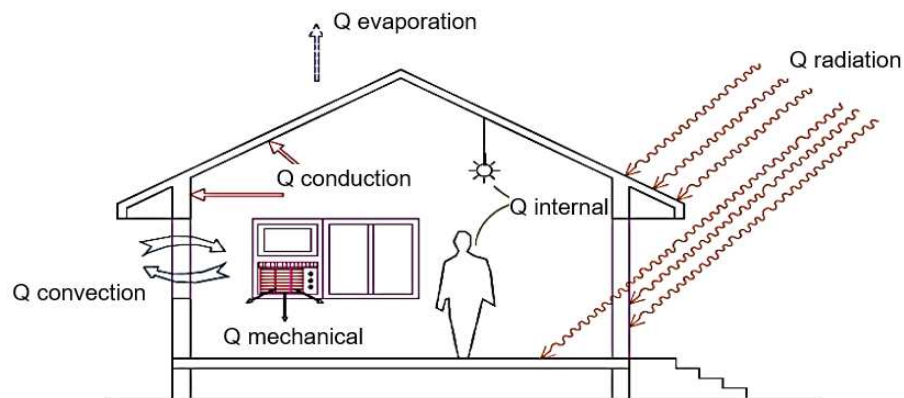


Figure 8.2. Heat exchange processes between a human body and the indoor environment (Nayak 2006).

To estimate the heat load in a building, the heat transfer coefficients of the different building elements, depending on the system properties i.e. material and thickness, are initially estimated, then a proper analysis on solar radiation geometry angles acting on each external wall is required. Validated formulas (Table 8.1) are finally adopted to estimate the total heat balancing the different

heat flows (heat flow due to ventilation Q_v , internal heat gain Q_I , solar heat gain Q_s , heat flow due to conduction Q_c , heat gain from infiltration Q_a):

$$Q_{total} = Q_v + Q_I + Q_s + Q_c + Q_a [W]$$

Table 8.1. Formulas adopted for the calculation of the different heat exchanges in a building.

Exchange process	Heat flow/gain calculation
Ventilation	<p>Heat flow rate due to ventilation of air between the interior of a building and the outside depending on the rate of air exchange:</p> $Q_v = \rho \cdot V_r \cdot C \cdot \Delta T$ <p>ρ is the air density, V_r is the ventilation rate, C is the specific heat of air, ΔT is the temperature difference.</p>
Internal	<p>The internal heat gain depends on people, lights, equipment present inside the buildings:</p> <p>- Heat gain from people:</p> $Q_{p,sensible} = N \cdot \text{Sensible Heat Gain/person} \cdot CLF$ $Q_{p,latent} = N \cdot \text{Latent Heat Gain/person}$ <p>N is the number of people, CLF is the Cooling Load Factors accounting for the delay before radiative gains become a cooling load.</p> <p>- Heat gain from lighting:</p> $Q_l = \text{Total wattage} \cdot \text{Ballastfactor} \cdot CLF$ <p><i>Ballastfactor</i> is equal to 1.2 for fluorescent lights and 1.0 for incandescent lights.</p> <p>- Heat gain from equipment:</p> $Q_{eq,sensible} = \text{Total wattage}$ $Q_{eq,latent} = \text{Total wattage}$
Solar	<p>Solar heat gain through transparent elements:</p> $Q_s = A \cdot SC \cdot SCL$ <p>SC is the shading coefficient, used to define how much of the solar radiant energy that strikes the outer window surface is transmitted through the window and into the space, SCL is the Solar Cooling Load Factor, used to estimate the rate at which solar heat energy radiates directly into the space and then is released to the space as a sensible heat gain.</p>

Exchange process	Heat flow/gain calculation
Infiltration	<p>Considering both sensible and latent contributions:</p> $Q_{a,sensible} = 1210 \cdot Airflow \cdot \Delta T$ $Q_{a,latent} = 3010 \cdot Airflow \cdot \Delta W$ <p>ΔW is the difference between the outdoor and indoor humidity ratio, $Airflow$ is the quantity of air infiltrating the place, ΔT is the temperature difference.</p>
Conduction	<p>The conduction through a shaded wall is calculated as:</p> $Q_c = U \cdot A \cdot \Delta T$ <p>U is the overall heat transfer coefficient of the surface, A is the area of the surface and ΔT is the temperature difference across the surface.</p> <p>The conduction through a Sunlit surface is:</p> $Q_c = U \cdot A \cdot CLTD$ <p>$CLTD$ is a term used to account for the added heat transfer due to the sun shining on exterior walls, roofs and windows, and the capacity of wall and roof to store heat.</p>

The resistance or transmittance of a system to the heat transfer must be calculated for each component to properly obtain the thermal balance. Heat conduction takes place from a region of higher temperature to a region of lower temperature and acts to equalize temperature differences. The heat flow through a component is defined using the total coefficient of thermal transmittance (U coefficient, in W/m^2K). This coefficient is defined from an elaboration of the heat conduction law, also known as Fourier's law, that from its differential or integral formulation can be simplified for a planar surface and a homogeneous wall composed of a single material layer as follows:

$$Q' = \frac{\lambda}{s} \cdot \Delta T = \frac{\Delta T}{R} [W/m^2]$$

$$U = \frac{1}{R} = \frac{\lambda}{s} [W/m^2K]$$

Where: Q' is the thermal energy crossing one square meter of planar surface, and far from the edges, in one second (thermal power per square meter of surface), s is the thickness of the wall, λ is the conductivity coefficient of the material forming the wall, ΔT is the temperature difference between the two sides of the wall, while R is the thermal resistance of the wall whose inverse represents the transmittance U . Generally, the U coefficient of a building system is influenced by

different phenomena: 1) the thermal transfer from the internal air to the element, described by the thermal coefficient h_i ; 2) the thermal flow inside the element, whose process is described by the thermal conductivity λ of the single materials forming the element; 3) the thermal transfer from the component to the external air, described by the thermal coefficient h_e (Figure 8.3, left).

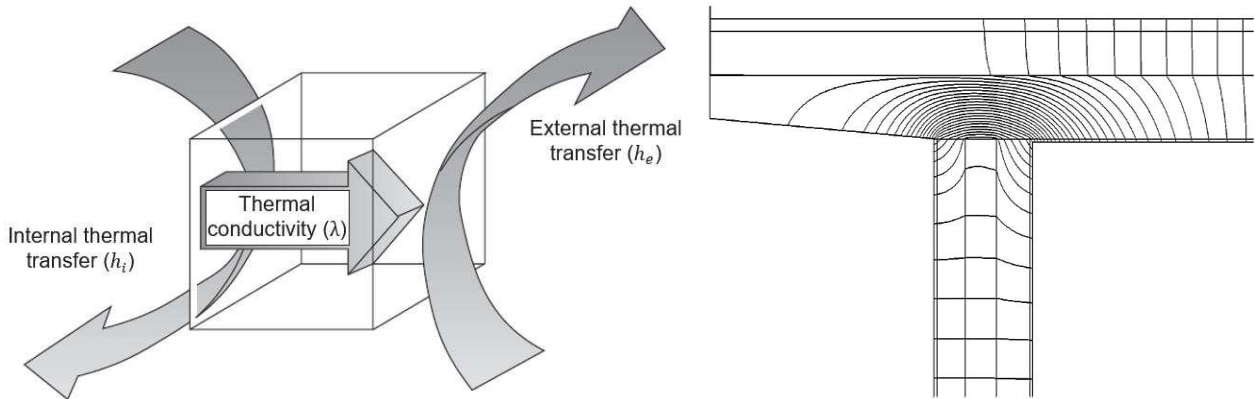


Figure 8.3. Left: Thermal transfers and conductivity affecting the calculations of the U coefficient; Right: Isotherms forming due to a thermal bridge between infill wall and planar roof (UFE 2001).

The two coefficients h_i and h_e are calculated summing convective and radiant thermal exchanges and using specific formulations, as presented in UNI EN ISO 6946 (1999). While, the material conductivity coefficients measure the resistance provided by materials against heat transfer and are generally specified by the manufacturing companies or from tables available in codes (e.g. UNI 10351 2015). The thermal conductivity λ represents the density of the thermal flow considering a thermal gradient of 1 Kelvin per meter for stationary conditions in a homogeneous material; lower is the value of λ , better is the thermal protection.

For an opaque multi-layer component, the U coefficient can be estimated using the following formula:

$$U = \frac{1}{\frac{1}{h_i} + \frac{s_1}{\lambda_1} + \frac{s_2}{\lambda_2} + \dots + R_g + \dots + \frac{s_n}{\lambda_n} + \frac{1}{h_e}} [W/m^2K]$$

Where: $s_1 \dots s_n$ are the thicknesses of the various layers, h_i , h_e represent the convection thermal coefficients, $\lambda_1 \dots \lambda_n$ are the thermal conductivities of the single materials, R_g is the resistance to the internal air flow.

In the evaluation of the thermal load in a building, for all the situations where the thermal flow is not represented by mono-dimensional heat propagation, i.e. where structural joints are located, the

hypotheses of thermal lines parallel and orthogonal to the surfaces are not valid (Figure 8.3, right) and is not possible to apply the previous formula. Thermal bridges can form due to inhomogeneity on the geometrical disposition of equal components or due to adjacent different components, as for the cases presented in Figure 8.4 or as classified in detail in UNI EN ISO 14683 (2008).

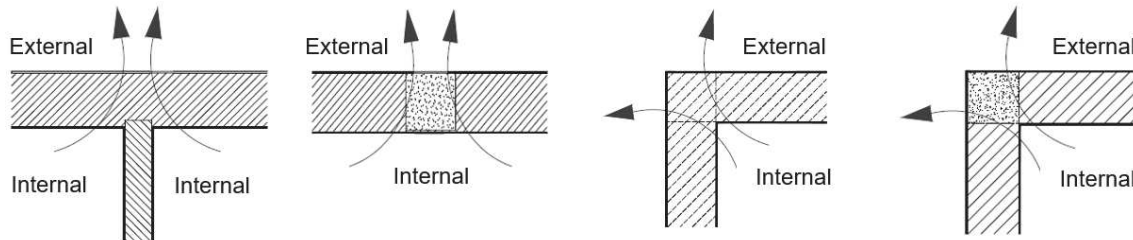


Figure 8.4. Examples of thermal bridging referring to horizontal disposition of walls/columns UNI EN ISO 14683 2008).

Although numerical modelling can be implemented to evaluate thermal bridging, different studies have been carried out using finite element modelling and results have been summarized through the so-called “linear thermal transmittance” Ψ_l , estimated for each typology of thermal bridging. Using these Ψ_l values, the formula developed to calculate the thermal dispersions due to each thermal bridge is presented below.

$$Q' = \Psi_l \cdot L \cdot \Delta T [W]$$

Where: L is the linear extension of the thermal bridge and ΔT is the temperature difference.

Thermal bridges reduce resistance to heat flow thus leading to high thermal losses. Therefore, it must be properly evaluated, and specific measurements must be adopted to limit their presence, as the solutions proposed in the final report of the 2012 Aia UPJohn Grant Research initiative.

8.2.2 Energy efficiency evaluation

Inspired by the 1997 Kyoto protocol, the Directive on the Energy Performance of Buildings (EPBD) of the European Parliament and Council forced in 2003 every member state to meet minimum requirements for the energy efficiency of both new constructions and renewed existing buildings. Different approaches are currently adopted in the European codes to encourage energy efficiency of buildings and most of them are based on indicators describing the global energy performance level of energy-consuming systems in a building.

E.g. in Italy, the so-called “Attestato di Prestazione Energetica” (APE) is adopted (DL 192 2005, DL 63 2013, DM 162 2015), that is a document certifying the energy consumptions of a building. A specific energy class is assigned to the structure (A indicates less energy consumptions while from B to G the consumptions increase; see Figure 8.5, left) in function of the global non-renewable energy performance index ($EP_{gl,nren}$), depending on different energy demands: 1) the summer ($EP_{H,nren}$) and winter ($EP_{C,nren}$) air conditioning system; 2) the hot domestic water ($EP_{W,nren}$); 3) the mechanical ventilation ($EP_{V,nren}$); 4) the lighting system ($EP_{L,nren}$); 5) people or equipment mobility ($EP_{T,nren}$).

$$EP_{gl,nren} = EP_{H,nren} + EP_{W,nren} + EP_{C,nren} + EP_{V,nren} + EP_{L,nren} + EP_{T,nren} [kWh/m^2year]$$

Therefore, the $EP_{gl,nren}$ index represents information on the entire construction in terms of thermal insulation, typology of fixtures, boiler efficiency, presence of renewable energy sources and exposure. The energy efficiency certification is mandatory for new buildings and for specific cases, i.e. sales contract, lease, real estate transfer, while allows the identification of the best retrofiting intervention for an existing construction. For interventions on the building enclosure the APE is also demanded for accessing to tax deduction of 65%.

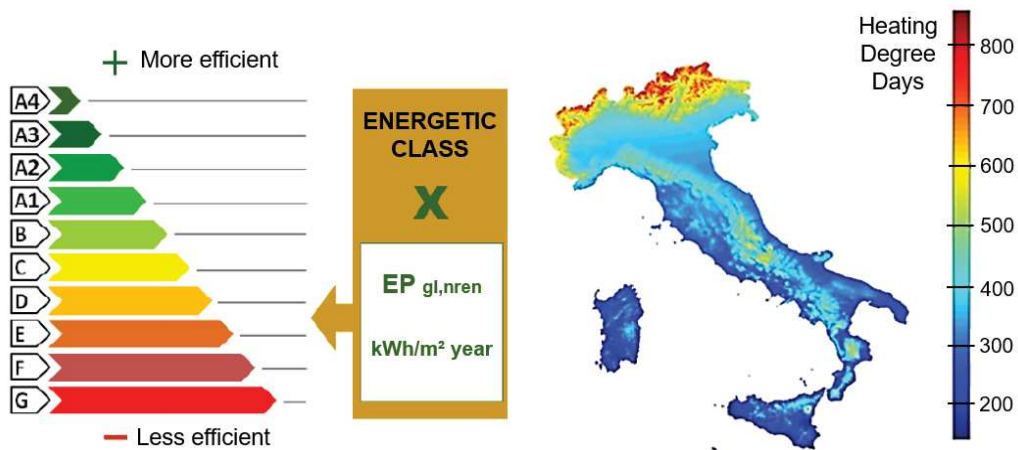


Figure 8.5. Left: Estimation of the global building energy performance from the Italian codes (APE); Right: Italian climatic zones referred to degree day units (source: ISPRA).

The external climate influences energy cost decisions and different solutions can be adopted for the same building located in different climatic zones. The common methodology used for defining the energy demand is based on the “Heating Degree Days” (HDDs), that is a measure reflecting the energy demand needed to heat a building. The daily average temperature gives an idea on the daily quantity of energy required for heating purposes. Assuming a conventional internal temperature of 18 °C, heating is required for any day having an average outdoor temperature less than this

conventional value and this energy demand can be computed by subtracting the daily average temperature from this 18 °C. The result is the number of heating degrees for that day or HDDs. Following this approach, the climatic zones in Italy are indicated in terms of degree day units, as shown in Figure 8.5, right.

The Italian code, such as the majority of the European standards, defines both the climatic zone and the time interval during which the heating system can be operating in a building, in order to reduce the energy consumptions. Using the same approach of HDDs, the energy demand for cooling can be also determined taking into account when the external temperature exceeds the conventional internal temperature. The HDDs are generally adopted with stationary energy simulations, however, different methodologies can be applied for the estimation of the energy demand, depending on the considered temporal unit (Figure 8.6).

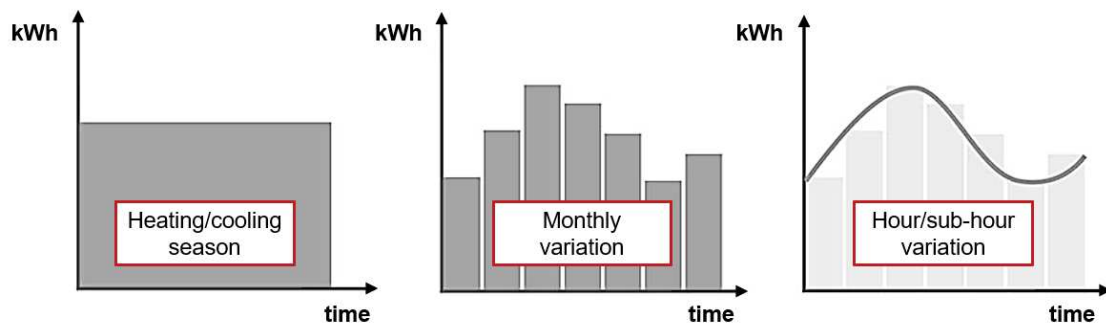


Figure 8.6. Alternative methods for building energy simulation: 1) stationary condition (left), 2) quasi-stationary condition (centre), 3) dynamic condition (right).

1. *Stationary energy simulation.* The temporal unit is the heating or cooling season. In this simplified method average external climatic values are considered and both the internal building conditions and facilities' functioning are assumed constant over time, thus the estimated energy consumptions represent average values;
2. *Quasi-stationary energy simulation.* The previous methodology differs significantly from the reality, therefore a quasi-stationary simulation based on the monthly energy demand can be implemented. However, quasi-stationary analysis is still a simplified procedure where the energy balance is developed comparing the internal and external temperatures separated by enclosure/envelopes characterized by a defined thermal transmittance, constant over time and assumed without mass or phase-shift. Consequently, this type of simulation should be adopted in the common practise for initial building energy evaluations, e.g. to identify energy issues in the initial phases of a project;

3. *Dynamic energy simulation.* This type of energy analysis is based on hour and sub-hour simulations thus, it represents the most accurate procedure for the estimation of energy consumptions. Although time-consuming analysis can be performed, the dynamic investigation allows to take realistically into account each factor influencing the results (i.e. the daily variation of temperature or lighting in a building) and accurate values of the energy demand can be obtained. An important aspect related to dynamic analysis is the capability of introducing all the thermal properties of the enclosure in the energy simulation, that is considering the capacity of heat storing of the massive components of the enclosure (thermal inertia of the opaque exterior enclosure).

8.2.3 Innovative energy efficiency solutions

Different solutions are available at global (building system) or local level (single components, such as external walls) to improve the thermal performance of a construction, consequently reducing the expected energy consumptions. These strategies/techniques are summarized and described within this section.

8.2.3.1 Energy-efficient solutions for buildings

Political, economic and ecological reasons are involved in the construction of very low-energy houses. Society should build these houses to take actions against climate change and reduce energy consumption, to lower the environmental impact of the buildings as well as the Life-Cycle Costs, to fulfil political agreements. Very low-energy buildings are realized optimising the building site, building layout, building envelope and the building services, reducing the heat losses and covering as much as possible of the remaining losses by heat gains. As described by Dokka (2006), different steps are generally recommended for low-energy design: 1) reducing heat losses (and need for cooling); 2) reducing electricity consumption; 3) utilising passive solar energy including daylight; 4) controlling and displaying energy use; 5) supplying the rest of the energy demand with renewable energy sources.

Building conceived following a low-energy design can be classified as:

- Low-energy House;
- Passive House;
- Net Zero Energy Building (NZEB);
- Plus-Energy Building;

- Green Building;
- Autonomous Building.

LOW-ENERGY HOUSE

Low-energy houses are constructions with higher energy performance when compared with buildings just meeting the mandatory building regulations. In Italy low-energy structures have an energy demand 50% less than buildings designed with the minimum thermal code requirements (e.g. a code-compliant building is in “B” energy class, while a low-energy structure is in “A” energy class).

In a low-energy house the following measures are introduced: thermal insulation of the exterior enclosure, controlled mechanical ventilation, efficient generating systems, low-temperature distribution systems, combination of photovoltaic and solar energy systems. In Figure 8.7 the concept of low-energy house and an example of on-site application can be found.

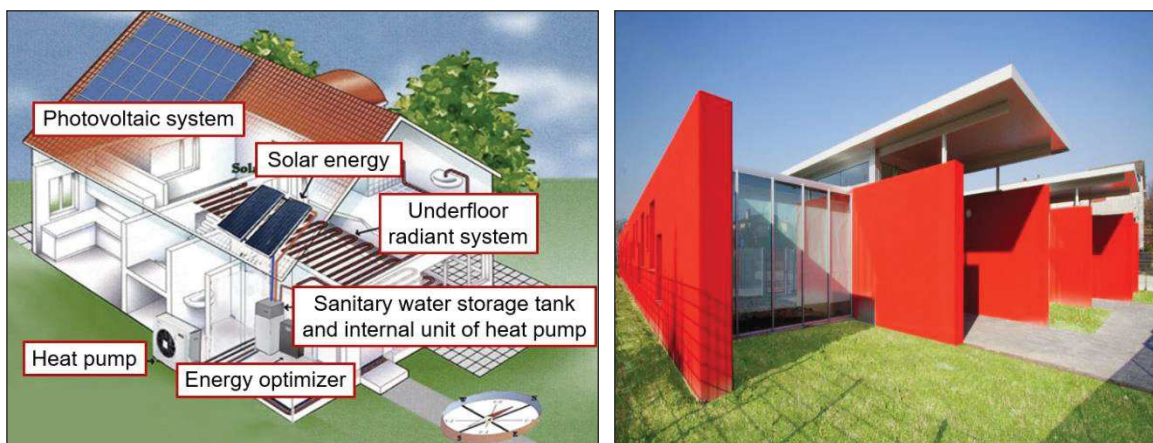


Figure 8.7. Low-energy house concept (left) and on-site application (right, Mantovani e Gonelli school in Mirabello (FE), Italy, A Energy class, Architect: Mario Cucinella).

PASSIVE HOUSE

Passive houses are built to achieve highest thermal comfort conditions at low total costs and are defined as buildings for which thermal comfort can be obtained solely by post-heating or post-cooling of the fresh air mass required to fulfil sufficient indoor air quality conditions without the need for re-circulated air. Therefore, the internal comfort is ensured without the use of facilities.

As described by the Passivhaus Institute in Germany, these buildings are characterized by the following limitations: space heating demand lower than 15 kWh/m²/a or heating load below 10 W/m², total primary energy demand lower than 120 kWh/m² year and air tightness less than 0.6 vol/h. The

measures to consider for the design of passive houses are thermal insulation of the opaque enclosure (0.1-0.15 W/m²K), thermal insulation of the windows (0.7-0.85 W/m²K), adoption of solutions for thermal bridging, use of thermal masses and sunscreens, exploitation of solar gains, optimal disposition of building on the site, possibility of introducing a small biomass chimney/stove (Figure 8.8, concept and on-site application).

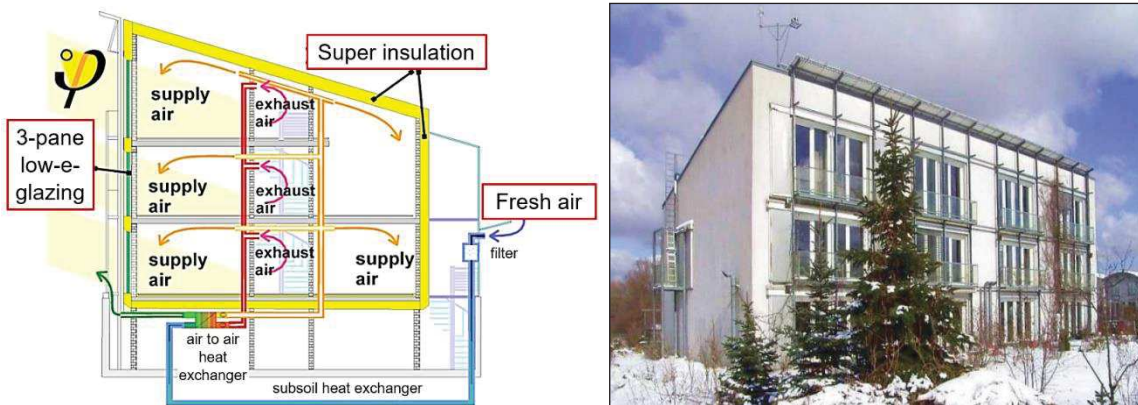


Figure 8.8. First passive house built in 1990/1991 in Darmstadt-Kranichstein, Germany (Architects: Bott, Ridder, Westermeyer): design concept (left) and on-site construction (right) (Feist 1999).

NET ZERO ENERGY BUILDING (NZEB)

A Net Zero Energy Building indicates a building with renewable energy supply equalling the energy demand in annual balance. Referring to the definition provided by the 2010/31/CE EPBD recast, the NZEB is a highly energy efficient building with a very low or around 0 kWh/m² energy demand, due to on-site renewable energy sources (e.g. solar water heating and solar electricity) completely covering the annual total energy consumption.

The NZEB has the capacity of producing thermal or electrical energy through the introduction of renewable energy systems inside the building boundaries (physical boundaries related to the building footprint or property borders; balance boundaries: energetic consumptions are due to heating, cooling, ventilation, sanitary hot water, lighting, domestic appliances). The house is capable of producing its own energy as much or more that it needs.

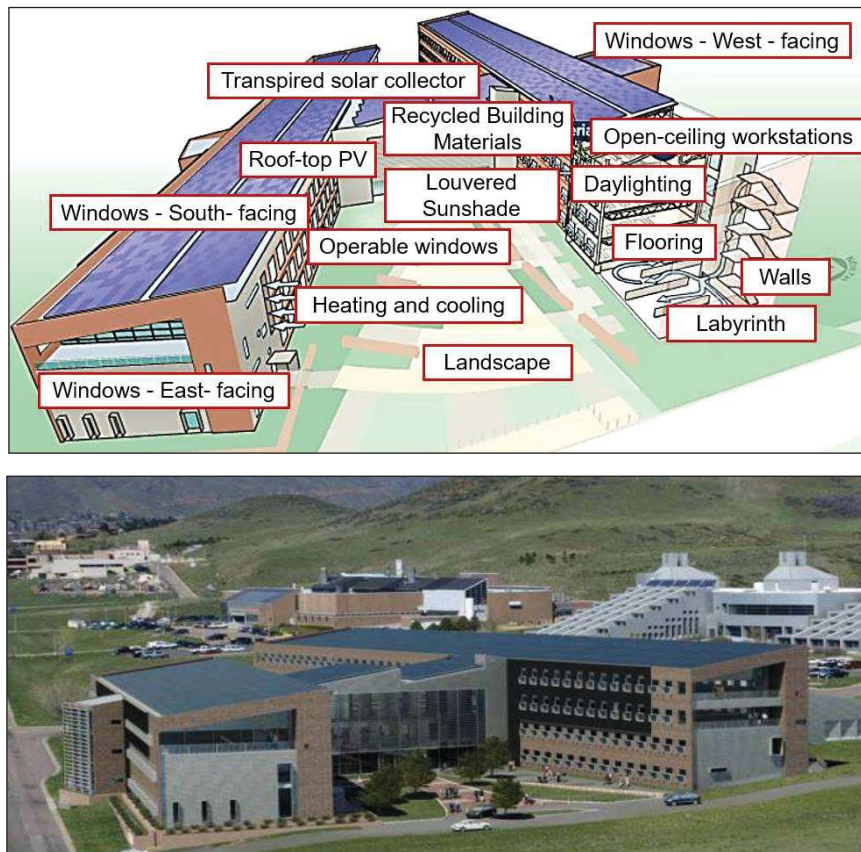


Figure 8.9. Example of NZEB: Research Support Facilities (RSF) at DOE's National Renewable Energy Laboratory (NREL) in Golden, Colorado (top - building concept; bottom - on-site construction) (Crawley et al. 2009).

PLUS-ENERGY BUILDING

Plus-Energy Buildings are constructions with renewable energy supply on the building, which more than equal the energy demand in annual balance. The energy balance between the exported and imported energy by an external energy source is positive (energy demand less than 0 kWh/m² year). 1) Energy exchange with the earth through the soil-source heat pumps, 2) safe and ecological materials with high insulation values, 3) use of the correct direction, 4) led lighting, daylight lighting, 5) venturi chimney with wind emitters and 6) hot water collectors are main elements composing a Plus-Energy Building.

The first Plus-Energy Building was built in Freiburg, Germany in 1994, the so-called Heliotrope house (Figure 8.10), and is a building physically rotating to follow the movement of the sun. The house is composed of 56 m² of photovoltaic systems, a geotherm source, a combined heat and power plant (CHP), solar panels producing hot water, thermal insulation, an autonomous system cleaning the wastewater and natural trash disposal through composting. The house produces 4-6 times the energy consumed during a year.



Figure 8.10. First Plus Energy Building: Heliotrope house built in Freiburg, Germany, in 1994 (Architect: Rolf Disch).

GREEN BUILDING

Green Buildings represent a design and construction practise aiming at reducing the overall impact of the built environment on human health and natural environment. The building design is based on the sustainability concept which is extended to all the environmental impacts of the building during the entire life. The design of these structures aims to minimize the use of resources, reduce the waste and negative environmental impacts, maximize occupant health and productivity and decrease the life-cycle costs.

A Green Building is resource-efficient during its life cycle and this is achieved through an efficient use of energy, materials and water, generating minimal or no waste, providing a healthy indoor environment for its occupant. For this reason, they generally incorporate sustainable materials in their construction (e.g. reused, recycled, or made from renewable resources), create healthy indoor environments (e.g. reduced product emissions), feature landscaping that reduces water usage (e.g. using native plants surviving without extra watering). Examples of on-site constructions of Green Buildings can be found in Figure 8.11. This typology of structures is not only energetically certified, but an environmental /sustainability certification is usually provided (Protocollo Itaca, Italy; LEED, United States/world; BREEM, United Kingdom/world, etc.).



Figure 8.11. Examples of on-site Green Building constructions with LEED certificate: Bosco Verticale, Milano, Italy (left, Architect: Boeri Studio) and Portland Community College, Oregon, United States (right, Architect: Renzo Piano).

AUTONOMOUS BUILDING

An Autonomous Building is a structure designed to be operating independently from infrastructural support services (i.e. electric power grid, gas grid, municipal water systems, sewage treatment systems, storm drains, communication services, and in some cases, public roads). Figure 8.12 (left) shows an example of on-site applications for this typology of solutions.

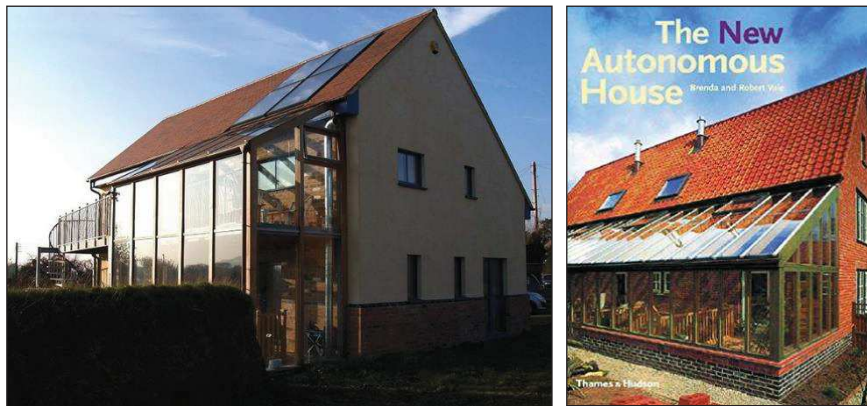


Figure 8.12. Left: Autonomous House in Cropthorne, Worcestershire, England (Architects: Mike Coe and Lizzie Stoodley); Right: cover of the Book “The New Autonomous House: Design and Planning for Sustainability” by Brenda and Robert Vale (2000).

Advantages of this design concept, which leads to 0 kWh/m² year energy demand, are reduced environmental impacts, increased security and lower costs of ownership (Nawale 2015). The basic functions of an autonomous building are: 1) functioning independently from external infrastructure, 2) neutral impact on the environment due to the used building materials and construction technologies.

As described by Brenda and Robert Vale (2000) (Figure 8.12, right), these buildings can be indicated as 'house with no bills', which would be comfortable without heating and cooling, which would make its own electricity, collect its own water and deal with its own waste, etc. These houses can be built using off-the-shelf techniques and their location is dictated by climatic conditions as well as field factors.

8.2.3.2 Energy-efficient solutions for components

Nowadays a huge variety of solutions are available for improving the energy performance of the building components. Innovative techniques or specific detailing or materials can be adopted for reducing the energy consumptions related to the envelope components (walls, windows, doors, roof, flooring systems), ventilation components (e.g. fans), heating components (e.g. heat pumps and distribution system) or other systems (household appliances). Focusing the study on the envelope components, some of the techniques adopted in low-energy buildings for improving the overall energy performance are herein presented. Reference is taken from what is described in the NorthPass project report (2012).

THERMAL INSULATION

A common technique for reducing the heat losses is improving the system thermal insulation of the exterior enclosure using materials such as mineral wool, fibreglass and cellulose, all of them fulfilling the recommended thermal conductivity 0.05 W/m K. Polystyrene and polyurethane are used quite frequently in low energy residential buildings, but mostly only as ground insulation and occasionally as roof insulation.

Vacuum insulation panels with a very low thermal conductivity are very efficient components (vacuum insulation panel 2-3 cm thick is equivalent to 10-15 cm of mineral wool) however these panels are currently rather expensive. Another insulation material with low thermal conductivity and higher cost is PIR (polyisocyanurate) insulation.

AIRTIGHTNESS PRODUCTS

Airtightness solutions and products of high quality must be used for vapour/air barriers, windows/doors, joining plastic vapour/air barriers, sill and foundation, sill and wall, floor structure lead-through, pipe through concrete, electrical outlets, spotlights, small pipes, between outer and inner pipes, ventilation ducts, stoves and connections to other materials. These products are needed

to ensure good airtightness to the building envelope, required to avoid draft, moisture problems and ensure that all ventilating air passes through the heat recovery system.

WINDOWS

Low energy windows ensure low heat losses and thermal comfort even if there are no radiators below the windows. High energy performance can be obtained using quadruple-glazed windows with a U-value of 0.6 W/m²K and daylight transmittance of 0.59, or triple-glazed windows with a U-value of 0.7 W/m²K and daylight transmittance of 0.71. Low-emissivity glass or low-e-glass can also be used in order to keep a building cool in the summer and reduce heat from escaping through the glass in the winter (Figure 8.13, left).

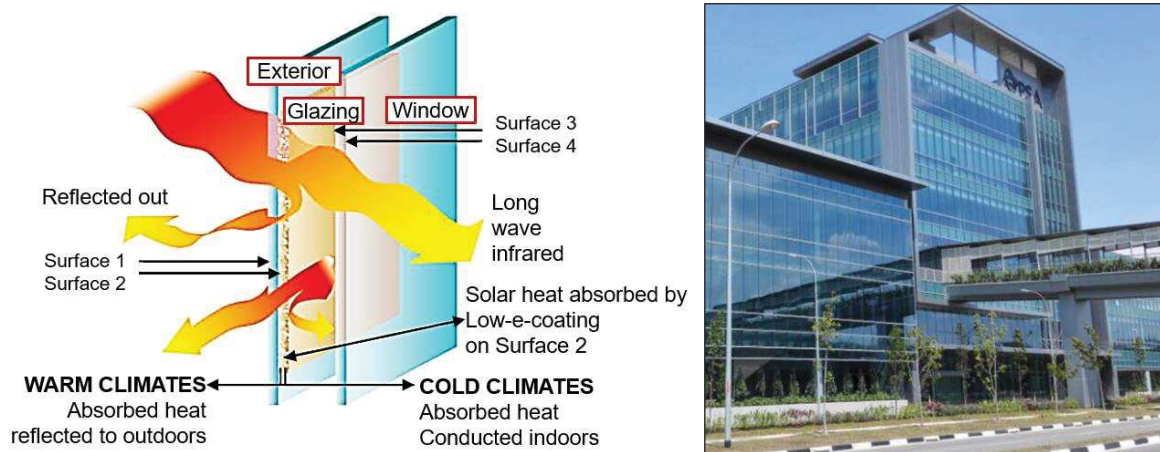


Figure 8.13. Schematic representation of low-emissivity glass window (left, Calvi et al. 2016) and example of on-site application (right, Singapore PSA).

The objective of a low-E coating is to improve comfort whilst reducing energy costs. The coatings are made of a series of almost invisible layers of various materials and rely on one or more precious metal layers (e.g. silver) to reflect exterior and interior heat. Windows with low-E coatings reduce the amount of heat transmitted through the glass. As well as reflecting heat, low-E coatings can also reduce fading by partially reflecting damaging UV-rays and acting as a sunscreen for artwork, furnishings and floors.

PASSIVE SOLUTIONS

The most common passive solution is the ventilated façade, represented by an outside wall cladding application in which the ventilation zone behind the cladding material is in contact with the atmosphere. At its most basic, a ventilated façade system consists of two layers of different facades separated by an air cavity. This cavity prevents rainwater from penetrating and diffuses water vapour

from the inside to the outside. While the external cladding serves to provide the majority of rain and wind protection, the air corridor between the support structure and the external cladding plays a major role in the ventilated façade system. A naturally ventilated façade results in a temperature difference between the face of the cladding panel and the air cavity behind. This, in turn, creates a variation in air density and causes air to flow upwards within the cavity according to the stack effect (chimney effect). The airflow transports heat from the cavity out through high level exhausts, aiding convection drying of any residual amounts of moisture accumulated within the air cavity.

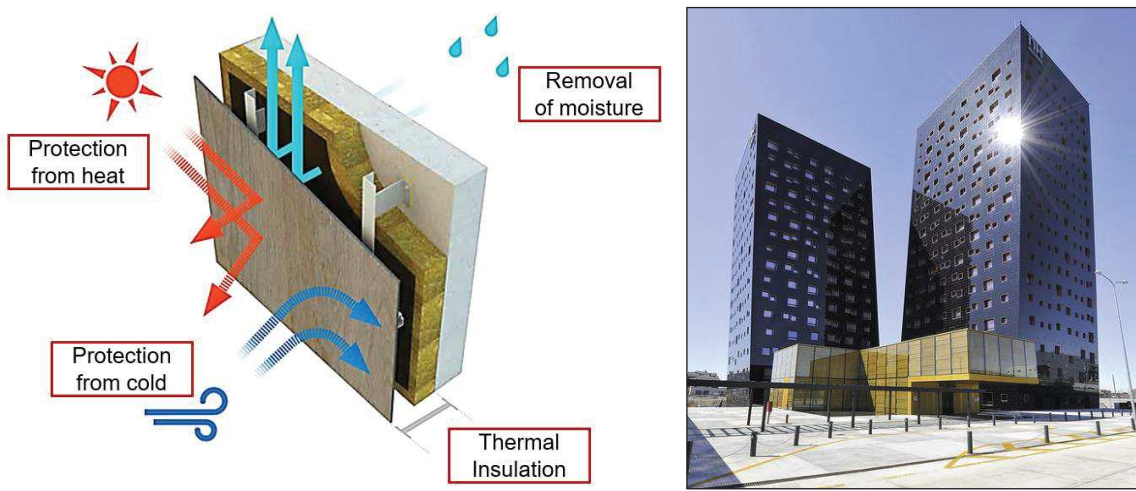


Figure 8.14. Concept of ventilated facade system (left) and on-site application (NH Hotel Tower, Polo di Rho Pero – Milan, Italy, Architect: Dominique Perrault Architecture).

This multi-layered system can guarantee long term functionality and insulates and protects the primary structure from weather exposure. The main advantages of this solution are: 1) high energy-efficiency through the use of insulating materials suitable for ventilated facades and innovative substructures which allow the achievement of almost any desired U-value; 2) a comfortable indoor climate thanks to a vapor diffusion coefficient decreasing from inside towards the outside, 3) cooling effect in summer due to the temperature barrier effect of the ventilation cavity dissipating the excess of heat, 4) thermal insulation in winter seasons due to the increased heat transition resistance of the ventilation cavity, 5) sustainable construction methods due to long life, low maintenance and the presence of separated layers, 6) reliable fire protection through the choice of proper system components and building materials' classes, 7) soundproofing, 8) lightning protection.

Other passive solutions for façade systems are the following:

1. *Solar Greenhouse*. Closed space separated from the external environment through glazing walls and connected to the construction using openings. The building roof can be in glass or

opaque material depending on the latitude and on the design objectives. The Solar Greenhouse absorbs as much as possible solar energy (sunlight during the day) in the winter season for the following gradual emission of accumulated solar energy for heating purposes (Figure 8.15, left).

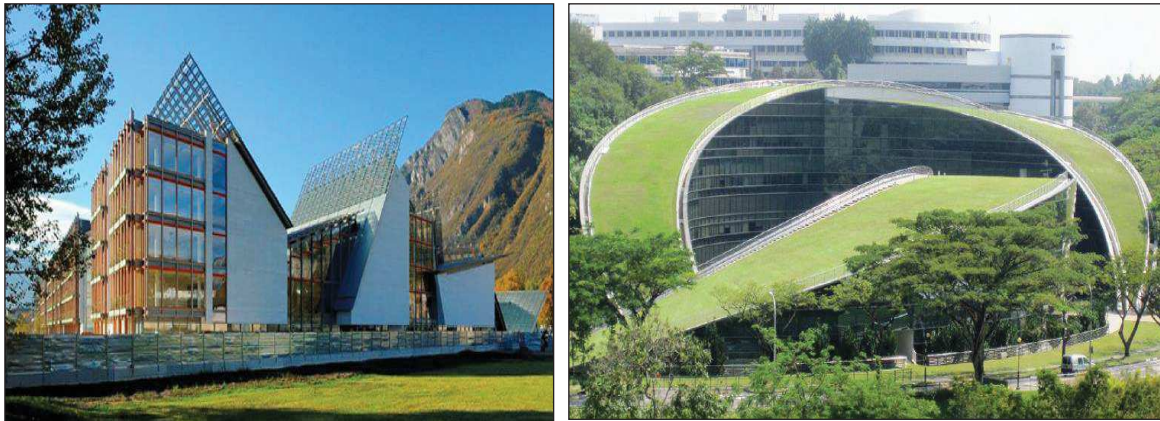


Figure 8.15. On-site applications of Solar Greenhouse (left, MUSE, Trento, Italy; Architect: Renzo Piano) and Green roof system (right, School of Art, Nanyang Technological University, Singapore, China; Architect: CGP Consultants).

2. **Green roofs/walls.** A green roof is a roof surface planted partially or completely with vegetation and a growing medium over a waterproof membrane. Green walls are external or internal vertical building elements which support a cover of vegetation rooted either in stacked pots or growing mats. The growing interest in green roof and wall constructions has been encouraged by the increasing availability of technologies making their construction easier and more economical. The benefits of green roofs include longer roof lifespan, improved sound insulation, reduced heating and cooling requirements, reduced and slowed stormwater runoff, capture of gaseous and particulate pollutants, alleviation of urban heat island effects, increased biodiversity. There is also the potential for green roofs to provide carbon sequestration.
3. **Reflective paint.** This energy-efficient solution can be used for the climatic zones where the sun radiation is very high representing a substantial part of the thermal balance. The colour of the external walls determines the quantity of solar radiation absorbed by the surfaces. Different colours can be used for the roof and walls depending on their orientation with the aim of reducing the surface temperature and the quantity of energy transferred to the internal building environment.

SOLAR SHADING

Solar shading system for the east, south and/or west facing windows are often needed to avoid high indoor temperatures during spring, summer and autumn. The systems are most efficient if installed on the outside and can be e.g. Venetian blinds for installation inside, outside or between the panes.

8.3 Integrated seismic & energy approach

The development of new solutions/technologies for natural hazard risk mitigation has evolved independently from considering sustainable development goals, keeping a disconnection between the different stakeholders. The need for a paradigm shift which allows the understanding of buildings' life-cycle costs from the "earthquake-induced environmental impact" point of view (Comber et al. 2012) is becoming fundamental. In the performance-based design as well as in the assessment procedures of buildings, a framework relating the seismic performance and energy performance must be developed. The definition of the optimal design solution or retrofit intervention on seismic risk must be driven considering an integrated approach taking into account a combined seismic and energy performance.

After a brief overview on the research developed in order to integrate seismic and energy performance evaluations, the combined approach is herein applied for the design of new buildings. Particularly, the same 5-storey case-study building analysed in Chapter 5 is considered and energy performance analyses are implemented. Results highlight the importance of considering both energy consumptions and seismic losses in the definition of the optimal building configuration (traditional vs. low-damage systems for seismic purpose; traditional vs. energy-efficiency solutions for energy purpose).

Finally, more studies are carried out focusing on the seismic & energy performance of façade systems. The aim of this investigation is to highlight that investing money for improving the energy efficiency of a façade only is not a convenient choice if substantial post-earthquake damage is expected for this component. While, simple modifications of the non-structural details, i.e. modify the connection system to the primary structure, can define a highly efficient system in terms of both the seismic and energy points of view.

8.3.1 Previous research

Concerning the overall construction system, different research recently aimed to define an integrated approach incorporating seismic risk analysis and its environmental impacts into a life-cycle assessment, considering the probabilistic distribution of possible building damage over a period of time. This research initially focused on the integration of the natural hazard risks and their mitigation in life-cycle analysis to assess sustainability of infrastructures (such as the work of Itoh et al. 2005; Padgett et al. 2009; Dennemann 2009; Ghosh et al. 2011; Tapia et al. 2011). Therefore, initial simplified attempts to join seismic risk and environmental impacts in an integrated approach started to be developed, however these studies were carried out for the specific case of bridges.

Regarding building constructions, Comber et al. (2012) proposed a methodology for quantifying the impacts of seismic damage of the building system considering both seismic loss estimation, developed through the Advanced Engineering Building Module (AEBM) of the Hazards US (HAZUS), and the Life-Cycle Analysis (LCA). However, the method does not include the energy efficiency in the calculation of the annualized environmental impact, while it incorporates impacts resulting from the expected seismic damage excluding the carbon footprint associated with consumed energy over the same time period.

Another procedure for quantifying the probable earthquake impacts adding them to the full building life-cycle assessment is the one which is developing within the ATC-86 Project (Court et al. 2012). Purpose of the project is to determine a performance-based environmental impact assessment methodology to be integrated into the P-58 procedures (FEMA P-58 2012) and its companion Performance Assessment Calculation Tool (PACT).

Calvi et al. (2016) also proposed an integrated energy efficiency and earthquake resilience assessment procedure. Referring to the Expected Annual Losses (EAL_S) that is one of the most important output for seismic risk assessments, an equivalent Energy Expected Annual Loss (EAL_E) can be determined using the building value as common ratio denominator.

$$EAL_S = \frac{\text{expected seismic loss}}{\text{total building value}}$$
$$EAL_E = \frac{\text{mean annual energy cost}}{\text{total building value}}$$

Where the mean annual energy cost represents the average annual cost of consumed energy for the building. Calvi et al. (2016) also define energy classes (from A+, lower energy consumptions

to G, higher energy consumptions) for classifying the energy performance. Building performance is finally categorized from both earthquake resilience and energy efficiency points of view using a common classification (GRI, *green and resilient* indicator, classification), as a function of EAL_S and EAL_E , respectively.

In the current research the integrated seismic & energy approach is proposed for the design of retrofit interventions of existing structures (such as for Italian cases: Calvi et al. 2016; Manfredi and Masi 2018; D'Angola et al. 2019). However, the integrated energy & seismic study should be also implemented to define the optimal system configuration during the design process of new buildings.

8.3.2 Application: seismic & energy cost/performance evaluation of building systems

Referring to the 5-storey reinforced concrete building presented in Chapter 5, an integrated seismic & energy cost/performance-based evaluation is herein implemented. Energy performance is evaluated through dynamic energy simulations and results in terms of energy consumptions are combined with the results obtained from the previous seismic loss estimations. The optimal building system configuration (traditional or low-damage structural/non-structural system with a traditional or energy-efficient exterior enclosure) is thus identified considering a total seismic & energy cost. This global cost is obtained combining the annual losses due to earthquakes with the annual energy losses due to energy consumptions.

The calculation of the seismic and energy performance follows a common approach, as highlighted in Figure 8.16, starting with the definition of the building site and related seismic/ energy hazard, then the building vulnerability to these external actions can be determined, and the building performance estimated.

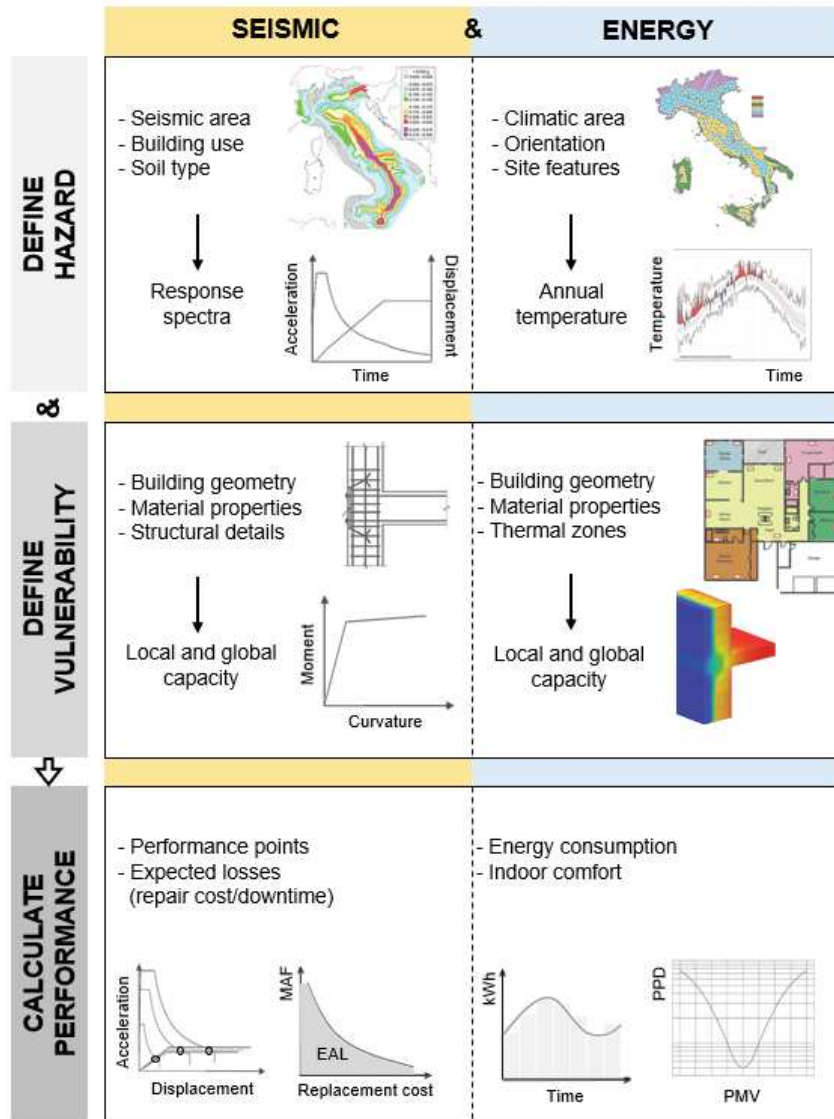


Figure 8.16. Schematic chart of the methodology used for the calculation of the seismic and energy building performance.

In this paragraph, a combined seismic & energy approach is applied to design a multi-storey building system, focusing the study on the exterior enclosures (façade system). In fact, different technologies are taken into account for improving either the seismic or the energy performance of these non-structural components, while the other building elements are considered the same for all the building configurations. If both the thermal and the seismic behaviour of the façade system as well as the total final seismic & energy cost are considered acceptable, the design of the façade can be concluded (Figure 8.17).

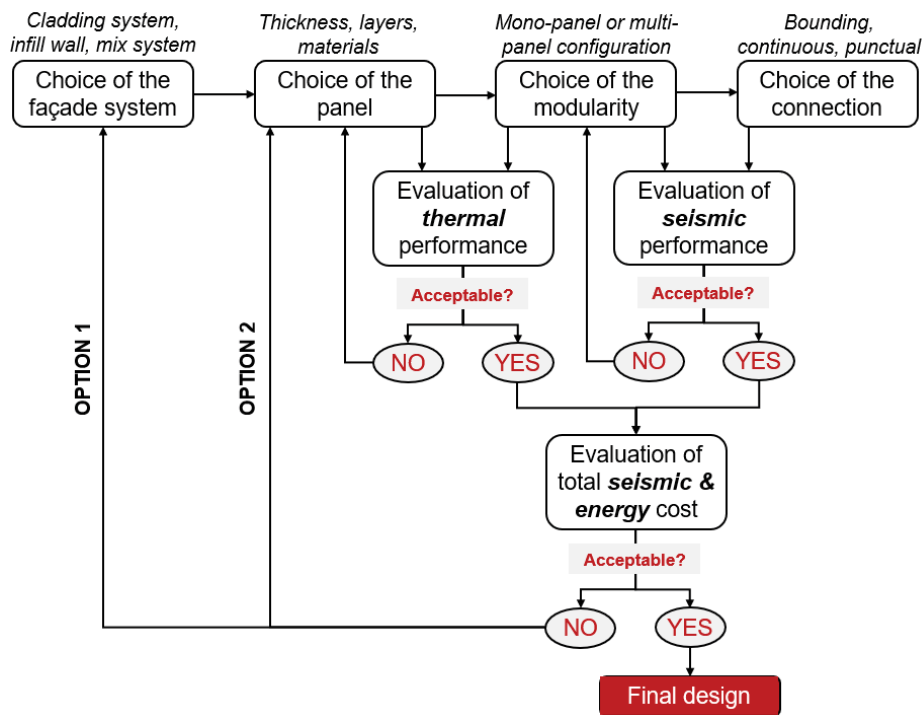


Figure 8.17. Flowchart for the combined seismic and energy design for façade systems.

8.3.2.1 Case-study building

The numerical investigation is carried out for the 5-storey building comprising alternative façade systems (precast concrete claddings, infill walls, spider glazing system) as analysed in the previous Chapter 5 and summarized in Figure 8.18. The building is located in Reggio Calabria (Italy) and the building use is commercial (office) for the first two floors and residential for the other two, while the top floor is a roof.

For implementing the dynamic energy simulation, the internal subdivision at each building floor and the use of every internal part (kitchen, living area, bathroom, etc.) must be known. This subdivision depends on the building architectural design and allows the definition of the thermal zones to be used for the energy analysis. Figure 8.19 presents the internal subdivision (units) of the case-study multi-storey building.

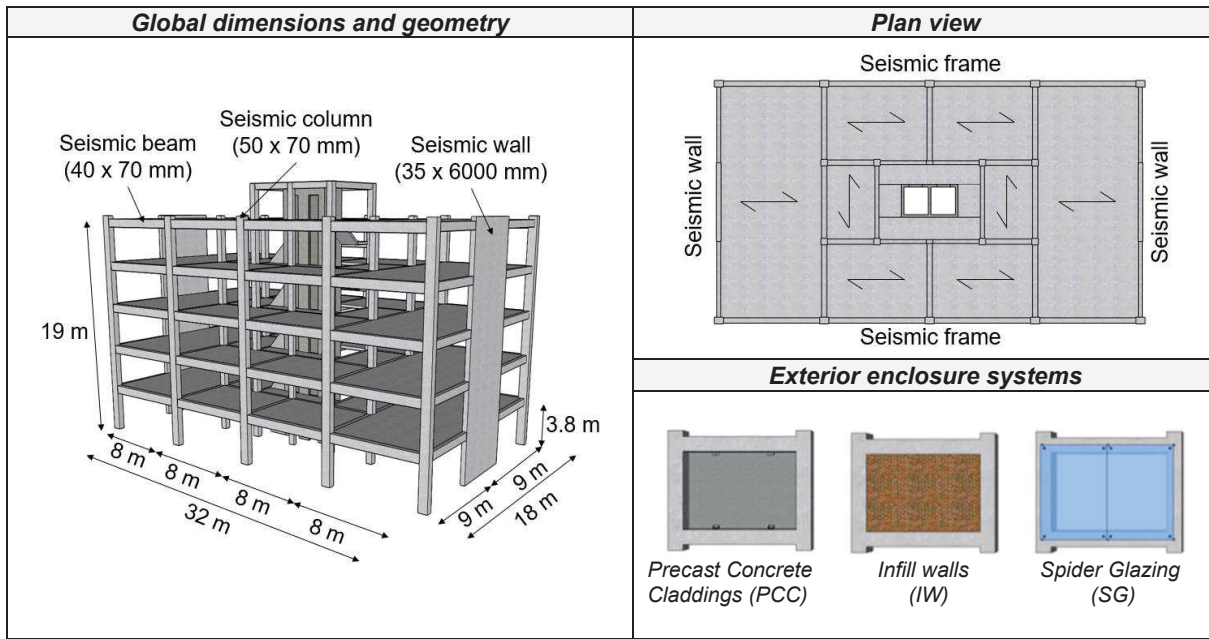


Figure 8.18. Dimensions and plan view of the structural system, and exterior enclosure configurations.

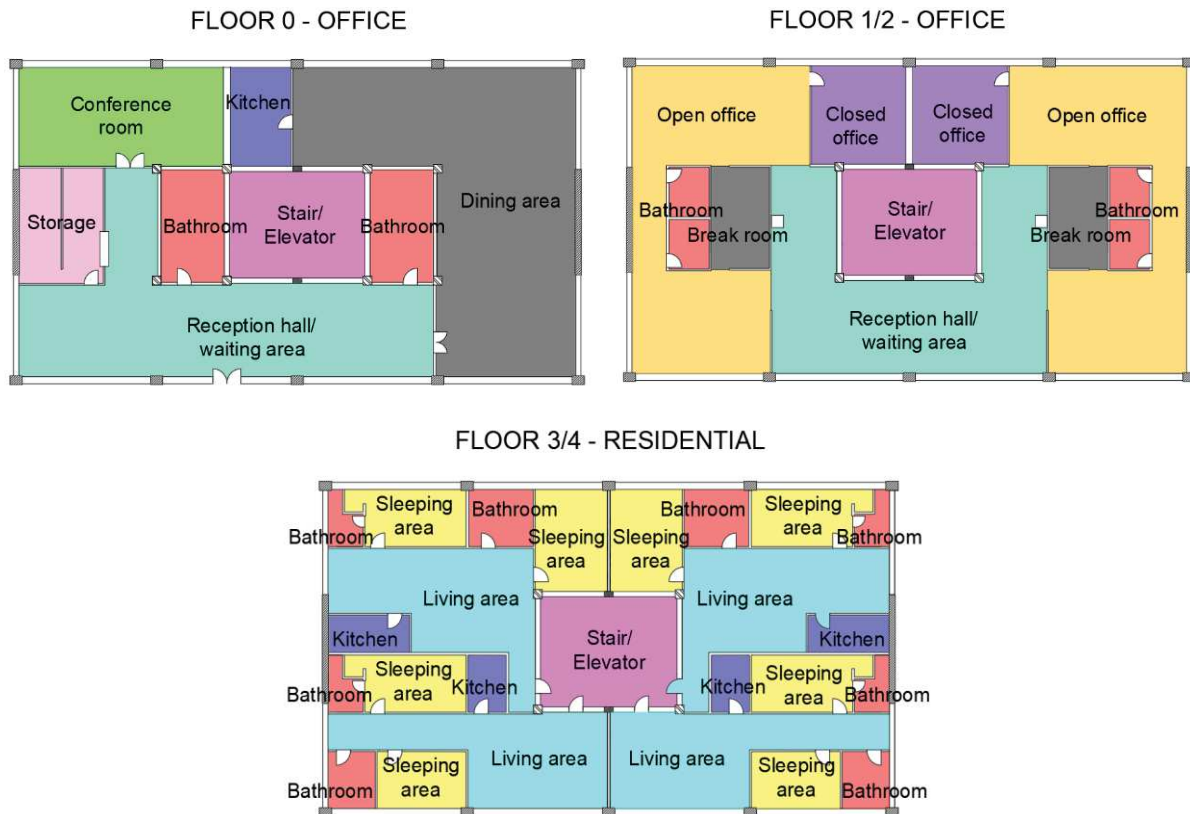
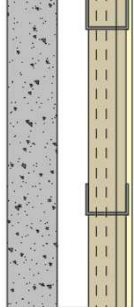
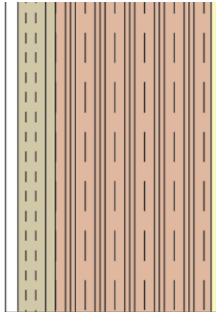

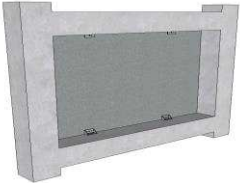
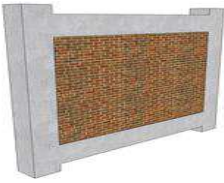

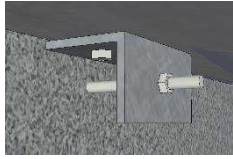

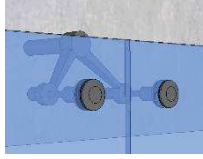


Figure 8.19. Different internal units characterizing the structure (floor 0, top - left; floors 1 and 2, top - right; floors 3 and 4, bottom - centre).

The design of the structural system has been already presented in Chapter 5 (design at the ULS - 475 years return period - following the Direct Displacement Based Design procedure by Priestley et al. 2007) considering both monolithic (cast-in-situ) members and PRESSS hybrid connections. While, more data on the façade systems' detailing (type of panel, modularity of the panel and connection to the structural system) can be found in Table 8.2.

Table 8.2. Details of the alternative façade systems.

Façade system	Precast concrete cladding system	Unreinforced masonry infill wall	Spider glazing curtain wall
Panel	 <p>Layer 1: 80 mm concrete Layer 2: 50 mm air Layer 3: 60 mm insulation + steel studs Layer 4: 10 mm plaster</p>	 <p>Layer 1: 20 mm adhesive Layer 2: 60 mm insulation Layer 3: 250 mm brick Layer 4: 10 mm plaster</p>	 <p>Layer 1: 10 mm glass Layer 2: 1.52 mm PVB Layer 3: 10 mm glass</p>
Modularity	 <p>Mono-panel</p>	 <p>Mono-panel</p>	 <p>Multi-panel</p>
Connection	 <p>Punctual (2 tie-back connections on the top; 2 bearing connections on the bottom)</p>	 <p>Bounding (bricks bounded by mortar)</p>	 <p>Punctual (spider connectors at each corner of the glass panel; 4 rotules for each glass panel)</p>

8.3.2.2 Seismic performance

As presented in Chapter 5, the building seismic performance has been investigated at global level through loss assessment analyses with Engineering Demand Parameters (EDS) from numerical investigations (Ruaumoko 2D) and a capacity spectrum approach. At local level a fragility study has been implemented to define the damage states and expected seismic behaviour of the different typologies of non-structural elements, i.e. façade systems, internal partitions, ceilings.

Regarding the investigations on the global seismic behaviour of the building, numerical analyses have been performed for both the bare-frame modelling (assumed as representative of the building behaviour when the precast concrete cladding facades and spider glazing curtain walls are considered as exterior enclosures) and the infilled-frame modelling. It has been observed that the presence of the masonry infill walls leads to an increase of stiffness and strength thus an increase in acceleration and decrease in the displacement demand of the performance points when compared to the equivalent skeleton configurations.

It is also worth noting that the assumption of considering the bare-frame modelling for the skeleton covered by precast concrete cladding systems can be considered acceptable as noticed from the analyses presented in section 5.3. In fact, it has been highlighted that modelling the concrete panels with tie-back connections on the top lead to a very limited interaction with the structural system (around 3% when comparing both stiffness and strength of the solution comprising long-threaded rod connections with the same parameters estimated for the sole structural skeleton). While, although no modelling has been implemented for the spider glazing configuration, the bare frame modelling can still be assumed as valid.

The study of the seismic vulnerability of the single non-structural elements has been instead conducted in terms of fragility functions. The mechanisms and damage states developing during earthquake motions have been collected for each non-structural component and the related fragility curves have been identified. These fragility functions have been adopted during the loss assessment investigations.

The seismic performance of the building has been improved through the application of low-damage solutions for both structural and non-structural systems. Focusing on the study of façade systems, this means modifying simple connection detailing for the cases of either precast concrete claddings or spider glazing systems, i.e. introduction of dissipative connections or internal horizontal/vertical gaps. While, for the masonry infill external walls the low-damage solution involves

the insertion of a steel sub-frame which modifies the modularity of the façade panel, i.e. the façade becomes an assembly of rocking-sliding vertical panels. However, as observed later, the introduction of this steel frame has direct effect on the thermal performance of the component.

8.3.2.3 Energy performance

Considering the traditional (monolithic) structural skeleton comprising the alternative façade systems previously described as well as all the non-structural elements included within the seismic analysis (partitions, ceilings, services, contents), the building energy performance at both local level, e.g. definition of transmittance and thermal bridging, and at global level, e.g. estimation of energy consumptions, have been investigated using *Rhinoceros3D/Grasshopper* software. *Grasshopper* is a visual programming language and environment running within the *Rhinoceros3D* (Rhino) computer-aided (CAD) design application (Figure 8.20). This graphical algorithm editor allows the implementation of energy performance simulations due to the links to other software packages, i.e. *Energy Plus* for the dynamic thermal simulation and *Therm* for the study of the transmittance of a component.

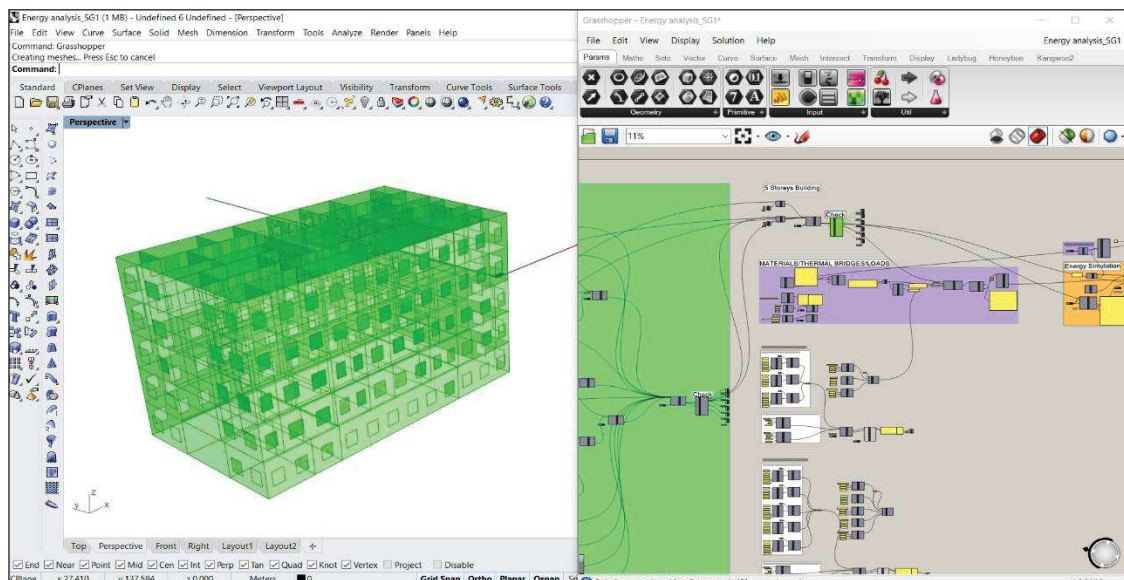


Figure 8.20. Typical working window of Grasshopper connected to Rhinoceros 3D.

The dynamic thermal simulation has been implemented as follows.

Step 1. Construction of the CAD model in *Rhinoceros3D* considering the internal subdivision characterizing the building at each floor level. The model is thus internalized within *Grasshopper*, particularly in the so-called *Honeybee* part of the software, and the different thermal zones are

identified. The geometry of the zones can be broken down by the surface type and this is very useful for previewing the zones, making sure that the surface type is correct (Figure 8.21).

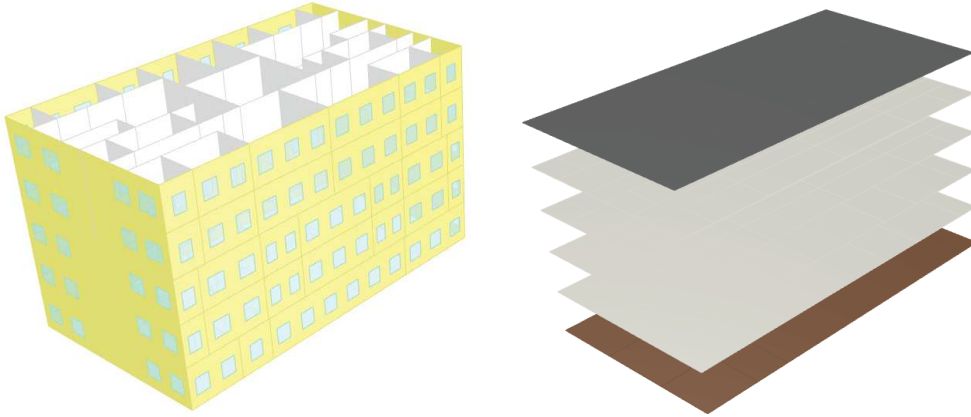


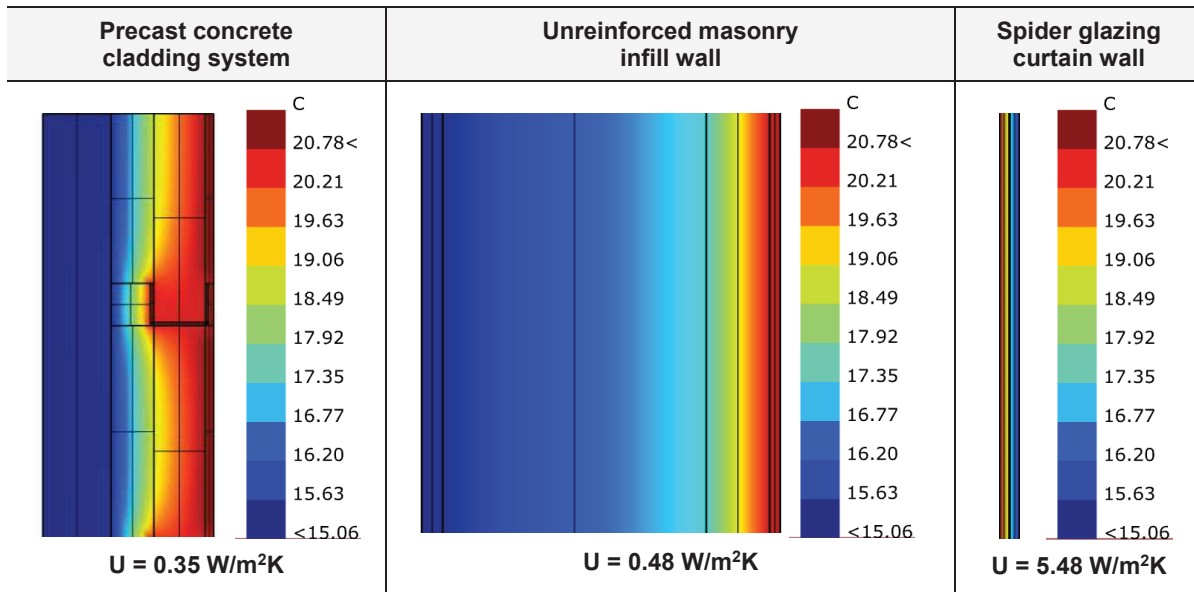
Figure 8.21. Preview in Rhinoceros 3D of the vertical (left) and horizontal (right) building enclosure components for the case of external infill walls.

Step 2. The material properties of each single layer defining a component or the *Energy Plus* construction typology, based on energy modelling standards, climate zone, surface type and building program, are assigned to each of these vertical and horizontal components. *Energy plus* constructions are attributed to window (double pane), internal walls (steel partition), roof (based on ASHRAE 90.1-2010 and climatic zone), floor (interior floor), while for the external walls the construction details depend on the façade system considered for the analysis. The thermal properties of the external walls are defined evaluating the correct transmittance of the wall. Through the link to *Therm* software, both the transmittance of the different façade systems and the thermal bridging can be defined, as presented in Table 8.3.

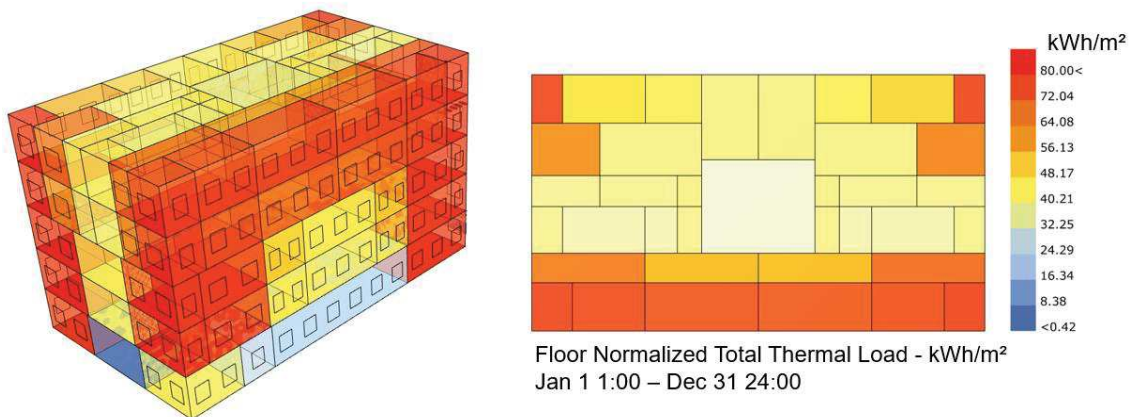
Step 3. Default values for the equipment, infiltration, lighting, occupancy, ventilation, etc. are assumed for each thermal zone, in function of the use of the zone.

Step 4. The building site (Reggio Calabria) is identified, i.e. the climatic zone of the area, and the energy simulation can be carried out.

Table 8.3. Temperature variation and transmittance values of the alternative façade systems.



The energy simulation provides different results which can be useful for the study of the thermal performance of a building, i.e. the energy use of the thermal zones such as heating, cooling, electricity for lights and for plug loads for each zone, or the building gains and losses such as people gains, solar gains, infiltration losses/gains, etc. and these results can be determined for each month, hour, sub-hour of the annual energy simulation. As example, in Figure 8.22 are shown the total thermal loads normalized considering the zone areas and the average operative temperature, useful for comfort estimations. For the Thesis scope, interest is focused on the thermal loads to be converted into annual energy consumption. Particularly, results are elaborated from the energy losses due to heating and cooling, mostly related to the thermal properties of the alternative typologies of façade systems included into the analysis.



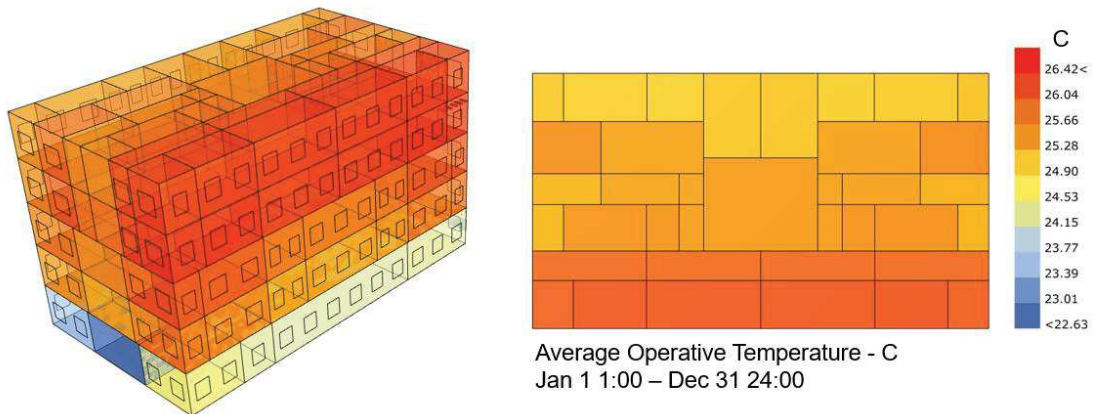


Figure 8.22. Results from the dynamic energy simulation: 3D and plan views of the normalized thermal load due to heating and cooling (top) and 3D and plan views of the average operative temperature (bottom) referred to the entire simulation time period (year).

Comparing the different alternatives of façade systems, results are presented in Figure 8.23 as total energy cost and kWh/m², while the influence of the heating and cooling thermal loads in the total building energy balance is also provided. Concerning the spider glazing solution, results are also influenced by the application of “brise soleil” systems, i.e. shading devices integrated into the building. These fixed devices are designed to allow the sun to penetrate only during predetermined times of the year. In winter, overhangs allow the low sun to enter south-facing windows, while in summer, the overhangs block the higher sun.

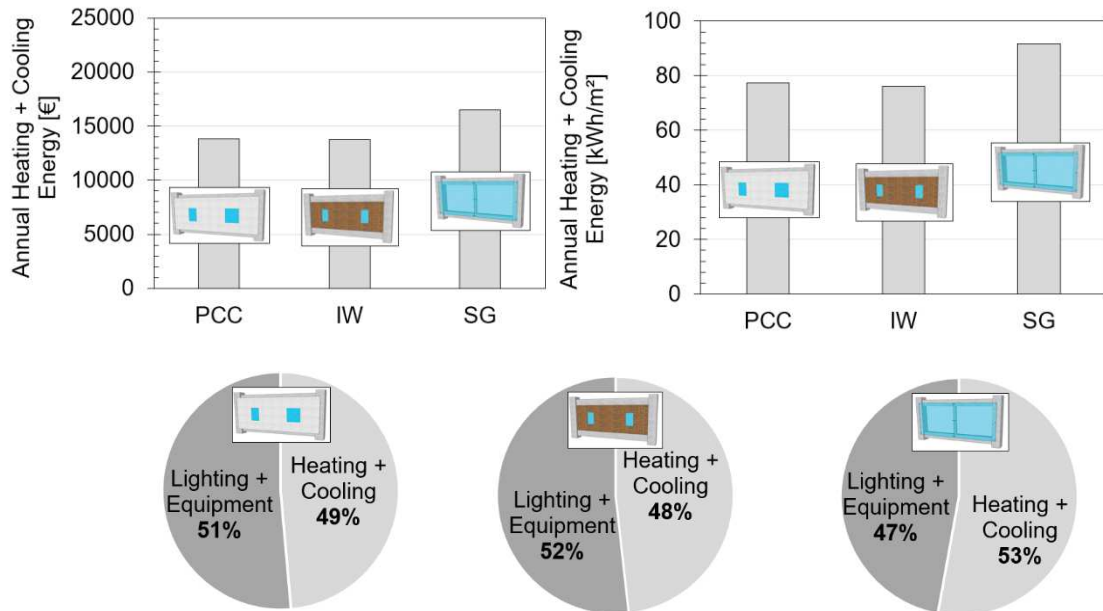


Figure 8.23. Results in terms of annual heating and cooling energy (top) and percentage of contribution to the total energy losses (bottom) for all the different façade solutions.

Referring to the work proposed by Tam et al. (2018), the cost implication of applying external façade systems can be defined considering different factors: 1) the construction cost, 2) the space heating and cooling cost, 3) the maintenance cost and 4) the rental loss due to the thickness of external façade systems. The most cost/effective façade system is herein identified referring to just the space heating and cooling cost (HC), estimated as proposed by Hasan (1999):

$$HC = 86400 \cdot U \cdot \frac{DD}{\eta} \cdot ER \text{ [€/m}^2\text{/year]}$$

Where: U is the thermal performance of the façade, DD is the degree day, η is the mechanical efficiency of space heating systems assumed as 1, ER is the electricity rate assumed as 0.18 €.

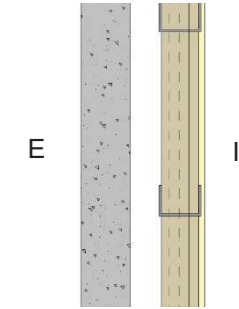
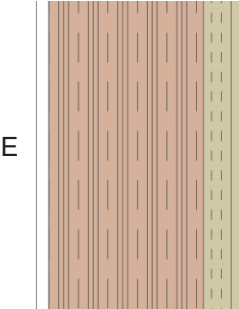
Applying this formula, the values in Table 8.4 are obtained for the different façade systems. It is observed that this method represents a simple way to compare facades' alternatives because it is directly related to the thermal properties (transmittance) of the component.

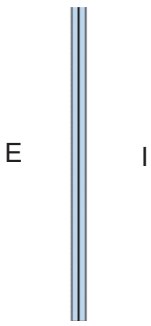
Table 8.4. Space heating and cooling cost for the different façade systems.

Façade system	Transmittance [W/m ² K]	Heating and cooling cost [€/m ²]
Precast concrete cladding systems	0.35	1.72
Unreinforced masonry infill wall	0.48	2.33
Spider glazing curtain walls	5.48	26.57

After the estimation of the thermal properties/performance of the building composed of the three different façade alternatives, additional solutions are proposed and studied for the same typology of external vertical enclosure, while the other building elements (internal partitions, facilities) are maintained equal when performing the different energy simulations: 1) three other solutions for the precast concrete cladding systems, defined considering simple modifications of the layers' thickness; 2) two additional solutions for the infill wall configuration, considering different strategies usually adopted for providing thermal insulation; 3) three other solutions for the spider glazing curtain walls, conceived adding layers or modifying the internal material of the layers. All these different façade configurations are described in Table 8.5, while the results obtained from the thermal investigation (*Therm*) can be found in **Appendix E**.

Table 8.5. Alternative configurations implemented for the energy simulation analysis.

Façade system	Description
<p>Precast concrete cladding systems</p> 	<p><u>TYPE 1 (Benchmark)</u></p> <p>Layer 1: 80 mm concrete Layer 2: 50 mm air Layer 3: 60 mm insulation + steel studs Layer 4: 10 mm plaster</p> <p>⇒ U = 0.354 W/m²K</p> <p><u>TYPE 2</u></p> <p>Layer 1: 120 mm concrete Layer 2: 50 mm air Layer 3: 60 mm insulation + steel studs Layer 4: 10 mm plaster</p> <p>⇒ U = 0.352 W/m²K</p> <p><u>TYPE 3</u></p> <p>Layer 1: 80 mm concrete Layer 2: 80 mm air Layer 3: 60 mm insulation + steel studs Layer 4: 10 mm plaster</p> <p>⇒ U = 0.278 W/m²K</p> <p><u>TYPE 4</u></p> <p>Layer 1: 80 mm concrete Layer 2: 50 mm air Layer 3: 80 mm insulation + steel studs Layer 4: 10 mm plaster</p> <p>⇒ U = 0.335 W/m²K</p>
<p>Unreinforced masonry infill wall</p> 	<p><u>TYPE 1 (Benchmark)</u></p> <p>Layer 1: 20 mm adhesive Layer 2: 250 mm brick Layer 3: 60 mm insulation Layer 4: 10 mm plaster</p> <p>⇒ U = 0.480 W/m²K</p> <p><u>TYPE 2</u></p> <p>Layer 1: 20 mm adhesive Layer 2: 60 mm insulation Layer 3: 250 mm brick Layer 4: 10 mm plaster</p> <p>⇒ U = 0.305 W/m²K</p> <p><u>TYPE 3</u></p> <p>Layer 1: 20 mm adhesive Layer 2: 120 mm brick Layer 3: 40 mm air Layer 4: 60 mm insulation Layer 5: 120 mm brick Layer 6: 10 mm plaster</p> <p>⇒ U = 0.279 W/m²K</p>

<p>Spider glazing curtain walls</p> 	<p>TYPE 1 (Benchmark)</p> <p>Layer 1: 10 mm glass Layer 2: 1.52 mm PVB Layer 3: 10 mm glass</p> <p style="text-align: right;">⇒ U = 5.478 W/m²K</p>
	<p>TYPE 2</p> <p>Layer 1: 10 mm glass Layer 2: 1.52 mm PVB Layer 3: 10 mm glass Layer 4: 1.52 mm PVB Layer 5: 10 mm glass</p> <p style="text-align: right;">⇒ U = 5.000 W/m²K</p>
	<p>TYPE 3</p> <p>Layer 1: 10 mm glass Layer 2: 1.52 mm PVB Layer 3: 10 mm glass Layer 4: 10 mm air Layer 5: 10 mm glass</p> <p style="text-align: right;">⇒ U = 1.744 W/m²K</p>
	<p>TYPE 4</p> <p>Layer 1: 10 mm glass Layer 2: 1.52 mm PVB Layer 3: 10 mm glass Layer 4: 10 mm argon Layer 5: 10 mm glass</p> <p style="text-align: right;">⇒ U = 1.323 W/m²K</p>

Considering all these alternative solutions, energy simulations are performed, and the obtained results are presented in Figure 8.24 in terms of annual energy cost of the entire building - left - (*Rhinoceros/Grasshopper/Energy Plus/Therm* software) and of the façade - right - (analytical formula).

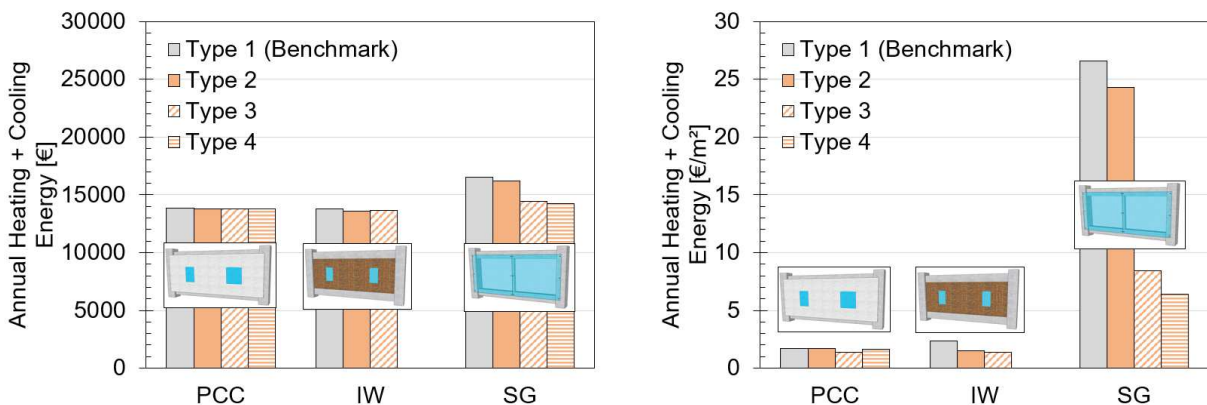


Figure 8.24. Annual heating and cooling cost of the entire building (left) and of the façade system (right) for the different typologies of external enclosures.

The previous graphs show that the energy losses are quite similar when precast concrete cladding systems and masonry infill wall solutions are adopted (in the range of 77-80 kWh/m² for the building energy consumption, in the range of 1.3-2.3 €/m² for the façade cost), at least when considering these specific multi-layer components with similar transmittance values applied to a building located in the same site. While, for the spider glazing facades results are more variable (in the range of 79-92 kWh/m² for the building energy consumption, in the range of 6.4-26.6 €/m² for the façade cost).

For the case of curtain wall systems, notwithstanding the reduction of the total building energy losses (more than 15%) and of the façade cost (more than 75%) due to the application of the most energy-efficient solution, energy costs are still high when compared to the other more economical typologies of façade systems, as also highlighted in Figure 8.25, where it is also reported the linear increasing of the façade cost due to the variation of the building site.

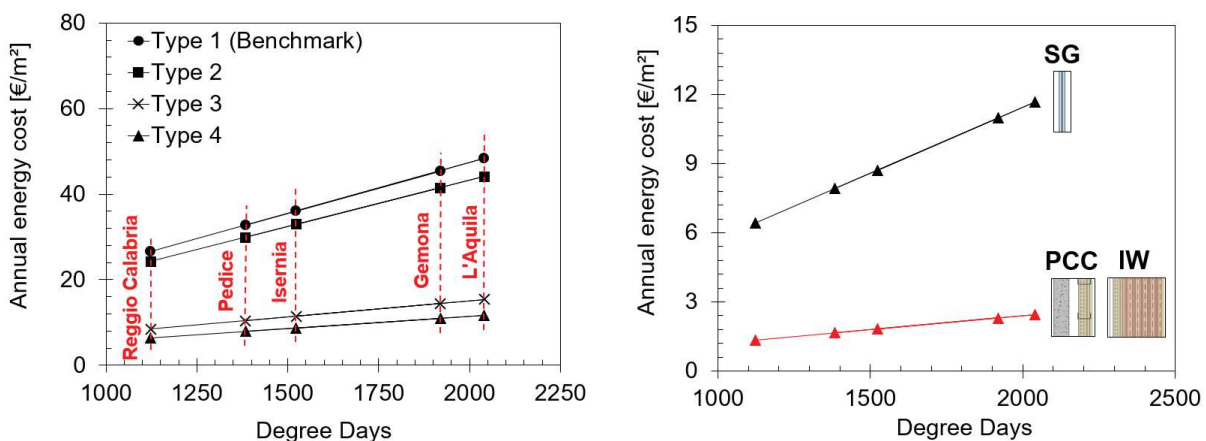


Figure 8.25. Determination of the annual energy façade cost for all the spider glazing solutions when varying the building site (left) and comparison between the most energy-efficient strategies for the different façade systems, that is type 4 of spider glazing system vs. type 3 of both precast concrete cladding and infill wall solutions (right).

However, it is observed that the energy consumptions could be further reduced if more energy-efficient solutions are applied to all the façade typologies. In fact, if the chosen systems for both precast concrete claddings and infill walls, all with good thermal performance being new design systems, lead to very similar values because no substantial modifications are introduced, the spider glazing configuration could be further improved using low-emissivity glass. However, the aim of the research is to provide evidence on the importance of taking into account the seismic performance/losses when designing the non-structural configuration, therefore these alternative systems are considered acceptable in terms of energy performance they provide.

8.3.2.4 Integrated seismic & energy performance

The results in terms of seismic and energy cost/performance can be combined to define a common approach helping in the definition of the optimal non-structural configuration. For the case-study building herein analysed, i.e. a 5-storey structure composed of three alternative façade systems, the proposed investigation aims to apply a procedure which can address the choice of the non-structural system and its detailing, also highlighting how this selection can be mostly influenced by the seismic performance analysis.

Concerning the overall building behaviour, the expected energy and seismic annual losses (EAL_E and EAL_S) can be used as performance measures to define the optimal structural and non-structural system during the design of new buildings as well as for making decisions on retrofit interventions of existing structures, as presented by Calvi et al. (2016). Referring to the energy classes proposed in the work previously cited and to the seismic classes defined in the DM 58 (2017), while focusing on new design, combined energy & seismic classes can be determined as shown in Figure 8.26 (left), where A+ indicates the class of ideal design while C represents the range for acceptable design. Consequently, when considering a preliminary building design, depending on the final target (increase the energy and/or the seismic performance of a building system) different paths can be followed (Figure 8.26, right).

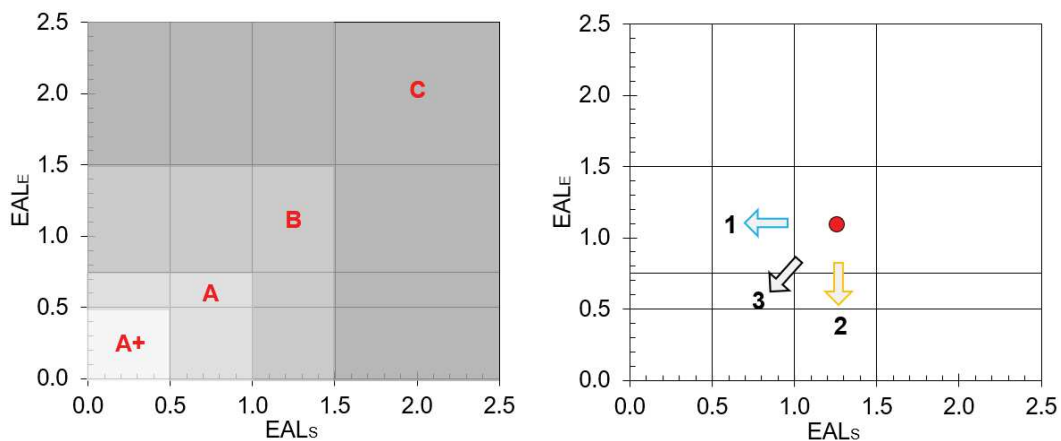


Figure 8.26. Combined classes for energy and seismic annual losses (left) and possible pathways for improving the system performance (right), i.e. increasing the seismic (1), energy (2) or seismic&energy (3) performance.

For the 5-storey monolithic (cast-in situ) structure consisting of alternative façade systems, when combining the results associated to the implementation of the low-damage or/and low-energy solutions previously presented, the values summarized in Table 8.6 are obtained. The building option with traditional energy & seismic façade systems (Trad + Type 1 for each typology of façade) is

compared to the case of : 1) best energy solution for that component and traditional non-structural detailing, 2) only low-damage non-structural system, 3) best energy solution for that component and low-damage non-structural detailing.

Table 8.6. Seismic and energy losses and savings in 50 years building life due to the application of the different seismic and energy solutions for all the façade systems taken into account.

Façade system	Seismic solution	Energy solution	EAL Seismic [%C]	EAL Energy [%C]	Seismic Losses [€/m ²]	Energy Losses [€/m ²]	Seismic Savings [%]	Energy Savings [%]
Precast concrete cladding systems	Trad	Type 1	0.73	0.68	302.0	241.6	-	-
	Trad	Type 3	0.73	0.68	302.0	240.9	-	0.3
	LD	Type 1	0.58	0.68	236.4	241.6	22	-
	LD	Type 3	0.58	0.68	236.4	240.9	22	0.3
Unreinforced masonry infill walls	Trad	Type 1	0.77	0.68	316.4	240.5	-	-
	Trad	Type 2	0.77	0.67	316.4	238.0	-	1.01
	LD	Type 1	0.30	0.68	175.47	241.6	45	-
	LD	Type 2	0.30	0.67	175.47	238.0	45	1.01
Spider glazing curtain walls	Trad	Type 1	0.67	0.81	277.0	288.4	-	-
	Trad	Type 4	0.67	0.70	277.0	248.9	-	16.4
	LD	Type 1	0.52	0.81	212.0	288.4	23	-
	LD	Type 4	0.52	0.70	212.0	248.9	23	16.4

It can be observed that greater savings are obtained when low-damage non-structural components are applied (22% for precast concrete claddings, 45% for masonry infill walls, 23% for spider glazing systems), while the application of low-energy solutions leads to high savings for the case of spider glazing curtain walls only and this can be justified as follows. When considering typical solutions adopted nowadays for providing thermal insulation for both the case of precast concrete claddings and masonry infill walls, these solutions already provide acceptable thermal performance, consequently trying to improve this performance through the application of economical strategies, e.g. modification of the thickness or of the material of the panel layers, leads to very limited savings. Therefore, in this specific cases, the modification of the only façade properties is not enough for moving the EAL_E towards better values (Figure 8.27, right), as happens for the spider glazing system (from class B to class A). While, the introduction of other energy-efficient components (i.e. controlled

mechanical ventilation, efficient generating systems, low-temperature distribution systems, combination of photovoltaic and solar energy systems) can produce a lower energy building.

Alternatively, when using common techniques (construction practice) for either the precast concrete claddings, i.e. connecting the panels to the structural skeleton using bearing connections on the bottom and tie-back or sliding connections on the top, or the unreinforced masonry infill walls, i.e. using monolithic panels where bricks are bounded using mortar, the seismic losses associated with these components' damage are more evident. Consequently, when applying high seismic performance solutions, which are simple modifications of non-structural detailing thus comparable or slightly greater as construction cost when compared to traditional solutions, the reduction of the expected annual losses EAL_S can be very high, e.g. for the case of infill walls the seismic class moves from A to A+ (Figure 8.27, left).

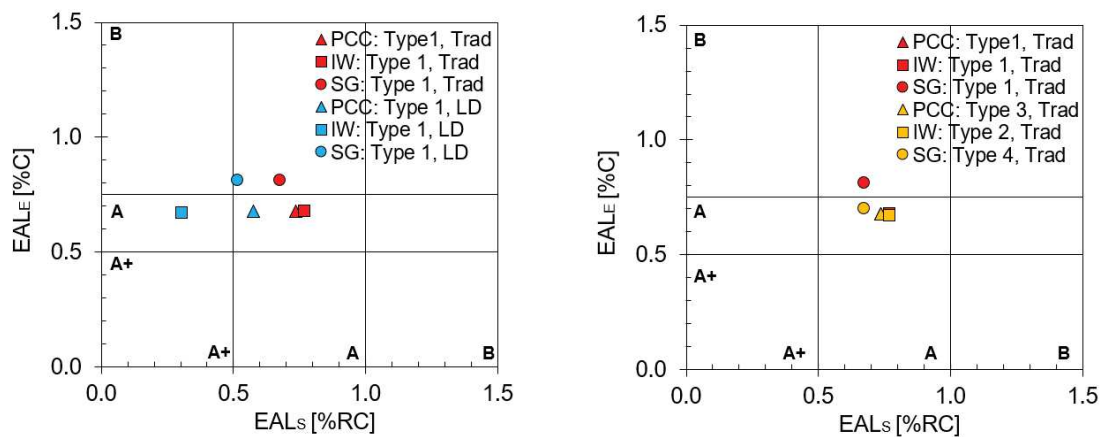
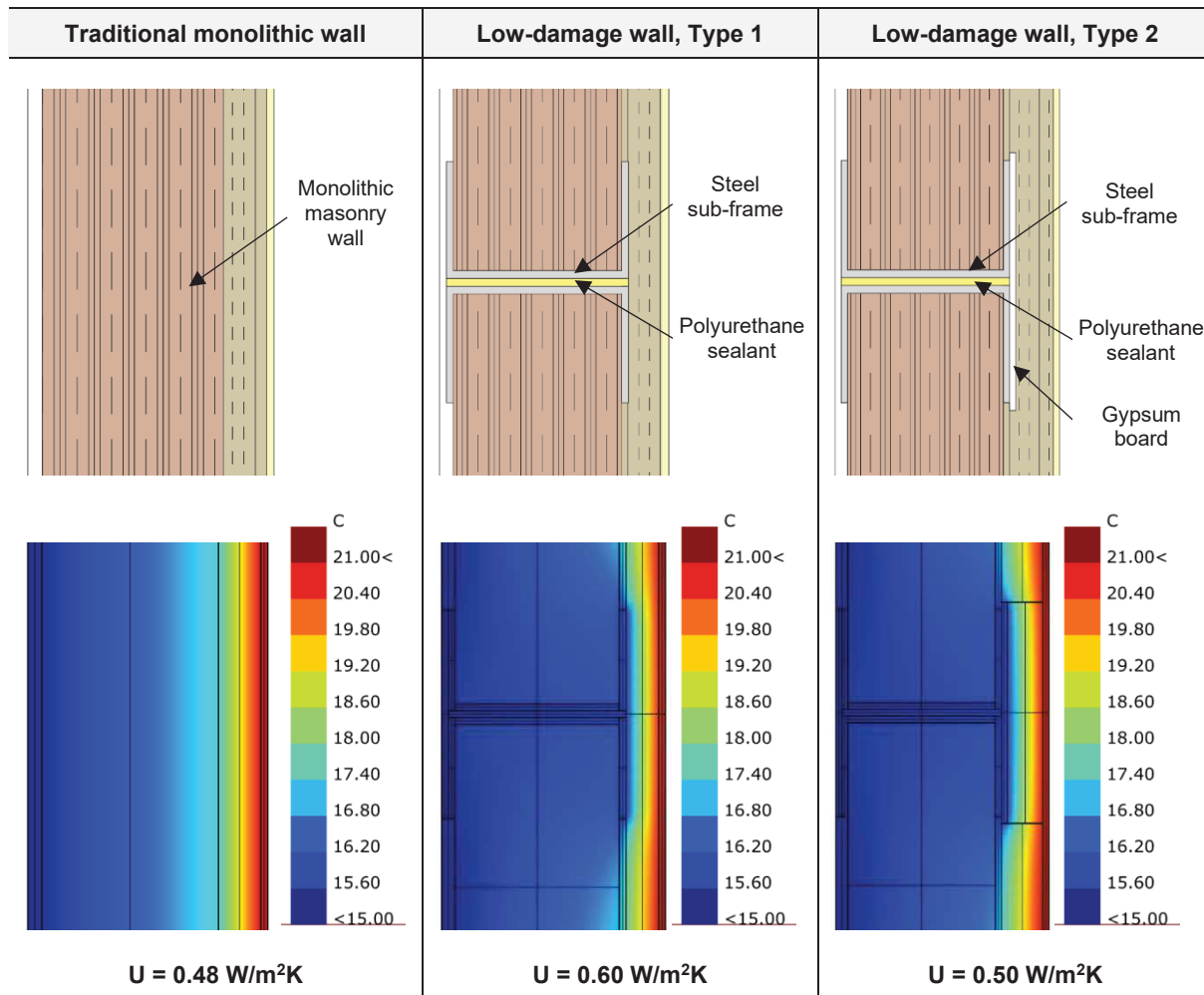


Figure 8.27. Identification of the EAL_{E+S} points for the traditional benchmark solutions when compared to the solutions with low-damage (LD) systems only (left) or low-energy systems only (right).

However, it is observed that for the case of infill walls, the low-damage solution comprises rocking walls built within steel frames which are separated by internal and lateral gaps filled using polyurethane foam and sealant. The introduction of steel profiles in the panel thickness leads to the formation of thermal bridging increasing the thermal transmittance of the component, consequently reducing its energy performance. Then, system modifications must be introduced for having at least the same energy performance of the traditional monolithic panel (Table 8.7), i.e. increasing the thickness of the insulation panel or the material providing insulation or adding strips of high insulation material to cover the steel profiles thus limiting the propagation of the heat flux. The steel frame also decreases the fire performance of the wall therefore a gypsum strip can be introduced to improve the resistance against fire. Another option for having comparable energy performance should be the use of a different material, such as timber, that is a sustainable material with better energy

properties compared to the steel. In any case, the timber frames must be properly designed for guaranteeing out-of-plane capacity against the inertia forces of the walls developing during seismic motions.

Table 8.7. Temperature variation and transmittance values of the alternative façade systems.



Summarizing, this study highlights how it is fundamental to include the evaluation of the seismic performance, herein described in terms of building post-earthquake losses, in the design or retrofitting process of a non-structural component and, more generally, of a building system. A total seismic & energy cost must be estimated to determine the total savings that can be achieved during the building life due to the application of a specific system. This total cost can be used to compare and select the best option within alternatives (Figure 8.28), thus defining the strategy to be adopted in function of the design targets.

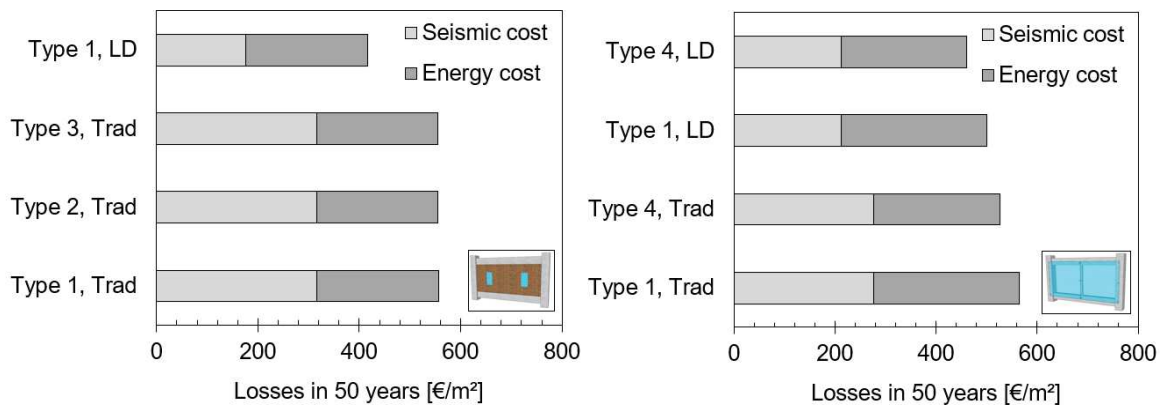


Figure 8.28. Comparison of solutions for masonry infill walls (left) and spider glazing systems (right), where: 1) Trad indicates the traditional non-structural detailing, while LD the low-damage seismic detailing; 2) Types from 1 to 4 represent the alternative configuration considered for improving the energy performance of the component, as indicated in Table 8.4.

A combined seismic & energy cost can be also developed on a component-based level. In fact, referring to the space heating and cooling cost of the façade defined by Hasan (1999) for the energy part, while considering the seismic losses due to the damage of the façade systems only as obtained from intensity-based estimations through the PACT software (FEMA P-58 2012), the seismic & energy cost of the different façade solutions can be determined to be compared. Table 8.8 summarizes the results in terms of total cost and savings due to the application of the best low-damage and low-energy solutions, among those proposed for each typology of façade, when compared to the traditional (benchmark) solution (Type 1, Trad). The seismic costs are here intended as the post-earthquake repair cost associated to the Life-Safety limit state condition (seismic design level).

Table 8.8. Seismic and energy costs and savings for different typologies of façade systems.

Façade system	Energy solution	Seismic solution	Seismic cost [€/m²]	Energy cost [€/m²]	Seismic saving [%]	Energy saving [%]
Precast concrete cladding systems	Type 1	Trad	23.75	1.72	-	-
	Type 3	LD	9.60	1.35	56.00	1.44
Unreinforced masonry infill walls	Type 1	Trad	103.45	2.33	-	-
	Type 3	LD	12.84	1.35	85.00	1.65
Spider glazing curtain walls	Type 1	Trad	4.47	26.57	-	-
	Type 4	LD	5.44	6.42	11.00	65.00

Focusing on the percentage of savings (Figure 8.29), representing the convenience of implementing the low-damage/low-energy solution when compared to the traditional system, as previously highlighted and justified for the total building savings, the seismic savings are still very high for either the precast concrete cladding or the infill wall configurations, with values up to 50% and 75% respectively. While, for the spider glazing facades the savings due to the application of the energy efficiency system are greater than the seismic ones. In fact, if the energy performance of the 10+1.52+10 mm glass panel needs to be adjusted to reduce energy consumptions, the seismic performance of a traditional spider glazing system is already high when compared to other façade solutions, thus the application of a better seismic system leads to a reduced percentage of savings.

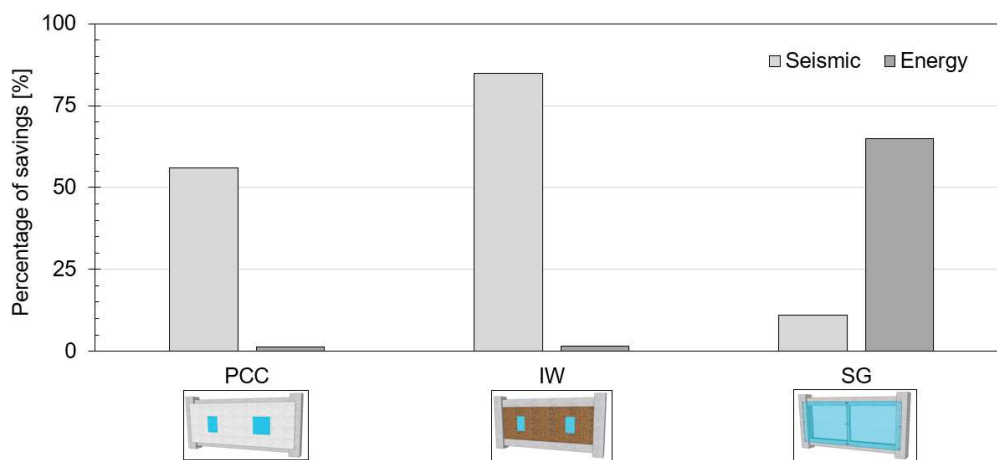


Figure 8.29. Percentage of savings due to the application of the best low-damage and low-energy solutions when compared to the traditional system for each typology of façade.

Finally, it is observed that the integrated seismic & energy performance analysis considers the seismic and energy expected losses or cost as performance measures, because more useful to decision makers. However, for the entire building system other comparisons can be implemented taking into account the building performance points, thus the related storey drift ratios and floor accelerations, while for the energy investigations the total energy balance and related thermal load. Concerning the component level, considering that the seismic performance is generally identified in terms of fragility curves, it is suggested to extend this concept to the case of energy performance. Therefore, fragility curves on an energy-based evaluation could be defined to be used to describe the expected energy performance of a building component. As example, Figure 8.30 presents the fragility functions obtained for the case of precast concrete claddings. The seismic vulnerability is expressed in terms of probability of reaching specific damage states, i.e. DS1 represents the formation of first visible cracking on the panels and DS2 indicates the condition of exceeding the maximum crack width for the serviceability limit state, as defined by Baird 2014. Similarly, the energy

vulnerability of a component can be expressed in terms of probability of reaching energy state conditions. Performing analyses in *Rhinoceros 3D/Grasshopper/Therm* software, parametrical studies are carried out assuming variation ranges to both the external conditions (temperature) and the component properties (conductivity of materials, thickness of layers) to determine the energy demand associated with the winter and summer conditions.

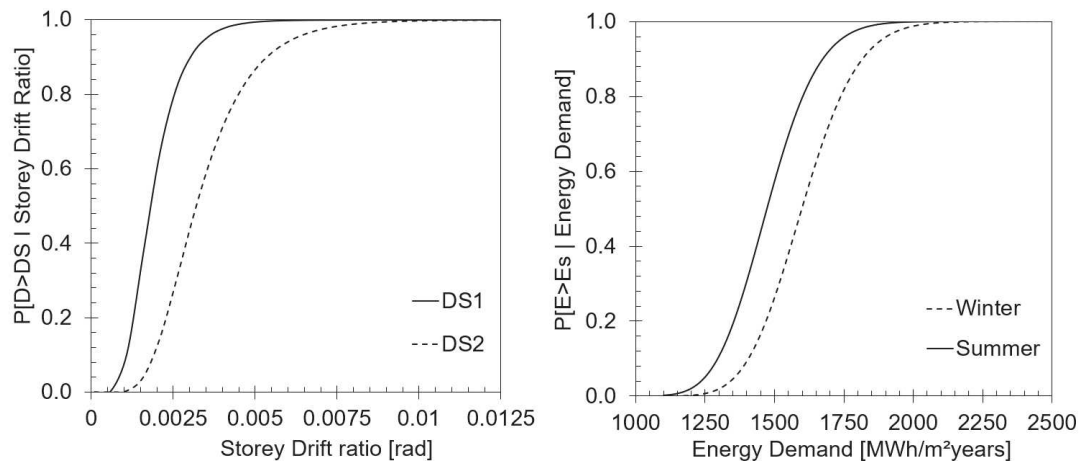


Figure 8.30. Fragility curves on both a seismic-based (left) and a energy-based (right) evaluation.

As for the seismic performance, the definition of energy-based fragility curves can be a valuable tool to compare alternative solutions and propose new solutions to improve the energy performance of a component.

8.4 Conclusions

This Chapter has presented a combined seismic and energy cost/performance-based evaluation of building configurations comprising different façade systems (traditional vs. low-energy and/or low-seismic solutions). Focusing on non-structural components, the design of these building elements should be developed considering a multi-performance investigation involving all the performance affecting these systems' behaviour, as described in the next Chapter.

After an initial background on the energy performance analysis of buildings as well as on the different energy-efficient solutions available nowadays, numerical investigations through *Rhinoceros3D/Grasshopper (Energy Plus and Therm)* software have been implemented to study the energy behaviour of a 5-storey reinforced concrete building composed of alternative façade systems (precast concrete claddings, masonry infill walls, spider glazing systems) and located in Reggio Calabria (Italy). Combining the energy performance study with the seismic investigation, already

presented in Chapter 5 for the same case-study structure, a multi-performance approach can be implemented to define the optimal design for, in this particular case, the façade system. The numerical results highlight the importance of applying this multi-performance analysis and, mainly, of including the seismic performance when decisions on non-structural detailing must be taken. In fact, non-structural elements are generally not designed to resist against seismic actions, whilst are design taking into account aesthetic criteria, thermal performance, etc. Nevertheless, the implemented study highlights how the seismic cost/losses can be very high when compared to the energy ones, especially for the case of unreinforced masonry infill walls. Therefore, the application of low-damage non-structural solutions, which are related to simple detailing modifications thus are cost-comparable to more traditional systems, can lead to substantial economical savings during the overall building life (around 45% for the configuration with external infill walls).

8.5 References

- ASHRAE 90-1 (2010). *Performance Rating Method Reference Manual*, ASHRAE Standard, Prepared for the U.S. Department of Energy, New York, USA.
- Baird A. (2014), Seismic Performance of Precast Concrete Cladding Systems, *Ph.D. Thesis*, University of Canterbury, Christchurch, New Zealand.
- Calvi G.M., Sousa L., Ruggeri C. (2016). Energy Efficiency and Seismic Resilience: A Common Approach, *Springer International Publishing Switzerland 2016*, P. Gardoni, J.M. LaFave (eds.), Multi-hazard Approaches to Civil Infrastructure Engineering.
- Comber M., Poland C., Sinclair M. (2012). Environmental Impact Seismic Assessment: Application of Performance-Based Earthquake Engineering Methodologies to Optimize Environmental Performance, *Structures Congress*, 910–921.
- Court A., Simonen K., Webster M., Trusty W., Morris P. (2012). Linking Next-Generation Performance-Based Seismic Design Criteria to Environmental Performance (ATC-86 and ATC-58), *Structures Congress*, 922–928.
- Crawley D., Pless S., Torcellini P. (2009). Getting to Net Zero, *ASHRAE Journal*, NREL/JA-550-46382, Atlanta, USA.
- D'Angola A., Manfredi V., Masi A., Mecca M. (2019), *Energy and Seismic Rehabilitation of RC Buildings through an Integrated Approach: An Application Case Study*, IntechOpen.
- DL 192 (2005). *Attuazione della direttiva 2002/91/CE relativa al rendimento energetico nell'edilizia*, Gazzetta Ufficiale n. 222 23/09/2005 - suppl. ord. n. 158, Rome, Italy.
- DL 63 (2013). *Disposizioni urgenti per il recepimento della Direttiva 2010/31/UE del Parlamento europeo e del Consiglio del 19 maggio 2010, sulla prestazione energetica nell'edilizia per la definizione delle procedure d'infrazione avviate dalla Commissione europea, nonché altre disposizioni in materia di coesione sociale*, Gazzetta Ufficiale serie generale n. 130 05/06/2013, Rome, Italy.
- DM 58 (2017). *Linee guida per la classificazione del rischio sismico delle costruzioni*, Rome, Italy.
- DM 162 (2015). *Linee guida nazionali per la certificazione energetica degli edifici*, Adeguamento del decreto del Ministro dello sviluppo economico, 26/06/2009 - (15A05200) in S.O. n. 39 Gazzetta Ufficiale, Rome, Italy.
- Dennemann K. L. (2009). *Life-cycle cost-benefit (LCC-B) analysis for bridge seismic retrofits civil and environmental engineering*, Houston, TX: Rice University.
- Dokka T.H., Hemstad K. (2006). *Energy efficient residential buildings for the future – a handbook for designing passive houses and low energy residential buildings*, IEA SHC Task 28/ECBCS Annex 38 Sustainable Solar Housing (in Norwegian).
- European Parliament and Council of the European Union (2010). *Energy Performance of Buildings Directive (EPBD recast)*, Directive 2010/31/EU, Bruxelles, Belgium.

- Federal Emergency Management Agency (2012). *Seismic Performance Assessment of Buildings, Volume 1 – Methodology*, Technical Report FEMA-P-58-1, Washington, D.C., USA.
- Feist W. (1999). *First steps: What can be a passive house in your region with your climate?*, Passivhaus Institute, Darmstadt, Germany.
- Ghosh, J., Tapia, C., Padgett, J. (2011). Life-cycle analysis of embodied energy for aging bridges subject to seismic hazards, *Proceedings of the 11th International Conference on Applications of Statistics and Probability in Civil Engineering*, ETH Zurich, Switzerland.
- Hasan A. (1999). Optimizing insulation thickness for buildings using life cycle cost, *Applied Energy*, 63: 115–124.
- Intelligent Energy Europe (2012). *Very Low-Energy House Concepts in North European Countries, NorthPass Project report*.
- Itoh Y., Wada M., Liu C. (2005). Lifecycle environmental impact and cost analyses of steel bridge piers with seismic risk, *9th International Conference on Structural Safety and Reliability, Rome, Italy*.
- Kats G. (2003). *Green Building Costs and Financial Benefits*, Massachusetts Technology Collaborative: Westborough, Massachusetts, USA.
- Manfredi V. and Masi A. (2018). Seismic Strengthening and Energy Efficiency: Towards an Integrated Approach for the Rehabilitation of Existing RC Buildings, *Buildings*, 8: 36.
- Nayak J.K., Prajapati J.A. (2006). *Handbook on Energy Conscious Buildings*, Prepared under the interactive R & D project no. 3/4(03)/99-SEC between Indian Institute of Technology, Bombay and Solar Energy Centre, Ministry of Non-conventional Energy Sources, Government of India.
- Nawale S. (2015). Autonomous Building, *International Journal of Engineering Research and Development*, 11(11): 22-24.
- Padgett J. E., Ghosh J., Tapia C. (2009). Sustainable infrastructure systems subjected to multiple threats, *TCLEE Conference*, Oakland, CA.
- Priestley M.J.N., Calvi G.M., Kowalsky M.J. (2007). *Direct Displacement-Based Seismic Design of Structures*, 1st edition, IUSS Press, Pavia, Italy.
- Tapia C., Ghosh J., Padgett J. (2011). Life cycle performance metrics for aging and seismically vulnerable bridges, *Proceedings of the 2011 Structures Congress*, Las Vegas, Nevada.
- Tam V. W.Y., Khoa L.N., Wang J.Y. (2018). Cost Implication of Implementing External Façade Systems for Commercial Buildings, *Sustainability*, 10, 1917.
- Ufficio Federale dell'Energia UFE (2001). *Calcolo del coefficiente U e catalogo degli elementi costruttivi per nuovi edifici*, Eds: svizzera energia.
- UNI 10351 (2015). *Materiali e prodotti per edilizia - Proprietà termoigrometriche - Procedura per la scelta dei valori di progetto*, Italian standards, Milan, Italy.
- UNI EN ISO 6946 (1999). *Building components and building elements, Thermal resistance and thermal transmittance, Calculation method*, Italian standards, Milan, Italy.

UNI EN ISO 14683 (2008). *Thermal bridges in building construction - Linear thermal transmittance - Simplified methods and default values*, Italian standards, Milan, Italy.

United Nations (2009). *Buildings and climate change: a summary for decision makers*, United Nations Environmental Programme, Sustainable Buildings and Climate Initiative, Paris, France.

Vale B., Vale R. (2000). *The Autonomous House: Design and Living for Self-Sufficiency*, Ed. Thames & Hudson, London, United Kingdom.

Zhang X., Platten A., Shen L.Y. (2011). Green property development practice in China: Costs and barriers, *Building Environment*, 46: 2153–2160.

9. Multi-criteria decision-analysis for non-structural components

9.1 Introduction

This Chapter describes the multi performance-based (multi criteria) approach which should be implemented in order to make decisions on new non-structural elements as well as on retrofit interventions for existing systems. A summary of the overall performance measures describing the behaviour of these building elements is provided, i.e. the structural, architectural and long-term properties already introduced in Chapter 2 and further described in the initial part of this Chapter. Particularly, more information can be found on the methods generally adopted for calculating the different performance quantities. Finally, an initial multi-criteria decision-making approach, comprising more technical criteria at this stage, is defined with the aim of driving the choice of new or retrofitted non-structural components.

9.2 Overall non-structural performance

Non-structural elements are subjected to various external actions during their life, that is environment actions or casual factors such as natural events. The non-structural performance correlated to each of these external loads needs to be determined in order to define the performance targets/levels to be included within a multi-criteria design process. Therefore, considering prescriptions from European and Italian codes/guidelines the parameters describing the component capacity are identified for all the performance herein listed.

- *Structural performance:*
Static, Dynamic, Fire;
- *Architectural performance:*
Thermal, Acoustic, Weather tightness;
- *Long-term performance:*
Durability, Sustainability.

The previous classification aligns with the one provided in Chapter 2 of this Thesis.

9.2.1 Static performance

Non-structural elements are primarily designed to support their own weight and the additional vertical loads planned during the building design. In fact, specific anchorage systems are designed to be connected to the structural skeleton for allowing the correct transfer of load to the primary structure. Apart from the self-weight, vertical non-structural elements (partitions, facades) are also designed to accommodate the live load deflection of the floor slab.

However, focusing on the façade systems (exterior enclosures) deflections due to temperature variations and wind loads need to be verified and contained. E.g. infill walls behaving like a cantilever in the out-of-plane direction typically include specific out-of-plane supports on the top (and possibly sides) of the panel or curtain wall systems usually have splice joints properly sized to allow for either the deflection or the thermal expansion.

In the common practice façade engineering, the exterior enclosures are designed for the maximum deflection they can achieve. Although more accurate procedures through numerical investigations are available, the deflection can be calculated referring to analytical formulations:

$$u_{wind} = k \cdot \frac{qh^4}{EI} [mm]$$

$$u_{thermal} = \alpha \cdot \Delta T \cdot h [mm]$$

Where: q is the wind load [N/mm²], h is the height of the mullion/panel [mm], I is the moment of inertia [mm⁴], k is the coefficient joint depending on the static scheme adopted for the façade (e.g. in Figure 9.1), α is the thermal dilatation [1/°C], ΔT is the increase in temperature of the mullion/panel [°C], h is the height of the mullion/panel [mm].

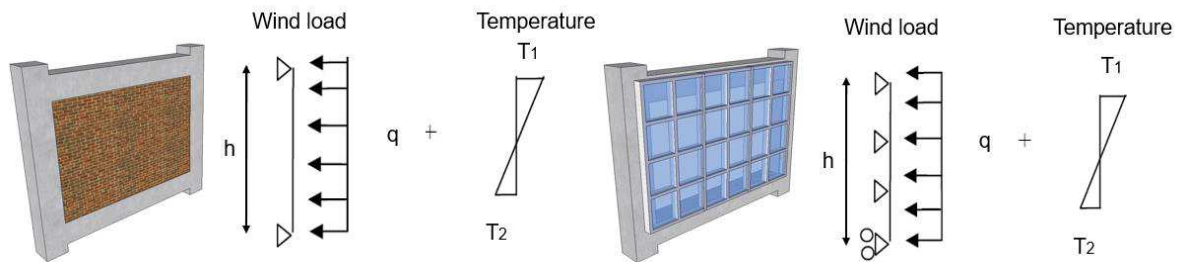


Figure 9.1. Example of static schemes for the infill wall façade system (left) and curtain wall solution (right).

Nevertheless, façade quality certifications already define the capacity of resisting against wind actions, thus of maintaining an allowable deflection and keeping the initial system properties, through the quantification of the design and safety pressure wind loads. The values of the pressure loads are obtained performing experimental wind testing on the façade, as described in the UNI EN 12179 (2002). The facade is subjected to a design wind action and, considering both positive and negative pressure zones, it should be able to completely transfer the action to the structural system through its anchorage devices. The design wind action is defined referring to the national code and the maximum elastic deflection, orthogonal to the wall, is checked to be less than $1/200$ of the distance between two anchorage points and however less than 15 mm, as prescribed in the UNI EN 13116 (2002). While, applying a wind load equal to 150% of the design load (safety load) in both pressure and suction sides, no deformation or permanent damage of the elements composing the façade should form (UNI EN 13116 2002).

According to what previously described, the deflection u can be considered as the parameter describing the static performance and, consequently, to be used for defining the rating system of this non-structural technical aspect.

9.2.2 Dynamic performance

The dynamic or seismic non-structural performance has been widely described in chapters of this Thesis (from Chapter 3 to Chapter 7), where the importance of including the seismic study in the typical design process of non-structural systems is ever highlighted. Depending on the sensitivity of the element, the peak floor acceleration a or the inter-storey drift ratio θ can be assumed as the parameter characterizing this non-structural behaviour. The non-structural seismic response can be expressed in terms of fragility functions, specifically developed to describe the seismic vulnerability as the exceeding of non-structural damage conditions.

When subjected to seismic actions the behaviour of non-structural components depends on the system properties (material properties, panel modularity) and the type of connection to the structural system (material properties, modularity and typology of connection, detailing). Although analytical formulations based on geometrical considerations are available, the seismic response can be accurately studied through numerical modelling or experimental investigations on unscaled or scaled elements, as described in Chapter 3.

Providing limiting values from international codes/guidelines to the inter-storey drift and/or floor acceleration (θ , a) to each typology of non-structural components, the seismic performance can be assessed. However, the so-defined limiting values are dependent on the considered level of seismic intensity, e.g. when assessing the performance for the Ultimate Limit State condition the expected performance/targets are different from the one associated with a Damage Control Limit State condition. Consequently, in order to provide a more general description the rating system for the seismic performance can be defined through an index describing the expected annual losses due to the sole non-structural damage.

9.2.3 Fire performance

The fire performance of a non-structural system is described in terms of fire-resistance rating, generally available from product catalogues. The fire-resistance rating is indicated as “REI” value and represents the duration for which a passive fire protection system can withstand a standard fire resistance test, without loss of its functionality. As defined within the Italian DM 16/02/2007, the REI factor takes into account the following aspects:

- Load bearing capacity, R, i.e. the ability of a building element to resist a fire when exposed on one or several sides and when supporting an external load during a time period without losing its stability. This capacity is related to components which are part of the structural skeleton and those providing support to other fire rated elements within the same or adjacent fire-cells, i.e. columns, beams, floors and walls;
- Integrity, E, i.e. the ability of a secondary element, when exposed to fire on one side, to prevent the passage through it of flames and hot gases and to prevent the occurrence of flames on the unexposed side. Secondary elements indicate fire separations being internal walls and floors, areas of external walls not permitted to be an unprotected area, and some areas of roofs when close to another building.

- Insulation, I, that is the ability of a primary or a secondary element when exposed to fire on one side, to restrict the temperature rise of the unexposed face to below specified levels. This property is required to fire separations and where the transmission of heat through the element may endanger occupants on the other side, or cause fire to spread to other fire-cells or adjacent buildings.

Limiting values for the REI factor for different typologies of component or material can be found in the DM 16/02/2007, however for the specific case of façade systems the CVVF 5043 (2013) can be taken into account for developing a rating system. With the aim of limiting the probability of fire to a façade and its subsequent propagation, due to a fire developing from the internal or external zone of a building, and in order to limit or avoid the possible detachments of façade parts which may be dangerous to people during the evacuation, the CVVF 5043 (2013) describes the different typologies of façade systems and indications on the non-structural detailing (e.g. length of air cavity) are provided for guaranteeing specific fire performance (e.g. in Figure 9.2).

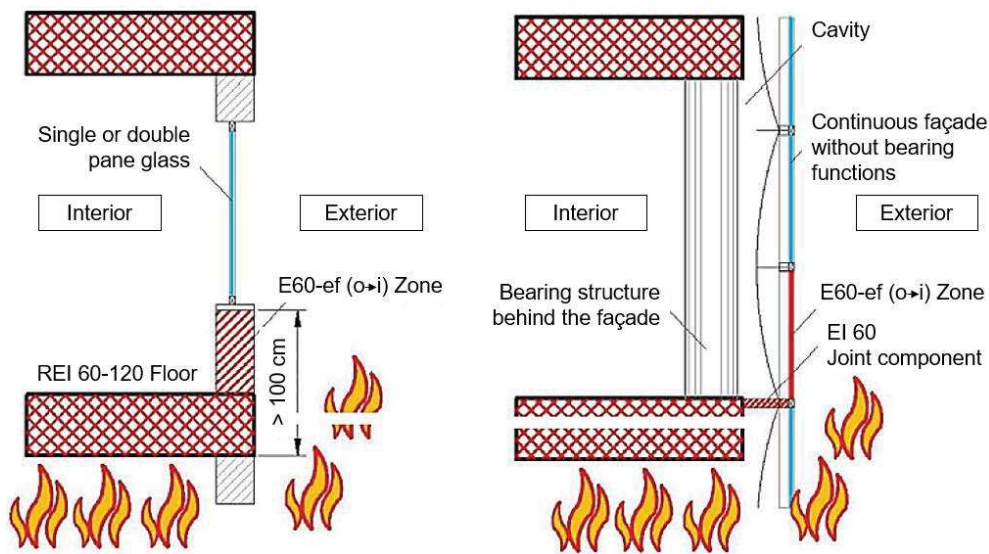


Figure 9.2. Examples of façade detailing for a simple façade (left) and a continuous façade solution (right) - CVVF.

The REI factor describing the fire performance of a component/system can be identified through numerical investigations on the building or performing fire tests on specific non-structural elements. The limiting values of this factor determine the fire performance levels to be included in the multi-performance decision-analysis.

9.2.4 Thermal performance

The thermal performance represents the resistance or transmittance of a system to the heat transfer. The previous Chapter has provided information on the key parameters influencing this aspect, on the methods and formulations generally used to evaluate the thermal behaviour of a component, as well as on existing solutions which can be nowadays adopted for improving the energy efficiency of a building or system. As shown in the previous Chapter, the thermal performance of a component is described in terms of thermal transmittance, U . Then, this parameter can be used for rating the energy efficiency of a non-structural component. Limiting values for the transmittance can be extrapolated from the UNI EN 13947 (2007) and from the Italian DPR 59/09 (2009), where U is defined in function of the Italian climatic zones.

9.2.5 Acoustic performance

The acoustic phenomenon consists of a perturbation of the atmospheric pressure which propagates inside an elastic component (gas, liquid, solid). The human response to the sound energy is calculated in terms of level of sound pressure, L_p , determined as:

$$L_p = 20 \log \frac{p}{p_0} [dB]$$

Where: p is the measured acoustic pressure while p_0 is the reference pressure equal to 20 μ Pa, corresponding to the minimum level of sound pressure perceived from an individual at 1000 Hz of frequency, that is 0 dB. However, in addition to the sound level, the human hearing is also sensitive to the sound frequency composition and the sensitivity is greater for the higher frequencies when compared to the lower ones.

For the specific case of noise propagation inside a building, the propagation medium is represented by the same building elements, such as walls or floors. As example, Figure 9.3 (left) presents the different propagation paths of the sound from the source chamber to the receiving chamber. The sound propagates by means of two different mechanisms: 1) propagation by air; 2) propagation through solid elements (elastic vibrations). Considering these mechanisms, the transmission can be: 1) direct, meaning a sound transmission through the only considered element; 2) lateral, meaning a sound transmission involving also other components adjacent to the considered element. Therefore, the acoustic insulation certified by laboratory measurements is generally higher than the real value due to the absence of lateral sound transmission.

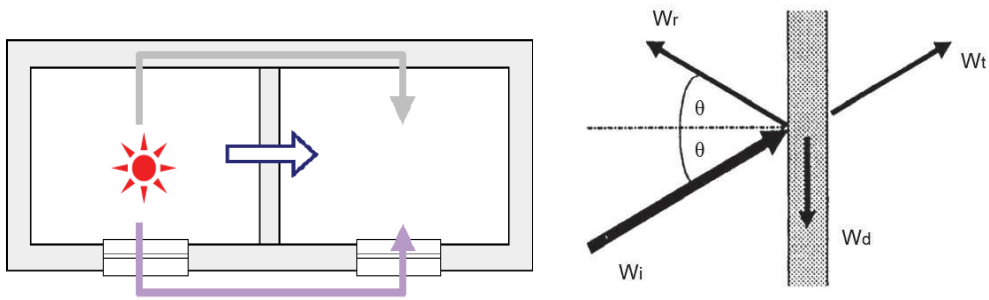


Figure 9.3. Left: sound transmission paths between two adjacent building zones. Right: decomposition of a sound wave through a wall (Mattevi 2005).

The acoustic insulation does not represent an intrinsic property of a system, while is a parameter conditioned by the configuration of the environment where it is measured. Particularly, among all the conditions influencing the sound level measurements there are: the acoustic properties of the component, the mechanical properties of the lateral walls, the sound absorption capacity of the materials composing the internal zone surface. The acoustic performance of a system can be described in terms of sound insulation D , defined as:

$$D = L_1 - L_2 \text{ [dB]}$$

Where: L_1 is the mean value of the sound pressure level of the “source” place, while L_2 is the mean value of the sound pressure level of the “receiving” place.

For understanding how a component can hinder the sound propagation, it is finally introduced the concept of sound reduction. Considering a sound wave acting on a wall, expressed in terms of sound power W_i , this wave decomposes into different components: a part is reflected to the source chamber (W_r) while another part passes through the wall, being transformed into vibrational energy, and, in turn, is separated into a part dissipating in heat (W_d) and another one transmitted to the receiving chamber (W_t). This decomposition is shown in the previous Figure 9.3 (right). The quantity of energy absorbed and transmitted depends on the material properties of the wall and the phenomenon is described using two parameters: 1) the acoustic absorption coefficient (α), indicating the absorbed fraction of energy and is equal to 0 if the sound is completely reflected or equal to 1 if all the energy is absorbed; 2) the acoustic transmission coefficient (τ), indicating the sound power passing through the element and defined, for the case of the tilt angle θ equal to zero, as:

$$\tau = \frac{W_t}{W_i}$$

Using the acoustic transmission coefficient τ , the sound reduction can be determined, for the zero θ value, applying the formulation which follows.

$$R(\theta) = 10 \log \frac{1}{\tau(\theta)} \text{ [dB]}$$

For the specific case of façade systems, as defined by the UNI EN ISO 12354-3 (2017) the acoustic insulation is measured as difference between the mean value of the sound pressure at 2 meters from the façade level ($L_{1,2m}$) and the mean value of the sound level in the receiving chamber (L_2), estimated referring to the conditions described in the DPCM 05/12/1997. In fact, this standard requires the calculation of the acoustic insulation normalized by the ‘reverberation time’ or ‘decay time’, as also indicated in the UNI EN ISO 717-1 (2013), with noise source represented by the vehicle traffic if predominant or by a speaker with inclined angle of 45°. Thus, this normalized sound insulation ($D_{2m,nT}$) is calculated as:

$$D_{2m,nT} = L_{1,2m} - L_2 + 10 \log \frac{T}{T_0} \text{ [dB]}$$

Where: T [s] is the reverberation time of the receiving place, T_0 [s] is the reference reverberation time assumed as 0.5 s.

The reverberation time (T_{60}) is the time required for having the sound pressure in a confined place equal to 60 dB, after that the sound source generating that level turns off. For environments with small dimensions, widespread sound and moderate sound absorption, the reverberation time can be estimated as:

$$T_{60} = \frac{0.16V}{A}$$

Where V [m³] is the volume of the considered environment, A [m²] is the equivalent absorption defined as:

$$A = \sum_{i=1}^n S_i \alpha_i \text{ [m}^2\text{]}$$

Where: n is the number of surfaces, each of area S_i and with sound absorption α_i .

Summarizing, the acoustic performance of a non-structural component is described in terms of sound reduction (R) or sound insulation index (D) and current standards define classes/levels for these parameters to be included within the multi-performance evaluation.

9.2.6 Weather tightness

Weather tightness performance is concerned with the penetration of air, water and vapor into the building envelope. As described in Chapter 2, different issues are related to weather tightness, e.g. moisture problems, noise transfer, smoke propagation, indoor air quality, therefore the resistance to air, water and vapor needs to be guaranteed for the building façade systems. Different codes (UNI EN 12153 2002, UNI EN 12155 2002, UNI EN 13050 2011, UNI EN 13051 2002) define the methods to be used for determining these properties through laboratory or in-situ testing, while other codes provide rating systems for classifying the weather tightness (UNI EN 12152 2003, UNI EN 12154 2001, UNI EN ISO 13788 2013).

Air leakage can occur through gaps and cracks in the fabric of the building envelope, allowing heat to escape, thus driving up heating bills and CO₂ production. Air tightness testing, also known as an air leakage testing, is a test indicating the cubic metres of air leakage per hour per square metre of the external area of the façade. It is experimentally measured by a blower-door test (Figure 9.4) consisting of a calibrated fan for determining an airflow rate and a pressure sensing device to measure the air pressure created by the fan flow. The blower-door system generally includes three main components: a calibrated fan, a door-panel system and a device for measuring fan flow and building pressure. The fan blows air into the structure and a pressure difference between inside and outside is created, consequently this pressure difference forces the air to pass through the gaps of the building envelope and the airtightness of the structure can be determined.

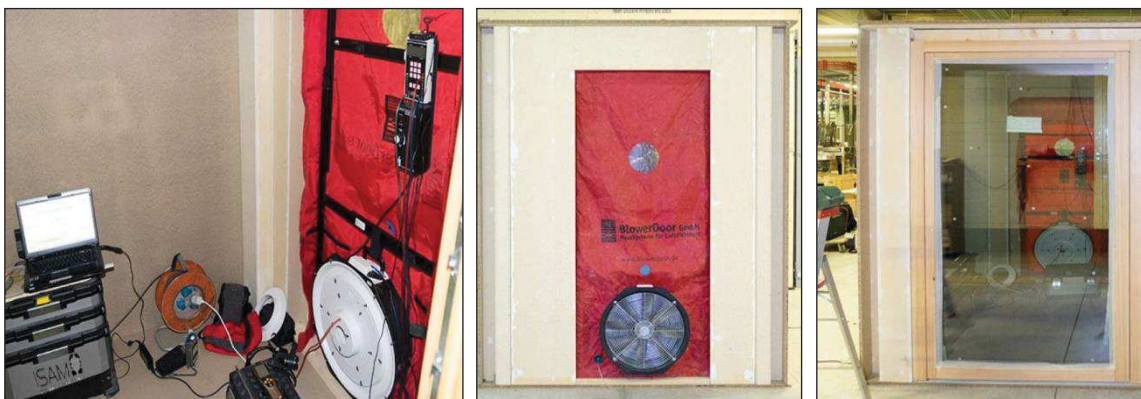


Figure 9.4. Example of blower-door test (source: www.isamsr.it).

Water tightness is the capacity of preventing water or other fluids from getting from one side of the wall to the other side. The main areas of concern when it comes to constructions and water tightness is the penetrations and joints, as well as the material itself used for the wall system. Porosity, representing the ratio for the volume of the voids with the total volume of the material, describes the storage capacity that a material has. The other key measurement associated with water tightness is the permeability of the materials composing the façade system.

Water tightness is measured through experimental or in-situ testing as the air tightness. The experimental test (e.g. in Figure 9.5) determines the pressure at which the infiltration of water in the frame happens, taking into account the air pressure associated with the infiltration, time of application of the artificial rain to the edge of the water leakage, quantity of water thrown on the outer surface during the test.



Figure 9.5. Examples of watertightness test performed in laboratory (source: www.tostem.com).

Concerning the vapor tightness, the vapour resistance of a material or component is a measure of the resistance to let water vapour passes through it. The vapour resistance of a material can be defined using the “water vapour resistance factor” (μ), which is a property of the material itself and independent of the thickness of the material in a specific construction. The lower is the μ value, the more breathable is the material. However, the vapor tightness of a component can be monitored using the water vapour diffusion “equivalent air layer thickness” (S_d), calculated as:

$$S_d = \mu \cdot s [m]$$

The S_d value is the thickness of a static layer of air in metres, which displays the same resistance to water vapour transmission as the building material in the thickness s with the resistance to water vapour transmission μ .

9.2.7 Durability performance

As defined in the ISO 15686-1 (2000), the durability represents the capability of a building or its parts to perform the required function over a specified period of time under the influence of the agents anticipated in service. In other words, durability is the capability of a material to perform at least as well as the level given by performance criteria.

An element undergoes a natural drop in the performance over time and beyond a certain threshold limit the performance of the component achieves values below which is no longer able to respond effectively in relation to the function required and this would put an end to its life. The estimation of the service life of materials and building components has been widely investigated in the research field and different international codes/guidelines provide a method to estimate this value. As indicated in the ISO 15686-1 (2000), the service life is the period of time after installation during which a building or its parts meet or exceed the performance requirements. Service life is thus dependent on both changes in performance and on the performance requirements (or criteria) made on the product.

Figure 9.6 shows the general effect of degradation, and that the performance level can be increased, at least temporarily, by maintenance. The performance curve is valid for some given confidence limit, and the dark area represents the instantaneous probability of failure at time t_1 . To be able to estimate the service life then, both the degradation process and changes in requirements must be predictable.

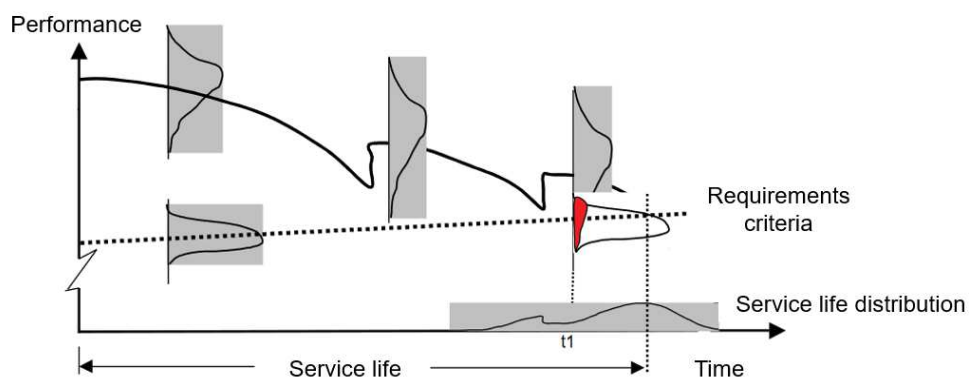


Figure 9.6. Performance and performance requirements over time (Marteinsson 2005).

The Estimated Service Life (*ESL*) can be calculated using the formulation provided by the same ISO 15686-1 (2000), provided below.

$$ESL = RSL \cdot A \cdot B \cdot C \cdot D \cdot E \cdot F \cdot G$$

Where: *RSL* represents the Reference Service Life, determined through experimental investigation in laboratory or in-situ following the method proposed by the UNI 11156-3 (2006) and based on the ISO 15686-2 (2001), while the different factors indicate:

- *A* describes the quality of the component, taking into account the construction phases as well as the transport and storage phases;
- *B* indicates the design quality, that is the care with which the component usage has been designed, e.g. if shelters from the atmospheric conditions have been considered;
- *C* defines the execution quality, thus considers the aspects related to the manpower quality, the climatic conditions during the construction and all the other aspects related to the construction site;
- *D* represents the conditions of the internal environment, e.g. possibility of forming condensation;
- *E* describes the external environment, taking also into account the micro-climatic conditions nearby the component, e.g. height of the buildings;
- *F* defines the usage conditions, considering the type of usage and the users of the environment, e.g. the presence of children increases the probability of ruptures due to improper usage;
- *G* indicates the maintenance level.

Concluding, the durability performance is described by the Estimated Service Life (*ESL*), which can be determined for each building element and classified considering the performance levels indicated within the UNI 11156 (2006).

9.2.8 Sustainability performance

As described in the ISO 14040 (1997), the heightened awareness of the importance of environmental protection and the possible impacts associated with products manufactured and consumed, has increased the interest in the development of methods to better determine and reduce these impacts. Sustainability is becoming a fundamental aspect to be taken into account when realizing a product, thus companies actually define sustainability goals trying to achieve them, therefore creating "green" or "sustainable" products, e.g. cutting emissions, lower energy usage, sourcing products from fair-trade organizations, and by ensuring their physical waste is disposed of properly and with as little carbon footprint as possible (Caruso et al. 2017).

Many assessment tools have been progressively developed to drive decision-making processes in the direction of achieving sustainability goals and these frameworks are nowadays part of international standards being mandatory or voluntary, i.e. Protocollo ITACA, LEED, SBTool, HQE, DGNB, BREEAM, GBC, CASBEE. One of the techniques being developed for analysing the environmental factors related to the entire life cycle of a building is the Life Cycle Assessment (LCA). LCA is a technique for assessing the environmental aspects and potential impacts associated with a product which studies the environmental aspects and potential impacts throughout the life of the product, from raw material acquisition through production, use and disposal. The main advantage of an LCA is that it makes possible to quantify the impacts on the environment not limited to energy or CO₂ emissions, but also considering the use of other renewable and non-renewable resources, covering the emission of many organic and non-organic compounds into the air, water, and soil, as well as ionizing radiation.

The phases of an LCA methodology are summarized in the next Figure 9.7, however more information on the procedure and its development can be found in ISO 14040 (1997).

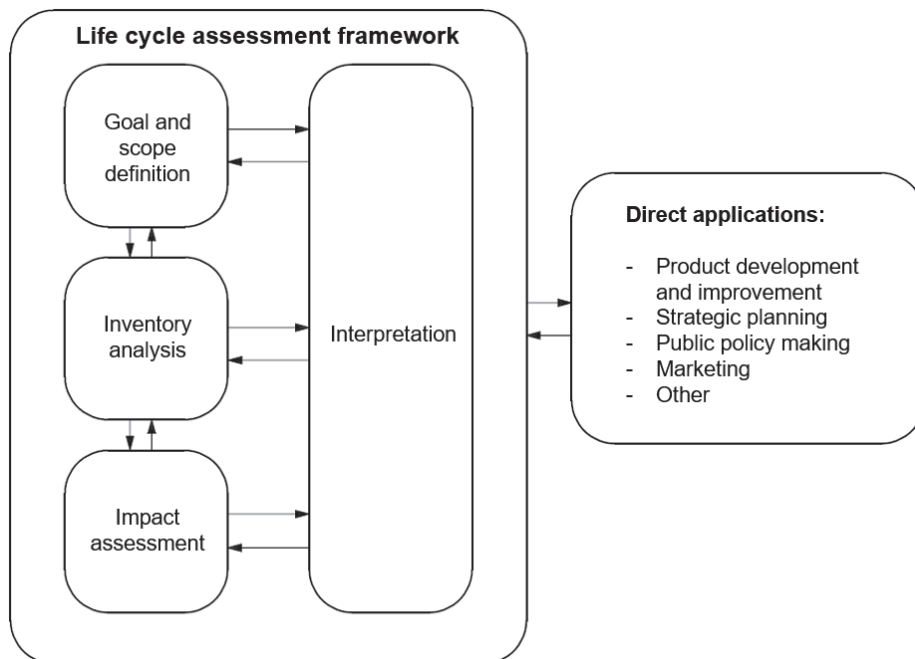


Figure 9.7. Stages of an LCA (from ISO 14040 1997).

For the specific study implemented in this Chapter of the Thesis, the sustainable performance of non-structural elements is herein defined calculating the emission of CO₂ and the embodied energy. Therefore, specific performance classes will be defined in functions of these factors for rating the sustainability performance of a component.

9.3 Multi-criteria decision-making approach

When designing non-structural components or retrofit interventions for these building elements, a multi-criteria decision analysis should be developed to identify the optimal solution among alternatives. This multi-criteria approach should include all the technical (performance) and non-technical aspects (installation cost, maintenance cost, duration of work, etc.) properly rated and weighted for driving the final decision. Therefore, after an initial description of the Multi-Criteria Decision-Making (MCDM), useful for solving different engineering problems, an initial approach is suggested for making decisions on non-structural elements. However, in this initial stage of the proposal, mainly technical aspects are included within the procedure, i.e. the criteria are represented by all the non-structural performance quantities previously described.

9.3.1 General aspects of MCDM

Decision making is the process of making choices by identifying a decision, gathering information and assessing alternative solutions and using a step-by-step decision-making process can help in making more deliberate decisions, thus determining the most satisfying possibility. The development of approaches for optimal decision making is very important and a prominent class of such problems is the Multi-Criteria Decision-Making (MCDM) dealing with the evaluation of a set of alternatives in terms of a set of decision criteria.

The multi-criteria decision problem consists of defining the best solution among alternatives, that is the solution showing the highest degree of desirability with respect to all the criteria. The multi-criteria decision analysis comprises different steps, easily summarized in Figure 9.8 and described below.

Step 1. Define the problem. The first step of the procedure consists in clearly defining the decision to make.

Step 2. Identify the criteria. After the definition of the problem to solve, the different criteria for making the decision are selected. Each MCDM problem is associated with multiple attributes, also referred as decision criteria representing the different dimensions from which the alternatives can be viewed. If the number of attributes is large, the criteria can be arranged in a hierarchical manner, thus some attributes are major attributes associated with several sub-attributes. Although some MCDM methods may explicitly consider a hierarchical structure in the attributes of a problem, most of them assume a single level of criteria.

Step 3. Decision framework. The several possible paths of action or alternative are identified and listed. Alternatives represent the different choices of action available to the decision maker and the set of alternatives is assumed to be finite.

Step 4. Rating the alternatives. Rating systems can be assigned to each attribute, e.g. 5 for excellent, 4 for good, 3 for satisfactory, 2 for below average and 1 for poor, and each alternative can be properly rated giving a score to the different criteria.

Step 5. Assign the weights. MCDM methods need the definition of a “weight” for each criterion expressing the relative importance of it in respect to the others. The definition of the weights is one of the most critical phases of the decision procedure requiring a quantitative measure of the decision maker’s preference about each performance target.

Step 6. Score the alternatives. Final step of the procedure consists in scoring the different alternatives, thus taking into account the different criteria, rating systems and weights. The optimal solution among all the possibilities is finally determined.

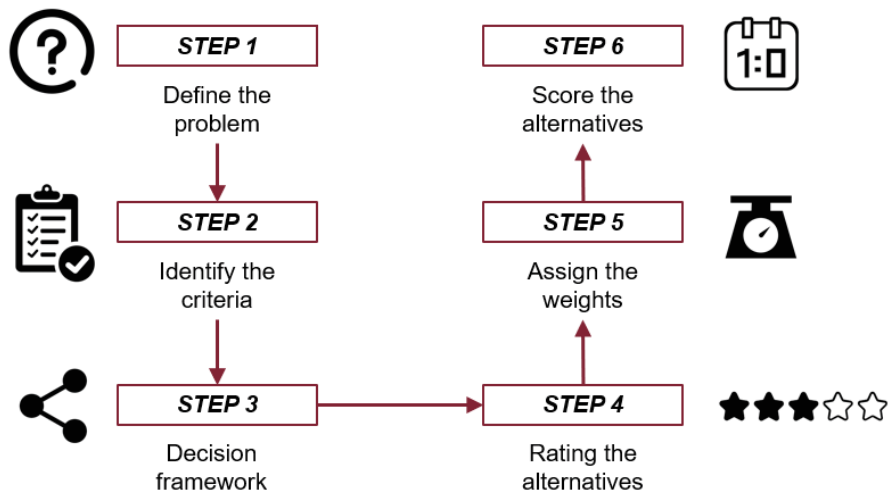


Figure 9.8. Steps of a Multi-Criteria Decision analysis.

9.3.2 MCDM for non-structural components

Multi-Criteria Decision analysis is a valuable tool to be applied to many complex decisions. Concerning structural engineering works, the procedure has been developed for both the design of new buildings (e.g. Balcomb and Curtner 2000; Mela et al. 2012; Mosalam et al. 2018) as well as for the retrofit of existing structures (e.g. Dan 2004; Caterino et al. 2008, 2009). While, about non-structural elements some research works can be specifically found on the design of façade systems (e.g. Zavadskas et al. 2013; Moghtadernejad et al. 2018).

Nevertheless, the MCDM can be used for decisions on each typology of non-structural element and the procedure should include among the criteria considerations on the seismic performance of the component. Therefore, a simplified approach based on technical aspects (non-structural performance) as decision criteria is herein presented to be used during feasibility studies of new components or retrofit solutions. In addition to the technical aspects, the non-technical condition related to the system construction is introduced within this initial multi-criteria evaluation.

Obviously, the proposed procedure can be improved because it does not take into account many other non-technical aspects, such as aesthetics, operating cost, maintenance work, which may influence the final result. The approach also uses the earliest and common weighted sum method, while more accurate estimations can be obtained using other methodologies, i.e. Analytical Hierarchy Process (Saaty 1980) or Technique for Order Preference by Similarity to Ideal Solutions - TOPSIS - (Hwang and Yoon 1981). Nevertheless, the multi-criteria procedure proposed in this Thesis has again the aim of highlighting the importance of considering the seismic performance as one of the selecting criteria, especially when decisions need to be taken for buildings located in high-seismicity areas as well as for structures for which the safety has a very important role.

Referring to the different steps characterizing an MCDM process, for the non-structural elements these steps can be adjusted as presented in Figure 9.9 and described as follows.

- **Step 1**

The decision opportunity is initially defined. Considering the design of a new component or the retrofit of an existing element, the goal of the procedure is the definition of the optimal non-structural system to be included within a building characterized by a specific use and located in a certain site. For example, the decision can be related to the choice of the optimal solution of a façade system to be used for covering a building skeleton.

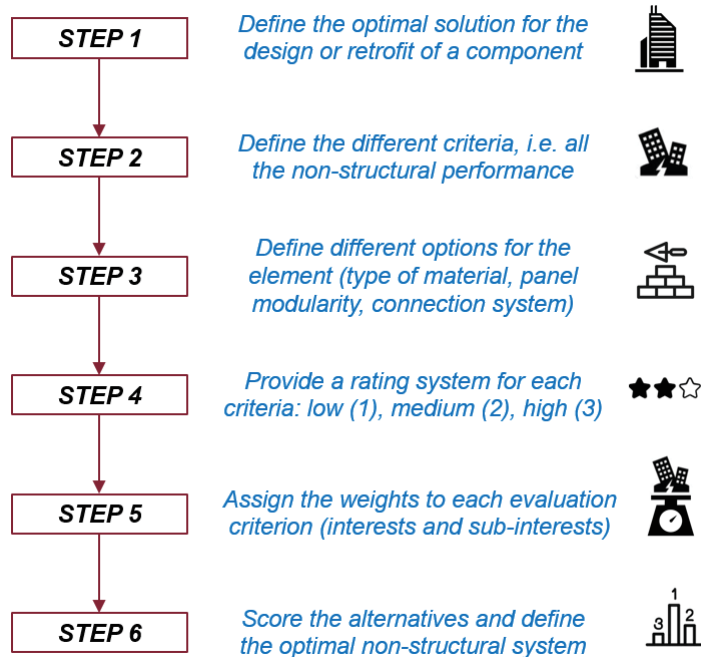


Figure 9.9. Sketch of the multi-criteria decision making procedure for the non-structural elements.

- **Step 2**

The different criteria to be included within the procedure are chosen as all the performance affecting the non-structural behaviour (structural, architectural, long-term). All these technical aspects do not belong to all the typologies of non-structural components, i.e. for defining the optimal solution for a new ceiling system, the resistance against wind or weather tightness are not taken into account, however, a general procedure is herein provided. Only the non-technical aspect related to the initial construction cost of the non-structural component is added to the other criteria. In fact, this aspect certainly drives the decision mainly during initial feasibility study of the problem.

- **Step 3**

The alternatives to be compared are identified. As example for the case of internal partitions the options can be determined considering different typologies of system, i.e. clay brick partition vs. metal partition vs. timber partition, or taking into account different solutions for the same typology, i.e. a standard partition can be compared to other solutions including detailing modifications (thickness, type of layers, connection to the skeleton, etc.).

- **Step 4**

A rating system is then assigned to each criterion. Three different levels of evaluation are identified for each performance and to each of this level a specific score is attributed (low = 1, medium = 2, high = 3). For defining how a specific criterion can be rated, i.e. to determine if it can be considered low, medium or high, limiting values of the performance measures are provided referring to the prescriptions found in the national or international codes/guidelines indicated in the previous section. The rating system to be used for each interest and sub-interest is summarized in the following Table 9.1.

Regarding the seismic performance, considering that the seismic behaviour of a system in terms of inter-storey drifts and floor accelerations can be rated in function of the considered seismic intensity level, i.e. a specific seismic response can be assessed as good or not depending on the intensity of the earthquake, the seismic performance is now described in terms of Expected Annual Losses associated with the non-structural component only, that is:

$$EAL_{nsc} = \frac{R_{nsc}}{RC_{nsc}}$$

Where: R_{nsc} is the annualized repair cost associated with the non-structural damage while RC_{nsc} represents the replacement cost of the non-structural element. This parameter allows the definition of more general ranges established basing on what can be found in the Italian seismic classification (DM 58 2017).

- **Step 5**

Then, one of the last steps of the analysis consists in assigning a weight to each criterion. This is related to personal preferences matter, so to each interest or sub-interest a specific weight is attributed. The criteria are classified from the most important to least important and 100 points are allocated among the interests. Weights are also assigned to the sub-interests considering values between zero and the value of the weight of the interest, as shown in the next Table 9.2.

Table 9.1. Rating system to be used for the different criterion.

Interest	Sub-interest		Key parameter	Level	Pts	Description	
Technical	Structural	Static	Deflection v_1 [mm]	Low	1	$v_1 \leq L_1^{(1)}/375$	
				Medium	2	$v_1 \leq L_1^{(1)}/500$	
				High	3	$v_1 \leq L_1^{(1)}/750$	
		Wind	Deflection v_2 [mm]	Low	1	$v_2 \leq L_2^{(2)}/150$	
				Medium	2	$v_2 \leq L_2^{(2)}/200$	
				High	3	$v_2 \leq L_2^{(2)}/300$	
		Dynamic	-	Expected Annual Losses EAL_{nsc}	Low	1	$EAL_{nsc} \geq 1.50$
					Medium	2	$0.50 \leq EAL_{nsc} \leq 1.50$
					High	3	$EAL_{nsc} \leq 0.50$
		Fire	-	Fire resistance EI	Low	1	$EI \geq 30$
	Medium				2	$EI \geq 60$	
	High				3	$EI \geq 90$	
	Architectural	Thermal	-	Transmittance U [W/m ² K]	Low	1	$U > 3.00^{(4)}$ $U > 0.32^{(5)}$
					Medium	2	$1.00 \leq U \leq 3.00^{(4)}$ $0.22 \leq U \leq 0.32^{(5)}$
					High	3	$U < 1.00^{(4)}$ $U < 0.22^{(5)}$
		Acoustic	-	Sound reduction R [dB]	Low	1	$R < 40$
					Medium	2	$40 \leq R \leq 55$
					High	3	$U > 55$
		Tightness	Air	Maximum pressure p_{max} [Pa]	Low	1	$p_{max} < 150$
					Medium	2	$150 \leq p_{max} \leq 600$
High					3	$p_{max} > 600$	
Water			Maximum pressure p_{max} [Pa]	Low	1	$p_{max} < 150$	
	Medium			2	$150 \leq p_{max} \leq 300$		
	High			3	$p_{max} > 300$		
Vapor	Equivalent air thickness S_d [mm]	Low	1	$S_d < 0.14$			
		Medium	2	$0.14 \leq S_d \leq 1.4$			
		High	3	$S_d > 1.4$			
Long-term	Durability	-	Estimated Service Life ESL [years]	Low	1	$ESL < 50$	
				Medium	2	$50 \leq ESL \leq 80$	
				High	3	$ESL > 80$	
	Sustainability	-	Embodied carbon EC [kg CO ₂ / kg material]	Low	1	$EC > 3.5$	
Medium				2	$2 \leq EC \leq 3.5$		
High				3	$EC < 2$		
Non-Technical	Cost	Construction cost	-	Cost C [% of total building cost]	Low	1	$C > 15\%$
					Medium	2	$5\% \leq C \leq 15\%$
					High	3	$C < 5\%$

⁽¹⁾ L_1 is the length of the horizontal element of the frame system supporting the component.

⁽²⁾ L_2 is the distance between two consecutive points where the component is connected to the structure.

⁽³⁾ For defining more general limiting values, the seismic performance is herein described in terms of EAL_{nsc} .

⁽⁴⁾ Transmittance limits for opaque vertical elements.

⁽⁵⁾ Transmittance limits for transparent vertical components.

Table 9.2. Chosen weights to be attributed to the different interests/sub-interests.

Interest		W_i	Sub interest	W_s
Technical	Structural	W_{str}	Static - Vertical	W_1
			Static - Wind	W_2
			Dynamic	W_3
			Fire	W_4
	Architectural	W_{arc}	Thermal	W_5
			Acoustic	W_6
			Air Tightness	W_7
			Water Tightness	W_8
			Vapor Tightness	W_9
	Long-term	W_{lt}	Durability	W_{10}
			Sustainability	W_{11}
Non-technical	Cost	W_{cc}	Construction cost	W_{12}

It is highlighted that the different weights to the various interests and sub-interests are assigned in function of the decision to make. E.g. considering the interests, if the building has commercial use more weight is attributed to the architectural aspects, while if the building is a health facility, more importance is given to the safety conditions thus a greater weight is assigned to the structural performance. E.g. concerning the sub-interests, for designing internal partitions, the decision is influenced by the building internal use thus more weight can be assigned to the acoustic criterion when compared to the other criteria if a good sound insulation is required (i.e. for a music academy) or more attention is given to the fire performance if the partitions delimit a library.

- Finally, a final score is assigned to each non-structural alternative as follows:

$$Score = \sum_{i=1}^n r_{ij} w_i \text{ for } j = 1, 2, 3$$

Where: n is the number of the decision criteria, r_{ij} represents the value (1, 2 or 3) of the i -th criterion, while w_i the weight of importance of each sub-criterion.

9.3.3 Application of the proposed MCDM

In this section, the proposed multi-criteria decision analysis is applied to identify the optimal façade system among various alternatives. Referring to the same case-study building - 5-storey reinforced concrete structure - analysed in Chapter 5 in terms of seismic performance whilst in Chapter 8 in terms of thermal behaviour, the decision will be related to the exterior vertical enclosure to use for covering the structural skeleton of this commercial and residential building comprising seismic frames in one direction and seismic walls in the opposite direction (see Chapter 5 for more details). Three alternative typologies of façade are compared: unreinforced masonry infill walls vs. precast concrete cladding systems vs. spider glazing curtain walls.

Following the MCDM procedure, the parameters describing each non-structural performance as well as the initial construction cost are initially estimated with the aim of rating the different sub-interests (Table 9.3).

Table 9.3. Rating the different alternative façade solutions.

Criteria parameter	Masonry Infill		Precast Concrete Cladding		Spider Glazing	
	Value	Pts	Value	Pts	Value	Pts
Deflection v_1 [mm]	0.60	3	0.72	3	0.18	3
Deflection v_2 [mm]	0.33	3	0.93	3	18.00	1
Expected Annual Losses EAL_{nsc} [%]	2.53	1	0.61	2	0.16	3
Fire resistance EI	120	3	120	3	60	2
Transmittance U [W/m ² K]	0.48	1	0.35	1	5.48	1
Sound reduction R [dB]	55	2	47	2	45	2
Equivalent air thickness S_d [mm]	2.25	3	6.40	3	>>	3
Estimated Service Life ESL [years]	50	2	50	2	50	2
Embodied carbon EC [kgCO ₂ / kg material]	2.30	2	3.75	1	2.64	2
Cost C [% of total building cost]	1.42	3	4.55	3	14.87	2

Apart from the seismic and thermal performance, already studied in previous investigations (Chapters 5 and 8), all the other values of Table 9.3 are calculated using the formulas presented in the initial section of this Chapter or assuming values from catalogues found on the different typologies of façade system. Concerning the embodied carbon calculation reference is made to the ICE V2.0 database, while for the estimation of the initial construction cost both the national price list for material components and suggestions from the contractors that supplied the material for the SERA research project are taken into account. It is also highlighted that regarding the weather tightness, only the vapor tightness is reported as value because the air and water tightness are assumed to be designed for guaranteeing medium performance for all the façade solutions, thus they do not influence the final decision.

Then, weights are assigned to all the interests and sub-interests as presented in Table 9.4. In this table more weight is now attributed to the architectural aspects because the building use is commercial for the first two floors and residential for the other two, while the weights of the different sub-criteria are defined taking into account considerations related to building site. It is observed that the weights are linked to the personal preferences, therefore each board member taking the decision assigns his/her own weight to each interest or sub-interest.

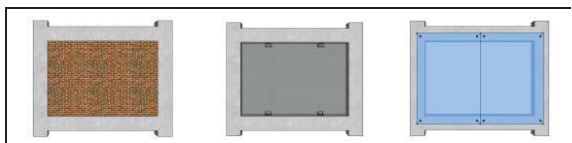
Table 9.4. Weights assigned to each interest and sub-interest.

Interest		W_i	Sub interest	W_s
Technical	Structural	30	Static - Vertical	30
			Static - Wind	20
			Dynamic	25
			Fire	25
	Architectural	40	Thermal	40
			Acoustic	30
			Air tightness	35
			Water tightness	35
			Vapor Tightness	15
	Long-term	10	Durability	10
			Sustainability	8
Non-technical	Cost	20	Construction cost	20

Finally, the final score can be calculated for each façade solution and the optimal system among all the alternatives can be identified (Table 9.5). For the assigned weights the best solution is now represented by the implementation of precast concrete cladding systems. The building envelopes compared in the table are the so-called traditional elements presented in Chapter 5, that is typical construction-practice systems for these typologies of façade: monolithic infill walls made of bricks bounded by mortar, precast panels connected to the structural system using bearing (bottom) and tie-back (top) connections, spider glazing curtain walls attached through X-shape spider connectors to the building skeleton.

Table 9.5. Determining the final score of each façade solution.

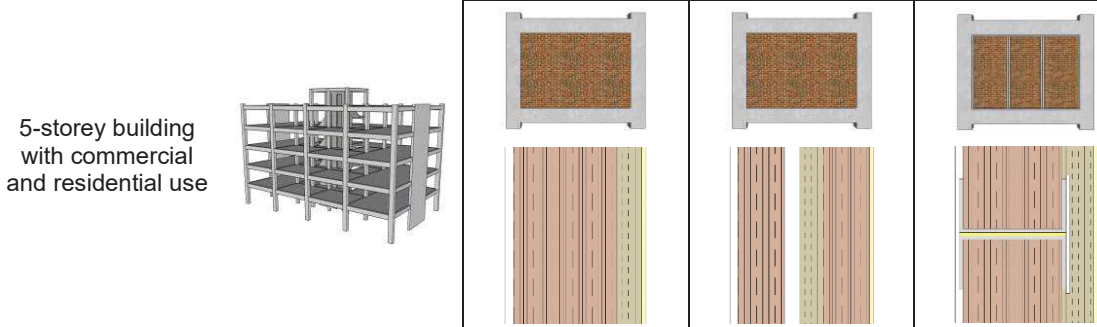
Sub interest	W _s	Rating			Score		
Static – Vertical load	30	3	3	3	90	90	90
Static – Wind load	20	3	3	1	60	60	20
Dynamic	25	1	2	3	25	50	75
Fire	25	3	3	2	75	75	50
Thermal	40	1	1	1	40	40	40
Acoustic	30	2	2	2	60	60	60
Air Tightness	35	2	2	2	70	70	70
Water Tightness	35	2	2	2	70	70	70
Vapor Tightness	15	3	3	3	45	45	45
Durability	10	2	2	2	20	20	20
Sustainability	8	2	1	2	16	8	16
Construction cost	20	3	3	2	60	60	40
					631	648	596



Focusing on the infill wall solution, it is now highlighted how simple detailing modifications can change the final decision. Particularly, comparing the traditional solution to the optimal energy

efficient solution proposed in Chapter 8 and to the low-damage rocking infill system described in Chapter 5 new results are obtained as presented in Tables 9.6 and 9.7.

Table 9.6. Rating the different alternatives of infill walls.



Criteria parameter	Traditional		Low-damage		Low-damage with internal cavity	
	Value	Pts	Value	Pts	Value	Pts
Deflection v_1 [mm]	0.60	3	0.60	3	0.66	3
Deflection v_2 [mm]	0.33	3	0.33	3	0.30	3
Expected Annual Losses EAL_{nsc} [%]	2.53	1	2.53	1	0.24	3
Fire resistance EI	120	3	120	3	90	3
Transmittance U [W/m^2K]	0.48	1	0.28	2	0.50	1
Sound reduction R [dB]	55	2	55	2	55	2
Equivalent air thickness S_d [mm]	2.25	3	2.25	3	2.25	3
Estimated Service Life ESL [years]	50	2	50	2	50	2
Embodied carbon EC [$kgCO_2/kg$ material]	2.30	2	2.30	2	3.67	1
Cost C [% of total building cost]	1.42	3	1.42	3	1.71	3

It is observed that the second option of infill wall system has the same weight of the traditional solution, the only difference is related to the presence of an internal air cavity in the wall which increases the thermal behaviour of the system, thus the corresponding rating value moves from 1 to 2. While, for the low-damage infill wall system the various performance parameters need to be re-determined, apart from the sound reduction, same of the traditional system because proper measures maintaining that level of performance are assumed to be introduced, as well as the equivalent air thickness and the estimated building life, equal for all the three alternatives. Nevertheless, the low-damage solution increases the score due to the seismic performance (from 1 to 3) whilst reduces the ones related to the thermal and sustainability performance (from 2 to 1), due

to the introduction of the steel sub-frame. However, as observed from Table 9.7, the final score provides as best result this low-damage solution, also if with a limited margin when compare to the second option.

Table 9.7. Determining the final score of different infill wall solutions.

Sub interest	W _s	Rating			Score		
Static – Vertical load	30	3	3	3	90	90	90
Static – Wind load	20	3	3	3	60	60	60
Dynamic	25	1	1	3	25	25	75
Fire	25	3	3	3	75	75	75
Thermal	40	1	2	1	40	80	40
Acoustic	30	2	2	2	60	60	60
Air tightness	35	2	2	2	70	70	70
Water tightness	35	2	2	2	70	70	70
Vapor Tightness	15	3	3	3	45	45	45
Durability	10	2	2	2	20	20	20
Sustainability	8	2	2	1	16	16	8
Construction cost	20	3	3	3	60	60	60
					631	671	673




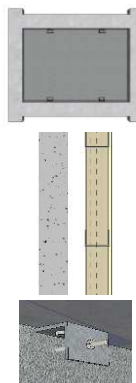
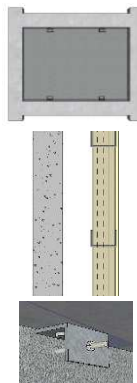
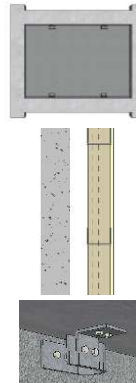
Summarizing, a solution not adding many additional construction costs could be implemented for increasing the building safety, consequently reducing the potential risk to life safety. Notwithstanding for the building use more weight is now assigned to the architectural performance, which can be however improved for the low-damage masonry wall by the introduction of a timber sub-frame instead of a steel system, the application of such type of solutions (low-damage technologies) can become important for those structures attributing more importance to the building safety, such as health facilities. In fact, in this case the weights can be re-assigned, and the final choice may change.

For example, considering the optimal façade system obtained for the 5-storey structure (precast concrete claddings), when applying the energy-efficient system proposed in Chapter 8, this solution becomes the optimal strategy (Table 9.8). While, if the building use changes and a health facility is considered the weights are re-assigned to the interests and sub-interests and the optimal solution becomes the cladding system comprising the upper energy dissipative connections (Table 9.9), as proposed in Chapter 5. The introduction of these devices creates a high seismic performance system comparable as cost to a traditional solution.

Table 9.8. Determining the final score of the precast concrete alternatives – Commercial/residential building.

5-storey building
with commercial
and residential use











Sub interest	W_s	Rating			Score		
Static – Vertical load	30	3	3	3	90	90	90
Static – Wind load	20	3	3	3	60	60	60
Dynamic	25	2	2	3	50	50	75
Fire	25	3	3	3	75	75	75
Thermal	40	1	2	1	40	80	40
Acoustic	30	2	2	2	60	60	60
Air tightness	35	2	2	2	70	70	70
Water tightness	35	2	2	2	70	70	70
Vapor Tightness	15	3	3	3	45	45	45
Durability	10	2	2	2	20	20	20
Sustainability	8	1	1	1	8	8	8
Construction cost	20	3	3	3	60	60	60
					648	688	673

Table 9.9. Determining the final score of the precast concrete alternatives – Health facility structure.

5-storey building
with health facility
function



Sub interest	W _s	Rating			Score		
Static – Vertical load	40	3	3	3	120	120	120
Static – Wind load	30	3	3	3	90	90	90
Dynamic	35	2	2	3	70	70	105
Fire	35	3	3	3	105	105	105
Thermal	30	1	2	1	30	60	30
Acoustic	20	2	2	2	40	40	40
Air tightness	25	2	2	2	50	50	50
Water tightness	25	2	2	2	50	50	50
Vapor Tightness	10	3	3	3	30	30	30
Durability	10	2	2	2	20	20	20
Sustainability	8	1	1	1	8	8	8
Construction cost	20	3	3	3	60	60	60
					673	703	708

As already highlighted, the decision to solve through the MCDM procedure is affected by the weights assigned to each criterion and sub-criterion and different aspects influence their definition. First of all, the weights are linked to the personal preferences of each decision maker, then different conditions can change the attribution of the weights, such as the site where the building is located or the building use or a specific request from the stakeholder/building owner asking for the problem.

9.4 Conclusions

The Chapter has provided an overview of all the performance measures describing the non-structural behaviour. The key parameters representing each performance are initially presented and references to the international/national codes and guidelines providing information on the methodology or formulas to be used for calculating these factors and for defining rating systems to the various performance are indicated. Then, an initial simplified Multi-Criteria Decision-Making (MCDM) analysis is proposed to be used for making decisions on the design or retrofit of non-structural components, i.e. for defining the best option among different alternatives. The suggested methodology includes as criteria and sub-criteria all the non-structural performance, however at least the non-technical aspect related to the component construction cost is introduced to influence the final decision. The proposed approach can be obviously improved using more refined MCDM procedures as well as introducing other non-technical considerations which are important for non-structural elements, such as the aesthetics of the component or the maintenance cost.

Therefore, this Chapter has highlighted the importance of implementing a multi-criteria analysis, developed considering a multi-performance evaluation, for making decisions on non-structural components. Different aspects influence this decision, nevertheless it is fundamental to include into the selecting criteria the seismic performance of the component, because this parameter can substantially influence the choice of the typology of component and its detailing when the building is located in either high or low seismicity areas.

9.5 References

- Balcomb J.D., Curtner A. (2000). Multi-Criteria Decision-Making - process for Buildings, to be presented at the *American Institute of Aeronautics and Astronautics Conference*, Las Vegas, Nevada.
- BREEAM, <http://www.breeam.org>.
- Caruso M.C., Menna C., Asprone D., Prota A., Manfredi G. (2017). Methodology for Life-Cycle Sustainability Assessment of Building Structures, *ACI Structural Journal*, 114(2).
- CASBEE, Comprehensive Assessment System for Built Environment Efficiency, Japan, <http://www.ibec.or.jp/CASBEE/english>.
- Caterino N., Iervolino I., Manfredi G., Cosenza E. (2008). Multi-criteria decision making for seismic retrofitting of RC structure, *Journal of Earthquake Engineering*, 12: 1–29.
- Caterino N., Iervolino I., Manfredi G., Cosenza E. (2009). Comparative Analysis of Multi-Criteria Decision-Making Methods for Seismic Structural Retrofitting, *Computer-Aided Civil and Infrastructure Engineering*, 24: 432–445.
- CVVF 5043 (2013). *Requisiti di sicurezza antincendio delle facciate negli edifici civili – Aggiornamento*, Lettera circolare, Dipartimento dei Vigili del Fuoco, del Soccorso Pubblico e della Difesa Civile, Rome, Italy.
- Dan M.D.B (2004). *Multi-criteria decision model for retrofitting existing buildings*. *Natural Hazards and Earth System Science*, Copernicus Publications on behalf of the European Geosciences Union, 4(4): 485-499.
- DGNB, German Sustainable Building Council, <http://www.dgnb.de/en>.
- DM 16/02/2007 (2007). *Classificazione di resistenza al fuoco di prodotti ed elementi costruttivi di opere da costruzione*, Suppl. Ord. G.U. n. 74 29/03/2007, Rome, Italy.
- DM 58 (2017). *Linee guida per la classificazione del rischio sismico delle costruzioni*, Decreto Ministeriale 58 del 28/02/2017, Rome, Italy.
- DPCM 05/12/1997 (1997). *Determinazione dei requisiti acustici passivi degli edifici*, Italian standards, Italy.
- DPR 59/09 (2009). *Regolamento di attuazione dell'articolo 4, comma 1, lettere a) e b), del decreto legislativo 19 agosto 2005, n. 192, concernente attuazione della direttiva 2002/91/CE sul rendimento energetico in edilizia*, Italian standards, Rome, Italy.
- EN 13116 (2001). *Curtain walling - Resistance to wind load - Performance requirements*, European standards, Brussels, Belgium.
- GBC, World Green Building Council, London, England, <http://www.worldgbc.org>.
- HQE, <http://www.behqe.com/5>. DGNB, German Sustainable Building Council, <http://www.dgnb.de/en>.
- Hwang C.L., Yoon K. (1981). *Multiple Attribute Decision Making: Methods and Applications, A State-of-the-Art Survey*, Springer-Verlag, New York.
- ICE V2.0 (2011). Inventory of Carbon & Energy database, <http://www.carbonsolutions.com>.
- International Initiative for a Sustainable Built Environment, SB Tool, <http://iisbe.org/sbtool-2012>.

- ISO 15686-1 (2000). *Buildings and constructed assets — Service life planning — Part 1: General principles*, International Organization for Standardization, Geneva, Switzerland.
- ISO 15686-2 (2012). *Buildings and constructed assets — Service life planning — Part 2: Service life prediction procedures*, International Organization for Standardization, Geneva, Switzerland.
- ISO 14040 (2006). *Environmental Management - Life Cycle Assessment - Principles and Framework*, International Standards Organization, Geneva, Switzerland.
- ITACA Italia Protocol, Roma, Italy, http://www.itaca.org/valutazione_sostenibilts.asp.
- Marteinsson B. (2005). *Service life estimation in the design of buildings - A development of the factor method*, PhD Thesis, Department of Technology and Built Environment, University of Gävle, Sweden.
- Mattevi L. (2005). *Requisiti acustici degli edifici – Metodi di calcolo, Normativa, Accorgimenti, Giurisprudenza. Manuale tecnico-pratico*.
- Mela K., Tiainen T., Heinisuo M. (2012). Comparative study of multiple criteria decision making methods for building design, *Advance Engineering Informatics*, 26(4): 726-726.
- Moghtadernejad S., Chouinard L.E., Mirza M.S. (2018). Multi-criteria decision-making methods for preliminary design of sustainable facades, *Journal of Building Engineering*, 19: 181-190.
- Mosalam K.M., Alibrandi U., Lee H., Armengou J. (2018). Performance-based engineering and multi-criteria decision analysis for sustainable and resilient building design, *Structural Safety*, 74: 1-13.
- Saaty T.L. (1980). *The Analytic Hierarchy Process*, McGraw-Hill, New York.
- UNI 11156-1 (2006). *Valutazione della durabilità dei componenti edilizi - Parte 1: Terminologia e definizione dei parametri di valutazione*, Italian standards, Milan, Italy.
- UNI 11156-3 (2006). *Valutazione della durabilità dei componenti edilizi - Parte 3: Metodo per la valutazione della durata (vita utile)*, Italian standards, Milan, Italy.
- UNI EN 12152 (2003). *Facciate continue - Permeabilità all'aria - Requisiti prestazionali e classificazione*, Italian standards, Milan, Italy.
- UNI EN 12153 (2002). *Facciate continue - Permeabilità all'aria - Metodo di prova*, Italian standards, Milan, Italy.
- UNI EN 12154 (2001). *Facciate continue - Tenuta all'acqua - Requisiti prestazionali e classificazione*, Italian standards, Milan, Italy.
- UNI EN 12155 (2002). *Facciate continue - Tenuta all'acqua - Prova di laboratorio sotto pressione statica*, Italian standards, Milan, Italy.
- UNI EN 12179 (2002). *Facciate continue - Resistenza al carico del vento - Metodo di prova*, Italian standards, Milan, Italy.
- UNI EN 13050 (2011). *Facciate continue - Tenuta all'acqua - Prova di laboratorio in condizioni dinamiche di pressione dell'aria e di proiezione d'acqua*, Italian standards, Milan, Italy.

UNI EN 13051 (2002). *Facciate continue - Tenuta all'acqua - Prova in sito*, Italian standards, Milan, Italy.

UNI EN 13116 (2002). *Facciate continue - Resistenza al carico del vento - Requisiti prestazionali*, Italian standards, Milan, Italy.

UNI EN 13947 (2007). *Prestazione termica delle facciate continue - Calcolo della trasmittanza termica*, Italian standards, Milan, Italy.

UNI EN ISO 12354-3 (2017). *Acustica in edilizia - Valutazioni delle prestazioni acustiche di edifici a partire dalle prestazioni dei prodotti - Parte 3: Isolamento acustico dal rumore proveniente dall'esterno per via aerea*, Italian standards, Milan, Italy.

UNI EN ISO 13788 (2013). *Prestazione igrotermica dei componenti e degli elementi per edilizia - Temperatura superficiale interna per evitare l'umidità superficiale critica e la condensazione interstiziale - Metodi di calcolo*, Italian standards, Milan, Italy.

UNI EN ISO 717-1 (2013). *Acustica - Valutazione dell'isolamento acustico in edifici e di elementi di edificio - Parte 1: Isolamento acustico per via aerea*, Italian standards, Milan, Italy.

U.S. Green Building Council, Washington, DC, <http://www.usgbc.org/leed>.

Zavadskas E.K., Antucheviciene J., Saparauskas J., Turskis Z., Multi-criteria Assessment of Facades' Alternatives: Peculiarities of Ranking Methodology, *Procedia Engineering*, 57: 107-112.

10. Conclusions and recommendations for future work

10.1 Introduction

Damage reports from past earthquakes have highlighted the poor seismic performance of non-structural components, typically designed for providing architectural functions only instead of being resistant to earthquake shakings. As either the earthquake engineering community or the public demand higher level of earthquake protection, it becomes fundamental to protect both the structural skeleton and the non-structural systems from extensive damage. Therefore, innovative damage-resistant solutions have been recently developed with the aim of improving the seismic performance of these building elements, consequently reducing the related socio-economic losses.

After an initial investigation on the seismic vulnerability of different typologies of non-structural systems, the Thesis has provided evidence on the benefits related to the implementation of low-damage non-structural techniques through either numerical (cost/performance-based evaluations) or experimental (shaking table tests) investigations. Finally, including the seismic performance within a more general design framework, the importance of applying a multi-performance approach for the design of new components or the retrofit of existing systems has been highlighted.

Going through the different research scopes and objectives, this Chapter summarizes the key outcomes of the work. Limitations to the research work are also identified while recommendations for future developments are suggested.

10.2 Research conclusions

Non-structural components are not generally designed for seismic loads, nevertheless their response can significantly affect the building functionality after earthquakes, even for low-intensity events. The seismic behavior of traditional non-structural elements can result in substantial economic losses and business interruption after earthquakes. Consequently, as further highlighted by recent seismic events, the damage of these components has severe impact in the post-earthquake building recovery in addition to the potential risk to life safety.

Improving the seismic performance of structural systems is not enough for raising the bar towards the earthquake-proof building that the current society awaits, and expectations of advanced seismic behaviour for non-structural components are also demanded. Therefore, within the performance-based seismic design philosophy the attention is nowadays focused on two main issues: 1) the harmonization of performances between structural and non-structural elements, 2) the development of damage-control or low-damage structural and non-structural innovative technological solutions.

The need for reduction of non-structural seismic risk is becoming evident not only in the academic or scientific research field but it is also being recognized fundamental in the decision-making process. Thus, the development of cost-effective, low-invasive and practical solutions for both the design and the retrofit of non-structural systems is urgently required.

This Thesis has intended to highlight the importance of including the investigation of the seismic performance into the design process of non-structural elements and mainly to provide evidence on the high benefits related to the implementation of innovative low-damage technologies for non-structural components. However, the key outcomes and limitations from the developed research are herein summarized.

10.2.1 Study of the seismic behaviour of non-structural elements

Summary

A literature review has been carried out to investigate the seismic response of non-structural components (facades, partitions, ceilings, building services and contents). Collecting information from past damage reports, laboratory testing, analytical/numerical investigations, a state-of-the-art overview of the mechanisms and damage states developing

in the non-structural systems during earthquake shakings is initially provided, then, fragility specifications are collected for some typologies of non-structural elements.

In order to facilitate the quantification of damage levels as well as the proposal of efficient damage-resistant technologies, a collection of key parameters (mechanisms, damage states, fragility curves) for each non-structural system is needed. In fact, in the definition of a non-structural damage-mitigation solution, the knowledge of the single-component/global-system behaviour is fundamental to help determining which parameters influence the failure modes and at which demand level a damage state is expected to be achieved (Figure 10.1).

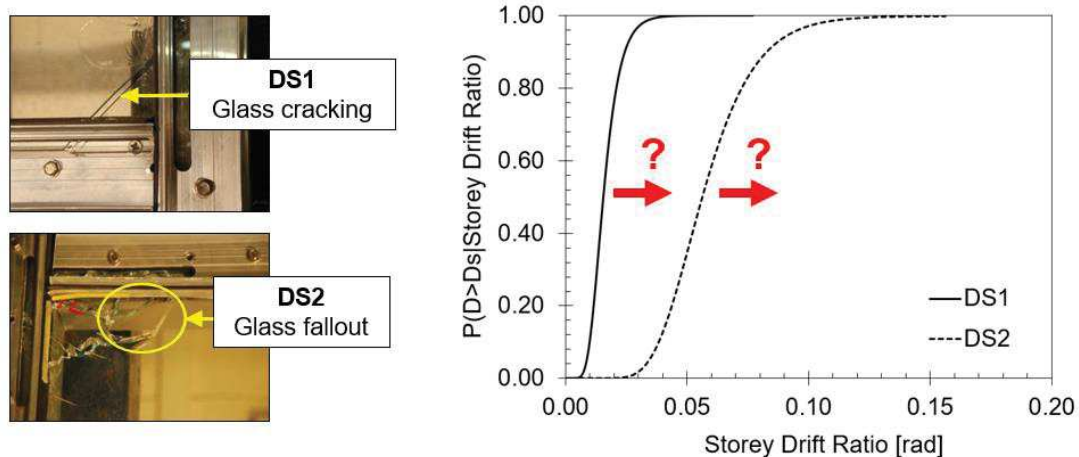


Figure 10.1. Example of fragility curves for a midrise stick-built curtain wall (source: FEMA P-58 2012) and pathway for improving the seismic behaviour.

Limitations

Due to the broad spectrum of alternative configurations available for each typology of non-structural system, mainly depending on the construction practice of the countries where the components are built, collecting fragility curves of non-structural components is not so simple. In fact, the fragility curves vary in function of the system details, i.e. the behaviour of a glass façade is influenced by the framing detailing, glass-to-frame clearance, system type, glass type, panel dimensions, glass thickness, and not for all the possible configurations experimental testing or other data are available for defining the fragility functions.

However, general considerations on the expected behaviour of a system can be identified taking into account the collected fragility specifications and, as previously anticipated, this knowledge can help in the proposal of new solutions.

10.2.2 Provide evidence on the benefits of innovative low-damage technologies

Summary

Numerical and experimental investigations have been carried out to prove the efficiency of low-damage solutions in improving the seismic performance (mitigating the risk to damage) and reducing the expected post-earthquake losses. The study has focused on either the non-structural elements or the overall integrated structural & non-structural system.

- **Cost/performance-based evaluation**

Regarding the numerical investigation, cost/performance-based evaluations of multi-storeys reinforced concrete buildings, comprising alternative combinations of traditional vs. low-damage solutions for both skeleton (frames and walls) and non-structural elements (heavy/light facades, heavy/light partitions, ceilings) have been performed. Loss assessment analyses, with input data provided by numerical push-over analyses and a capacity spectrum approach, confirm the significant benefits of implementing damage-mitigation technologies for buildings located in both high and low seismicity zones, in terms of either time-based results (Expected Annual Losses) or intensity-based results, i.e. repair costs, downtime and resilience curves at different intensity levels.

The integrated low-damage structural/non-structural systems, for example, can provide savings in the range of 150-300 €/m² during the 50-years building-life and downtime reductions at ULS in the order of 2-7 months. However, notwithstanding the benefits in the use of the sole damage-resistant structural members are evident, low-damage non-structural elements lead to a considerable reduction of repair costs and downtime, especially for heavy infill walls for the condition of low-seismicity design (i.e. direct savings of about 220 €/m² in a 50-years building life; a downtime reduction of about 8 months under the design level earthquake).

Within the performance-based study, risk assessment analyses of precast concrete cladding systems have also been implemented, i.e. Incremental Dynamic Analyses (IDA)

performed to define the fragility curves of cladding systems composed of traditional vs. low-damage connections. Thus, the convenience of implementing the damage-resistant solution can be further shown in terms of probability of damage levels not being exceeded.

- **Experimental testing on damage-resistant solutions**

Two different experimental campaigns have been carried out to prove the high seismic performance of low-damage techniques. The first campaign has involved 1D shaking table testing on post-installed fasteners, which commonly represent the weakest part of restraint non-structural systems, while the second campaign has involved 1D/2D/3D shaking table tests of a half scaled low-damage structural/non-structural building system (SERA Project).

The experimental campaign on post-installed fasteners has been performed to confirm the beneficial effects of the concept of dissipative anchor rod to seismically protect the non-structural components for a greater variety of fastening systems (expansion and chemical anchors) in both un-cracked and cracked concrete. A low-damage solution (EQ-Rod 2.0) has been proposed and studied through shaking table testing developed at the University of Rome “La Sapienza” (Figure 10.2, left).



Figure 10.2. Left: Experimental campaign carried out at the Structural Laboratory of the University of Rome on post-installed anchors; Right: Experimental campaign carried out at the Laboratório Nacional de Engenharia Civil (LNEC) in Lisbon - Phase 3 of experimental testing.

Experimental results have shown that the proposed solution is able to reduce the accelerations and forces onto the connected non-structural component, with values of 10-40% of reduction when compared to the traditional system, thus it can be considered a damage-control solution for such type of applications.

The second experimental campaign has focused on the shake table tests of a 1:2 scale two storey-two bay low-damage building system, consisting of a low-damage timber-concrete structural skeleton (frames in one direction and walls in the other) and alternative non-structural components/envelopes (Figure 10.2, right). The design of the specimen and its detailing (structural/non-structural), the manufacturing and construction processes, the preliminary results (global and local seismic response) are presented in Chapters 6 and 7 of the Thesis, focusing the description on the non-structural systems tested during all the different project phases. The experimental investigation has highlighted the benefits of applying low-damage and high-performance solutions for different typologies of non-structural systems (gypsum and masonry partitions, GFRC and glass facades) as well as the convenience of implementing an integrated low-damage structural/non-structural system. The project has intended to promote a research effort within the European environment for the wider industry/community uptake of an integrated low damage solution, including skeleton and non-structural components, for the next generation of buildings.

Limitations

- **Cost/performance-based evaluation**

The results of the cost/performance-based investigations are obtained through 2D pushover analysis and a capacity spectrum approach, however they can be further improved by the implementation of 3D numerical models and carrying out time-history non-linear analyses. Nevertheless, as highlighted in **Appendix B**, the numerical push-over approach provides acceptable estimations of the post-earthquake losses when compared to more sophisticated time-history analyses.

Further investigations are also required to develop ad-hoc consequence functions for low-damage structural and non-structural systems. In fact, the consequence time and cost functions are fundamental in order to obtain good estimations of repair costs and time, and these functions have not been yet defined for low-damage technologies, apart from the ones found in literature for precast concrete systems. Nevertheless, considering that the consequence functions used for the cost/performance-based evaluations have been developed from the curves available for traditional solutions taking into account the achievement of specific damage conditions, results can be considered acceptable for the non-structural components. While, reduced post-earthquake losses can be obtained if ad-hoc functions for the low-damage structural members are defined. In fact, the expected repair

actions (replacement of external dissipaters) are surely less invasive when compared to the traditional monolithic solution.

- **Experimental testing on damage-resistant solutions**

The experimental campaigns have been carried out following specific test matrices, properly defined in order to achieve specific scopes and to respect pre-determined timelines. For the second experimental campaign, just preliminary results are presented within the Thesis, however more investigations on the experimental study are expected to be developed in the future work.

10.2.3 Definition of a multi-performance design approach for non-structural components

Summary

Non-structural components are generally designed for architectural performance, such as thermal or weather tightness for a façade, while the seismic performance is typically neglected in the common design practice or is less considered when compared to the other performance quantities.

- **Integrated seismic&energy cost/performance-based analysis**

With the aim of highlighting the importance of including the study of the seismic behaviour when designing a non-structural system, a combined seismic and energy cost/performance-based evaluation has been implemented. Numerical investigations through *Rhinoceros 3D/Grasshopper (Energy Plus and Therm)* software have been carried out to study the energy performance of a multi-storey reinforced concrete building located in Reggio Calabria and comprising alternative façade solutions. The energy study has been combined with the seismic investigation to determine the optimal design for the non-structural detailing. The study has highlighted that the seismic losses can be very high when compared to the energy losses and that the seismic response can rule the design. Therefore, the application of low-damage non-structural solutions, related to simple detailing modifications and cost-comparable to traditional systems, can lead to substantial economical savings during the overall building life (around 45% for the configuration with external masonry infill walls).

- **Multi-Criteria Decision Analysis for non-structural design**

Non-structural systems should be designed following a multi-criteria approach including the overall performance of the component (thermal, acoustical, weather tightness, seismic, fire, wind, durability, sustainability). This approach is not yet applied in the common practice, while it can bring to the identification of the optimal non-structural detailing depending on the priority given during the design (criteria weights assigned to each performance) and mainly related to the building site and use.

An initial simplified Multi-Criteria Decision-Making (MCDM) analysis is thus proposed to be used for making decisions on the design or retrofitting of non-structural components, i.e. to define the best option among various alternatives. The suggested analysis includes as criteria and sub-criteria all the non-structural performance parameters (Figure 10.3), and the non-technical aspect related to the initial construction cost. Some examples of application of such type of approach are provided to demonstrate how the MCDM, depending on the assigned weights, can influence the choice of the component detailing.

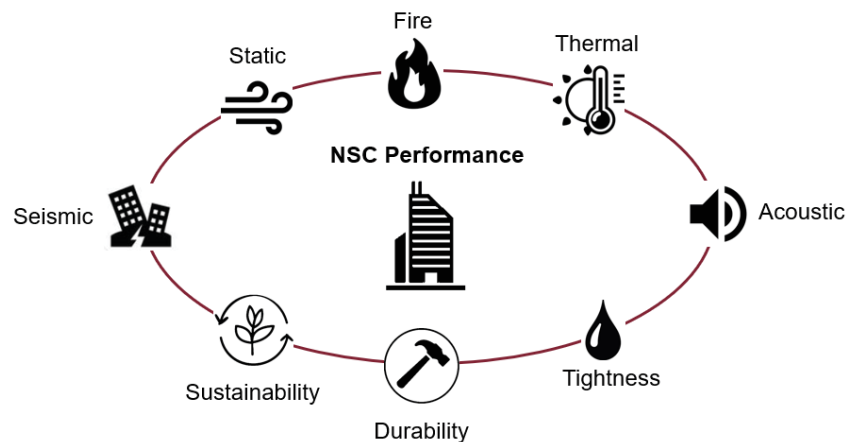


Figure 10.3. Performance characterizing the non-structural behaviour.

Limitations

- **Integrated seismic&energy cost/performance-based analysis**

The energy study has been carried out through dynamic simulations and finite element methods, which are the most refined methodologies adopted for estimating the thermal load and energy losses of a building. The results of these analyses have been combined with the results from the seismic investigation implemented using push-over analysis and an ADRS

approach, which, as anticipated, provide good results, however, they do not represent the most refined methods to be used for estimating the seismic losses.

It is also observed that the energy performance analysis has been developed assuming default values for the heating systems, cooling systems, etc., whose behaviour highly influence the energy losses of a building, as well as applying “energy efficiency” solutions defined from simple detailing modifications to façade systems already characterized by good thermal performance, apart from the glass façade. While, alternative and more efficient technologies could be applied at both global (building) and local (enclosure) levels to obtain more energy savings. Nevertheless, the implemented investigation has aimed to show how simple detailing modifications, i.e. a solution cost-comparable to the initial system, cannot be useful to improve the energy response whilst can be very efficient in achieving higher levels of seismic performance.

- **Multi-Criteria Decision Analysis for non-structural design**

As already observed in the previous Chapter, the proposed Multi-Criteria Decision-Making analysis should be improved to be applicable in the common practice. In fact, a more refined MCDM procedure should be used as well as other non-technical criteria introduced. If more refined MCDM approaches are already available from literature to be implemented, regarding the introduction of additional criteria and sub-criteria, they could be defined considering suggestions from building owners/stakeholders and architects who commonly make decisions on such type of problems. However, the proposed procedure is simple to be applied in feasibility studies of new or retrofitted non-structural solutions. Furthermore, it has been developed to prove the importance of including the seismic study within this complete approach.

10.3 Future developments

The research developed within this Thesis suggests the following studies, herein recommended as main future works. As a continuous of the Thesis, part of this research is already developing.

➤ *Collection of fragility specifications for the Italian cases*

The fragility databases used nowadays for implementing loss assessment analysis refer to fragility and consequence functions of American construction-practice components. Therefore, for the aim of the research, that is comparing different solutions looking at the savings in the total building life or the downtime reduction, the application of such database is suitable. While, if the scope is estimating the post-earthquake losses of a building, the fragility specifications should be related to the specific components included within the building system. For the specific case of Italian solutions, it is recommended to work in the future for gathering all the data available from literature and build a new fragility database for the Italian solutions. E.g. consequence functions of the Italian cases can be build referring to the documentation developed after past and more recent earthquakes (e.g. “White Book” after L’Aquila earthquake). The same consideration can be made when considering the estimation of the downtime whose “impeding factor” curves are now available for just the American situation. While, also in this case specific curves can be determined for the Italian case taking into account data from available documentations.

➤ *Development of a fragility-based design*

The seismic design of non-structural systems should be carried out considering a fragility-based approach. Thus, work in the future is recommended for defining a procedure which can allow to design the non-structural detailing taking into account the inter-storey drift ratios or floor accelerations (demand parameters) expected to be achieved for the specific component at different seismic intensity levels. This fragility-based design should include not only in-plane damage states, but also out-of-plane failure considerations, generally neglected in fragility studies while, as also highlighted from experimental testing, the out-of-plane behaviour can highly influence the seismic behaviour of a building component.

➤ *Development of practical user manuals on the low-damage technologies*

Merging considerations on the non-structural performance with economical aspects, a practical, technical and economical user manual to be useful for designers and constructors as well as for owners/stakeholders of the building/facilities should be developed. In fact, notwithstanding the low-damage systems have been studied in different past research works (numerical/experimental), they are not yet applied in the common construction practice, because a standardized design and construction procedure is missing. Looking at the system detailing, standardized practical and efficient damage details/measurements can be defined while additional economical investigations should be implemented for estimating the construction cost/time, thus also providing evidence on the economical convenience related to the implementation of these solutions. These documents can be very useful to help engineers and constructors in building these technologies as well as to address decisions on non-structural seismic risk.

➤ *Convenience of implementing low-damage technologies through a resilience-based approach*

The convenience of applying low-damage technologies has been shown through the comparison of resilience-based curves (first attempt). However, more studies are suggested towards this direction in order to define a procedure that will allow to design a system depending on the level of resilience to be achieved.

➤ *Calibration of numerical modelling and additional studies from the experimental results*

The results from both the experimental campaigns, i.e. the shaking table tests on the post-installed traditional or innovative fasteners and the shaking table tests on the 1:2 scaled integrated structural/non-structural low-damage building system, should be further elaborated. Particularly, numerical models should be properly calibrated basing on the experimental results of both campaigns. Then, more investigations should be carried out for the SERA project results, due to the various non-structural systems included in the low-damage structural skeleton. In fact, more studies on the structural/non-structural interaction, the floor spectra and the behaviour of each non-structural component should be developed. Finally, based on these investigations improvements of the available non-structural detailing can be proposed.

➤ *Refine the combined energy-seismic approach for the design of building systems*

Recent research is moving towards the development of an integrated energy/seismic performance-based approach for selecting the optimal retrofit strategies for structural and non-structural systems. However, this combined approach should also be used in the design of new building systems, especially when different alternatives are available at early stage of the project. Specifically, for non-structural systems this approach is fundamental for driving the final decision. For example, thermal bridging analysis can quantify the decrease of the thermal performance of the low-damage rocking infill walls, whose detailing need to be properly adjusted for maintaining the same level of transmittance.

➤ *Development of a fragility-based analysis for the overall non-structural performance*

For making comparison between alternative non-structural solutions, fragility curves can be a valuable tool. Therefore, as initially proposed for the combined seismic and energy study, fragility functions should be developed to describe the different non-structural behaviour. In fact, taking into account the demand parameters affecting each non-structural response, fragility curves can be derived for the different performance quantities, joint fragility functions determined, and acceptable design levels identified.

➤ *Definition of a Multi-Criteria cost-benefit approach for supporting decisions on non-structural systems*

Future work is recommended to improve the simplified procedure suggested in Chapter 9 of the Thesis. Both technical criteria related to the multi-performance characterizing the non-structural components (i.e. static, dynamic, fire, thermal, acoustic, weather tightness, durability, sustainability) and non-technical criteria, i.e. financial aspects associated with the implementation of non-structural systems, should be included within an ad-hoc cost-benefit analysis approach to facilitate the selection of non-structural systems.

APPENDIX A:

Shake-table tests on post-installed fasteners: Testing procedure and experimental results

A.1 Introduction

This Appendix provides additional information on the testing procedure adopted for the experimental campaign (1D shake table tests) on post-installed anchors (Traditional, Traditional with additional damping - EQ-Rod 2.0 -, Traditional with mortar fillings) in both uncracked and cracked concrete (project report: Pampanin et al. 2017). Particularly, the complete Test Matrix followed during the tests as well as the testing protocols used for the correct installation of either expansion or chemical fasteners in uncracked or cracked concrete can be found.

Finally, tables summarizing the results obtained from the shake-table tests (ground motions) in terms of driving mass accelerations, displacements and forces can be found. The experimental data are elaborated to highlight the reduction of these parameters due to the application of the two different solutions (additional damping, mortar filling) when compared to the traditional system.

A.2 Testing procedure

The test matrices describing the planned series of tests in uncracked and cracked concrete blocks, included in Phase I and II of the experimental campaign are shown (Tables A.1 and A.2). Three different expansion anchors (FAZ II Traditional, FAZ II EQ-Rod and FAZ

II Traditional with Mortar Filling) and three different chemical anchors (Superbond Traditional, Superbond EQ-Rod and Superbond Traditional with Mortar Filling) were tested considering five input motions ($EQ_i + EQ_{i_50}$), i.e. three Far Field earthquake records and two Near Field earthquake records and their simulated aftershocks, assumed as 50% (amplitude-only reduction, same duration) of the input motion, as also described in Tables 4.1 and 4.2 of Chapter 4 of the Thesis. In total, the test matrix consisted of a total number of 360 shake table tests (input + aftershocks), 180 for uncracked concrete and 180 for cracked concrete.

Table A.1. Test Matrix for uncracked concrete blocks.

Concrete	N. Block	N. Line	FAZII			Superbond			Input motion	
			Trad	EQ-Rod	MF	Trad	EQ-Rod	MF		
Uncracked	Block 1	line 1	X	X	X				$EQ_1 + EQ_{1_50}$	
		line 2	X	X	X				$EQ_1 + EQ_{1_50}$	
		line 3	X	X	X				$EQ_1 + EQ_{1_50}$	
	Block 2	line 1	X	X	X				$EQ_2 + EQ_{2_50}$	
		line 2	X	X	X				$EQ_2 + EQ_{2_50}$	
		line 3	X	X	X				$EQ_2 + EQ_{2_50}$	
	Block 3	line 1	X	X	X	PHASE 1			$EQ_3 + EQ_{3_50}$	
		line 2	X	X	X				$EQ_3 + EQ_{3_50}$	
		line 3	X	X	X				$EQ_3 + EQ_{3_50}$	
	Block 4	line 1	X	X	X				$EQ_4 + EQ_{4_50}$	
		line 2	X	X	X				$EQ_4 + EQ_{4_50}$	
		line 3	X	X	X				$EQ_4 + EQ_{4_50}$	
	Block 5	line 1	X	X	X				$EQ_5 + EQ_{5_50}$	
		line 2	X	X	X				$EQ_5 + EQ_{5_50}$	
		line 3	X	X	X				$EQ_5 + EQ_{5_50}$	
	Block 6	line 1				X	X	X	$EQ_1 + EQ_{1_50}$	
		line 2				X	X	X	$EQ_1 + EQ_{1_50}$	
		line 3				X	X	X	$EQ_1 + EQ_{1_50}$	
	Block 7	line 1				X	X	X	$EQ_2 + EQ_{2_50}$	
		line 2				X	X	X	$EQ_2 + EQ_{2_50}$	
		line 3				X	X	X	$EQ_2 + EQ_{2_50}$	
	Block 8	line 1				PHASE 2	X	X	X	$EQ_3 + EQ_{3_50}$
		line 2					X	X	X	$EQ_3 + EQ_{3_50}$
		line 3					X	X	X	$EQ_3 + EQ_{3_50}$
	Block 9	line 1				X	X	X	$EQ_4 + EQ_{4_50}$	
		line 2				X	X	X	$EQ_4 + EQ_{4_50}$	
		line 3				X	X	X	$EQ_4 + EQ_{4_50}$	
	Block 10	line 1				X	X	X	$EQ_5 + EQ_{5_50}$	
		line 2				X	X	X	$EQ_5 + EQ_{5_50}$	
		line 3				X	X	X	$EQ_5 + EQ_{5_50}$	

Table A.2. Test Matrix for cracked concrete blocks.

Concrete	N. Block	N. Line	FAZII			Superbond			Input motion	
			Trad	EQ-Rod	MF	Trad	EQ-Rod	MF		
Cracked	Block 1	line 1	X	X	X				EQ ₁ + EQ _{1_50}	
		line 2	X	X	X				EQ ₁ + EQ _{1_50}	
	Block 2	line 1	X	X	X				EQ ₁ + EQ _{1_50}	
		line 2	X	X	X				EQ ₂ + EQ _{2_50}	
	Block 3	line 1	X	X	X				EQ ₂ + EQ _{2_50}	
		line 2	X	X	X				EQ ₂ + EQ _{2_50}	
	Block 4	line 1	X	X	X				EQ ₃ + EQ _{3_50}	
		line 2	X	X	X			PHASE 1	EQ ₃ + EQ _{3_50}	
	Block 5	line 1	X	X	X				EQ ₃ + EQ _{3_50}	
		line 2	X	X	X				EQ ₄ + EQ _{4_50}	
	Block 6	line 1	X	X	X				EQ ₄ + EQ _{4_50}	
		line 2	X	X	X				EQ ₄ + EQ _{4_50}	
	Block 7	line 1	X	X	X				EQ ₅ + EQ _{5_50}	
		line 2	X	X	X				EQ ₅ + EQ _{5_50}	
	Block 8	line 1	X	X	X				EQ ₅ + EQ _{5_50}	
		line 2					X	X	X	EQ ₁ + EQ _{1_50}
	Block 9	line 1					X	X	X	EQ ₁ + EQ _{1_50}
		line 2					X	X	X	EQ ₁ + EQ _{1_50}
	Block 10	line 1					X	X	X	EQ ₂ + EQ _{2_50}
		line 2					X	X	X	EQ ₂ + EQ _{2_50}
	Block 11	line 1					X	X	X	EQ ₂ + EQ _{2_50}
		line 2					X	X	X	EQ ₃ + EQ _{3_50}
	Block 12	line 1					X	X	X	EQ ₃ + EQ _{3_50}
		line 2					X	X	X	EQ ₃ + EQ _{3_50}
	Block 13	line 1					X	X	X	EQ ₄ + EQ _{4_50}
		line 2					X	X	X	EQ ₄ + EQ _{4_50}
	Block 14	line 1					X	X	X	EQ ₄ + EQ _{4_50}
		line 2					X	X	X	EQ ₅ + EQ _{5_50}
	Block 15	line 1					X	X	X	EQ ₅ + EQ _{5_50}
		line 2					X	X	X	EQ ₅ + EQ _{5_50}

Commenting the previous tables:

- **Table A.1.** 10 concrete blocks were available for the shaking table tests in uncracked concrete of both expansion and chemical anchors. Three parallel lines were identified for each concrete block and per each line the three alternative anchors were installed (see the following Figure A.1). It is also observed that for each earthquake, to have more reliability in the results tests were performed on

three different anchors of the same typology (Traditional, *Trad*, with supplemental damping, *EQ-Rod*, with Mortar Filling, *MF*).

- **Table A.2.** For the tests on cracked concrete, 15 concrete blocks were used. Due to the presence of two parallel cracks in each concrete block (see the following Figure A.3), for each line the three types of anchor were installed and tested. As before, also for cracked concrete more reliable results were obtained performing for each earthquake tests on three different anchors of the same typology (Traditional, *Trad*, with supplemental damping, *EQ-Rod*, with Mortar Filling, *MF*).

As already described in Chapter 4, the shaking table tests were carried out in two different phases:

- *Phase 1*, all the tests were performed on uncracked and cracked concrete as well as considering the different types of expansion (FAZ II) fastener;
- *Phase 2*, all the tests were performed on uncracked and cracked concrete as well as considering the different types of chemical (Superbond) fastener.

The installation of the anchors in the concrete blocks was a crucial phase for the experimental campaign. In fact, test results are directly affected by the installation operation of the fasteners, therefore for each typology of anchor the installation procedure was applied in a rigorous manner. These procedures are described below for both expansion and chemical anchors and are valid for post-installed fasteners in both uncracked and cracked concrete blocks (see Chapter 4 for the procedure followed for cracking the concrete blocks).

➤ **Expansion anchors (FAZ II)**

Traditional anchor

Phase 1: Drilling. Holes of 120 mm depth and 12 mm diameter were prepared using a drill into the concrete block. Each hole was 150 mm spaced from the others (Figure A.1, left).

Phase 2: Cleaning. The cleaning of the holes was made by a special pump to remove pieces of concrete and dust developed during the drilling and to guarantee the spread of stresses from the concrete to the anchor (Figure A.1, right).

Phase 3: Installation. The anchor was installed by hitting with a hammer for an effective depth (or H_{eff}) of 70 mm. The 12mm-thick steel plate was then placed on the anchor rod using the 14mm-diameter hole (1 mm of gap between anchor and steel plate). A torque of 60

Nm was initially applied to the nut by a torque meter to guarantee the expansion of the anchor, while after 10 minutes the torque was reduced to 30 Nm to simulate the long-term losses of tightening torque. The anchor was thus ready for the shake table test.

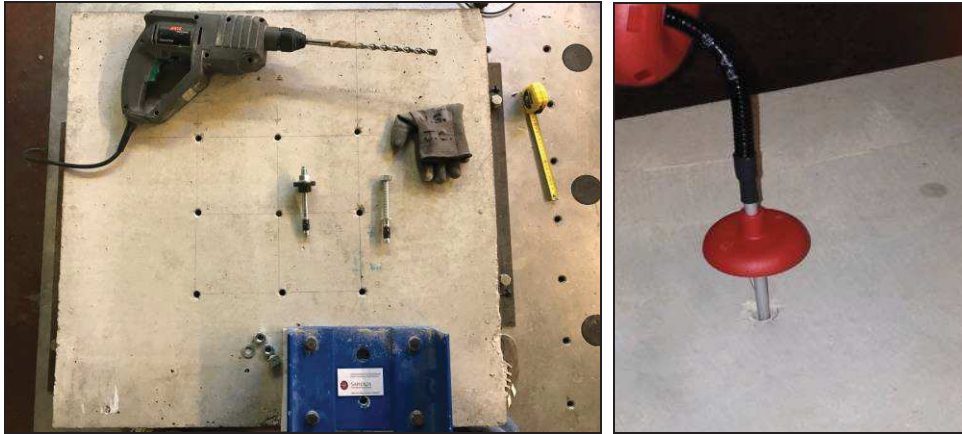


Figure A.1. Installing phases for the traditional expansion anchors: drilling (left) and cleaning of the holes (right).

Traditional anchor with Mortar Filling

The installation procedure was the same described above for the traditional anchors, however in Phase 3 the following modification was applied. After positioning the 12mm-thick steel plate, a washer and an additional piece comprising a hole for the injection of the mortar were positioned under the nut, as can be seen in Figure A.2, left. Then the torque of 60 Nm was applied and the injection of mortar through the hole on the steel piece was made using a special gun. After 10 minutes the torque was reduced to 30 Nm and after the hardening of the mortar the anchor was ready to be tested.



Figure A.2. Installation of the Traditional FAZ II with Mortar Filling (left) and with EQ-Rod 2.0 (right).

Traditional anchor with EQ-Rod 2.0 solution

The installation procedure for the EQ-Rod 2.0 solution was the same described for traditional anchor. The only difference was that the 24mm-diameter hole of the 12mm-thick steel plate was used for installing this anchor (Figure A.2, right).

➤ **Chemical anchors (Superbond)**

Traditional anchor

Phase 1: Drilling. Holes of 110 mm depth and 14 mm diameter were prepared by drilling into the concrete block. Each hole was 150 mm spaced from the others.

Phase 2: Cleaning. Cleaning the holes using special accessories (hole cleaning pump + metal cleaning brush), see Figure A.3.



Figure A.3. Accessories used for the installation of the chemical anchors.

Phase 3: Installation. After filling the hole in the concrete with mortar, the anchor rod was screwed into this hole. When the mortar became harder, the steel plate was positioned using the available 14mm-diameter hole, the nut was inserted, and a torque of 40 Nm was finally applied. After 10 minutes the torque was reduced to 20 Nm, thus the anchor was ready to be tested.

Traditional anchor with Mortar Filling

The installation procedure was the same described above for the traditional anchors, however in Phase 3 the following modification was applied.

After the positioning of the steel plate, a washer and an additional piece comprising a hole for the injection of the mortar were positioned under the nut. Then the torque of 40 Nm was applied and the injection of mortar through the hole on the plate was made using a special gun. After 10 minutes the torque was reduced to 20 Nm and after the hardening of the mortar the anchor was ready for the experimental test.

Traditional anchor with EQ-Rod 2.0 solution

The installation procedure for the EQ-Rod 2.0 solution - applied to the Superbond anchor - was the same of traditional anchor. The only difference was that the 24mm-diameter hole of the 12mm-thick steel plate was used for installing the EQ-Rod.

A.3 Test results

In this part of the Appendix different tables (from Table A.3 to Table A.26) can be found summarizing the experimental results in terms of Driving Mass (non-structural component) Acceleration DMA, Driving Mass Displacement DMD and Driving Mass Force DMF from the two testing phases. For each phase the output data are reported for both the conditions of uncracked and cracked concrete as well as considering the tests under the ground motions (100% input) and the related aftershocks (50% input).

The reductions due to the application of the supplemental damping (Trad/EQ-Rod) and due to the presence of the mortar filling (Trad/MF) are also calculated and presented in these tables. Statistics can be implemented for each typology of anchor and earthquake from the three different tests carried out in the same conditions and mean/standard deviation values of these reductions can be determined. Moreover, the influence of the earthquake properties (frequency range) in the results can be evaluated (see Pampanin et al. 2017). However, in this Appendix only a statistical study on the global test results (DMA and DMF), i.e. including all the earthquakes, is shown to compare the traditional system with the EQ-Rod solution (Figure A.4).

Note that the terms “positive” and “negative” indicated in the following tables refer to the directions of loading/motions.

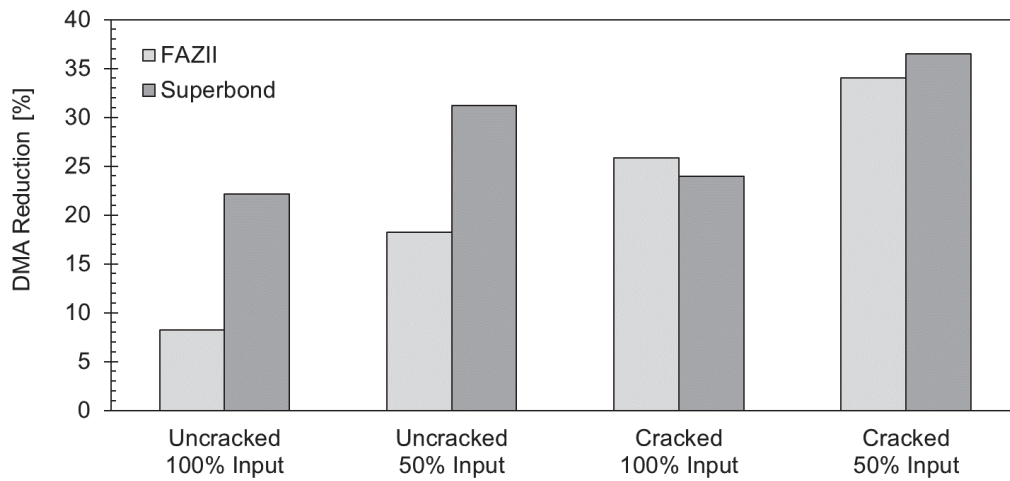


Figure A.4. Mean values of Driving Mass Acceleration (DMA) Reductions from all the experimental tests when comparing the traditional system to the EQ-Rod solution.

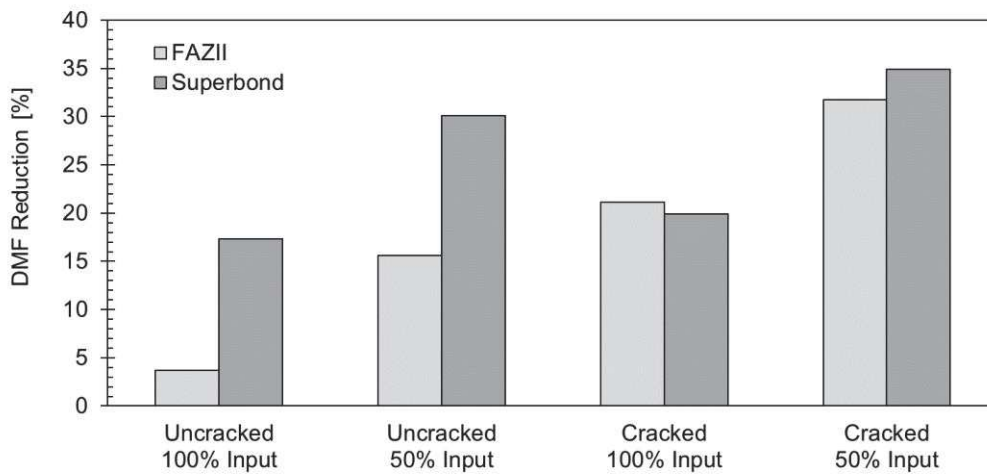


Figure A.5. Mean values of Driving Mass Force (DMF) Reductions from all the experimental tests when comparing the traditional system to the EQ-Rod solution.

PHASE 1: SHAKING TABLE TESTS ON FAZ II ANCHORS

Table A.3. **Uncracked concrete, 100% Input:** summary of test results in terms of Driving Mass Acceleration and its reductions.

	Test	Peak DMA [g]						Ratio [%]			
		Positive			Negative			Positive		Negative	
		Trad	EQRod	MF	Trad	EQRod	MF	Trad/ EQRod	Trad/ MF	Trad/ EQRod	Trad/ MF
EQ ₁	1	0.63	0.74	0.38	1.05	0.96	0.46	-17.61	39.61	8.57	56.19
	2	1.02	0.78	0.37	1.08	0.97	0.43	23.53	63.73	10.19	60.19
	3	0.81	0.66	0.57	0.94	0.83	0.76	18.52	29.63	11.70	19.15
EQ ₂	1	0.89	0.89	0.48	0.98	0.79	0.55	0.00	46.07	19.39	43.88
	2	1.08	0.86	0.41	1.08	0.79	0.42	20.37	62.04	26.85	61.11
	3	0.96	0.92	0.46	1.11	0.81	0.65	4.17	52.08	27.03	41.44
EQ ₃	1	1.00	0.97	0.68	1.13	1.25	0.86	3.00	32.00	-10.62	23.89
	2	1.14	1.05	0.84	1.60	1.30	1.12	7.89	26.32	18.75	30.00
	3	0.87	0.96	0.82	1.17	1.17	1.20	-10.34	5.75	0.00	-2.56
EQ ₄	1	1.74	1.29	1.03	1.38	1.26	0.90	25.86	40.80	8.70	34.78
	2	1.64	1.25	0.56	1.40	1.21	0.50	23.78	65.85	13.57	64.29
	3	1.52	1.25	0.72	1.40	1.20	0.73	17.76	52.63	14.29	47.86
EQ ₅	1	0.86	1.03	0.42	0.94	0.88	0.44	-19.77	51.16	6.38	53.19
	2	0.79	0.85	0.53	0.79	0.78	0.46	-7.59	32.91	1.27	41.77
	3	0.85	0.80	0.39	0.71	0.74	0.47	5.88	54.12	-4.23	33.80

Table A.4. **Uncracked concrete, 100% Input:** summary of test results in terms of Driving Mass Displacement and its reductions.

	Test	Peak DMD [mm]						Ratio [%]			
		Positive			Negative			Positive		Negative	
		Trad	EQRod	MF	Trad	EQRod	MF	Trad/ EQRod	Trad/ MF	Trad/ EQRod	Trad/ MF
EQ ₁	1	4.16	3.72	0.31	2.65	5.38	0.23	10.58	92.55	-103.02	91.32
	2	1.90	3.50	0.16	4.40	6.81	0.13	-84.21	91.58	-54.77	97.05
	3	2.17	4.73	0.67	4.54	4.74	1.79	-117.97	69.12	-4.41	60.57
EQ ₂	1	8.62	3.12	0.19	6.39	5.55	0.08	63.81	97.80	13.15	98.75
	2	4.19	4.33	0.15	2.17	3.99	0.15	-3.34	96.42	-83.87	93.09
	3	2.15	3.53	1.04	4.09	5.65	0.67	-64.19	51.63	-38.14	83.62
EQ ₃	1	3.19	4.31	1.85	4.78	6.17	1.16	-35.11	42.01	-29.08	75.73
	2	3.65	5.08	2.16	3.76	8.03	1.09	-39.18	40.82	-113.56	71.01
	3	5.18	2.90	2.32	3.49	5.38	0.61	44.02	55.21	-54.15	82.52
EQ ₄	1	4.61	5.17	1.32	2.44	5.07	1.13	-12.15	71.37	-107.79	53.69
	2	3.83	4.54	0.18	3.36	5.08	0.19	-18.54	95.30	-51.19	94.35
	3	2.69	4.63	1.03	4.18	4.66	0.27	-72.12	61.71	-11.48	93.54
EQ ₅	1	4.30	2.09	0.23	1.21	6.99	0.34	51.40	94.65	-477.69	71.90
	2	1.94	2.47	0.93	3.24	5.08	0.30	-27.32	52.06	-56.79	90.74
	3	3.26	3.39	0.12	2.02	3.52	0.15	-3.99	96.32	-74.26	92.57

Table A.5. **Uncracked concrete, 100% Input:** summary of test results in terms of Driving Mass Force and its reductions.

	Test	Peak DMF [kN]						Ratio [%]			
		Positive			Negative			Positive		Negative	
		Trad	EQRod	MF	Trad	EQRod	MF	Trad/ EQRod	Trad/ MF	Trad/ EQRod	Trad/ MF
EQ ₁	1	10.37	9.75	3.95	6.24	7.83	3.38	5.98	61.91	-25.48	45.83
	2	10.06	10.00	4.00	9.40	8.36	3.30	0.60	60.24	11.06	64.89
	3	10.00	8.58	7.19	7.40	6.51	5.61	14.20	28.10	12.03	24.19
EQ ₂	1	9.37	8.51	5.89	9.13	9.06	4.83	9.18	37.14	0.77	47.10
	2	10.71	8.35	4.13	10.29	8.64	4.02	22.04	61.44	16.03	60.93
	3	10.77	8.67	5.91	9.31	9.24	4.72	19.50	45.13	0.75	49.30
EQ ₃	1	12.78	13.87	9.13	9.95	10.02	7.16	-8.53	28.56	-0.70	28.04
	2	15.27	14.19	10.72	12.27	10.94	8.04	7.07	29.80	10.84	34.47
	3	12.56	12.62	11.33	9.30	10.01	8.21	-0.48	9.79	-7.63	11.72
EQ ₄	1	13.01	13.06	8.72	16.79	13.32	10.97	-0.38	32.97	20.67	34.66
	2	13.87	12.40	5.11	16.20	13.53	5.79	10.60	63.16	16.48	64.26
	3	13.36	12.64	7.58	14.56	13.03	7.33	5.39	43.26	10.51	49.66
EQ ₅	1	9.47	9.26	4.76	8.67	11.05	4.21	2.22	49.74	-27.45	51.44
	2	8.21	7.68	4.91	8.33	9.37	5.36	6.46	40.19	-12.48	35.65
	3	7.52	8.19	4.99	8.67	8.68	3.84	-8.91	33.64	-0.12	55.71

Table A.6. **Uncracked concrete, 50% Input:** summary of test results in terms of Driving Mass Acceleration and its reductions.

	Test	Peak DMA [g]						Ratio [%]			
		Positive			Negative			Positive		Negative	
		Trad	EQRod	MF	Trad	EQRod	MF	Trad/ EQRod	Trad/ MF	Trad/ EQRod	Trad/ MF
EQ ₁	1	0.52	0.74	0.24	0.74	0.96	0.33	-42.31	53.85	-29.73	55.41
	2	0.74	0.53	0.27	0.83	0.67	0.31	28.38	63.51	19.28	62.65
	3	0.68	0.44	0.49	0.77	0.60	0.48	35.29	27.94	22.08	37.66
EQ ₂	1	0.63	0.57	0.29	0.70	0.52	0.26	9.52	53.97	25.71	62.86
	2	0.77	0.64	0.28	0.81	0.55	0.25	16.88	63.64	32.10	69.14
	3	0.73	0.67	0.32	0.77	0.60	0.42	8.22	56.16	22.08	45.45
EQ ₃	1	0.62	0.63	0.52	0.82	0.79	0.57	-1.61	16.13	3.66	30.49
	2	0.66	0.63	0.64	0.92	0.56	0.98	4.55	3.03	39.13	-6.52
	3	0.57	0.63	0.63	0.76	0.85	0.81	-10.53	-10.53	-11.84	-6.58
EQ ₄	1	1.12	0.77	0.74	1.18	0.75	0.55	31.25	33.93	36.44	53.39
	2	1.16	0.75	0.37	1.02	0.72	0.28	35.34	68.10	29.41	72.55
	3	1.10	0.72	0.49	0.90	0.65	0.46	34.55	55.45	27.78	48.89
EQ ₅	1	0.68	0.56	0.23	0.72	0.46	0.23	17.65	66.18	36.11	68.06
	2	0.73	0.41	0.26	0.59	0.49	0.25	43.84	64.38	16.95	57.63
	3	0.61	0.27	0.28	0.47	0.42	0.25	55.74	54.10	10.64	46.81

Table A.7. *Uncracked concrete, 50% Input: summary of test results in terms of Driving Mass Displacement and its reductions.*

	Test	Peak DMD [mm]						Ratio [%]			
		Positive			Negative			Positive		Negative	
		Trad	EQRod	MF	Trad	EQRod	MF	Trad/ EQRod	Trad/ MF	Trad/ EQRod	Trad/ MF
EQ ₁	1	2.65	3.72	0.28	3.91	5.38	0.18	-40.38	89.43	-37.60	95.40
	2	3.27	4.85	0.12	2.92	4.40	0.11	-48.32	96.33	-50.68	96.23
	3	1.50	3.66	0.61	4.73	4.66	1.79	-144.00	59.33	1.48	62.16
EQ ₂	1	4.45	4.57	0.08	11.10	3.36	0.07	-2.70	98.20	69.73	99.37
	2	3.06	3.14	0.11	3.23	4.70	0.14	-2.61	96.41	-45.51	95.67
	3	3.32	3.43	0.93	2.75	5.32	0.66	-3.31	71.99	-93.45	76.00
EQ ₃	1	1.65	3.09	1.23	5.70	6.53	1.46	-87.27	25.45	-14.56	74.39
	2	2.46	3.83	2.19	4.50	6.78	0.96	-55.69	10.98	-50.67	78.67
	3	3.19	4.15	2.03	4.62	3.29	0.80	-30.09	36.36	28.79	82.68
EQ ₄	1	5.42	4.34	1.16	1.47	4.61	1.00	19.93	78.60	-213.61	31.97
	2	3.50	4.24	0.13	3.46	4.14	0.10	-21.14	96.29	-19.65	97.11
	3	2.89	4.40	0.86	3.82	3.33	0.29	-52.25	70.24	12.83	92.41
EQ ₅	1	2.53	2.30	0.09	2.80	5.37	0.19	9.09	96.44	-91.79	93.21
	2	1.60	1.74	0.55	3.58	4.67	0.33	-8.75	65.63	-30.45	90.78
	3	1.51	2.01	0.06	3.38	3.20	0.07	-33.11	96.03	5.33	97.93

Table A.8. *Uncracked concrete, 50% Input: summary of test results in terms of Driving Mass Force and its reductions.*

	Test	Peak DMF [kN]						Ratio [%]			
		Positive			Negative			Positive		Negative	
		Trad	EQRod	MF	Trad	EQRod	MF	Trad/ EQRod	Trad/ MF	Trad/ EQRod	Trad/ MF
EQ ₁	1	7.21	9.75	2.92	5.41	7.83	2.45	-35.23	59.50	-44.73	54.71
	2	7.94	7.24	3.03	7.17	5.57	2.39	8.82	61.84	22.32	66.67
	3	7.47	6.34	4.66	6.39	4.63	5.10	15.13	37.62	27.54	20.19
EQ ₂	1	7.31	5.63	2.59	6.62	6.32	2.57	22.98	64.57	4.53	61.18
	2	8.41	6.13	2.50	7.81	6.45	2.55	27.11	70.27	17.41	67.35
	3	7.53	6.35	4.02	7.38	6.99	3.35	15.67	46.61	5.28	54.61
EQ ₃	1	8.83	8.64	5.95	6.36	6.25	5.27	2.15	32.62	1.73	17.14
	2	10.25	6.45	8.84	6.27	6.39	6.47	37.07	13.76	-1.91	-3.19
	3	8.84	8.77	7.66	6.06	6.71	6.33	0.79	13.35	-10.73	-4.46
EQ ₄	1	11.67	7.99	5.52	11.32	8.04	7.33	31.53	52.70	28.98	35.25
	2	10.36	6.99	2.81	12.04	8.18	3.70	32.53	72.88	32.06	69.27
	3	9.19	7.27	4.86	11.26	7.56	5.13	20.89	47.12	32.86	54.44
EQ ₅	1	7.21	4.94	2.48	7.08	6.22	2.35	31.48	65.60	12.15	66.81
	2	6.35	5.25	2.68	7.57	4.53	2.80	17.32	57.80	40.16	63.01
	3	5.27	4.35	2.52	6.35	2.81	2.65	17.46	52.18	55.75	58.27

Table A.9. **Cracked concrete, 100% Input:** summary of test results in terms of Driving Mass Acceleration and its reductions.

	Test	Peak DMA [g]						Ratio [%]			
		Positive			Negative			Positive		Negative	
		Trad	EQRod	MF	Trad	EQRod	MF	Trad/ EQRod	Trad/ MF	Trad/ EQRod	Trad/ MF
EQ ₁	1	0.75	0.31	0.43	1.43	0.74	0.48	58.67	42.67	48.25	66.43
	2	0.69	0.24	0.43	1.10	0.56	0.48	65.22	37.68	49.09	56.36
	3	0.73	0.37	0.44	1.30	0.43	0.77	49.32	39.73	66.92	40.77
EQ ₂	1	0.98	0.61	0.42	0.83	0.73	0.47	37.76	57.14	12.05	43.37
	2	1.02	0.69	0.37	1.23	0.76	0.37	32.35	63.73	38.21	69.92
	3	1.01	0.77	0.44	0.97	0.76	0.38	23.76	56.44	21.65	60.82
EQ ₃	1	1.29	1.01	0.50	1.83	1.35	0.91	21.71	61.24	26.23	50.27
	2	1.18	0.95	0.56	1.59	1.23	0.55	19.49	52.54	22.64	65.41
	3	1.23	1.01	0.50	1.59	1.27	0.90	17.89	59.35	20.13	43.40
EQ ₄	1	1.63	1.28	0.65	1.70	1.17	0.57	21.47	60.12	31.18	66.47
	2	1.62	1.22	0.58	1.63	1.22	0.60	24.69	64.20	25.15	63.19
	3	1.82	1.27	0.69	1.45	1.23	0.62	30.22	62.09	15.17	57.24
EQ ₅	1	0.81	0.84	0.43	0.73	0.89	0.48	-3.70	46.91	-21.92	34.25
	2	1.02	0.85	0.41	0.85	0.81	0.46	16.67	59.80	4.71	45.88
	3	0.98	0.91	0.49	0.82	0.88	0.41	7.14	50.00	-7.32	50.00

Table A.10. **Cracked concrete, 100% Input:** summary of test results in terms of Driving Mass Displacement and its reductions.

	Test	Peak DMD [mm]						Ratio [%]			
		Positive			Negative			Positive		Negative	
		Trad	EQRod	MF	Trad	EQRod	MF	Trad/ EQRod	Trad/ MF	Trad/ EQRod	Trad/ MF
EQ ₁	1	3.93	2.30	0.13	1.76	2.78	0.05	41.48	96.69	-57.95	97.16
	2	3.35	1.69	0.07	1.59	2.96	0.06	49.55	97.91	-86.16	96.23
	3	4.36	0.09	1.07	1.65	2.84	0.91	97.94	75.46	-72.12	44.85
EQ ₂	1	3.59	3.47	0.05	1.29	4.05	0.06	3.34	98.61	-213.95	95.35
	2	3.29	2.33	0.77	3.00	4.44	0.25	29.18	76.60	-48.00	91.67
	3	3.34	3.18	0.13	2.32	4.70	0.14	4.79	96.11	-102.59	93.97
EQ ₃	1	5.07	4.75	1.41	2.28	4.87	0.81	6.31	72.19	-113.60	64.47
	2	2.14	4.62	0.13	4.51	5.37	0.21	-115.89	93.93	-19.07	95.34
	3	2.18	3.09	1.35	4.91	6.12	0.83	-41.74	38.07	-24.64	83.10
EQ ₄	1	5.64	3.80	0.34	2.42	5.42	0.33	32.62	93.97	-123.97	86.36
	2	4.61	4.82	0.27	3.13	5.31	0.19	-4.56	94.14	-69.65	93.93
	3	4.34	5.23	0.38	4.10	4.25	0.23	-20.51	91.24	-3.66	94.39
EQ ₅	1	4.66	3.46	0.26	1.27	4.15	0.23	25.75	94.42	-226.77	81.89
	2	3.39	4.22	0.23	2.74	3.81	0.16	-24.48	93.22	-39.05	94.16
	3	3.31	5.03	0.47	2.86	3.77	0.70	-51.96	85.80	-31.82	75.52

Table A.11. **Cracked concrete, 100% Input:** summary of test results in terms of Driving Mass Force and its reductions.

	Test	Peak DMF [kN]						Ratio [%]			
		Positive			Negative			Positive		Negative	
		Trad	EQRod	MF	Trad	EQRod	MF	Trad/ EQRod	Trad/ MF	Trad/ EQRod	Trad/ MF
EQ ₁	1	13.13	7.82	4.17	7.53	3.09	4.05	40.44	68.24	58.96	46.22
	2	10.22	5.73	4.02	6.93	2.35	4.06	43.93	60.67	66.09	41.41
	3	12.65	4.35	7.05	7.54	3.55	4.25	65.61	44.27	52.92	43.63
EQ ₂	1	8.19	7.79	4.38	9.62	6.64	4.06	4.88	46.52	30.98	57.80
	2	12.15	8.27	3.68	10.06	7.15	3.62	31.93	69.71	28.93	64.02
	3	9.67	8.31	3.99	10.20	7.80	4.11	14.06	58.74	23.53	59.71
EQ ₃	1	16.94	14.74	8.95	12.52	10.34	5.09	12.99	47.17	17.41	59.35
	2	15.73	13.31	5.53	12.03	10.10	5.69	15.38	64.84	16.04	52.70
	3	16.00	13.83	9.22	12.10	10.05	5.45	13.56	42.38	16.94	54.96
EQ ₄	1	17.08	12.33	5.69	16.14	12.95	6.14	27.81	66.69	19.76	61.96
	2	15.25	13.51	5.55	15.89	12.82	5.63	11.41	63.61	19.32	64.57
	3	14.97	13.33	6.31	17.89	13.62	6.46	10.96	57.85	23.87	63.89
EQ ₅	1	7.81	9.16	5.07	8.16	9.43	4.19	-17.29	35.08	-15.56	48.65
	2	8.34	8.68	4.90	10.12	9.29	4.11	-4.08	41.25	8.20	59.39
	3	8.48	9.13	4.42	10.13	9.95	5.10	-7.67	47.88	1.78	49.65

Table A.12. **Cracked concrete, 50% Input:** summary of test results in terms of Driving Mass Acceleration and its reductions.

	Test	Peak DMA [g]						Ratio [%]			
		Positive			Negative			Positive		Negative	
		Trad	EQRod	MF	Trad	EQRod	MF	Trad/ EQRod	Trad/ MF	Trad/ EQRod	Trad/ MF
EQ ₁	1	0.51	0.15	0.29	0.83	0.30	0.31	70.59	43.14	63.86	62.65
	2	0.39	0.15	0.29	0.59	0.25	0.33	61.54	25.64	57.63	44.07
	3	0.48	0.25	0.23	0.98	0.49	0.42	47.92	52.08	50.00	57.14
EQ ₂	1	0.55	0.33	0.32	0.27	0.37	0.35	40.00	41.82	-37.04	-29.63
	2	0.48	0.40	0.21	0.82	0.32	0.27	16.67	56.25	60.98	67.07
	3	0.65	0.48	0.27	0.48	0.39	0.23	26.15	58.46	18.75	52.08
EQ ₃	1	0.72	0.54	0.30	0.97	0.73	0.55	25.00	58.33	24.74	43.30
	2	0.89	0.55	0.35	1.16	0.67	0.34	38.20	60.67	42.24	70.69
	3	0.64	0.54	0.29	0.99	0.74	0.52	15.63	54.69	25.25	47.47
EQ ₄	1	0.86	0.76	0.44	0.90	0.66	0.31	11.63	48.84	26.67	65.56
	2	1.09	0.66	0.40	1.12	0.70	0.30	39.45	63.30	37.50	73.21
	3	1.08	0.80	0.48	0.96	0.67	0.36	25.93	55.56	30.21	62.50
EQ ₅	1	0.70	0.40	0.31	0.63	0.45	0.23	42.86	55.71	28.57	63.49
	2	0.74	0.43	0.28	0.62	0.47	0.25	41.89	62.16	24.19	59.68
	3	0.64	0.38	0.32	0.66	0.51	0.27	40.63	50.00	22.73	59.09

Table A.13. **Cracked concrete, 50% Input:** summary of test results in terms of Driving Mass Displacement and its reductions.

	Test	Peak DMD [mm]						Ratio [%]			
		Positive			Negative			Positive		Negative	
		Trad	EQRod	MF	Trad	EQRod	MF	Trad/ EQRod	Trad/ MF	Trad/ EQRod	Trad/ MF
EQ ₁	1	1.67	0.83	0.07	3.62	1.49	0.06	50.30	95.81	58.84	98.34
	2	1.91	0.42	0.05	2.69	1.22	0.03	78.01	97.38	54.65	98.88
	3	2.34	3.58	0.85	3.41	2.44	0.79	-52.99	63.68	28.45	76.83
EQ ₂	1	1.07	3.24	0.04	1.63	3.11	0.04	-202.80	96.26	-90.80	97.55
	2	3.60	2.77	0.49	2.19	3.21	0.16	23.06	86.39	-46.58	92.69
	3	2.00	3.16	0.07	3.34	3.68	0.09	-58.00	96.50	-10.18	97.31
EQ ₃	1	3.40	3.64	1.08	2.30	4.64	0.49	-7.06	68.24	-101.74	78.70
	2	2.31	4.55	0.08	4.23	3.87	0.13	-96.97	96.54	8.51	96.93
	3	4.02	5.01	0.93	2.55	3.10	0.66	-24.63	76.87	-21.57	74.12
EQ ₄	1	5.05	4.40	0.24	2.31	3.55	0.26	12.87	95.25	-53.68	88.74
	2	3.40	5.05	0.22	4.15	3.45	0.11	-48.53	93.53	16.87	97.35
	3	3.10	4.17	0.23	4.81	4.15	0.24	-34.52	92.58	13.72	95.01
EQ ₅	1	4.71	1.39	0.19	1.13	4.81	0.12	70.49	95.97	-325.66	89.38
	2	1.76	1.90	0.11	4.17	4.78	0.13	-7.95	93.75	-14.63	96.88
	3	2.67	1.39	0.38	3.13	5.68	0.57	47.94	85.77	-81.47	81.79

Table A.14. **Cracked concrete, 50% Input:** summary of test results in terms of Driving Mass Force and its reductions.

	Test	Peak DMF [kN]						Ratio [%]			
		Positive			Negative			Positive		Negative	
		Trad	EQRod	MF	Trad	EQRod	MF	Trad/ EQRod	Trad/ MF	Trad/ EQRod	Trad/ MF
EQ ₁	1	7.86	2.99	3.00	5.22	1.13	2.77	61.96	61.83	78.35	46.93
	2	5.78	2.16	2.79	3.91	1.49	2.94	62.63	51.73	61.89	24.81
	3	9.49	5.08	3.70	5.46	2.77	2.38	46.47	61.01	49.27	56.41
EQ ₂	1	2.74	4.07	3.07	5.52	3.57	3.06	-48.54	-12.04	35.33	44.57
	2	8.23	3.73	2.56	5.36	4.31	2.30	54.68	68.89	19.59	57.09
	3	4.82	3.91	2.31	6.85	5.48	2.66	18.88	52.07	20.00	61.17
EQ ₃	1	9.32	7.93	5.04	7.33	5.62	3.24	14.91	45.92	23.33	55.80
	2	11.50	7.08	3.34	8.89	5.57	3.20	38.43	70.96	37.35	64.00
	3	10.48	8.13	5.29	6.62	5.84	3.03	22.42	49.52	11.78	54.23
EQ ₄	1	9.18	6.79	3.40	8.99	8.26	4.31	26.03	62.96	8.12	52.06
	2	10.79	7.79	3.54	11.33	6.92	3.73	27.80	67.19	38.92	67.08
	3	10.26	7.15	3.70	11.17	8.48	4.50	30.31	63.94	24.08	59.71
EQ ₅	1	6.37	4.59	2.37	7.40	4.47	3.07	27.94	62.79	39.59	58.51
	2	6.37	4.91	2.56	7.70	4.75	2.62	22.92	59.81	38.31	65.97
	3	6.74	5.55	2.89	6.70	3.83	3.25	17.66	57.12	42.84	51.49

PHASE 2: SHAKING TABLE TESTS ON SUPERBOND ANCHORS

Table A.15. **Uncracked concrete, 100% Input:** summary of test results in terms of Driving Mass Acceleration and its reductions.

	Test	Peak DMA [g]						Ratio [%]			
		Positive			Negative			Positive		Negative	
		Trad	EQRod	MF	Trad	EQRod	MF	Trad/ EQRod	Trad/ MF	Trad/ EQRod	Trad/ MF
EQ ₁	1	0.73	0.44	0.41	1.26	0.78	0.46	39.73	43.84	38.10	63.49
	2	0.58	0.32	0.50	1.02	0.66	0.55	44.83	13.79	35.29	46.08
	3	0.75	0.74	0.36	1.21	0.81	0.46	1.33	52.00	33.06	61.98
EQ ₂	1	0.92	0.70	0.43	1.02	0.60	0.41	23.91	53.26	41.18	59.80
	2	0.75	0.69	0.44	0.99	0.65	0.43	8.00	41.33	34.34	56.57
	3	0.76	0.68	0.49	1.00	0.67	0.52	10.53	35.53	33.00	48.00
EQ ₃	1	1.11	0.91	0.55	1.47	1.22	0.54	18.02	50.45	17.01	63.27
	2	1.20	1.01	0.52	1.42	1.31	0.54	15.83	56.67	7.75	61.97
	3	1.20	0.84	0.62	1.38	1.07	0.66	30.00	48.33	22.46	52.17
EQ ₄	1	1.56	1.33	0.66	1.46	1.14	0.61	14.74	57.69	21.92	58.22
	2	1.53	1.35	1.19	1.40	1.27	0.85	11.76	22.22	9.29	39.29
	3	1.49	1.35	0.64	1.43	1.01	0.59	9.40	57.05	29.37	58.74
EQ ₅	1	0.88	0.75	0.47	0.92	0.68	0.45	14.77	46.59	26.09	51.09
	2	0.84	0.80	0.44	0.94	0.65	0.47	4.76	47.62	30.85	50.00
	3	0.95	0.82	0.47	0.96	0.73	0.45	13.68	50.53	23.96	53.13

Table A.16. **Uncracked concrete, 100% Input:** summary of test results in terms of Driving Mass Displacement and its reductions.

	Test	Peak DMD [mm]						Ratio [%]			
		Positive			Negative			Positive		Negative	
		Trad	EQRod	MF	Trad	EQRod	MF	Trad/ EQRod	Trad/ MF	Trad/ EQRod	Trad/ MF
EQ ₁	1	1.71	2.04	0.17	1.33	2.40	0.15	-19.30	90.06	-80.45	88.72
	2	1.68	0.53	0.06	1.21	3.20	0.04	68.45	96.43	-164.46	96.69
	3	1.68	1.81	0.06	1.48	3.60	0.02	-7.74	96.43	-143.24	98.65
EQ ₂	1	1.79	2.13	0.07	1.36	2.54	0.11	-18.99	96.09	-86.76	91.91
	2	2.13	1.97	0.06	0.79	2.71	0.08	7.51	97.18	-243.04	89.87
	3	1.64	3.06	0.04	1.39	2.02	0.25	-86.59	97.56	-45.32	82.01
EQ ₃	1	1.63	2.74	0.16	2.05	3.62	0.24	-68.10	90.18	-76.59	88.29
	2	1.61	3.60	0.09	1.97	2.98	0.26	-123.60	94.41	-51.27	86.80
	3	1.26	2.37	0.04	2.33	3.43	0.10	-88.10	96.83	-47.21	95.71
EQ ₄	1	1.74	3.19	0.29	2.41	3.59	0.21	-83.33	83.33	-48.96	91.29
	2	3.04	3.82	1.73	1.19	2.85	1.06	-25.66	43.09	-139.50	10.92
	3	3.14	2.56	0.19	0.90	4.04	0.14	18.47	93.95	-348.89	84.44
EQ ₅	1	1.53	2.31	0.10	1.60	2.58	0.10	-50.98	93.46	-61.25	93.75
	2	1.91	3.51	0.11	1.30	1.55	0.11	-83.77	94.24	-19.23	91.54
	3	1.63	2.36	0.07	1.48	2.68	0.04	-44.79	95.71	-81.08	97.30

Table A.17. **Uncracked concrete, 100% Input:** summary of test results in terms of Driving Mass Force and its reductions.

	Test	Peak DMF [kN]						Ratio [%]			
		Positive			Negative			Positive		Negative	
		Trad	EQRod	MF	Trad	EQRod	MF	Trad/ EQRod	Trad/ MF	Trad/ EQRod	Trad/ MF
EQ ₁	1	11.33	7.35	3.87	7.25	4.85	4.11	35.13	65.84	33.10	43.31
	2	9.15	6.42	4.56	5.76	3.20	4.89	29.84	50.16	44.44	15.10
	3	11.00	7.83	3.93	7.38	7.60	3.49	28.82	64.27	-2.98	52.71
EQ ₂	1	9.76	6.30	3.91	8.58	7.09	4.03	35.45	59.94	17.37	53.03
	2	9.21	6.86	4.19	7.75	7.14	4.42	25.52	54.51	7.87	42.97
	3	9.26	6.77	4.84	7.84	7.15	4.90	26.89	47.73	8.80	37.50
EQ ₃	1	13.86	12.70	5.56	11.06	9.74	5.30	8.37	59.88	11.93	52.08
	2	13.61	13.38	5.23	11.28	10.45	5.25	1.69	61.57	7.36	53.46
	3	12.80	11.03	6.01	12.00	9.12	5.73	13.83	53.05	24.00	52.25
EQ ₄	1	14.10	11.57	5.87	15.43	13.88	6.47	17.94	58.37	10.05	58.07
	2	13.74	12.89	8.47	15.25	13.43	11.76	6.19	38.36	11.93	22.89
	3	13.51	10.44	5.84	14.66	13.87	6.29	22.72	56.77	5.39	57.09
EQ ₅	1	8.66	6.87	4.82	8.79	7.78	4.54	20.67	44.34	11.49	48.35
	2	8.77	6.65	5.03	8.55	8.41	4.14	24.17	42.65	1.64	51.58
	3	9.75	7.44	4.66	9.28	8.61	4.60	23.69	52.21	7.22	50.43

Table A.18. **Uncracked concrete, 50% Input:** summary of test results in terms of Driving Mass Acceleration and its reductions.

	Test	Peak DMA [g]						Ratio [%]			
		Positive			Negative			Positive		Negative	
		Trad	EQRod	MF	Trad	EQRod	MF	Trad/ EQRod	Trad/ MF	Trad/ EQRod	Trad/ MF
EQ ₁	1	0.54	0.18	0.29	0.77	0.36	0.35	66.67	46.30	53.25	54.55
	2	0.14	0.16	0.33	0.33	0.28	0.37	-14.29	-135.71	15.15	-
	3	0.48	0.42	0.25	0.73	0.43	0.27	12.50	47.92	41.10	63.01
EQ ₂	1	0.64	0.33	0.31	0.64	0.24	0.26	48.44	51.56	62.50	59.38
	2	0.55	0.35	0.30	0.67	0.25	0.31	36.36	45.45	62.69	53.73
	3	0.56	0.42	0.34	0.63	0.30	0.41	25.00	39.29	52.38	34.92
EQ ₃	1	0.64	0.50	0.32	0.94	0.69	0.38	21.88	50.00	26.60	59.57
	2	0.63	0.51	0.35	0.97	0.70	0.46	19.05	44.44	27.84	52.58
	3	0.68	0.48	0.37	0.94	0.66	0.43	29.41	45.59	29.79	54.26
EQ ₄	1	0.96	0.73	0.43	0.93	0.56	0.34	23.96	55.21	39.78	63.44
	2	0.96	0.74	0.89	0.90	0.69	0.47	22.92	7.29	23.33	47.78
	3	0.97	0.75	0.41	0.93	0.65	0.31	22.68	57.73	30.11	66.67
EQ ₅	1	0.67	0.52	0.34	0.62	0.40	0.23	22.39	49.25	35.48	62.90
	2	0.67	0.50	0.35	0.63	0.40	0.23	25.37	47.76	36.51	63.49
	3	0.53	0.50	0.34	0.59	0.40	0.25	5.66	35.85	32.20	57.63

Table A.19. **Uncracked concrete, 50% Input:** summary of test results in terms of Driving Mass Displacement and its reductions.

	Test	Peak DMD [mm]						Ratio [%]			
		Positive			Negative			Positive		Negative	
		Trad	EQRod	MF	Trad	EQRod	MF	Trad/ EQRod	Trad/ MF	Trad/ EQRod	Trad/ MF
EQ ₁	1	0.38	0.87	0.12	2.48	2.55	0.11	-128.95	68.42	-2.82	95.56
	2	0.26	0.75	0.04	2.05	0.89	0.02	-188.46	84.62	56.59	99.02
	3	1.59	1.50	0.02	1.32	3.00	0.02	5.66	98.74	-127.27	98.48
EQ ₂	1	2.71	2.19	0.07	0.32	1.55	0.07	19.19	97.42	-384.38	78.13
	2	1.49	1.97	0.06	1.23	1.72	0.05	-32.21	95.97	-39.84	95.93
	3	1.25	1.67	0.02	1.54	2.44	0.03	-33.60	98.40	-58.44	98.05
EQ ₃	1	1.15	2.12	0.13	2.27	3.15	0.15	-84.35	88.70	-38.77	93.39
	2	2.05	1.70	0.15	1.28	3.81	0.12	17.07	92.68	-197.66	90.63
	3	1.81	3.18	0.03	1.58	1.73	0.06	-75.69	98.34	-9.49	96.20
EQ ₄	1	1.89	2.21	0.20	1.90	3.34	0.16	-16.93	89.42	-75.79	91.58
	2	2.78	1.90	1.42	1.12	3.75	0.93	31.65	48.92	-234.82	16.96
	3	1.41	3.48	0.14	2.37	2.14	0.09	-146.81	90.07	9.70	96.20
EQ ₅	1	0.95	1.13	0.07	2.06	3.11	0.05	-18.95	92.63	-50.97	97.57
	2	0.77	1.19	0.07	2.29	3.13	0.04	-54.55	90.91	-36.68	98.25
	3	0.33	1.06	0.02	2.45	3.17	0.02	-221.21	93.94	-29.39	99.18

Table A.20. **Uncracked concrete, 50% Input:** summary of test results in terms of Driving Mass Force and its reductions.

	Test	Peak DMF [kN]						Ratio [%]			
		Positive			Negative			Positive		Negative	
		Trad	EQRod	MF	Trad	EQRod	MF	Trad/ EQRod	Trad/ MF	Trad/ EQRod	Trad/ MF
EQ ₁	1	7.05	3.61	2.92	5.43	2.19	2.92	48.79	58.58	59.67	46.22
	2	3.01	2.72	3.32	1.47	1.30		9.63	-	11.56	125.17
	3	6.53	4.14	2.40	4.97	4.66	2.43	36.60	63.25	6.24	51.11
EQ ₂	1	6.45	2.48	2.49	6.58	3.64	3.06	61.55	61.40	44.68	53.50
	2	6.27	2.79	3.06	5.98	3.60	2.91	55.50	51.20	39.80	51.34
	3	6.19	2.90	3.72	6.13	4.42	3.50	53.15	39.90	27.90	42.90
EQ ₃	1	9.59	7.10	3.60	6.47	4.93	3.04	25.96	62.46	23.80	53.01
	2	9.84	7.56	4.29	6.38	5.18	3.39	23.17	56.40	18.81	46.87
	3	9.27	6.86	4.17	7.01	4.69	3.35	26.00	55.02	33.10	52.21
EQ ₄	1	9.28	5.74	3.53	9.99	7.71	4.28	38.15	61.96	22.82	57.16
	2	9.08	7.60	4.79	9.94	7.71	8.85	16.30	47.25	22.43	10.97
	3	9.14	6.46	3.24	10.07	8.02	4.08	29.32	64.55	20.36	59.48
EQ ₅	1	6.16	3.98	2.26	7.05	5.51	3.38	35.39	63.31	21.84	52.06
	2	5.99	3.96	2.37	6.91	5.38	3.23	33.89	60.43	22.14	53.26
	3	6.08	4.05	2.44	5.42	5.36	3.43	33.39	59.87	1.11	36.72

Table A.21. **Cracked concrete, 100% Input:** summary of test results in terms of Driving Mass Acceleration and its reductions.

	Test	Peak DMA [g]						Ratio [%]			
		Positive			Negative			Positive		Negative	
		Trad	EQRod	MF	Trad	EQRod	MF	Trad/ EQRod	Trad/ MF	Trad/ EQRod	Trad/ MF
EQ ₁	1	0.62	0.59	0.43	1.23	0.88	0.49	4.84	30.65	28.46	60.16
	2	0.79	0.36	0.53	1.20	0.63	0.58	54.43	32.91	47.50	51.67
	3	0.68	0.69	0.40	1.19	0.82	0.47	-1.47	41.18	31.09	60.50
EQ ₂	1	0.98	0.74	0.50	1.00	0.70	0.43	24.49	48.98	30.00	57.00
	2	0.77	0.66	0.47	1.04	0.74	0.40	14.29	38.96	28.85	61.54
	3	0.93	0.67	0.37	1.01	0.63	0.35	27.96	60.22	37.62	65.35
EQ ₃	1	1.01	1.02	0.55	1.25	1.16	0.55	-0.99	45.54	7.20	56.00
	2	1.07	0.70	0.50	1.31	1.00	0.52	34.58	53.27	23.66	60.31
	3	1.20	0.92	0.58	1.35	1.16	0.66	23.33	51.67	14.07	51.11
EQ ₄	1	1.42	1.18	0.67	1.38	1.08	0.59	16.90	52.82	21.74	57.25
	2	1.43	1.24	0.74	1.36	1.13	0.61	13.29	48.25	16.91	55.15
	3	1.21	0.72	0.58	1.38	0.71	0.52	40.50	52.07	48.55	62.32
EQ ₅	1	1.01	0.71	0.52	0.72	0.74	0.45	29.70	48.51	-2.78	37.50
	2	0.86	0.66	0.44	0.94	0.52	0.41	23.26	48.84	44.68	56.38
	3	0.72	0.60	0.45	0.64	0.52	0.42	16.67	37.50	18.75	34.38

Table A.22. **Cracked concrete, 100% Input:** summary of test results in terms of Driving Mass Displacement and its reductions.

	Test	Peak DMD [mm]						Ratio [%]			
		Positive			Negative			Positive		Negative	
		Trad	EQRod	MF	Trad	EQRod	MF	Trad/ EQRod	Trad/ MF	Trad/ EQRod	Trad/ MF
EQ ₁	1	1.44	1.79	0.10	1.87	2.86	0.11	-24.31	93.06	-52.94	94.12
	2	1.29	1.54	0.03	1.94	2.34	0.02	-19.38	97.67	-20.62	98.97
	3	1.73	1.99	0.11	1.29	2.99	0.11	-15.03	93.64	-131.78	91.47
EQ ₂	1	1.68	1.91	0.01	1.69	3.19	0.10	-13.69	99.40	-88.76	94.08
	2	1.95	2.29	0.09	1.22	2.53	0.09	-17.44	95.38	-107.38	92.62
	3	1.46	1.88	0.05	1.87	2.62	0.10	-28.77	96.58	-40.11	94.65
EQ ₃	1	1.37	2.71	0.03	2.30	3.49	0.04	-97.81	97.81	-51.74	98.26
	2	2.16	2.51	0.11	1.94	2.51	0.15	-16.20	94.91	-29.38	92.27
	3	1.76	2.01	0.09	1.99	4.28	0.07	-14.20	94.89	-115.08	96.48
EQ ₄	1	2.17	2.35	0.06	2.21	3.34	0.12	-8.29	97.24	-51.13	94.57
	2	2.11	3.58	0.00	2.38	2.72	0.26	-69.67	100.0 0	-14.29	89.08
	3	2.23	1.56	0.05	1.56	2.17	0.06	30.04	97.76	-39.10	96.15
EQ ₅	1	1.18	1.57	0.00	1.90	2.78	0.10	-33.05	100.0 0	-46.32	94.74
	2	1.79	2.34	0.02	1.30	1.54	0.09	-30.73	98.88	-18.46	93.08
	3	0.95	1.18	0.05	2.11	3.04	0.03	-24.21	94.74	-44.08	98.58

Table A.23. **Cracked concrete, 100% Input:** summary of test results in terms of Driving Mass Force and its reductions.

	Test	Peak DMF [kN]						Ratio [%]			
		Positive			Negative			Positive		Negative	
		Trad	EQRod	MF	Trad	EQRod	MF	Trad/ EQRod	Trad/ MF	Trad/ EQRod	Trad/ MF
EQ ₁	1	11.68	8.65	4.58	5.70	5.63	3.89	25.94	60.79	1.23	31.75
	2	10.96	6.51	5.08	7.59	3.38	5.12	40.60	53.65	55.47	32.54
	3	11.04	8.30	3.97	6.76	6.93	4.04	24.82	64.04	-2.51	40.24
EQ ₂	1	9.34	7.17	4.07	9.87	7.90	5.10	23.23	56.42	19.96	48.33
	2	10.03	7.63	3.81	7.61	7.20	4.71	23.93	62.01	5.39	38.11
	3	9.45	6.52	3.24	9.37	7.10	3.66	31.01	65.71	24.23	60.94
EQ ₃	1	11.88	12.30	5.33	10.43	10.18	5.29	-3.54	55.13	2.40	49.28
	2	12.62	10.36	5.37	10.67	7.33	5.07	17.91	57.45	31.30	52.48
	3	13.24	12.09	5.75	11.75	9.84	5.69	8.69	56.57	16.26	51.57
EQ ₄	1	14.15	10.92	6.17	14.45	11.94	6.53	22.83	56.40	17.37	54.81
	2	13.56	11.68	6.05	14.44	12.42	7.17	13.86	55.38	13.99	50.35
	3	13.78	7.36	5.27	12.30	7.41	5.73	46.59	61.76	39.76	53.41
EQ ₅	1	7.31	8.11	4.94	9.72	7.36	5.04	-10.94	32.42	24.28	48.15
	2	9.87	5.89	4.86	8.50	6.80	3.93	40.32	50.76	20.00	53.76
	3	6.45	5.69	4.66	6.80	5.99	4.45	11.78	27.75	11.91	34.56

Table A.24. **Cracked concrete, 50% Input:** summary of test results in terms of Driving Mass Acceleration and its reductions.

	Test	Peak DMA [g]						Ratio [%]			
		Positive			Negative			Positive		Negative	
		Trad	EQRod	MF	Trad	EQRod	MF	Trad/ EQRod	Trad/ MF	Trad/ EQRod	Trad/ MF
EQ ₁	1	0.26	0.29	0.30	0.48	0.40	0.36	-11.54	15.38	16.67	25.00
	2	0.55	0.14	0.37	0.71	0.27	0.40	74.55	32.73	61.97	43.66
	3	0.46	0.35	0.28	0.73	0.46	0.31	23.91	39.13	36.99	57.53
EQ ₂	1	0.59	0.54	0.33	0.64	0.39	0.33	8.47	44.07	39.06	48.44
	2	0.54	0.44	0.29	0.68	0.39	0.27	18.52	46.30	42.65	60.29
	3	0.62	0.45	0.29	0.61	0.34	0.25	27.42	53.23	44.26	59.02
EQ ₃	1	0.58	0.49	0.32	0.80	0.66	0.36	15.52	44.83	17.50	55.00
	2	0.60	0.31	0.29	0.89	0.56	0.35	48.33	51.67	37.08	60.67
	3	0.64	0.55	0.35	0.87	0.70	0.39	14.06	45.31	19.54	55.17
EQ ₄	1	0.90	0.63	0.41	0.92	0.47	0.34	30.00	54.44	48.91	63.04
	2	0.95	0.68	0.43	0.87	0.56	0.37	28.42	54.74	35.63	57.47
	3	0.82	0.35	0.39	0.93	0.22	0.32	57.32	52.44	76.34	65.59
EQ ₅	1	0.62	0.21	0.38	0.59	0.19	0.27	66.13	38.71	67.80	54.24
	2	0.51	0.22	0.30	0.54	0.19	0.23	56.86	41.18	64.81	57.41
	3	0.51	0.43	0.29	0.36	0.32	0.24	15.69	43.14	11.11	33.33

Table A.25. **Cracked concrete, 50% Input:** summary of test results in terms of Driving Mass Displacement and its reductions.

	Test	Peak DMD [mm]						Ratio [%]			
		Positive			Negative			Positive		Negative	
		Trad	EQRod	MF	Trad	EQRod	MF	Trad/ EQRod	Trad/ MF	Trad/ EQRod	Trad/ MF
EQ ₁	1	0.33	2.28	0.07	2.50	1.58	0.08	-590.91	78.79	36.80	96.80
	2	1.57	0.73	0.02	1.51	1.58	0.01	53.50	98.73	-4.64	99.34
	3	1.13	2.11	0.08	1.66	1.97	0.08	-86.73	92.92	-18.67	95.18
EQ ₂	1	2.69	2.88	0.02	0.40	1.44	0.03	-7.06	99.26	-260.00	92.50
	2	1.42	1.16	0.06	1.54	2.99	0.06	18.31	95.77	-94.16	96.10
	3	1.66	1.86	0.04	1.43	1.97	0.05	-12.05	97.59	-37.76	96.50
EQ ₃	1	2.52	3.10	0.02	0.86	2.02	0.06	-23.02	99.21	-134.88	93.02
	2	2.77	1.19	0.06	0.98	2.79	0.10	57.04	97.83	-184.69	89.80
	3	2.30	2.98	0.03	1.14	2.72	0.06	-29.57	98.70	-138.60	94.74
EQ ₄	1	2.43	2.61	0.05	1.56	1.96	0.04	-7.41	97.94	-25.64	97.44
	2	3.18	2.68	0.04	0.95	2.53	0.04	15.72	98.74	-166.32	95.79
	3	2.00	0.99	0.03	1.52	1.46	0.03	50.50	98.50	3.95	98.03
EQ ₅	1	0.45	0.19	0.00	2.46	1.62	0.06	57.78	100.0 0	34.15	97.56
	2	0.38	0.21	0.03	2.41	1.29	0.03	44.74	92.11	46.47	98.76
	3	0.42	1.06	0.02	2.52	2.65	0.02	-152.38	95.24	-5.16	99.21

Table A.26. **Cracked concrete, 50% Input:** summary of test results in terms of Driving Mass Force and its reductions.

	Test	Peak DMF [kN]						Ratio [%]			
		Positive			Negative			Positive		Negative	
		Trad	EQRod	MF	Trad	EQRod	MF	Trad/ EQRod	Trad/ MF	Trad/ EQRod	Trad/ MF
EQ ₁	1	5.03	4.30	3.45	2.58	3.11	2.77	14.51	31.41	-20.54	-7.36
	2	6.85	2.93	3.60	5.66	1.01	3.61	57.23	47.45	82.16	36.22
	3	6.64	4.34	3.03	4.69	3.88	2.89	34.64	54.37	17.27	38.38
EQ ₂	1	6.34	4.06	3.14	5.89	5.61	3.35	35.96	50.47	4.75	43.12
	2	6.82	4.03	2.62	5.58	4.74	2.99	40.91	61.58	15.05	46.42
	3	5.82	3.41	2.52	6.66	4.61	2.93	41.41	56.70	30.78	56.01
EQ ₃	1	8.22	7.17	3.51	5.80	4.78	3.00	12.77	57.30	17.59	48.28
	2	9.03	6.09	3.33	6.21	3.17	2.92	32.56	63.12	48.95	52.98
	3	9.11	7.38	3.77	6.40	5.70	3.13	18.99	58.62	10.94	51.09
EQ ₄	1	9.38	5.06	3.49	9.37	6.54	4.02	46.06	62.79	30.20	57.10
	2	9.11	5.93	3.80	9.83	7.04	4.33	34.91	58.29	28.38	55.95
	3	9.41	2.28	3.45	8.38	3.41	3.70	75.77	63.34	59.31	55.85
EQ ₅	1	6.11	1.91	2.56	6.23	2.13	3.77	68.74	58.10	65.81	39.49
	2	5.88	2.02	2.63	5.19	2.09	2.64	65.65	55.27	59.73	49.13
	3	3.62	3.43	2.56	5.03	4.42	2.92	5.25	29.28	12.13	41.95

A.4 References

Pampanin S., Bianchi S., Ciurlanti J. (2017). *Shake table tests of post-installed anchors with supplemental damping (EQ-Rod 2.0)*, Report prepared for Fischerwerke Artur Fischer GmbH & Co. KG, Sapienza University of Rome, Rome, Italy.

APPENDIX B:

SLaMA-based analytical procedure for the cost/performance-based evaluation of buildings

B.1 Introduction

This Appendix focuses on the implementation of an analytical procedure based on the Simplified Lateral Mechanism Analysis of NZSEE 2017 for the cost/performance evaluation of reinforced concrete buildings. The proposed methodology is validated comparing the results from this simplified procedure with the results obtained implementing more rigorous methods (numerical non-linear static and dynamic analyses). The comparison shows that the SLaMA-based approach can be a useful tool for the daily use of practicing engineers for a rapid evaluation of economic losses for both the seismic assessment of existing buildings as well as for initial feasibility studies of new structures.

This research led to the development of a conference paper to which this Appendix refers (Bianchi et al. 2019).

B.2 Evaluation of building response within the PBEE methodology

The seismic design philosophy is based on controlling the building response under low-to-high intensity earthquakes, including both structural and non-structural components. Traditionally the design aimed to prevent the damage of these elements under low-intensity earthquakes, to reach repairable conditions in medium-intensity shakings and to avoid

building collapse under high-intensity earthquakes. However, past earthquakes highlighted very high economic losses in terms of repair costs and business interruption even for code-compliant buildings, leading in the mid-1990s to the development of the performance-based earthquake engineering (PBEE) concept (Cornell et al. 2002, Krawinkler et al. 2004).

SEAOC Vision 2000 (1995) is one of the first documents where there is evidence of this new philosophy. Different structural and non-structural performance levels at various intensity demands (frequent, occasional, rare, and very rare) are described and classified as fully operational, operational, life safety, and near collapse, thus design objectives for building typologies are identified through the combination of performance levels and seismic hazard. Following this original concept, a series of additional documents were published considering the same design philosophy and representing the first generation of PBEE (ATC 40, FEMA 273, FEMA 356).

Nevertheless, the initial PBEE procedures were deterministic-based and affected by many shortcomings. Therefore, a more rigorous and probabilistic methodology was developed by the Pacific Earthquake Engineering Research (PEER) Center. The PEER methodology allows the direct evaluation (estimation) of performance measures such as economic losses, downtime and casualties that are relevant to stakeholders to manage decisions about seismic risk mitigation. For the practical implementation of the probabilistic procedure, the US Federal Emergency Management Agency (FEMA) commissioned to the Applied Technology Council (ATC) the development of an electronic tool to apply this methodology, referred to as Performance Assessment Calculation Tool (PACT) and provided with the publication of the FEMA P-58 Document (FEMA P-58 2012).

The application of the PBEE procedure is primary for the seismic loss evaluation of new buildings as well as for taking decisions on intervention/retrofit strategies of existing structures. However, the fully probabilistic procedure can be time-consuming in its implementation, because it also requires the definition of numerical models to evaluate the building response through non-linear static and dynamic analyses. Structural analysis is conducted to determine the building response to earthquake shaking, obtaining values for those key parameters that are predictive of structural and non-structural damage (floor accelerations, floor velocities, story drift ratios and residual drift ratios).

Alternative procedures can be used to estimate the peak values of these parameters:

1. *Simplified procedures.* Linear models and static analyses are implemented to estimate the lateral yield strength, generate median demand values, thus determine the building response at each floor through simplified and numerically calibrated formulas;
2. *Non-linear static analyses.* They allow the definition of the building capacity curve from numerical modelling as well as the performance points for the various seismic intensity (i.e. Capacity Spectrum Method), giving more accurate predictions than the previous ones;
3. *Non-linear response (time) history analyses.* These analyses represent the most sophisticated method. The structure is numerically modelled in its full non-linear cyclic and dynamic behaviour, sets of demand parameters are generated from sets of earthquake input motions and are used to develop statistics (median values and dispersions) for each parameter of interest.

Among all the aforementioned analysis methods, the non-linear static procedures (pushover) are the best compromise between accuracy and simplicity.

In the recently developed New Zealand Seismic Assessment Guidelines (NZSEE 2017) an analytical non-linear static analysis procedure has been proposed for the seismic assessment of reinforced concrete existing buildings, the Simplified Lateral Mechanism Analysis (SLaMA), schematically shown in Figure B.1. This assessment method, mandatory for every assessment prior to carry out any numerical modelling, is able to predict the building capacity curve (pushover) through an analytical study that, starting from the local section and member analysis and through the hierarchy of strengths evaluation of subassemblies, evaluates the local and global building mechanisms.

Notwithstanding the SLaMA procedure has been primarily implemented for the assessment existing structures, it can be applied, for the sake of simplicity, to rapidly estimate the seismic response of new reinforced concrete buildings, because it can be very useful for initial feasibility studies. In the case of a new building, the procedure can be modified and simplified as follows: a) in terms of input data, the building characteristics are not already available but obtained from a preliminary building design that aims to already respect the hierarchy of strengths determining a final beam-sway mechanism, as required by the seismic codes; b) the capacity curve of such type of building mechanism is analytically

determined considering the results from the section analysis evaluation; c) finally, introducing the capacity curve into the Acceleration-Displacement Response Spectra and combining it with the demand spectra, the expected maximum accelerations and displacements at different seismic intensities can be determined.

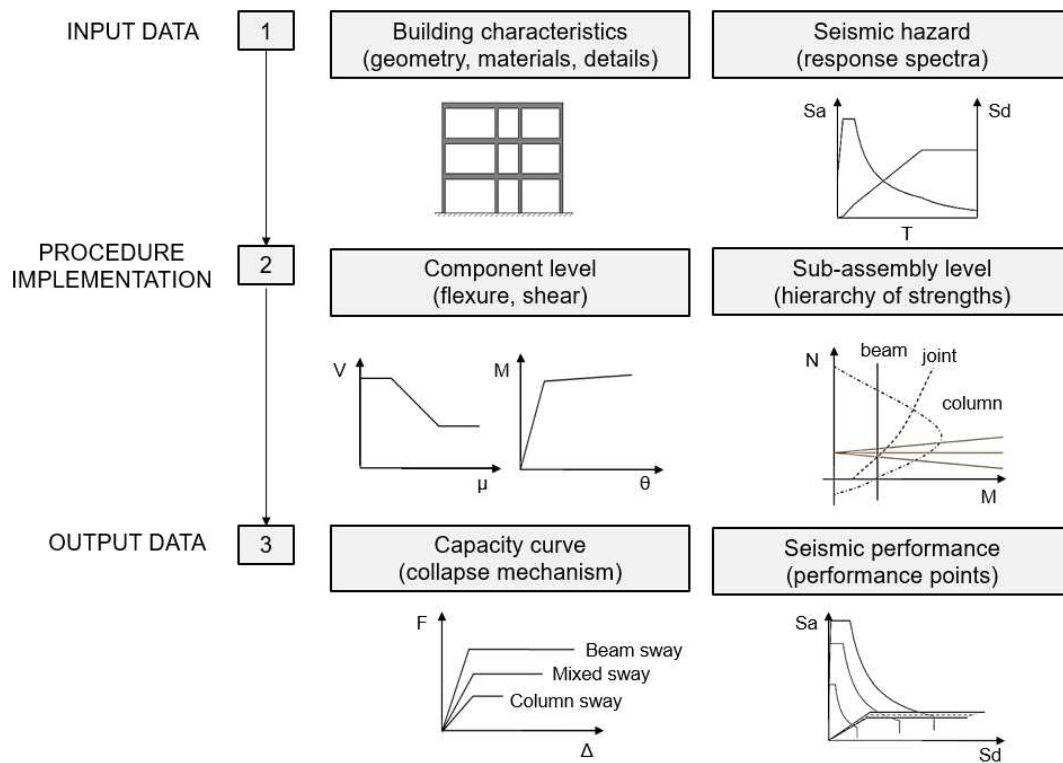


Figure B.1. SLAMA assessment procedure for reinforced concrete buildings.

B.3 Validation of the SLAMA-based analytical procedure

Apart from the seismic assessment process of existing buildings, the need for loss estimation in the common design process is starting to spread, therefore practical and efficient tools must be developed to be used by engineers. As alternative to more sophisticated procedures based on non-linear dynamic analyses, more rapid estimations of post-earthquake losses can be determined through non-linear static (pushover) evaluations, especially as part of an initial feasibility study of the building design features. Therefore, it is proposed the application of an analytical non-linear static analysis procedure, based on the Simplified Lateral Mechanism Analysis (SLAMA), for the rapid evaluation of post-earthquake losses of buildings without the need of more complicated numerical models.

Cost/performance evaluations are implemented for a set of multi-storey buildings considering different approaches: the proposed SLaMA-based analytical procedure and numerical analyses through both non-linear Push-Over and Time-History analyses. These numerical investigations are carried out with the aim of validating the analytical approach and confirming whether acceptable results in terms of economic losses can be expected from the SLaMA evaluation when compared to more sophisticated numerical results.

B.3.1. Case-study buildings

The procedure is implemented referring to a 5-storey monolithic reinforced concrete building located in a high seismic zone in Italy (Soil type C, PGA of 0.35 g at the Life-Safety Limit State), that is the same structure used for the full study presented in Chapter 5. From this case-study structure, referred as *Case1*, other structures are derived by varying: the beam span length in both seismic directions (*Case2*); the inter-storey height to 4.5 m (*Case3*); both the beam span length and the inter-storey height (*Case4*). Figure B.2 presents the plan view of the benchmark building (*Plan1*) and its variation (*Plan2*), while all the case-study structures are summarized in Figure B.3.

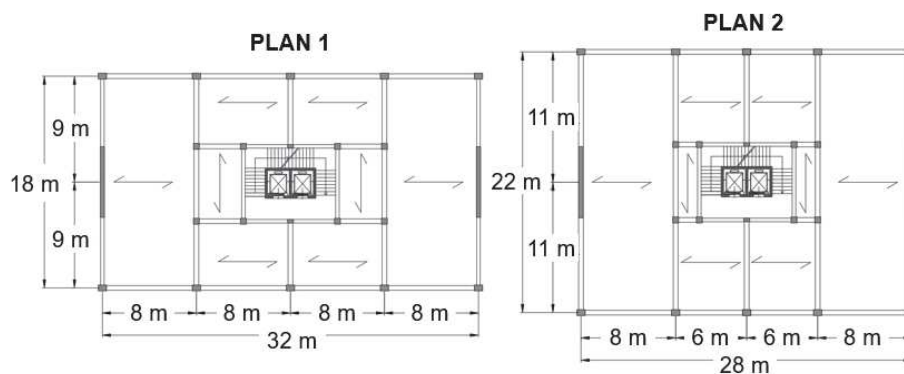


Figure B.2. Plan view and dimensions of the benchmark building (*Plan 1*, left) and modified plan (*Plan 2*, right).

In terms of dimensions of the structural members: the seismic beams and columns have same dimensions for both building plan (400 x 700 mm and 500 x 700 mm, respectively); while the wall is 6 m long, but its thickness varies depending on the plan configuration (350 mm for *Plan1* and 400 mm for *Plan2*). Finally, the gravity beams connecting the wall are 300 x 600 mm and 400 x 700 mm, respectively for *Plan 1* and *Plan 2*.

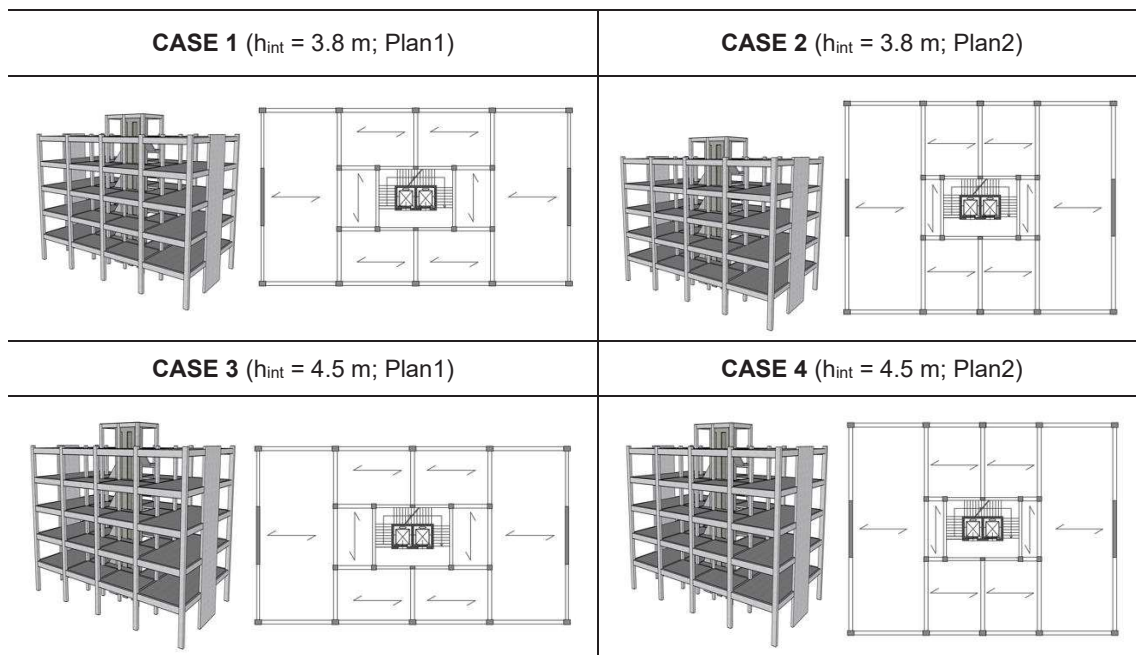


Figure B.3. Case-study structures considered for the investigation.

B.3.2. Design of structural system

Referring to this structural scheme, geometry and related gravity loads, all the buildings are designed following the Direct Displacement Based Design (DDBD) procedure (Priestley et al. 2007; Pampanin et al. 2010). The DDBD procedure has been performed at the ULS limit state (Life-Safety) considering an appropriate value for the inter-storey drift limit, i.e. 2% for the frame direction and 1.2% for the wall direction for all case-study structures (Table B.1).

Table B.1. Parameters from the DDBD procedure for all the case-study buildings.

Parameter	Case 1		Case 2		Case 3		Case 4	
	Frame	Wall	Frame	Wall	Frame	Wall	Frame	Wall
Δ_y [mm]	62.17	50.29	62.15	50.26	73.38	70.14	73.36	70.10
Δ_d [mm]	223.80	163.19	223.74	163.13	264.36	192.63	264.28	192.56
m_e [t]	2760.15	2627.80	2914.20	2774.46	2834.12	2698.27	2991.83	2848.42
H_e [m]	13.24	13.60	13.24	13.60	15.63	16.05	15.62	16.05
ξ_{eq} [%]	19.19	18.35	19.19	18.35	19.19	16.90	19.19	16.90
T_e [s]	2.65	1.91	2.65	1.91	3.13	2.22	3.13	2.21
K_e [kN/m]	15533.5	28383.0	16409.6	29987.5	11429.8	21705.3	12072.43	22928.2
V_b [kN]	3476.42	4631.94	3671.44	4891.99	3021.56	4181.03	3190.55	4415.01

Distributing the base shear obtained by the DDBD throughout each structure, the internal actions in the structural members are determined and the required steel reinforcement of each component can be designed.

B.3.3. Building seismic response

The building response is initially estimated through the SLaMA procedure described in the New Zealand code (NZSEE 2017). The seismic design considers capacity design principles, thus it is sufficient to evaluate the capacity curves related to the beam-sway mechanism. Converting the base shear/displacement relationships into acceleration/displacement responses and considering the demand spectra from the Italian Code (NTC 2018) of either elastic or ultimate limit states - SLO, SLD, SLV, SLC, or, respectively Immediate Operational, Damage Control, Life Safety and Collapse Prevention -, the building performance points at each intensity level can be identified in the Acceleration Demand Response Spectrum (ADRS) domain. The demand spectra of the ultimate limit states are reduced considering the equivalent viscous damping evaluated through the formulation proposed by Priestley et al. 2007. The SLaMA capacity curves are compared to those obtained from numerical non-linear static analyses (e.g. Figure B.4 for Case 2).

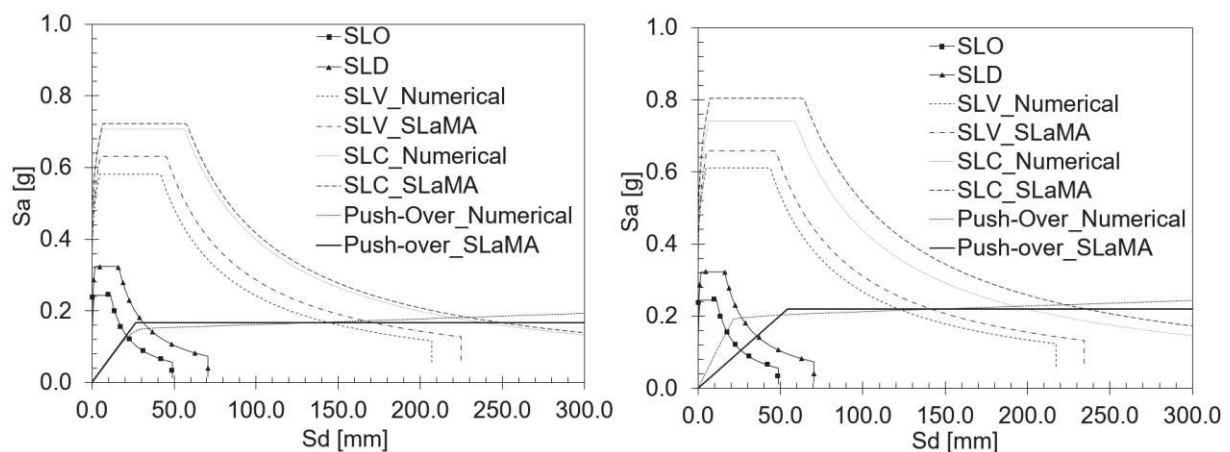


Figure B.4. Analytical and numerical capacity curves in the ADRS domain for one case-study structure (Case 2) considering both frame (left) and wall (right) directions.

Numerical models of each building are implemented using Ruaumoko 2D analysis program (Carr 2003) through a lamped-plasticity approach. Applying the Capacity Spectrum Method (ATC 40) where the equivalent viscous structural damping is directly evaluated from push-pull analyses, the performance points can be also evaluated for this analysis approach.

From the previous graphs it can be noticed that the analytical curves well predict the building seismic behaviour. Very similar performance points are obtained from the analytical and numerical procedure for all the case study-buildings in the frame directions, apart from the collapse limit state because of the increasing slope of the numerical curve and the inherent limit of the analytical curve itself which is not modelling the collapse point. Regarding the wall directions, the main differences in the performance points are obtained for the lower limit states (fully operational and operational) because of the modelling of the wall as equivalent frame which produces a very high initial stiffness when compared to the one from the analytical procedure.

In order to further validate the accuracy of the SLaMA method as a loss-modelling simplified procedure, non-linear time history analyses are also performed using sets of 7 accelerograms obtained from REXEL (Iervolino et al. 2009) for each seismic intensity. The accelerograms, extrapolated from the European Strong Motion database, are properly scaled to guarantee the spectro-compatibility to each demand spectrum. E.g. for the Life-Safety intensity level, the response spectra related to the 7 accelerograms, the average and target spectra, the lower and upper tolerances, as well as the range of periods (0.15 s ÷ 2 s) selected for the spectro-compatibility can be found in Figure B.5.

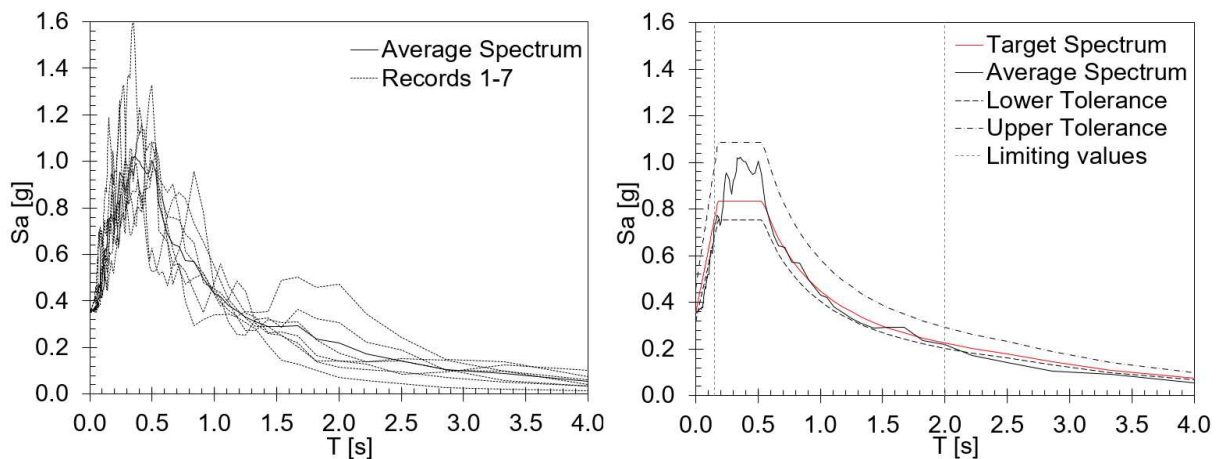


Figure B.5. Spectro-compatibility at Life-Safety intensity level.

A direct estimation of the floor accelerations and inter-storey drift ratios can be determined from time-history analyses. As example, results in terms of storey drift ratios are presented for one case-study structure and one seismic intensity level in Figure B.6. These key engineering demand parameters are direct input data for the loss assessment investigations, while for the analytical and numerical non-linear static assessments they are

estimated from the performance points, representing the behaviour of the equivalent SDOF system, at each seismic intensity. In fact, considering the effective building height these parameters can be estimated at each floor assuming proper displacement and acceleration profiles for the SLaMA procedure or the exact profiles from the numerical Push-Over results.

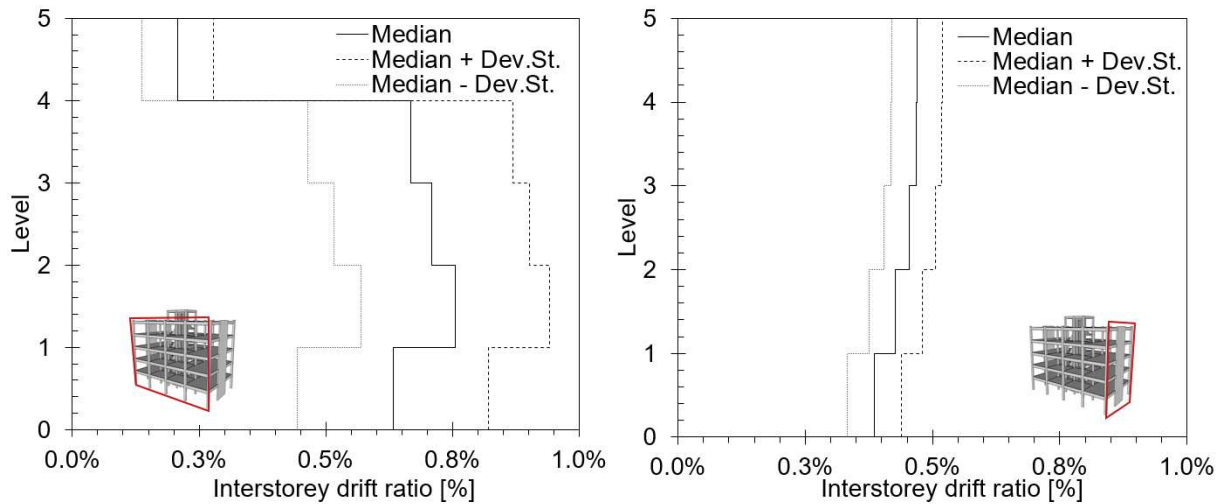


Figure B.6. Time-history results in terms of storey drift ratios at Life-Safety demand level for both frame and wall directions of Case2 structure.

B.3.4. Loss assessment analysis

Loss assessment estimations are performed using the PACT software (FEMA P-58 2012) where all the case-study buildings are implemented. The input data for the analysis are: 1) the total replacement cost and time, calculated referring to 338 euro/m³ and estimating the proper number of man-days; 2) the population model of the building, provided by the software depending on the building use; 3) the component fragilities, considering all the structural members, non-structural components, building services and contents present into the building; 4) the seismic building response, estimated using the different structural analyses methods; 5) finally, the seismic hazard, whose function is built referring to the demand intensity levels reported in the Italian Code (NTC 2018) ($T_R=30$ years, Fully Operational; $T_R=50$ years, Operational; $T_R=475$ years, Life-Safety; $T_R=975$ years, Near Collapse).

Regarding the non-structural systems, it is assumed that all the structural skeletons are covered by external curtain walls, while interior components include lightweight partitions, suspended ceilings, electrical and mechanical services and contents. All the structural and

non-structural components are defined using the fragility curves and consequence functions already available in the fragility database. The results obtained for all the case-study buildings considering the alternative structural analyses are reported in Figure B.7 and Table B.2.

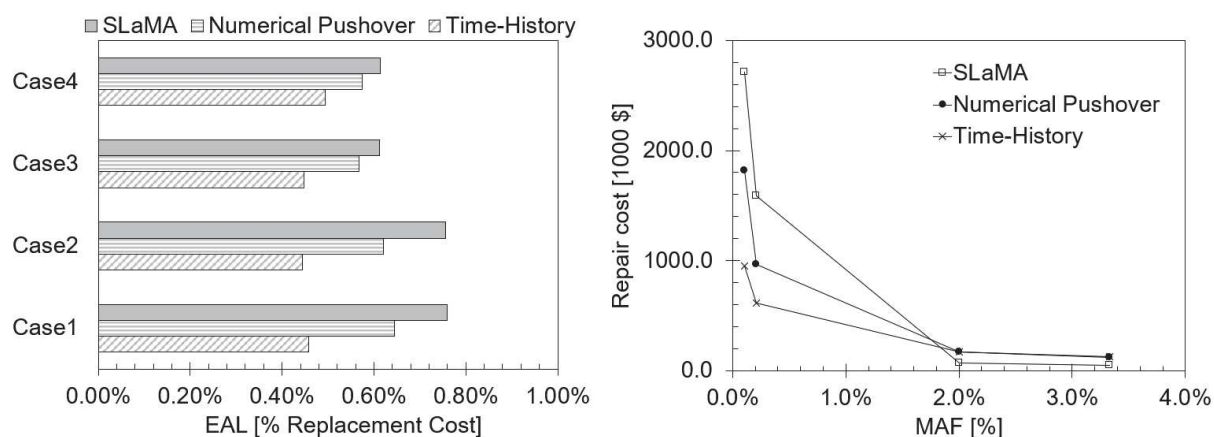


Figure B.7. EAL values for all the four case-study buildings considering different structural analysis results (left) and Repair cost/Median Annual Frequency functions (right) for one case-study structure (Case 2).

Table B.2. EAL values from different non-linear analyses results: SLaMA versus numerical Push-Over (PO) versus Time-History (TH).

	Case 1	Case 2	Case 3	Case 4
EAL _{SLaMA} [%RC]	0.759	0.755	0.612	0.614
EAL _{PO} [%RC]	0.644	0.621	0.567	0.573
EAL _{TH} [%RC]	0.457	0.444	0.447	0.493
Δ EAL _{SLaMA / PO}	15.16	17.79	7.31	6.70
Δ EAL _{SLaMA / TH}	39.76	41.18	26.84	19.75
Δ EAL _{PO / TH}	28.98	28.44	21.07	14.02

SLaMA vs Pushover

The loss estimations are carried out considering the floor accelerations and inter-storey drift ratios from: 1) for the SLaMA approach, these parameters are evaluated assuming a proper displacement profile for the building beam-sway mechanism, as suggested in NZSEE Guidelines (NZSEE 2017) and considering the floor acceleration profile proposed by FEMA P-58 (2012) for simplified procedures, 2) for the numerical analysis, the floor accelerations and inter-storey drift ratios are determined from the performance points considering both the displacement and acceleration profiles resulting from the numerical investigation. All the loss estimations have been performed, in this initial validation of the SLaMA procedure, without

including the effects of the building collapse fragility or the residual drift into the results. As observed from the previous table, the application of SLaMA gives quite satisfactory results in terms of Expected Annual Losses (EAL) when compared to the results obtained from the numerical investigations, i.e. approximately 7-18% higher (conservative side).

Estimations of direct economic losses can be also developed through the simplified procedure presented in the Italian Guidelines for Seismic Risk Classification (DM 58 2017). This document describes a simple methodology to determine the expected annual losses, that is generally applied for the seismic assessment of existing buildings to investigate the benefits of retrofit strategies and regulate financial incentives provided to private owners to improve the risk/losses of their building. While, herein the same approach is applied to new buildings. The building analytical and numerical capacity curves are the starting points of this procedure, which requires the determination of the median annual frequencies, MAF, associated with the achievement of specific limit states in the structure. Particularly, in this study, two limit states (Damage Control and Life-Safety) are identified taking into account just the structural behaviour (achievement of yielding and ultimate rotations of structural members). These conditions are used to estimate the other limit states related to the structural and non-structural system, as explained in the Guidelines (DM 58 2017). The results from this simplified methodology are presented in Table B.3 and Figure B.8.

Table B.3. EAL (as a percentage of the Replacement Cost, RC) values from the simplified procedure Italian Guidelines for Seismic Risk Classification (DM 58 2017) using the building capacity curves from analytical (SLaMA) and numerical (PO) Pushover analyses.

	Case 1		Case 2		Case 3		Case 4	
	X Dir.	Y Dir.	X Dir.	Y Dir.	X Dir.	Y Dir.	X Dir.	Y Dir.
EAL _{SLaMA} [%RC]	0.810	0.717	0.892	0.669	0.789	0.631	0.865	0.595
EAL _{PO} [%RC]	0.872	0.749	0.920	0.704	0.849	0.648	0.891	0.623
Δ EAL _{PO/SLaMA}	7.17	4.22	2.99	4.94	7.27	2.68	2.91	4.49

As it can be observed from the previous table, the differences between the EAL values from the SLaMA-based approach and numerical analysis are less, in the range of 3-7% for both building directions. It is also noticed that the EALs associated to the numerical Pushover curves are now higher than those derived from the simplified SLaMA procedure, then it seems that the estimation is not on the conservative side. This can be justified considering that the elastic and ultimate limit state points are identified on the numerical capacity curves respectively for lower and greater accelerations compared to the same points on the

simplified elasto-plastic capacity curves. In any case, the differences are relatively low and well acceptable, thus the SLaMA method can be considered a valuable alternative tool to numerical methods for an initial cost-based building evaluation.

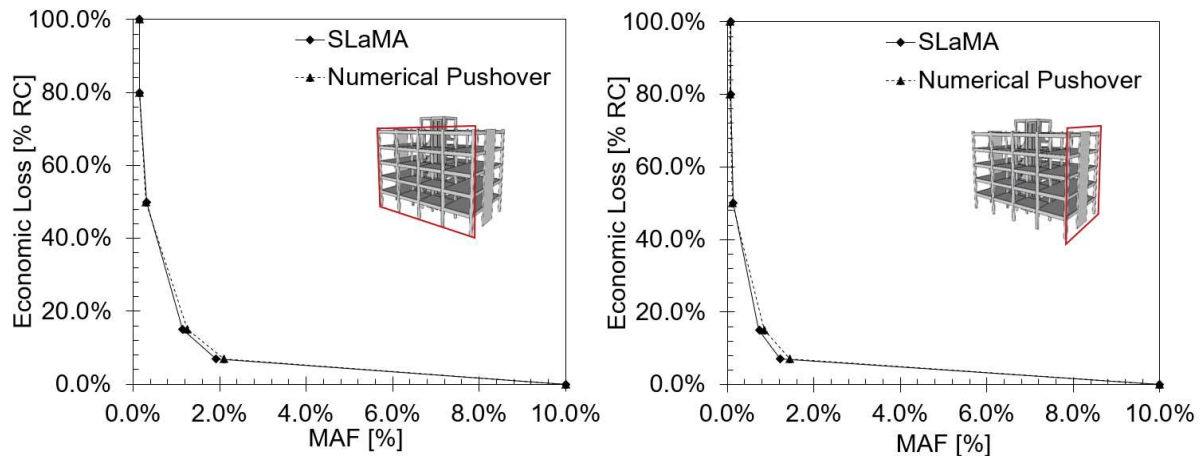


Figure B.8. Economic loss/Median Annual Frequency functions estimated following the Italian Guidelines for Seismic Risk Classification (DM 58 2017) for Case 2 and both building directions referring to the capacity curves obtained from SLaMA or numerical studies.

SLaMA vs Pushover vs Time-history

As shown in the previous Table B.2, the percentage difference between the EAL values from SLaMA approach and Time-History analysis is in the range of 20-40%, while between numerical Pushover and Time-History results a difference of 15-30% is estimated. Notwithstanding the differences between the EAL values from the simplified SLaMA procedure and the sophisticated Time-History investigation are in this case not negligible, the SLaMA method still produces acceptable results and, in any case, more accurate than those obtained from a linear static analysis suggested within the FEMA P-58 as an alternative simplified investigation to the non-linear response history analysis.

B.4 Conclusions

In the engineering community the estimation of performance metrics, such as repair costs or downtime, relevant to management decisions for seismic risk mitigation is becoming more consolidated not only for the assessment of existing buildings and thus for the evaluation of optimal retrofit strategy, whilst also in the seismic design of new buildings.

Probabilistic methodologies have been proposed to implement socio-economic loss estimations, which need as input data engineering demand parameters, i.e. floor accelerations and inter-storey drift ratios. The latter are usually obtained from simplified linear or non-linear analyses, requiring the implementation of simple or more-sophisticated numerical building models. The more complex the model the more accurate are typically expected to be the results in terms of seismic response, although very time-consuming modelling and analyses are required (i.e. Non-linear Time-History analyses).

With the aim of avoiding the implementation of un-necessary complex numerical models and knowing that non-linear static procedures are a very valuable compromise between accuracy and simplicity, the application of an analytical non-linear static analysis procedure, based on the Simplified Lateral Mechanism Analysis (SLaMA), is proposed for the cost/performance-based evaluation of buildings. The procedure is validated considering four multi-storey reinforced concrete structures. The Expected Annual Losses are estimated referring to different structural analyses (SLaMA, numerical Pushover, Time-Histories) and loss assessment methodologies (FEMA P-58 2012; DM 58 2017).

Notwithstanding the study represents an initial investigation, results highlighted that the SLaMA-based approach can provide satisfactory and acceptable results when compared to more complex numerical procedures. The method can be a promising tool for the daily use of practicing engineers for a rapid evaluation of the post-earthquake losses and it can be suggested both for the seismic assessment of existing buildings and retrofit interventions as well as part of the design feasibility study of new reinforced concrete structures.

B.5 References

- American Society of Civil Engineers (2000). *Prestandard and Commentary for the Seismic Rehabilitation of Buildings*, FEMA 356. ASCE for the Federal Emergency Management Agency, Washington.
- Applied Technology Council (1996). *Seismic evaluation and retrofit of concrete buildings, Volume 1, Technical Report ATC 40*, Redwood City, California, USA.
- Bianchi S., Ciurlanti J., Pampanin S. (2019). A SLAMA-based analytical procedure for the cost/performance-based evaluation of buildings, *7th ECCOMAS Thematic Conference on Computational Methods in Structural Dynamics and Earthquake Engineering*, Crete, Greece.
- Carr A.J. (2003). *Ruaumoko Program for Inelastic Dynamic Analysis – User Manual*, University of Canterbury, Christchurch, New Zealand.
- Cornell C. A., Jalayer F., Hamburger, R.O. Foutch, D.A. (2002). Probabilistic basis for 2000 SAC Federal Emergency Management Agency steel moment frame guidelines, *ASCE Journal of Structural Engineering*, 128 (4): 526-533.
- DM 58 (2017). *Linee guida per la classificazione del rischio sismico delle costruzioni*, Decreto Ministeriale 58 del 28/02/2017, Rome, Italy.
- Federal Emergency Management Agency (1997). *NEHRP Guidelines for Seismic Rehabilitation of Buildings*, FEMA-273, Building Seismic Safety Council, Washington, D.C.
- Federal Emergency Management Agency (2012). *Seismic Performance Assessment of Buildings, Volume 1 – Methodology, Technical Report FEMA-P-58-1*, Washington, D.C.
- Iervolino I., Galasso C., Cosenza E. (2009). REXEL: computer aided record selection for code-based seismic structural analysis, *Bulletin of Earthquake Engineering*, 8(339-362): 2009.
- Krawinkler H., Miranda E. (2004). *Performance-based earthquake engineering. Earthquake Engineering: from engineering seismology to performance-based engineering*, Bertero VV (eds), CRC Press: Boca Raton.
- New Zealand Society for Earthquake Engineering (2017). *The Seismic Assessment of Existing Building – Technical Guidelines for Engineering Assessments*, NZSEE 2017, New Zealand
- NTC (2018). *Aggiornamento delle Norme Tecniche per le Costruzioni*, Supplemento ordinario n°8 alle G.U. n° 42 del 20/02/2018, serie generale, Rome, Italy.
- Pampanin S., Marriott D., Palermo A. and New Zealand Concrete Society (2010). *PRESSS Design Handbook*, Auckland, New Zealand.
- Priestley M.J.N., Calvi G.M., Kowalsky M.J. (2007). *Direct Displacement-Based Seismic Design of Structures*, 1st edition, IUSS Press, Pavia, Italy.
- Structural Engineers Associate of California (1995). *Performance-based seismic engineering*, SEAOC Vision 2000, Sacramento, California, USA.

APPENDIX C:

Shake-table tests on an integrated low-damage building system (SERA Project): Seismic design and structural verifications of the Test Building

C.1 Introduction

This Appendix provides more information on the design of the specimen structural skeleton. The properties of the Test Building (geometry, sections, hybrid connections) were defined scaling the Prototype system through the Cauchy-Froude similitude, however, a complete Direct-Displacement Based Design was also implemented as further verification and this design procedure is herein presented. A summary of all the structural verifications implemented for each component is also reported, as well as the dimensional tolerances and the total specimen mass.

C.2 Test Building design

C.2.1 Building data

For implementing the design procedure, data on the Test Building in terms of geometry and sectional dimensions, materials and total seismic mass as well as the seismic demand need to be known.

- Building and section geometry.

These properties were defined scaling the dimensions of the Prototype Building and are summarized in Figure C.1 and Table C.1.

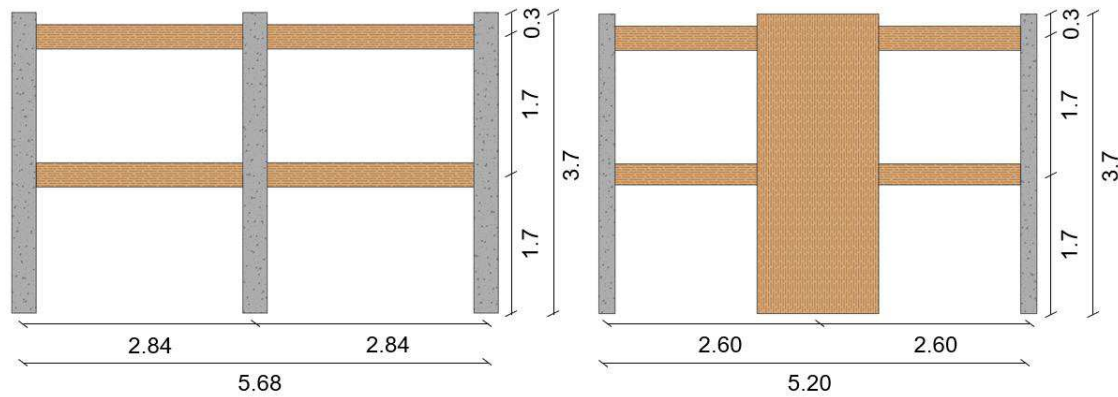


Figure C.1. Global dimensions of the Test Building in the frame - or longitudinal - (left) and wall - or transversal - (right) directions.

Table C.1. Section properties of the seismic resistant components.

Section property	Beam	Column	Wall
Height [m]	0.3	0.3	1.5
Width [m]	0.2	0.2	0.158
Height of internal hole [m]	0.08	-	0.2
Width of internal hole [m]	0.04	-	0.04
Area [m ²]	0.06	0.06	0.23
Inertia Moment I_x [m ⁴]	0.00045	0.00045	0.04441

- Material properties

The Test Building was realized using different typologies of material. The structural frames in the longitudinal direction consisted of Glulam 32h timber beams with horizontal post-tensioned tendons (1/2' for the first floor and 3/8' for the second floor) and S 235 mild steel external dissipaters, while the columns were made of C 35/45 concrete with B 450C reinforcement bars and S 235 mild steel external dissipaters. For the transversal direction, the XLam C24 timber walls were designed to have Dywidag 18 WR post-tensioned bars and S 235 mild steel external dissipaters. The other gravity beams as well as the timber joists and the timber parts of the 3PT slab were made of Glulam 32h, while C 35/45 concrete was also used for the concrete slab of the first floor and for making the concrete blocks of the second level.

The properties of the different materials of the structural members can be found in the following tables (from Table C.2 to Table C.9).

Table C.2. Concrete properties of all the concrete structural members.

CONCRETE C35/45 (EN1992-1-1 2004, NTC 2018)	
Mean secant modulus of elasticity E_{cm} ,	34077 MPa
Mean shear modulus G_{cm}	14199 MPa
Specified characteristic cylinder compressive strength f_{ck}	35 MPa
Mean concrete cylinder compressive strength f_{cm}	43 MPa
Mean density γ_m	25 kN/m ³
Poisson coefficient ν	0.2

Table C.3. Steel reinforcement properties of the concrete components (columns, slab).

STEEL B 450 C (NTC 2018)	
Modulus of elasticity E_s	210000 MPa
Specified characteristic yield strength f_{yk}	450 MPa
Specified characteristic ultimate tensile strength f_{tk}	540 MPa
Mean density γ_m	78.5 kN/m ³
Poisson coefficient ν	0.3

Table C.4. Timber properties of all the timber components, apart from the walls.

TIMBER GL32h (UNI EN 1194 2000, UNI EN 14080 2013)	
Mean value of modulus of elasticity $E_{m,o}$ (parallel to the grains)	14200 MPa
Mean value of modulus of elasticity $E_{m,90}$ (orthogonal to the grains)	300 MPa
Mean value of shear modulus G_m	650 MPa
Bending strength $f_{m,k}$	32 MPa
Compression strength (parallel to the grains) $f_{c,0,k}$	32 MPa
Compression strength (orthogonal to the grains) $f_{c,90,k}$	2.5 MPa
Tensile strength (parallel to the grains) $f_{t,0,k}$	25.6 MPa
Shear strength $f_{v,k}$	3.5 MPa
Mean density γ_m	4.81 kN/m ³

Table C.5. Timber properties of the seismic walls.

TIMBER Xlam 24 (UNI EN 338 2016, UNI EN 14081-1 2016)	
Mean value of modulus of elasticity $E_{m,o}$ (parallel to the grains)	11000 MPa
Mean value of modulus of elasticity $E_{m,90}$ (orthogonal to the grains)	370 MPa
Mean value of shear modulus G_m	690 MPa
Bending strength $f_{m,k}$	24 MPa
Compression strength (parallel to the grains) $f_{c,0,k}$	21 MPa
Compression strength (orthogonal to the grains) $f_{c,90,k}$	2.5 MPa
Tensile strength (parallel to the grains) $f_{t,0,k}$	14 MPa
Shear strength $f_{v,k}$	4 MPa
Mean density γ_m	4.12 kN/m ³

Table C.6. Steel properties of the external dissipaters.

STEEL S235 (EN 1993-1-1 2005, NTC 2018)	
Modulus of elasticity E_s	210000 MPa
Specified characteristic yield strength f_{yk}	235 MPa
Specified characteristic ultimate tensile strength f_{tk}	360 MPa
Mean density γ_m	78.5 kN/m ³
Poisson coefficient ν	0.3

Table C.7. Steel properties of the beam post-tensioned cables (from Anchelor-Mittal catalogue) - First floor.

Φ 1/2 - 7 WIRE STRANDS (ASTM A 416/A 416 M)	
Modulus of elasticity E_s	201000 MPa
Ultimate strength f_u	1860 MPa
Minimum breaking strength	183.7 kN
Yield strength minimum load at 1% extension	165.3 kN

Table C.8. Steel properties of the beam post-tensioned cables (from Anchelor-Mittal catalogue) - Second floor.

Φ 3/8 - 7 WIRE STRANDS (ASTM A 416/A 416 M)	
Modulus of elasticity E_s	201000 MPa
Ultimate strength f_u	1860 MPa
Minimum breaking strength	102.3 kN
Yield strength minimum load at 1% extension	92.1 kN

Table C.9. Steel properties of the wall post-tensioned bars (from Dywidag catalogue).

18WR THREADED BAR (EN1992-1-1 2004)	
Modulus of elasticity E_s	205000 MPa
Ultimate strength f_u	1050 MPa
Characteristic breaking load	255 kN
Maximum initial stressing force	204 kN
Maximum overstressing force	219 kN

- Loads and total building mass

Apart from the self-weight of all the structural components, the gravity loads of the two flooring systems as well as the additional load from the non-structural components were calculated to be included within the design procedure.

The floor gravity load included the dead weight (G_1 and G_2) and the live load (Q) of the floor systems, which are summarized in Table C.10. The Q values were obtained scaling the live loads of the Prototype Building, characterized by a commercial use in the first building floor and a not-accessible roof in the second building floor. While, Table C.11 lists the weight of each typology of non-structural component. It is observed that the non-structural weight was defined basing on the values provided by each industry supplier.

Table C.10. Gravity loads of the two flooring systems.

Section property	First level	Second level
Dead load G_1 [kN/m ²]	0.85	0.91
Super imposed dead load G_2 [kN/m ²]	0.50	0.50
Live load Q [kN/m ²]	1.00	0.25

Table C.11. Non-structural weight.

Element	Total weight [t]
GFRC facades	2.16
Spider glazing facades	1.90
Fiber-reinforced gypsum partitions	1.00
Masonry partition	0.62

Referring to these vertical loads, the total seismic mass was determined. This mass was taken into account for the implementation of the seismic design, thus, it had to include all the steel assemblies required for forming the hybrid connections and for connecting the different structural members. Not knowing at the beginning of the project the detailing of these steel assemblies, this additional mass was included assuming an increase of 20% of the mass. The specimen seismic mass (weights + driving masses) considered for the Test Building design, i.e. referring to the heaviest system configuration (*Option 2*), is summarized in Table C.12.

Table C.12. Seismic mass of the Test Building.

Level	Element	Total driving mass [t]	Total weight [t]
First floor	Seismic beams	0.325	0.325
	Seismic columns	1.72	1.72
	Seismic walls	0.42	0.42
	Gravity beams	0.15	0.15
	Edge beams	0.19	0.19
	TCC floor	5.83	2.52
	GFRC facades	-	1.08
	Spider glazing facades	-	0.87
	Masonry partition	-	0.62

Level	Element	Total driving mass [t]	Total weight [t]
Second floor	Seismic beams	0.325	0.325
	Seismic columns	1.17	1.17
	Seismic walls	0.29	0.29
	Edge beams	0.19	0.19
	3PT floor	4.99	2.71
	GFRC facades	-	0.54
	Spider glazing facades	-	0.59

C.2.2 Seismic demand

The DDBD procedure of the Test Building was implemented with reference to the response spectra of Figure C.2 (scaled from the spectra of Figure 6.3 of Chapter 6), representing the ULS acceleration and displacement elastic spectra (5% damping, 475 years return period). These design spectra were evaluated implementing the NTC 2018 formulations and using the parameters reported in Table C.13, obtained as mean values from 5 different high seismicity zones.

Table C.13. Parameters used for the definition of the design spectra.

Element	Value
Horizontal ground acceleration on type A soil a_g [g]	0.267
Amplification factor F_o	2.368
Reference value for the beginning of the constant velocity range T_{c^*} [s]	0.367
Soil type	C
Topography type	T1
Soil factor S	1.320
Lower limit of the period of the constant spectral acceleration branch T_B [s]	0.127
Upper limit of the period of the constant spectral acceleration branch T_C [s]	0.380
Beginning of the constant displacement response range T_D [s]	1.887

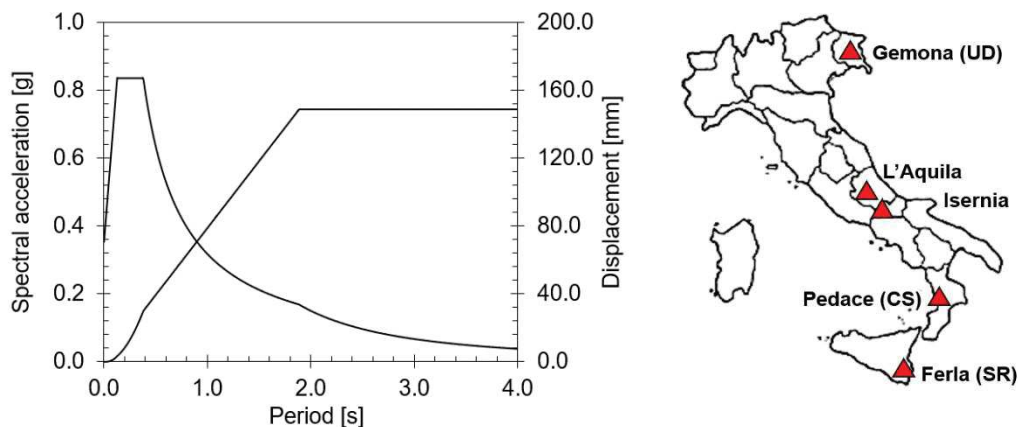


Figure C.2. Left: Elastic acceleration and displacement spectra at ULS for the scaled structure. Right: 5 locations contributing in the definition of the seismic demand parameters.

C.2.3 DDBD procedure

The design was carried out following the Direct-Displacement Based Design (DDBD) procedure, originally proposed by Priestley (1993) and further refined in the last decades (Priestley et al. 2007, Pampanin et al. 2010), which allows the determination of the internal forces to be used for the design of the hybrid connections. Considering an appropriate inter-storey drift limit suggested by material strain limits for both building directions, the procedure reduces the structure to a SDOF system, and its base shear is obtained through the following step-by-step procedure:

- The design displacement at each building level is determined from the imposed inter-storey drift:

$$\Delta_i = \theta_d \cdot H_i$$

- Using the MDOF parameters (Δ_i, m_i, H_i), the effective mass m_e and the displacement of the effective mass Δ_d at the effective height H_e can be evaluated:

$$\Delta_d = \frac{\sum_{i=1}^n (m_i \cdot \Delta_i^2)}{\sum_{i=1}^n (m_i \cdot \Delta_i)}$$

$$m_e = \frac{\sum_{i=1}^n (m_i \cdot \Delta_i)}{\Delta_d}$$

$$H_e = \frac{\sum_{i=1}^n (m_i \cdot \Delta_i \cdot H_i)}{\sum_{i=1}^n (m_i \cdot \Delta_i)}$$

- The ductility of the system can be calculated as:

$$\mu = \frac{\Delta_d}{\Delta_y}$$

Where Δ_d is the design displacement previously evaluated and Δ_y is the yield displacement defined from the yield rotation θ_y as:

$$\Delta_i = \theta_y \cdot H_i$$

$$\Delta_y = \frac{\sum_{i=1}^n (m_i \cdot \Delta_i^2)}{\sum_{i=1}^n (m_i \cdot \Delta_i)}$$

- From the system ductility, the equivalent structural damping (ξ_{eq}) can be calculated. Assuming a value for the re-centering or over-turning moment ratio λ , that is the ratio between the moment contribution provided by the post-tensioned tendons (M_{pt}) and by axial load (M_n) and the moment contribution from the energy dissipation devices (M_s):

$$\lambda = \frac{M_{pt} + M_n}{M_s} = \frac{\alpha_{OTM}}{\beta_{OTM}}$$

The structural damping can be determined as:

$$\xi_{eq} = \xi_{hyst} + \xi_{el};$$

$$\xi_{el} = 5 \cdot \mu^{-0.43}$$

$$\xi_{hyst} = \frac{(2 - 2 \cdot \alpha_{OTM}) \cdot (\mu - 1)}{(\pi \cdot \mu \cdot (1 + r \cdot (\mu - 1))) \cdot 65}$$

Where r is the post-yielding stiffness factor equal to 0.1 for the frame system and 0.2 for the wall system.

- Introducing the η spectral reduction factor by *Priestley et al. (2007)* which is applied to the 5% elastic spectrum, the building effective period (T_e) can be determined from the target displacement (Δ_d).

$$\eta = \left(\frac{7}{2 + \xi_{eq}} \right)^{\alpha_{SF}}$$

Where α_{SF} is taken equal to 0.25 representing sites located close to a major fault with ground motions comprising of near-fault.

- Therefore, the building base shear is calculated multiplying the secant stiffness of the SDOF system by the target displacement:

$$K_e = \frac{4 \cdot \pi^2 \cdot m_e}{T_e^2}$$

$$V_b = K_e \Delta_d$$

And distributing this base shear throughout the building, the internal forces acting on each structural member can be determined, and the elements (beams, columns and walls) and their connections can be designed using capacity design principles.

For the DDBD of the Test Building, the following assumptions were made:

1. The design inter-storey drift ratios were assumed to be 1.5% and 1.0% for the frame and wall directions, respectively;
2. The system ductility was estimated using the formulation previously indicated for the frame system, while it was assumed to be 4 for the wall system;
3. The re-centering ratio λ was considered equal to 1.50 (60% unbonded post-tensioned tendons, 40% dissipative devices) for the structural wall while equal to 1.25 (56% unbonded post-tensioned tendons, 44% dissipative devices) for the structural frame.

C.2.3.1 Frame system

The DDBD parameters obtained for the specimen frame direction are listed in the following Table C.14, while the determination of the effective period from the elastic spectrum and the base shear-displacement curve resulting from the DDBD are shown in Figure C.3. The base shear can be distributed within the frame and the hybrid connections can be finally designed.

Table C.14. Parameters obtained from the DDBD for the frame direction.

Parameter	Value
Design inter-storey drift θ_d [%]	1.50%
Design displacement Δ_d [mm]	41.43
Yielding Displacement Δ_y [mm]	10.46
Effective mass m_e [t]	23.37
Effective height H_e [m]	2762.06
Ductility η	3.96
Equivalent viscous damping ξ_{eq} [%]	13.37
Effective period T_e [s]	0.64
Effective stiffness K_e [kN/m]	2252.28
Total base shear V_b [kN]	93.31
Number of frames	2
Base shear $V_{b,fr}$ [kN]	46.66

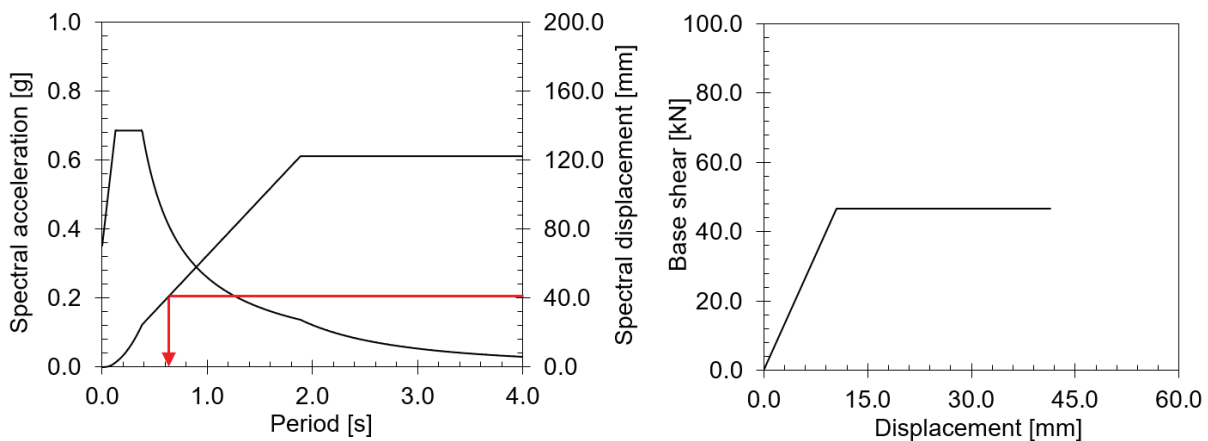


Figure C.3. Left: identification of the effective period from the displacement design spectrum; Right: base shear-displacement curve for the frame system.

➤ COLUMN/FOUNDATION CONNECTION

The earthquake-induced axial load (N_E) in the columns can be estimated as follows:

$$N_E = \frac{OTM - 0.6 V_B H_i}{L_{base}}$$

This axial load can be added to the one provided by the vertical loads to determine the total axial load to be taken into account for each column to properly design the base connection. Assuming one direction for the earthquake excitation, the axial loads on each column are summarized in Table C.15.

Table C.15. Column axial loads.

	Exterior Column A	Interior Column B	Exterior Column C
Axial load due to gravity N_{G+Q} [kN]	20.56	61.69	20.56
Earthquake-induced axial load N_E [kN]	14.7	0.0	14.7
Total axial load N_{TOT} [kN]	5.83	61.69	35.29

Then, assuming that the average re-centring ratio on the columns is equal to the global (system) re-centring ratio β , the moment and shear demands can be identified:

$$M_{col,A/C} = \left(\frac{N_{col,A/C}}{N_{col,B}} + \frac{1}{\beta} - 1 \right) \cdot \beta \cdot M_{col,B}$$

$$M_{col,B} = \frac{0.6 \cdot V_b H_i}{\left(\frac{N_{col,A}}{N_{col,B}} + \frac{N_{col,C}}{N_{col,B}} + \frac{n_{col}}{\alpha_{OTM}} - 2 \right)} \cdot \alpha_{OTM}$$

$$V_{col,A} = \frac{1}{2 \cdot n_{col} - 2} \left[V_b + \frac{(2 \cdot n_{col} - 3) \cdot M_{col,A}}{L_{col}} - \frac{1}{L_{col}} \cdot \sum_{i=B}^C M_{col,i} \right]$$

$$V_{col,B} = 2 \cdot V_{col,A} - 2 \cdot \frac{M_{col,A}}{L_{col}} + \frac{M_{col,B}}{L_{col}}$$

$$V_{col,C} = V_{col,A} - \frac{M_{col,A}}{L_{col}} + \frac{M_{col,C}}{L_{col}}$$

The moment and shear demands calculated from these formulations are listed in Table C.16 and Table C.17.

Table C.16. Moment demands for the concrete columns.

Level	Exterior Column A [kN m]	Interior Column B [kN m]	Exterior Column C [kN m]
1	10.5	21.1	16.1
	7.9	15.9	7.9
2	4.7	9.4	4.7
	8.3	16.6	8.3

Table C.17. Shear demands for the concrete columns.

Level	Exterior Column A [kN m]	Interior Column B [kN m]	Exterior Column C [kN m]
1	10.8	21.7	14.1
2	7.6	15.3	7.6

Considering these internal actions, the column section analysis was carried out at different connection limit states (yielding of the dissipaters, design condition, collapse of dissipaters) and the mild steel external dissipaters could be properly designed. The moment-rotation relationships of the designed column/foundation connections can be found in Figure C.4, while Table C.18 and Figure C.5 indicate the characteristics of the external column dissipaters.

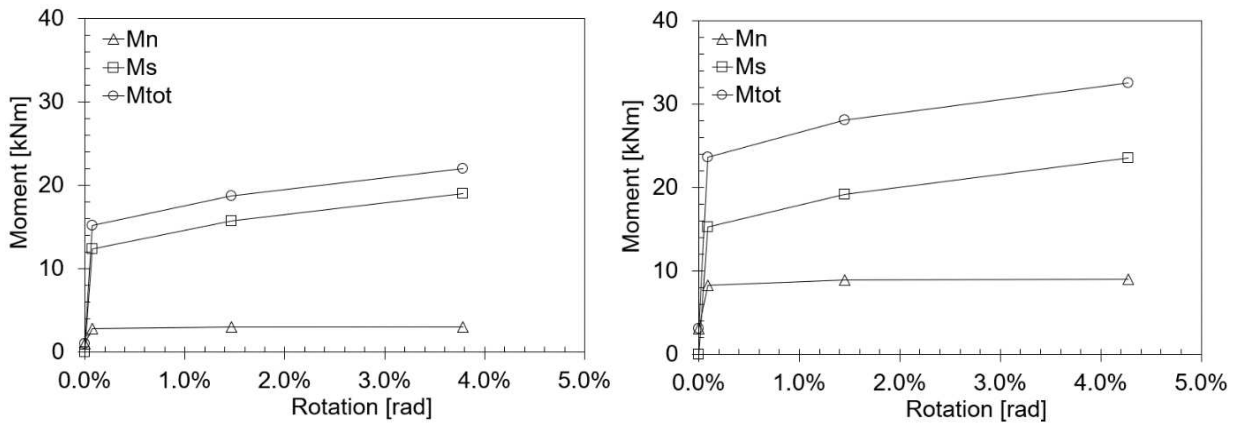


Figure C.4. Moment-rotation relationships of the external (left) and internal (right) columns where: M_n is the axial load contribution, M_s the contribution from the external dissipaters, M_{tot} is the total resulting moment.

Table C.18. Properties of the external dissipaters - Columns.

Parameter	Exterior Columns	Interior Columns
Fuse diameter ϕ_{fuse} [mm]	14.0	15.6
Fuse area A_{fuse} [mm ²]	153.9	191.1
Fuse slenderness λ_{fuse}	60.0	60.0
Fuse length L_{fuse} [mm]	210.0	234.0

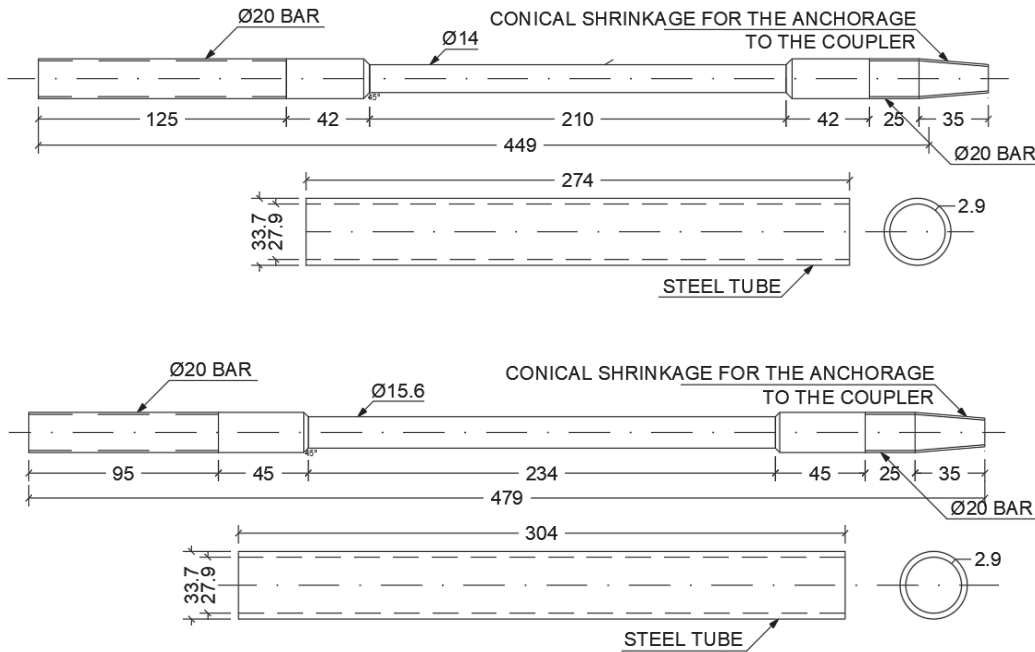


Figure C.5. External dissipater of the exterior columns - top - and interior columns - bottom - .

➤ **BEAM/COLUMN CONNECTION**

Distributing the seismic base shear (F_t) into the structure using the equivalent static analysis method defined by NZS1170.5 (2004) and considering the distribution of the seismic shear based on the equilibrium approach, the beam shear and moments can be determined:

$$F_i = F_t + 0.92 \cdot V_b \frac{W_i H_i}{\sum W_i H_i}$$

Where $F_t = 0.08 \cdot V_b$ at the top level and zero elsewhere. Therefore, applying the following formulas the moment and shear demands on the beams can be estimated:

$$OTM = \sum F_i \cdot H_i$$

$$OTM = N_E \cdot L_{base} + \sum_{i=1}^{n_{col}} M_{b,col}^i$$

$$V_{b,i} = N_E \cdot \frac{V_{s,i}}{V_{s,tot}}$$

$$M_{b,i} = V_{b,i} \cdot \frac{L_b}{2}$$

$$M_{b,i}^* = M_{b,i} \cdot \left(1 - \frac{h_c}{L_b}\right)$$

$$V_{b,i \text{ Average}} = N_E \cdot \frac{\text{average}(V_{s,1}, V_{s,2})}{V_{s,tot}}$$

$$M_{b,i \text{ Average}} = V_{b,i \text{ Average}} \cdot \frac{L_b}{2}$$

$$M_{b,i \text{ Average}}^* = M_{b,i \text{ Average}} \cdot \left(1 - \frac{h_c}{L_b}\right)$$

Where H_i is the inter-storey height, L_{base} is the centreline distance between the exterior columns, $V_{s,i}$ is the storey shear, L_b is the beam length and h_c is the height of the column section. Following this approach, the moment values ($M_{b,i}^*$) summarized in Table C.19 were determined for the Test Building.

Table C.19. Internal actions on the seismic beams.

Level	Shear $V_{b,i}$ [kN]	Moment $M_{b,i}^*$ [kN m]
1	8.9	11.3
2	5.8	7.4

The design of the mild steel dissipaters and of the post-tensioned tendons through analytical section analysis at different beam limit states (yielding of the dissipater, design condition, collapse of dissipater, yielding of the post-tensioned tendon) was thus implemented. The moment-rotation relationships of the designed beam/column connections can be found in Figure C.6, while Table C.20 defines the characteristics of the external dissipaters (see also Figure C.7) and of the internal post-tensioned wire strands.

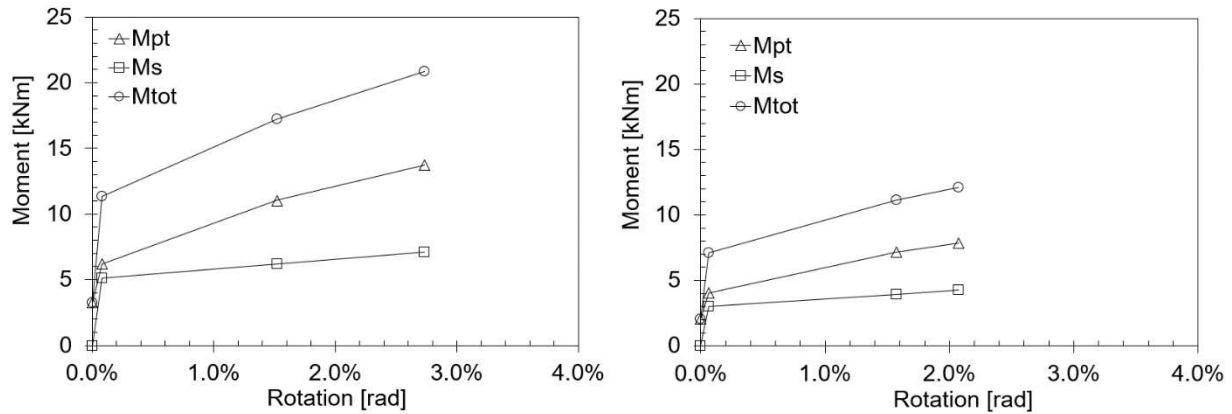
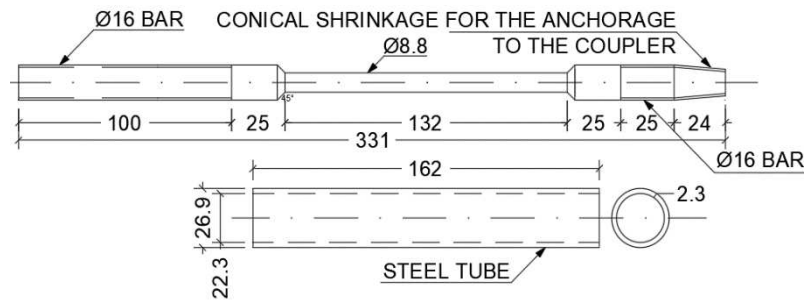


Figure C.6. Moment-rotation relationships of the beams of the first floor (left) and of the second floor (right) where: M_{pt} is the contribution of the post-tensioned tendons, M_s the contribution from the external dissipaters, M_{tot} is the total resulting moment.

Table C.20. Properties of the external beam dissipaters - First configuration - Beams.

Parameter	First level	Second level
Fuse diameter φ_{fuse} [mm]	8.8	6.8
Fuse area A_{fuse} [mm ²]	60.8	36.3
Fuse slenderness λ_{fuse}	60.0	60.0
Fuse length L_{fuse} [mm]	132.0	102.0



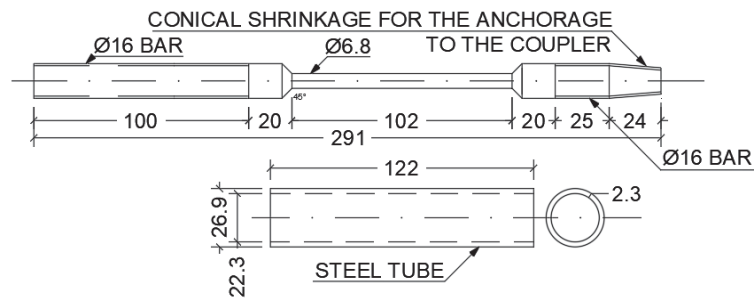


Figure C.7. External dissipaters of the beams of the first floor - top - and of the second floor - bottom - .

It is finally observed that a second configuration of dissipaters was also designed to be tested for the timber beams of both building levels. The properties of this second configuration are summarized in Table C.21.

Table C.21. Properties of the external dissipaters - Second configuration - Beams.

Parameter	First level	Second level
Fuse diameter φ_{fuse} [mm]	8.0	7.6
Fuse area A_{fuse} [mm ²]	50.3	45.4
Fuse slenderness λ_{fuse}	60.0	60.0
Fuse length L_{fuse} [mm]	120.0	114.0

C.2.3.2 Wall system

The DDBD parameters obtained for the wall direction are listed in the following Table C.22.

Table C.22. Parameters obtained from the DDBD procedure for the wall direction.

Parameter	Value
Design inter-storey drift θ_d [%]	1.00%
Design displacement Δ_d [mm]	27.60
Yielding Displacement Δ_y [mm]	2.10
Effective mass m_e [t]	23.37
Effective height H_e [m]	2762.06
Ductility η	4.00
Equivalent viscous damping ξ_{eq} [%]	14.69
Effective period T_e [s]	0.44
Effective stiffness K_e [kN/m]	4880.86
Total base shear V_b [kN]	134.57
Number of walls	2
Base shear $V_{b,fr}$ [kN]	67.29

While, the determination of the effective period from the elastic spectrum as well as the base shear-displacement curve resulting from the DDBD procedure are shown in Figure C.8. Calculating the internal action on the timber wall, the external *Plug&Play* dissipaters (internal fuse dimensions) and the internal post-tensioned bar (typology and initial force) could be designed.

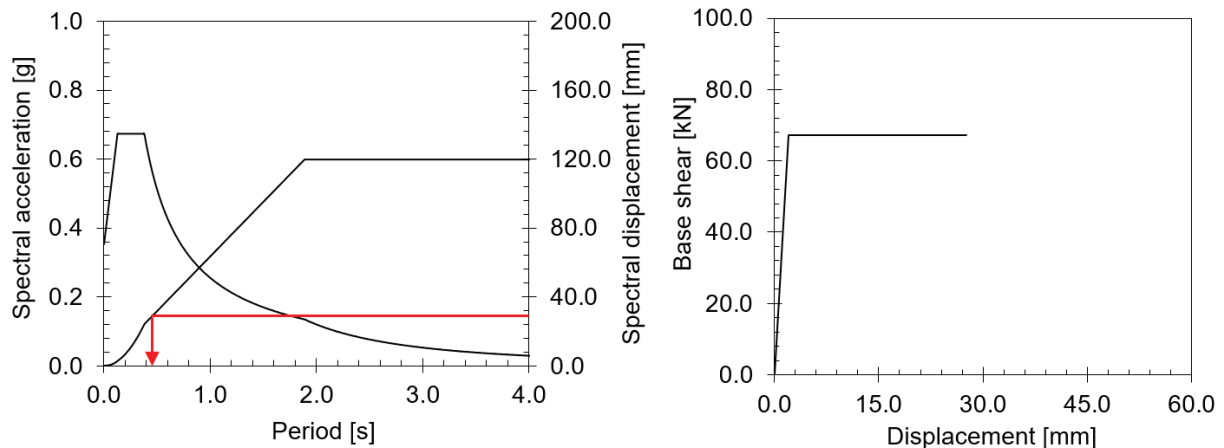


Figure C.8. Left: identification of the effective period from the displacement design spectrum; Right: base shear-displacement curve for a wall system.

➤ **WALL/FOUNDATION CONNECTION**

The internal actions used for designing the wall/foundation connection are summarized in the following Table C.23.

Table C.23. Internal actions on the timber wall.

Level	Shear [kN]	OTM [kN m]
1	67.3	39.5
2	44.1	149.8
Tot	111.3	189.3

The moment-rotation relationships of the designed wall/foundation connections as well as the variation of the neutral axis in function of the rotation can be found in Figure C.9, while Table C.24 defines the characteristics of the external dissipaters (see also Figure C.10) and of the internal post-tensioned bar.

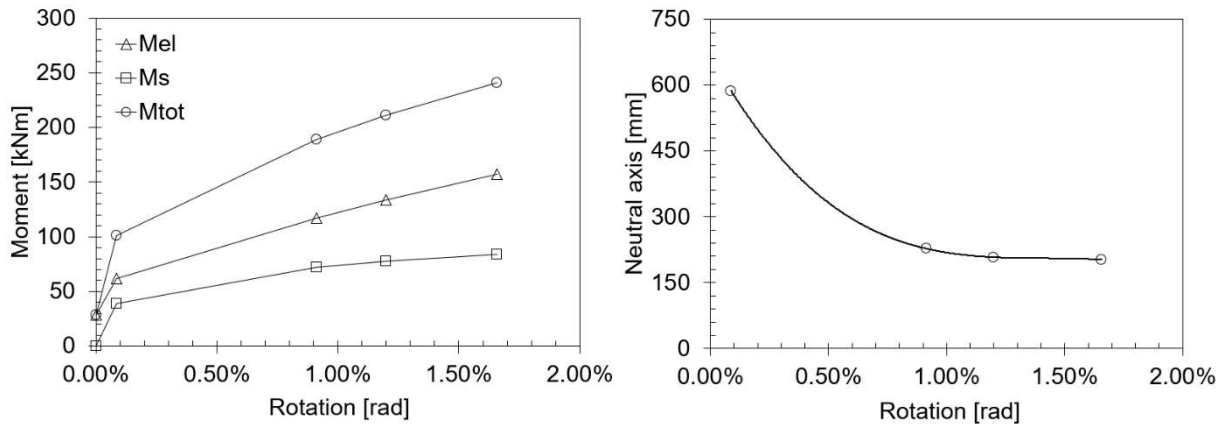


Figure C.9. Left: moment-rotation relationships of the wall where M_{el} is the axial load and post-tensioned bar contribution, M_s is the contribution from the external dissipaters, M_{tot} is the total resulting moment. Right: variation of the neutral axis in function of the rotation.

Table C.24. Properties of the external dissipaters - Wall.

Parameter	Wall
Fuse diameter ϕ_{fuse} [mm]	11.0
Fuse area A_{fuse} [mm ²]	95.0
Fuse slenderness λ_{fuse}	60.0
Fuse length L_{fuse} [mm]	165.0

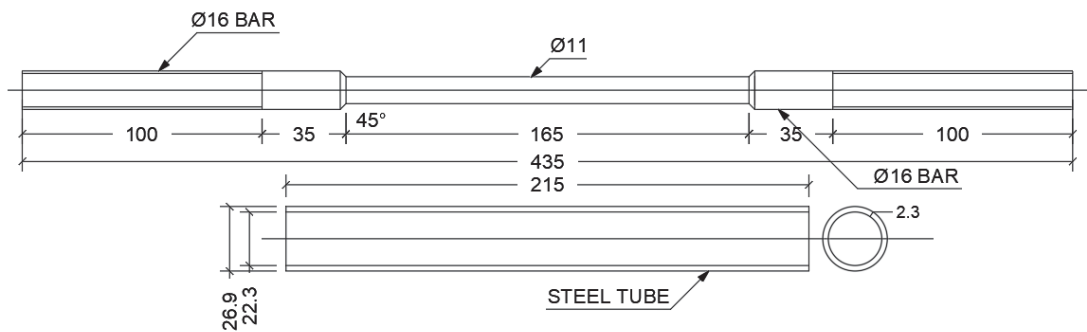


Figure C.10. External dissipater of the walls.

C.2.4 Initial numerical analysis

After the specimen design, initial numerical analyses were implemented for checking the seismic design and predicting the seismic behaviour of the Test Building. Lumped-plasticity numerical models were developed in Ruaumoko 2D software (Carr 2003) for both building directions, considering moment-rotational springs at the beam-column interfaces and column/wall bases to simulate the response of the hybrid connections. The re-centering action of the post-tensioning and

the energy dissipation capability provided by the *Plug&Play* external replaceable dissipaters were described using multi-linear elastic and Ramberg-Osgood hysteresis rules, respectively.

Then, non-linear static push-over and push-pull analyses were preliminary performed to determine the capacity curves and hysteresis behaviour for both building directions and estimate the equivalent viscous damping affecting the system behaviour. Following a Capacity Spectrum Method (ATC 40 1996), the push-over curves were converted into an acceleration-displacement function and introduced into the Acceleration-Displacement Response Spectra (ADRS) domain. Introducing into the same graph the design spectra associated to various Limit States, performance points at different intensity levels could be determined. The evaluation of the maximum accelerations and displacements expected at considered intensity levels allowed a preliminary estimation of the floor acceleration and inter-storey drift ratios and thus of the behaviour of the hybrid connections at the various demand levels. Then, non-linear time history analyses were performed to obtain blind predictions of the Test Building seismic behaviour. Dynamic response to each seismic intensity included within the Test Matrix (see Chapter 7) was determined to evaluate according to a blind-prediction approach the transient and residual response expected from the experimental tests.

Results from this blind prediction can be found in an initial conference paper on the research (Pampanin et al. 2019), while are not herein reported because refinements of the numerical modelling should be introduced for having better comparison with the experimental results. In fact, as partly observed in Chapter 6, different system modifications were introduced during the construction phases of the Bare Frame (e.g. the value of the post-tensioning force) and these variations should be considered for re-calibrating a proper numerical model.

C.3 Test Building detailing



Specific structural details were designed for realizing the low-damage structural skeleton. The system detailing plays a fundamental role for the correct functioning of such type of structural system, therefore all the components of the skeleton (members and steel assemblies) were properly verified using formulations from national or international codes (Italian code, Eurocode, New Zealand Standards).



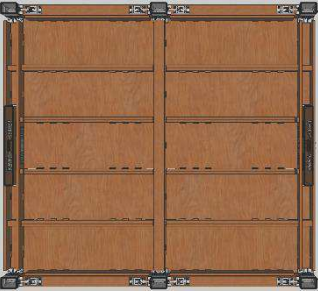
This session does not report all the calculations implemented for verifying the system elements, however a summary of the main verifications carried out can be found in Table C.25. Depending on the typology of structural verification, the following codes/standards were taken as reference: EN

1995-1-1 2004; EN 1993-1-8 2005; EN 1993-1-1 2005; NTC 2018; NZS 3404-1,2 1997; NZS 3404-1 2009; NZS 3101-1,2 2006; NZS 3603 1993; STIC 2012; STIC 2013; AS/NZS1170 2002.

It is highlighted that in the following table no indications can be found for the second-floor slab (3PT flooring system, Palermo 2017). In fact, this type of floor was proposed and designed by the research group from the University of Canterbury, Christchurch (NZ) which collaborated to the SERA project introducing this innovative floor solution. This typology of high seismic performance flooring system has been recently studied and tested in the New Zealand laboratory through quasi-static testing, while the SERA Project allowed to test it under earthquake motions. However, it is observed that some modifications of the initial design of the 3PT floor were required during the construction phases, also if no additional detail is provided within this Thesis, and the initial design of the pre-stressed floor was changed into a post-tensioned floor.

Table C.25. Structural verifications implemented for the different Test Building components/assemblies.

Component/assembly	Type of verification
<p>Seismic beams</p> 	<ul style="list-style-type: none"> ➤ Member verifications (bending, shear) ➤ Dissipater steel assembly: <ol style="list-style-type: none"> 1. Steel plates: <ul style="list-style-type: none"> - Bolts (shear) - Nails (shear) - Plate (tension, bearing) 2. Tension Bolts (tension) 3. Bearing plates (bearing) 4. Welded plates (stress) ➤ Post-tensioning endplates (stress, deflection) ➤ Shear keys (shear, bending)
<p>Seismic columns</p> 	<ul style="list-style-type: none"> ➤ Member verifications: (compression + bending, shear) ➤ Foundation steel assembly: <ol style="list-style-type: none"> 1. Steel plate: <ul style="list-style-type: none"> - Plate (tension, punching, bearing) - Bolts (shear, tension, shear-tension) 2. Steel shoes (tension, stress) ➤ Dissipater steel assembly: <ol style="list-style-type: none"> 1. Steel plates: <ul style="list-style-type: none"> - Bolts (shear) - Plate (tension, punching) 2. Tension Bolts (tension) 3. Bearing plates (bearing) 4. Welded plates (stress)

Component/assembly	Type of verification
<p>Seismic walls</p> 	<ul style="list-style-type: none"> ➤ Member verifications: (compression + bending, shear, buckling) ➤ Foundation steel assembly: <ol style="list-style-type: none"> 1. Steel plate: <ul style="list-style-type: none"> - Plate (tension, punching, bearing) - Bolts (shear, tension, shear-tension) 2. Steel shoes (tension, stress) ➤ Dissipater steel assembly: <ol style="list-style-type: none"> 1. Steel plates: <ul style="list-style-type: none"> - Bolts (shear) - Nails (shear) - Plate (tension, punching) 2. Tension Bolts (tension) 3. Bearing plates (bearing) 4. Welded plates (stress) ➤ Floor connections: <ol style="list-style-type: none"> 1. Pin (shear, bearing) 2. Bowties: <ul style="list-style-type: none"> - Plate (tension, bearing) - Nails (shear) ➤ Post-tensioning endplates (stress, deflection)
<p>Gravity beams (central and edge beams)</p> 	<ul style="list-style-type: none"> ➤ Member verifications (bending, shear, torsion) ➤ Gravity supports: <ol style="list-style-type: none"> 1. Plate (bearing, punching, tension) 2. Bolts (shear, tension, shear-tension) ➤ Rectangular plates for pinned connection: <ul style="list-style-type: none"> - Plate (tension, bearing) - Nails (shear)
<p>Timber-Concrete Composite (TCC) floor</p> 	<ul style="list-style-type: none"> ➤ Joist verifications (bending, shear, stress, displacement) ➤ Connectors (shear) ➤ Concrete slab (shrinkage and temperature, shear, diaphragm, elongation)

The structural verifications were carried out considering the material properties already presented from Table C.2 to Table C.9, however for the additional elements introduced during the detailing design the properties summarized in the following tables (from Table C.26 to Table C.30) were taken into account.

Table C.26. Steel properties of the bolts.

GRADE 8.8 (EN 1993-1-8 2005)	
Yield strength f_y	1050 MPa
Ultimate strength f_u	255 kN

Table C.27. Steel properties of the Anker nails (by Rothoblaas catalogue) – 4mm diameter.

LBA 4 (EN 1995-1-1 2004)	
Yield characteristic moment $M_{y,k}$	6500 N mm
Tensile characteristic strength $f_{tens,k}$	6.9 kN
Withdrawal characteristic strength $f_{ax,k}$	7.5 kN

Table C.28. Steel properties of the Anker nails (by Rothoblaas catalogue) – 6mm diameter.

LBA 6 (EN 1995-1-1 2004)	
Yield characteristic moment $M_{y,k}$	19000 N mm
Tensile characteristic strength $f_{tens,k}$	11.4 kN
Withdrawal characteristic strength $f_{ax,k}$	7.5 kN

Table C.29. Steel properties of Anker nails (by Rothoblaas catalogue) – 4mm diameter.

KOP8 (EN 1995-1-1 2004)	
Yield characteristic moment $M_{y,k}$	16900 N mm
Tensile characteristic strength $f_{tens,k}$	15.9 kN
Withdrawal characteristic strength $f_{ax,k}$	12.9kN

Table C.30. Steel properties of the plates.

STEEL S355 (EN 1993-1-1 2005, NTC 2018)	
Modulus of elasticity E_s	210000 MPa
Specified characteristic yield strength f_{yk}	355 MPa
Specified characteristic ultimate tensile strength f_{tk}	510 MPa
Mean density γ_m	78.5 kN/m ³
Poisson coefficient ν	0.3

After the structural verifications on the specimen skeleton, structural drawings were prepared to be sent to the different industry suppliers. The structural drawings, prepared by *J. Ciurlanti* and *S. Bianchi* and reviewed by *Prof. S. Pampanin*, of the Bare Frame system and its detailing are not reported within this Thesis.

Finally, after the definition of the Test Building configurations, the non-structural components were properly designed to be adapted to the existing structural skeleton:

1. The Fiber-Reinforced Gypsum partition walls were only fitted to the skeleton, due to non-structural detailing already defined by the supplier;
2. The Glass-Fiber Reinforced Concrete (GFRC) precast cladding panels were completely designed by the supplier, so the usual design was adapted to such type of structural system;
3. The spider glazing facades were designed following a practical guide provided by the company and suggestions from the industry supplier. However, the connections to the primary building (steel assemblies) were designed and verified following the EN 1995-1-1 (2004) and EN 1993-1-8 (2005);
4. The low-damage infill wall was designed and verified as indicated by Tasligedik and Pampanin (2016).

Non-structural drawings were finally prepared by the same authors for helping during the construction phases.

The following dimensional tolerances from national/international codes were also provided to the different suppliers for fabricating the different components:

- For the glulam components the tolerances can be found in the code UNI EN 14080 (2013) and are summarized in Table C.31, while for the cross-laminated timber tolerable dimensions are provided within the EN 336 (2013), that is for Class 2 components ± 1.5 mm for dimensions between 100 mm and 300 mm and ± 2 mm for dimensions greater than 300 mm.

Table C.31. Tolerances for nominal dimensions of glulam elements.

Nominal sizes for	Maximum deviations
Length of member	± 2 mm
Width of cross section	± 2 mm
Depth of cross section	± 2 mm
Angle deviation of the cross section from the right angle	± 1 mm
Squareness of elements	± 1 mm

- For the concrete elements, referring to the UNI EN 13369 (2013) and considering the more rigid requirements for the tolerance class 2, the squareness of the precast concrete elements was defined to be less than 4 mm.
- For the steel components, for the hot rolled steel plates 3 mm and above, the BS EN ISO 18286 (2010) provides specific requirements for the width, length and thickness. For the mild steel dissipaters, the BS 970-3 (1991) gives the tolerances for the bars used to create the external dissipaters: the squareness tolerance is 1/1000 while the diameter tolerance is - 0.07 mm for diameters between 6 mm and 18 mm and - 0.085 mm for diameters between 18 and 30 mm. Concerning the holes into the steel plates for bolts, screws or nails, references can be found in EN 1993-1-8 (2005), Table 3.3 of the code, and EN 1995-1-1 (2004), Table 8.2 of the code. Concerning the bolts of the steel plates, the minimum edge distances, both parallel and orthogonal to the applied load, is $1.2d_0$ and the minimum spacing between bolts in the direction parallel to the load is $2.2d_0$, while in the opposite direction is $2.4 d_0$ where d_0 is the nominal diameter of the bolt. For the Anker nails, the minimum spacing and edge distances in the direction parallel and perpendicular to the grains are obtained from the values of Table 8.2 of EN 1995-1-1 (2004) multiplied by 0.7, as the code suggests for steel-timber connections. Catalogues provide indications about the minimum values for the distances for positioning the Anker nails and the coach screws in the steel plates.

The knowledge of all the structural and non-structural components/detailing allowed the calculation of the total specimen mass (Table C.32) to be supported by the shaking table (maximum allowable capacity of 40 tons).

Table C.32. Total specimen mass.

Configuration	Mass [t]
Bare Frame	28.44
Option 1	29.44
Option 2	33.12

The total mass indicated in the previous table does not include the additional mass provided by the steel foundation of the laboratory, that is around 9 tons. Therefore, adding the foundation weight, the total mass on the table becomes greater than the maximum capacity of 40 tons for the integrated system (*Option 2*). However, this mass was still considered acceptable for performing the shaking table testing.

C.4 References

- AS/NZS 1170 (2002). *Australian/New Zealand Standard 1170*, Standards Australia/Standards New Zealand.
- ASTM A 416/A 416M (2012). *Specification for Steel Strand, Uncoated Seven-wire for Prestressed Concrete*, International Building Code.
- Applied Technology Council (1996). *Seismic evaluation and retrofit of concrete buildings, Volume 1*, Technical Report ATC 40, Redwood City, California, USA.
- BS 970-3 (1991). *Specification for wrought steels for mechanical and allied engineering purposes. Bright bars for general engineering purposes*, British standards.
- BS EN ISO 18286 (2010). *Hot-rolled stainless steel plates. Tolerances on dimensions and shape*, British standards.
- Carr A.J. (2003). *Ruaumoko Program for Inelastic Dynamic Analysis – User Manual*, University of Canterbury, Christchurch, New Zealand.
- EN 1992-1-1 (2004). *Eurocode 2: Design of concrete structures - Part 1-1: General rules and rules for buildings*, The European Union Per Regulation 305/2011, Directive 98/34/EC, Directive 2004/18/EC.
- EN 1993-1-1 (2005). *Eurocode 3: Design of steel structures - Part 1-8: Design of joints*, The European Union Per Regulation 305/2011, Directive 98/34/EC, Directive 2004/18/EC.
- EN 1993-1-8 (2005). *Eurocode 3: Design of steel structures - Part 1-1: General rules and rules for buildings*, The European Union Per Regulation 305/2011, Directive 98/34/EC, Directive 2004/18/EC.
- EN 1995-1-1 (2004). *Eurocode 5: Design of timber structures - Part 1-1: General - Common rules and rules for buildings*, The European Union Per Regulation 305/2011, Directive 98/34/EC, Directive 2004/18/EC.
- NTC (2008). *Norme Tecniche per le Costruzioni*, Supplemento ordinario n°30 alle G.U. n° 29 del 14/01/2008, serie generale, Rome, Italy.
- NZS 1170.5 (2004). *Structural Design Actions - Part 5: Earthquake design actions - New Zealand*, Standards New Zealand.
- NZS 3101-1 (2006). *Concrete structures standard - The design of concrete structures*, Development Sponsored by the Earthquake Commission (EQC) and Department of Building and Housing (DBH), Standards New Zealand.
- NZS 3101-2 (2006). *Concrete structures standard – Commentary*, Development Sponsored by the Earthquake Commission (EQC) and Department of Building and Housing (DBH), Standards New Zealand.
- NZS 3404-1 (2009). *Steel structures Standard Part 1: Materials, fabrication, and construction*, Supersedes in part NZS 3404 Parts 1 and 2:1997, P 3404 Committee for the Standards Council established under the Standards Act 1988, Standards New Zealand.
- NZS 3404-1,2 (1997). *Steel structures Standard*, P 3404 Committee for the Standards Council established under the Standards Act 1988, Standards New Zealand.

- NZS 3603 (1993). *Timber Structures Standard*, Standards New Zealand.
- Palermo A., Pampanin S. (2017). Pre-stressed beams or panels (3PT), *United States Patent n. US9809979B2* (filed in 2014), *Japan Patent n. JP6373975B2* (filed in 2014), *Canada Patent n. CA2909402C*.
- Pampanin S., Marriott D., Palermo A. and New Zealand Concrete Society (2010). *PRESSS Design Handbook*, Auckland, New Zealand.
- Pampanin S., Ciurlanti J., Bianchi S., Palmieri M., Grant D., Granello G., Palermo A., Correia A. (2019). Overview of SERA Project: 3D shaking table tests on an integrated low-damage building system, *Proceedings of 4th International Workshop on the Seismic Performance of Non-Structural Elements (SPONSE)*, Pavia, Italy.
- Priestley M.J.N. (1993) Myths and fallacies in earthquake engineering-conflicts between design and reality, *Bulletin NZSEE*, 26(3): 329-341.
- Priestley M.J.N., Calvi G.M., Kowalsky M.J. (2007). *Direct Displacement-Based Seismic Design of Structures*. 1st edition, IUSS Press, Pavia, Italy.
- Structural Timber Innovation Company (2012). *Design Guide Australia and New Zealand – Timber Concrete Composite Floor Systems*, STIC, New Zealand.
- Structural Timber Innovation Company (2013). *Design Guide Australia and New Zealand – Timber Rivet Connections Design Guide*, STIC, New Zealand.
- UNI EN 1194 (2000). *Strutture di legno - Legno lamellare incollato - Classi di resistenza e determinazione dei valori caratteristici*, Italian standards, Milan, Italy.
- UNI EN 13369 (2013). *Regole comuni per prodotti prefabbricati di calcestruzzo*, Italian standards, Milan, Italy.
- UNI EN 14080 (2013). *Strutture di legno - Legno lamellare incollato e legno massiccio incollato – Requisiti*, Italian standards, Milan, Italy.
- UNI EN 14081-1 (2016). *Strutture di legno - Legno strutturale con sezione rettangolare classificato secondo la resistenza - Parte 1: Requisiti generali*, Italian standards, Milan, Italy.
- UNI EN 336 (2013). *Legno strutturale - Dimensioni, scostamenti ammissibili*, Italian standards, Milan, Italy.
- UNI EN 338 (2016). *Legno strutturale - Classi di resistenza*, Italian standards, Milan, Italy.

APPENDIX D:

Shake-table tests on an integrated low-damage building system (SERA Project): Construction of the non-structural systems

D.1 Introduction

The construction/assembly of the all the non-structural components tested during Phase 2 and Phase 3 of the experimental campaign, i.e. the two different partition systems (fibre-reinforced ceramic gypsum and masonry partitions) and the two exterior envelopes (Glass Fibre Reinforced Concrete and glass facades), are further described through additional photos.

D.2 Fiber reinforced gypsum walls (Option 1)



Figure D.1. Partition in the wall direction - connection of the horizontal channel of the steel sub-frame to the first floor: detail of the steel profile at the base of the opening (left) and nearby the concrete column (right).



Figure D.2. Partition in the wall direction - connection of the horizontal track of the steel sub-frame to the timber-concrete beams of the second floor: view (left); additional steel pieces introduced for the connection to the timber part due to the presence of the internal hole for the wire strands (centre); telescopic joint of the steel studs of the openings connected to the upper horizontal channel (right).



Figure D.3. Partition in the wall direction: timber frame forming a door in the partition wall (top - left and right); detail of the connection of the steel studs forming the openings to the bottom horizontal profile (bottom - left); steel assembly above the timber frame (bottom - right).



Figure D.4. Partition in the frame direction: additional L-shape profiles attached to the horizontal track on the bottom for the insertion of plants (top - left and right); detail of the connection of the horizontal track to the timber wall (bottom - left); complete assemblage of the steel frame (bottom - right).

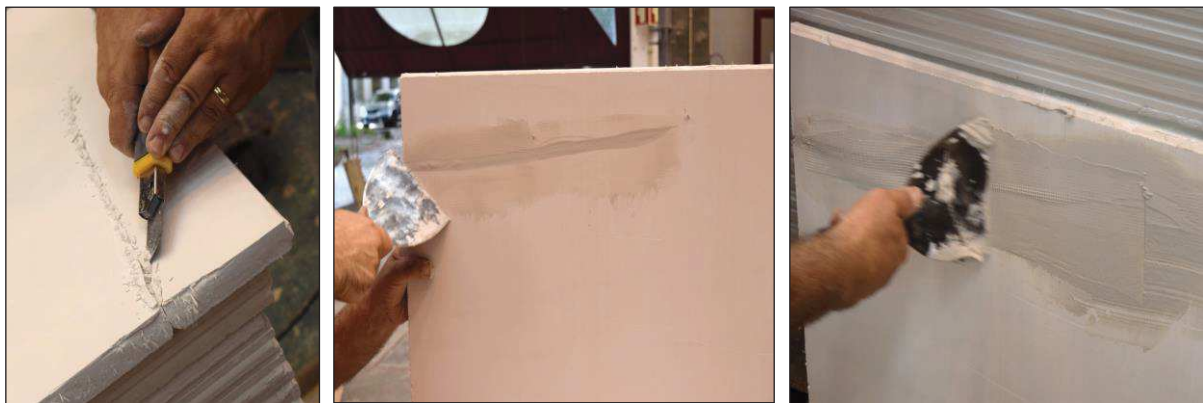


Figure D.5. Repairing actions of a gypsum panel damaged during the material transportation from Italy to Lisbon: cutting of the damaged zone (left); introduction of adhesive glue in the zone (centre); insertion of joint tape and additional adhesive glue for completing the repair (right).



Figure D.6. Partition in the wall direction - realization of the gypsum wall connecting the ceramic panels through their male-female joints and adding adhesive glue between the panels.



Figure D.7. Partition in the frame direction: complete assembly of the wall (left); gap between the two orthogonal walls (centre); gap between the partition and the timber wall (right).



Figure D.8. Application of the sealant foam in the lateral gaps of both partition walls.



Figure D.9. Final configuration of the two partition walls in the wall (left) and in the frame (right) directions.

D.3 Glass fiber reinforced concrete facades (Option 2)



Figure D.10. Top anchorage system of the GFRC facades bolted on the concrete columns.



Figure D.11. Checking the position of the panels in the upper level (left) and fixing of the anchorage devices to the specimen foundation (right).



Figure D.12. Completion of the façade in the North side of the Test Building: assembly of the panels in the West part (left); lifting in place of the bottom panel in the East side (centre); final configuration of the façade (right).



Figure D.13. Details of the GFRP panel: internal opening (left), connection of the external panel to the steel frame (centre) and sliding anchorage on the top of the system (right).



Figure D.14. Completion of the façade in the South side of the Test Building: assembly of the first level (left), final configuration of the system (right).



Figure D.15. Filling of the bottom anchorages using fast-setting mortar.

D.4 Spider glazing facades (Option 2)

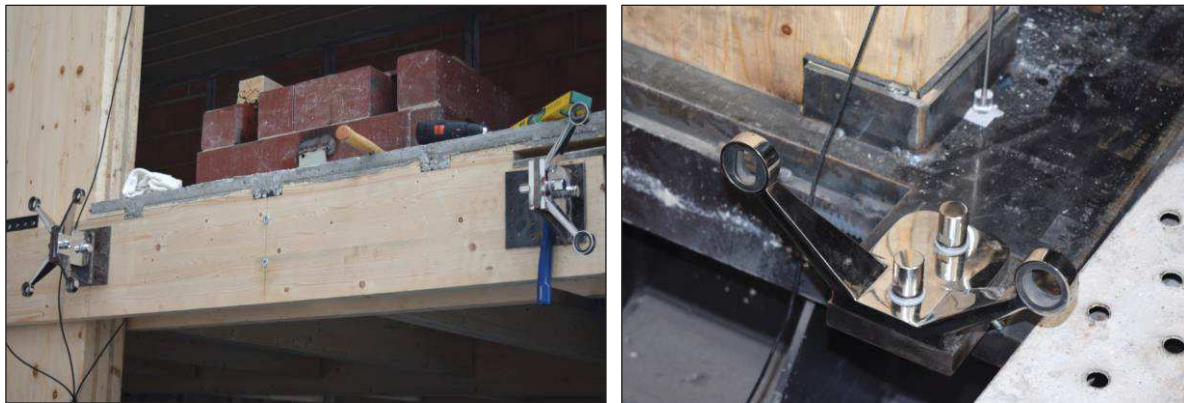


Figure D.16. Positioning of the steel anchorage assembly on the edge beams (left) and of the spider connectors on the steel foundation (right).

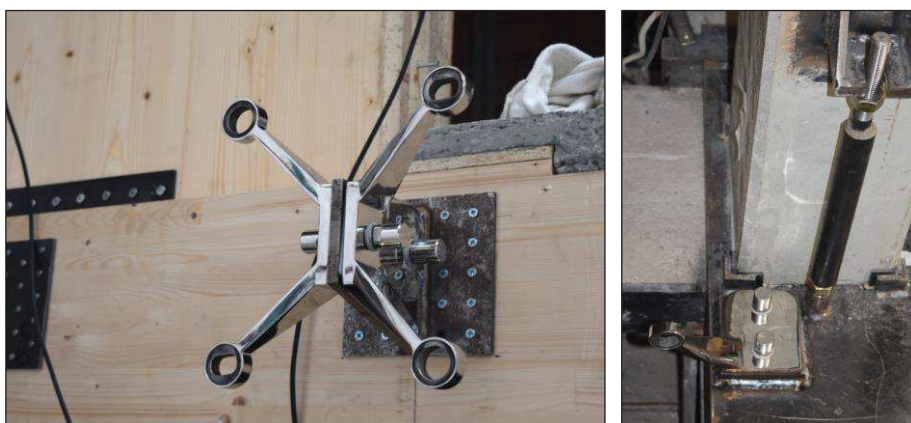


Figure D.17. Connection of the steel plate to the edge timber beams through screws (left) and welding of the spider connectors to the specimen foundation (right).



Figure D.18. Articulated screw (rotule) to be fixed to both the glass and the spider connector (left); different parts composing the system and tools used for fixing the rotules (right).

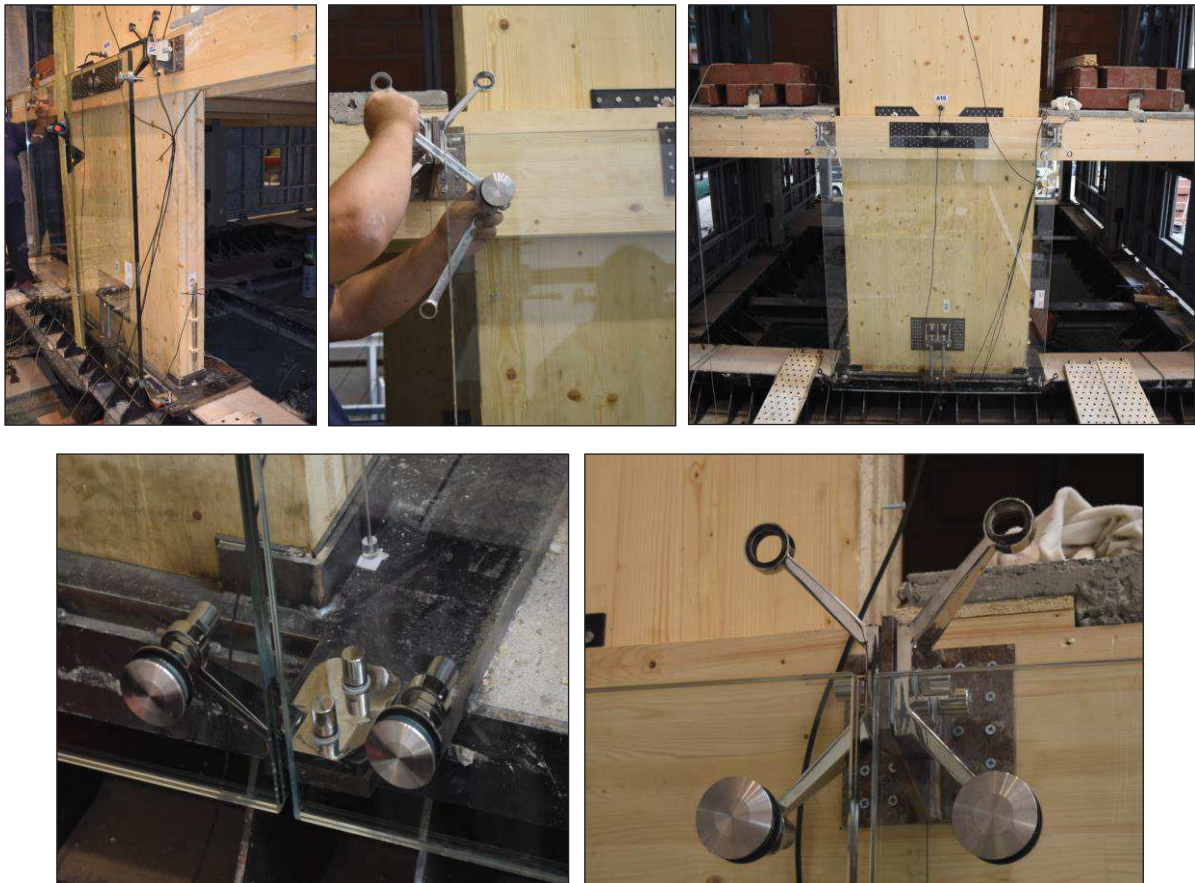


Figure D.19. Assembly of the central panel of the East-side facade: lifting in place of the panel (top - left), fixing the rotules to the spider connector (top - centre), final configuration of the central panel (top - right), spider connector welded on the foundation base (bottom - left), plate/connector assembly screwed to the timber beam (bottom - right).



Figure D.20. Assembly of all the first level of the East-side façade: connection of the South-side panel (left) and of the North-side panel (right).



Figure D.21. Assembly of all the second level of the East-side façade: connection of the top-left panel (left), final configuration of the glass wall (centre) and particular of an internal connection system (right).

D.5 Masonry infill partition (Option 2)



Figure D.22. Measurement of the horizontal alignment on the South (left) and on the North (right) sides before constructing the internal wall.



Figure D.23. Non structural detailing: gap between the column and the horizontal track on the first building level (top - left); gap between the column and the horizontal track connected to the second floor (top - centre); gap between the concrete column and the first vertical steel stud (top - right); internal gap between two vertical studs (bottom - left); detail of the bottom part of the internal steel studs (bottom - centre); introduction of an adhesive tape on the internal part of the steel profiles (bottom - right).



Figure D.24. Final configuration of the steel sub-frame.



Figure D.25. Construction of the infill wall: construction of the infill panel in the North side (top - left); construction of the first brick line of the second wall from the North side (top - right); positioning of the first brick line in the central infill wall (centre - left); completion of the first three panels from the North side (centre -right); construction of the second wall from the South side (bottom - left); introduction of polyurethane foam in the lateral gaps after completing the wall (bottom - right).

APPENDIX E:

Thermal performance analysis of façade systems

E.1 Introduction

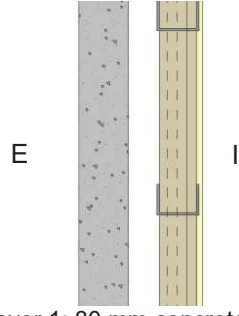
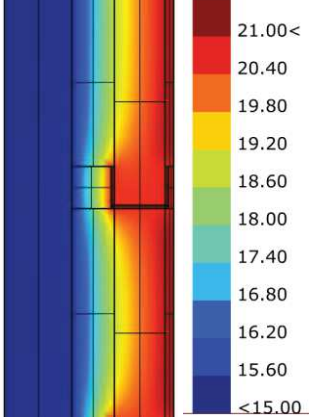
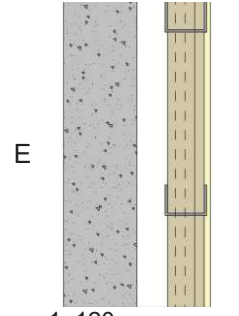
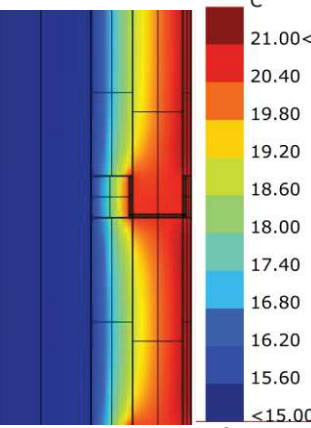
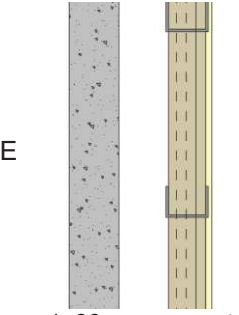
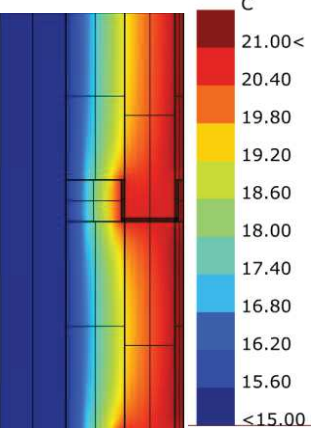
This Appendix provides additional results on the thermal analysis implemented in *Therm* software for each typology of façade system analysed in Chapters 5 and 8 of this Thesis. Particularly, the results are presented in terms of heat propagation inside the walls, transmittance values, while final graphs correlating the annual energy or seismic cost to the relative demand (degree days or return period) can be found.

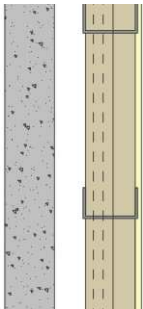
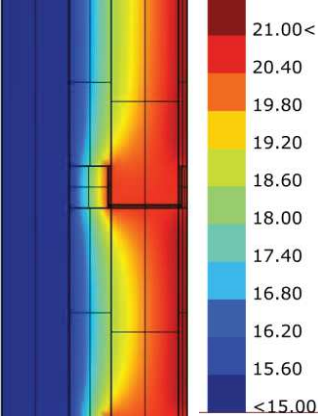
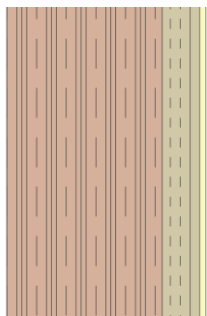
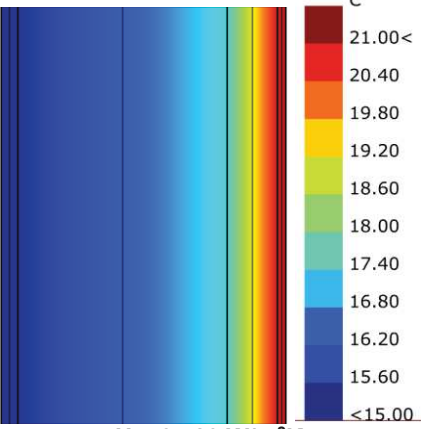
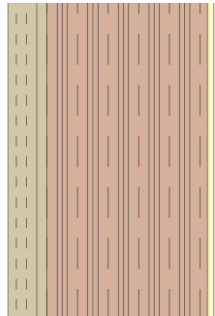
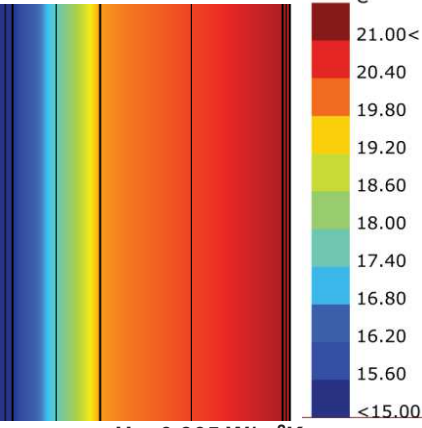
E.2 Thermal analysis

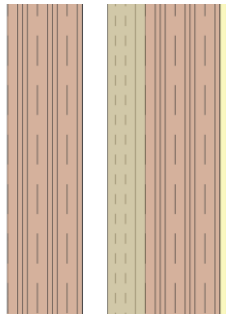
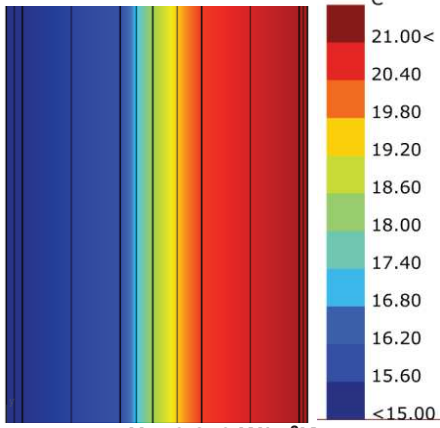


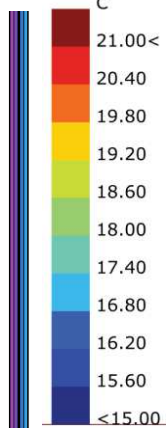
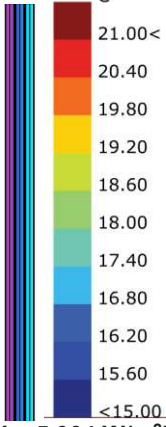
The thermal study has been carried out using *Therm* software from the *Grasshopper* platform. This program is based on a finite-element method and allows to perform two-dimensional conduction heat-transfer analysis, consequently evaluating a product energy efficiency and local temperature patterns.

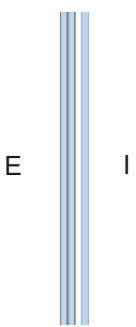
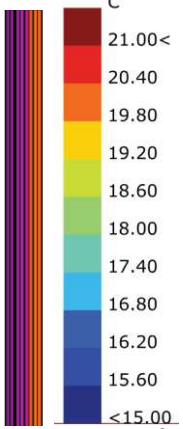
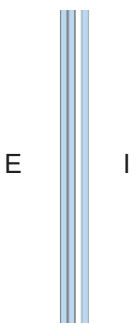
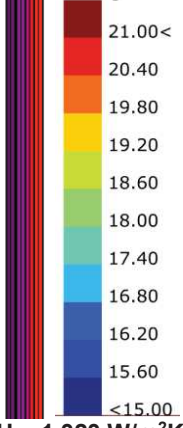
Table E.1 summarizes the results obtained for each façade solution considered in the seismic&energy cost/performance-based analysis of Chapter 8. The thermal properties are presented in terms of temperature patterns and the final value of transmittance representing the thermal behaviour of the façade system can be found.

Table E.1. Thermal properties estimated for each façade system.

Façade system	Panel geometry	Thermal properties
Precast concrete cladding systems	<p>TYPE 1 (BENCHMARK)</p>  <p>Layer 1: 80 mm concrete Layer 2: 50 mm air Layer 3: 60 mm insulation + steel studs Layer 4: 10 mm plaster</p>	<p>TYPE 1 (BENCHMARK)</p>  <p>$U = 0.354 \text{ W/m}^2\text{K}$</p>
	<p>TYPE 2</p>  <p>Layer 1: 120 mm concrete Layer 2: 50 mm air Layer 3: 60 mm insulation + steel studs Layer 4: 10 mm plaster</p>	<p>TYPE 2</p>  <p>$U = 0.352 \text{ W/m}^2\text{K}$</p>
	<p>TYPE 3</p>  <p>Layer 1: 80 mm concrete Layer 2: 80 mm air Layer 3: 60 mm insulation + steel studs Layer 4: 10 mm plaster</p>	<p>TYPE 3</p>  <p>$U = 0.278 \text{ W/m}^2\text{K}$</p>

Façade system	Panel geometry	Thermal properties
<p>Precast concrete cladding systems</p>	<p>TYPE 4</p>  <p>Layer 1: 80 mm concrete Layer 2: 50 mm air Layer 3: 60 mm insulation + steel studs Layer 4: 10 mm plaster</p>	<p>TYPE 4</p>  <p>$U = 0.335 \text{ W/m}^2\text{K}$</p>
<p>Unreinforced masonry infill wall</p>	<p>TYPE 1 (BENCHMARK)</p>  <p>Layer 1: 20 mm adhesive Layer 2: 250 mm brick Layer 3: 60 mm insulation Layer 4: 10 mm plaster</p>	<p>TYPE 1 (BENCHMARK)</p>  <p>$U = 0.480 \text{ W/m}^2\text{K}$</p>
	<p>TYPE 2</p>  <p>Layer 1: 20 mm adhesive Layer 2: 60 mm insulation Layer 3: 250 mm brick Layer 4: 10 mm plaster</p>	<p>TYPE 2</p>  <p>$U = 0.305 \text{ W/m}^2\text{K}$</p>

Façade system	Panel geometry	Thermal properties
<p>Unreinforced masonry infill wall</p>	<p>TYPE 3</p>  <p>E I</p> <p>Layer 1: 20 mm adhesive Layer 2: 120 mm brick Layer 3: 40 mm air Layer 4: 60 mm insulation Layer 5: 120 mm brick Layer 6: 10 mm plaster</p>	<p>TYPE 3</p>  <p>C</p> <p>21.00< 20.40 19.80 19.20 18.60 18.00 17.40 16.80 16.20 15.60 <15.00</p> <p>U = 0.279 W/m²K</p>
<p>Spider glazing curtain walls</p>	<p>TYPE 1 (BENCHMARK)</p>  <p>E I</p> <p>Layer 1: 10 mm glass Layer 2: 1.52 mm PVB Layer 3: 10 mm glass</p> <p>TYPE 2</p>  <p>E I</p> <p>Layer 1: 10 mm glass Layer 2: 1.52 mm PVB Layer 3: 10 mm glass Layer 4: 1.52 mm PVB Layer 5: 10 mm glass</p>	<p>TYPE 1 (BENCHMARK)</p>  <p>C</p> <p>21.00< 20.40 19.80 19.20 18.60 18.00 17.40 16.80 16.20 15.60 <15.00</p> <p>U = 5.478 W/m²K</p> <p>TYPE 2</p>  <p>C</p> <p>21.00< 20.40 19.80 19.20 18.60 18.00 17.40 16.80 16.20 15.60 <15.00</p> <p>U = 5.004 W/m²K</p>

Façade system	Panel geometry	Thermal properties
Spider glazing curtain walls	<p style="text-align: center;"><u>TYPE 3</u></p>  <p style="text-align: center;">E I</p> <p>Layer 1: 10 mm glass Layer 2: 1.52 mm PVB Layer 3: 10 mm glass Layer 4: 10 mm air Layer 5: 10 mm glass</p>	<p style="text-align: center;"><u>TYPE 3</u></p>  <p style="text-align: center;">C</p> <p style="text-align: center;">21.00< 20.40 19.80 19.20 18.60 18.00 17.40 16.80 16.20 15.60 <15.00</p> <p style="text-align: center;">U = 1.744 W/m²K</p>
	<p style="text-align: center;"><u>TYPE 4</u></p>  <p style="text-align: center;">E I</p> <p>Layer 1: 10 mm glass Layer 2: 1.52 mm PVB Layer 3: 10 mm glass Layer 4: 10 mm argon Layer 5: 10 mm glass</p>	<p style="text-align: center;"><u>TYPE 4</u></p>  <p style="text-align: center;">C</p> <p style="text-align: center;">21.00< 20.40 19.80 19.20 18.60 18.00 17.40 16.80 16.20 15.60 <15.00</p> <p style="text-align: center;">U = 1.323 W/m²K</p>

Finally, using the same analytical approach described in the section 8.2.3.5 for the energy analysis of façade systems and referring to the results obtained from the seismic loss assessment estimation presented in Chapter 5, additional graphs (Figures E.1, E.2, E.3) can be found correlating the annual energy or seismic cost of the different typology of façade to the related energy or seismic demand. The considered non-structural configurations refer to the systems presented in the previous table for the energy part, while to the traditional vs. low-damage solutions for the seismic part.

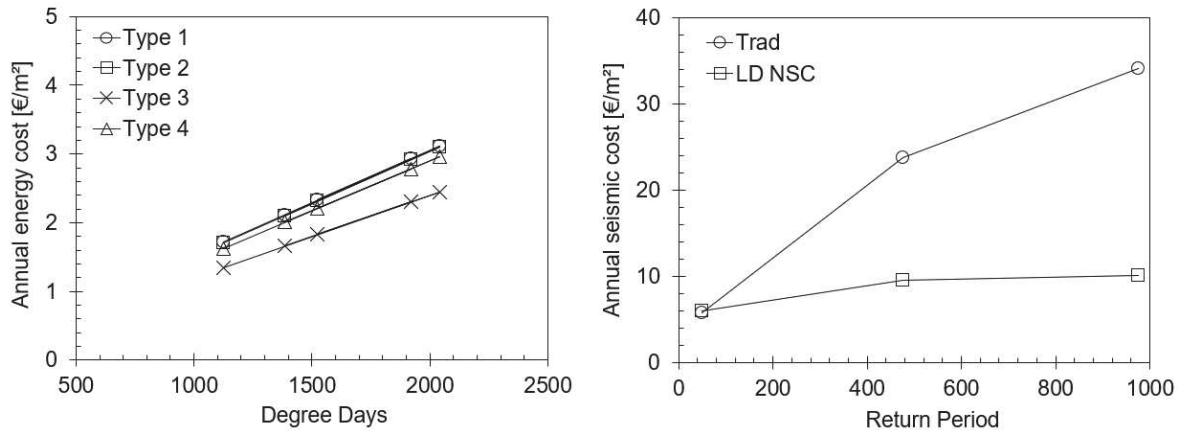


Figure E.1. Annual energy (left) and seismic (right) cost of the different typologies of precast concrete panels.

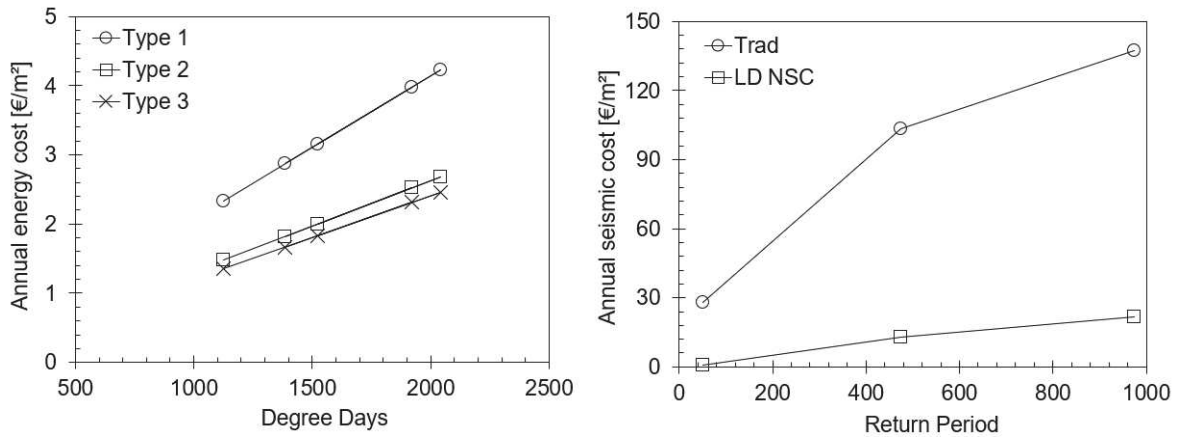


Figure E.2. Annual energy (left) and seismic (right) cost of the different typologies of infill wall systems.

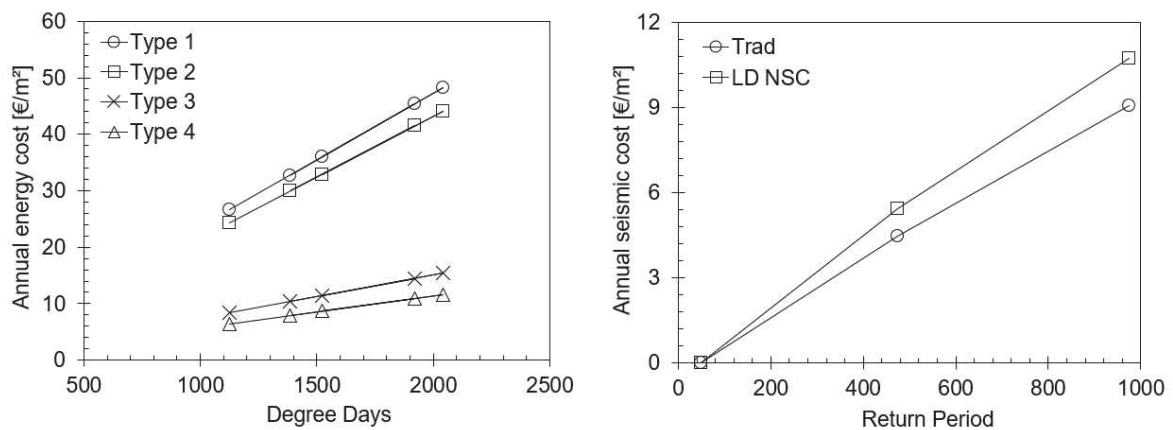


Figure E.3. Annual energy (left) and seismic (right) cost of the different typologies of spider glazing curtain walls.